

University of Nottingham
UK | CHINA | MALAYSIA

Applications of Photo-oxidation With $^1O_2$ In Multistep Reactions

Lingqiao Wu, Msc

Thesis submitted to The University of Nottingham for the degree of Doctor of Philosophy

May 2019

Abstract

There is an increasing drive to perform chemical synthesis in a greener and more environmentally friendly way, particularly on an industrial scale. Usually, this can be achieved by designing new routes to higher value chemicals, by using low hazardous solvents and avoiding the emission of high quantities of waste in an existing process. This Thesis mainly describes the progress towards the applications of dense carbon dioxide as a solvent for conducting the continuous flow reaction with photochemically generated singlet oxygen in a multistep synthesis process. This method helps to achieve a green and efficient way to produce versatile chemicals on a relatively large scale to meet the demand for the production of personalised pharmaceuticals.

Chapter 1 provides the new challenges in the chemical and pharmaceutical industry and the applications of continuous flow photochemistry in dense carbon dioxide to meet the demand for the new challenges in Pharma, as well as singlet oxygen, including a review of its known reactions. A brief introduction to green chemistry is also included. Chapter 2 describes the batch and flow reactors that are used to carry out the high-pressure experiments discussed in this Thesis.

The experimental results are discussed in three chapters: Chapter 3, Chapter 4, and Chapter 5. Chapter 3 describes the four versatile compounds, (1R, 3S)-cyclopent-4-ene-1,3-diol, 4-hydroxy-2-cyclopentenone, 4,5-epoxy-*cis*-2-pentenal, and furfuryl alcohol, were successfully synthesised from a single feedstock, cyclopentadiene, in the high-pressure continuous flow reactor on a relatively larger scale, which successfully combines the photochemistry with thermal chemistry. These experiments include the reaction conducted in dense carbon dioxide, in traditional solvents at atmospheric pressure and in a vortex reactor, with in-line analysis by FT-IR and NMR for the kinetics study of photo-oxidation of cyclopentadiene in supercritical carbon dioxide also being discussed in this chapter. Chapter 4 presents

the photo-oxidation of fulvenes to synthesise the unsaturated caprolactone in a daisy-chained high-pressure flow reactor. This method provides a new route to introducing oxygen functional group into a hydrocarbon compound. The valorisation of these lactones by hydrogenation or photochemistry processes is also discussed. Chapter 5 describes the continuous flow synthesis of 1,2,4-trioxane chemicals in supercritical carbon dioxide. Dearomatisation of *para*-alkyl phenols with singlet oxygen is a key step in this synthesis followed by the cyclisation of peroxides with aldehydes with the help of solid acid catalysts. This Chapter also presents the multistep processes were adapted and optimised for the scale-up of a series of synthetic 1,2,4-trioxanes in the high-pressure continuous flow reactor.

Finally, Chapter 6 summarises the work described in this Thesis and demonstrates the progress has been successfully achieved in a continuous high-pressure flow carbon dioxide reactor. A summary of potential research directions for further study is also discussed.

Acknowledgements

Firstly, I would like to thank my supervisors Professors Martyn Poliakoff and Mike George for giving me the opportunity to study in the Clean Technology Group and for their support and guidance throughout my PhD. I would also like to thank the Vice-Chancellor's Scholarship and the Photo-Electro Project for financial support.

I am grateful to Dr Jie Ke for his mentorship in introducing me to the world of high-pressure chemistry and for his patient help with the assembly and maintenance of high-pressure equipment and general lab works. I would also like to thank Dr Rowena Howie, who gives me the advice for the operations of high-pressure equipment.

Many thanks to Dr Darren Lee and Dr Zahra Abada for their invaluable advice of my experiments and organic chemistry, and for helping me improving my ability of analysing NMR data. Also, I am grateful to Dr Charlotte Clark for her expertise in FT-IR and to Dr Hamza Boufroura for his advice in organic chemistry.

For technical support, I would like to thank the workshop and Analytical Services departments in the University of Nottingham, in particular Mark Guyler, David Litchfield in equipment maintenance, Butler Kevin and Shazad Aslam in NMR analysis.

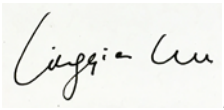
I wish to thank all my friends and colleagues at the University of Nottingham, for making my time here enjoyable. I would like to thank the project students, Judith Barwise, Clarke-Knowles Samuel and PhD student, Bruna Abreu, for their hard working. I am extremely thankful to Jing and Emilia, who always help me solve different problems in first time at the start of my PhD. Many thanks to Amy, Chris, Erica, Inès, Jonny, Jorge, Sam(s), and for their enthusiasm for difficulties. Many thanks will go to my friends in Nottingham, Zhong, Zhimin and Xue, who spend with

me a happy period. I would also like to thank all the members of the Poliakoff and George groups, past and present, for their company.

Last but no means least, I would like to thank my parents, all of my family, and my boyfriend, for their continued love, support and encouragement through whatever I've thrown at them over the years. Sadly I cannot express my gratitude to my grandpa in person now.

Declaration

I declare that the work presented in this Thesis is a record of my own work for the period of September 2015 to May 2019. Where any work has been carried out in collaboration, the relevant researcher or researchers have been acknowledged. This Thesis has not been accepted in partial or complete fulfilment of any other degree or personal qualification.



Lingqiao Wu, 28th of May 2019

Table of Contents

Abstract i

Acknowledgements iii

Declaration v

Table of Contents vii

Nomenclature xiii

Chapter 1. Introduction……. 1

1.1 The chemical and pharmaceutical industry 1

1.1.1 Chemical Industry 1

1.1.2 New Challenging in Pharma 2

1.2 Photochemistry 3

1.3 Continuous flow photochemistry 9

1.4 Singlet oxygen 12

1.4.1 Origin of singlet oxygen 12

1.4.2 Generation of singlet oxygen 15

1.4.3 Reactivity of Singlet Oxygen 19

1.4.4 The lifetime of Singlet Oxygen 26

1.5 Dense CO_2 as an alternative solvent 28

1.5.1 The choice of alternative solvents 28

1.5.2 Supercritical carbon dioxide 29

1.6 Green chemistry and sustainable chemistry 34

Thesis aims 38

Chapter 2. Experimental…..... 39

2.1 High-pressure apparatus 39

2.1.1 Batch high-pressure rig for monitoring by FT-IR..... 40

2.1.2 General diagram for high-pressure continuous flow reactor 43

2.1.3 Devices used for high-pressure equipment 49

2.2 Analytic techniques 54

2.2.1 Auto-sample Flash Chromatography..... 54

2.2.2 General Practices 55

2.2.3 Fourier Transform Infrared Spectroscopy (FT-IR)..... 55

2.3 Materials 56

Chapter 3. Scale-up of Selective Production from Photo-oxidation of Cyclopentadiene in CO_2…….....57

3.1 Introduction 58

3.1.1 Continuous flow process with photochemistry..... 58

3.1.2 Oxidation of 3.1 in a traditional solvent 60

3.2 Experimental Strategy..... 62

3.3 Investigating the reaction of Cyclopentadiene with $^1O_2$ 64

3.3.1 FT-IR monitoring in a high-pressure batch cell 64

3.3.2 NMR monitoring in atmospheric pressure 69

3.4 Development of Daisy-Chain in Flow 72

3.5 Synthesis of products in liquid CO_2 75

3.5.1 Production of Cyclopent-4-ene-1,3-diol..... 75

3.5.2 Production of 4-hydroxycyclopent-2-en-1-one in CO_2 79

3.6 Synthesis of products in supercritical CO_2 81

3.6.1 Production of cis-3-(oxiran-2-yl)acrylaldehyde (3.5) in $scCO_2$ 81

3.6.2 Production of furfuryl alcohol (3.6) in $scCO_2$ 82

3.7 The effect of CO_2 on the synthesis..... 85

3.8 Conclusion..... 88

3.9 Experimental 89

3.9.1 General information 89

3.9.2 Determination of FTIR kinetics and NMR kinetics 90

3.9.3 High-Pressure Rig operation 91

3.9.4 Characterisation of NMR data..... 96

3.9.5 Representative ^{1}H and ^{13}C NMR spectra 98

3.9.6 Optimisation of HCP 105

3.9.7 Acid catalysts screening for the production of 3.6 107

Chapter 4. Synthesis of Unsaturated lactones from the Photo-oxidation of Fulvenes…….. 113

4.1 Background 114

4.1.1 Properties of Fulvenes..... 114

4.1.2 Caprolactones 115

4.2 Process development from Cyclopentadiene to Fulvene 119

4.3 Optimisation of the photo-oxidation of 6,6-dimethyl fulvene 122

4.4 The scope of different fulvene derivatives..... 127

4.5 The investigation into methods to add further value to the caprolactones 132

4.5.1 Hydrogenation of lactone..... 132

4.5.2 Further reactions 133
4.6 Conclusions and further work 134
4.7 Experimental 136
4.7.1 Synthesis of different fulvene derivatives 136
4.7.2 High pressure setup using CO_2 as a solvent 136
4.7.3 Procedures for further value studies 140
4.7.4 Characterisation 140
Chapter 5. Flow Approaches for Dearomatisation of Phenols with $^1O_2$ 149
5.1 Background 151
5.1.1 General aspects of phenols 151
5.1.2 Oxidation of *p*-alkyl phenol derivatives with transition-metal catalyst 153
5.1.3 Photosensitised dearomatisation of *p*-substituted phenols 155
5.2 Photo-oxidation of *p*-cresol in Batch 158
5.2.1 Screening of different organic solvents 159
5.2.2 The screen of different co-catalysts 160
5.3 Dearomatisation of *p*-cresol in high pressure setup 161
5.3.1 High Pressure Setup 161
5.3.2 Oxidation of *p*-alkyl phenol derivatives by hypervalent iodine 162
5.3.3 The yield of peroxide dependence on the co-catalysts 166
5.3.4 The effect of concentration of *p*-cresol in MeOH 169
5.3.5 The scope of different phenol derivatives 172
5.4 The application of *p*-peroxyquinol 175
5.4.1 Access to 1,2,4-trioxane 175

5.4.2 The reactivity of *p*-peroxyquinol with an aldehyde in methanol 177

5.5 Dearomatisation of 5.1a using EtOAc as co-solvent 178

5.6 The reactivity of *p*-peroxyquinol 5.2a with an aldehyde in EtOAc 180

5.6.1 The reactivity of 5.2a using EtOAc as co-solvent 180

5.6.2 The reactivity of 5.2a using MeCN/ EtOAc as co-solvent 183

5.6.3 The reactivity of 5.2a dependent on the residence time 184

5.6.4 The scope of different substrates using EtOAc as co-solvent .. 187

5.7 The effect of HFIP on the dearomatisation of 5.1b 193

5.8 The scope of different aldehydes reacting with 5.2a 195

5.9 Conclusion and Future work 197

5.10 Experimental data..... 198

5.10.1 Procedure for batch reaction 198

5.10.2 Procedure for the high-pressure setup..... 199

5.10.3 Phase Behaviour study..... 205

5.10.4 NMR Data..... 208

Chapter 6. Conclusion and Future Work 213

6.1 Aim 1 and Aim 3 214

6.1.1 Rationale 214

6.1.2 Progress 215

6.1.3 Further directions..... 216

6.2 Aim 2 217

6.2.1 Rationale 217

6.2.2 Progress 219

6.2.3 Future Directions 221
6.3 Aim 4 222
6.3.1 Rationale 223
6.3.2 Progress 223
6.3.3 Future Directions 224
6.4 Aim 5 225
6.4.1 Rationale 225
6.4.2 Progress 226
6.4.3 Future directions 227
6.5 Final Words 227
Reference…… 229
Appendix…….. 261
Standard Operation Procedure for Batch cell Reaction in CO_2 261
Standard Operating Procedure for Flow photo-oxidation 264
Crystal Data 267
NMR Data (Chapter 4) 287
NMR Data (Chapter 5) 320
Excel spreadsheet for data caculations 340
Publications 341

Nomenclature

ACTs: Artemisinin-based Combination Therapies

Amb-15: Amberlyst-15

ART: Artemisinin

APIs: Active Pharmaceutical Ingredients

BTI: [bis(trifluoroacetoxy)iodo]benzene

m-CPBA: 3-Chloroperbenzoic acid

DHAA: dihydroartemisinic acid

EtOAc: ethyl acetate

FEP: Fluorinated ethylene propylene

FTIR: Fourier Transform Infrared Spectroscopy

HFIP: Hexafluoro-2-propanol

IBX: 2-iodoxybenzoic acid

ISC: Intersystem crossing

MeOH: Methanol

NBS: N-Bromosuccinimide

PS: Photosensitiser

PIDA: phenyliodoso diacetate

Pd/C: Palladium on carbon catalyst

PTFE: Polytetrafluoroethylene

S_0: Ground state

S_1: First singlet state

Sn: Singlet excited state

T_1: Triplet state

TEA: Triethylamine

TPFPP: 5,10,15,20-tetrakis-(pentafluorophenyl)porphyrin

VOCs: Volatile Organic Compounds

Chapter 1. Introduction

1.1 The chemical and pharmaceutical industry

1.1.1 Chemical Industry

The chemical industry plays a key role in converting raw materials into desirable products that we use in our daily life and is one of the largest manufacturing industries in all developed and emerging countries.[1] These chemical products, divided into basic chemicals, speciality chemicals and consumer chemicals, have an impact on several facets of our life such as healthcare, hygiene, food, decor, agriculture, environment and transportation and so on.[2] (see Table 1-1)

Table 1-1 Chemical products in the industry value chain.

Categories	Basic Chemicals	Speciality Chemicals	Consumer Chemicals
Examples	methanol, ethane, polycarbonate, ammonia	additives, pigments, dispersions	pharma intermediates, flavours& fragrances
Applications	foils, fertiliser, plastic bottles	coatings, inks, colourants	herbicides, food and nutrition

For example, chemicals are important in our food. Flavours, taste enhancers and preservatives all help the food to be palatable and increase their shelf life. This helps distribute food to different parts of the world because the preservatives maintain the quality of the food. The chemistry industry is also an essential partner for communication and automotive industry, for example, the use of screens and batteries in cell phones, as well as tyres and coatings on cars. Parallel to this, it is the

essential role in the medical professions particularly in the production of a wide range of pharmaceuticals.

The chemical industry is not only important from a scientific and societal perspective, but also from a business point of view that it continues to be a vital contributor to the global Gross Domestic Product (GDP). In 2018, it was estimated that sales of chemicals amounted to $3500 billion worldwide.[3] This means every man, woman and child in the world, averagely uses $500 worth of chemicals per year. The UK is one of the world's top countries with global chemicals and pharmaceutical industries. In the same year, the chemical and pharmaceutical businesses in the UK give over £15 billion a year Added Value to the UK's GDP. In the UK, the exports of chemicals were £40.7 billion, which together accounted for ca. 20 % of all UK manufactured exports in 2014.[4]

1.1.2 New Challenging in Pharma

The pharmaceutical industry is responsible for the development, production and marketing of medication. The industry has already contributed to significant improvements in patient well-being and today's European citizens can expect to live up to 30 years longer than they did a century ago.[5] Thus, its huge importance as a global sector is irrefutable. In 2014, total pharmaceutical revenues worldwide had exceeded 1000 billion U.S. dollars for the first time, which increased to 1,143 billion U.S. dollars in 2017.[6] As is shown above, the exports of pharmaceutical industries account for 46 % sales of all UK chemical industries in 2014.[5] The pharmaceutical industry plays a critical role in producing Active Pharmaceutical Ingredients (APIs) for the drugs and medicine.

Recently, the term "Industrie 4.0" was coined by the German federal government in a political scenario to advocate the computerisation of manufacturing.[7] It represents the fourth industrial revolution on the way to the internet of things, data, and service connected in a cyber-physical network. One of the key benefits of Industrie 4.0 is that

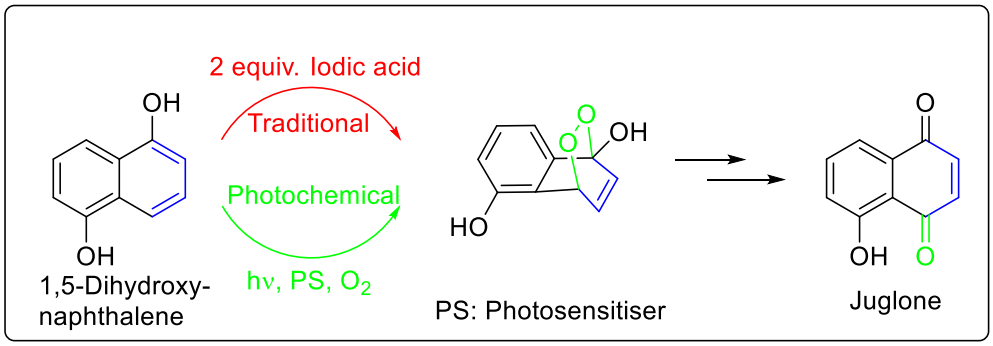
it can solve the issues associated with the increasing need of individualised products by enabling the flexible pre-configuration with the help of the smart technology so that the productivity can be dramatically improved.

This “Industrie 4.0” brought the “Pharma 4.0” to us in the viewing of the current state of pharmaceutical manufacturing. “Pharma 4.0” has more challenges associated with pharmaceutical manufacturing and quality compared to decades ago.[8] One of the reasons is that there is a shift from a “one drug fits all” approach towards more individualised therapies. Thus, one of the aims of “Pharma 4.0” is producing personalised medicine with specialised drugs for smaller targeted patient groups to improve the effectiveness of treatments.[9] During this process, a more sustainable and efficient pharmaceutical supply chain should be employed to meet the demand for the future operations and management in the full life cycle.[10] Instead of producing large amounts of the same medicine in a fixed specification, more flexible, efficient, interchangeable equipment and patient-centred suppliers for individulised medicine should be involved, such as using continuous flow process replacing batch-based mass production, as well as reducing the waste and pollution in different stages.[11] Moreover, photochemistry is known as an efficient method to access chemicals that are difficult to obtain by traditional methods.[12] All these aspects should be performed under the traditional consideration criteria, such as cost, quality, risk assessment, etc.[13]

1.2 Photochemistry

Sunlight is a readily available source of energy and is green, efficient, renewable and sustainable. But up until recently, it has not been fully utilised to produce industrially relevant chemicals.[14-15] Therefore, many researchers have thought out new ideas to utilise solar energy to catalyse chemical reactions,[16-17] giving access to reaction pathways that are not possible under thermal conditions, or require a

relatively harsh condition. A good example is the photo-oxidation of 1,5- dihydroxynaphthalene to juglone (Scheme 1-1). Harsh and toxic oxidants such as iodic or chromic acids were used in the traditional synthesis for the production of juglone from 1,5-dihydroxynaphthalene.[18] Under photochemical conditions, the reaction occurred without using iodic acid, and water is the only side product during this photochemical process.[19-20]



Scheme 1-1 Comparison of traditional and photochemical methods to prepare juglone from 1,5-dihydroxynaphthalene.

The utilisation of photochemistry provides a green and efficient process for chemistry.[21] The first reported photochemical reaction, dates back to the work of Giacomo Ciamician a century ago (Figure 1-1).[22-23] He proposed that photochemistry could offer a "cleaner" path for chemical synthesis since a clean reagent such as light is used instead of aggressive chemical reagents or elevated temperature.[24-25]

A photochemical reaction occurs when an atom or molecule absorbs "light" (Grotthuss-Draper law, also called the Principle of Photochemical Activation) at optical frequencies. Furthermore, one photon of light can only activate one molecule (Stark-Einstein law[26]). In the past few years, visible light has emerged as an initiator for the photochemical reaction of small molecules, using organic dyes to harvest visible light photons and convert this energy to an electrochemical potential, thus facilitating subsequent energy transfer or single electron transfer with organic substrates.[27-29] Photons are clean reagents, without residues left after participating

reactions, improving the atom economy. The absorption of photons is crucial to carry out photochemical reactions.

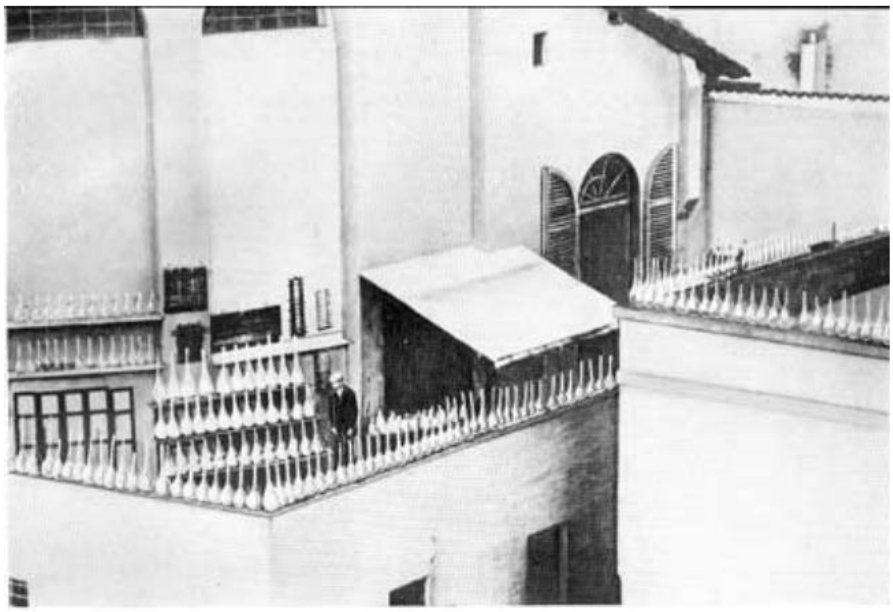


Figure 1-1 Giacomo Ciamician was surveying his collection of tubes and flasks being exposed to the sun on the roof of his laboratory. (Courtesy, Margherita Venturi), images are taken from ref.[23]

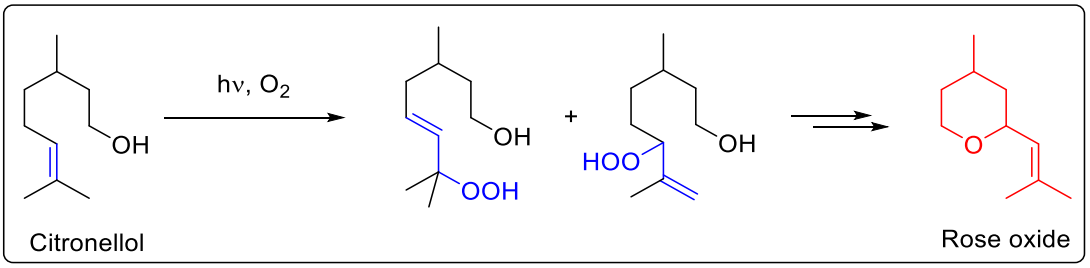
However, not every photon will activate the transformation of one molecule of the relevant material, since excited states can decay to their ground state by radiative or nonradiative processes (e.g. heating). The efficiency of a photochemical process can be qualified by its quantum yield, as presented below:

$$\Phi = \frac{number\ of\ molecules\ of\ product\ formed}{number\ of\ photons\ absorbed\ by\ reactive\ medium}$$

The quantum yield is located between 0 and 1 for nonchain mechanisms.[30]

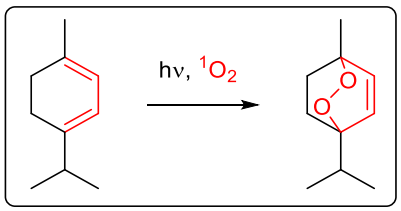
One more important “green” role for photochemistry is in improving the atom economy and efficiency. An excellent example of this is the avoidance of stoichiometric amounts of oxidants such as chromium oxide, used in the oxidation reactions. The fragrance chemical, rose oxide, has been synthesised from citronellol by a route involving singlet oxygen photochemically generated, using a

photosensitiser such as Rose Bengal under visible light (Scheme 1-2).[31-32] More details of photo-oxidation with singlet oxygen will be discussed in Section1.4.



Scheme 1-2 Synthesis of rose oxide in the photochemical process using $^1O_2$ as oxidant.

Other than the synthesis of rose oxide from citronellol with singlet oxygen, another important example of this efficient singlet oxygen oxidation to produce APIs is the well-known preparation of ascaridole from *α*-terpinene, as shown in Scheme 1-3. Ascaridole was a natural compound found in a Peruvian plant, which can be used as APIs in anthelmintic[i] drugs.[33] However, attempts to synthesis ascaridole was not successful in the 1910s until Schenck and Ziegler in 1944 discovered that light can activate *α*-terpinene to this valuable ascaridole in the presence of oxygen and chlorophyll.[34]

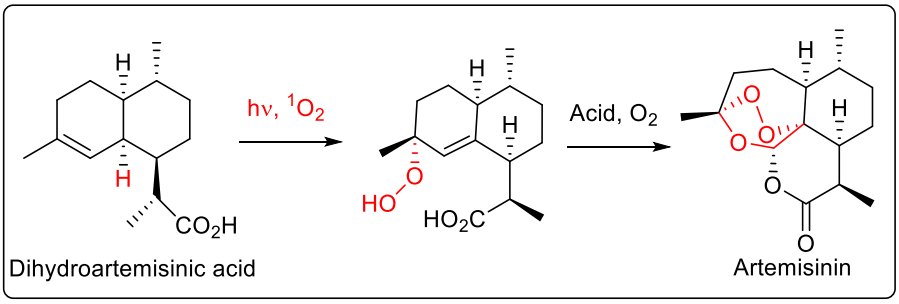


Scheme 1-3 Synthesis of ascaridole from α-terpinene with singlet oxygen.

Artemisinin was extracted in 1972 in a Chinese plant *Artemisia annua* (*qinghao*, sweet wormwood) and used as a main antimalarial drug.[35-36] A key step of the

[i] Anthelmintic drugs are a group of antiparasitic drugs that expel parasitic worms and other internal parasites from the body by either stunning or killing them and without causing significant damage to the host.

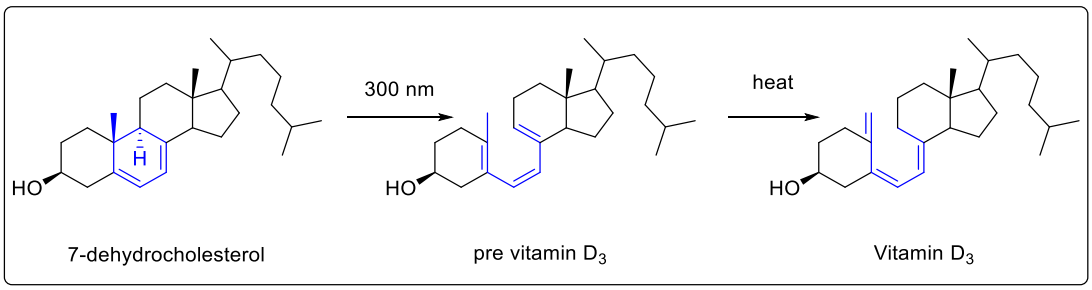
chemical method for the synthesis of artemisinin was the singlet oxygen reaction of dihydroartemisinic acid,[37-39] as shown in Scheme 1-4.



Scheme 1-4 Synthesis of Artemisinin via singlet oxygen reacting with dihydroartemisinic acid.

Moreover, a photoinitiated process has potential advantages even when compared to the reaction initiated by using catalysts. Since the energy for the reaction is more directed, reaction temperatures are usually lower, which can give higher selectivity, reducing side products from competing pathways. A critical feature of all light-promoted transformations is the involvement of electronically excited states, generated upon absorption of photons. This generates transient reactive intermediates and alters the reactivity of chemical compounds.[40-41]

Another “green” credential of photochemistry is that the photochemical method provides a new process leading to products that would be difficult to achieve by other traditional routes, such as the production of vitamin D_3 in the industrial photochemical process (Scheme 1-5). This process involves a photochemical electrocyclic ring opening of 7-dehydrocholesterol followed by a thermal 1,7-hydride shift, and there is no viable alternative thermal process.



Scheme 1-5 Vitamin D3 synthesis using a photochemically method in the first step.

Over the time of this PhD, there has been an ever increasing interest in organic photochemistry, as demonstrated by the number of recent reviews.[21, 42-46] Although academic research on photochemistry dates back many years, its applications in industry have been limited, as a result of there being significant unsolved engineering problems. Reactor fouling is a common problem in chemical manufacturing. Moreover, in photochemical processes even small amounts of fouling on the window or reactor wall, through which the light has to pass, can completely prevent the reaction occurring because phochemical reactions are driven by the absorption of photons. In addition, since the power of transmitted light drops off as the square of the distance from the light, the reactants must be as close as possible to the light source.[47] This has practical implications for the special design of industrial reactors to access light as efficiently as possible. The most likely problem to hinder the application in large scale is that light penetration is not efficient in traditional batch reactors. The large volume of batch reactor leads to insufficient light penetrating through the reaction mixture due to the increased path length, as shown in Beer-Lambert Law (Eq Chapter 1.1).

$$A = log_{10}T = log_{10}\frac{I_0}{I} = \varepsilon cl \qquad \text{(Chapter 1.1)}$$

This equation shows that the correlation between light absorption (*A*) and the molar extinction coefficient (ε) of the light absorbing molecules, their concentrations (c) and the path length of light penetration (l). T represents transmittance, and I and I_0 represents the transmitted light intensity and incident light intensity, respectively.

According to the key parameters for photochemistry, continuous flow photochemical reactors have many advantages over batch reactors when used in industry. These will be discussed as follows.

1.3 Continuous flow photochemistry

Some aspects of the chemistry involved with the design of the “greener” routes and products have been discussed along with the photochemical technique and preventing waste as well as improving the atom economy. Most of them are focused on what chemists can do, but engineering also makes a big step for “greener” chemistry and Pharma 4.0.

Increasing the productivity of chemical reactions to industrial scale has proven to be a great challenge for chemists and chemical engineers since scale-up from the laboratory is not always straightforward. The reactions that may appear to be a green and efficient on the bench may not result in a green and safe process in the industry without appropriate development, such as the correct choice of the reactor and other necessary equipment. Chemical processes can be divided into two types, batch and continuous flow process. Continuous photochemistry has many advantages over the traditional batch reactors.

Firstly, photochemical flow reactors can improve the efficiency of irradiating the reaction mixture. As discussed in Section 1.2, photochemical reactions are driven by the absorption of photons. It is important that a homogeneous energy distribution inside a photoreactor leads to high yields and high selectivities. The Beer-Lambert Law implications (Eq Chapter 1.1) are well-known that the irradiation distribution will not be uniform in a reactor due to the absorption effects. To obtain a good irradiation distribution and thus maximise the efficiency of the photochemical process, it is better to use a small reactor to achieve uniform light penetration.[48]

In this case, photochemical flow reactors also provide more reliable scale-up. Scale-up of photochemistry in the industry is problematic due to the Beer-Lambert limitation of photon transfer, even in a large laboratory scale. The advantages of photochemical synthesis on a small scale are difficult to be fully employed on a larger scale when using a traditional dimension-enlarging strategy. This results in applications of photochemical transformations in the pharmaceutical and fine chemical industry being severally impeded.[49-50] The diameter of photoreactor should be as small as possible to achieve better light penetration. Therefore, microreactor technology is prevalent for the scale-up of photochemical productions.[51-53] Essential strategies are mainly focused on two kinds of micro-photoreactors: (1) longer the irradiation time by numbering-up (2) increasing the throughout by increasing the flow rates.[54-55] The numbering-up flow micro-photoreactor provides a chance to do library synthesis (Figure 1-2),[56] but the productivity is difficult to reach very large scale due to the size of microreactor.

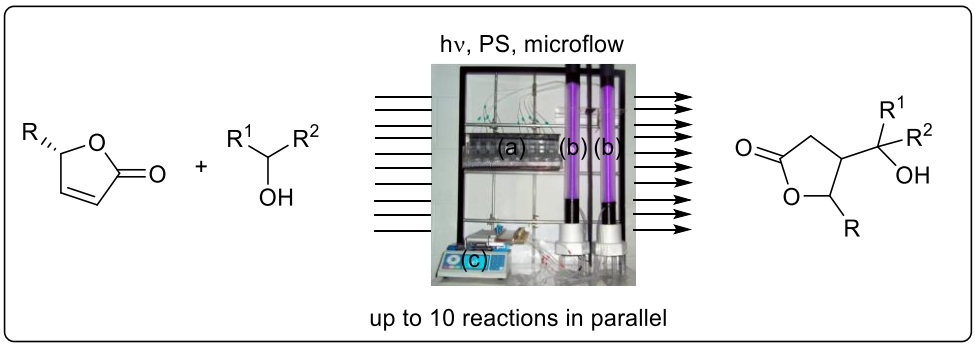
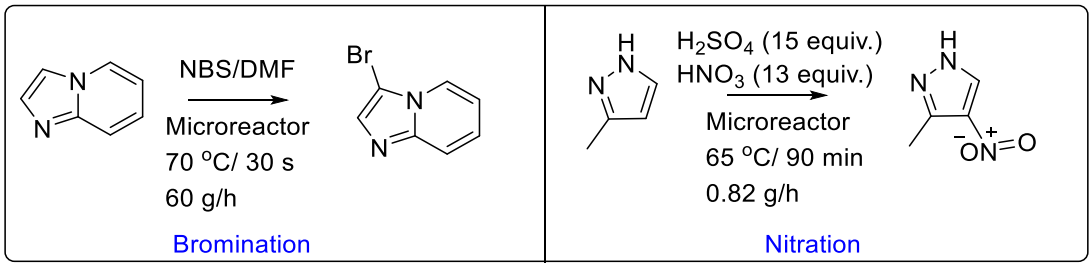


Figure 1-2 Mulitimicrocapillary flow reactor for the synthesis of furanone derivatives: (a) collection flasks; (b) FEP microcapillaries; (c) 10 syringe pump. "PS" represents photosensitisers.

Moreover, continuous flow reactions are much safer than batch reactions because the quantity of reaction occurring at any time is minimised. Smaller reactor volumes can usually be used in continuous flow processes to improve reaction selectivity and reproducibility while maintaining high throughput. These benefits are often attributed to the enhanced mass-, heat- and photon-transfer phenomena

observed in microchannels, which offers a high reproducibility of the reaction.[57] Usually, smaller flow reactors can be operated under pressure and without an air chamber, and so volatile gases of toxic and explosive nature (e.g. Hydrogen azide(HN_3)[58] and hydrogen cyanide[59]) can be kept in solution during the reaction, both increasing the reaction rate and in some cases preventing gases reaching a lower explosion concentration. Furthermore, the hazardous reagents can be treated in-line if necessary rather than requiring extra risky disposal procedure; and once neutralisation has been done can be disposed of following the standard procedures.[60-61] Researchers at AstraZeneca reported the facile, fast, and safe process development of bromination and nitration reactions using a Syrris microreactor continuous reactor (Scheme 1-6).[62] Due to the increased safety, reaction conditions which are impossible to carry out in a batch reactor can be carried out in the flow. This safety assessment is especially true for photochemical reactions with singlet oxygen, due to the potentially explosive character of O_2 storage and handling on a large scale.



Scheme 1-6 Nitration and Bromination in Microreactor at AstraZeneca. NBS represents N-bromosuccinimide.[62]

Fast heat exchange and mass transfer in photochemical reactions are important to keep the reaction temperature inside the reactor stable and to avoid by-product formation by thermal pathways, as well as good selectivity with minimum concentration gradient.[63] For photochemical processes, the reaction temperature can increase due to heating from the light source and exothermic reaction, e.g. singlet oxidation reactions.

Continuous flow process also can enable much faster reaction optimisation, thereby reducing costs and saving chemists' valuable time. The reasons are that the conditions in a continuous flow chemistry reactor are usually easy to vary; such as reaction time by varying the total flow rate, the reaction temperature due to good mass transfer, the concentration by varying the flow rate ratio of reagents being pumped. This merit is in accordance with the Pharma 4.0, pursuing the aim of individualised drugs production, and as a result large numbers of reactions need to be optimised. Readily employing in-line analysis in the flow system to give the timely feedback and results can be realised much more accessible than in batch reactor.

Moreover, immobilised catalysts can be used in continuous flow reactors,[21] the reactors are filled with supported catalyst before the other chemicals are pumped through because immobilisation of photocatalysts on the wall of reactors is an interesting way of recycling the catalyst to increase the economic viability of the photocatalytic process.[64] These photocatalysts can be irradiated from the front and back sides of the reactor.[65] Another advantage of continuous flow over a traditional batch process is that multi-step reactions can be conducted in a continuous sequence because the reagents required for subsequent steps can be added downstream.[66-67]

1.4 Singlet oxygen

1.4.1 Origin of singlet oxygen

Multiple oxygen atom sources for photo-oxidation are present, but molecular oxygen is an attractive oxidant because of its atom efficiency, reduced cost and sustainable nature.[68] The chemistry of singlet oxygen ($^1O_2$) has been of considerable interest[69-70] because of its importance in atmospheric, biological,[71] and photodynamic therapy (PDT) of cancer,[72] and particularly its use as a reagent in organic chemistry.

The history of research on photo-oxidation involving $^1O_2$ dates back to the 19th century. In the late 18th century, a biologist discovered that dyes and oxygen, with the help of light, are toxic to some organisms due to photochemical process *via* an unknown mechanism.[73-74] It was not until 1924 that Lewis proposed that ground state molecular oxygen was a triplet diradical species.[75]

The properties and behaviour of oxygen reflect its unique electronic structure. Molecular oxygen orbital descriptions of different states were provided in the late 1920s, as shown in Figure 1-3.[76] Unlike many other homonuclear molecules, molecular oxygen's electronic ground state, $^3O_2$ or O_2 ($^3\Sigma_g$), is a spin triplet state. One of the molecular oxygen's excited electronic states, O_2 ($^1\Delta_g$), is a spin singlet state, called "singlet oxygen or $^1O_2$".[69, 77-78]

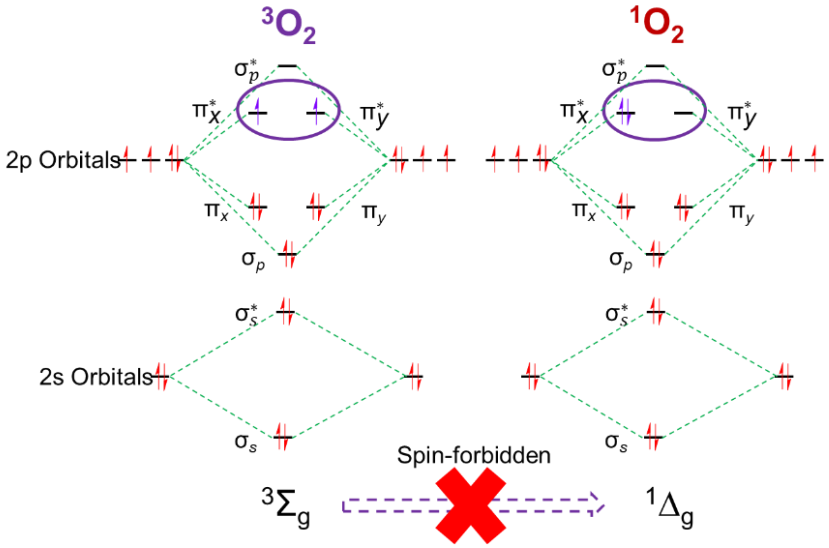


Figure 1-3 The molecular orbital diagrams for ground state molecular oxygen, $^3O_2$ or O_2 ($^3\Sigma_g$), and its excited singlet states, $^1O_2$ or O_2 ($^1\Delta_g$).[77-78]

Electronic configurations of these states differ only by the structure of the *π*–antibonding orbitals. Two electrons with parallel spin occupied in two separate *π*–antibonding orbitals in molecular oxygen ground state; in O_2 ($^1\Delta_g$) state, the two electrons occupied a single π–antibonding orbital with antiparallel spins.[78, 79]

However, the transition from the O_2 ($^1\Delta_g$) state (95 kJ/mol) to the O_2 ($^3\Sigma_g$) state (ground state) is spin forbidden, thus the O_2 ($^1\Delta_g$) is a relatively long-lived species.[69]

As shown in Figure 1-4, the second excited state of oxygen, O_2 ($^1\Sigma_g$) state (157 kJ/mol) is short-lived due to a spin-allowed transition to the O_2 ($^1\Delta_g$) state, and there are two electrons with antiparallel spins occupied in two separate π–antibonding orbitals in the O_2 ($^1\Sigma_g$) state. This difference in stability between O_2 ($^1\Delta_g$) state and O_2 ($^1\Sigma_g$) state is confirmed by the radiative lifetimes of O_2 ($^1\Sigma_g$) to O_2 ($^1\Delta_g$), which are 2700 seconds and 7-12 seconds in the gas phase,[80] and 10^{-6}-10^{-3} seconds and 10^{-11}-10^{-9} seconds in solution.[81] O_2 ($^1\Sigma_g$) rapidly decays into O_2 ($^1\Delta_g$) because of collisions between oxygen and solvent molecules.[82] These results provide the evidence for identifying the excited species involved in the photo-oxidation being O_2 ($^1\Delta_g$) rather than O_2 ($^1\Sigma_g$).[83-84]

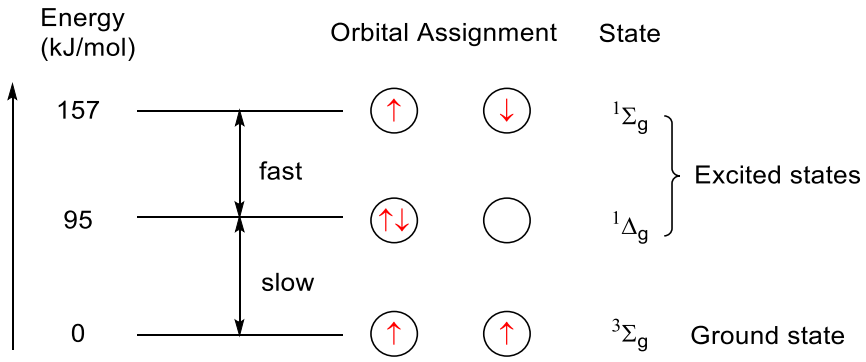


Figure 1-4 Primitive representations of molecular oxygen lowest singlet and triplet states.[78]

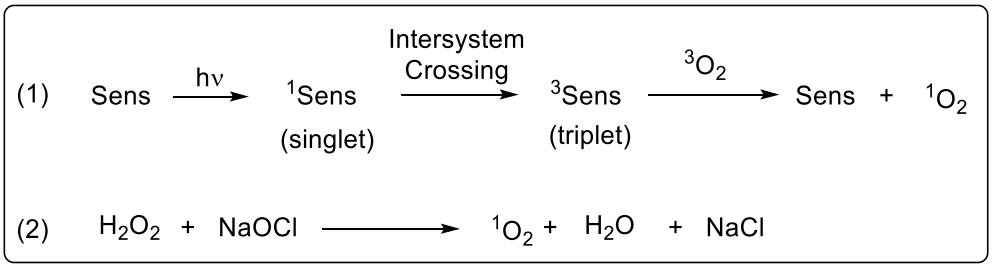
It was not until the 1960s that the idea that O_2 ($^1\Delta_g$) is an intermediate involved in the photo-oxidation was widely accepted, when Kautsky and Schenck reported a short-lived sensitizer-oxygen adduct (·Sensistiser-OO·) of the $^1O_2$ "ene" reaction of alkenes to give an allylic hydroperoxides[85] and Kasha and Khan detected the red chemiluminescence of $^1O_2$ in NaOCl-H_2O_2 systems and attributed this to the emission of pairs of $^1O_2$ molecules.[86-88] Kautsky's idea of a dye-sensitised photochemical route to O_2 ($^1\Delta_g$) was demonstrated in 1964.[89-90] Finally, singlet oxygen luminescence was established in the gas and condensed phases, where $^1O_2$ decays to $^3O_2$ + hν at 1268 nm.[91-93]

1.4.2 Generation of singlet oxygen

Mechanism of $^1O_2$ generation

As mentioned above, transitions between one of these excited states and the ground state are forbidden due to electric-dipole selection rules.[94] This forbidden characteristic usually prohibits the direct generation of $^1O_2$ from molecular oxygen to react with chemical acceptors.[95-96]

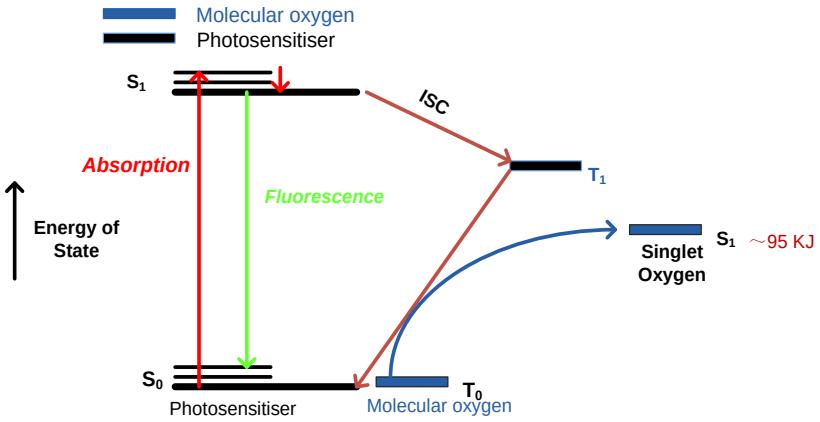
As shown in Scheme 1-7, $^1O_2$ usually can be generated *via* two independent routes: (1) a photochemical method in dye-sensitised photo-oxidation, and (2) a chemical method involving NaOCl and H_2O_2.[87, 89-90]



Scheme 1-7 Two general methods to generate $^1O_2$; "Sens" means photosensitiser; (1) A photochemical route to generate $^1O_2$; (2) A chemical route to generate $^1O_2$.

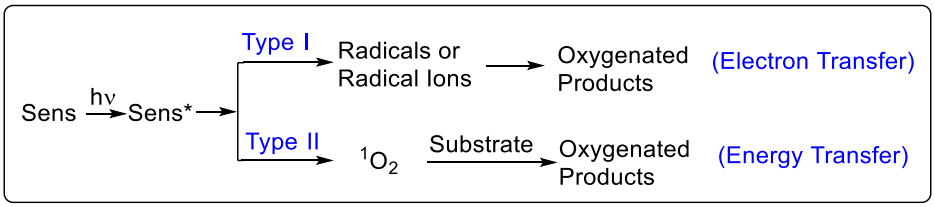
The photochemical generation of $^1O_2$, namely photosensitisation as it is termed nowadays, is the most prevalent.[73, 97] Photosensitised generation is a simple and controllable method for the production of $^1O_2$. As shown in Scheme 1-8, this method requires only oxygen, light of an appropriate wavelength, and a photosensitiser being capable of absorbing that light and exciting the molecular oxygen to its singlet state. Photosensitiser excitation is generally initiated *via* a one-photon transition ($h\nu$) from the ground state, S_0, to a singlet excited state S_n. Relaxation of the S_n state yields the lowest excited singlet state of the photosensitiser, its first singlet excited state, S_1. Then, the S_1 state of photosensitiser will pass to its triplet state (T_1) *via* an intersystem crossing (ISC) process.

$^1O_2$ is generated *via* an energy transfer process during a collision of the excited sensitiser (T_1 state) with molecular oxygen, namely generated in the process of relaxation of the photosensitiser from its T_1 state to the S_0 state, transferring the remaining energy to $^3O_2$, as shown in Scheme 1-8. Each photosensitiser molecule can typically produce 10^3-10^5 moles of $^1O_2$ before being degraded through photo bleaching or by some other process (refer to Section 1.4.4).[78]



Scheme 1-8 A Jablonski diagram describing the generation of the photosensitiser excited states and the reactive dioxygen species for Type II photo-oxidation.[78]

Apart from the generation of $^1O_2$ in this photochemical process, other reactive species also can be generated. Therefore, there are two understood modes of photosensitised oxidations: Type I and Type II (Scheme 1-9), which were firstly proposed by Foote.[98] The distinction between Type I and Type II modes depends on the nature of the intermediates produced.[85] In both cases, the photosensitiser in its ground state, S_0, absorbs light and is excited to the S_1. Intersystem crossing generates the sensitiser triplet state, T_1. The lifetime of the T_1 state is longer (μs) than that of the S_1 state (ns) allowing the triplet state to further react in one of the two ways, namely Type I and Type II mechanisms.



Scheme 1-9 The methods of Type I and Type II for the photosensitised oxidation. Sens means photosensitiser.

In the case of Type I mechanism, the excited state T_1 photosensitiser reacts with an organic substrate through an electron transfer, yielding free radicals. These radicals can react with oxygen to form active oxygen species such as the superoxide radical anion,[69] as shown in Figure 1-5. While in a Type II mechanism,[99] the T_1 state of the photosensitiser activates ground state molecular oxygen to $^1O_2$ *via* energy transfer, which has been explained above. Thus the spin restriction is removed, increasing the oxidising ability of $^1O_2$ compared to ground state O_2.

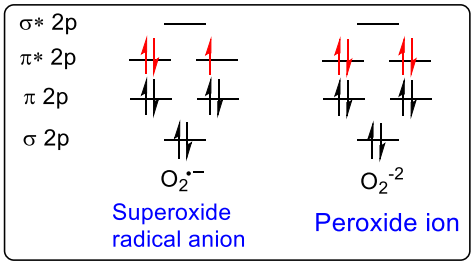
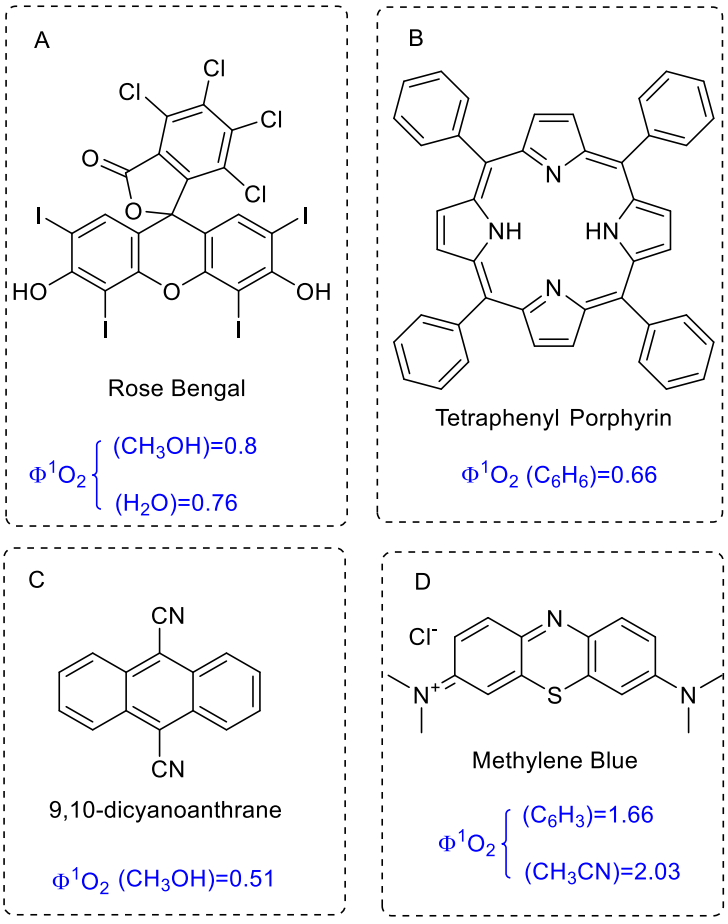


Figure 1-5 Molecular orbital diagrams from the superoxide radical anion $O_2^{\bullet -}$ and the peroxide ion O_2^{-2}.

There are three main factors which lead to the $^1O_2$ generation as the dominant mechanism of the photosensitisation.[100] Firstly, molecular oxygen has an uncommon electronic structure with two low excited singlet states and is a small molecule with a high diffusion coefficient. Secondly, the lowest triplet state of many photosensitisers has sufficient energy to excite oxygen to its singlet states in spin-allowed transitions. Finally, the concentration of oxygen in the atmosphere is high.

Photosensitisers

An appropriate photosensitiser is also very important for the efficient production of singlet oxygen. An ideal photosensitiser should be, therefore, thermally and photochemically stable, and have a solvent-independence. They usually include a high extinction coefficient at the required wavelength of light and high quantum yield for the production of a triplet state with a lifetime, sufficiently long to generate the O_2 ($^1\Delta_g$) state. Almost all families of dyes can be used for generating $^1O_2$ upon irradiation by light with suitable wavelength. There are some commonly used and commercial photosensitisers listed in Scheme 1-10, such as rose bengal, methylene blue, tetraphenylporphyrin, and 9,10-dicyanoanthrane. The triplet state energies for these photosensitisers are higher than the $^1O_2$ state energy (94.2 kJ/mol) to excite the ground state molecular oxygen.



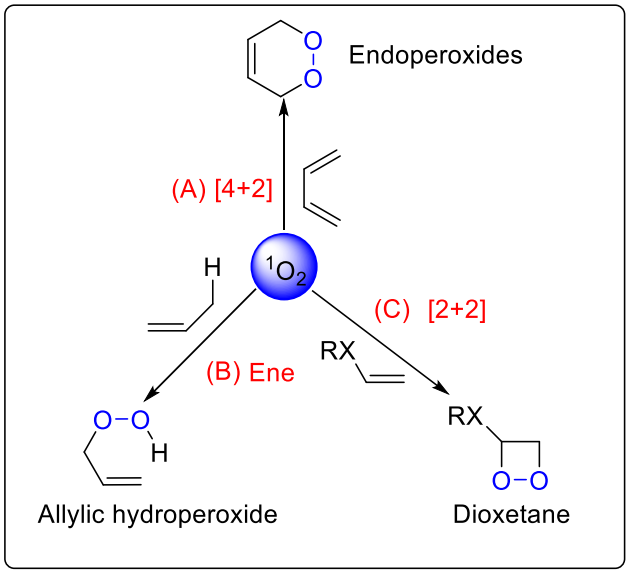
Scheme 1-10 Four commercially available photosensitisers.

There are other chemical methods generating singlet oxygen, such as two oxidants system (NaOCl and H_2O_2)[101-102] and chemical decompositions typically *via* decomposition of either phosphite ozonides[103] or an endoperoxide.[104-105] Chemical methods are useful for providing a well-defined quantity of $^1O_2$ but they often need stoichiometric, or more than stoichiometric quantities, of precursors whose byproducts need to be separated from the reaction mixtures, making the process more expensive and laborious. In addition, the procedure for NaOCl and H_2O_2 cannot be used for substrates that react with hydrogen peroxide or cannot tolerate water or alcohol as solvents.[102]

For the work discussed in this Thesis, $^1O_2$ has only been generated *via* a photochemical method since it provides a clean and efficient route to obtain $^1O_2$ and is readily scalable in a continuous flow reactor.

1.4.3 **Reactivity of Singlet Oxygen**

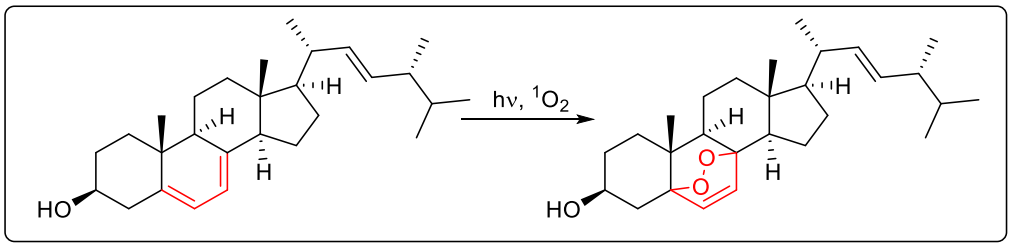
As explained above, the ground state of molecular oxygen is a triplet state with two parallel spins. Its reaction with closed-shell singlet organic molecules is spin forbidden. By contrast, $^1O_2$ is in a singlet state and is highly electrophilic due to its vacant molecular orbital, and is known to participate in a number of different reaction types with unsaturated molecules.[89, 106] The majority of the $^1O_2$ reactions with olefins can be divided into three major pathways: (i) conjugated dienes react preferably by [4+2] cycloaddition to form endoperoxides;[107-108] (ii) unactivated olefins with allylic hydrogen atom undergoes ene-type reaction to form allylic hydroperoxides;[109-111] (iii) electron-rich olefins preferably give 1,2-dioxetanes by the [2+2] cycloaddition.[110] (Scheme 1-11)



Scheme 1-11 The main reactions of singlet oxygen with alkene compounds.

[4+2] Cycloaddition

In 1928, the first photo-oxygenation by $^1O_2$ was discovered, the [4+2] cycloaddition of ergosterol, when a bridged peroxide compound was isolated (Scheme 1-12).[66, 112]

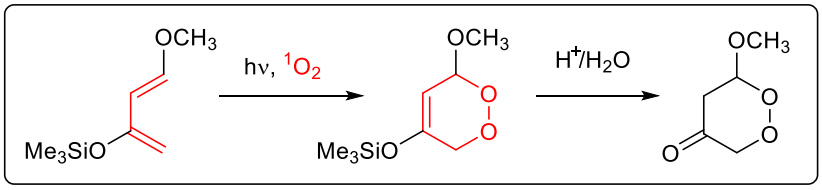


Scheme 1-12 The first photo-oxidation of ergosterol to a bridged peroxide using a photochemicaly way producing $^1O_2$.[66]

Since then, numerous examples of Diels-Alder-type additions of $^1O_2$ have been reported.[54, 108, 113-115] $^1O_2$ reacts with electron rich s-*cis* dienes to form endoperoxides in a process analogous to the Diels-Alder reaction. A well-known example for [4+2] cycloaddition is the photo-oxidation of α–terpinene to ascaridole, as already shown in Scheme 1-3 above.[34]

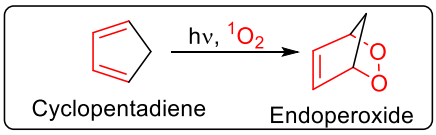
1,3-butadienes undergo [4+2] cycloadditions with singlet oxygen have been classified into five different categories: nonhomoannular 1,3-dienes, homoannular aliphatic dienes, alkenyl arenes, heterocyclic 1,3-dienes and nonheterocyclic aromatic dienes.[116]

Non-homoannular 1,3-dienes are acyclic dienes which react to form monocyclic endoperoxides. These dienes often contain aliphatic, aromatic, or heteroatom substituents. As shown in Scheme 1-13, 1,3-diene is a nonhomoannular diene bearing a trimethylsiloxyl group which functions as an inherent carbonyl.[117-118]



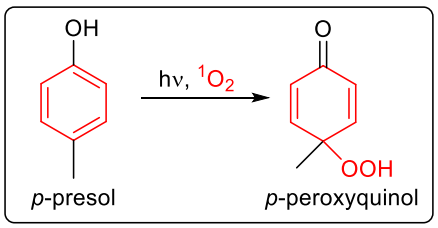
Scheme 1-13 An example of [4+2] cycloaddition of non-homoannular 1,3-diene with $^1O_2$.[117]

Homo-annular aliphatic dienes have both double bonds endocyclic in the same aliphatic ring and react with $^1O_2$ to give bicyclic rather than monocyclic endoperoxides. For example, cyclopentadiene reacts with $^1O_2$ to form 2,3-dioxabicyclo[2.2.1]endoperoxide (Scheme 1-14), which is the reactive motif of prostaglandin endoperoxide.[119-121]



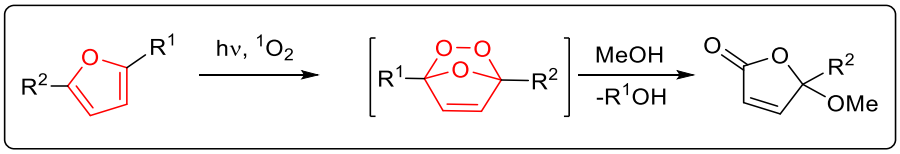
Scheme 1-14 Homo-annular aliphatic dienes react with $^1O_2$ to give bicyclic endoperoxides.[120]

Alkenyl arenes are also acyclic dienes but in which one of the conjugated double bonds is also part of an aromatic system (Scheme 1-15). The aromatic part can be phenyl, naphthyl, or heteroaromatic such as furyl.[122-124]



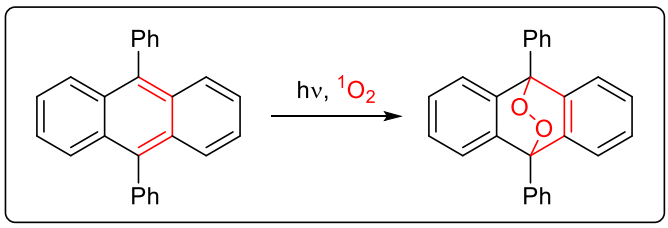
Scheme 1-15 Photo-oxidation of alkenyl arenes in an aromatic system with $^1O_2$.

Heterocyclic 1,3-dienes can either be aromatic such as furans (Scheme 1-16)[125-127] or nonaromatic such as pyran.[128]



Scheme 1-16 Photo-oxidation of furan with $^1O_2$ via [4+2] cycloaddition.[127]

The final 1,3-diene category is **non-heterocyclic aromatic dienes** as exemplified by the photo-oxidation of 9,10-diphenylanthracene,[129] as shown in Scheme 1-17. Mononuclear aromatics must be heavily substituted to react, such as hexamethylbenzene.[130]



Scheme 1-17 Photo-oxidation of non-heterocyclic aromatic diene, 9,10-diphenylanthracene.[129]

The synthetic importance of 1,3-dienes reacting with singlet oxygen *via* [4+2] cycloaddition results from the number of versatile transformations that can be done from endoperoxides,[131] and some of these transformations are present in Figure 1-6. These secondary transformation products can be used in active pharmaceutical

ingredients,[70, 132-134] such as prostangladins[119] and artemisinin[39, 135-137] synthesis of natural products,[42] and in bioscience.[121, 138]

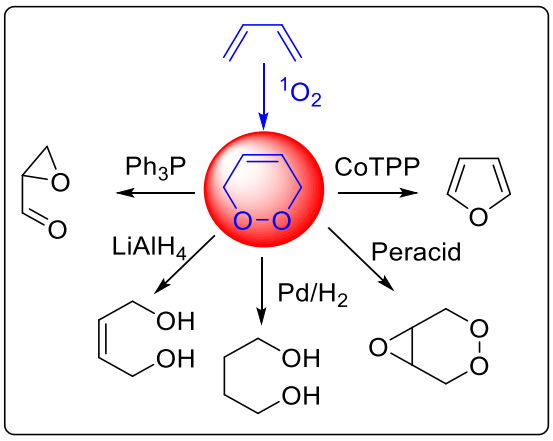
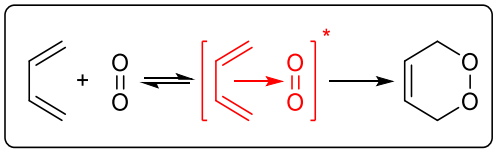


Figure 1-6 Some synthetic transformations of endoperoxides.[131]

Mechanisms of the [4+2] cycloaddition with singlet oxygen

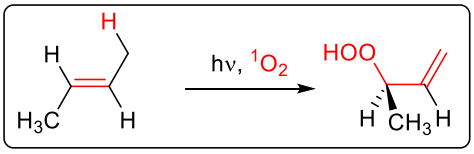
In terms of the versatile [4+2] cycloaddition, a concerted reaction mechanism was initially postulated analogous to the classical Diels-Alder reaction.[139] However, further studies including computational calculations[140] and kinetic isotope effects on the stereochemical,[141] as well as the evidence for the formation of an exciplex intermediate[142] have been performed to give a more accurate description for the mechanism of [4+2] cycloaddition with $^1O_2$, as shown in Scheme 1-18. Moreover, this intermediate with a loose structure is consistent with the observation that many [4+2] cycloadditions with singlet oxygen occur stereospecifically.[143]



Scheme 1-18 An exciplex intermediate formed in the [4+2] cycloaddition with $^1O_2$.[140-142, 144]

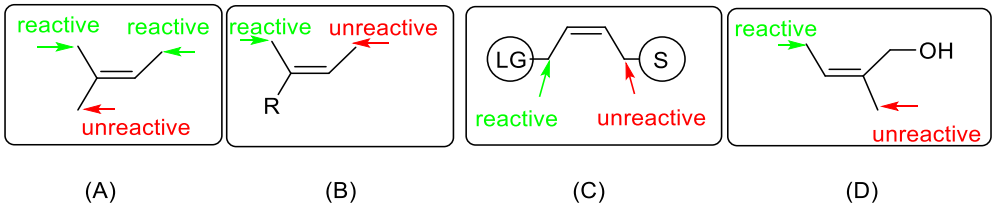
Ene reaction

The singlet oxygen ene reaction (Scheme 1-19) was first reported in the 1940s by Schenck to produce an allylic hydroperoxide,[34] formed by the addition of oxygen to a carbon of the alkene substrate and abstraction of hydrogen from a distal allylic carbon.



Scheme 1-19 An ene reaction performed in the 1940s by Schenck.[34]

These allylic hydroperoxides can also be readily reduced to synthetically important alcohols,[124, 133, 145-146] due to its controllable stereo- and regiochemistry. This control depends on four main factors: (A) mechanistic constraints;[147] (B) hydrogen bonding;[148] (C) electronic perturbations;[149-150] (D) steric perturbations.[151] These high stereo-controlling effects have been further investigated recently in Griesbeck's group.[152]

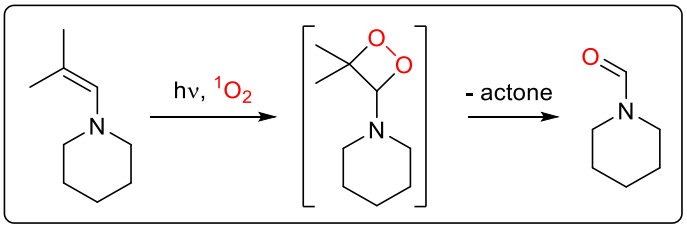


Scheme 1-20 Singlet oxygen ene regiodirecting effects: (A) "cis"-site selectivity; (B) gem-selectivity, R is electron withdrawing group; (C) "Large-group non-bonding" effect and "S" means small group; (D) allylic alcohol directing effect.[152]

The diastereoselective ene reaction with singlet oxygen is the first step of multi-step processes and introduces a tertiary hydroperoxide motif *via* an exo-selective attack of $^1O_2$ onto the alkene bond of an artemisinic acid derivative,[39, 153] as shown in previous Scheme 1-4. Further oxidative transformations including Hock cleavage and enol oxidation by molecular oxygen followed.[154] More details of ene reactions are discussed in Dr. Jessica Hall's Thesis.[155]

[2+2] Cycloaddition

[2+2] cycloadditions of singlet oxygen react with electron-rich alkenes to give dioxetanes. These alkenes can also undergo both ene and [4+2] cycloaddition in some cases.[156] In most cases, the singlet oxygen ene reaction is predominant. However, there are three main cases where [2+2] cycloaddition are prevailing to form dioxetanes. The first one is that no allylic hydrogen is available;[157] also, the allylic hydrogens are not optimally positioned perpendicular to the π–π system in the alkene,[158] as well as singlet oxygen is driven by an allylic heteroatom to a side without available allylic hydrogen.[159] The [2+2] cycloaddition of singlet oxygen coupled with thermal decomposition of dioxetane is a useful method to oxidatively cleave a carbon-carbon double bonds (Scheme 1-21).[160-161]



Scheme 1-21 [2+2] cycloaddition of $^1O_2$ coupling with a thermal reaction to cleave carbon-carbon double bond.[161]

The reaction rate of these types of chemical reactions usually depends on the competitive singlet oxygen deactivation routes. These deactivation routes include nonradiative electronic-to-vibrational energy transfer to solvent and physical quenching which occurs in the presence of an added quencher, an impurity or the substrate itself.[82, 162] $^1O_2$ also can decay via a radiative channel in solution but its rate is very slow compared to other deactivation methods.[163]

1.4.4 **The lifetime of Singlet Oxygen**

The lifetime of $^1O_2$ is determined by the relaxation rates to the ground electronic state of oxygen, O_2 ($^3\Sigma_g$).[82] One of the major breakthroughs in the singlet oxygen scientific community was the development of methods to directly detect rates of the $^1O_2$ decay by its characteristic phosphorescence emission at 1275 nm by time-resolved experiments.[164] This technique allow one to detect the accurate $^1O_2$ decay rate constant (k_Δ) or its reciprocal parameter, the $^1O_2$ lifetime (τ_Δ) in different media. The results reveal that the $^1O_2$ decay kinetics are highly dependent on the environment where it is located.[165] The k_Δ can be expressed as below:

$$k_\Delta = \tau_\Delta^{-1} = k_{\Delta,\,r} + k_{\Delta,\,NR} + k_{\Delta,\,R}$$

Where $k_{\Delta,\,r}$ is the rate constant for chemical reaction quenching of $^1O_2$, $k_{\Delta,\,NR}$ is the rate constant for the nonradiative $^1O_2$ deactivation and $k_{\Delta,\,R}$ is the rate constant for the radiative $^1O_2$ deactivation. We should recognise that the inequality $k_{\Delta,\,NR} \gg k_{\Delta,\,R}$ is applicable for most solvents of practical consequence.[82]

Radiative deactivation of singlet oxygen

The purely radiative lifetime of $^1O_2$ is relatively long, approximately 2700 s as it is a forbidden electric dipole process in terms of spin, parity and angular momentum.[166] However, it varies from microseconds in the gas phase to only a few nanoseconds in solution.[163, 167] The solvent has an effect on the lifetime of $^1O_2$ and it has been observed that there is a reasonable correlation between $k_{\Delta,\,R}$ and the solvent polarisability expressed as a function of the solvent refractive index, where $k_{\Delta,\,R}$ increased with the polarisability of the solvent.[167]

Nonradiative deactivation of singlet oxygen

Other than the chemical reactions, there are three pathways of interaction leading to the nonradiative deactivations of $^1O_2$:[168] (a) charge-transfer quenching,[169-170] (b) electronic to vibrational energy transfer[171-172] and (c) electronic energy transfer to

solutes[i] molecules such as carotenoids.[173-174] In homogenous solution, the factor that electronic to vibrational energy transfer is mainly responsible for the lifetime of $^1O_2$.[82] In order to undergo electronic to vibrational energy-transfer deactivation, $^1O_2$ must transfer its energy to a vibrational mode of the solvent. The better that energy of this vibrational mode matches with that of the $^1O_2$ deactivation energy, and the faster that this process will occur. The deactivation of $^1O_2$ is favoured in O-H containing solvents, e.g. H_2O, whereas it is clearly reduced in C-H and C-F comprising solvents, as shown in Table 1-2.[175] Similarly, the lifetimes are considerably increased in deuterated solvents because of a poor match with the $^1O_2$ vibrational deactivation.

Table 1-2 Rate constants for the electronic to vibrational energy transfer of $^1O_2$ to different X-Y bonds in solutions.[176]

X-Y	$k_{\Delta, NR}$, $M^{-1}S^{-1}$	X-Y	$k_{\Delta, NR}$, $M^{-1}S^{-1}$
O-H	2900	O-D	132
N-H	1530	C-Cl	0.181
C-H	309	C-F	0.049

The lifetime of singlet oxygen in different solvents

The lifetime of $^1O_2$ depends considerably on its environment; in particular, it varies from solvent to solvent as described above. It has been widely studied and described over the last 20-30 years. A large number of τ_Δ have been reported (Table 1-3 overleaf), which have been collected in extensive reviews.[82, 165, 168, 177-180]

The effect of solvent on the lifetime of $^1O_2$ is important in determining the efficiency of reactions. The lifetimes of $^1O_2$ in CCl_4, CS_2 and C_6F_6 are relatively long compared to other solvents (Table 1-3 overleaf). However, these solvents are not recommended for use in the pharmaceutical manufacturing since they have a serious effect on human health and environment.[181-183] Looking for alternative solvents is an

[i] In particular, it protects the organism from photo-oxidative damage and are accessory light-harvesting pigments in the antenna systems.

urgent goal to develop a better route to perform these reactions efficiently and environmentally.

Table 1-3 Lifetime of singlet oxygen in various solvents.[82, 165, 168, 177-180]

Solvent	τ_Δ/μs
H_2O	3.3±0.5
D_2O	66±2
CH_3OH	9.9±0.5
CH_3OD	240±10
$(CH_3)_2CO$	50.5±4
CH_2Cl_2	101±39
$CHCl_3$	235±30
$CDCl_3$	650±150
CCl_4	73000±14000
CH_3CN	66.7±13.5
Pentane	29±6
THF	23±2.6
Cyclohexane	21±4
CS_2	37000±8000
C_6F_6	12000±8000
C_6H_6	32±3.3
C_6D_6	665±95
Toluene	27±2

1.5 Dense CO_2 as an alternative solvent

1.5.1 The choice of alternative solvents

Solvents have played a key role in many chemical processes,[184-185] which are frequently used to enable homogeneous reactions, speeding up reactions through improving mixing and heat transfer. Particularly, in terms of singlet oxygen reactions, solvents affect the lifetime of $^1O_2$ seriously. Deuterated and halogenated solvents give the longest $^1O_2$ lifetime, but they are expensive and often harmful to aquatic organisms and human health.[186] Therefore, the correct choice of solvent is significant in chemical processes.[187] Solvents often have an important effect on the cost,

environment and safety of chemical and pharmaceutical industries as well. The number of solvents used, in many chemical reactions as well as separation processes, exceed the total of feedstocks, reagents and products used in the reaction.[10] They typically make up more than 80 % of the material used for APIs manufacture[188] and account for 50 % of the post-treatment green-house gas emissions.[189]

Volatile Organic Compounds (VOCs) frequently used as solvents, usually with low molecular weight and high volatility have the potential for greater exposure, more risks, and also some of them with toxic,[190] resulting in environmental issues when they are released into the environment. They can cause a number of adverse health effects because of their ability to form low-level ozone and smog through free-radical air oxidation processes.[191]

Total elimination of volatile organic solvents from the chemical manufacturing processes is desirable but there may be other problems, such as poor heat and mass transfer and/or viscosity limitations. These would result in more energy or organic solvents being used in the subsequent purification steps. Therefore, some common alternatives solvents to substitute VOCs have been proposed, such as water-based processes, ionic liquids, fluorous biphasic solvents and supercritical fluids.[192-196]

1.5.2 Supercritical carbon dioxide

A supercritical fluid (SCF) can be defined as a compound that is above its critical pressure (P_c), and its critical temperature (T_c)， as shown in *Figure 1-7*. SCFs possess properties of both liquids and gases.[197] They can diffuse through solids like a gas, and dissolve materials like a liquid. In addition, close to the critical point, small changes in pressure or temperature lead to large changes in density, so that many properties of a supercritical fluid can be tunable. SCFs possess most of the properties of a gas and a liquid, such as low viscosity, high diffusivity and relatively high density, which allow them to be applied as suitable solvents.[198]

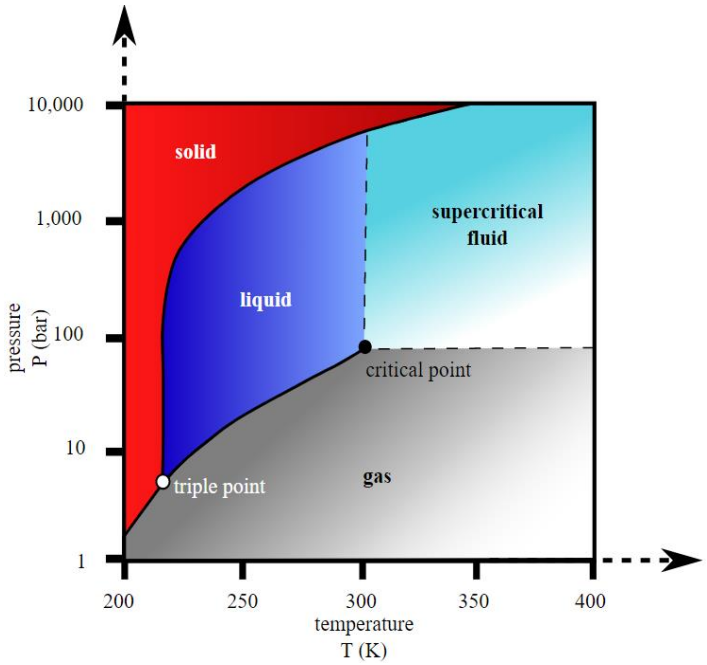


Figure 1-7 Pressure-temperature phase diagram of carbon dioxide.

The critical parameters (P_c = 73.9 bar and T_c =304.25 *K*) of supercritical CO_2 ($scCO_2$) are mild and are easy to achieve in the lab or in industry. $scCO_2$ has the general advantages of supercritical fluids, as well as additional attractive properties in terms of its high abundance and low toxicity. Also, $scCO_2$ is non-flammable and thermodynamically stable for a variety of processes including oxidations using molecular oxygen,[199] which can be fully miscible in $scCO_2$.[200] This avoids the mass transfer limitations typically observed in biphasic systems.

In addition, the lifetime of $^1O_2$ in $scCO_2$, 5100 μs at 314 K and 147 bar, is longer than in most of the traditional organic solvents.[201] Worral also reported that the lifetime of $^1O_2$ in CO_2 was a function of temperature and pressure, as shown in *Figure 1-8*. It shows that there was no sudden change in the lifetime of $^1O_2$ for the transition between liquid and supercritical CO_2.

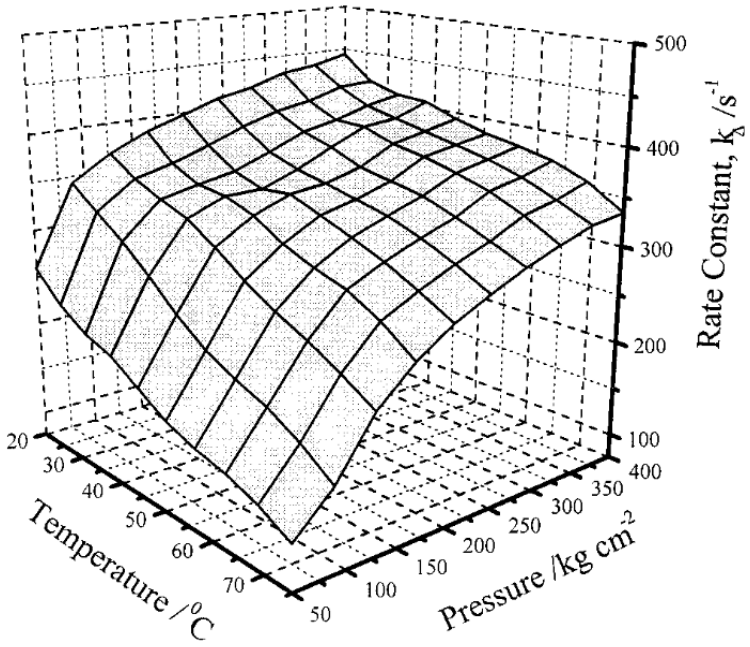
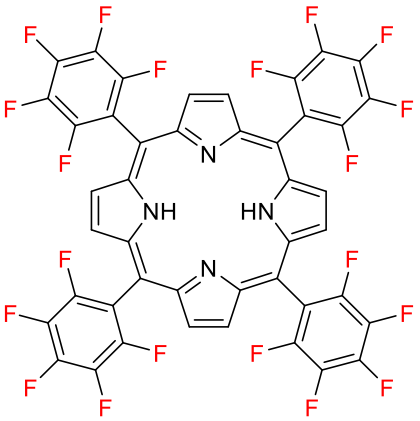


Figure 1-8 The dependence of the rate constant for the decay of $^1O_2$ on temperature and pressure in supercritical CO_2, reproduced from Ref 201.

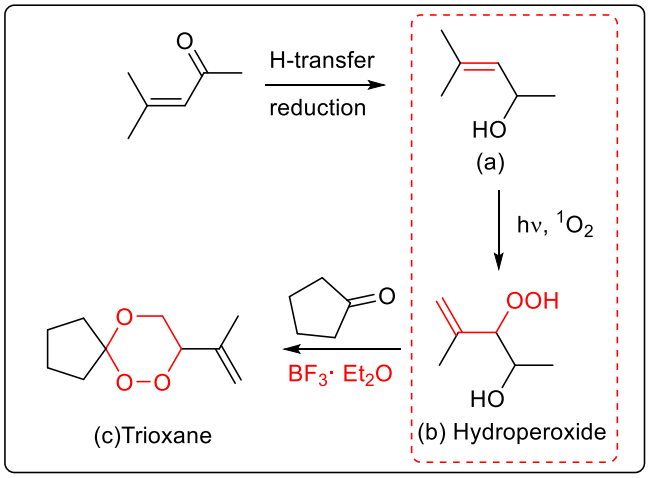
In terms of photosensitiser, mainly TPFPP, 5,10,15,20-tetrakis (pentafluorophenyl) porphyrin (*Scheme 1-22*), was used for the generation of $^1O_2$ throughout this Thesis. It is a fluorinated analogue of the more traditionally used tetraphenylporphyrin (TPP), as described in Scheme 1-10. Unlike TPP, this fluorinated photosensitiser, TPFPP, has been shown[202] to be soluble in $scCO_2$, which is pivotal for an efficient generation of $^1O_2$ as well as for scaling-up in a continuous flow CO_2 reactor.

Based on this work, our group at the University of Nottingham has made use of the relatively long lifetime of $^1O_2$ in $scCO_2$ to perform the photo-oxidation of α-terpinene in both batch and flow reactors, using $scCO_2$ as the solvent (Scheme 1-3 above).[203] Following the successful results of the batch process, Bourne and Han developed a continuous flow reactor with high turnover frequency when using either homogeneous or heterogeneous photosensitisers.[204-205] Later, Bourne and Hall further developed and redesigned the sapphire tube to achieve better light irradiation.[206] The details[202] of the redesigned apparatus will be discussed in



Scheme 1-22 The structure of 5,10,15,20-Tetrakis (pentafluorophenyl) porphyrin, TPFPP, as a $scCO_2$-soluble photosensitiser.

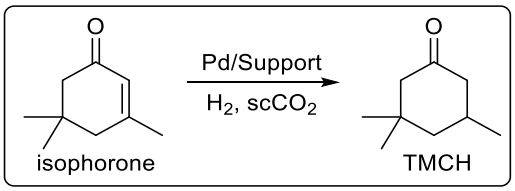
Chapter 2. Hall synthesised a number of potentially antimalarial trioxanes (*Scheme 1-23* (c)) *via* photo-oxidation of allylic alcohol to its hydroperoxides (b) in $scCO_2$, which represents the key step in the antimalarial trioxane synthesis process.[206] These hydroperoxides can be further reacted with cyclic ketones, catalysed by $BF_3{\cdot}Et_2O$, to yield potentially antimalarial trioxanes after 12 hours in CH_2Cl_2. Since CH_2Cl_2 is not a "green" solvent, a solvent-free flow system, using a packed bed of silica/BF_3 instead of $BF_3{\cdot}Et_2O$ in a batch reactor, was employed for the hydroperoxides transformation to trioxanes, as shown in *Scheme 1-23*. Unfortunately, the BF_3 leached into the solution and the conversion dropped off after 20 min.



Scheme 1-23 Synthetic route to spirobicyclic trioxanes in $scCO_2$, with Lewis acid, highlighting the photo-oxidation step.[206]

In terms of clean technology, $scCO_2$ has another advantage. Upon pressure release, CO_2 returns to its gaseous state allowing facile product separation and purification, leading to reduced costs associated with product clean-up.[207] As a result of its tunable solvent properties, $scCO_2$ has been used as a clean extraction medium for a variety of natural products.[208] In particular, it is used on an industrial scale as a replacement for dichloromethane in the decaffeination of coffee.[209]

There have been successful industrial-scale hydrogenation processes in $scCO_2$. One was using a multi-purpose plant built by Thomas Swan & Co. Ltd. in collaboration with the Clean Technolgy group at Nottingham.[210] The Thomas Swan plant was a technical success in the hydrogenation of isophorone, as shown in *Scheme 1-24*. The product trimethylcyclohexanone (TMCH) was obtained sufficiently pure that it could be sold without any downstream purification. The success of this led to increased interest in $scCO_2$ as a solvent in the production of many chemicals.



Scheme 1-24 Hydrogenation of isophorone to TMCH, one of the few reactions to be carried out on a commercial scale in $scCO_2$.[210]

The use of $scCO_2$ as a safer solvent, with enhanced solubility of O_2 and better mass transfer, as well as relatively long lifetime of singlet oxygen, has led to good results. However, the suitability for scaling-up remains to be demonstrated, as most of the research in photo-oxidation was performed on small scales. In addition, daisy-chaining of reactions has not been studied yet. Hence, this Thesis aims to establish whether multistep experiments are worth scaling up and being further explored for the transformations of products obtained in photo-oxidation step, in order to determine scalability and opportunity for daisy-chaining.

1.6 Green chemistry and sustainable chemistry

As previously stated in the discussion of photo-oxidation with $^1O_2$ in continuous CO_2 systems, both "green" and "sustainable" chemistry methods should be employed in the full life cycle of chemicals, including the feedstocks, synthesis, purification, utilisation and "end of life". As shown in *Figure 1-9*, green chemistry attempts to solve the issues about the chemicals themselves and their technical problems, whereas sustainable chemistry is related to social, economic and other aspects of manufacturing and applications of the chemicals.[211-212]

A new approach to sustainability: "A Moore's Law for Chemistry (MLFC)" was proposed recently by Mike George, Martyn Poliakoff and Pete Licence.[213] The concept of "MLFC" is that sustainable chemists should endeavour to produce a given effect by a factor of two by reducing the amount of a chemical demanded over a fixed period, and this process should be repeated in a number of cycles.

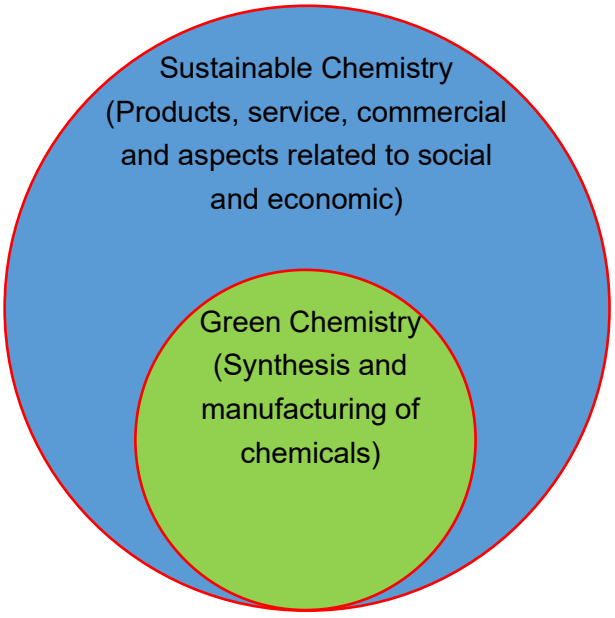


Figure 1-9 The relationship between green chemistry and sustainable chemistry.

The term, "Green Chemistry", which was coined by Anastas in the late 1990s, is familiar to most of us.[214] It involves "reducing or eliminating the use or generation of a hazardous substance in the design, manufacture and application of chemical

products".[215] Nowadays, environmentally benign processes have been developed[216-218] increasingly following on the well-known twelve principles of green chemistry in order to counter the negative effects of chemical manufacturing on our environment. In the last two decades, green chemistry has become perceived as both a culture and a methodology for accessing sustainability.[219] The concept of green chemistry is used not only in the final reaction product but also applied to the whole life cycle of the products. It can be grouped into seven "fundamental aspects" below (*Figure 1-10*).[214]

Waste: It is better to prevent waste than to treat it after it has been created. The Environmental Factor (E-factor) is a useful metric to measure the amount of waste generated in a process.[220] It has been intensively used in academic labs and industry. E-factor is defined by a weight ratio, which is the weight of generated waste to the final product achieved (Chapter 1.2).

$$E\text{-}factor = \frac{Weight\ (total\ waste)}{Wieght\ (final\ products)} \qquad \text{(Chapter 1.2)}$$

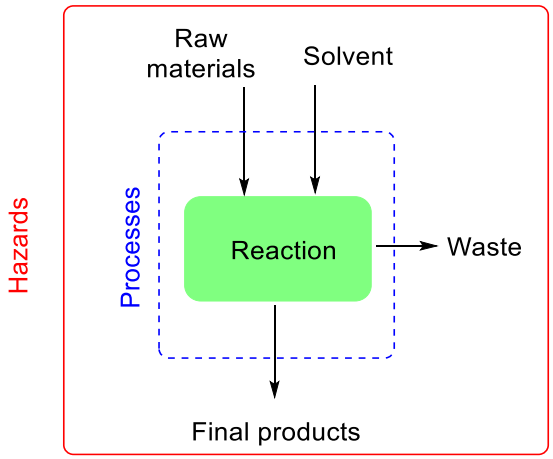


Figure 1-10 Seven fundamental aspects combined from 12 principles of green chemistry, adapted from Ref[218].

Raw materials: A raw material or feedstock should be renewable instead of being derived from depleting petroleum feedstock or natural gas, and also they can be maximised into the final products.[217]

Solvents and Auxiliaries: The auxiliaries (solvents or purification solutions) should be used as less as possible and, when used, should be innocuous to human health and the environment.

Final products: Chemical products with atom efficiency should be designed to keep the efficacy of the function while reducing toxicity and should be degradable at the end of the function without harming the environment.[221-222]

Reactions: Synthesis methodologies should be designed to use and generate compounds with the least toxicity to creatures at any time, and also working under the basis of atom economy to have a better efficiency.[216, 223] Moreover, catalysts should be used and as selective as possible, rather than using stoichiometric reagents.

Processes: Energy consumption should be minimised in all processes; if possible, experiments should be performed at ambient temperature and pressure.

Hazards and Toxicity: The raw materials/feedstocks and final products should be non-toxic, and have no impact on human health and safety as well as the environment, they should be non-toxic. The final product's hazard and toxicity should be assessed. A hazard is defined as the ability of any agent that is detrimental to both human health and the environment. Both hazard and exposure can be used for defining the risk, which is crudely defined as in *Figure 1-11*.

$$\text{Risk} = \text{Hazard} \times \text{Exposure}$$

Figure 1-11 Risk is a function of hazard and exposure.[224]

The Twelve Principles of Green Chemistry have played a crucial role in the development of this discipline and explaining its aims. It has been further extended by Neil Winterton[225] with his twelve more green chemistry and Paul Anastas and Julie Zimmerman's principles of green engineering.[211]. In 2005， Poliakoff and co-workers proposed much simpler statements of these 12 principles, the acronym of which is "PRODUCTIVELY",[226] and which can be presented in a single slide, conveying similar meaning.

With a brief introduction of prior knowledge, based on continuous flow photochemistry as well as alternative solvents, the principal aim of this Thesis is to use a green reagent, singlet oxygen, and green solvent, supercritical CO_2, to scale up synthesis of a number of higher value products in an efficient method. To do so, this would involve flow photochemistry as well. This is a promising methodology for fulfilling the new challenges in the pharmaceutical industry: to produce small quanlities amount of personalised drugs suited to each individual, rather than making a large amount of more general drugs.

Thesis aims

From the brief overview given above, it can be seen that pharmaceutical industries play a pivotal role in our daily life, but with new challenges constantly arising as the demand for personalised medicines increases.

The overall aims of the work discussed in this Thesis are to explore a green methodology for a relatively large-scale synthesis of individualised, valuable medicine-related compounds in a multistep, high-pressure continuous flow photoreactor. $^1O_2$ is used as a green reagent, and dense CO_2 as green solvent. Therefore, reactions combining $^1O_2$ and CO_2 in a continuous flow reactor to prepare medicinal chemicals were investigated in this Thesis. To explore and produce more different valuable medicinal chemicals, the main goals of the work described are:

1. To improve and rebuild a safer high-pressure continuous flow photo-oxidation reactor in order to perform multistep experiments.
2. To investigate the synthesis of a range of valuable products from a single feedstock in a new daisy-chained reactor, such as from combining the photoreactor and thermal reactor in series.
3. To investigate the principle of how to efficiently perform a multistep experiment to realise high reaction yields and productivities, such as synthesis of a range of individualised chemicals.
4. To explore a green photochemical route as an alternative to the traditional, harsh method (using stoichiometric reagents to obtain high efficiency), reactions such as the dearomatisation of phenols *via* photo-oxidation.
5. To investigate the heterogeneous catalyst in continuous fixed-bed thermal reactor daisy-chaining with photoreactor in order to conduct a sequence of steps to give a target molecule, such as the synthesis of 1,2,4-trioxanes following dearomatisation of phenols.

Chapter 2. Experimental

This Chapter describes details of the experimental equipment, procedures, and analytic techniques used in the Thesis. The continuous flow setup and operating procedures are presented in Section 2.1, as well as a high-pressure batch reactor for FT-IR monitoring is shown in Section 2.1.1. This equipment was used for high-pressure experiments. Therefore appropriate training is required before any experiments were conducted in these high-pressure rigs. Details about the analytical techniques are given in Section 2.2. This is followed by a description of the materials used throughout this Thesis.

2.1 High-pressure apparatus

High-pressure reaction systems in $scCO_2$ have been designed, built and utilised at the University of Nottingham for nearly 20 years.[227] More recently, a method was developed for allowing known amounts of required gases to be dosed into the supercritical fluid stream at high pressure.[228]

Batch and continuous flow reactor systems with $^1O_2$ in $scCO_2$ have been built by generations of researcher,[203-205, 229] and further details are provided in this section. These sapphire tube reactors for continuous flow systems were further improved by Bellamy in later years.[155, 228] The work presented in this Thesis aims to expand the existing technologies and the author developed and rebuilt them to adapt them for the current project.

The batch and continuous flow reactor systems use a Jasco CO_2 pump to compress CO_2 to supercritical or liquid CO_2. High–performance liquid chromatography (HPLC) pumps are used to deliver liquids into the reactors at set volumetric flow rates. Oxygen is dosed using a Rheodyne™ dosage unit and mixed with CO_2. All the chemicals and gases are mixed in a pre-heater before reaching the reactor. The pressure is controlled using a back pressure regulator (BPR). The diagrams are shown in Section 2.1.1 and Section 2.1.2.

2.1.1 Batch high-pressure rig for monitoring by FT-IR

The small scale batch photo-oxidation rig is mainly made up of two parts illustrated in Figure 2-1: a continuous flow section for the preparation of a CO_2/O_2 mixture and the batch cell (described in detail later). The CO_2 and O_2 are mixed in the static mixer (typically 40 °C). The BPR is used to control the desired system pressure. (120 bar)

After an equilibration period and the cell reaching the required temperature, the gas mixture is allowed to slowly (at the rate of 3-5 psi/s) fill the batch cell which has been preloaded with the substrate and the photosensitiser. Gradual filling of the cell was achieved by opening V6 and V7 slowly. Once the desired pressure had been reached, the cell was isolated from the rest of the rig between V6 and V7. Photolysis and further analysis of the reaction were performed as described at the end of this section.

High-Pressure Batch Cell

A high-pressure cell is used for the small scale photo-oxidation in $scCO_2$, which was specially designed at Nottingham and built to be easily dismantled and reassembled. The cell was initially used for Fourier Transform Infrared Spectroscopy

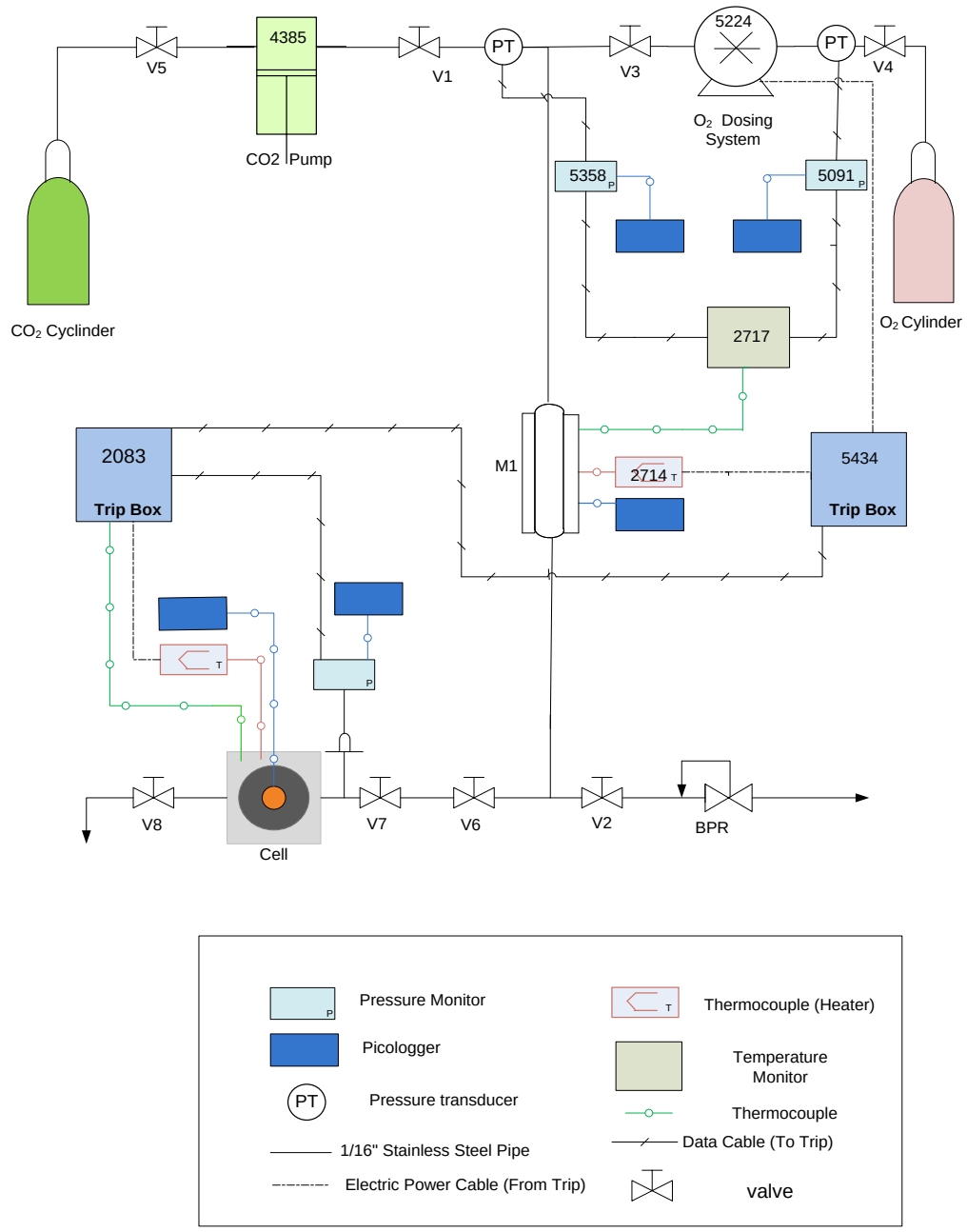


Figure 2-1 This high-pressure batch system is for small scale photo-oxidation with $^1O_2$ in $scCO_2$ and used for the FT-IR monitoring.The rig consists of two parts: one is for the mixing of CO_2 and O_2; another part is for the photo-oxidation in the batch cell. M1: static mixer; Cell: batch photo-oxidation cell, the temperature of temperature is controlled using an external heating block. Compressed CO_2 is pumped using a Jasco™ PU-1580-CO_2 unit, O_2 is delivered directly from an O_2 cylinder via a dosage unit, see Section 2.1.3 for further details. The cell (see below for details) should be heated to the desired temperature and filled with reaction solution before filling CO_2 and O_2 mixer. CO_2 and O_2 mixed well in the static mixer and then feed into the cell, which has temperature and pressure monitors.

(FT-IR) and Raman spectroscopy in supercritical fluids.[230] The cell is made of stainless steel, and consists of a body and a window holder, as shown in Figure 2-2. Calcium fluoride windows (CaF_2 window, 0.6 inches diameter, 0.4 inches thickness) are glued into the window holder. The path length of the cell can be changed by using different window holders, which vary the depth of the window in the holder. The port used to fill the cell with substrate also holds an internal thermocouple. There was a Polytetrafluoroethylene (PTFE) spacer between the inside surface of the holder and the inside of the body, which come in two sizes, narrow or wide thickness according to the position of the safety pressure release hole under the batch cell. The position of the PTFE spacer is very important to be used to exclude different reasons for leaking. If it has been used for a long time since the batch cell has not been used, the next user should change a new spacer.

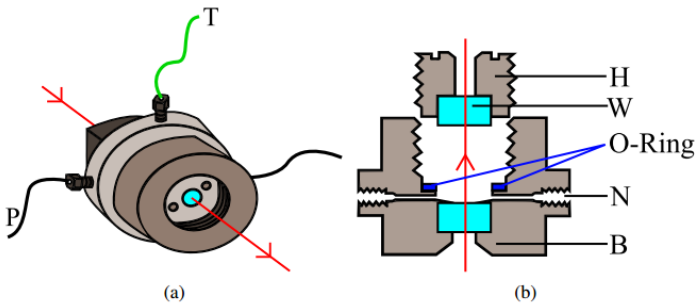


Figure 2-2 (a) External 3D view and (b) cross-section view of a stainless steel high-pressure batch cell. ***P****: the pipe connecting to the other part of system;* ***T****: internal thermocouple;* ***H****: the stainless steel window holder;* ***W****: CaF_2 window which can be irradiated using UV/Visible light and is also transparent to IR;* ***O-rings****: PTFE spacer;* ***N****: screw rut;* ***B****: stainless steel body; This figure is reproduced from ref [155, 230].*

The cell is suitable for white LED light because of the CaF_2 window and can be used for reaction monitoring by FTIR. An external aluminium heating block (controlled *via* a Tempatron TC4800 temperature controller) surrounds the batch cell, and the temperature is typically maintained at 40 °C before the introduction of chemicals.

White LED light for batch photo-oxidation

The batch cell was irradiated by a single white light emitting diode (LED array) (1000 lumen, OSTAR; part code: LEUWE3B-PZQZ-4C8F), which is made of a cluster of six individual diodes, shown in Figure 2-3. These LED sets are mounted on an aluminium block with a cooling fan at the back. The size of light source is the same as the aperture of the batch cell, ensuring efficient irradiation can be achieved.

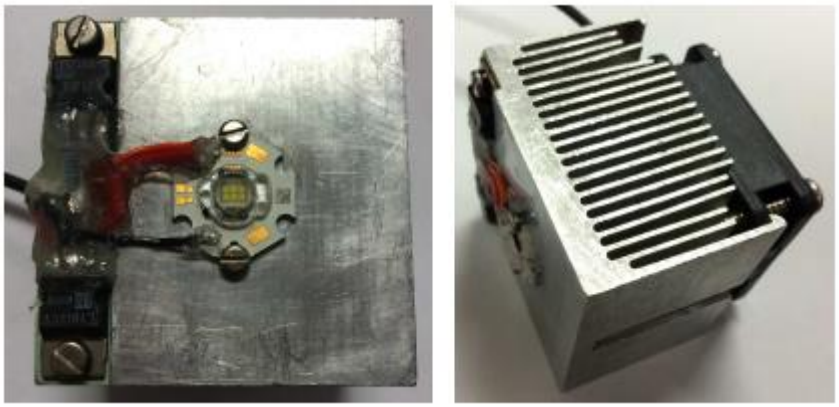


Figure 2-3 Photograph of LED units for high-pressure batch photo-oxidation.

2.1.2 General diagram for high-pressure continuous flow reactor

This high-pressure continuous flow equipment (Figure 2-4) was built for the photo-oxidation in CO_2. Details about the pumps, connecting tubes, mixers, sapphire tube reactor (new design in Jessica Hall's PhD thesis,[155] see more details later in

Figure 2-6), cooling bath and BPR are described in Section 2.1.3. Compressed CO_2 and O_2 are mixed in the first static mixer, **M1**, and then the organic stream is added, and mixed with the gases in the second mixer, **M2**, the temperatures for the two mixers are typically at approximately 40 °C. The fluid entered into the sapphire tube in an up-flow method, irradiated with visible light (three 5 × LEDs mounted on an aluminium blocks) controlled by a LED controller, details shown in Figure 2-8. Due to the heat generated by the LED lights, a secondary cooling bath is used to pump

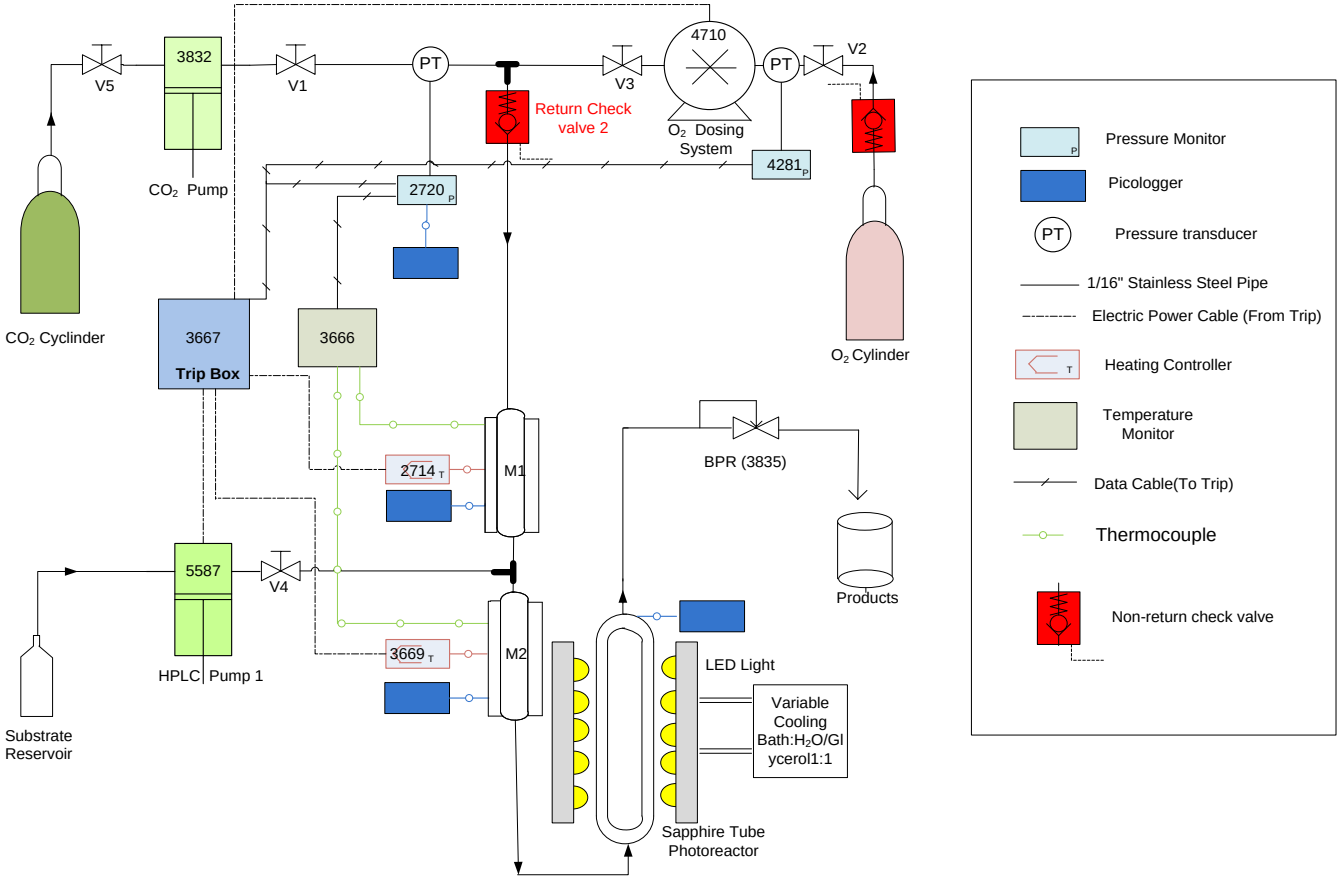


Figure 2-4 This rig is used for continuous flow high pressure photo-oxidation with $^1O_2$ in $scCO_2$. M1 and M2 are static mixers, and M1 is use for mixing CO_2 and O_2. Then the organic substrate is mixed in the second mixer, M2. LED arrays are positioned around the sapphire tube reactor.

between the sapphire tube and Lexan™ tube to ensure that the desired temperature is set for the reactor, typically approximately 40 °C is maintained. The water removes excess heat from the system during irradiation such that the LEDs can be positioned as close as possible to the sapphire tube reactor for the more efficient irradiation. The system pressure is controlled by a BPR located after the sapphire tube reactor. Once the reaction mixture passes the BPR, the products can be collected for further analysis. The high-pressure apparatus was assembled and installed with isolatable components, so it can be readily modified to adapt to different photo-oxidation experiments. Any changes are explained in the relevant chapters. A photograph of the high-pressure continuous flow reactor is shown in Figure 2-5. The maximum temperature rating for the apparatus is 121 °C, and the maximum pressure rating for the apparatus at 121 °C is 200 bar.

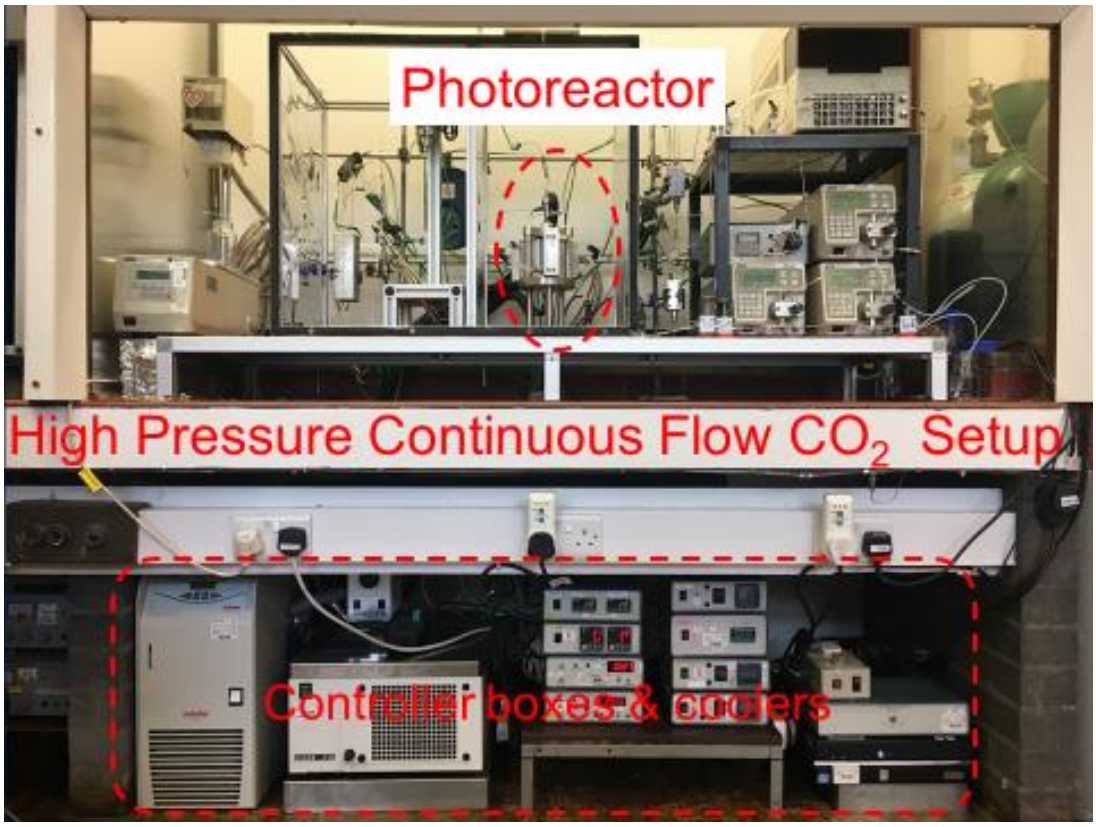


Figure 2-5 A photography of the high-pressure continuous flow reactor, which shows the real setup in Figure 2-4.

A standard operating procedure for the use of the continuous flow setup is given at the end of this section.

Sapphire Tube Reactor

A new sapphire tube reactor has been designed and constructed in our group to increase the efficiency of high-pressure continuous flow reactor, as shown in Figure 2-6. The design consists of a sapphire tube held between two stainless steel plates with connections to the high-pressure apparatus. A Lexan™ (polycarbonate, 18 mm *o.d.*, 2 mm wall thickness and 95 mm in length) tube surrounds the sapphire tube and is sealed at either end with EPDM O-rings. Water or a water/glycol mixture is circulated into the minimal space (*ca.* 2 mm) between the Lexan™ and sapphire tubes using connectors at either end. The stainless steel struts hold the two plates together, at either end of the reactor, can be exchanged to give longer struts and hence a longer sapphire/Lexan combination can be incorporated. Only EPDM O-rings can be used to seal the sapphire tube for the current photo-oxidation experiments.

The LEDs are placed close to the sapphire tube for maximum irradiation. The positions of LEDs are secured in pre-formed grooves to ensure that conditions are consistent for each experiment. This reactor is also able to be readily modified for the incorporation of longer sapphire tubes; different reactors are used in different chapters, which are detailed as required.

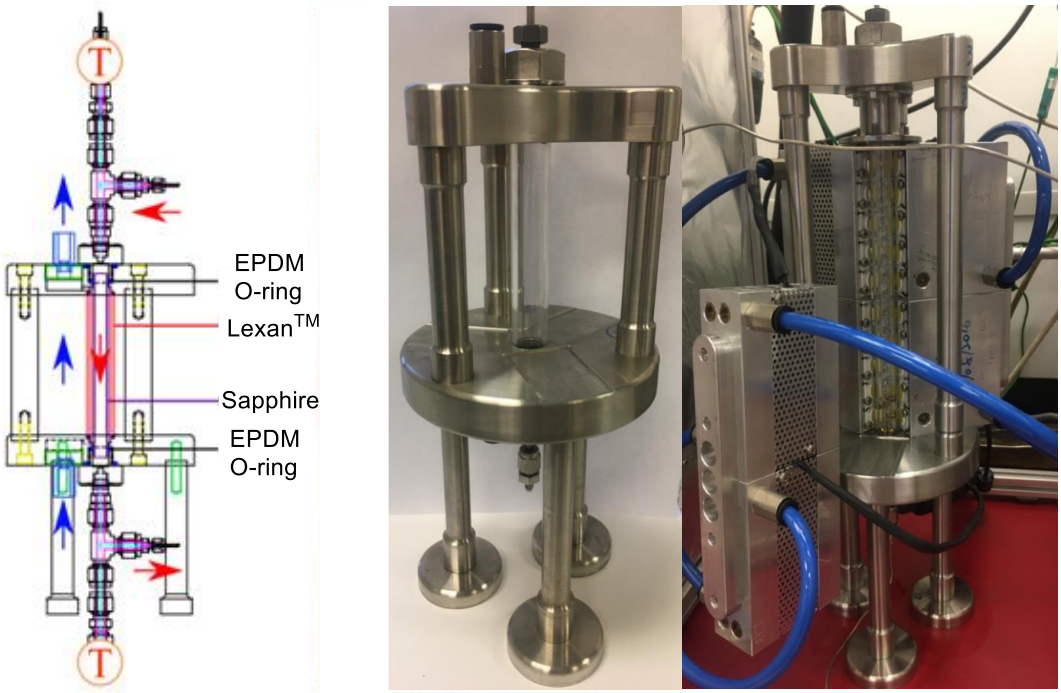


Figure 2-6 (a) Schematic of Sapphire tube reactor (Saint-Gobain Crystals, 10 mm o.d., 1 mm wall thickness, 120 mm long);[155] (b) Photograph of the stand-alone reactor. The body of the reactor is constructed from 316 stainless steel and is machined at the University of Nottingham. Red Flow = direction of high pressure fluid stream; Blue Flow = direction of coolant for LED arrays. The other ports at the top and bottom of the reactor are for thermocouples to monitor the internal reactor temperature. Grooves are cut into the stainless steel base of the reactor to hold the LED units in place being described later, and these are secured using a grub screw at the top. (c) Photograph of the longer sapphire tube reactor by switching the struts holding the top and bottom plates together, it's same with Reactor (b) except with difference length of the reactor (Saint-Gobain Crystals, 10 mm o.d., 1 mm wall thickness, 240 mm long).

Sapphire Tube Reactor Installing Tool

The sapphire tube is fragile and at risk of cracking if overtightened against the stainless steel frame, particularly in the case that the sapphire tube is not in the correct orientation. Therefore, there is a special tool newly designed at the workshop in The University of Nottingham, as shown in Figure 2-7 overleaf. This tool can be screwed into either the top or bottom plates to allow the sapphire tube to be positioned correctly

before tightening both sides. When fixing either side of the sapphire tube with the help of the tool, we can remove the tool and then mount the other fittings as normal.

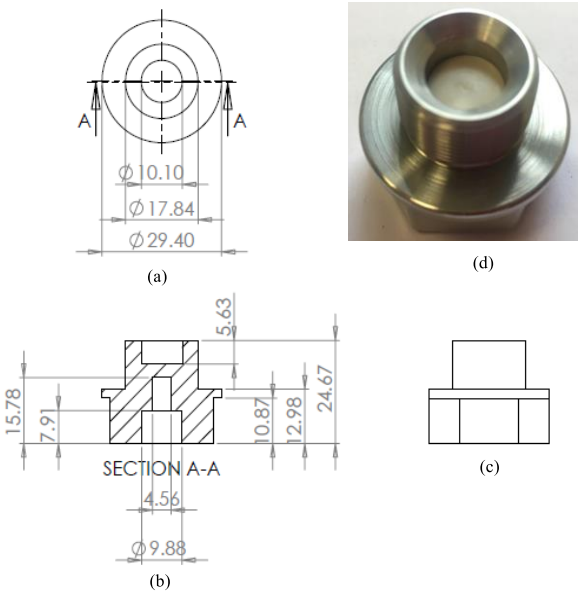


Figure 2-7 Diagrams for the sapphire tube installing tool. (a) Bird's-eyeview of the tool; (b) cross-section drawn of the tool; (c) front view of the tool; (d) a photograph of the tool.

Liquid Cooled LED Unit

White light LEDs (5×Citizen Electronics Co. Ltd 1000 lumen) were used to irradiate with visible light to a particular photochemical reaction with photosensitiser, shown in Figure 2-8. In the blocks, there are channels built for the coolant (typically glycerol: water (v/v) = 1:1, at 35 °C). All three LED units can be controlled by a single controller box, and the brightness can be varied through a variable resistor connected to a control knob. Different LEDs were employed in Chapter 5, which has been described later. The LED chips set are covered by waterproof glue in case of condensation when the temperature of the coolant is below 0 °C. Usually, three sets of LED blocks are provided for all the continuous high-pressure flow

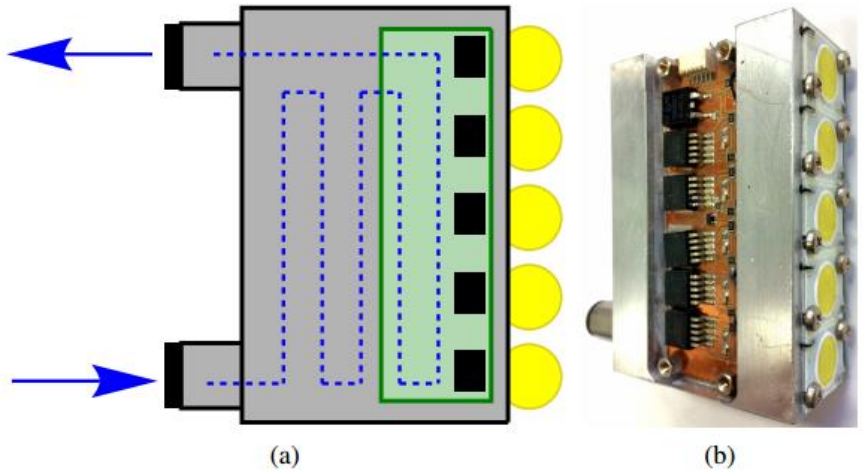


Figure 2-8 (a) A schematic and (b) A photograph of the LED unit which are designed for the sapphire tube reactor. Blue arrows represent the direction of the coolant. Dashed blue lines show the channel for the coolant in the aluminium heating blocks. The image is reproduced from ref.[155].

sapphire tube reactor (Saint-Gobain Crystals, 10 mm o.d., 1 mm wall thickness, 120 mm long), and six sets for 240 mm long reactor and twelve sets for 480 mm length reactor.

2.1.3 **Devices used for high-pressure equipment**

Both the batch and high-pressure flow equipemnt utilised in this Thesis are connected by a series of tubes, connecting parts, valves, pumps, Rheodyne and a BPR. The temperature monitors and controllers, pressure transducers and monitors, Picolog, trip box, cooling bath and LED light are also used for the rigs working properly. The sapphire tube reactors and different stainless steel tubes are included as well. For convenience, the details for some components are presented as follows.

Connecting Tubing and Valves

Swagelok® fittings are used to connect the 316 stainless steel tubing in both systems. Currently, these fittings are mainly used to connect 1/16'' pipe, which all are stainless steel tubes provided by Swagelok®. The temperature and pressure ratings

of Swagelok tubings are dependent on the tubing diameter and wall thickness. Unless stated otherwise, the High Pressure Equipment Company (HiP 15-11 AFI) or Scientific System, Inc (SSI, flat valves) were used as the manual valves. Both HiP and SSI valves were connected in a way that the fluid flowed in from the bottom inlet and flowed out from the top outlet. For the tubing being used for delivering oxygen, check valves should be installed properly to avoid the organic stream flowing back to the oxygen stream and oxygen cylinder.

HPLC Pumps and CO_2 Pump

Compressed CO_2 is fed into the reactor system using a Jasco™ PU-1580-CO_2 pump where it is cooled to *ca.* -7 °C to ensure that the CO_2 is compressed in the liquid state before being pumped into the pre-heater and reactor. The efficiency of the CO_2 pump should be tested regularly using a mass flow meter. It is very important to know the precise flow rate of CO_2 to keep the desired amount of molecular oxygen in the photo-oxidation reactor because the concentration of oxygen is pivotal in oxidation reactions. Before conducting any experiments, the dense CO_2 was pressurised against a closed valve, to a higher pressure than the desired one and to ensure it worked correctly. At any time, the CO_2 pump is filled with CO_2 to reduce frequently warming and cooling cycles; when not in use, the CO_2 pump should be isolated from other parts of the system using a HiP/SSI valve. The over-pressure of the CO_2 pump is typically set at *ca*. 200 bar.

Liquids are pumped into the system using Jasco™ PU-980 high-performance liquid chromatography (HPLC) pumps. The efficiency of the organic pumps should be tested regularly by recording the amount of time required to fill a volumetric flask at a specific flow rate. Before every experiment, the pump is pressurised to a higher pressure than the system pressure to ensure it can work at the desired pressure. The HPLC over-pressure of the pump is typically set at *ca*. 200 bar.

Rheodyne®-Oxygen Dosage Unit

For safe operation, the concentration of O_2 in the CO_2 should be kept below *ca.* 8 mol % in CO_2 system to ensure that being under its flammability point.[231] Therefore, each photo-oxidation rig is equipped with an oxygen dosing unit which delivers the oxygen at cylinder pressure into the system, *via* the pressure difference. The cylinder pressure of oxygen is always higher than the system pressure to block any backflow of organic material into the oxygen cylinder. One check valve is located between the oxygen cylinder and Rheodyne®, and another is located between static mixer 1 and Rheodyne®, which further prevent organic material from flowing back into the oxygen stream. During initial experiments, the O_2 source for the continuous flow rig was equipped with a dosage unit, coupled to a source of compressed air, as shown in Han Xue's PhD thesis.[232] However, because of its instability for providing desired amount of oxygen, another dosage unit was used. This unit is equipped with a six-port HPLC (modified Rheodyne® 7000L or a Vici® equivalent) switching valve,[155] shown in Figure 2-9. This unit has two small sample loops, which contain oxygen at cylinder pressure. The 3-slot rotor seal has two positions to join pairs of ports together so that, at any one position, one of the loops is filled with oxygen from the O_2 cylinder, while, another loop is providing O_2 to the system due to the pressure gradient and then is empty. The rotor position is then switched such that the 3-slot rotor joins with another empty sample loop and this process is repeated. The concentration of O_2 in the CO_2 stream can be varied by adjusting the volume of the sample loops (*ca.* <300 μL) and the value of pressure difference, such that the switching time is around 4-14 seconds. If the switching rate is too slow, the diffusion of O_2 will result in uneven mixing with other materials. On the contrary, if the switching rate is too fast, then insufficient O_2 diffusion from the loop into the system may lead to a lower O_2 concentration than the required amount.[233]

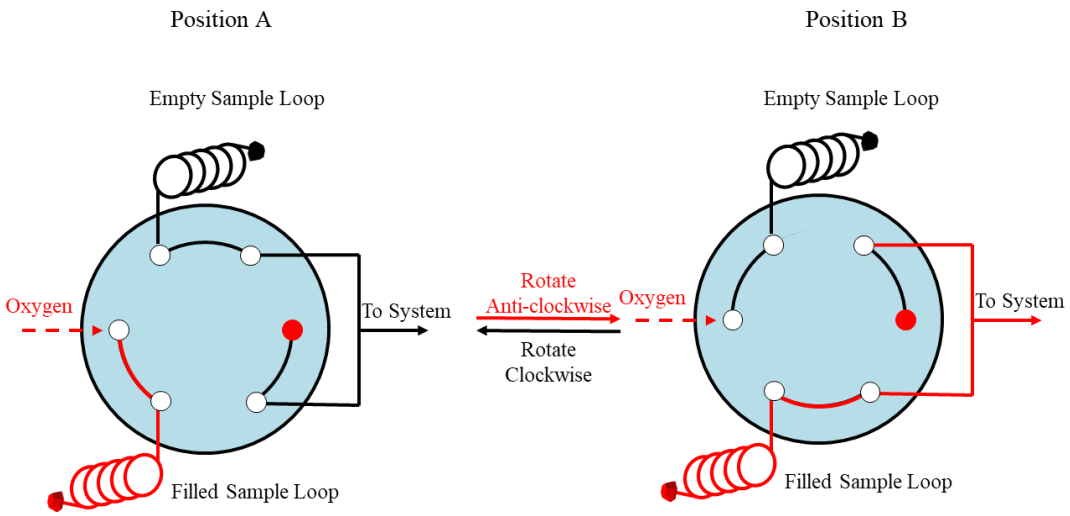


Figure 2-9 A basic schematic of the inside of the O_2 dosage unit used for supplying O_2 to high pressure photo-oxidation systems.

Mixing chambers and pre-heaters

The standard mixing chamber consists of a stainless steel tube ((1/4" o.d., 0.049" wall thickness, 3.1" in length) loaded with sand, which is used for mixing O_2 and CO_2, or with organic materials. In the high-pressure batch system, there is just one mixer for the mixing of O_2 and CO_2, but in the case of high-pressure continuous flow reactor, there are two, one mixer for mixing gases and another for mixing the organic materials and the gases. The pre-heaters are heated to *ca.* 40 °C and maintained by the aluminium heating blocks placed around the stainless steel tubes (heating cartridge inside).

Temperature and Pressure monitors

Both temperature monitor and temperature controllers are used for keeping the desired temperature of the operating system. The temperature of the heating blocks were controlled by temperature controllers by receiving the temperature signal from the temperature monitors, shown in Figure 2-1 and Figure 2-4. This internal and external temperatureswere measured by thermocouples (Type-K). These units were connected to a trip box. The setting values of heating controllers are typically 10 ˚C

higher than the set number on the heating monitor. The temperature of photoreactor was kept stable by a cooling bath.

Pressure monitors should be calibrated frequently at atmospheric pressure, especially when turning them on. Two pressure monitors were installed on the high-pressure continuous flow rig. One pressure monitor box was used for monitoring the system pressure and another for the oxygen pressure. The system over-pressure is set approximately 20 bar higher than the desired system pressure (120 bar) and the low-pressure oxygen trip is set at least approximately 20 bar higher than the desired system pressure to prevent back-flow into the oxygen cylinder. The oxygen over-pressure trip values are typical *ca*. 20 bar higher than the projected value (180 bar).

BPR

The system pressure is controlled by a Jasco™ BP-1580-81 back pressure regulator (BPR), and the temperature can be adjusted at the point of depressurisation to assist in blockage prevention.

Picologger

Useful data, *i.e.* system pressure, mixers temperature and reactor temperature, was recorded on the rigged computer using a Pico® Technology TC-08 Picologger *via* Pico software. The picolog is important during continuous flow experiments or injecting the batch cell with gases mixtures as it can indicate the time of a system trip, a variation of pressure and temperature, and enable identification of the cause.

Trip box and emergency shutdown button

The high-pressure apparatus should be tripped in the event of an over-pressure or over-temperature, and the reactor system shut down in case of potential risks. The rigs also can be shut down in an emergency situation by manually pressing the red shutdown button on the trip box. Trips setting rules are described in the relevant

sections. The power of the trip box for high-pressure continuous flow rig was 3000 W; an extra trip box was installed for the high-pressure batch cell during the FTIR monitoring. Prior to each experiment, the trip should be tested. When the trip is initiated, the organic pumps, heating controllers, light sources, and oxygen dosage unit should switch off, but the CO_2 pump, BPR and cooling bath, as well as temperature and pressure monitors, should remain on. The remaining CO_2 pump can remove the blockages in time and dilute the oxygen in the system, eventually removing the rest of the oxygen from the rig. The BPR is open when the trip is initiated, which can be fully open and vent the remaining solution from the rig. The trip box should be reset once the problems have been solved, returing the rig back to working condition.

2.2 Analytic techniques

2.2.1 **Auto-sample Flash Chromatography**

Thin layer chromatography (TLC) using pre-coated glass plates from AnalTech covered with 0.20 mm silica gel with fluorescent indicator visualised upon UV irradiation (λ = 254 nm) or $KMnO_4$ stain, was used for reaction monitoring and product detection.

For the purification of new compounds, flash chromatography was used for some compounds, using cyclohexane/EtOAc or n-pentane/EtOAc as eluent solvents. Two methods were used, flash chromatography and auto-sampler flash chromatography. The auto-sampler flash chromatography machine was purchased from TELEDYNE ISCO (P/N 69-3873-244). The procedure for the auto-sampler column as follows: firstly, two different eluent solvents as chosen were primed to the system; then a dry pre-loaded solid load cartridge with silica was placed into the solid sample position; a desired Redi*Sep* Rf Gold® silica gel column was loaded on to the system; a new

method was created, then running the separation. Different fractions were obtained. Further identification was made after removing the solvents.

2.2.2 General Practices

Proton nuclear magnetic resonance (^{1}H NMR) spectra and proton-decoupled carbon nuclear magnetic resonance (^{13}C / ^{1}H NMR) spectra were recorded at 25 °C (unless stated otherwise) on Bruker AV-400 (400 MHz), AV (III) 400 (400 MHz) or AV (III) 500 (500 MHz) spectrometers at the University of Nottingham nuclear magnetic resonance facility. Chemical shifts for proton are reported in parts per million downfield from tetramethylsilane and are referenced to the residual proton in the NMR solvent according to values reported in the literature.[234]

Chemical shifts for carbon are reported in parts per million (ppm) downfield from tetramethylsilane and are referenced to the carbon resonances of the solvent. The solvent peak was referenced to 3.31 ppm for ^{1}H and 49.00 ppm for ^{13}C in CD_3OD, or 7.26 ppm for ^{1}H and 77.16 ppm for ^{13}C in $CDCl_3$. All the NMR samples were performed at room temperature.

Data are represented as follows: chemical shift, integration, multiplicity (s = singlet, d = doublet, t = triplet, q = quartet, dd = doublet doublet, ddd = doublet doublet doublet, dt = doublet triplet, tdt = triplet doublet triplet, m = multiplet), coupling constants in Hertz (Hz). In the case of compounds containing fluorine atoms, it should be noted that ^{13}C NMR experiments were obtained without ^{19}F decoupling. NMR spectra were processed with MestReNova Software.

All samples for mass spectrometry were recorded on an EI-GC machine, using MeCN as a solvent.

2.2.3 Fourier Transform Infrared Spectroscopy (FT-IR)

The infrared region of the electromagnetic spectrum extends from 14,000 cm^{-1} to 10 cm^{-1}. The mid-infrared region (4,000 cm^{-1} to 400 cm^{-1}) is the region most interest

to chemists. The spectrum corresponds to vibrational energy changes within the molecules. Therefore, it can be used to identifying certain functional groups in a particular sample and can monitor the changes during the progress of a chemical reaction.[235]

The design of the high pressure batch photo-oxidation cell is described in Section 2.1.1. In this batch reaction, we assume that once irradiation is ceased, the reaction stops. This can be done because the $^1O_2$ used in this reaction is very reactive, and the intermediates that are formed are assumed to be long-lived enough to be observed. As such, the FT-IR absorption spectrum for monitoring of the reaction kinetics can be obtained by irradiating the solution for a certain time and then recording the FTIR spectrum. In this work, spectra were recorded by placing the cell into Avatar 370 FTIR spectrometer with a dry air purge. The scan rate is 32, the resolution is 4, and the path length of the cell is 1 mm. A DTGS detector was used, and data processing was performed with Omnic (Version 6.1a) software. Typically, a background at pressure or the solution itself as background were collected before recording the spectra at different times.

2.3 Materials

All the reagents and solvents used in this Thesis were obtained from commercial suppliers and used without additional purification unless stated otherwise. The CO_2 was supplied by BOC Gases (99.8 %, food grade). The niobium pentoxide hydrate ($\mathbf{Nb_2O_5 \cdot nH_2O}$) and niobium phosphate ($\mathbf{Nb_3O_{20}P_5}$) (w = 0.98) were supplied by Companhia Brasileira de Metalurgia e Mineração in Brazil.

Chapter 3. Scale-up of Selective Production from Photo-oxidation of Cyclopentadiene in CO_2

As discussed in Chapter 1, an idea of a green chemical process would involve sustainable reagents or at least 'green' solvents, which are environmental-friendly, resulting in less pollution to the environment.[214, 236] The application of dense CO_2 as a reaction medium satisfies this objective up to a point: the solvent is readily removed from the reaction by simply releasing the pressure and it is not detrimental to nature, apart from consider allows of climate change. Organic synthesis in dense CO_2 has been studied widely in the past. Dense CO_2 is an ideal reaction medium for oxidation because its total inertness towards oxidation offers safety. It also provides high concentrations of the oxidant and reduces mass transfer limitations. It is also suited to flow processes, which are attractive in the industry for scaling up and can be performed in a relatively small volume to avoid the build-up of hazardous chemicals.

This Chapter describes how four potentially valuable chemicals can be synthesised from a single feedstock, cyclopentadiene, on a relatively large scale in high-pressure continuous flow system, using dense CO_2 as a solvent.[237] Section 3.1 presents a brief introduction to photo-oxidation with singlet oxygen in a continuous flow reactor, as well as the oxidation of cyclopentadiene in traditional solvents. Then,

Section 3.2 describes the concept of the valorisation of cyclopentadiene in a daisy-chained mode. Section 3.3 presents the initial results obtained by monitoring of photo-oxidation of cyclopentadiene with FT-IR and NMR. Section 3.4 describes the high-pressure continuous flow daisy-chain setup. This includes the first step of daisy-chain reactions, accessing the endoperoxides from cyclopentadiene reacting with singlet oxygen after irradiation with visible light.

Section 3.5 outlines that endoperoxide (**3.2**) is produced from the photo-oxidation of **3.1**. It can react with different quenching reagents to synthesise 1,3-diol (**3.3**) and cyclopentanone (**3.4**) in liquid CO_2, respectively. Section 3.6 describes the synthesis of aldehyde (**3.5**) and furfuryl alcohol (**3.6**) in supercritical CO_2. Here, the aldehyde (**3.5**) was formed from intermediate (**3.2**) at 40 °C with a quantitative yield. Furfuryl alcohol (**3.6**), which was produced *via* a daisy chained reaction (photo-oxidation of **3.1**, thermal isomerisation of **3.2**, following the acid cyclisation step of **3.5**), are discussed in Section 3.6 as well. Later on, Section 3.7 discusses the effect of CO_2 on the daisy-chained reactions of cyclopentadiene to synthesise four different products. This section also includes the comparison of the productivities of these compounds in a flow reactor with results obtained in batch reactors using traditional solvents.

Finally, the conclusion and high-pressure reactor information are presented in Section 3.8 and Section 3.9. Moreover, the optimisation experiments for producing compound (**3.4**) and (**3.6**) are described in Section 3.9.

3.1 Introduction

3.1.1 **Continuous flow process with photochemistry**

The implementation of more sustainable processes for the production of chemicals or active pharmaceutical intermediates recently has received growing attention.[212, 238-239] Reducing environmental impact has become one aim to achieve

that goal by controlling reaction conditions as well as reducing the use of hazardous compounds. Therefore, green chemistry combined with the use of continuous systems has allowed several issues[i] to be tackled[240-244] and parameters to be varied to reach high productivity and efficiency.[245-246]

Continuous flow reactors have an inherently smaller volume than the corresponding batch reactor for a given rate, which can be allowed to operate above ambient conditions more safely than batch processes. In addition to this, reactions can be more finely tuned in continuous flow than in batch mode because flow reactors can be employed under a wider variety of conditions than in batch reactors. Flow systems allow chemists to work with minimum quantities of hazardous materials inside the reactor at any given instant, reducing exposure risks for the chemists, and scale-up will be possible for the products.[247-248] A more detailed discussion of the advantages of flow reactors has been given in Section 1.3.

As discussed in Section 1.4, oxygenation of compounds is synthetically interesting and industrially important.[63] Molecular oxygen is a widely available, inexpensive and environmentally friendly reactant and is considered as a highly attractive oxidant. The photochemical generation of singlet oxygen ($^1O_2$), a relatively reactive species, from molecular oxygen, has gained interest in contemporary organic synthesis over the last decade,[42, 249] providing a green and sustainable route to access higher oxidation state chemicals with high atom efficiency. $^1O_2$ can then undergo a variety of useful reactions, mainly [4+2] cycloadditions with alkenes and similar systems. From a green chemistry aspect, the route to $^1O_2$ using low energy visible light with an appropriate catalytic photosensitiser (xanthones, anthracene or porphyrins) is the most convenient and cleanest process.[250] $^1O_2$ reacts with 1,3-dienes *via* a [4+2] photocycloaddition process to form endoperoxides. A highly active species easily converted into higher value compounds.[251] However, due to the highly

[i] Such as better light penetration in photochemistry and avoiding the build-up of hazardous chemicals, further details have been discussed in Section 1.3.

reactive nature of $^1O_2$, the choice of suitable solvents for the scale-up of such photo-oxidation is limited as they are required to be non-flammable and inefficient $^1O_2$ quenchers.[82] Thus new approaches are demanded so that photo-oxidation with $^1O_2$ can be realised with its full potential in *Green Chemistry*.

The problems can be partially mitigated by using supercritical CO_2 ($scCO_2$) or liquid CO_2 ($liqCO_2$) in continuous flow processes as an alternative solvent to traditional organic solvents. $scCO_2$ provides many attractive properties for oxidation as it is fully-oxidised, non-flammable and non-toxic. Using inert supercritical gases as reaction solvents is a greener alternative to using traditional, flammable or toxic solvents.[252, 209] Moreover, gaseous O_2 is entirely miscible with CO_2, which has a lower viscosity, and higher diffusivity than more conventional solvents.[253] Also, photophysical experiments have demonstrated that $^1O_2$ can be effectively generated in $scCO_2$ with an extended lifetime compared to many traditional solvents.[229, 254-256] Further details of using CO_2 as a solvent are discussed in Section 1.5.

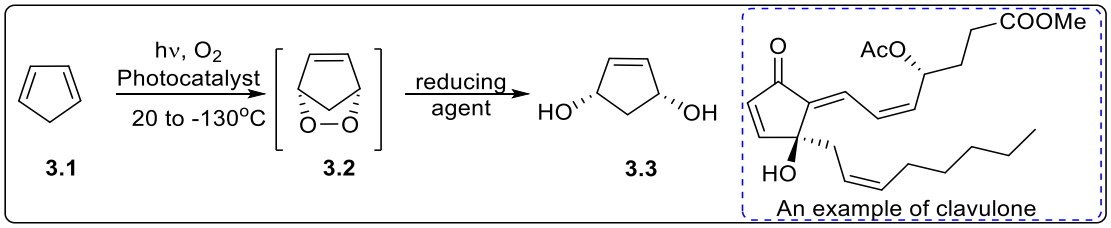
Our group has developed the use of $scCO_2$, as an alternative solvent, enabling photo-oxidation to be carried out safely in a non-flammable and non-toxic solvent.[203, 205] Reactions include etherification[257] and acid-catalysed alkylation,[258] as well as hydrogenation,[259] which was successfully scaled up to 1000 tons/yr.[260] The photo-oxidation of *α*-terpinene with $^1O_2$ in $scCO_2$ has been conducted from a small volume batch reactor to a larger flow reactor, with excellent space-time yield.[204] Recently, the photochemical synthesis of artemisinin was published in the strategy combining liquid CO_2 and a dual-functional solid acid/photosensitiser.[39]

3.1.2 **Oxidation of 3.1 in a traditional solvent**

In 2010, our group studied the hydrogenation of furfural in $scCO_2$.[261] It has been demonstrated that the principle of real-time switching between multiple products with a tandem flow-reactor setup to generate five products from a single feedstock is possible. This work inspired us to apply the ‘vending machine’ concept to the photo-

oxidation of cyclopentadiene (**3.1**) with $^1O_2$ in CO_2 to obtain a number of products selectively.

The photochemical oxidation of **3.1** is a relatively well-known reaction. It proceeds *via* a [4+2] cycloaddition reaction of $^1O_2$, as shown in Scheme 3-1.[262] These reactions have been discussed in literature, concerning the generation of the endoperoxide, 3-dioxabicyclo[2.2.1]hept-5-ene (**3.2**), after irradiation by visible light at a low temperature *i.e.* -20 to -130 °C.[263] Compound **3.2** is a key intermediate for the production of the *meso*-cyclopent-4-ene-1,3-diol (**3.3**), a precursor for the synthesis of prostaglandins.[264,265] Compound **3.3** also has been recognised as a significant motif of clavulones[i] controlling a number of significant physiological processes,[266] such as remarkable anticancer activity.[267]



*Scheme 3-1. Synthesis of (1R,3S)-cyclopent-4-ene-1,3-diol (**3.3**) in the literature.*[262]

However, in order to isolate the endoperoxide (**3.2**), the irradiation and work-up had to be carried out at *ca*. -100 °C due to the instability of the endoperoxide (**3.2**) (decomposed at *ca*. -30 °C).[268] Such demanding reaction conditions are difficult to implement for larger preparative purpose. The lifetime of $^1O_2$ is short-lived in most organic solvents, except in halogenated solvents.[82] Therefore the one-step synthesis of **3.3** by photo-oxidation of compound **3.1** has been modified[269,270] to use CH_2Cl_2 or CCl_4 as a solvent, which increases the lifetime of $^1O_2$, although this is at the expense of the 3rd (Less hazardous chemical syntheses) and the 5th (Safer solvents and auxiliaries) principle of *Green Chemistry*.[226] Jähnisch and Ehrich *et al.* reported a falling-film microreactor for the photo-oxidation of **3.1**, the yield of product **3.3** was

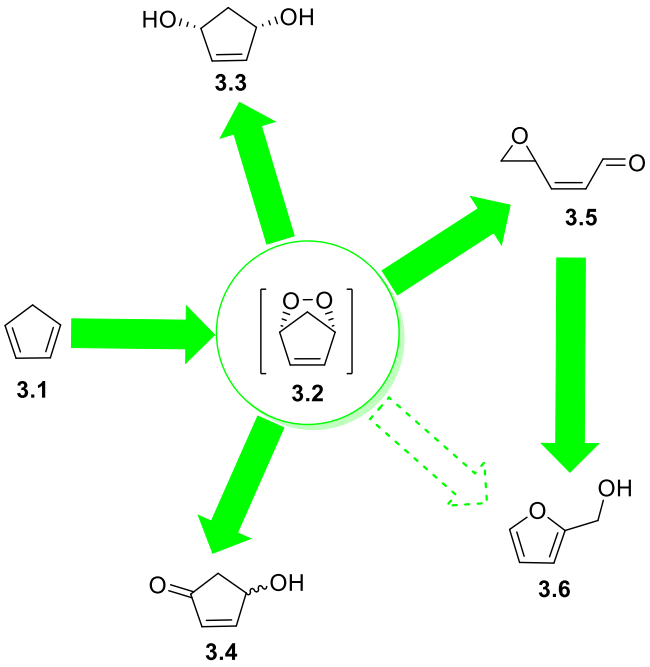
[i] Isolated from the Okinawa soft corals Calvularia viridis Quoy and Gaimard.

only 20 % after reduction with thiourea.[271] Moreover, a low concentration, *e.g.* 0.01M, was required under the optimised reaction conditions, which therefore results in low productivity. These conditions were necessary due to the rather unstable nature of explosive endoperoxide intermediate **3.2**, requiring a dilute solution and the relatively long lifetime of $^1O_2$ in halogenated solvents, *e.g.* CH_2Cl_2 or CCl_4. However, it is no longer acceptable to use such solvents from an environmental standpoint, by *EU Directives* 1999/45/EC.[272] To meet these demands, it is believed that a greener and safer process should be employed.

3.2 Experimental Strategy

Production of product **3.3** prompts us to try different quenching reagents to treat active intermediate **3.2** in order to produce valuable chemicals following a daisy-chain reaction. We demonstrated this concept using **3.1** as a single feedstock. This photo-oxidation of **3.1** was catalysed by 5,10,15,20-tetrakis-(pentafluorophenyl)porphyrin (TPFPP), a highly fluorinated analogue of *meso*-tetraphenylporphyrin (TPP), the CO_2-soluble homogeneous photosensitiser.[205, 203]

Interestingly, apart from the synthesis of **3.3** from **3.1**, intermediate **3.2** can undergo facile transformations upon treatment under a variety of conditions. 4-hydroxy-2-cyclopentenone, HCP, **3.4** was allegedly formed when the photo-oxidation of **3.1** was carried out in dilute alkaline alcoholic solutions at atmospheric pressure and room temperature.[273] Additionally, active 4, 5-epoxy-*cis*-2-pentenal, (**3.5**) (shown in Scheme 3-2) obtained from the thermal isomerisation of **3.2**, can be produced at an appropriate temperature, further treatment of an aqueous solution of **3.5** with H_2SO_4 yielded furfuryl alcohol, FA, **3.6**.[274]



*Scheme 3-2. Compounds of interest in the different treatment after the photo-oxidation of **3.1**: Cyclopentadiene, **3.1**, 2, 3-dioxabicyclo[2.2.1]hept-5-ene, (**3.2**), meso-cyclopent-4-ene-1,3-diol, (**3.3**), 4-hydroxy-2-cyclopentenone, (**3.4**), 4,5-epoxy-cis-2-pentenal, (**3.5**), and furfuryl alcohol, (**3.6**).*

Other than the production of the diol **3.3** from **3.1**, the other compounds mentioned above have been relatively less studied. The enantiomers of **3.4** are attractive to organic chemists due to their interesting features, possessing three different functional groups on a small cyclopentyl molecule. They have been the key starting materials for a variety of applications, most notably in one of the popular routes to prostaglandins.[275-276] They are derived enzymatically from the fatty acid, arachidonic acid.[277] Compound **3.5** has a unique structure comprising of different active sites (such as, α,β-conjugated ketone and a terminal epoxide), susceptible to undergoing a reaction to useful compounds, such as furfuryl alcohol, FA, **3.6**, a versatile compound being used as a fuel.

We adopted a two stage strategy. First, kinetic studies were conducted in the batch using FT-IR and NMR. Then, the production of these chemicals was scaled-up in the high-pressure continuous flow setup.

3.3 Investigating the reaction of Cyclopentadiene with $^1O_2$

3.1 is very easily dimerised at room temperature, and it was freshly prepared before each experiment. It was obtained by the distillation of dicyclopentadiene at 170 °C, being collected in a flask cooled by an ice bath.

3.3.1 FT-IR monitoring in a high-pressure batch cell

An investigation by FT-IR *in-situ* analysis in a high-pressure batch cell was carried out. The experimental details were described in Chapter 2. The small scale batch photo-oxidation rig is made up of two parts (Figure 3-1): a continuous flow section for the preparation of the CO_2/O_2 mixture and the batch cell illustrated in Figure 3-1. The system pressure was maintained at 120 bar, the volume of the *multi*-purpose

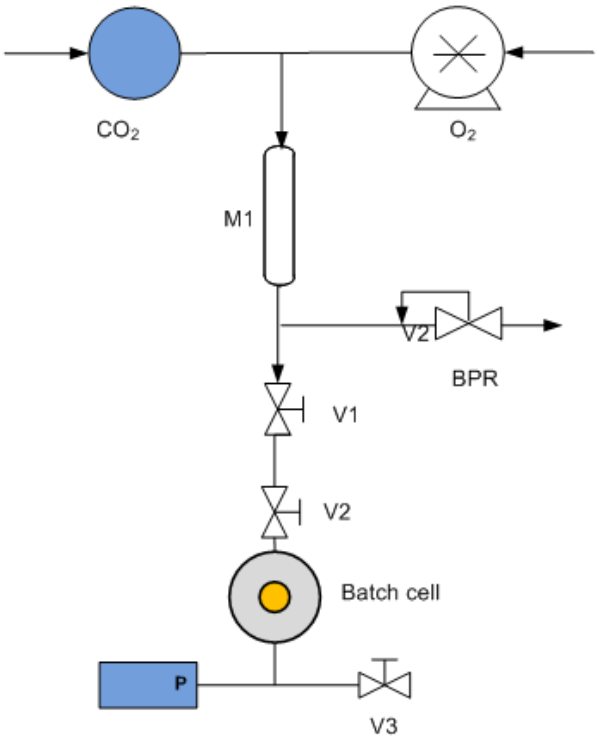


Figure 3-1 Schematic of high-pressure batch cell. The rig consists of two parts: one is for the mixing of CO_2 and O_2; another part is for the photo-oxidation in the batch cell. M1: static mixer; Cell: batch photo-oxidation cell which is temperature controlled using an external heating block. The cell would be positioned as a normal sample loaded in the FT - IR after disconnecting between V1 and V2.

photochemical and spectroscopic cell was 0.78 mL, with CaF_2 windows and the path length was 1 mm. The cell was filled with CO_2 and O_2 such that the molar ratio of O_2 to the substrate was 5:1, and TPFPP was dissolved in **3.1** with a concentration of 4 mg/mL, at 40 °C. 15 µL of the mixture of TPFPP and **3.1** was fed into the cell and then filled with CO_2 and O_2 by opening V1 and V2 until the cell reached the desired pressure reading from the pressure monitor, *P*. Finally, the cell was disconnected between V1 and V2 before closing V1 and V2. This design was based on the apparatus used previously for the photo-oxidation of α-terpinene in $scCO_2$.[205, 278] The high-pressure mixture was then irradiated for the time indicated, FT-IR spectra were recorded after each interval of photolysis, before depressurisation.

Since the intermediate **3.2** is unstable and is difficult to isolate at room temperature, an investigation of *in-situ* FT-IR analysis of photo-oxidation of **3.1** to **3.2** was conducted in the batch cell.

The cell was maintained at 40 °C during the experiments by using aluminium heating blocks. Firstly, the spectrum of **3.1** was recorded in the high-pressure batch cell. 8 µL **3.1** was injected into the cell using an syringe (SGE 10R-S-0.63, 10 µL), the cell was then filled with CO_2 to 120 bar at 40 °C. The spectrum was shown in Figure 3-2. The peak at 1369 cm^{-1} represents the C-H bond bending, which is an intensive peak due to two C-H bonds. The represented peaks at 2896-3100 cm^{-1} are assigned to C=C bond vibration and C-H bond symmetrical stretching.

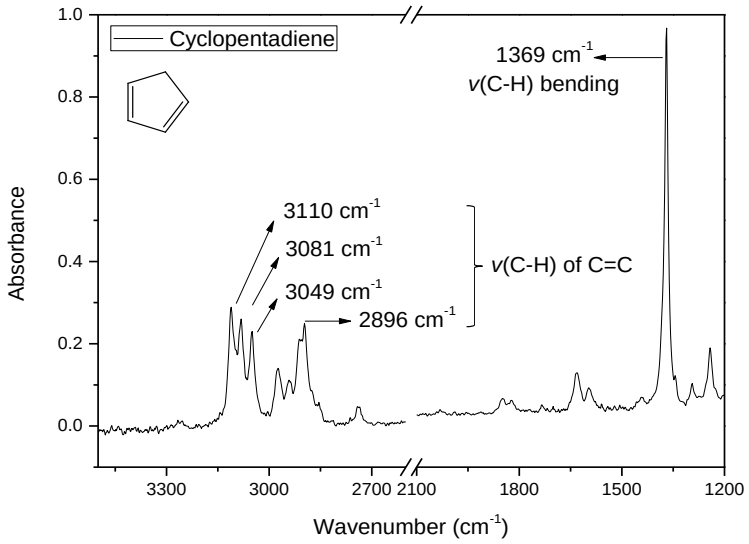


*Figure 3-2 FTIR spectrum of **3.1** recorded in the high-pressure batch cell. 8µL **3.1** was injected into the batch cell using an syringe (SGE 10R-S-0.63 10µL). The cell was then filled with CO_2 to 120 bar at 40 °C.*

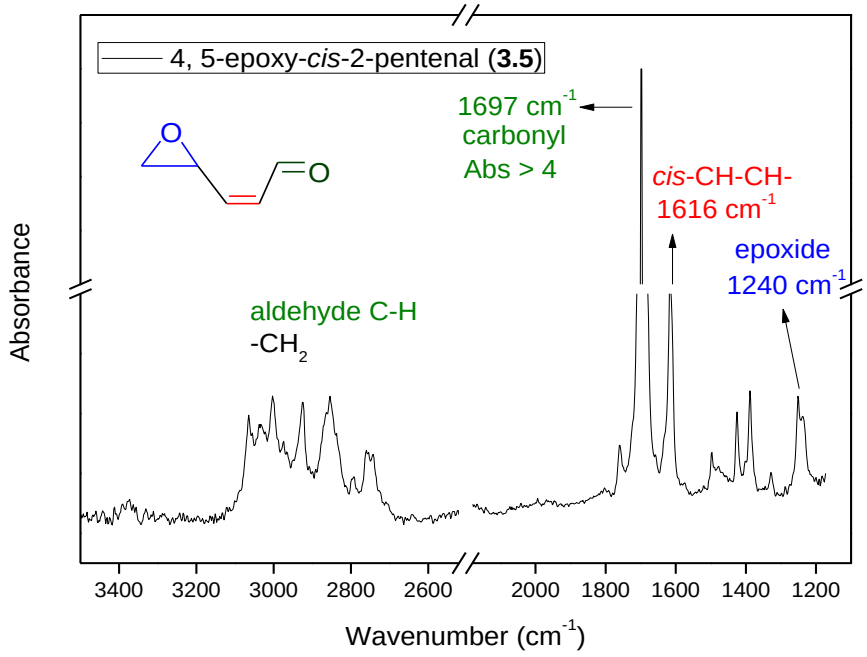


*Figure 3-3 FT-IR spectrum of 4, 5-epoxy-cis-2-pentenal (**3.5**) recorded in a high-pressure batch cell. 8µL (**3.5**) was injected into the batch cell using an syringe (SGE 10R-S-0.63 10µL). The cell was then filled with CO_2 to 120 bar at 40 °C.*

Then the spectrum of product, 5-epoxy-*cis*-2-pentenal (**3.5**) were recorded as well under the same condition with that of **3.1**, which is shown in Figure 3-3. The peaks of 1697 cm^{-1}, 1616 cm^{-1} and 1240 cm^{-1} were assigned to the carbonyl group, C-H bond bending and epoxide group of product **3.5**, respectively.[279] The peaks of *ca*. 3000 cm^{-1} were assigned to C-H bond of an aldehyde group, with C-H bond stretching.

Then, the spectrum of photo-oxidation of **3.1** with singlet oxygen using CO_2 as a solvent was recorded in the batch cell. Freshly prepared solution of TPFPP solublising

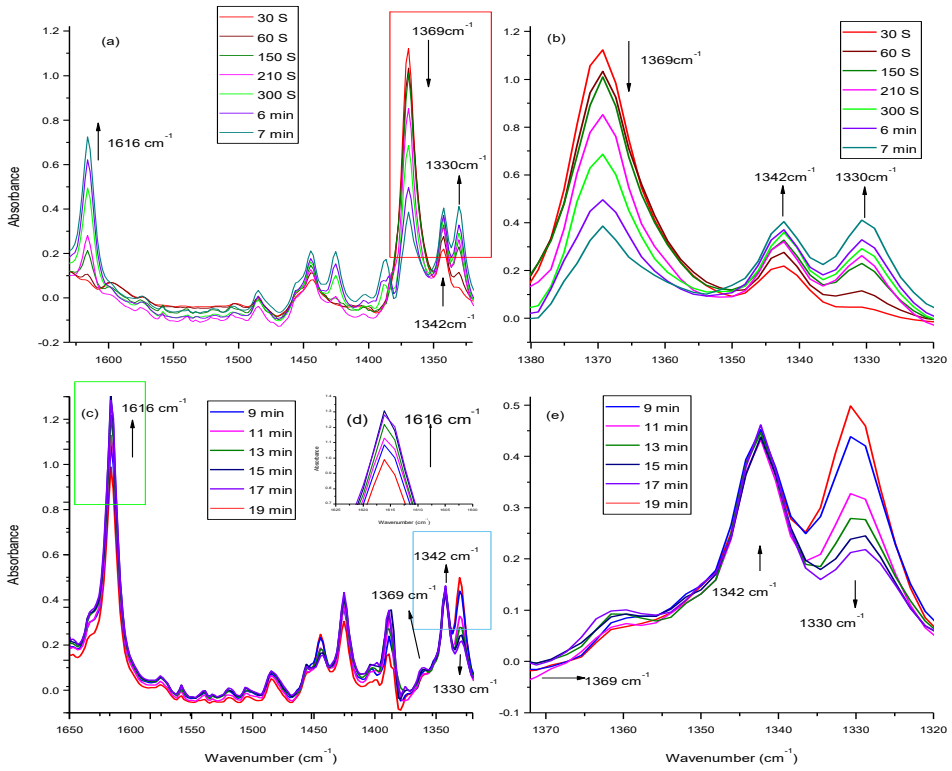
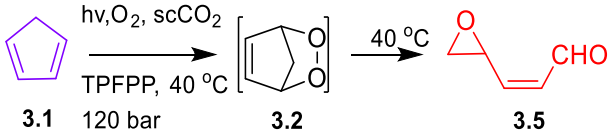


*Figure 3-4 FT-IR monitoring of reaction of **3.1** with O_2 in $scCO_2$ at 40 °C using TPFPP at 120 bar during irradiation (300 W xenon lamp with a filter to cut out UV irradiation). (a) From the start of the reaction to 7 min, shows the spectra from 1650 cm^{-1} to 1320 cm^{-1}; (b) At the same time range, zoom in the Red part in (a); (c) From 9 min to 19 min, the 1650 cm^{-1} to 1320 cm^{-1} region; (d) The enlarged Green region of (c) from 1630 cm^{-1} to 1600 cm^{-1};(e) The enlarged Blue region of (c) from 1380cm^{-1} to 1320 cm^{-1}. For a schematic of the reactor, please see the previous publication in our group.[203]*

in **3.1** was filled in the cell as described above, following feeding the CO_2/O_2 to 120 bar at 40 °C, irradiated by a single white LED array (1000 lumen, OSTAR, part code: LEUWE3B-PZQZ-4C8F) every 20 seconds after disconnecting between V1 and V2. Figure 3-4 shows that quantitative conversion of **3.1** to **3.2** and **3.5** can be observed using TPFPP as photosensitiser with 6.8 % O_2 in $scCO_2$ during the irradiation for 19 min. The reaction was confirmed using FT-IR spectroscopy, and the peak height at 1369 cm^{-1} was assigned to the *v*(C-H) bending of the starting material, **3.1**. It was observed to decrease as the photolysis time increased. Additionally, the peaks at 1616 cm^{-1} and 1330 cm^{-1} increased in size and can be assigned to the aldehyde *v*(CO) *cis*-CH=CH of product **3.5** and C-H of intermediate **3.2**, respectively. These results are consistent with the spectra of **3.1** and **3.5** recorded in $scCO_2$ (See Figure 3-2 and Figure 3-3). Based on the assignment preceding, the peak height at 1616cm^{-1} and 1330 cm^{-1} grew in size from 0 to 7 min photolysis time, until **3.1** was close to complete conversion, seen from the decay of the peak at 1369 cm^{-1}.



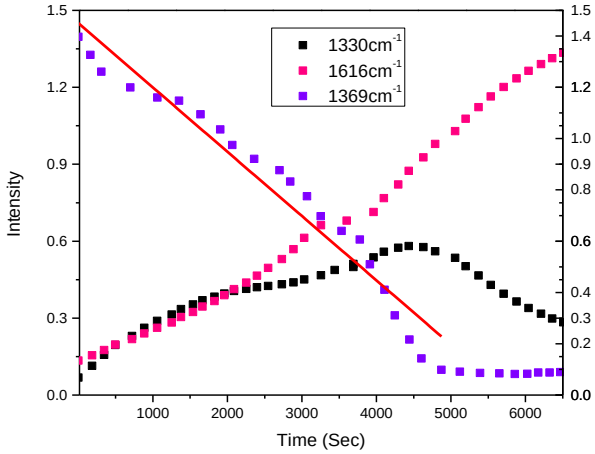


*Figure 3-5 Spectra were recorded at 20 s intervals showing: (**3.1**), loss of starting material (1369 cm^{-1}); (**3.2**), endoperoxide (1330 cm^{-1}) and (**3.5**), epoxyaldehyde (1616 cm^{-1}).*

Upon more extended irradiation period from 9 min to 19 min, the peak height at 1616 cm^{-1} increased in size, but the peak height at 1330 cm^{-1} decreased, although there was no starting material left during this period. Due to this, it can be inferred that intermediate **3.2** was converted to **3.5** at 40 °C. The kinetics of photo-oxidation of **3.1** to **3.2** was followed using the intensity of the 1369 cm^{-1} (**3.1**) and 1330 cm^{-1}(**3.2**) bands, Figure 3-4.

The reaction was found to proceed with zero order kinetics (See Experimental Section 3.9.2) under these conditions and the rate constant was 0.00251 $mol^{-1}{\cdot}L{\cdot}s^{-1}$ as fitting line showing in Figure 3-5. The monitoring of the reaction demonstrated that: (ⅰ) Product **3.2** and **3.5** were produced under these conditions (120 bar, 40 °C); (ⅱ) **3.2** can be detected before decaying into **3.5**, which is in agreement with the observation from the nuclear magnetic resonance (NMR) results in the next section.

3.3.2 NMR monitoring in atmospheric pressure

After the monitoring of photo-oxidation of **3.1** using $scCO_2$ as a solvent in the batch cell by FT-IR, we can know the kinetics for the photo-oxidation of **3.1** to **3.2**. Now, the isomerisation of **3.2** to **3.5** was monitored by NMR at 20 °C, atmospheric pressure. The photo-oxidation of **3.1** to **3.2** was conducted in a thick NMR tube at -78 °C, to monitor the reaction rate of **3.2** isomerising to **3.5** during this process. $CDCl_3$ was used as the solvent, the concentration of **3.1** in $CDCl_3$ was 2.6 mM, with TPFPP (4 mg/mL of **3.1**), and oxygen was provided by a balloon filled with pure oxygen. The tube, then, was transferred to NMR machine carefully after a time period of 1 h irradiation. The spectra have been recorded for 5 h, shown in Figure 3-6. Chemical shifts at 10.18~10.22 ppm and 5.29~5.32 ppm represent compound **3.5** and **3.2**, respectively. The concentration of **3.5** increases as that of **3.2** decreases. The results show that this thermal isomerisation was the first order reaction (See Experimental Section 3.9.2), and the half-life is a couple of hours at 20 °C. These

results helped decide the appropriate volume of the thermal isomerisation reactor to provide the desired residence time in the flow process.

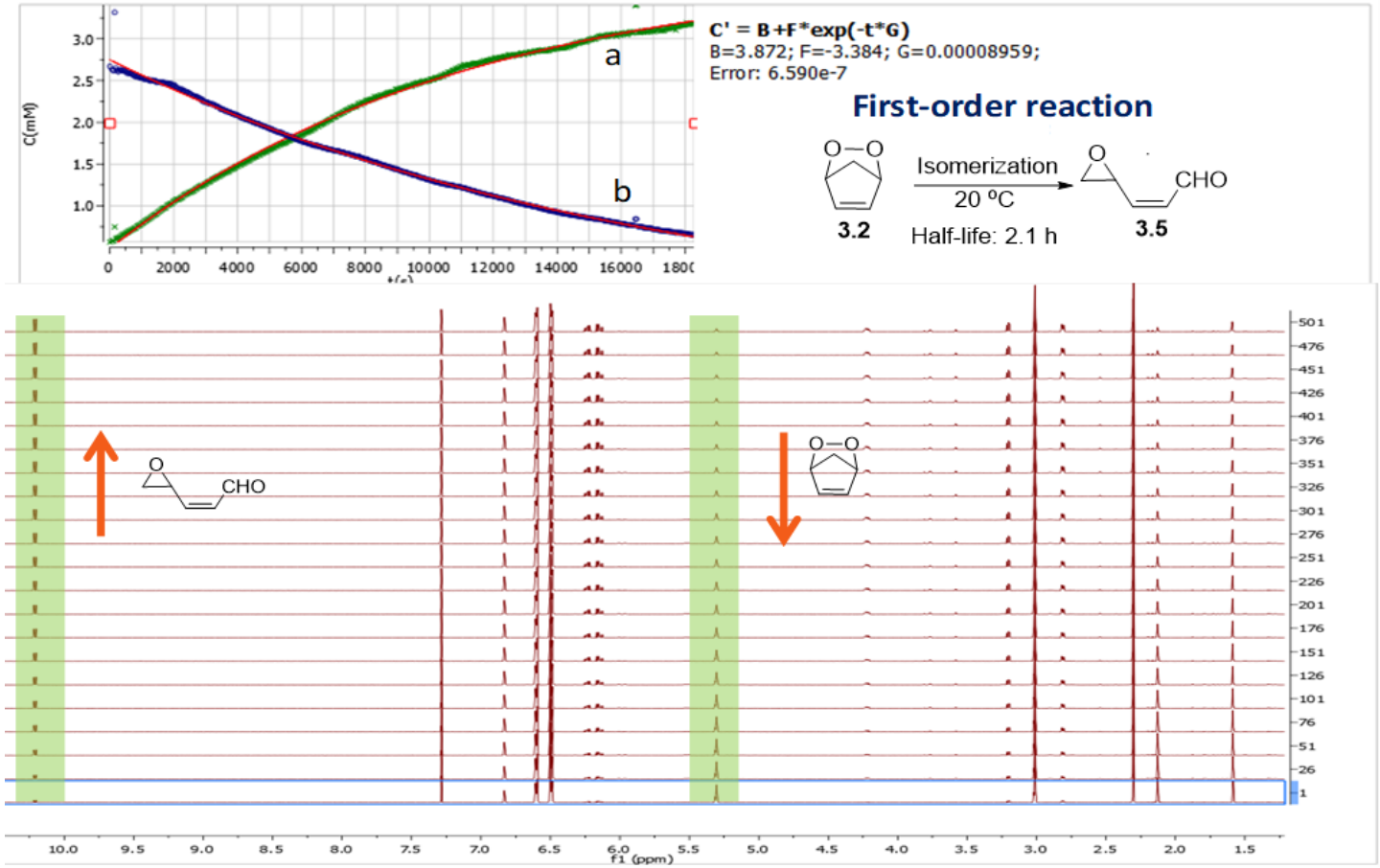


*Figure 3-6 Results for the monitoring of intermediate **3.2** to product **3.5** by NMR (500 MHz) within 5 h. Compound **3.2** was prepared freshly before monitoring, the concentration was 2.6 mM in $CDCl_3$, at 20 °C. The traces, (a) and (b), represented the peaks changing at δ10.18~10.22 ppm (**3.5**) and δ 5.29~5.32 ppm (**3.2**), respectively.*

3.4 Development of Daisy-Chain in Flow

Following the small-scale batch reactions and the monitoring experiments in the high-pressure spectroscopic cell, these results suggested that it might be possible to synthesise products **3.3**, **3.4**, **3.5** and **3.6** after the photo-oxidation of **3.1** in $scCO_2$ in a scaled-up daisy-chain continuous flow setup. The reason is that the important endoperoxide intermediate **3.2** was found to have a lifetime of the order of several minutes, in $scCO_2$ under a range of conditions at a temperature as high as 40 °C. A schematic diagram of the reactor system for continuous photo reactions is shown in Figure 3-7.

A key engineering challenge for safe operation is to ensure efficient mixing because the organic substrate is flammable, even if the CO_2 solvent is not itself flammable. It can be seen from Figure 3-7 that we premix the O_2 and CO_2 and pass them through a static mixer (a stainless steel tube, filled with sand) before they contact the organic stream containing starting material **3.1**. The combined streams are then passed through a second static mixer before entering the photo-reactor. This strategy has previously been successfully used for catalytic thermal oxidation.[280] After the photo-reactor, different arrangements of additional reactors and mixers, as well as a quenching reagent feed, can be employed depending on the desired product (different configurations are shown in Figure 3-7 with dashed lines). Three sets of LED lights were used in the high-pressure experiments of this chapter, and the details about the LED have been discussed in Chapter 2.

Initially, the photo-oxidation of **3.1** was carried out in the continuous flow photo-reactor where complete consumption of the starting material was achieved over a range of conditions (Table 3-1). Under both liquid CO_2 and supercritical conditions (Table 3-1, entries 4-6), complete conversion of **3.1** was observed. The products were

a mixture of **3.2** and **3.5**, however, which were often obtained in different ratios due to the unstable nature of **3.2** above -30 °C.

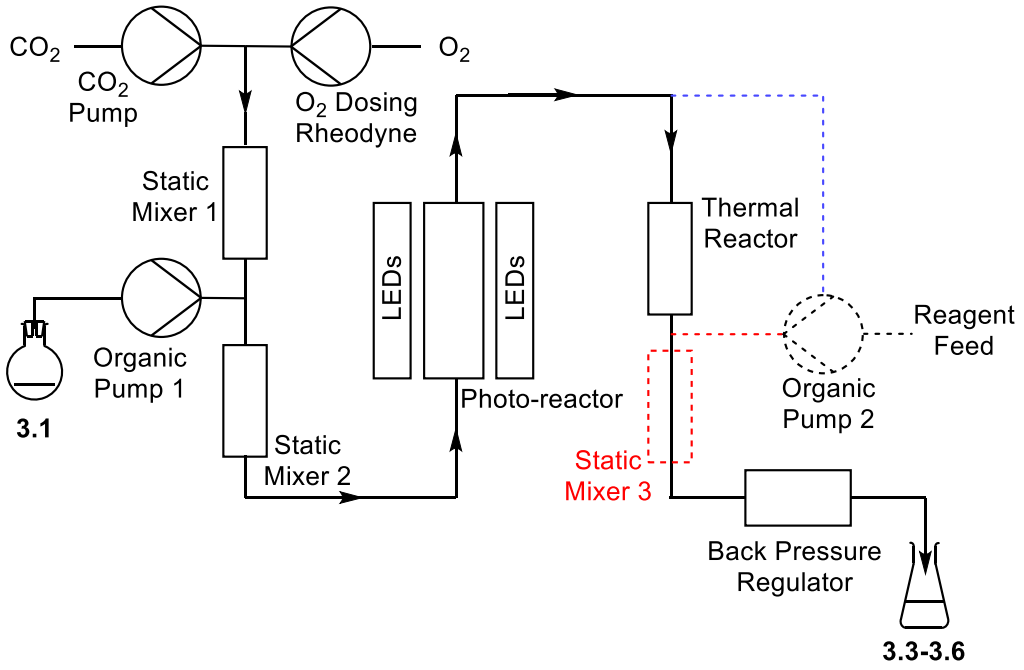
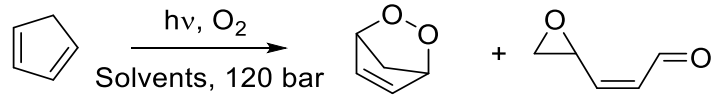


Figure 3-7 Simplified schematic of the high pressure continuous flow setup. CO_2 is delivered from a chilled CO_2 pump and O_2 is dosed at a known rate via a Rheodyne dosage unit. Static mixer 1 consists of a stainless steel tubular reactor filled with sand and provides mixing for the CO_2 and O_2. Static mixer 2, which is also a steel tube filled with sand provides mixing for the organic feed and the gases. Organic pump 1 is used to pump a mixture of 1 and photosensitizer. The mixture is then passed into a high pressure sapphire tube reactor, which is irradiated by LEDs in an upward flow. The sapphire tube is filled with glass balls (6 mm diameter) to provide mixing. After the photoreactor is a thermal reactor which consists of 4 × tubular reactors (1/4" O.D. 0.049" wall thickness, 150 mm length) filled with glass beads (710-1180 µm) in series which could be heated with an aluminium heating jacketed.[243, 281] A second organic pump is added either before (shown in blue) or after (shown in red) the thermal reactor depending on the reaction and in some cases a third static mixer is added in (shown in red). (A full diagram of each set-up is shown in the experimental).

Table 3-1 Optimisation of the photo-oxidation of cyclopentadiene in the high-pressure continuous flow reactor.[a]



3.1 **3.2** **3.5**

Entry	Solvent	TPFPP (mol %)	Flow Rate (mL/min)		O_2 molar ratio	Temp. (°C)	Conv. (%)[b]
			CO_2	3.1			
1	$scCO_2$	0.002	1	0.05	2:1	40	33
2	$scCO_2$	0.002	1	0.3	2:1	40	-[c]
3[d]	$liqCO_2$	0.002	0.5	0.1	0.1:1	0	10
4	$liqCO_2$	0.008	0.5	0.05	2:1	0	>99
5	$scCO_2$	0.008	0.25	0.05	1:1	40	>99
6[e]	MeOH/ $scCO_2$	0.008	0.25	1	2:1	40	>99

[a]: All the experiments were carried out at 120 bar unless stated otherwise. Three sets of white light LEDs were used for these experiments, and the details about LEDs have been talked in Chapter 2. [b]: Conversions of **3.1** were calculated by ^{1}H NMR Spectroscopy using biphenyl as an internal standard. [c]: At this flow rate, blockages in the system occurred. [d]: System pressure was 1 bar. [e]: **3.1** was pumped as a solution in MeOH (0.1 M).

To ensure that all of the endoperoxide **3.2** was converted to the Z-aldehyde **3.5**, a simple thermal reactor was added downstream after the photoreactor. This reactor consisted of 4 × tubular reactors in series which were filled with glass beads and heated to 40 °C to promote the isomerisation of **3.2** to **3.5**. The optimal conditions from the photo-oxidation (Table 3-1, entry 5) were run with this additional reactor, which gave quantitative conversion to the aldehyde **3.5**.

3.5 Synthesis of products in liquid CO_2

3.5.1 Production of Cyclopent-4-ene-1,3-diol

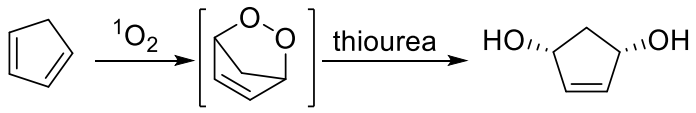
Cleavage of the O-O bond of an endo-peroxide to yield a *syn*-diol, which is an attractive motif present in a range of prostaglandins,[275] is often facilitated using thiourea as a reducing agent.[282] In 2003, the production of **3.3** from **3.1** had been studied,[269] a biphasic system was used for quenching the intermediate **3.2** directly with thiourea during the photo-oxidation process in CH_2Cl_2/H_2O, a good yield of **3.3** was obtained. The results of the photo-oxidation of **3.1** to **3.3** in batch reactor using methanol as solvent at 1 atm, 0 °C showed that the yield of **3.3** was 61 % after 2 h irradiation, with full conversion.

Synthesis of diol 3.3 in liqCO_2

In order to synthesise **3.3** following the photo-oxidation of **3.1** in the continuous CO_2 photo-reactor, an additional reagent stream was added downstream of the photoreactor (See Figure 3-7, with an organic pump 2 in the blue configuration). A number of parameters were investigated in this continuous flow reactor, the substrate, **3.1**, that TPFPP dissolving well in it was mixed with CO_2 and O_2 (7.6 mol%), irradiated by LED light, then treated by different quenching solution to obtain various products after flowing out from BPR. The results shown in Table 3-2 demonstrate that all the concentrations of TPFPP, **3.1** and O_2, solvent have effects on the yield of **3.3**. The photo-oxidation was examined at 40 °C, 120 bar (Table 3-2, entries 1 - 2), to be sure that CO_2 was in a supercritical condition (critical point of CO_2: 31 °C, 73.8 bar),[283] but the elevated temperature required for the supercritical conditions resulted in inconsistent yields throughout the experiments as the endoperoxide **3.2** can decompose to **3.5** at the high temperatures before it could react with thiourea. Lowering the temperature to 0 °C to increase the lifetime of the endoperoxide **3.2** (Table 3-2, entries 3-4) meant operating in liqCO_2, but, under these conditions, a slight

increase in the yield of the diol **3.3** was observed. Diluting **3.1** by the addition of a co-solvent proved to be successful in increasing the yield of **3.3**, in both $scCO_2$ and $liqCO_2$ (Table 3-2, entries 5-7). Using THF as solvent proved slightly detrimental compared to MeOH as the lower solubility of thiourea occasionally led to blockages.

*Table 3-2 Synthesis of diol (**3.3**) from **3.1** in a continuous flow reactor.*[a]



3.1 **3.2** **3.3**

Entry	Solvent	Co-solvent	TPFPP: CPD (mol %)	Flow Rate (mL·min^{-1})			Yield[b] of 3.3 (%)
				CO_2	3.1	Thiourea	
1	$scCO_2$	-	0.002	1	0.2	1	22
2	$scCO_2$	MeOH	0.008	1	1(0.1M)	1	60
3	$liqCO_2$	-	0.002	1	0.2	2	33
4	$liqCO_2$	-	0.002	0.5	0.05	2	30
5	-	MeOH	0.008	0.5	1(0.1M)	0.5	91[c]
6	$liqCO_2$	MeOH	0.008	0.5	1(0.1M)	0.5	94[c]
7	$liqCO_2$	THF	0.008	0.5	0.1(0.1M)	0.8	80[c]

[a]: All experiments were conducted at 120 bar unless otherwise stated. Three sets of LED light were involved, and the details have been discussed in Chapter 2. Thiourea (1 M) was dissolved well in methanol before pumping into the system. $liqCO_2$: Liquid CO_2. TPFPP was dissolved well in substrate **3.1** before pumping. [b]: Yield was calculated by ^1H NMR, biphenyl as an internal standard. [c]: Full conversion. The amount of thiourea was in excess than the required amount of quenching (**3.2**). Entry 1: The molar ratio of O_2 to **3.1** was 1:1; entries 2 to 7: The molar ration of O_2 to **3.1** was 2:1. The temperature for photoreactor was 40 °C (entries 1 and 2); was 0 °C (entries 3 to 7).

Synthesis of 3.3 in Vortex Reactor

The synthesis of diol (**3.3**) was conducted in a Vortex reactor[55] working at atmospheric pressure to compare with the results in a high-pressure continuous flow reactor. This reactor was designed in our group (Figure 3-8), which uses a shaft rapidly rotating to generate Taylor vortices for continuous flow thermal and photochemical reactions. For reactions with oxygen, the reactor offers an alternative to traditional setups as it efficiently draws in air from the lab without the need specifically to pressurise with oxygen, the further details can be found in the previous publication.[55]

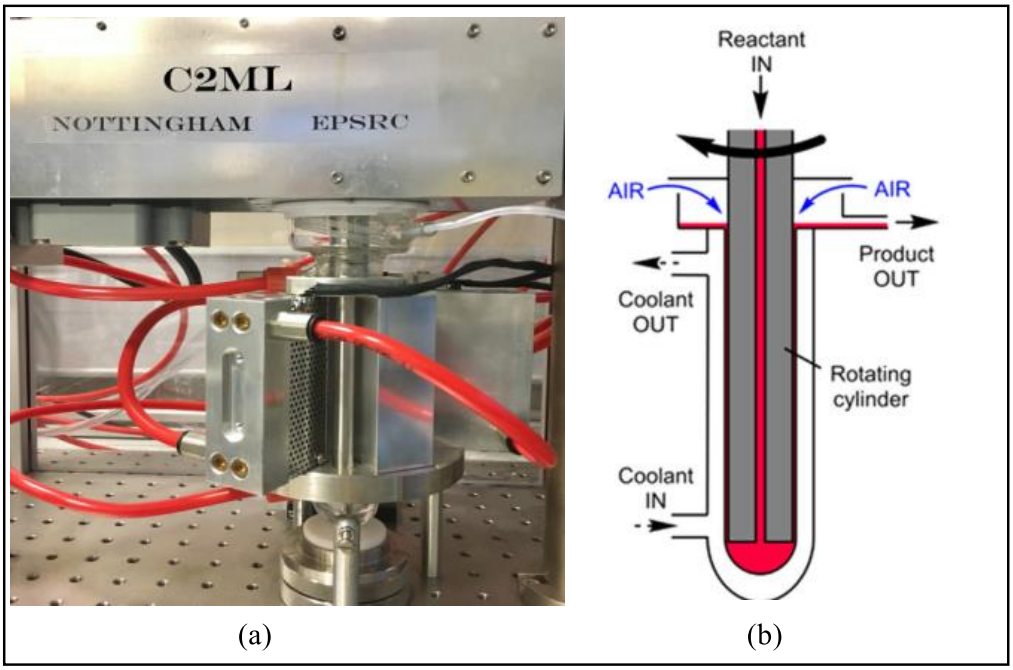
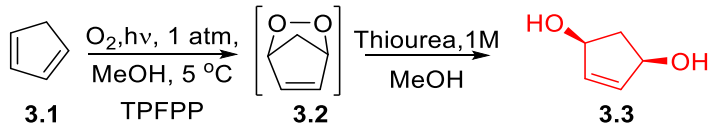


Figure 3-8 Vortex Reactor (a): Showing the LEDs and mirror blocks mounted placed around the reactor. (b): A cross-section (not to scale) of the reactor showing the delivery and removal of reagents and the intake of oxygen.[55]

One of the differences between a high-pressure sapphire tube reactor and a vortex reactor is that the vortex reactor is surrounded by LED lights, holding a shaft in the middle. The shaft can spin at a very high speed to form Taylor vortices, oxygen

in the air will be trapped to react with the substrate (**3.1**), and then products would be pumped out. The volume of the vortex reactor was 8 mL.

Figure 3-9 shows that the yields of **3.3** are dependent on the flow rates, the concentrations of **3.1** as well as the orders of adding thiourea. The spin rate of cylinder maintained at 4000 r/min, and the photo-oxidation intermediate **3.2** reduced by thiourea solution after flowing out of MasterFlex pump, unless otherwise stated. The yield of **3.3** decreased on increasing both the concentration of **3.1** from 0.05 M to 0.2 M and the flow rate from 0.5 mL/min to 1.5 mL/min, since the residence time is reduced in the photoreactor when increasing the flow rate. The yield of **3.3** peaked at 98 % when the concentration was 0.05 M at the flow rate of 0.5 mL/min. However, the yield decreased when adding thiourea into the starting material at the beginning.



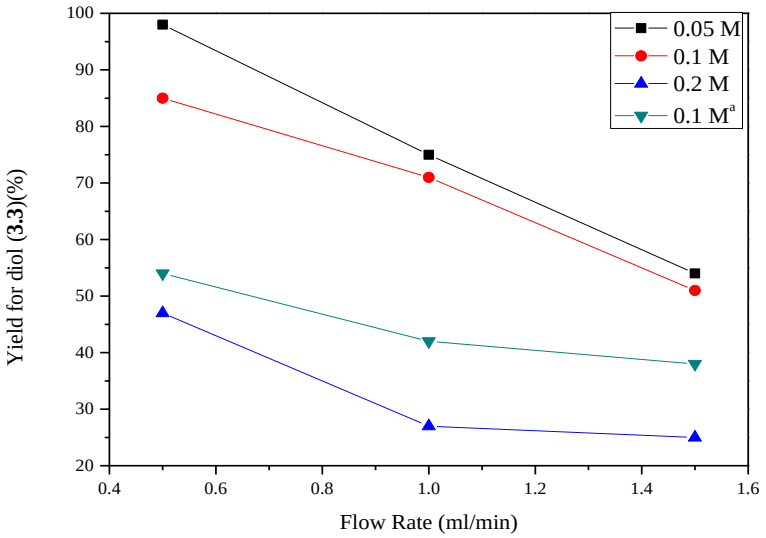


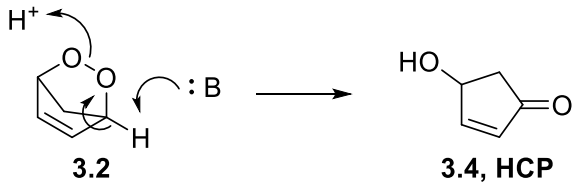
*Figure 3-9 Synthesis of diol (**3.3**) in the vortex reactor. Treating endoperoxide (**3.2**) with thiourea after photoreactor, unless other stated. [a]: Adding thiourea into the starting material solution (1.2 M).*

These resulted from less light penetration due to the fouling around the reactor, as sulfur was produced from the reacting of endoperoxide **3.2** with thiourea.

The productivity is the highest at 4.26 mmol/h under the conditions of 0.1 M, 1.0 mL/min although the highest yield was obtained at the state of 0.05 M, 0.5 mL/min, and the productivity at the latter condition is 1.47 mmol/h. The reason is that there is inadequate oxygen to react at a high concentration and high flow rate.

3.5.2 **Production of 4-hydroxycyclopent-2-en-1-one in CO_2**

Treatment of endoperoxides with a base leads to the formation of an α, β-unsaturated carbonyl moiety containing an attached hydroxyl group (Scheme 3-3). This type of reaction has been demonstrated enantioselectively using cobalt complexes *via* Kornblum-DelaMare rearrangement[284], and more recently with chiral cinchona alkaloid derived organocatalysts.[285-286]

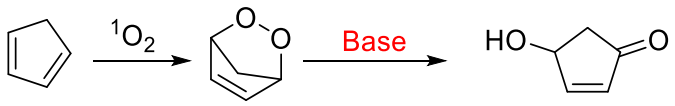


*Scheme 3-3 Treatment of endoperoxides with base and the resultant product **3.4**.*

Initial treatment of **3.2** with a strong base such as NaOH yielded mainly a polymeric material, which is unsurprising given that the product is a Michael acceptor with a nucleophilic hydroxyl group (Table 3-3, entry 1). To prevent decomposition of **3.4** by the basic catalyst, a heterogeneous catalyst Amberlite (IR 120 Na^+ form) was employed, which contains a mildly basic sulfonate group. Also having the catalyst immobilised prevents further reaction of **3.4**. While this catalyst is commonly used as an ion exchange resin, it presented moderate activity for this transformation. However, the system quickly blocked due to the build-up of polymeric compounds on the fixed catalyst bed when liqCO_2 was used as a solvent, since this polymeric material was insoluble in liqCO_2 (Table 3-3, entry 2). Repeating the experiments using a polar co-

solvent (methanol) removed the build-up of the polymeric material, but gave an only moderate yield of only 18 % of **3.4** after the reactor. More positive results were obtained when switching to a homogeneous base, trimethylamine (TEA). TEA solution was fed in downstream of the photo-reactor (see Figure 3-7, organic pump 2 in the blue configuration) and was passed through a reactor at ambient temperature (Figure 3-7, static mixer 3) which was loaded with glass beads (710-1180 μm). An excellent yield of **3.4**, 81 % was obtained when a concentration of 0.8 M TEA in MeOH was employed, delivered at a flow rate of 0.5 mL/min when pure **3.1** was pumped by organic pump 1 at a flow rate of 0.05 mL/min (Table 3-3, entry 4).

*Table 3-3 Synthesis of HCP (**3.4**) from **3.1** in liqCO_2.*[a]



3.1 **3.2** **3.4, HCP**

Entry	Solvent	Catalyst	Flow Rate (OP2, mL/min)	3.1	[c]Yield for HCP, 3.4
1	MeOH	NaOH (aq, 0.01 M)	1	0.1 M	Polymer + diol
2[d]	liqCO_2	Amberlite IR 120 Na^+ form	-	Neat[b]	Blockage
3[d]	MeOH	Amberlite IR 120 Na^+ form	-	0.1 M	18%
4[e]	liqCO_2	TEA (0.8 M)	0.2	Neat[b]	81%
5	MeOH	TEA (0.5 M)	0.5	0.1 M	84%

[a]: All of these experiments were conducted under the condition: the ratio of O_2 to **3.1** was 2:1, the concentration of TPFPP was 0.008 % mol of **3.1**, CO_2 flow rate: 0.5 mL·min^{-1}, organic pump 1 flow rate: 0.05 mL·min^{-1} (liqCO_2 as solvent), 1 mL·min^{-1} (MeOH used as solvent), the temperature of photo-reactor was 0 °C, three sets of white light LEDs were employed; [b]: Neat: Only TPFPP was dissolved well in **3.1**, no co-solvent was used; [c]: Yields were calculated by ^{1}H NMR spectroscopy, mesitylene as internal standard; [d]: 1 g Amberlite IR 120 Na+ form catalyst was loaded in the thermal reactor before experiment starting. [e]: Optimisation reactions are referred to Section 3.9.

Increasing the flow rate, and hence the concentration of base, led to a reduction in yield of **3.4**, possibly as the results of the combination of decreasing the residence time in the reactor and a higher flow rate of polymerisation of the product. Diluting **3.1** in methanol (0.1 M), further increasing the yield to 84 % when reacting 0.5 M TEA solution at a flow rate of 0.5 mL/min (Table 3-3, entry 5). (see Table 3-7, Table 3-8, Table 3-9, Table 3-10 in Section 3.9) The crude solution was neutralised by HCl aqueous solution (1 M) and extracted by diethyl ether after removing MeOH. Following on, the remaining water phase isolated from the previous extraction was extracted by EtOAc (50 mL, 3 times), a yellow oil product HCP was obtained after concentrating EtOAc phase.

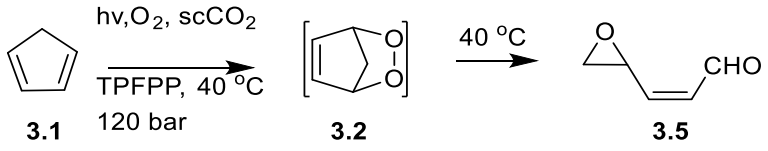
3.6 Synthesis of products in supercritical CO_2

The production of **3.5** and **3.6** from **3.1** will be discussed here. As mentioned above, **3.5** and **3.6** are versatile compounds for organic synthesis. Compound **3.5** was obtained from the thermal isomerisation of endoperoxide **3.2**.

3.6.1 Production of cis-3-(oxiran-2-yl)acrylaldehyde (3.5) in $scCO_2$

A quantitative yield of **3.5** was achieved in the continuous flow reactor, shown in Figure 3-7 when using $scCO_2$ as a solvent. The temperature of both the photoreactor and the thermal reactor was 40 °C, at 120 bar, three sets of white light LEDs were used for the photoreactor, which are presented in Table 3-4. This yield is much higher than that obtained in the published work (^{1}H NMR yield: 65 %),[287] also very promising for the production of **3.6** in the next step.

*Table 3-4 The synthesis of **3.5** in $scCO_2$.*[a]



3.1 **3.2** **3.5**

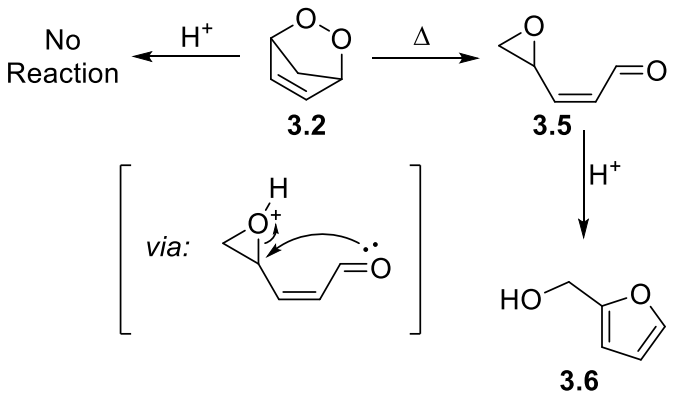
Solvent	TPFPP: CPD (mol %)	CO_2 (mL·min^{-1})		O_2: 3.1 (mol)	*T* *I*(°C)[b]	[c]Yield of 3.5
		CO_2	3.1			
$scCO_2$	0.008	0.25	0.05	1:1	40	>99%

[a]: This reaction was conducted at 40 °C, 120 bar, using $scCO_2$ as a solvent.
[b]: Both the temperature of photo-reactor and thermal reactor were 40 °C;
[c]: Yields were calculated by ^{1}H NMR spectroscopy, mesitylene was used as an internal standard.

3.6.2 **Production of furfuryl alcohol (3.6) in $scCO_2$**

Later on, the use of an acid catalyst instead of a basic catalyst was investigated in this high-pressure continuous flow reactor. In this case, the intermediate **3.2** was not reacted. However, the aldehyde **3.5**, produced from the thermal reaction of **3.2**, reacted instead. Furfuryl alcohol **3.6** was observed as the primary product in the initial batch experiments (Table 3-11 in Experimental Section 3.9). Presumably, this was formed *via* an acid-catalysed opening of the epoxide by the aldehyde, which undergoes subsequent rearrangement to yield **3.6** (Scheme 3-4). Product **3.6** is traditionally produced from the hydrogenation of furfural at high temperature (more than 200 °C) and catalysed by a metal catalyst, e.g. Pd.[288]

Two different strategies were used for the conversion of **3.1** to **3.6** through photo-oxidation, thermal isomerisation and acid catalysed cyclisation (Figure 3-10). The first step was the photo-oxidation with singlet oxygen using visible light (white light LEDs) to produce endoperoxide **3.2**, followed by step 2: thermal isomerisation giving the product **3.5**, then going through step 3: acid catalysed cyclisation to the ending



*Scheme 3-4 Reaction of **3.2** and **3.3** conducted under acidic conditions and proposed intermediate for the formation of **3.6**.*

product, **3.6**. The first strategy was a daisy-chain reaction with three reactors: photoreactor, thermal reactor (see Figure 3-7, Thermal reactor) and acid cyclisation reactor (see Figure 3-7, Static mixer 3). Strategy 2 was a "one-pot" reaction from CPD using a dual-functional acid-photocatalyst packed in a sapphire tube reactor. This dual-catalyst has been prepared by anchoring a *meso*-tetraphenylporphyrin (TPP) onto the sulfonated cross-linked polystyrene ion-exchange resin Amberlyst-15 (Amb-15) providing both Brønsted acidic and photo-catalytic functions to convert **3.1** into **3.6** in one step.

Initially, photosensitisers supported on solid acid catalyst (a dual-functional catalyst) were investigated since this approach had proved successful before.[39, 229] In the reaction with **3.1**, the photosensitisers quickly bleached when using TPP supported on Amberlyst-15 because when the photoreactor was irradiated, the outer layer of the catalyst bleached rapidly and the mixture yielded only a trace of the product (Figure 3-22). A longer path reactor would be required to increase the residence time in photoreactor that provides more mixing.[55, 289]

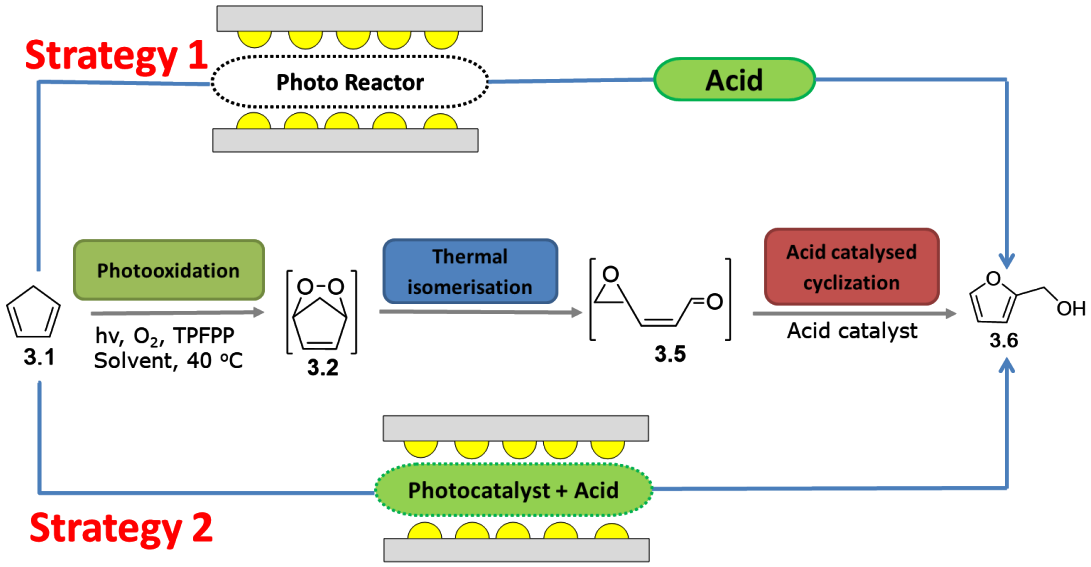
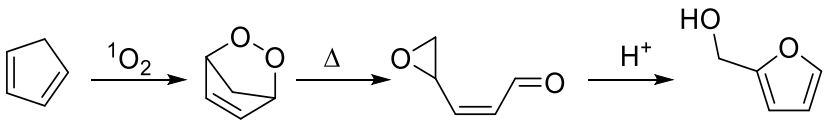


*Figure 3-10 Outline of two strategies for the synthesis of furfuryl alcohol (**3.6**).*

As explained in strategy 1, a tubular reactor filled with a heterogeneous acid catalyst was added downstream of the thermal reactor; this set-up facilitated complete conversion of **3.1** to **3.5** before reacting with the acid catalyst (see Figure 1, organic pump 2 and static mixer 3 in red configuration). Amberlyst-15 gave a poor yield for **3.6** while switching to the more acidic niobium phosphate ($NbOPO_4$), and niobium oxide (NbO_5) gave minor improvements in yield. Exchange of the solid acid catalyst reactor with a tubular reactor filled with glass beads for mixing allowed switching to a homogeneous acid and the addition of trifluoroacetic acid (TFA) feed gave an excellent yield of the furfuryl alcohol **3.6**, 85% (Table 3-5). PhMe, rather than methanol diluted TFA was used above, as **3.5** can be converted to its acetal form compound under the acidic condition in the presence of a protic solvent, methanol. In some cases, prolonged exposure time to TFA led to further reaction of **3.6** to form the trifluoroacetate ester of **3.6**. (Section 3.9.7)

*Table 3-5 Production of **3.6** from CPD in the continuous flow reactor.*



3.1 **3.2** **3.5** **3.6**

Entry	Solvent	OP1 Flow Rate (mL/min)[b]	Acid Catalyst[c]	Yield of 3.6[d]
1	$scCO_2$	0.05	Amberlyst-15	24%
2	$scCO_2$	0.05	$Nb_3O_{20}P_5$	34%
3	$scCO_2$	0.05	Nb_2O_5	30%
4[e]	$scCO_2$	0.05	TFA	85%

[a]: Conditions: system pressure: 120 bar, both the photo-oxidation and thermal isomerisation temperature: 40 °C, TPFPP (0.008 mol % of **3.1**), the ratio of O_2 to **3.1** was 1:1, CO_2 flow rate was 0.25 mL·min^{-1}, three sets of white light LEDs were used in these experiments, unless otherwise stated. [b]: Flow Rate of Organic Pump 1; [c]: 1 g solid catalysts were loaded in static mixer 3 (Figure 3-7) before starting experiment; [d]: Yields were calculated from ^{1}H NMR spectroscopy with mesitylene as internal standard; [e]: Liquid TFA (50 mM) in PhMe was pumped by organic pump 2 at a flow rate of 0.5 mL·min^{-1}.

3.7 The effect of CO_2 on the synthesis

All these four products **3.3** - **3.6** can be synthesised in both traditional solvents and $scCO_2$ or liquid CO_2 with different productivities. As we know, CO_2 is in a full oxidised mode and non-flammable, which provides the advantage to be used as a solvent, especially for the dangerous oxidation reaction as well as endoperoxide exiting condition, CO_2 provides a much safer route for these reactions.

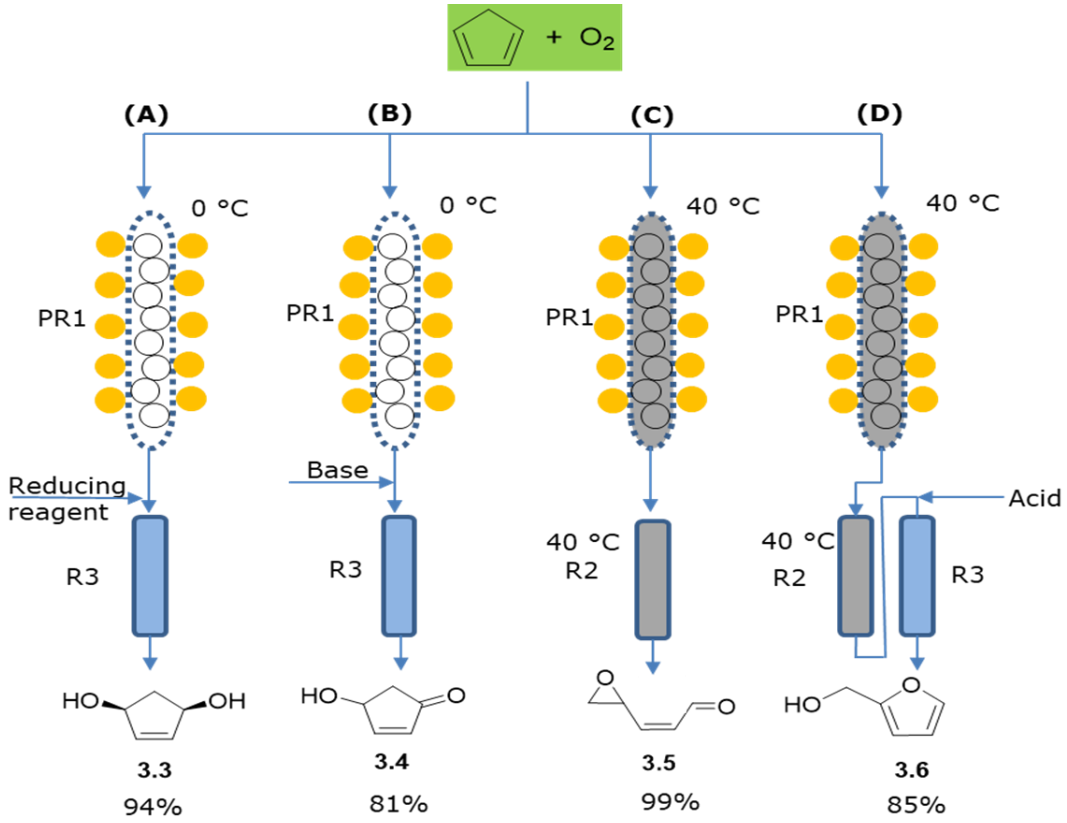


*Figure 3-11 A summary of the best yields achieved in CO_2 for the synthesis of products (**3.3**), (**3.4**), (**3.5**) and (**3.6**) using the apparatus shown in Figure 3-7. The temperatures are indicated.* **PR1** *was loaded with glass beads (Diameter: 6 mm), and R2 was empty unless otherwise stated. R2 was a thermal isomerisation reactor, which was employed in process (C) and (D). As indicated in the diagram, different quenching reagents were introduced before reactor 3 (R3), not in process (C). R3 was at room temperature, and R2 was at 40 °C.*

Figure 3-11 shows the optimum results obtained in CO_2, and all the photo-oxidation steps in the above reactions were catalysed by 0.008 mol % TPFPP, followed by the quenching step: catalysed by thiourea in the process (A), TEA in the process (B) and TFA in the process (D), respectively. All the four compounds, **3.3** to **3.6**, could be produced in high yield (>80% for all products) by merely tuning the temperature of reactors and the reagents pumped from organic pump 2. In contrast

Table 3-6 The comparison of productivity in organic solvent and CO_2.[a]

Entry	Product	Conc. Of 3.1[b]	OP 1 Folw Rate[c] (mL/min)	Productivity (mmol/h)[d]	
				In Organic solvent	In CO_2
1	(**3.3**)	0.1 M	0.1	3.06[e]	5.94[f]
2	(**3.4**)	Neat	0.05	5	30.9
3	(**3.5**)	Neat	0.05	0.65[g]	36.3
4	(**3.6**)	Neat	0.05	1.2	31.6

[a]: All these data were obtained in the work unless otherwise stated; the system pressure was 120 bar, the concentration of TPFPP was 0.008 mol %; [b]: Concentration of **3.1** in co-solvent; [c]: Flow Rate of Organic Pump 1; [d]: Productivity=Concentration of Substrate × Flow rate of organic pump 1 × Yield/ Reaction Time (h); Pure: no co-solvent used; [e]: Data was reproduced from Ref42. [f]: Methanol was used as co-solvent; [g]: Data was printed from Ref 287.

*to the reaction carried out in batch reaction or traditional organic solvents, the photo-oxidation of **3.1** and the quenching step in CO_2 exhibit higher productivity (*

Table 3-6), providing photo-oxidation step in CO_2 with higher $^1O_2$ lifetime, compared to other solvents screened (MeOH, PhMe). These allowed a higher concentration of feedstock in our continuous CO_2 system. Additionally, the productions of **3.3** and **3.6** were solvent dependent, as **3.3** was preferably prepared in polar solvents, such as methanol, due to the solubility of thiourea. Instead, **3.6** was preferentially formed in aprotic solvents, such as PhMe, as the side reaction was hinderred. It is challenging to find an appropriate polar aprotic solvent, that is, greener as well as having a long lifetime with $^1O_2$, however, CO_2 can be employed as the efficient solvent in both polar and aprotic conditions.

3.8 Conclusion

In this Chapter, four important compounds, *meso*-cyclopent-4-ene-1,3-diol (**3.3**), 4-hydroxy-2-cyclopentenone (**3.4**), 5-epoxy-*cis*-2-pentenal (**3.5**) and furfuryl alcohol (**3.6**), were successfully synthesised from a single feedstock, cyclopentadiene in the continuous flow reactor. The kinetics of photo-oxidation of (**3.1**) were monitored by FT-IR and NMR. Both good yields and productivities were achieved by merely tuning the quenching reagents or reaction temperature. The productivities using supercritical or liquid CO_2 as solvents are higher than that in the traditional solvents, methanol, PhMe or THF. The yield of **3.3** and **3.4** is 94 % and 81 % in liquid CO_2, respectively. The yield of **3.5** was more than 99% in $scCO_2$, with *ca.* 50 times more productivity than that using methanol instead of $scCO_2$.

In the future, a thermal reactor could be added before the photoreactor to realise the cracking of dicyclopentadiene to **3.1** directly, due to its easy dimerisation to its dimer at room temperature, there will be no extra distillation required before the reaction, and useful products can be produced from cheap dicyclopentadiene. Moreover, more functionalised cyclopentadiene derivatives will be explored in the high-pressure continuous flow reactor using CO_2 as a solvent. Investigating the chiral base for the production of HCP (**3.4**) enantiomers is also worth doing since there is the possibility of building a chiral centre in compound **3.4**, which is a valuable motif for prostaglandins and antibiotics. Product **3.5** is also a good imine precursor with an amine to synthesise pyrrole derivatives.

3.9 Experimental

3.9.1 General information

TPFPP, thiourea, Amberlyst-15, triethylamine (TEA), 2,2,2-trifluoroacetic acid (TFA) were purchased from Sigma Aldrich and used as received. Dicyclopentadiene was purchased from Sigma Aldrich and distilled using standard distillation setup. Pure cyclopentadiene distilled from dicyclopentadiene was stored at -20 °C.[290] Desired amount of TPFPP was dissolved in **3.1** before pumping into the system. During the reaction, starting material with TPFPP and internal standard were kept in the ice bath. Biphenyl or mesitylene was used as an internal standard for quantification. IR spectra were recorded on an Avatar 320 FT-IR spectrometer.

Procedures for Batch reactions

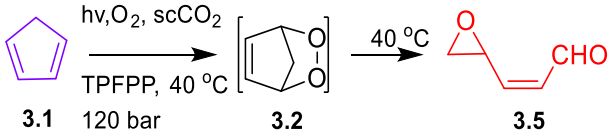
Freshly distilled cyclopentadiene(1 mL, 12 mmol), TPFPP (1 mg, 0.001 mmol) and biphenyl (10 mol % or 1 equiv.) were dissolved in methanol (60 mL, 0.1 M). The flask was placed in an ice bath to reach 0 °C, and a condenser was adapted, then irradiated with LED lights while 0.1 bar oxygen was bubbled through the solution. The progress of the reaction was checked by ^{1}H NMR spectroscopy, and the yields of the various products were obtained from the integration against the standard internal signals.

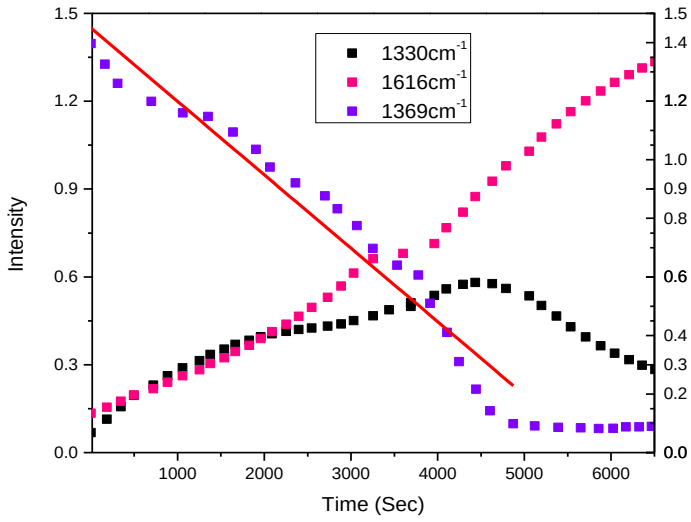
3.9.2 **Determination of FTIR kinetics and NMR kinetics**

FT-IR monitoring

As specified in Section 3.3.1, 15 μL **3.1** solution solubilising TPFPP (4 mg/mL) was injected into 0.78 mL cell, then filling with CO_2 and O_2. The molar ratio of CO_2: O_2: **3.1** was 91.8 %: 6.81 %: 1.36 %. In this photooxidation process, $^1O_2$ was formed from TPFPP and O_2 acitivated by LED light.

Although the data are not particularly good, the figure below is consistent with a zero order reaction because the rate does not change significantly over quite a long period of time (e.g. the rate only depends on the intensity of the light). This has been seen previously with *α*-terpinene.[203]





According to the decreasing of concentration of starting material **3.1** on the FT-IR spectrum, we can obtain the reaction rate for the photo-oxidation of **3.1** is :

$$-\frac{d[\mathbf{3.1}]}{dt} = 0.00251$$

Therefore, the photo-oxidation of **3.1** under this condition was a zero order reaction, and the rate constant is 0.00251 ($mol^{-1} \cdot L \cdot s^{-1}$).

NMR Monitoting

The isomerisation of **3.2** to **3.5** was monitored by NMR at 20 °C, atmospheric pressure. The photo-oxidation of **3.1** to **3.2** was conducted in a thick NMR tube at -78 °C, to monitor the reaction rate of **3.2** isomerising to **3.5** during this process. $CDCl_3$ was used as the solvent, the concentration of **3.1** in $CDCl_3$ was 2.6 mM, with TPFPP (4 mg/mL of **3.1**), and oxygen was provided by a balloon filled with pure oxygen. The tube, then, was transferred to NMR machine carefully after a time period of 1 h irradiation. The spectra have been recorded for 5 h, shown in Figure 3-6.

Based on the NMR spectrum in Section 3.3.2, the fitting equation was obtained according to the increasing concentration of **3.5**:

$$Y=3.872 – 3.384\exp(-8.96*10^{-5}t)$$

So, the rate constant is 3.384 s^{-1}, this is a first-order reaction. The rate law is:

$$\frac{d[\mathbf{3.5}]}{dt} = 8.96 \times 10^{-5}([\mathbf{3.2}]_0 - [\mathbf{3.2}])$$

3.9.3 **High-Pressure Rig operation**

The high pressure continuous flow rig was built for the photo-oxidation using HPLC pumps, connecting tubes, mixers, sapphire tube reactor, cooling bath and BPR (Back Pressure Regulator). Compressed CO_2 and O_2 are mixed in the first static mixer, and then the organic stream is added, and mixed with the gases in the second mixer, the temperature in the two mixers were typically at 40 °C. The fluid entered into the sapphire tube in an up-flow method, irradiated with visible light by three 5 × LEDs mounted on an aluminium blocks controlled by a LED controller. Due to the heat generated by the LED lights. A secondary cooling bath is used to pump around the sapphire tube to ensure that the desired temperature was set in the reactor, typically at ca. 40 °C was maintained. The water removed excess heat from the system during irradiation such that the LEDs can be positioned as close as possible to the sapphire and internal high-pressure stream for the high efficient irradiation. The system

pressure was controlled by a BPR located after the sapphire tube reactor. Once the reaction mixture passes the BPR, the products can be collected for further analysis.

The general operation was stated below. **CO_2** was delivered from a chilled CO_2 pump, and **O_2** was dosed at a known rate *via* a Rheodyne dosage unit. **M1** and **M2** (78 mm, ¼ inch O. D., SS316 tubes at 40 °C) represent the mixers loaded with sands. The **CO_2** and **O_2** were passed through **M1** and then mixed with organic solution pumped by organic pump 1 in the mixer 2, **M2**; **OP1** and **OP2** represent the Jasco™ organic pump 1 and Jasco™ organic pump 2, respectively. **OP2** was used to pump variable reagents for different products. Then, the mixture going through preheater 2 and/or reactor 3 were flowed out continuously via a Jasco™ BP-1580-81 back pressure regulator, **BPR**, before irradiated in a high-pressure sapphire tube reactor, **Photoreactor 1** (Saint-Gobain Crystals, 10 mm 0.d., 1 mm wall thickness, 120 mm long), which were collected in a vessel and then analysed by ^{1}H NMR. **LED lights**: 5×Citizen Electronics Co. Ltd 1000 lumen). Reactor 2 was four 156 mm ¼ inch SS316 tubes. 40 °C. **Reactor 3** was 156 mm ¼ inch SS316 tubes, room temperature. The total pressure was 120 bar unless otherwise stated. Solid catalysts were loaded in **Reactor 3** before starting the reaction. All continuous flow experiments were carried out in this rig unless otherwise stated. The set-up was slightly different when different products were produced. Product **3.3** and **3.4** were synthesised in rig 1, shown in Figure 3-12, product **3.5** was produced in rig 2, shown in Figure 3-13, and product **3.6** was synthesised in rig 3, shown in Figure 3-14.

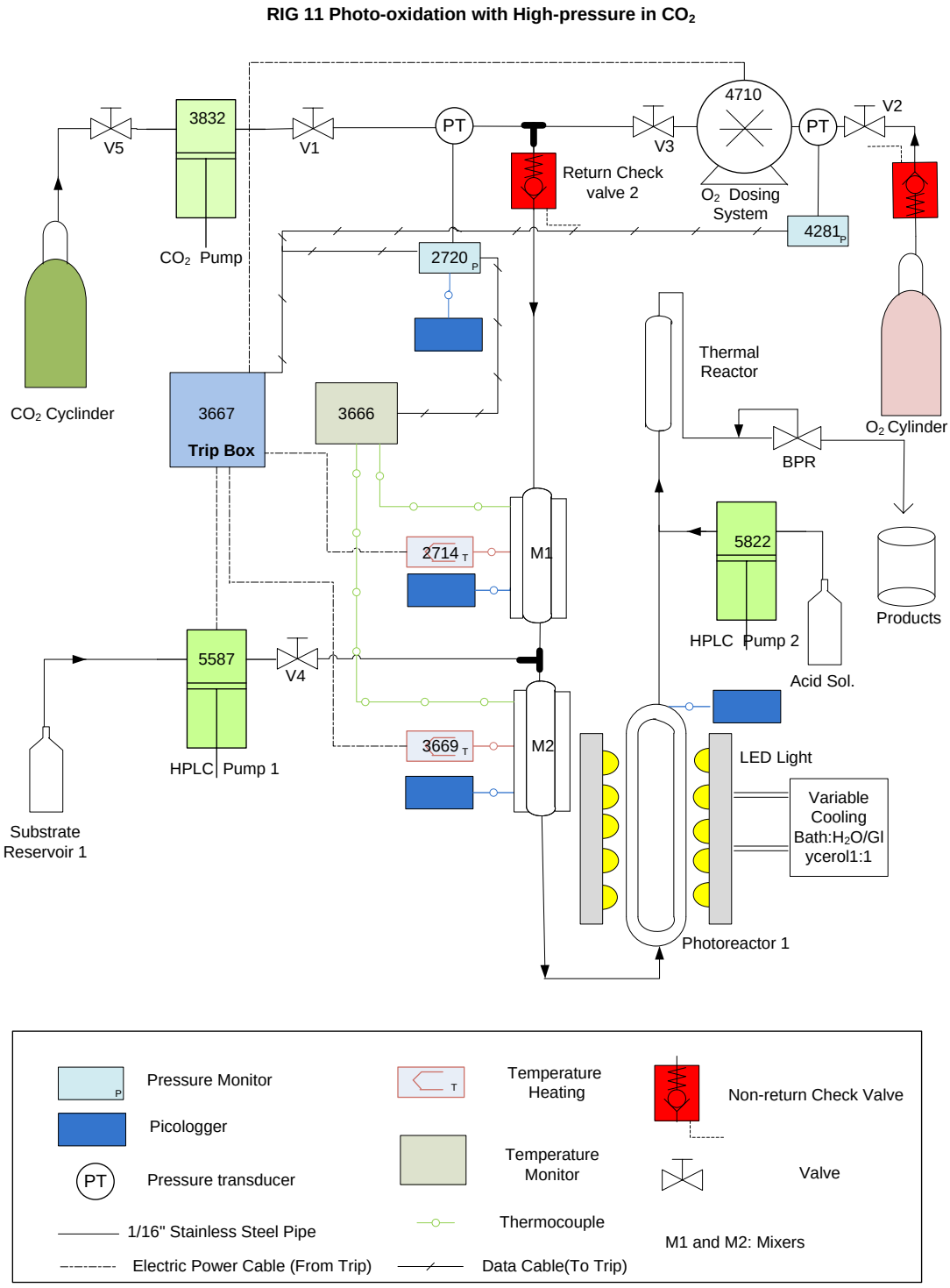


*Figure 3-12 Diagram of rig 1 for the synthesis of products **3.3** (pumping thiourea from organic pump 2) and **3.4** (pumping TEA from organic pump 2). An extra organic pump 2 and thermal reactor (one tubular reactor, 156 mm in length) were added based on the general diagram in the Experimental (Figure 2-4).*

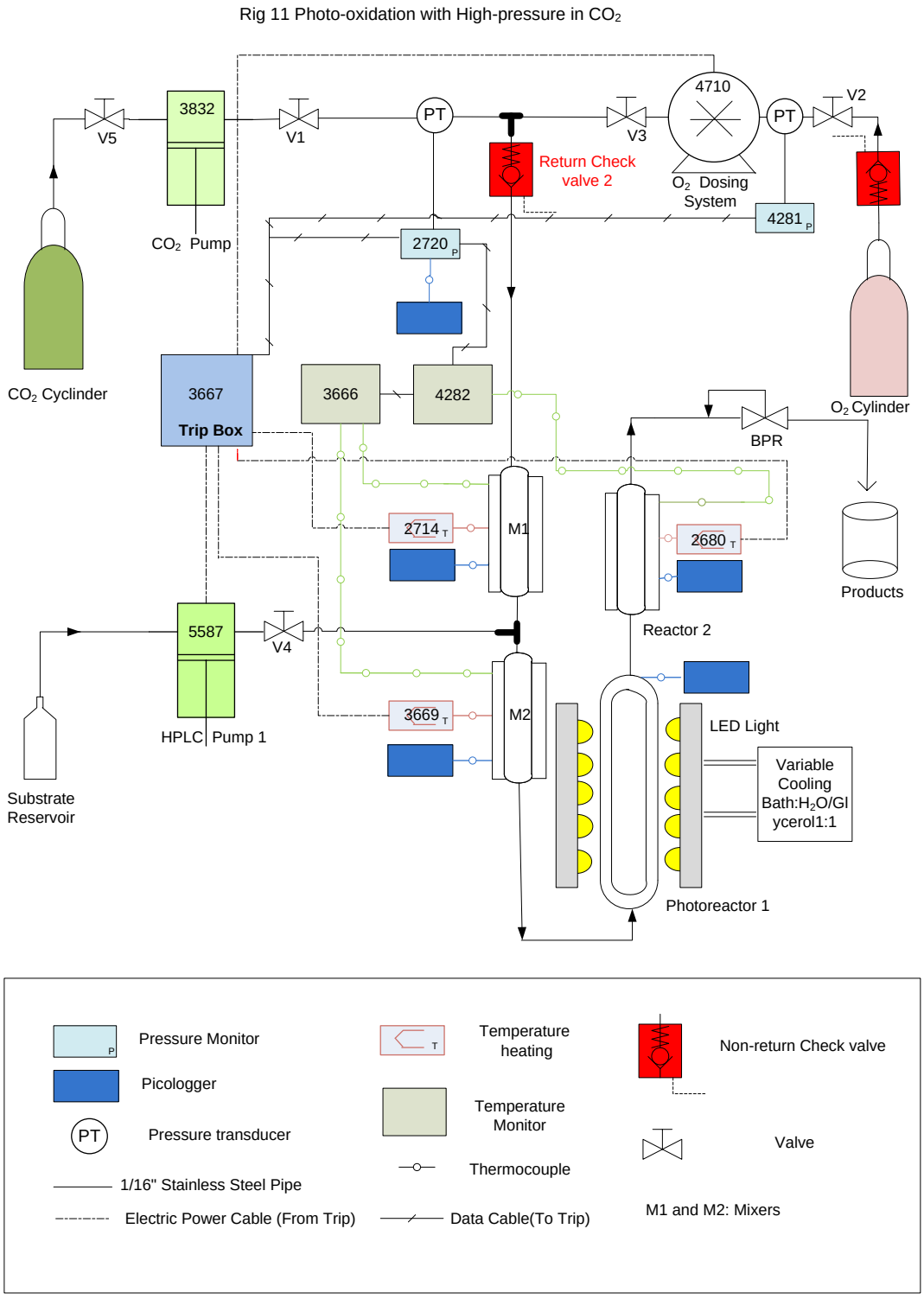


*Figure 3-13 Diagram of rig 2 for the synthesis of product **3.5**. An extra thermal reactor (4× tubular reactor, 156 mm in length) was added between photoreactor and BPR.*

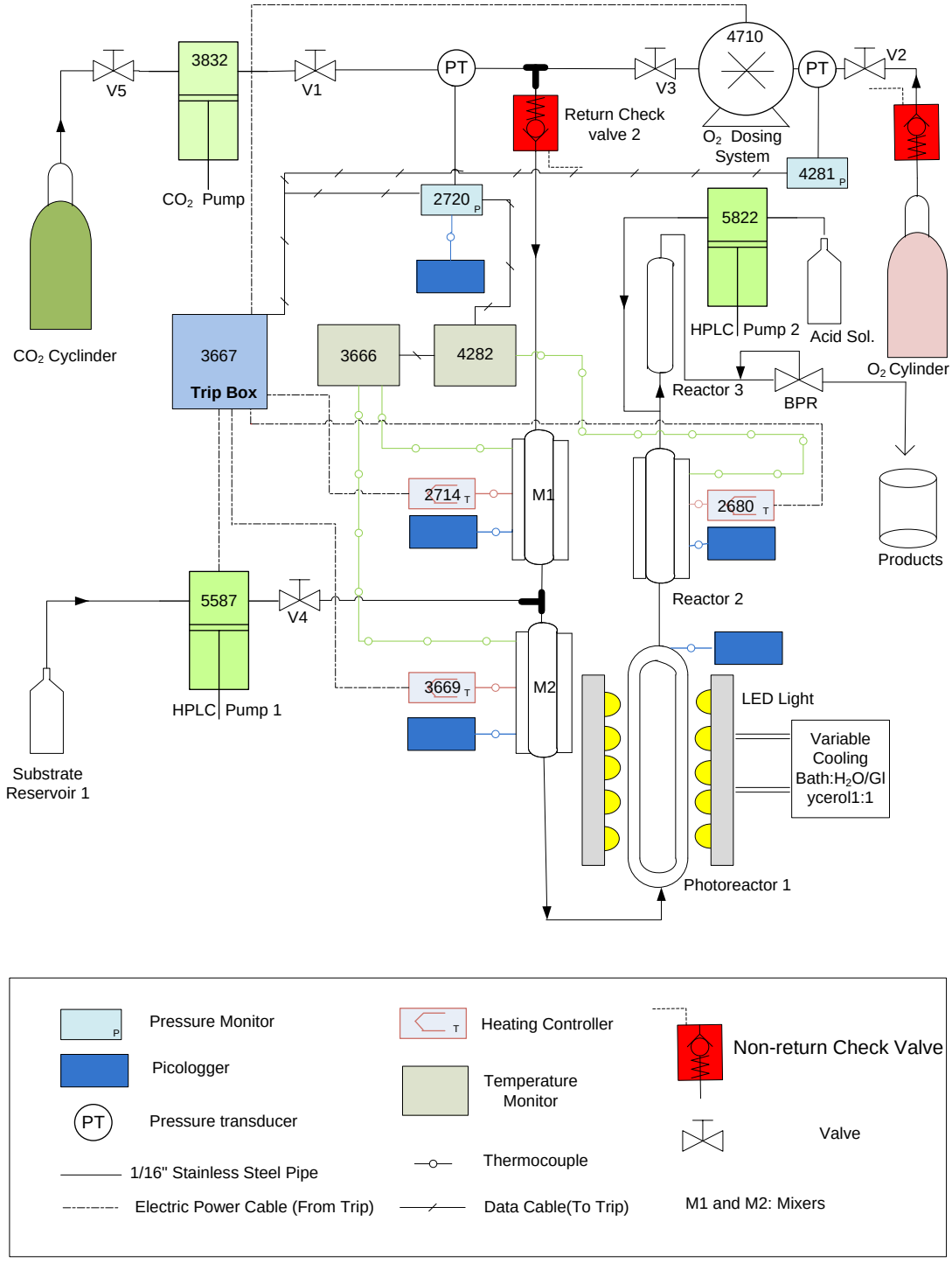
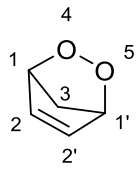


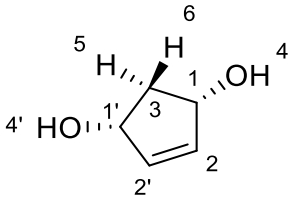
*Figure 3-14 Diagram of rig 3 for the synthesis of product **3.6**. Two more tubular reactors and one extra organic pump was added between photoreactor and BPR based on the general diagram in Chapter 2 (Figure 2-4).*

3.9.4 **Characterisation of NMR data**



2,3-dioxabicyclo[2.2.1]hept-5-ene (**3.2**)

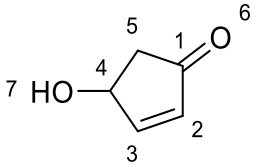
^{1}H NMR (300 MHz, Chloroform-*d*) δ 6.47 (t, J = 2.1 Hz, 2H, H2 + H2'), 5.27 (m,, 2H, H1 + H1'), 2.10 (t, J = 1.7 Hz, 2H, 2×H3).



Meso-cyclopent-4-ene-1,3-diol(**3.3**)

^{1}H NMR (300 MHz, Chloroform-*d*) δ 6.01 (s, 2H, H2 + H2'), 4.66 (m, 2H, H1 + H1'), 2.72 (d, J = 14.3, 7.2 Hz, 1H, H5), 1.55 (d, J = 14.3, 3.7 Hz, 1H, H6).

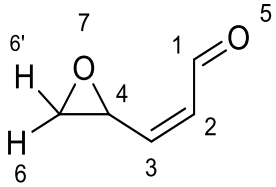
^{13}C NMR (300 MHz, Chloroform-*d*) δ 136.7 (C2 + C2'), 75.2 (C1 + C1'), 44.0 (C3). The data is agreement with the literature.[269]



4-hydroxycyclopent-2-en-1-one (**3.4**)

^{1}H NMR (300 MHz, Chloroform-*d*) δ 6.47 (t, J = 2.1 Hz, 2H, H2 + H3), 5.27 (m,, 2H, H4), 2.10 (t, J = 1.7 Hz, 2H, 2×H5).

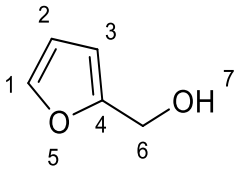
^{13}C NMR (300 MHz, Chloroform-*d*) δ 207.5 (C1), 163.1 (C2), 135.1 (C3), 70.5 (C4), 44.4 (C5). The data is agreement with commercially obtained samples.



(Z)-3-(oxiran-2-yl)acrylaldehyde (**3.5**)

^{1}H NMR (300 MHz, Chloroform-*d*) δ 10.17 (d, J = 6.6 Hz, 1H, H1), 6.24 – 6.05 (m, 2H, H2 + H3), 4.23 – 4.11 (m, 1H, H4), 3.16 (dd, J = 5.4, 4.2 Hz, 1H, H6), 2.77 (dd, J = 5.4, 2.5 Hz, 2H, H6').

^{13}C NMR (101 MHz, Chloroform-*d*) δ 190.2 (C1), 148.0 (C2), 133.2 (C3), 48.9 (C5), 47.5 (C4).The data is agreement with the literature.[291]



furan-2-ylmethanol (**3.6**)

^{1}H NMR (400 MHz, $CDCl_3$) δ 7.40 (dd, J = 1.9, 0.7 Hz, 1H, H1), 6.34 (dd, J = 3.2, 1.9 Hz, 1H, H2), 6.29 (dd, J = 3.2, 0.7 Hz, 1H, H3), 4.61 (d, J = 5.0 Hz, 2H, 2×H6). The data is agreement with commercially obtained samples.

3.9.5 **Representative ^{1}H and ^{13}C NMR spectra**

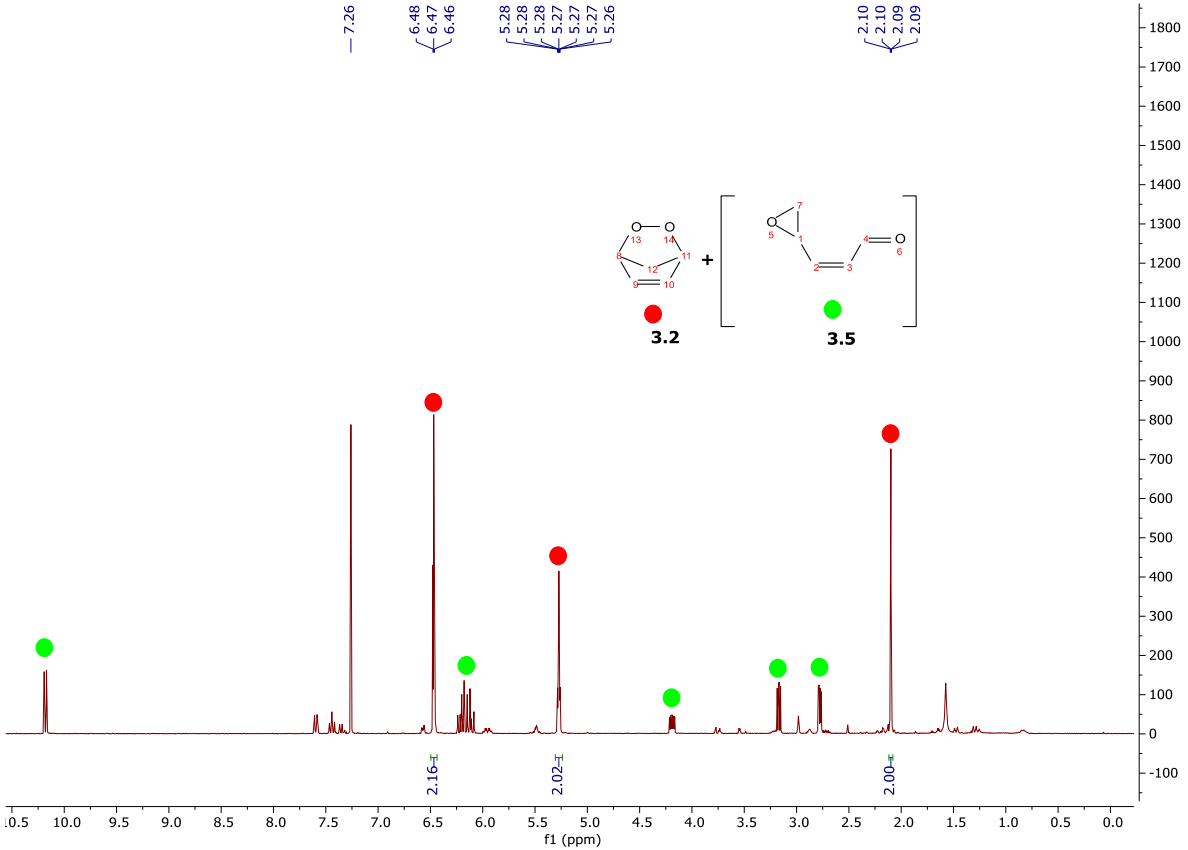


*Figure 3-15 ^{1}H NMR of mixture **3.2** and **3.5** in $CDCl_3$.*

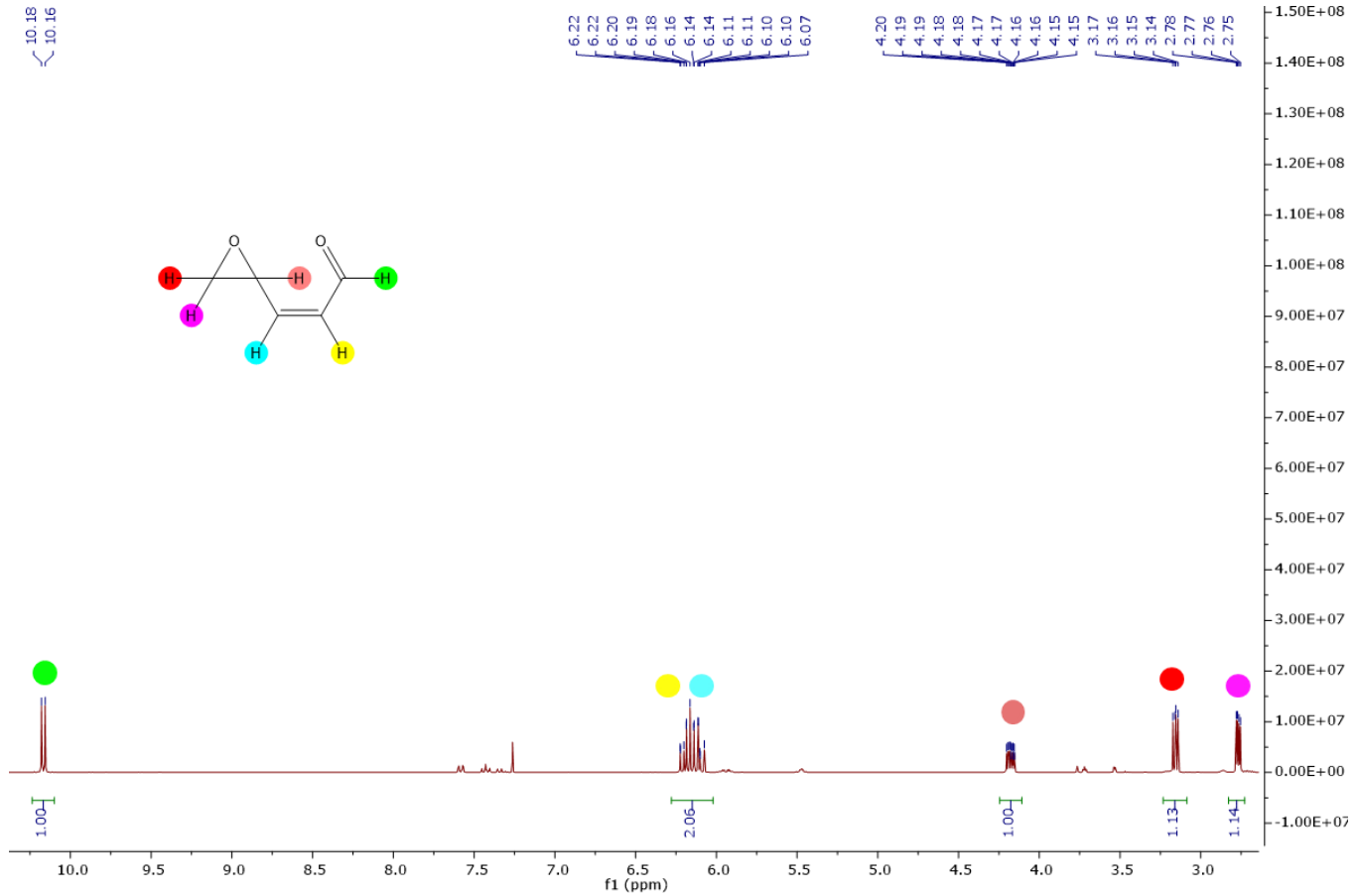


*Figure 3-16 ^1H NMR of compound **3.5** in $CDCl_3$.*

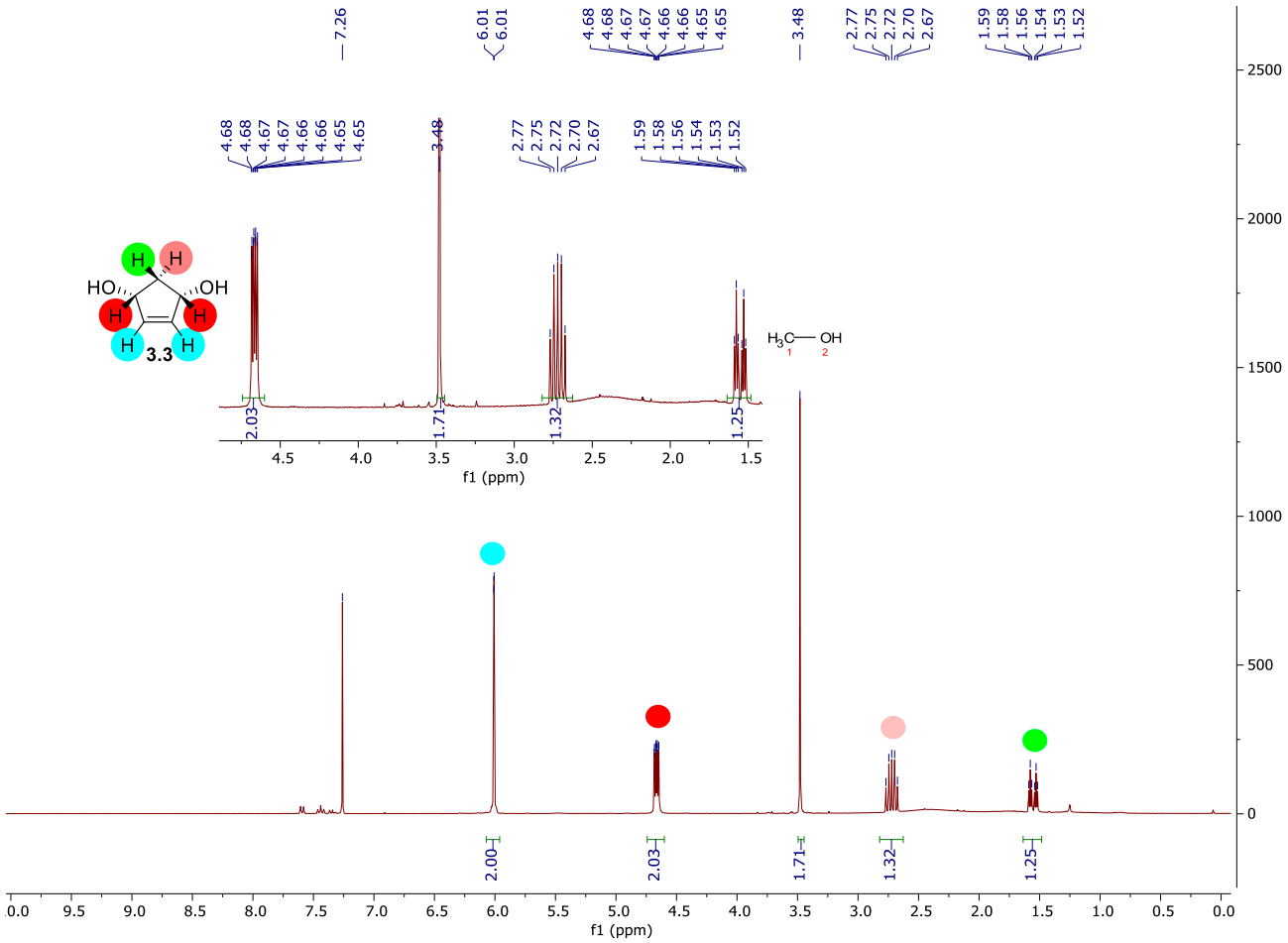


*Figure 3-17 ^{1}H NMR of compound **3.3** in $CDCl_3$.*

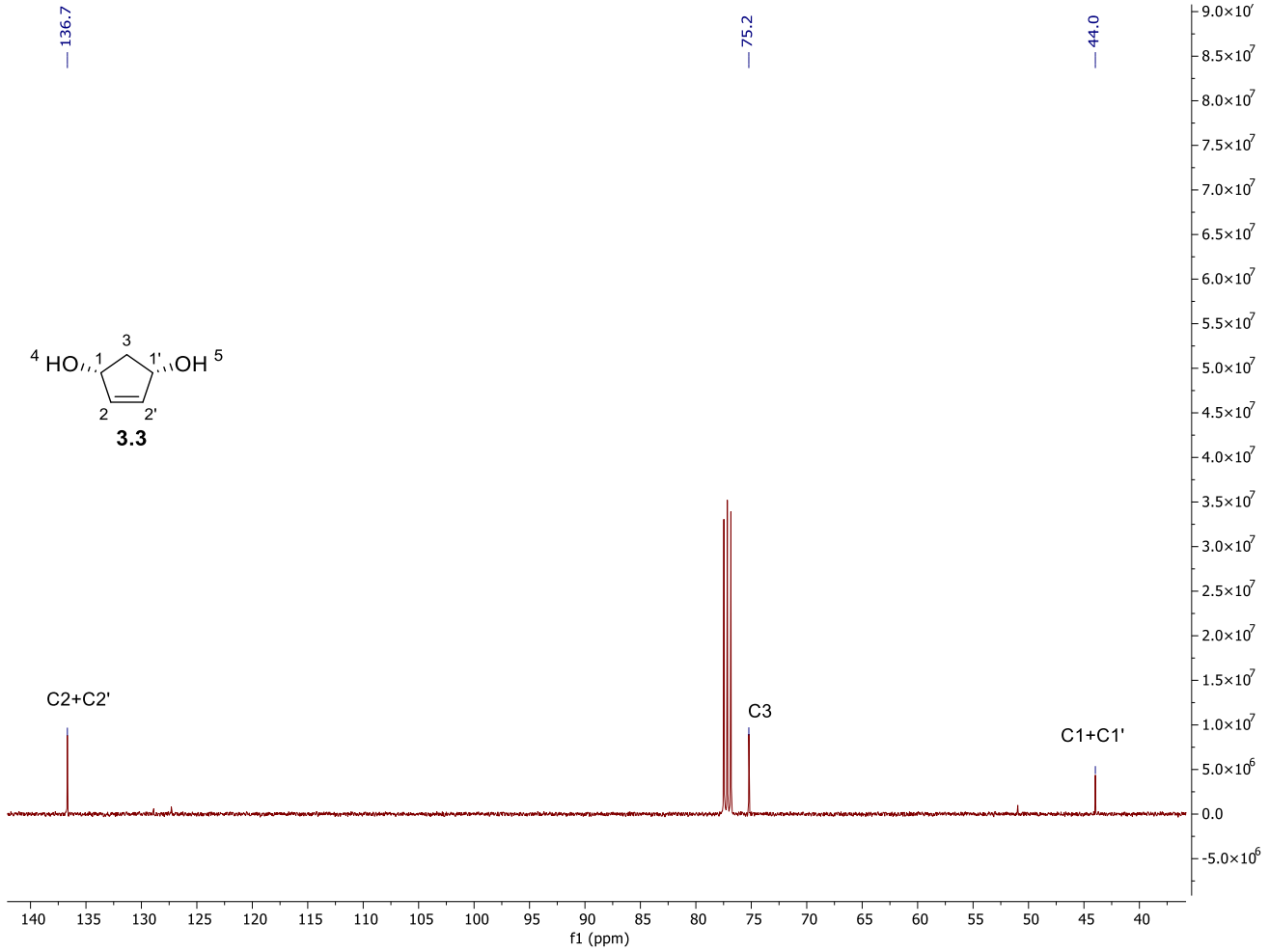


*Figure 3-18 ^{13}C NMR of compound **3.3** in CDCl3.*

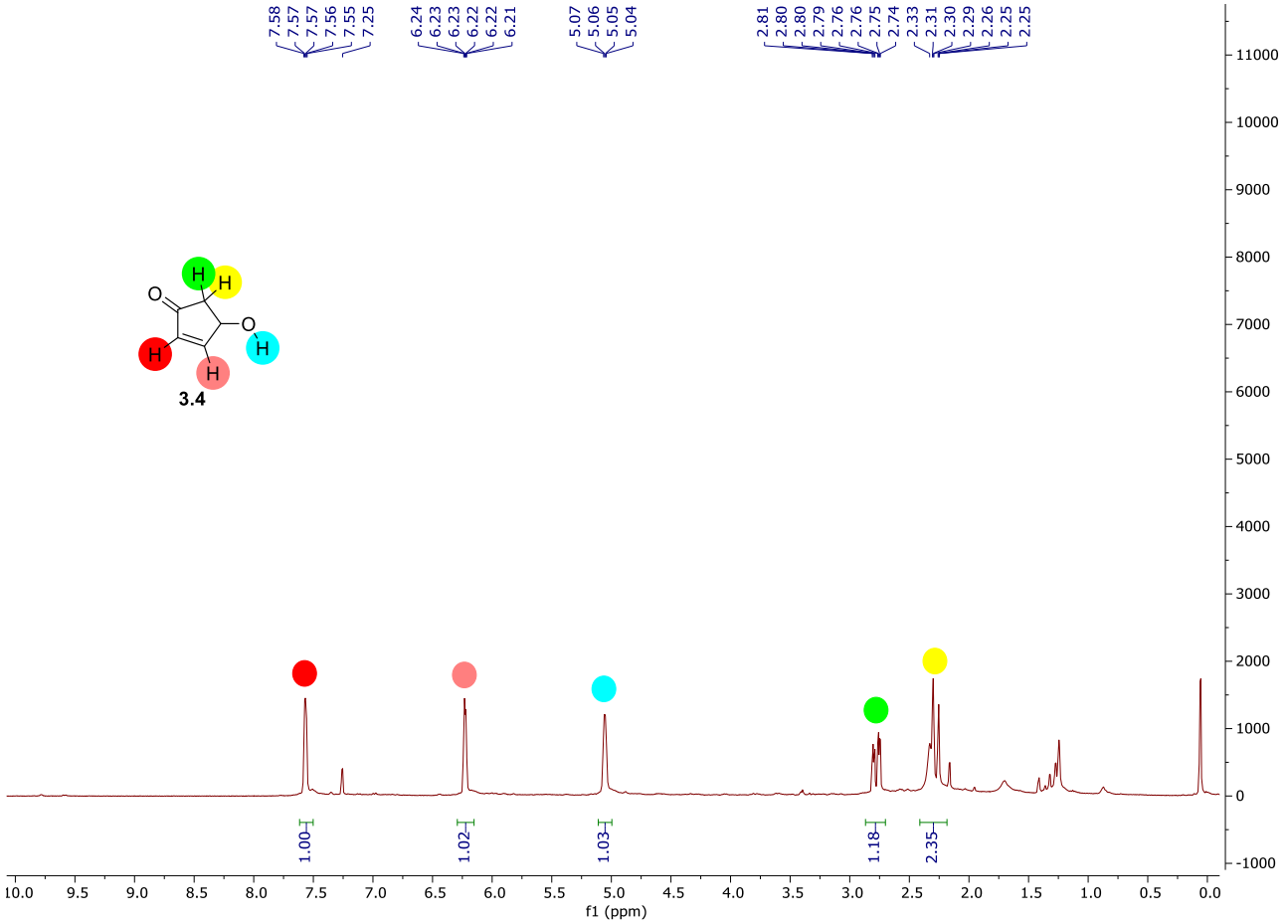


*Figure 3-19 ^{1}H NMR of compound **3.4** in $CDCl_3$.*

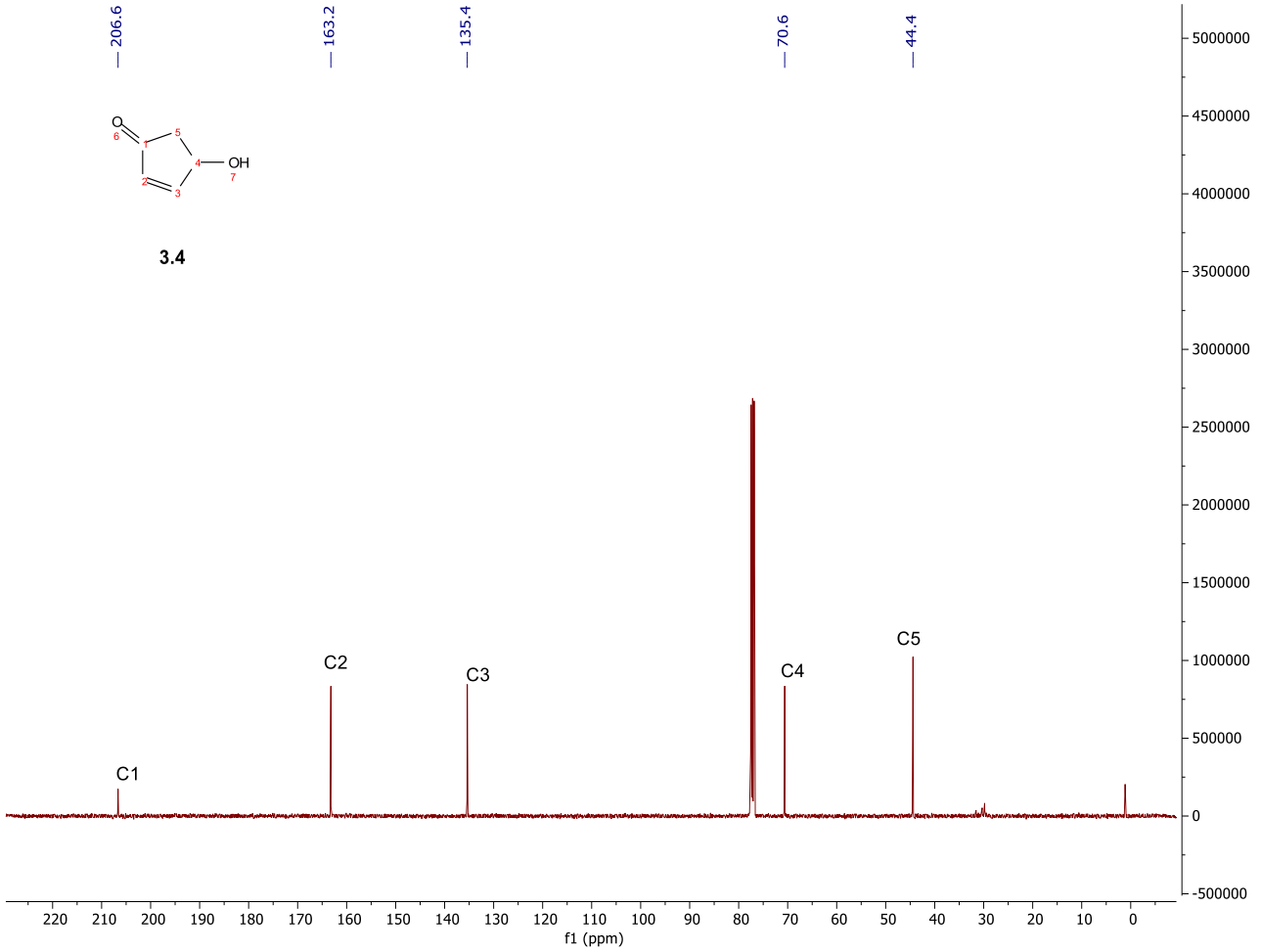


*Figure 3-20 ^{13}C NMR of compound **3.4** in $CDCl_3$.*

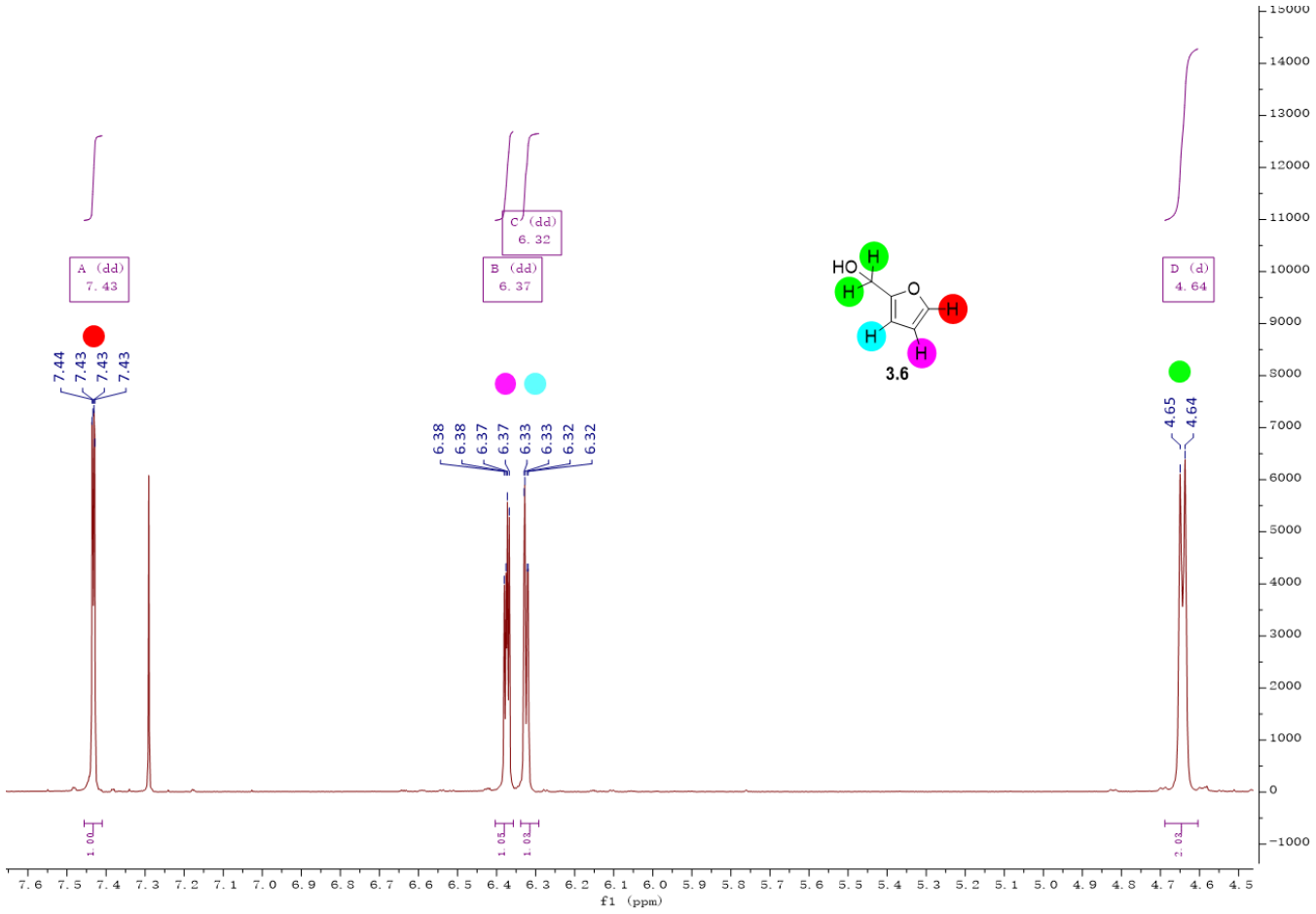
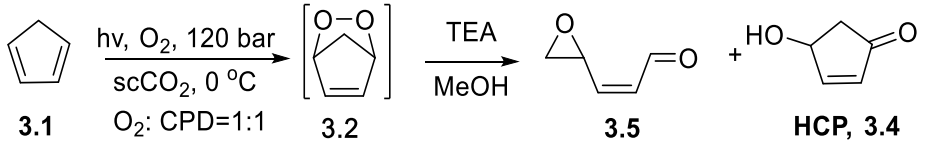


*Figure 3-21 ^{1}H NMR of compound **3.6** in $CDCl_3$.*

3.9.6 **Optimisation of HCP**

*Table 3-7 The NMR yield of HCP dependent on the concentration of TEA and flow rate. The molar ratio of O_2 to **3.1** was 1:1.*



3.1 3.2 **3.5** **HCP, 3.4**

Entry	TEA Conc.	CO_2 FR (ml·min^{-1})	Org. Pump 1(ml·min^{-1})	Org. Pump 2(ml·min^{-1})	Yield (%)		
					HCP	3.2	3.5
1	0.15 M	0.25	0.05	1	3	33	7
2	0.15 M	0.25	0.05	0.5	44	1	7
3	0.15 M	0.25	0.05	0.3	41	1	20
4	0.15 M	0.25	0.05	0.2	25	14	13
5	0.15 M	0.25	0.05	0.1	38	<1	24
6	0.15 M	0.5	0.05	0.1	33	<1	44
7	0.3 M	0.25	0.05	0.5	37	3	10
8	0.3 M	0.25	0.05	0.8	53	1	15
9	0.6 M	0.5	0.05	0.3	43	0	22
10	0.6 M	0.5	0.05	0.5	62	<1	7

*Table 3-8 The NMR yield of HCP dependent on the concentration of TEA. The molar ratio of O_2 to **3.1** was 1:1.*

Entry	TEA Conc.	CO_2 FR (mL/min)	Org. Pump 1(mL/min)	Org. Pump 2(mL/min)	Yield (%)		
					HCP	3.2	3.5
1	0.6 M	0.5	0.05	1.0	62	0	21
2	0.6 M	0.5	0.05	0.8	48	0	8
3	0.6 M	0.5	0.05	0.5	56	0	7
4	0.6 M	0.5	0.05	0.3	56	0	11
5	0.8 M	0.5	0.05	0.3	56	0	9
6	0.8 M	0.5	0.05	0.5	49	0	6
7	0.8 M	0.5	0.05	0.8	47	0	5
8	0.8 M	0.5	0.05	1.0	47	0	10
9	1.0 M	0.5	0.05	1	48	0	19
10	1.0 M	0.5	0.05	1.2	46	0	5
11	1.0 M	0.5	0.05	0.8	42	0	1
12	1.0 M	0.5	0.05	0.5	43	0	3

*Table 3-9 The NMR yield of HCP dependent on the concentration of TEA. The molar ratio of O_2 to **3.1** was 2:1.*

Entry	$(Et)_3N$ Conc.	CO_2 ($ml \cdot min^{-1}$)	Org. Pump 1($ml \cdot min^{-1}$)	Org. Pump 2($ml \cdot min^{-1}$)	Yield (%)		
					HCP	3.2	3.5
1	0.6 M	0.5	0.05	0.3	54	<1	10
2	0.6 M	0.5	0.05	0.5	49	<1	8
3	0.6 M	0.5	0.05	0.8	47	<1	6
4	0.6 M	0.5	0.05	1	42	<1	1
5	0.6 M	0.5	0.05	1.2	48	<1	1
6	0.8 M	0.5	0.05	0.1	66	0	16
7	0.8 M	0.5	0.05	0.3	52	0	4
8	0.8 M	0.5	0.05	0.5	50	0	9
9	0.8 M	0.5	0.05	0.8	42	0	6
10	0.8 M	0.5	0.05	1	45	0	6
11	1.0 M	0.5	0.05	1	42	0	1
12	1.0 M	0.5	0.05	0.8	47	0	8
13	1.0 M	0.5	0.05	0.5	45	0	1
14	1.0 M	0.5	0.05	0.3	52	0	8

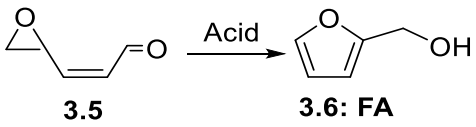
*Table 3-10 The NMR yield of HCP dependent on the concentration of TEA. The molar ratio of O_2 to **3.1** was 2:1.*

Entry	TEA Conc.	CO_2 FR (ml/min)	Org. Pump 1(ml/min)	Org. Pump 2(ml/min)	Yield (%)		
					HCP	3.2	3.5
1	No	0.5	0.05	-	0	86	14
2	0.8 M	0.5	0.05	0.2	81	0	<1
3	1.0 M	0.5	0.05	0.1	58	0	12
4	1.0 M	0.5	0.05	0.2	78	0	3
5	1.0 M	0.5	0.05	0.25	58	0	6
6	1.5 M	0.5	0.05	0.1	53	0	8
7	1.5 M	0.5	0.05	0.2	51	0	5
8	1.5 M	0.5	0.05	0.3	62	0	4
9	1.2 M	0.5	0.05	0.3	48	0	2
10	1.2 M	0.5	0.05	0.2	55	0	2
11	1.2 M	0.5	0.05	0.1	62	0	3

3.9.7 **Acid catalysts screening for the production of 3.6**

Procedure for the solid acid catalyst screen: **3.5** was used as starting material (17 mg, 0.17 mmol) added in a flask with 1 mL concentrated H_2SO_4 (Entry 1) or 17 mg solid acid catalyst (Entry 2 to Entry 6), 5 mL H_2O as solvent, stirring 2 hours, room temperature. The results are depicted in Table 3-11.

Table 3-11 Screen of various solid acid catalysts to produce FA in batch conditions.



3.5 **3.6: FA**

Entry	Acid Catalyst	Substrate	Selectivity		
			FA: HCP	FA (3.6)	HCP(3.4)
1[a]	0.01%Wt H_2SO_4	**3.5**	-	major	trace
2	Amb-15	**3.5**	3:1	-	-
3	NbP	**3.5**	-	major	trace
4	NbO	**3.5**	-	trace	trace
5	TPP@Amb-15	**3.5**	1:3	-	-

[a]*Tetrahedron*, 1971, **27**, 2631-2637; Full conversion was achieved in all experiments.

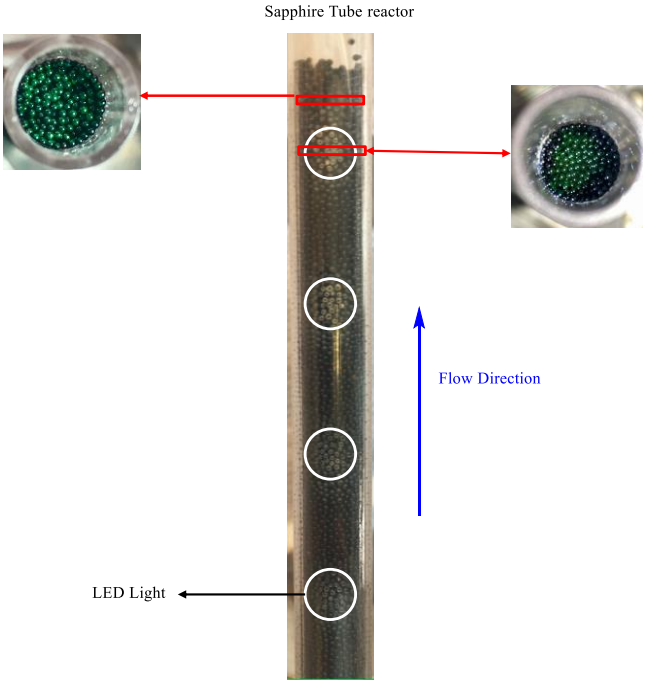
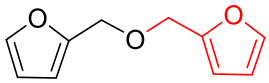


*Figure 3-22 Synthesis of **3.6** in Strategy 2. This picture shows that the LED light only stayed on the outer layer of packed TPP supported Amberlyst-15, which was difficult to penetrate into the inner part of TPP supported Amberlyst-15. This explains why this photo-oxidation of **3.1** was not efficient.*

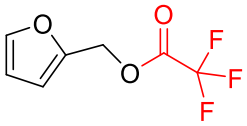
Study for the byproduct

'difurfuryl ether (2,2'-(oxybis(methylene))difuran)' or 'furan-2-ylmethyl 2,2,2-trifluoroacetate'?



2,2'-(oxybis(methylene))difuran

(a)



furan-2-ylmethyl 2,2,2-trifluoroacetate

(b)

*Scheme 3-5 Scheme of possible by-product in the synthesis of **3.6***

The 2D NMR results (Figure 3-23) showed that: the left black parts of compound (a) (Scheme 3-5) exists, and further investigation should be done to confirm the right red part. ^{1}H NMR (400 MHz, *Chloroform*-d) *δ* 7.50 (dd, *J* = 1.9, 0.8 Hz, 1H), 6.57 (d, *J* = 3.2 Hz, 1H), 6.43 (dd, *J* = 3.3, 1.8 Hz, 1H), 5.34 (s, 2H); or ^{1}H NMR (400 MHz, *Chloroform*-d) *δ* 7.50 (dd, *J* = 1.9, 0.8 Hz, 2H), 6.57 (d, *J* = 3.2 Hz, 2H), 6.43 (dd, *J* = 3.3, 1.8 Hz, 2H), 5.34 (s, 4H). ^{13}C NMR (400 MHz, *Chloroform*-d) *δ*=157.6, 144.3, 112.6, 110.6, 60.5.[274]

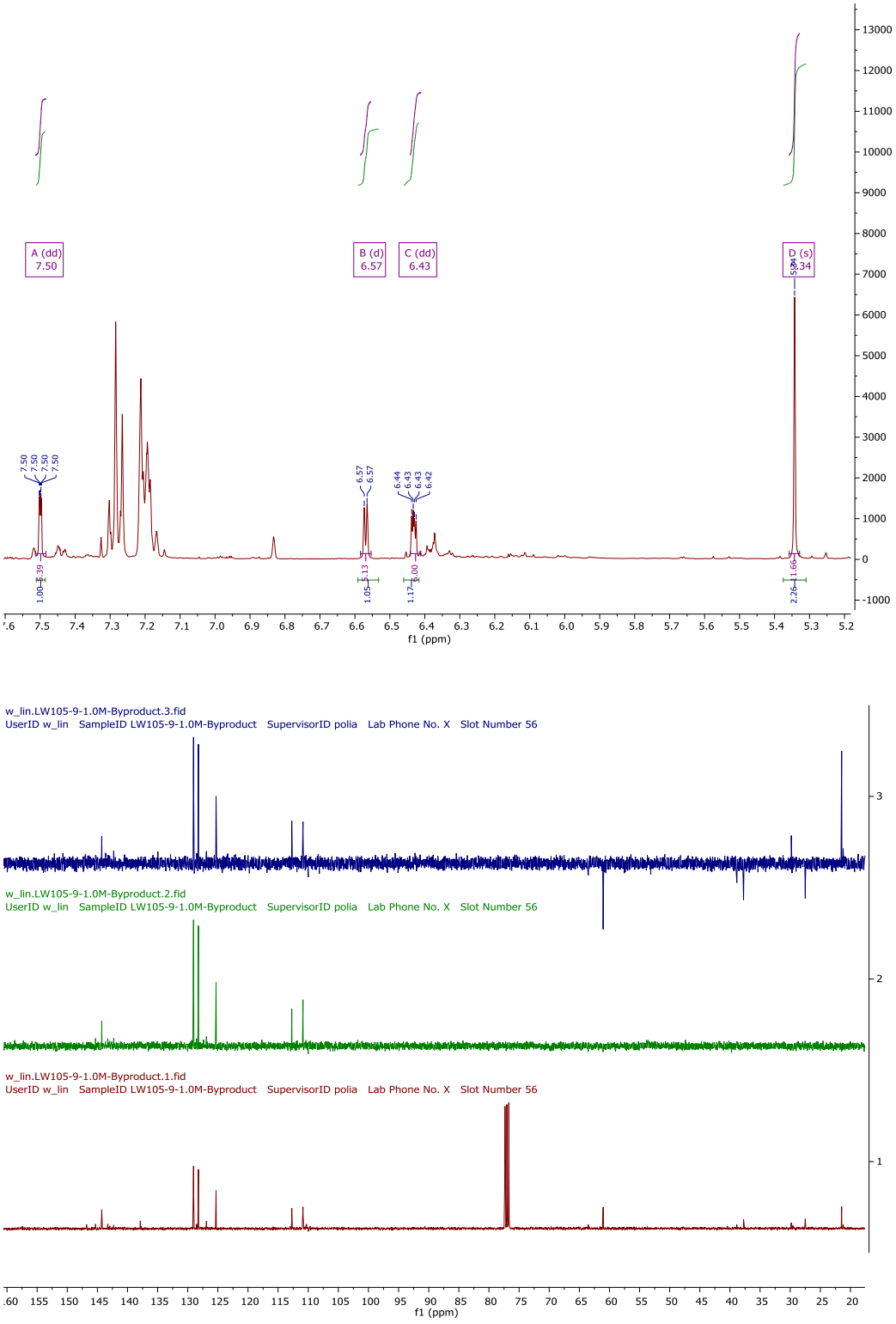


Figure 3-23 NMR results for the analysis of by-product in crude solution.

So, for the identification of the by-product, normally, first, we can use GC-MS to confirm it, but the proper concentration of sample for GC-MS should be prepared.

Second, we ran the ^{19}F NMR (Proton decoupled) to see the fluorinated by-product. The result was shown in Figure 3-24. When further to convert furfuryl alcohol to the by-product, we found furfuryl alcohol always existed. It might be an equilibrium reaction happened, as shown in Scheme 3-6. If H_2O was removed during this reaction when enough dry molecular sieve with micropore in the surface added, furfuryl alcohol should disappear at last, and pure by-product can be obtained to do further analysis and confirmation.

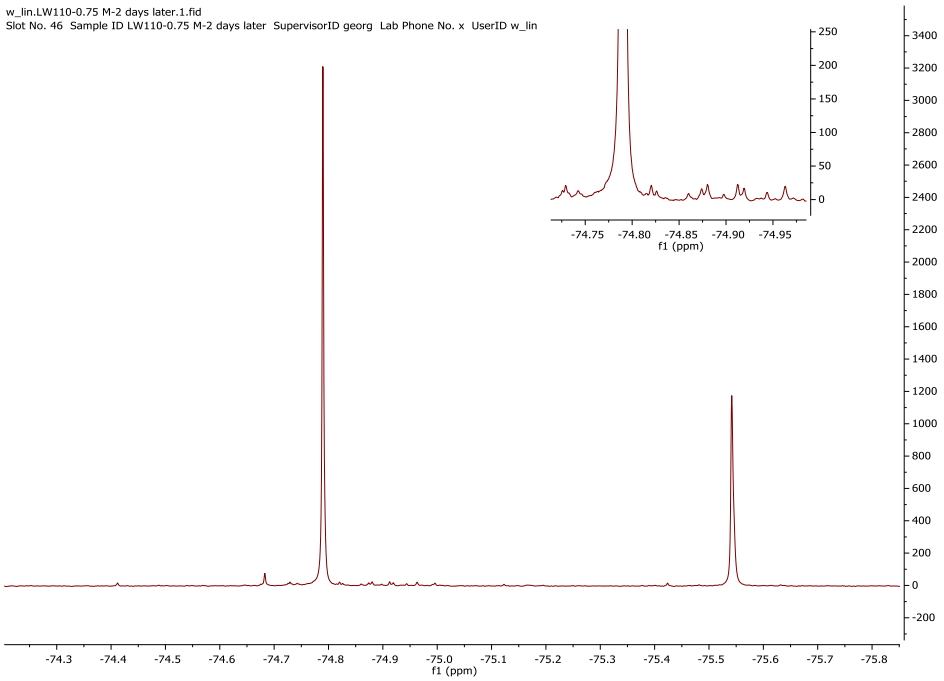
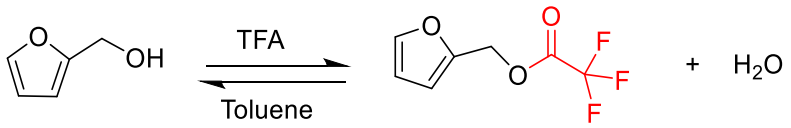


*Figure 3-24 ^{19}F NMR (proton decoupled) results in $CDCl_3$ of by-product in the process of synthesis of **3.6**.*



Scheme 3-6 A possible equilibrium for the by-product when 0.1 mmol of furfuryl alcohol was added into 10 mL Toulene with 0.5 M TFA stirring for overnight.

The results for the reaction with molecule sieve demonstrated that the unknown by-product should include a fluorine atom, but cannot be detected by 2D NMR, which is hard to confirm the trifluoroacetate group. It is still mystery that the by-product is

difurfuryl ether (2,2'-(oxybis(methylene))difuran) or furan-2-ylmethyl 2,2,2-trifluoroacetate. Therefore, FTIR is more sensitive to the ester group and ether group and was used to analyse the by-product further. The spectrum was shown in

Figure 3-25, which showed that the ester group was existing in this by-product. The ether group was included as well. Combining the NMR and FT-IR results, we can confirm that the by-product is furan-2-ylmethyl 2,2,2-trifluoroacetate.

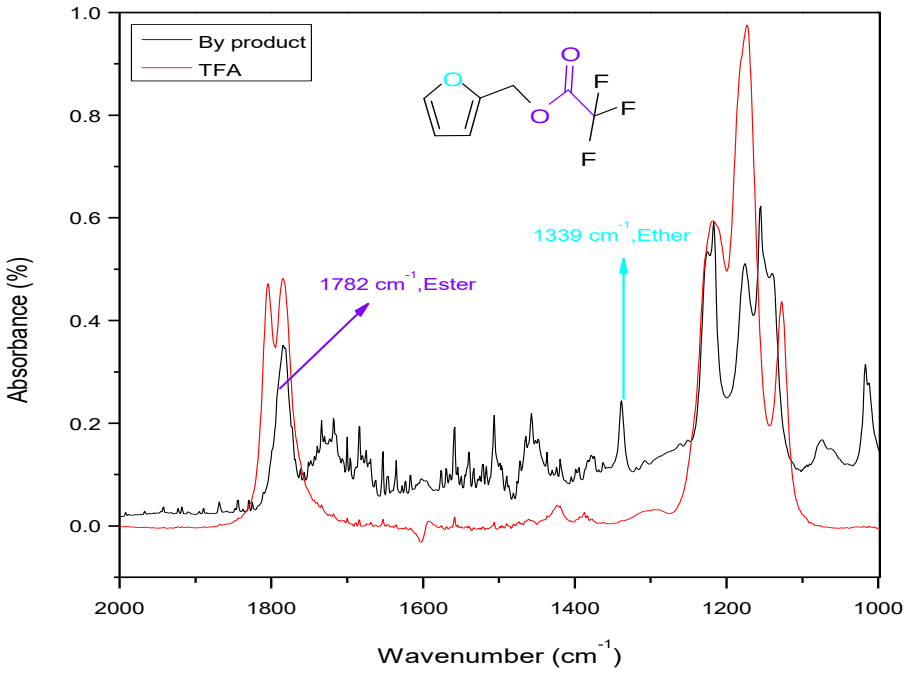


Figure 3-25 FT-IR spectrum recorded as a thin film. The pathlength was 200 μm. By-product was dissolved in Heptane.

Chapter 4. Synthesis of Unsaturated lactones from the Photo-oxidation of Fulvenes

In this Chapter, a new route is proposed to synthesise a range of unsaturated caprolactones in our high-pressure continuous flow photoreactor using supercritical CO_2 as a solvent. Caprolactones are mainly used as a monomer for the manufacture of specialised polymers, and its market demand is beyond 60 kilotons annually.[292] It is mostly synthesised in industry by the Baeyer-Villiger oxidation of cyclohexanone with an equivalent of peracetic acid.

An introduction to the background of fulvenes and lactones is presented in Section 4.1, including a description of typical Bayer-Villiger oxidation procedure for the synthesis of lactones. Section 4.2 explains the process development for the photo-oxidation of fulvenes, synthesised from cyclopentadiene with aldehydes or ketones, to access lactones.

Section 4.3 presents initial results obtained from the photo-oxidation of 6,6-dimethylfulvene (**4.1a**) leading to the caprolactone (**4.2a**). These results include the optimisation for the synthesis of **4.2a**, dependence on the co-solvent and flow rate of CO_2, as well as other competing pathways in this process. Section 4.4 investigates the scope of fulvenes with different functional groups. The presence of functional

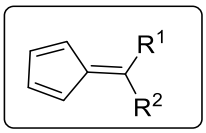
groups on the fulvenes including alkyl groups, sterically bulky groups, aromatic groups as well as other electron donating groups and electron withdrawing groups affect the photo-oxidation step of this reaction, hence gave different yields of the corresponding lactones. One of the lactones obtained contained a spiro centre. Ways to add further value to some of these lactones are explored in Section 4.5.2. These consist of the valorisation of product lactones *via* hydrogenation or additional photochemistry.

It should be noted that the experiments described in this Chapter were carried out in collaboration with Dr Darren S. Lee and Dr Hamza Boufroura. Most of the work in this Chapter has been published.[293] The role of the author was to carry out all the high-pressure photo-oxidation reactions and the UV reactions for further value investigations. The batch and flow procedures are described in Section 4.7.

4.1 Background

4.1.1 Properties of Fulvenes

Fulvenes constitute an important class of organic compounds that present a unique *π*-electron system due to their cyclic cross-conjugated structure (Scheme 4-1), [294] in which the R^1 and R^2 may be alkyl, hydrogen, aryl or other groups. Fulvene itself is an unsubstituted compound, C_6H_6, where $R^1 = R^2 = H$.



Scheme 4-1 Generalised structure of fulvenes.

Fulvene is an isomer of benzene but has very different colour and reactivity. The history of fulvenes began with the discovery of pentafulvenes at the beginning of the

20th century by a German chemist, Johannes Thiele.[295] Fulvenes are mainly synthesised *via* two different methods: (a) by condensation of cyclopentadiene with carbonyl compounds in the presence of a small amount of base, proposed by Thiele;[296] and (b) by use of Grignard reagents (RMgX) to catalyse the reaction of an aldehyde with cyclopentadiene.[297] In method a, the base acts both as a deprotonating agent and also as a catalyst in the dehydration step. The reaction is fast and easily monitored by the appearance of a yellow to red colour. Method b gives products which are somewhat easier to purify than Thiele's method, but the yields are considerably lower.[298]

Fulvenes are of general synthetic interest and are recognised as valuable synthons for the construction of a wide range of compounds[132, 294, 299-301] because they display multiple cycloaddition profiles. All the fulvenes are intensely coloured and their colour is due to "cross-conjugation"[i] since the aromatic isomer itself is colourless.[302] The most prominent feature of fulvenes is the relatively high polarisation of the exocyclic olefin and the resulting electropositive character at the exocyclic carbon atom. In terms of their bonding and reactivity, fulvenes occupy a position intermediate between open-chain olefinic molecules and delocalized aromatic systems.[303-304] Fulvenes can undergo many different reactions, such as Diels-Alder reactions,[305] hydrogenations,[306] the addition of halogens and oxygen[307] as well as polymerisation.[308]

4.1.2 **Caprolactones**

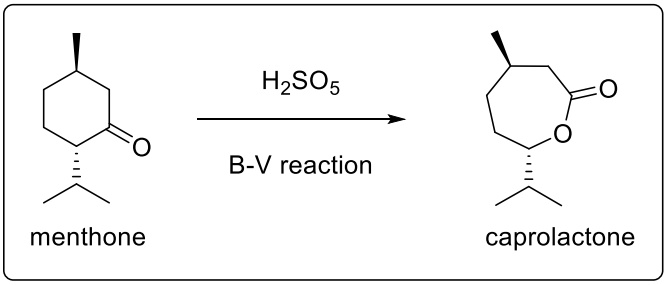
Lactones have found broad application as critical molecules for the synthesis of important bioactive compounds, natural products and polymers; and represent a valuable family of synthons for various organic transformations.[309] They are a

[i] Cross-conjugation is a special type of conjugation in a molecule, when in a set of three Pi bonds only two pi-bonds interact with each other by conjugation, the third one is exclude from interaction.

common structural motif within the chemical compounds that are used for transmission of information (semiochemicals) in different creatures, such as insects[310] or bacteria.[311] For example, 40 of the 436 structures listed in a recent review on insect pheromones are lactones.[310] Lactones are also found in a family of flavours and fragrances leading to an increasing demand for these substances.[312-313]

Aliphatic polyesters are a group of remarkably biocompatible and biodegradable polymers and are widely used in biomedical applications.[314] To date, the 7-membered ring monomer ε–caprolactone has been the most widely studied lactone in enzymatic polymerisation.[315] One of the reasons that these polymers have been received considerable attention is its good biodegradability, biocompatibility and thermoplastic properties. They have been investigated extensively in many groups, such as Shiro[316-318], Zhao[319], Matsumura[320], Spinella[321], Meijer[322], Heise[323-324], Katja[325]. Hence, it is important to consider how the monomer ε - caprolactone is being synthesised.

Since the Baeyer-Villiger reaction (B-V reaction) was first reported in 1899, it has been a useful method for converting ketones (readily available building blocks in organic chemistry) into higher value and complex esters or lactones.[326] In this early work, Caro's acid (H_2SO_5) was used to provide the oxygen for the oxidation of menthone to the corresponding lactone (Scheme 4-2). This Caro's acid version of the Baeyer-Villiger reaction is highly attractive for practical applications because the catalytic transformation simplifies the processing conditions while using minimal reactants as well as producing fewer pollutants. Further benefits were expected by the use of current, more sustainable oxidants, which mainly consist of organic peracids (such as 3-chloroperbenzoic acid and peracetic acid),[327-328] bis(trimethylsilyl) peroxide[329] and hydrogen peroxide[330-331]. Due to the high cost and sensitivity, instability and potential explosiveness, the applications of these peracids were difficult to extend.[332] Various heterogeneous[333-334] or homogeneous[335-338] catalytic system have been reported in recent years. For example, Corma and co-workers developed



Scheme 4-2 Oxidation of menthone with Caro's acid (Baeyer-Villiger reaction).[326]

an efficient and stable Sn-zeolite beta catalyst for the Baeyer-Villiger oxidation of saturated as well as unsaturated ketones by hydrogen peroxide, which showed good catalytic performance.[339] In addition to the catalyst, the use of solvent could also play an important role in Baeyer-Villiger oxidation,[340] such as the use of perfluorinated alcoholic solvents like 1, 1, 1, 3, 3, 3-hexafluoro-2-propanol (HFIP) in the absence of catalysts allowed electrophilic activation of hydrogen H_2O_2 toward epoxidation of alkenes and the Baeyer-Villiger oxidation of ketones.

Molecular oxygen has also been employed in the production of lactones, and in this case, the sacrificial agents are required, such as aldehydes that are converted to acids after the reaction. Both Li's and Ishii's groups have studied the oxidation of a mixture of cyclohexanol and cyclohexanone to caprolactone with molecular oxygen using $Ce(NH_4)_2(NO_3)_6$ as a catalyst.[334, 341] In this conversion, the sacrificial agent is cyclohexanol, which it is oxidised with O_2 to cyclohexanone, with hydrogen peroxide produced, then into caprolactone rather than byproducts. It was found that the cerium could perform both as a good radical initiator and an activator for the hydrogen peroxide in the oxidation step for the production of caprolactone (Figure 4-1).

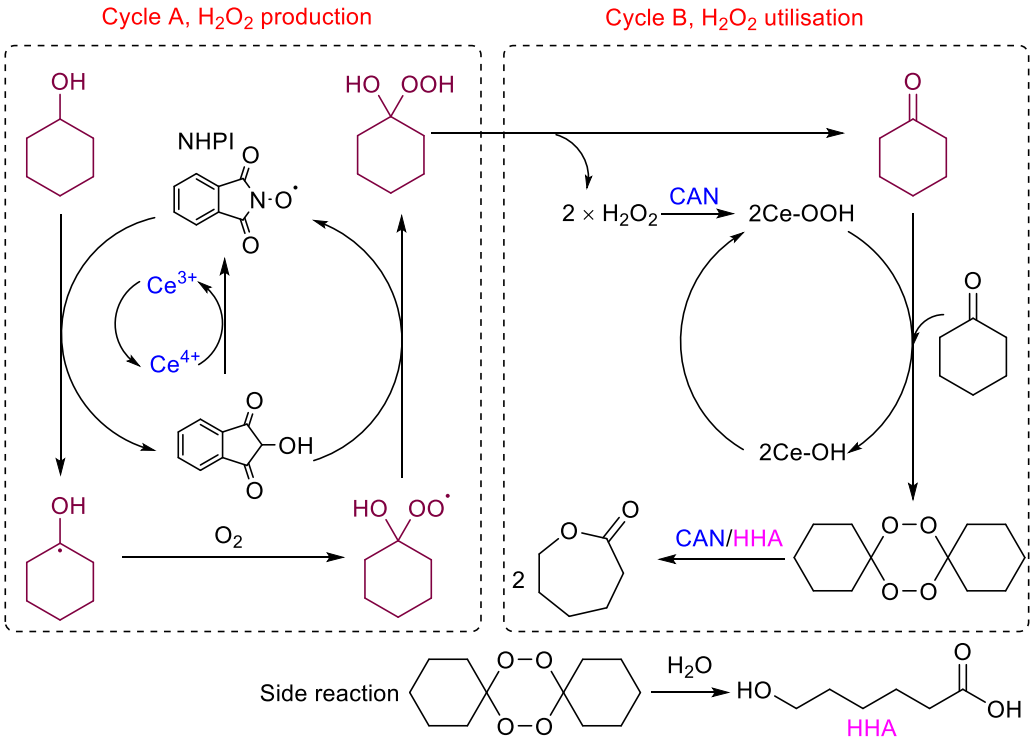


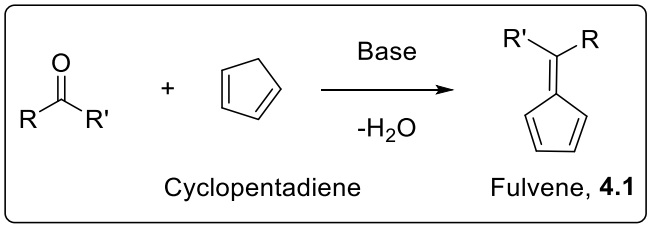
Figure 4-1 Proposed mechanism of aerobic oxidation of a mixture of cyclohexanol and cyclohexanone to caprolactone catalysed by NHPI and CAN.[341] CAN represents Ceric ammonium nitrate.

Most production methods for ε-caprolactone have applied the principles of the Baeyer-Villiger reaction, which requires the use of organic peracids or organometallic catalysts. It also has a high economic and environmental cost, together with a high risk of explosion due to the need for organic solvents and unstable reagents. As the demand for sustainable chemistry increases, an alternative method for the production of caprolactone is worth developing. The transformation of fulvenes to unsaturated lactones has been reported by Genf and co-workers, using a photochemical method on a small scale.[342]

Hence, the application of this methodology to the synthesis of caprolactones is proposed as a greener/sustainable alternative route.

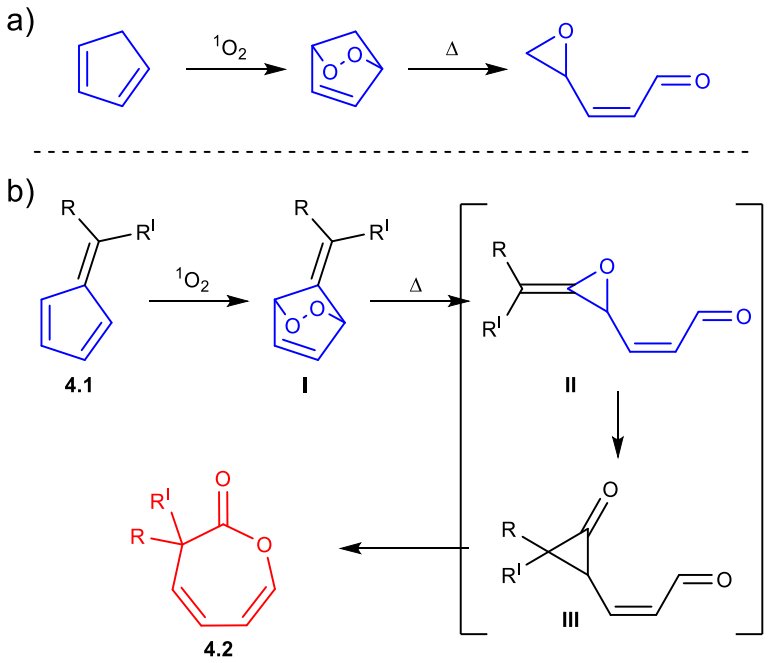
4.2 Process development from Cyclopentadiene to Fulvene

Fulvenes are composed of one conjugated odd-numbered ring and an exocyclic cross-conjugated double bond (Scheme 4-3). The structure of these molecules has many similarities to that of cyclopentadiene, the photo-oxidation of which has been successfully investigated in high-pressure continuous flow CO_2 reactor, as described in Chapter 3. In fact, fulvenes were first observed by Thiele when he was investigating the reactivity of cyclopentadienes.[343] He found that cyclopentadiene is reactive towards condensation with aldehydes and ketones with the help of a base (Scheme 4-3).[296, 344] This condensation reaction between cyclopentadiene and aldehydes or ketones is still, more than 100 years later, the most popular used procedure for the preparation of fulvenes and has also been used in the work presented in this chapter.



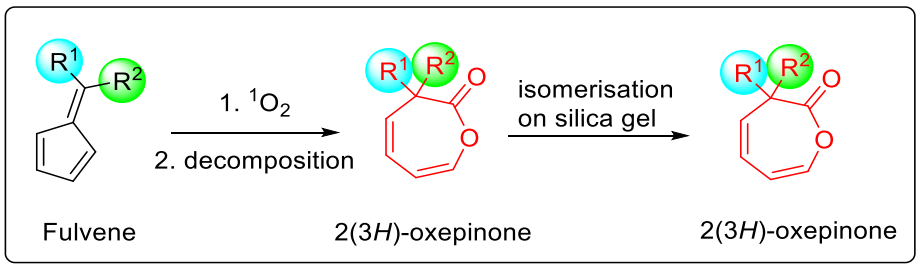
Scheme 4-3 General scheme for the synthesis of 6,6-disubstituted fulvenes.

The structure of fulvenes (Scheme 4-3, **4.1**) are closely related to cyclopentadiene, and hence the photo-oxidation of such derivatives also leads to unstable peroxide intermediates, as shown in Scheme 4-4. The endoperoxides of fulvene derivatives decompose *via* a radical based opening of the peroxide to form a *Z*-enal containing an epoxide moiety (**II**), much like what is seen for cyclopentadiene (Scheme 4-4). The additional functional group of fulvenes leads to further transformation products (**III**), the arrangement of which ultimately yields a 7-membered lactone containing a *Z*, *Z*-diene (**4.2**), which is a structure of caprolactone.[342]



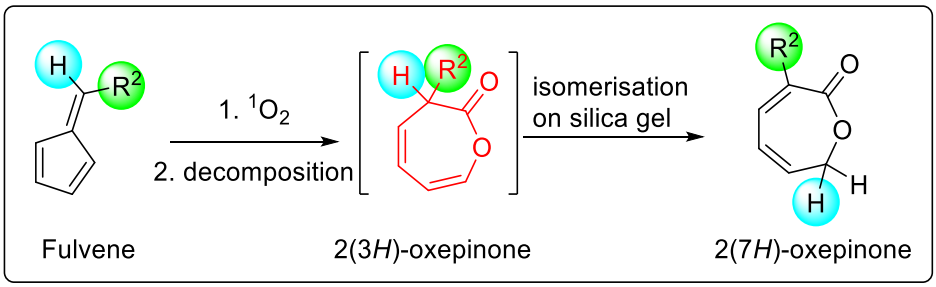
Scheme 4-4 The photo-oxidation and thermal degradation products of a) cyclopentadiene and b) fulvenes.

Previous reports of these reactions and the decomposition products have primarily been conducted on a small or analytical scale. In 1972, Uda and co-workers investigated the photosensitised oxidation of 6, 6-disubstituted fulvenes irradiated at room temperature, using benzene as solvent for 8 hours, forming a 7-membered ring containing compound, 2(3*H*)-oxepinone derivative (19 %), shown in Scheme 4-5.[345] Studies into solvent dependence in the photochemical oxidation of 6,6-dimethylfulvene were also performed in the same group.[346] They observed that the



Scheme 4-5 Photo-oxidations of 6,6-disubstituted fulvenes have been studied previously.[347]

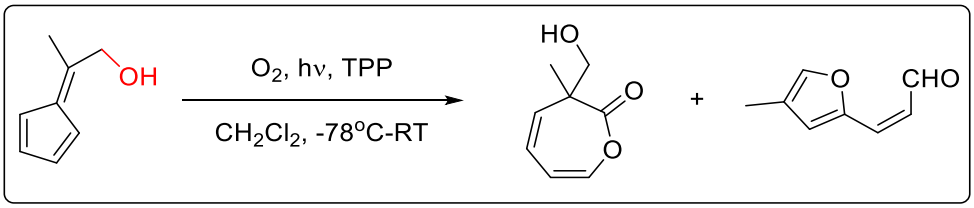
synthesis of productive 2(3*H*)-oxepinone *via* an allene oxide intermediate, was more effective when directly irradiated by UV in benzene, carbon disulfide, chloroform or acetone, than in methanol, and among the solvents used acetone seems to be the most suitable solvent for the preparation of the oxepinone. However, as acetone is highly reactive with the intermediated endoperoxides (**I**), this can also yield unstable trimer forms as studied previously.[347] Treatment of these fulvenes (300 mg scale) in alkaline methanol solution yielded furan derivatives after irradiation with a high-pressure mercury lamp for 20 hours.[348-349] Interestingly, it has been observed that a monosubstituted 2(3*H*)-oxepinone, synthesised from the reaction a 6-monosubstituted fulevene, can isomerise to 2(7*H*)-oxepinone during the purification on silica gel (*Scheme 4-6*).[350]



Scheme 4-6 Photo-oxidation of 6-monosubstituted fulvenes and purification.[350]

Previously studied photo-oxidation of fulvenes into 2(*3H*)-oxepinone and subsequent rearrangement to 2(*7H*)-oxepinone, the most notable feature common to fulvene endoperoxides is the fact that the rupture of the labile O-O bond leads to reactive intermediates such as allene oxides and cyclopropanones (Scheme 4-4). The latter had been implicated as likely precursors of oxepinones *via* electrocyclisation of the transient cyclopropane derivatives; the proposed mechanism was verified by trapping experiments with cyclic 1,2-dienes.[351-353] Recently, an unusual hydroxyl effect on fulvene endoperoxide decomposition was observed in the presence of a hydroxyl group on an alkyl or aryl group attached to the fulvene

exocyclic double bond.[354] As well as yielding oxepinone, furan was formed as an unexpected second product. (Scheme 4-7)



Scheme 4-7 photo-oxidation of fulvene with a hydroxyl group leading to oxepinone and furan. RT: Room Temperature.

Continuous flow reaction offers several advantages when generating compounds that are either highly reactive or unstable.[240] Reactors and systems can easily be engineered to allow for the addition of quench streams or reagent feeds, meaning that unstable intermediates can quickly be reacted to form more stable compounds, and more efficient for scaling up. Furthermore, parameters such as temperature and pressure can be monitored at multiple points throughout the system to match with the necessity of the desired experiment. In this project, our high-pressure continuous photoreactor was employed to the photo-oxidation of fulvenes to exploit this relatively underutilised transformation enabling the production of potentially scalable quantities of these useful synthetic building blocks.

4.3 Optimisation of the photo-oxidation of 6,6-dimethyl fulvene

The high-pressure equipment used in this study has been presented in Section 3.4, and the same setup was used for the production of epoxyaldehyde (**3.5**). A simplified diagram of this setup is shown in Figure 4-2.

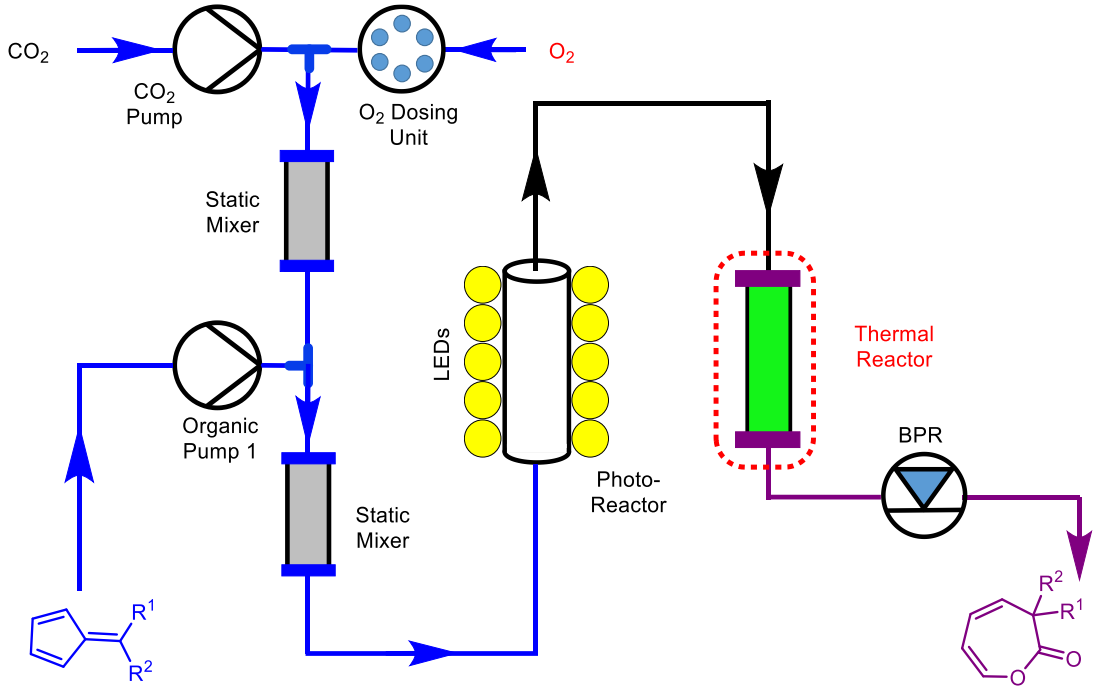
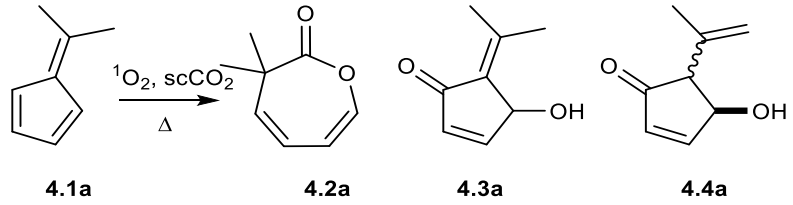


Figure 4-2 Simplified schematic of high pressure continuous flow setup.[293] CO_2 is delivered from a chilled CO_2 pump and O_2 is dosed at a known rate via a Rheodyne dosage unit. The gases are then mixed in a stainless steel tubular reactor filled with sand (Static Mixer 1) before the organic reagents are introduced and the components remixed (Static Mixer 2; consisting of a stainless steel tube filled with sand). Organic Pump 1 is an HPLC pump which delivers a solution of photosensitiser and fulvene. The photoreactor consists of an upward flow sapphire tube which is filled with glass balls (6 mm diameter) and is irradiated from the outside using white light LEDs. Downstream of the photoreactor is a Thermal Reactor, consisting of four stainless steel tubular reactors linked in series and housed in an aluminium heating block. The Back Pressure Regulator is used to maintain the system pressure and to release the reaction mixture continuously. Further details are provided in the experimental Section 4.7.

The investigation began with 6,6-dimethylfulvene **4.1a** as the model substrate because this fulvene is a liquid at ambient temperature and can be synthesised quickly on a large scale from acetone and cyclopentadiene.[355-356] The conditions which have been explored in Chapter 3 for the photo-oxidation of cyclopentadiene were used as a starting point.[237] The CO_2-soluble photosensitiser TPFPP was chosen as the catalyst for the reaction as it had been successfully applied in the previous system.[203] As **4.1a** is quite a viscous oil, a co-solvent was utilised so that the mixture

could be pumped with minimal blockages; initially, methanol was chosen. The first reaction was conducted at 120 bar and 40 °C, and the flow rates of the CO_2 and organic pump 1 were 0.25 mL/min and 0.1 mL/min, respectively; the concentration of **4.1a** in methanol was 0.1 M. The photo-oxidation of **4.1a** and subsequent decomposition of the endoperoxide in methanol led to a full conversion of the fulvene and a mixture of products with the expected lactone **4.2a** as the major product Scheme 4-8.



4.1a **4.2a** **4.3a** **4.4a**

*Scheme 4-8 Photo-oxidation of **4.1a** in supercritical CO_2.*

As highlighted in Table 4-1, different products ratios of **4.2a**: **4.3a**: **4.4a** could be obtained merely by changing the parameters of the flow reactor. A possible explanation for these products is presented below. Increasing the concentration of **4.1a** from 0.1 M to 1.0 M resulted in a slight drop in conversion (94 %) and decreased amount of **4.2a** (Table 4-1, entry 2). The yield of **4.2a** and **4.4a** dropped with decreasing temperature of the photoreactor and thermal reactor from 40 °C to 20 °C, but the yield of **4.3a** increased slightly (Table 4-1, entry 3). Diluting the reaction mixture by increasing the CO_2 flow rate (hence lowering the concentration of **4.1a** in the reactor as the organic flow rate remained constant) increased the yield of **4.2a** to 52 % and 55 % at 0.5 mL/min and 0.75 mL/min of CO_2, respectively (Table 4-1, entries 4-5). Reducing the concentration of **4.1a** in methanol also improved the yield and selectivity towards **4.2a** (Table 4-1, entry 6). Replacing methanol with the aprotic solvent EtOAc appeared to inhibit the formation of **4.3a** and also led to a slight increase in the yield of **4.2a** (Table 4-1, entry 7). Increasing the temperature of the thermal reactor to 80 °C provided a further increase in the yield of **4.2a** to 66 % (Table 4-1, entry 8).

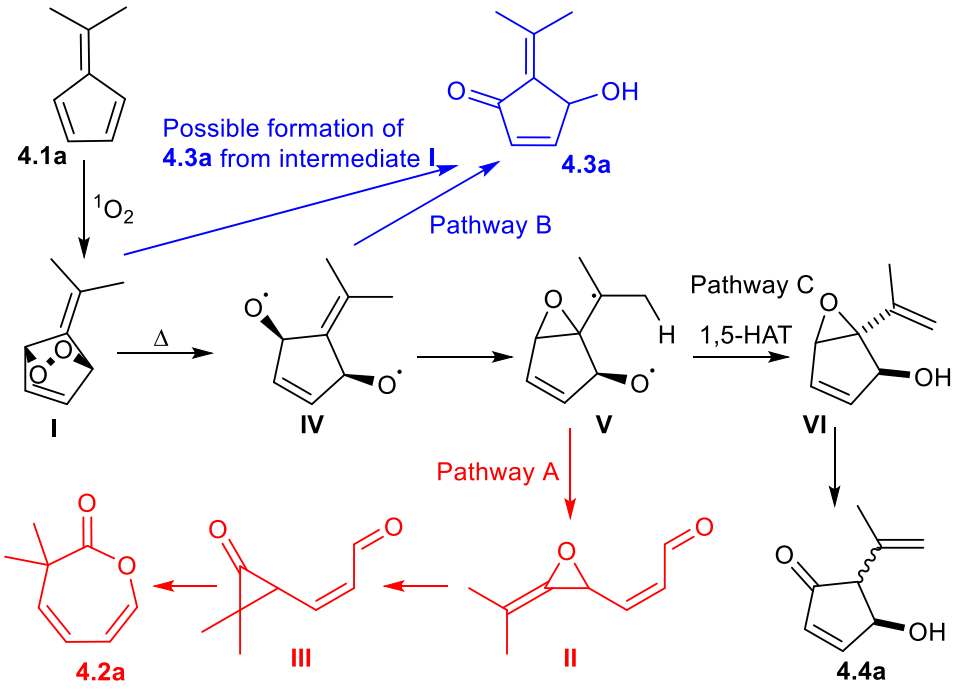
*Table 4-1 Conditions in high-pressure continuous flow reactor affecting the ratio of formation of **4.2a**, **4.3a** and **4.4a** from **4.1a**.*[a]

Entry	Conc. (M)	CO_2 Flow Rate (mL/min)	Temp. (°C)[b]	Co-solvent	Yield (%)		
					4.2a	4.3a	4.4a
1	0.1	0.25	40/40	MeOH	37	14	49
2[c]	1.0	0.25	40/40	MeOH	28	13	35
3	0.1	0.25	20/20	MeOH	34	17	34
4	0.1	0.5	40/40	MeOH	52	10	33
5	0.1	0.75	40/40	MeOH	55	8	22
6	0.05	0.5	40/40	MeOH	76	22	<1
7	0.1	0.75	40/40	EtOAc	57	-	18
8	0.1	0.75	40/80	EtOAc	66	-	14
9[d]	0.25	0.75	40/40	EtOAc	44	4	<1

[a]: 0.1 mol-% TPFPP as a catalyst, the flow rate of the organic pump was 0.1 mL/min; system pressure was 120 bar; and the switching time of Rheodyne for oxygen was 15.9 seconds, conversion >99%, conversion and yield were measured by ^{1}H NMR using mesitylene as an internal standard, unless otherwise noted. [b]: Photoreactor/Thermal reactor temperatures. [c]: Conversion = 94%. [d]: Starting mixture contained 1 equivalent TEA; conversion was 81 %.

The formation of **4.4a** as a *ca*. 1:1 mixture of diastereoisomers was observed in all reactions starting from **4.1a** regardless of the solvent choice. This results suggest that the formation of **4.4a** is not an intermolecular process interacting with solvents. Instead, **4.4a** is likely to be formed from a competing rearrangement facilitated by an intramolecular hydrogen proton transfer (Scheme 4-9). Decomposition of endoperoxide **I** leads to the bi-radical intermediate **IV** and **V** which can then proceed through one of two competing pathways. Pathway A is dominant, with the formation of allene oxide **II** and cyclopropanone **III** *via* cleavage of C-C bond in the cyclopentane ring (Scheme 4-9, shown in red arrows), and leads to the ultimately to the formation of lactone **4.2a**. Pathway C (Scheme 4-9, shown in black arrows) proceeds *via* abstraction of an allylic hydrogen atom and rearrangement to form the bicyclic epoxide intermediate **VI** which should be produced as a single diastereoisomer based on the stereochemistry setup by addition of singlet oxygen. Recently, a similar 1,7-

hydrogen atom transfer (HAT) mechanism and the isolation of compounds similar to **VI** have been reported for oxygenated fulvene derivatives.[354] Intermediate **VI** was neither isolated nor observed by ^{1}H NMR in any of these experiments. In this case, the formation of **4.4a** from **VI** probably proceeds *via* a hydrogen transfer mechanism that racemises the quaternary chiral centre. A possible cause for the loss of one of the chiral centres is that this hydrogen atom transfer event proceeds primarily *via* an intermolecular process, perhaps involving a second molecule of **V** (or involving methanol if it is used as the solvent) acting as a hydrogen atom donor/acceptor. It is possible that the conversion of **V** to **VI** is reversible because, when the reaction was diluted with CO_2 and an aprotic co-solvent used, selectivity towards the major product **4.2a** was increased and towards **4.4a** decreased. In this case, it is likely that the conversion of **VI** to **4.4a** is impeded. Further experiments to clarify this mechanism are currently in progress.

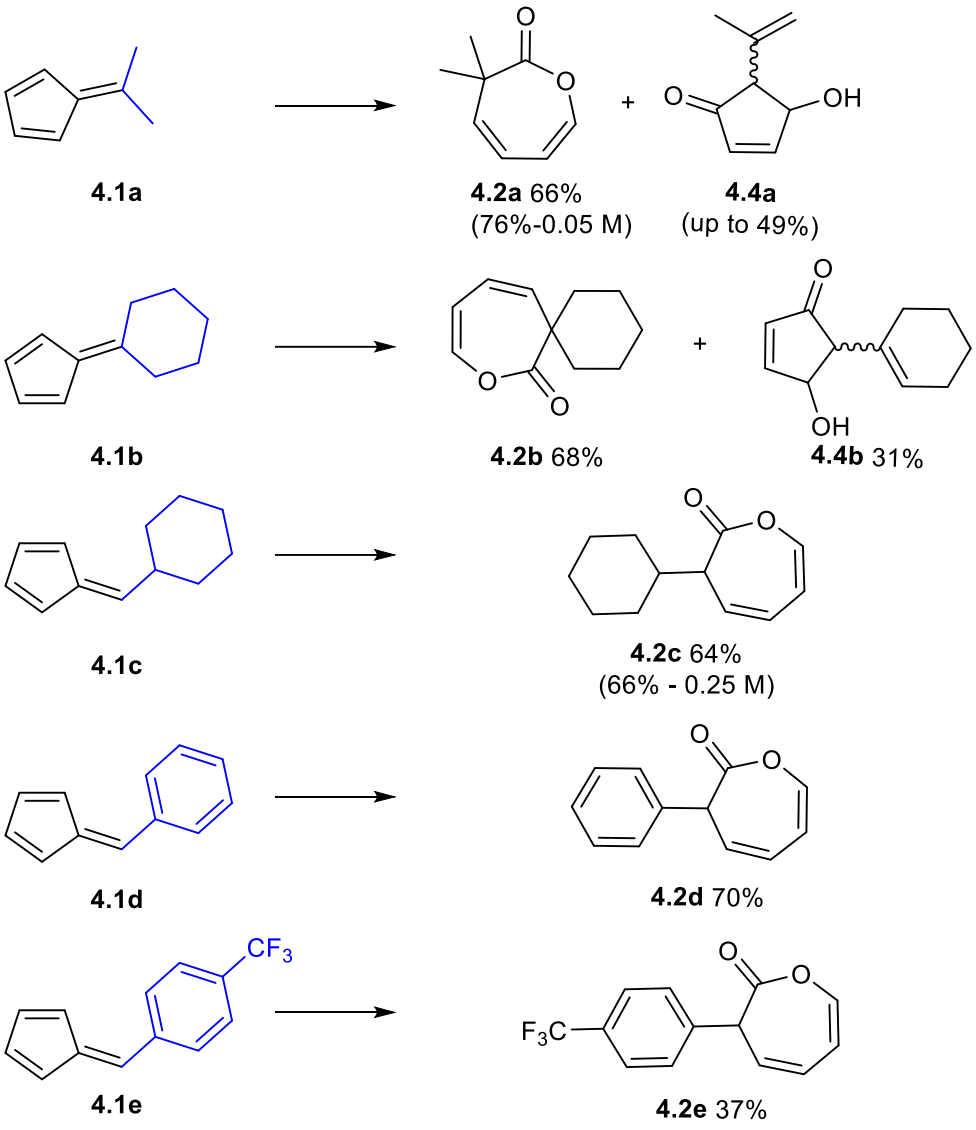


*Scheme 4-9 Proposed competing mechanistic pathways for the formation of **4.2a** (Pathway A), **4.3a** (Pathway B) and **4.4a** (Pathway C) from **4.1a**, HAT represents Hydrogen Atom Transfer.*

As observed in Table 4-1, product **4.2a** was the major product under most conditions (Table 4-1, entries 1 and 4-9). Minor product **4.3a** is a motif that is often achieved after treating a cyclic endoperoxide with a catalytic base.[357] Indeed the corresponding hydroxyenone is formed when the endoperoxide of cyclopentadiene is treated with trimethylamine (Section 3.5). In the case of **4.1a**, however, there is no base added but, it is possible, that methanol can act as a facilitator of hydrogen transfer because of the increased reactivity of the fulvene endoperoxide (**I**) compared to that of cyclopentadiene. When methanol was replaced with an aprotic solvent such as ethyl acetate or toluene, the formation of **4.3a** was suppressed to a level that was not detectable in the crude products, suggesting that a protic solvent such as methanol plays a key role in the formation of **4.3a**. Treatment with the stronger base, triethylamine (TEA, 0.25 M; 1 equivalent) in an attempt to alter selectivity towards **4.3a** resulted in a loss of efficiency for the photo-oxidation (Table 4-1, entry 9). However, **4.2a** was still observed as a primary product. It is possible that the TEA, as it is a strong electron donor, could inhibit the formation of $^1O_2$,[358] therefore, reducing the efficiency of photo-oxidation step, and leading to a loss of the final product **4.2a**. It is also possible that the formation of **4.3a** does not proceed *via* a base catalysed process and instead through a bi-radical intermediate (**IV**, Pathway B, Scheme 4-9) where a hydrogen abstraction mechanism involving methanol produces **4.3a**.

4.4 The scope of different fulvene derivatives

Given that there are several competing pathways when reacting **4.1a** with $^1O_2$, moving to a substrate that lacks an easily removed allylic hydrogen atom should inhibit this competing pathway and selectively give only the lactone product. These reactions were generally carried out in the aprotic solvent, ethyl acetate, so the formation of **4.3a** derivatives was not expected.



Scheme 4-10 Substrate scope using the high-pressure photoreactor with $^1O_2$ in $scCO_2$ and the products formed. *Yields were determined by ^1H NMR using mesitylene as an internal standard. Unless otherwise stated these experiments were carried out in high-pressure continuous flow reactor with $scCO_2$ as solvent and with EtOAc as co-solvent; the concentration of substrate in EtOAc was 0.1 M; 120 bar, 40 °C; the flow rate of CO_2 pump and organic pump 1 was 0.25 mL/min and 0.1 mL/min, respectively; the switching time of Rheodyne for oxygen was 15.9 seconds.*

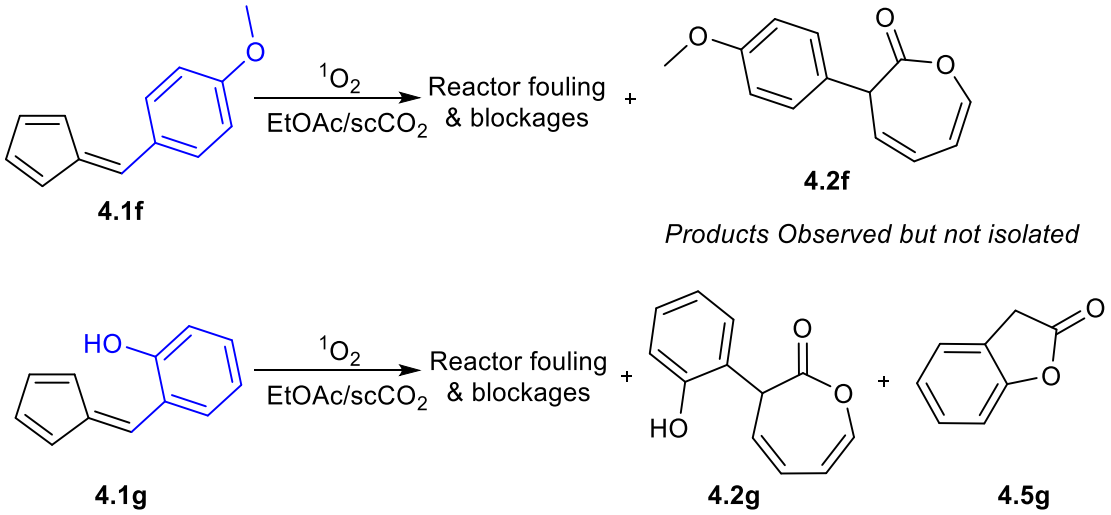
Therefore, several fulvenes with different substituted groups were synthesised and subjected to the high-pressure flow reactor (120 bar, 40 °C) to investigate their reactivity (Scheme 4-10). Further details of the conditions used can be found in the experimental section 4.7.2 at the end of this chapter. Using a similar substrate to **4.1a**,

the cyclohexyl derivative **4.1b** formed bicyclic lactone **4.2b** containing a spiro centre as the major product and also gave the hydroxyenone **4.4b** (up to 48 % by NMR) as a competing product. Unfortunately, **4.4b** could not be isolated in all cases and appeared to decompose in the presence of SiO_2 or Al_2O_3 during purification.

Fulvene **4.1c** which has a more hindered allylic proton yielded the lactone (**4.2c**) exclusively in EtOAc and no competing products were observed, suggesting that the hydrogen abstraction pathway was suppressed as explained in Scheme 4-9, since a bulky group with one allylic group was attached to the exocyclic double bond.

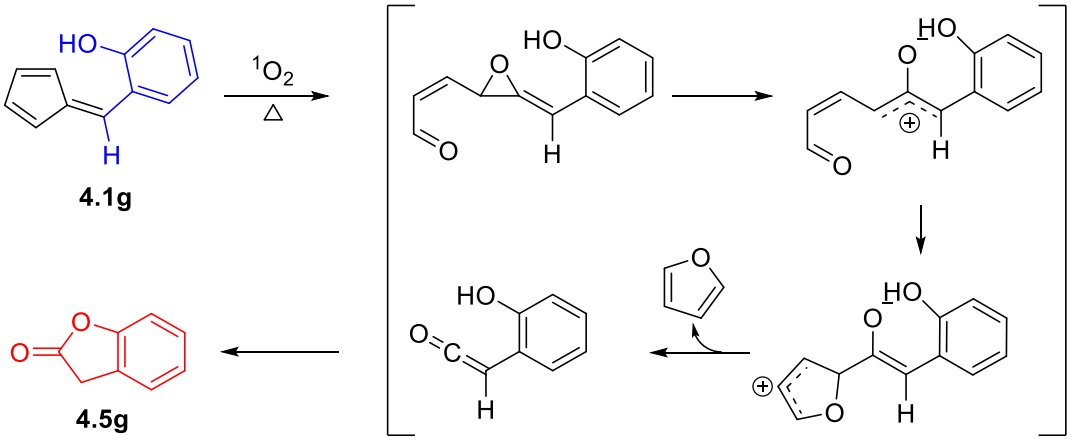
When substrates containing aromatic groups were used, the products formed from the photo-oxidation were dependent on the electron density of the aromatic group. For example, when the fulvene **4.1d**, which does not contain an allylic proton next to the exocyclic bond, was reached a peak yield of 70 % of lactone **4.2d** was obtained. When an aromatic substrate containing an electron withdrawing group (**4.1e**) was subjected to the reaction at the same condition, the conversion of the fulvene remained high; however, the overall yield of the lactone suffered (37 % for **4.2e**) and no side products can be observed.

Furthermore, for a substrate containing an electron donating group (**4.1f**) the reaction was complicated by the formation of a polymeric mixture which fouled the photoreactor and resulted in blockages when EtOAc was used as co-solvent (Scheme 4-11). These blockages could be prevented by using a 1:1 (v:v) mixture of EtOAc/MeOH; however, useful yields of **4.2f** could not be obtained (<12 %) and the product could not be isolated by column chromatography on silica gel or Al_2O_3.



*Scheme 4-11 Reactions of the substrate containing electron donating group (**4.1f-g**). Unless otherwise stated these experiments were carried out in high-pressure continuous flow reactor with scCO$_2$ as solvent and with EtOAc as co-solvent; the concentration of substrate in EtOAc was 0.1 M; 120 bar, 40 °C; the flow rate of CO$_2$ pump and organic pump 1 was 0.25 mL/min and 0.1 mL/min, respectively; the switching time of Rheodyne for oxygen was 15.9 seconds.*

Another substrate with an electron donating group (**4.1g**) was reacted in the flow reactor in scCO$_2$, with complete conversion of the starting material. However, much like substrate **4.1f**, the reaction again resulted in the formation of large quantities of polymeric material in the photoreactor with a low yield of **4.2g**, along with *ca.* 20 % yield of 2-coumaranone (**4.5g**) (Scheme 4-11). The production of **4.5g** from fulvene **4.1g** is not surprising as Erden and Gronet have demonstrated that fulvenes containing aromatic hydroxyl groups can be used to obtain **4.5g** *via* photo-oxidation and decomposition.[354] The proposed mechanism for the formation of 2-coumaranone **4.5g** is shown in Scheme 4-12 for convenience.



*Scheme 4-12 Mechanism for the formation of **4.5g** from photo-oxidation of **4.1g**.*[354]

Supercritical CO_2 is relatively non-polar in terms of its properties as a solvent; therefore it is possible that, for some of the substrates containing more polar heteroatomic functional groups (**4.1e-g**), probably the products or intermediates formed in the photoreactor are less soluble or even insoluble in supercritical CO_2 and are precipitating within the photoreactor, hence leading to blockages. No definite identification of the solid material from the photoreactor fouling and blockages could be obtained when the analysis was attempted.

For all products of type 2 (**4.2c-e**) that were derived from fulvenes (**4.1c-e**), i.e. containing an H-atom at the 3-position, prolonged exposure to silica or alumina led to isomerisation of the diene to form conjugation with the carbonyl (from 2(3*H*)-oxepinone to 2(7*H*)-oxepinone) as described in *Scheme* 4-6. However, flash chromatography on a short timescale could be used to purify these compounds before significant isomerisation occurred (<10%).

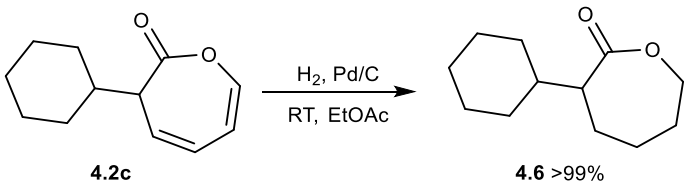
4.5 The investigation into methods to add further value to the caprolactones

A range of unsaturated caprolactones were successfully synthesised in the supercritical CO_2 system, using EtOAc as co-solvent. Caprolactones have wide applications in the synthesis of bioactive materials, natural products and are also used as monomers for the manufacture of specialty polymers,[292, 309] which have been discussed in Section 4.1.2. In addition, unsaturated compounds are generally more reactive than saturated compounds and were used broadly in chemical synthesis;[359-360] and are very useful in organic synthesis, as the diene group often can be used for the hydrogenation,[361] Diels-Alder reactions,[362] UV reaction[363] and so on. In an attempt to increase the synthetic usefulness of these unsaturated caprolactones, further variable reactions were carried out in this section.

4.5.1 Hydrogenation of lactone

To briefly test the reactivity of the lactones **4.2**, small scale reactions were carried out as batch reactions. Hydrogenation of the lactones **4.2c** gave saturated 7-membered rings, which have potential value as functionalised polycaprolactone monomers.[364-367] Taking **4.2c** as an example and submitting it to a palladium on carbon catalyst (Pd/C) in EtOAc under an atmosphere of H_2 yielded pure **4.6**, which can be isolated without any further purification (Scheme 4-13).

Hydrogenation reactions in $scCO_2$ have been reported extensively by our group including in continuous flow.[259, 261, 368-370] However the coupling of a supercritical photo-oxidation reactor with supercritical hydrogenation reactor presents several challenges, not least the possibility of having high-pressure mixtures of H_2 and O_2. Nevertheless, we aim to explore the streaming of this process in the future.

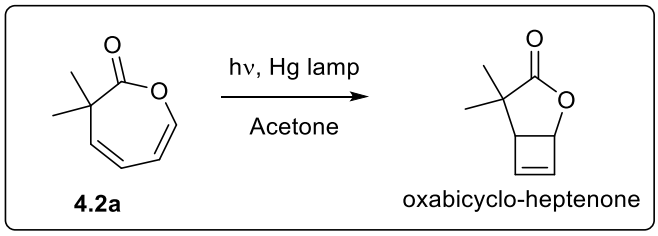


*Scheme 4-13 Quantitative hydrogenation of **4.2c** to **4.6**.*

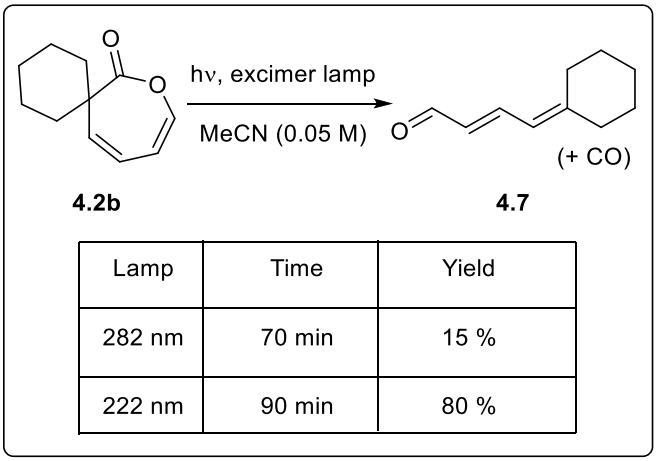
4.5.2 Further reactions

Submitting **4.2c** to another exposure to singlet oxygen did not yield any further reaction. This supports the apparent stability of the unsaturated lactones to further photo-oxidation observed in the first run through the photoreactor because no further oxidation products were observed in any of the continuous flow experiments. Further explanation would be required to determine the reason for the stability of **4.2c** with singlet oxygen.

a) Previous work:



b) This work:



Lamp	Time	Yield
282 nm	70 min	15 %
222 nm	90 min	80 %

*Scheme 4-14 a) Compound **4.2a** was irradiated by high-pressure mercury in acetone;[371] b) Submitting **4.2b** into batch UV reaction to form **4.7**, the yield of product **4.7** depends on the choice of lamp and irradiation time.*

When the UV reactivity of lactone **4.2b** was investigated interestingly, a new compound **4.7** was observed, as shown in Scheme 4-14 (b). This compound was observed when lactone **4.2b** (1.5 mmol, 0.05 M in acetonitrile) was irradiated in a batch excimer lamp reactor, irradiated by an excimer lamp (282 nm or 222 nm).[372] This contrasts with the results of a previous paper in 1984,[371] where when **4.2a** as a solution in acetone was subjected to irradiation by a high-pressure mercury lamp, an oxabicyclo-heptanone compound was obtained (Scheme 4-14 (a)).[371] One possible reason for the observed difference in reactivity is that the excimer lamps used in this investigation procedure light at discrete wavelengths (282 nm or 222 nm), which may activate different functional groups within the molecule, than those activated by the broad wavelengths emitted by a mercury lamp. Despite the difference in observed reactivity, this photochemical reaction is highly promising as it provides a potential procedure for synthesising conjugated aldehydes in a single step.[373]

Diels-Alder reactions of lactone **4.2a** with 1,4-benzoquinone in toluene did not proceed with the diene when stirred at room temperature for 16 h. Heating the mixture at reflux for 24 h gave no conversion, and the starting materials were obtained unchanged.

The ring-opening polymerisation of **4.2c** in toluene, using benzyl alcohol as the initiator and tin(II)-2-2ethylhexanoate as the catalyst at 110 °C for 24 hours, was examined and no polymers were observed by NMR or Size Exclusion Chromatography; some oligomers may have formed, but the conversion was very low. This experiment was in collaboration with Dr Andrea Hufendiek.

4.6 Conclusions and further work

A high-pressure continuous flow photoreactor was employed to carry out the photo-oxidation of fulvenes. By using the continuous flow reactor and $scCO_2$ as an inert solvent, photo-oxidation of different fulvene derivatives was achieved in good

yields. Coupling a thermal reactor to the photoreactor allowed for the efficient transformation of the reactive endoperoxides formed by reaction with singlet oxygen to ε-caprolactone derivatives, instead of involving H_2SO_5 in traditional Baeyer-Villiger reaction. These ε-caprolactones are promising as monomer precusors to polymers, which may be biodegradable.

The model substrate 6, 6-dimethylfulvene (**4.1a**) presented interesting reactivity, forming several different compounds *via* competing pathways. The ratios of variable products from **4.1a** depended on both the choice of co-solvent and the flow rate of CO_2. Other substrates, which lacked the allylic hydrogen atoms of the model substrate gave the desired caprolactone exclusively as the major product. The projected productivities for all of these caprolactones were up to grams per day, as much as with 9 grams for **4.2a**. However, processing issues such as reactor fouling and blockages occurred when substrates with more polar functional groups were employed.

Further exploring the usefulness of the synthesised lactones, some interesting products were obtained. One lactone (**4.1b**) was hydrogenated using Pd/C, demonstrating a potentially useful route to functionalised caprolactone derivatives. Moreover, synthesis of a conjugated aldehyde was achieved *via* UV initiated reaction of lactone **4.2b** in an excimer lamp reactor with different lamps; and this is good for the further investigating new and facile methods for the synthesis of conjugated aldehydes.

Further investigating the UV and visible properties of these caprolactones should be done in the future to explore more interesting reactions initiated by light. Scale-up can be studied by the larger the volume of the photoreactor. Also, polymerisation should be explored further using these unsaturated caprolactones or reduced caprolactones as starting materials.

4.7 Experimental

4.7.1 Synthesis of different fulvene derivatives

Typical procedure A to synthesise fulvenes 4.1b and 4.1c:

To a solution of aldehyde or ketone (1 equiv.) and freshly distilled cyclopentadiene (2.5 equiv.) in methanol (1 $mol \cdot L^{-1}$) was added dropwise under stirring pyrrolidine (1.5 equiv.). The mixture was then stirred under argon at room temperature. After completion, determined by TLC analysis, acetic acid (1.6 equiv.) was added to the yellow solution. The reaction mixture was diluted with diethyl ether and water. The aqueous layer was washed with diethyl ether and the combined organics were washed with water, brine, dried over $MgSO_4$ and concentrated under reduced pressure to afford the desired product.

Typical procedure B to synthesise fulvenes 4.1d - 4.1f:

To a solution of aldehyde or ketone (1 equiv.) and cyclopentadiene (1.2 equiv.) in $MeOH/H_2O$ (4/1) pyrrolidine (10 mol %) was added dropwise. The reaction mixture was then stirred under argon atmosphere until completion. The mixture was transferred to an ice-cold mixture of brine solution and 10 mol% acetic acid and then diluted with dichloromethane. The aqueous layer was extracted with methylene chloride. The combined organic layers were dried over $MgSO_4$, filtered, and concentrated under reduced pressure. The crude product was purified by flash chromatography on silica gel eluting with the corresponding solvent mixture to afford the desired product.

4.7.2 High pressure setup using CO_2 as a solvent

The high pressure continuous flow rig for photo-oxidation was built using HPLC pumps, connecting tubes, mixers, sapphire tube reactor and cooling baths. Temperatures were controlled *via* cooling baths and heaters, monitored by thermocouples, and system pressure was set and controlled by a back-pressure regulator. System pressure, CO_2 pressure and O_2 pressure were monitored by the

pressure transducer. All continuous flow experiments described in this paper were carried out using the rig described below. The rig diagram is shown in Figure 4-3. Further details of this setup can be found in Chapter 2.

Compressed CO_2 was delivered from a chilled CO_2 pump (JascoTM PU-1580-CO_2 pump), and O_2 was dosed at a known rate via a Rheodyne dosage unit.

Mixers M1 and M2 (78 mm, ¼ inch O. D., SS316 tubes) were loaded with one gram of sand each. CO_2 and O_2 were mixed in the first static mixer M1, and then the organic stream was added by OP1 (organic pump 1, JascoTM PU-980 HPLC pump) into the gases mixture before entering into the second mixer M2.

The fluid mixture then entered into the high-pressure sapphire tube reactor (Saint-Gobain Crystals, 10 mm O.D., 1 mm wall thickness, 120 mm long; loaded with 17 glass beads, 6 mm O. D.) following an up-flow method. The sapphire tube was irradiated with visible light by LEDs, which were controlled by a LED controller. LED lights were composed of three banks of liquid-cooled LED aluminium blocks each containing five chips (Citizen Electronics Co. Ltd) irradiating for 1000 lumen per chip. The blocks were cooled with a chiller. Due to the heat generated by the LED lights, a secondary cooling bath was used to pump coolant around the sapphire tube to ensure the desired temperature in the reactor. Thus, LEDs can be positioned as close as possible to the sapphire tube, without increasing the reaction temperature, assuring high efficient irradiation.

The startup procedure and shut-down procedure for this setup were described in Chapter 2.

The general conditions for the scope of different fulvene derivatives in the high-pressure setup

All the experiments for the investigation of the scope were conducted at this high-pressure setup, at 120 bar in supercritical, using EtOAc as co-solvent unless otherwise stated. The temperatures of a photoreactor and the thermal reactor was

kept at 40 °C, maintained by cooling baths and heaters. The concentrations of each substrate in co-solvent was 0.1 M, and 0.1 mol % of TPFPP to the substrate was employed. The switching time for the oxygen introducing was 15.9 seconds unless otherwise stated. The starting solution was dissolved well before being introduced into the system. More operating procedure details are presented in Chapter 2.

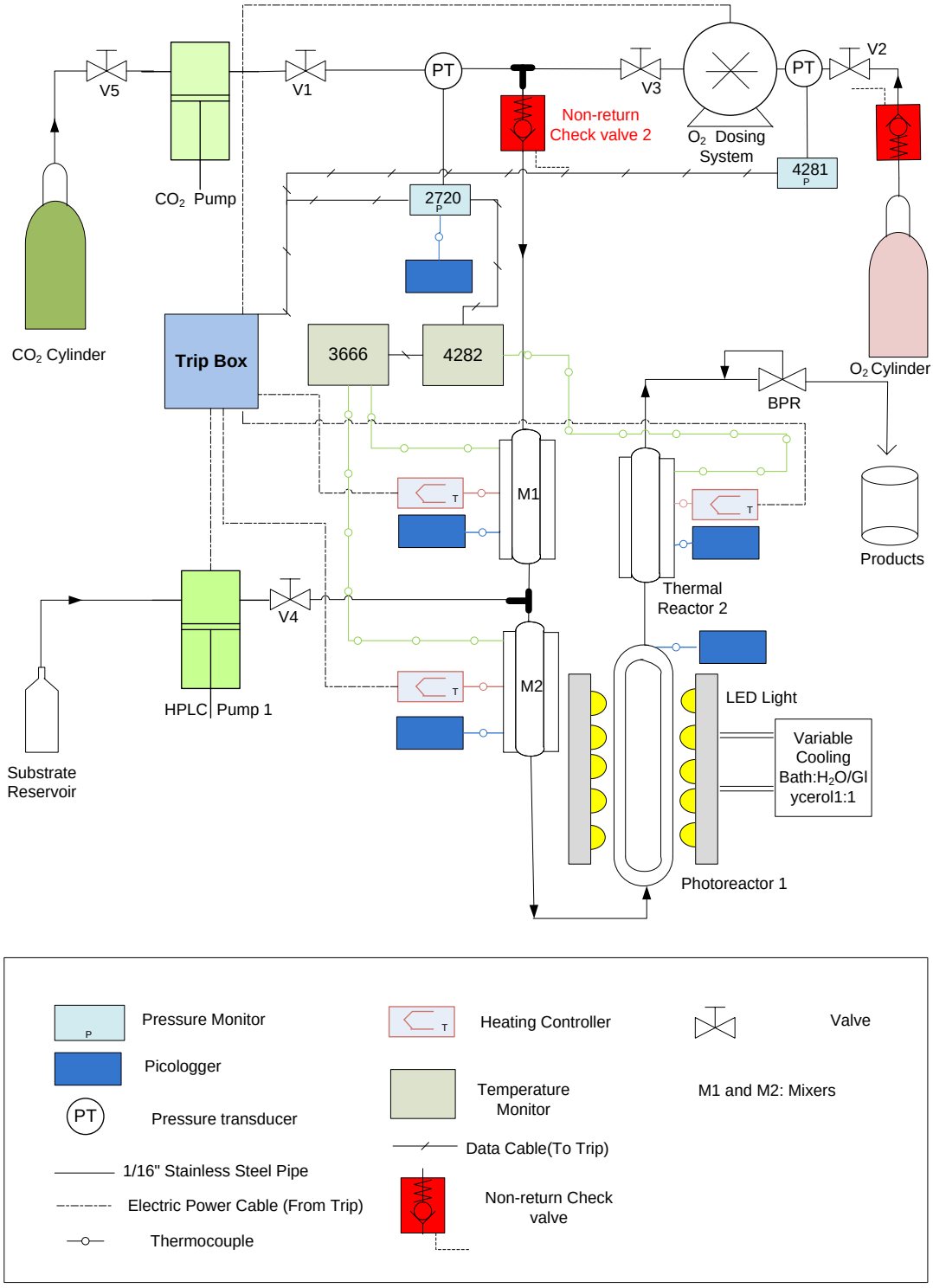


*Figure 4-3 Diagram of the rig for the synthesis of products **4.2a-4.2g** from **4.1a-4.1g**. An extra thermal reactor (1/4" O.D. 0.049" wall thickness, 150 mm length) was added downstream of photoreactor.*

4.7.3 Procedures for further value studies

UV reaction of 4.2b in batch excimer lamp reactor

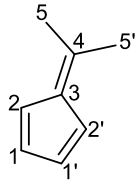
A solution of caprolactone **4.2b** (1.5 mmol) dissolved in MeCN (0.05 M) was added into the batch excimer lamp reactor. The temperature for the photoreactor was kept at 20-22 °C by a circulating cooling bath (10 °C). The reaction mixture was irradiated by excimer lamp (282 nm or 222 nm) for the desired time. The conjugated aldehyde product was obtained and analysed after column chromatography. This reaction was carried out with the help of Amy Flinn, a PhD student (a year below me) in the research group.

Both photo-oxidation of 4.2a and 4.2b

Lactone and TPFPP were dissolved in 5 mL EtOAc (0.05 mol·L^{-1}), and then irradiated by LED light. Oxygen was provided *via* a balloon; no reaction occurred even after irradiation with the visible light for 4 h at -70 °C. After increasing the irradiation reaction temperature to 25 °C, a tiny amount of decomposition of the lactone was observed after irradiation for 10 h, but most of the starting material was unreacted.

4.7.4 Characterisation

5-(Propan-2-ylidene)cyclopenta-1,3-diene[356] (4.1a)



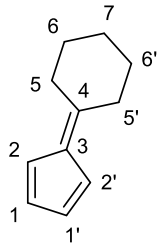
To a solution of cyclopentadiene (33 g, 0.5 mol) and acetone (14.7 mL, 0.20 mol) in methanol (500 mL) under argon atmosphere was added dropwise pyrrolidine (51 mL, 0.60 mol) at room temperature. After 1 h, acetic acid (18.8 mL, 0.32 mol) was added and stirred for 10 minutes. The mixture was poured on cold water, and diethyl ether was added. The aqueous layer was extracted twice with diethyl ether, and the organic layer was washed with cold water, dried over $MgSO_4$, filtered and concentrated under reduced pressure to afford **4.1a** as a yellow oil (48.9 g, 0.46 mol). The desired product was then used without any further purification. The isolated yield was 92 %.

^{1}H NMR (400 MHz, CD_3OD) δ = 6.43–6.59 (m, 2H, H2 + H2'), 6.30–6.46 (m, 2H, H1 + H1'), 2.19 (s, 6H, 2× CH3).

^{13}C NMR (400 MHz, CD_3OD) δ = 149.8 (C4), 144.0 (C3), 131.3 (C1 + C1'), 121.5 (C2 + C2'), 22.9 (C5 + C5').

HRMS (ESI): for C_8H_{10}, $[M+]^+$ calculated *m/z* = 106.0777, found *m/z* = 106.0772.

Cyclopenta-2,4-dien-1-ylidenecyclohexane (4.1b)



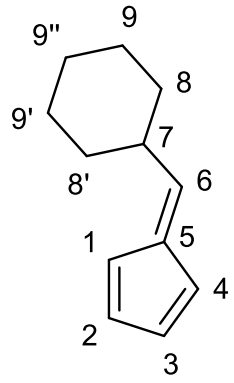
Cyclopenta-2,4-dien-1-ylidenecyclohexane (**4.1b**) was obtained using the **typical procedure A** using cyclohexanone (5.3 mL, 50.9 mmol), cyclopentadiene (12.2 mL, 127.25 mmol), pyrrolidine (7 mL, 76.35 mmol), methanol (127 mL) and acetic acid (4.7 mL). The isolated yield was 80 %.

^{1}H NMR (400 MHz, CD_3OD) δ = 6.56 – 6.52 (m, 2H, H2 + H2'), 6.45 – 6.39 (m, 2H, H1 + H1'), 2.66 (dd, *J* = 6.9, 5.0 Hz, 4H, 2×H5 + 2×H5'), 1.79 – 1.66 (m, 6H, 2×H6 + 2×H6' + 2×H7).

^{13}C NMR (101 MHz, CD_3OD) δ = 157.8 (C4), 141.0 (C3), 131.5 (C1 + C1'), 120.9 (C2 + C2'), 34.5 (C5 + C5'), 30.0 (C6 + C6'), 27.6 (C7).

HRMS (ESI): for $C_{11}H_{14}$, $[M+]^+$ calculated *m/z* = 146.1090, found *m/z* = 146.1095.

(Cyclopenta-2,4-dien-1-ylidenemethyl)cyclohexane[344] (4.1c)



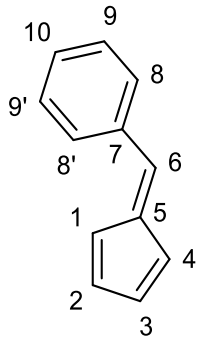
(Cyclopenta-2,4-dien-1-ylidenemethyl)cyclohexane (**1c**) was obtained using **typical procedure A** using cyclohexanecarboxyaladehyde (2.2 mL, 17.8 mmol), cyclopentadiene (3.7 mL, 44.6 mmol), methanol (17.8 mL), pyrrolidine (2.2 mL, 26.7 mmol), acetic acid (1.6 mL, 28.48 mmol). Isolated yield was 85 %.

^{1}H NMR (400 MHz, CD_3OD) δ 6.52 – 6.47 (m, 2H, H3 + H4), 6.40 (m, 1H, H1), 6.22 (m, 1H, H2), 6.15 (m, 1H, H6), 2.71 (m, 1H, H7), 1.84 – 1.67 (m, 4H, 2×H8 +2×H8'), 1.49 – 1.22 (m, 6H, 2×H9 + 2×H9' +2×H9'').

^{13}C NMR (101 MHz, CD_3OD) δ 148.3 (C5), 145.8 (C6), 133.8 (C4), 131.4 (C1), 126.9 (C2), 120.1 (C3), 41.2 (C7), 34.3 (C8 + C8‘), 26.9 (C9 + C9‘), 26.6 (C9‘‘).

HRMS (ESI): for $C_{12}H_{16}$, $[M+]^+$ calculated m/z = 160.1247, found m/z = 160.1243.

Cyclopenta-2,4-dien-1-ylidenemethyl)benzene[355] (4.1d)



Cyclopenta-2,4-dien-1-ylidenemethyl)benzene (**1d**) was obtained using **typical procedure B** using benzaldehyde (1.9 mL, 18.8 mmol), cyclopentadiene (1.9 mL, 22.6 mmol), pyrrolidine (240 µL, 1.8 mmol), methanol (15 mL) and water (3.8 mL). Isolated yield was 90 %.

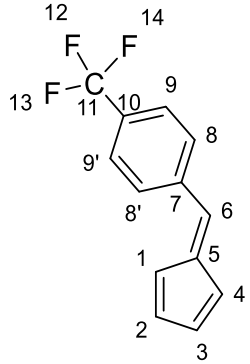
^{1}H NMR (400 MHz, CD_3OD) δ = 7.65 – 7.59 (m, 2H, H8 + H8’), 7.46 – 7.35 (m, 3H, H9 + H9’ + H10), 7.24 (s, 1H, H6), 6.72 – 6.62 (m, 2H, H3 + H4), 6.47 (m, 1H, H1), 6.32 (m, 1H, H2).

^{13}C NMR (101 MHz, CD_3OD) δ = 146.8 (C5), 138.8 (C6), 136.4 (C7), 131.7 (C8 + C8‘), 131.5 (C4), 130.1 (C1), 129.8 (C9 + C9‘ + C10), 128.4 (C2), 121.1 (C3).

HRMS (ESI): for $C_{12}H_{10}$, $[M+]^+$, calculated *m/z* = 154.0777, found *m/z* = 154.0773.

1-(cyclopenta-2,4-dien-1-ylidenemethyl)-4-(trifluoromethyl)benzene [355] (4.1e)

1-(cyclopenta-2,4-dien-1-ylidenemethyl)-4-(trifluoromethyl)benzene (**1e**) was obtained using **typical procedure B.** using 4-(trifluoromethyl)benzaldehyde (3.9 mL, 28.7 mmol), cyclopentadiene (3.1 mL, 34.5 mmol), pyrrolidine (375 µL, 2.87 mmol), methanol (28.7 mL) and molecular sieve 3Å (8.6 g). Isolated yield was 40 %.



^{1}H NMR (500 MHz, CD_3OD) δ = 7.80 – 7.70 (m, 4H, H8 + H8’ + H9 + H9’), 7.27 (s, 1H, H6), 6.69 – 6.64 (m, 2H, H3 + H4), 6.51 (m, 1H, H1), 6.33 (m, 1H, H2).

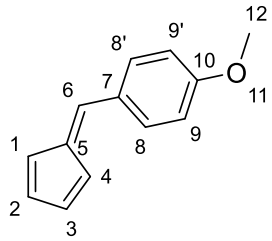
^{13}C NMR (126 MHz, CD_3OD) δ = 148.7 (C5), 141.9 (C6), 137.5 (C4 + C1), 136.4 (C3 + C2), 132.6 (C8 + C8‘), 132.0 (C9 + C9‘), 128.3 (C2), 126.6 (C11, q, J^{C-F} = 4.01 Hz), 121.0 (C10).

^{19}F NMR (376.4 MHz, CD_3OD) δ = -62.72.

HRMS (ESI): for $C_{13}H_9F_3$, $[M - H]^-$ calculated *m/z* = 221.0584, found *m/z* = 221.0584.

1-(Cyclopenta-2,4-dien-1-ylidenemethyl)-4-methoxybenzene[355] (4.1f)

1-(Cyclopenta-2,4-dien-1-ylidenemethyl)-4-methoxybenzene **(4.1f)** was obtained using **typical procedure B**. Isolated yield was 95 %.

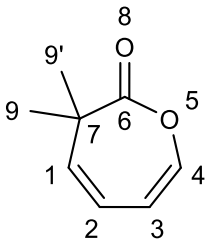


^{1}H NMR (400 MHz, CD_3OD) δ = 7.65 – 7.58 (m, 2H, H8 + H8’), 7.16 (d, *J* = 1.4 Hz, 1H, H6), 7.03 – 6.97 (m, 2H, H9 + H9’), 6.75 – 6.72 (m, 1H, H2), 6.62 (m, 1H, H1), 6.42 (m, 1H, H4), 6.29 (d, *J* = 5.1, 1H, H3), 3.86 (s, 3H, CH3).

^{13}C NMR (101 MHz, CD_3OD) δ = 162.4 (C10), 138.8 (C5), 135.8 (C6), 133.5 (C8 + C8‘), 130.9 (C1), 130.3 (C4), 128.6 (C3), 120.7 (C2), 115.4 (C9 + C9‘), 55.8 (CH3).

HRMS (ESI): for $C_{13}H_{12}O$, $[M + H]^+$ calculated *m/z* = 185.0961, found *m/z* = 185.1025.

3,3-Dimethyloxepin-2(3H)-one[342] (4.2a)



- Organic concentration solution feedstock: 0.05 mol/L

  CO_2 Flow rate: 0.5 mL/min; [**4.1a**/O_2/MeOH/CO_2] molar ratio: (0.0314 /3.14 / 7.76 / 89.07) Yield for **4.2a**: 62%

- Organic concentration solution feedstock: 0.1 mol/L

  CO_2 Flow rate: 0.75 mL/min [**4.1a**/O_2/EtOAc/CO_2] molar ratio: (0.044 / 2.20 / 4.53 /93.23) Yield for **4.2a**: 75%;

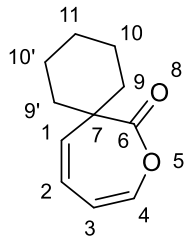
Isolated using flash chromatography with cyclohexane/EtOAc (8:2) as the eluent.

^{1}H NMR (400 MHz, CD_3OD) δ = 6.53 (d, *J* = 7.0 Hz, 1H, H4), 6.12 (dd, *J* = 10.2, 6.2 Hz, 1H, H2), 5.81 (dd, *J* = 7.0, 6.2 Hz, 1H, H3), 5.58 (dd, *J* = 10.2 Hz, 1H, H1), 1.35 (s, 6H, 2×CH3).

^{13}C NMR (400 MHz, CD_3OD) δ = 170.3 (C6), 141.6 (C4), 135.1 (C1), 126.1 (C2), 110.1 (C3), 46.3 (C7), 22.9 (C9 + C9‘).

HRMS (ESI): for $C_8H_{11}O_2$, $[M + H]^+$ calculated *m/z* = 139.0754, found *m/z* = 139.0755.

8-Oxaspiro[5.6]dodeca-9,11-dien-7-one (4.2b)



- Organic concentration solution feedstock: 0.1 mol/L

[**4.1b**/O_2/ EtOAc /CO_2] molar ratio: (0.044 / 2.20 / 4.53 / 93.23) in mol%. Yield obtained for **4.2b**: 66 %

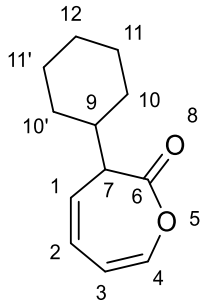
Isolated using flash chromatography with pentane/EtOAc (95:5) as the eluent.

^{1}H NMR (400 MHz, CD_3OD) δ = 6.51 (d, *J* = 6.9 Hz, 1H, H4), 6.15 (dd, *J* = 10.3, 6.2 Hz, 1H, H2), 5.78 (dd, *J* = 6.9, 6.2 Hz, 1H, H3), 5.50 (dd, *J* = 10.3, 0.7 Hz, 1H, H1), 1.93 (m, 2H, 2×H9), 1.74 (m, 2H, 2×H9’), 1.59 – 1.49 (m, 6H, 2×(H10 + H10’ + H11)).

^{13}C NMR (101 MHz, CD_3OD) δ = 168.3 (C6), 141.5 (C4), 133.3 (C1), 125.8 (C2), 109.4 (C3), 51.4 (C7), 31.6 (C9 + C9‘), 26.8 (C10 + C10‘), 23.8 (C11).

HRMS (ESI): for $C_{11}H_{14}O_2$, $[M + H]^+$ calculated m/z = 179.1067, found m/z = 179.1060.

3-Cyclohexyloxepin-2(3H)-one (4.2c)



- Organic concentration solution feedstock: 0.1 mol/L

[**4.1c**/O_2/EtOAc/CO_2] molar ratio: (0.044 / 2.20 / 4.53 / 93.23) in mol%. Yield obtained for **4.2b**: 64 %

- Organic concentration solution feedstock: 0.25 mol/L

[**4.1c**/O_2/EtOAc/CO_2] molar ratio: (93.11 / 2.20 / 4.58 / 0.1099) in mol%. Yield obtained for **4.2b**: 66%

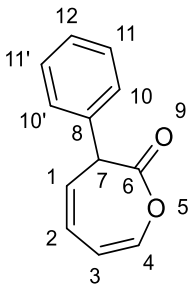
Isolated using flash chromatography with cyclohexane/EtOAc (9:1) as the eluent.

^{1}H NMR (400 MHz, CD_3OD) δ = 6.68 (d, *J* = 6.4 Hz, 1H, H4), 6.29 (dd, *J* = 9.4, 5.1, 2.1 Hz, 1H, H2), 6.02 (ddd, *J* = 6.4, 5.1, 1.1 Hz, 1H, H1), 5.72 (dd, *J* = 9.4, 5.6, 0.6 Hz, 1H, H3), 2.33 – 2.28 (m, 1H, H7), 2.12 – 2.01 (m, 1H, H9), 1.87 – 1.71 (m, 4H, 2×H10 + 2×H10'), 1.48 – 1.30 (m, 4H, 2×H11 + 2×H11'), 1.03 (m, 2H, 2×H12).

^{13}C NMR (101 MHz, CD_3OD) δ = 166.9 (C6), 141.5 (C4), 128.1 (C1), 126.7 (C2), 113.26 (C3), 53.2 (C7), 37.9 (C8), 32.5 (C10), 31.2 (C10'), 27.5 (C11), 27.2 (C11'), 27.0 (C12).

HRMS (ESI): for $C_{12}H_{16}O_2$, $[M + H]^+$ calculated m/z = 193.1229, found m/z = 193.1220.

3-Phenyloxepin-2(3H)-one[350] (4.2d)



- Organic concentration solution feedstock: 0.25 mol/L

[**4.1d**/O_2/EtOAc/CO_2] (in mol%) molar ratio (0.1099/ 2.20 / 4.58 /93.11) in mol%. Yield obtained for **4.2d**: 70 %

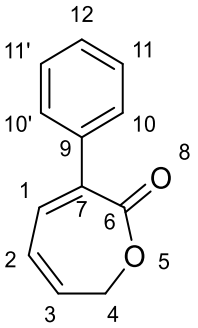
Isolated using flash chromatography with pentane/EtOAc (95:5) as the eluent.

^{1}H NMR (400 MHz, CD_3OD) δ = 7.45 – 7.38 (m, 5H, H attached benzene group), 6.78 (d, *J* = 6.8 Hz, 1H, H4), 6.38 (dd, *J* = 9.3, 5.2 Hz, 1H, H2), 6.11 (dd, *J* = 6.8, 5.2 Hz, 1H, H3), 5.97 (dd, *J* = 9.3, 5.2, Hz, 1H, H1), 3.90 (m, 1H, H7).

^{13}C NMR data and tentative assignment (101 MHz, CD_3OD) δ = 167.8 (C6), 142.1 (C4), 137.9 (C1), 132.9 (C8), 130.4 (C10 + C10'),129.6 (C11 + C11'), 128.7 (C12), 126.9 (C2), 113.7 (C3), 53.0 (C7).

HRMS (ESI): for $C_{12}H_{10}O_2$, $[M+]^+$ calculated *m/z* = 186.0681, found *m/z* = 186.0629.

3-Phenyloxepin-2(7H)-one (4.2d')



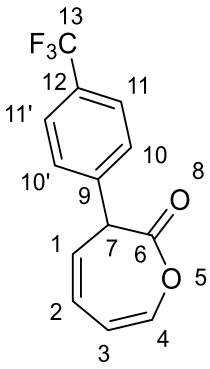
Isolated using flash chromatography on SiO_2 with pentane/EtOAc (95:5) as the eluent. Isolated yield was 20 %.

^{1}H NMR (400 MHz, CD_3OD) δ = 7.57 – 7.53 (m, 2H, H10 + H10'), 7.41 – 7.35 (m, 3H, H11 + H11' + H12), 7.05 (d, *J* = 5.6 Hz, 1H, H1), 6.71 (dd, J = 10.0, 5.6 Hz, 1H, H2), 6.57 (dt, J = 10.0, 6.2 Hz, 1H, H3), 4.64 (d, *J* = 6.2 Hz, 2H, CH2).

^{13}C NMR (101 MHz, CD_3OD) δ = 171.5 (C6), 139.8 (C8), 139.2 (C1), 134.7 (C7), 134.3 (C2), 132.9 (C3), 129.6 (C12), 129.5 (C10 + C10'), 129.2 (C11 + C11'), 63.6 (C4).

HRMS (ESI): for $C_{12}H_{10}O_2$, $[M + H]^+$ calculated *m/z* = 187.0759, found *m/z* = 187.0755.

3-(4-(Trifluoromethyl) phenyl)oxepin-2(3H)-one (4.2e)



- Organic concentration solution feedstock: 0.1 mol/L

[**4.1e**/O_2/EtOAc/CO_2] molar ratio (0.044/ 2.20 / 4.53 / 93.23) in mol%. Yield obtained for **4.2e**: 37 %

Isolated using flash chromatography with pentane/EtOAc (95:5) as the eluent.

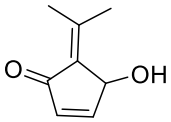
^{1}H NMR (400 MHz, CD_3OD) δ = 7.75 – 7.59 (m, 4H, H attached benzene group), 6.81 (d, *J* = 2.2 Hz, 1H, H4), 6.42 (ddd, *J* = 9.4, 5.2, 2.2 Hz, 1H, H2), 6.14 (dd, *J* = 5.2, 1.1 Hz, 1H, H3), 5.98 (dd, *J* = 9.4, 5.2 Hz, 1H, H1), 4.09 – 4.01 (m, 1H, H7).

^{13}C NMR data and tentative assignment (101 MHz, CD_3OD) δ = 167.2 (C6), 142.2 (C4), 136.1 (C9), 134.3 (C10), 133.9 (C10'), 131.3 (C11 + C11'), 130.0 (C1), 129.0 (C2), 127.3 (C12), 126.3 (C13, J^{C-F} = 3.86 Hz , 113.8 (C3), 52.6 (C7).

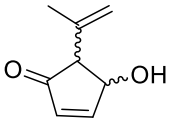
^{19}F NMR (376.4 MHz, CD_3OD) δ = -64.03.

HRMS (ESI): for $C_{13}H_9F_3O_2$,[M+H]$^+$calculated *m/z* = 255.0627, found *m/z* = 255.0641.

4-Hydroxy-5-(propan-2-ylidene)cyclopent-2-enone[345] (4.3) and 4-Hydroxy-5-(prop-1-en-2-yl)cyclopent-2-enone[354] (4.4a and 4.4a')



(4.3a)



(4.4a) and **(4.4a')**

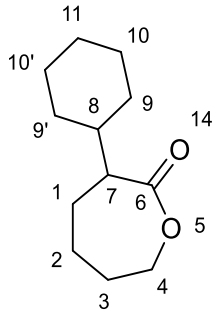
4-Hydroxy-5-(prop-1-en-2-yl)cyclopent-2-enone (**4.3a**) and 4-hydroxy-5-(propan-2-ylidene)cyclopent-2 enone (**4.4a**) and (**4.4a'**) were isolated as an inseparable mixture by flash chromatography (using pentane/EtOAc 9:1 as the eluent). Each peak was assigned and the data was in accordance with the literature referred above. NMR yield of **4.4a** and **4.4a**' was 49 %.

^{1}H NMR (400 MHz, CD_3OD) δ = 7.69 (dd, *J* = 5.8, 2.4 Hz, 1H, **4.4a**), 7.65 (dd, *J* = 5.8, 2.4 Hz, 1H, **4.4a'**), 7.39 (dd, *J* = 6.0, 2.5 Hz, 1H, **4.3a**), 6.27 (dd, *J* = 5.7, 1.5 Hz, 1H, **4.4a**), 6.25 (dd, *J* = 4.5, 1 Hz, 1H, **4.3a**), 6.21 (dd, *J* = 5.7, 1.5 Hz, 1H, **4.4a'**), 5.18 (d, *J* = 2.4 Hz, 1H, **4.3a**), 5.03 (ddd, *J* = 6.2, 2.4, 1.4 Hz, 1H, **4.4a'**), 4.99 (ddd, *J* = 6.2, 2.4, 1.4 Hz, 1H, **4.4a**), 5.03 (q, *J* = 1.6 Hz, 1H, **4.4a'**), 4.99 (q, *J* = 1.6 Hz, 1H, **4.4a**), 4.84 – 4.81 (m, 1H, **4.4a** and **4.4a'**), 3.26 (dd, *J* = 6.3, 0.7 Hz, 1H, **4.4a**), 2.88 (dd, *J* = 6.3, 0.7 Hz, 1H, **4.4a'**) 2.29 (s, 3H, **4.3a**), 2.08 (s, 3H, **4.3a**), 1.69 (dd, *J* = 1.5, 0.9 Hz, 3H, **4.4a**), 1.68 (dd, *J* = 1.5, 0.9 Hz, 3H, **4.4a'**).

^{13}C NMR (101 MHz, CD_3OD) δ = 210.3 (**4.4a**), 208.1 (**4.4a'**) 198.1 (**4.3a**), 166.0 (**4.4a**), 165.2 (**4.4a'**), 158.4 (**4.3a**), 152.4 (**4.3a**), 141.8 (**4.4a**), 137.55 (**4.4a**), 135.2 (**4.4a**), 134.6 (**4.4a'**), 132.8 (**4.3a**), 116.8 (**4.4a**), 115.6 (**4.4a'**), 76.1 (**4.3a**), 73.2 (**4.4a'**), 73.1 (**4.4a**) 72.0 (**4.3a**), 64.9 (**4.3a**), 59.8 (**4.4a**), 23.8 (**4.4a'**), 22.5 (**4.4a**), 20.4 (**4.3a**), 20.4 (**4.3a**).

HRMS (ESI): for $C_8H_{10}O_2$, [M + H]$^+$ calculated m/z = 139.0759, found m/z = 139.0755.

3-Cyclohexyloxepan-2-one (4.6)



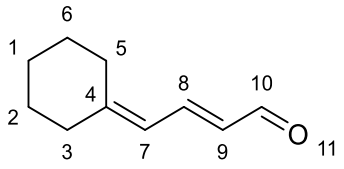
A solution of 3-cyclohexyloxepin-2(3H)-one (**4.2c**) (30 mg, 0.16 mmol) in 2 mL of EtOAc was hydrogenated over 5% Pd/C (34 mg) at atmospheric pressure for 3 h. After filtration through a pad of silica and evaporation, the desired product was obtained as an oil in a quantitative yield.

^{1}H NMR data and tentative assignment (400 MHz, CD_3OD) δ 4.43 – 4.19 (m, 2H, 2×H4), 2.56 (m, 1H. H7), 2.00 – 1.86 (m, 4H, 2×H9 + 2×H9'), 1.81 – 1.62 (m, 6H, 2×H1 + 2×H2 + 2×H3), 1.41 – 1.14 (m, 6H, 2×H10 + 2×H10' + 2×H11).

^{13}C NMR data and tentative assignment (101 MHz, CD_3OD) δ = 180.0 (C6), 69.5 (C4), 40.4 (C7), 32.0 (C1), 29.9 (C8), 28.8 (C2), 27.7 (C3), 27.6 (C9 + C9'), 27.5 (C10 + C10'), 27.0 (C11).

HRMS (ESI): for $C_{12}H_{20}O_2$, $[M + H]^+$ calculated *m/z* = 197.1536, found *m/z* = 197.1537.

(E)-4-Cyclohexylidenebut-2-enal (4.7)



^{1}H NMR yield was 80 %.

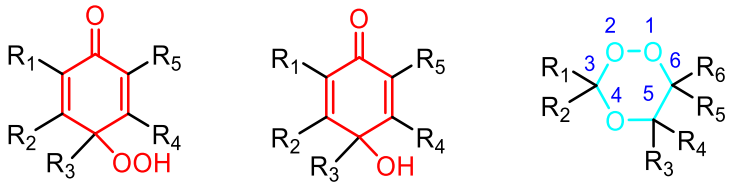
^{1}H NMR (400 MHz, CD_3OD) δ 9.52 (d, *J* = 8.1 Hz, 1H, H10), 7.70 (dd, *J* = 14.9, 11.6 Hz, 1H, H8), 6.17 (dq, *J* = 11.6, 1.1 Hz, 1H, H7), 6.09 (dd, *J* = 14.9, 8.1 Hz, 1H, H9), 2.58 – 2.45 (m, 2H, 2×H5), 2.37 – 2.27 (m, 2H, 2×H3), 1.73 – 1.61 (m, 6H, 2×H2 + 2×H6 + 2×H1).

^{13}C NMR data and tentative assignment (101 MHz, CD_3OD) δ = 196.6 (C10), 159.5 (C4), 150.7 (C8), 131.0 (C9), 122.3 (C7), 39.0 (C5), 30.9 (C3), 29.9 (C2), 29.3 (C6), 27.5 (C1). Isolated yield: 20 % for 45 mg.

HRMS (ESI): for $C_{10}H_{14}O$, $[M + H]^+$ calculated *m/z* = 151.1117, found *m/z* = 151.112.

Chapter 5. Flow Approaches for Dearomatisation of Phenols with $^1O_2$

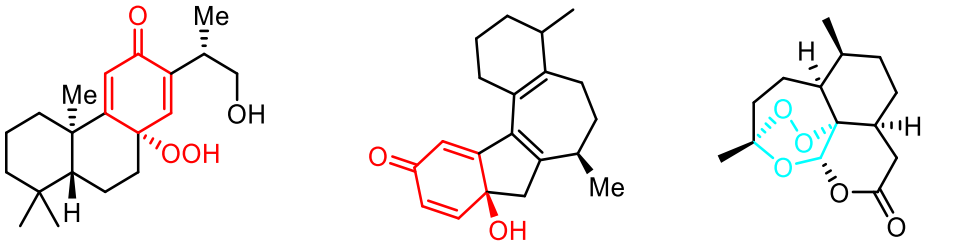
This Chapter describes the experiments performed in an attempt to realise an efficient and green continuous flow process for the dearomatisation of phenol derivatives and the synthesis of simple 1,2,4-trioxanes. The 4-alkyl-4-hydroperoxy-2,5-cyclo-hexadienones (***p*-peroxyquinols**) and 4-alkyl-4-hydroxy-2,5-cyclohexadienones (***p*-quinols**) are the dearomatisation products *via* photo-oxidation of *para*-phenol derivatives. The core structure of these products and further producing 1,2,4-trioxanes are presented in Scheme 5-1. The dearomatisation of *para*-alkyl phenols to *p*-peroxyquinols and *p*-quinols is of huge interest due to the presence of such derivatives in some natural products,[374-375] being valuable building blocks in organic synthesis[376] as well as novel therapeutic agents[377], taking natural products in Scheme 5-2 as an example. Many 1,2,4-trioxanes have demonstrated excellent



p-peroxyquinol *p*-quinol 1,2,4-trioxane

Scheme 5-1 The core structures are presented in some antimalarial and anticancer medicine, which are the focus of the work presented in this chapter.

antimalarial activity, such as natural product artemisinin in Scheme 5-2, which has been discussed previously in our group.[39] Herein, the methods for dearomatisation of *para*-alkyl phenol derivatives and a continuous daisy-chain process for the synthesis of 1,2,4-trioxane are focused on in this Chapter, such that a readily scalable process could be achieved.



Glutinosin C
p-Peroxyquinol

Frondosin C
(*p*-Quinol)

Artemisinin, **ART**

Scheme 5-2 Examples of natural p-peroxyquinol and p-quinol structures. Artemisinin is the example for the natural product antimalarial bearing a 1,2,4-trioxane pharmacophore.

An introduction to the dearomatisation of *para*-phenol derivatives is presented in Section 5.1, which includes the importance of dearomatisation of *para*-phenols with singlet oxygen ($^1O_2$) and the demand for the synthesis of 1,2,4-trioxanes compounds.

Starting with dearomatisation of *p*-cresol (**5.1a**) in the batch reaction in Section 5.2, followed by being scaled up experiments in high pressure continuous flow CO_2 system using methanol as co-solvent in Section 5.3 and the optimisation experiments are discussed. A scope of *para*-phenol derivatives with different functional groups with $^1O_2$ is conducted in the optimised condition of **5.1a**.

The subsequent daisy-chain cyclisation of photo-oxidation products with an aldehyde to synthesise 1,2,4-trioxane are discussed in Section 5.4, which demonstrated that acetal compounds were produced in protic solvent methanol and CO_2 system in the presence of acid. The alternative aprotic solvent ethyl acetate (EtOAc) as co-solvent is discussed for dearomatisation and cyclisation in Section 5.5 and Section 5.6. Finally, the effect of hexafluoro-2-propanol (HFIP) on the

dearomatisation and cyclisation with aldehyde catalysing by Amberlyst-15 are depicted in high pressure EtOAc and CO_2 system. Conclusions and future work for this Chapter are presented in Section 5.9.

5.1 Background

Phenol and its derivatives are pervasive in natural products, bioactive molecules and lignin, and also the most frequently utilised substrates for dearomatisation en route to exploiting their potential fully for complex natural products.[378-380] Phenols are the typical aromatic starting materials that have served over the years for the development of dearomatisation protocols. Thus, numerous methodological tactics have been implemented to accomplish this chemical task by relying on oxygenation, reduction, and cycloaddition reactions, and so on.[381-382]

5.1.1 General aspects of phenols

Phenols constitute an essential class of antioxidants that inhibit the oxidative degradation of organic materials. They also can be considered as the enol of cyclohexadienones, which are more acidic than aliphatic alcohols. With oxidising agents, a free radical could be readily formed from phenols, which can be oxidised to form dihydroxybenzenes and quinones.[383] The intriguing chemical properties have captured the attention of chemists from both industry and academia for centuries. Phenols are sensitive towards oxidation, because they are a class of electron-rich arenes containing a hydroxyl group bonded directly to the aromatic ring with an electronic subsystem that consists of 50 electrons. Due to that, phenols usually react further in three modes. They are susceptible to one-electron oxidation into delocalized phenoxy radical species, and can also be transformed into cationic electrophiles of the phenoxenium type or their equivalents by two-electron oxidation or activation through the use of “phenolophile” metal - or halogen-based reagents. Their non-

aromatic cyclohexadienones tautomers can also be stabilised through the formation of transition metal - arene complexes, which can then render them prone to cycloaddition and nucleophilic addition processes. Depending on their substitution pattern and functionalities, these phenols can be dearomatised into various reactive species such as quinones, quinone methides, and other quinone or quinol compounds (Figure 5-1).[384-386] In particular, it provides an efficient way *via* oxidation with phenolophile reagents to construct highly functionalised cyclohexadienones, which often appear in diverse biologically active natural products and pharmaceuticals.[387]

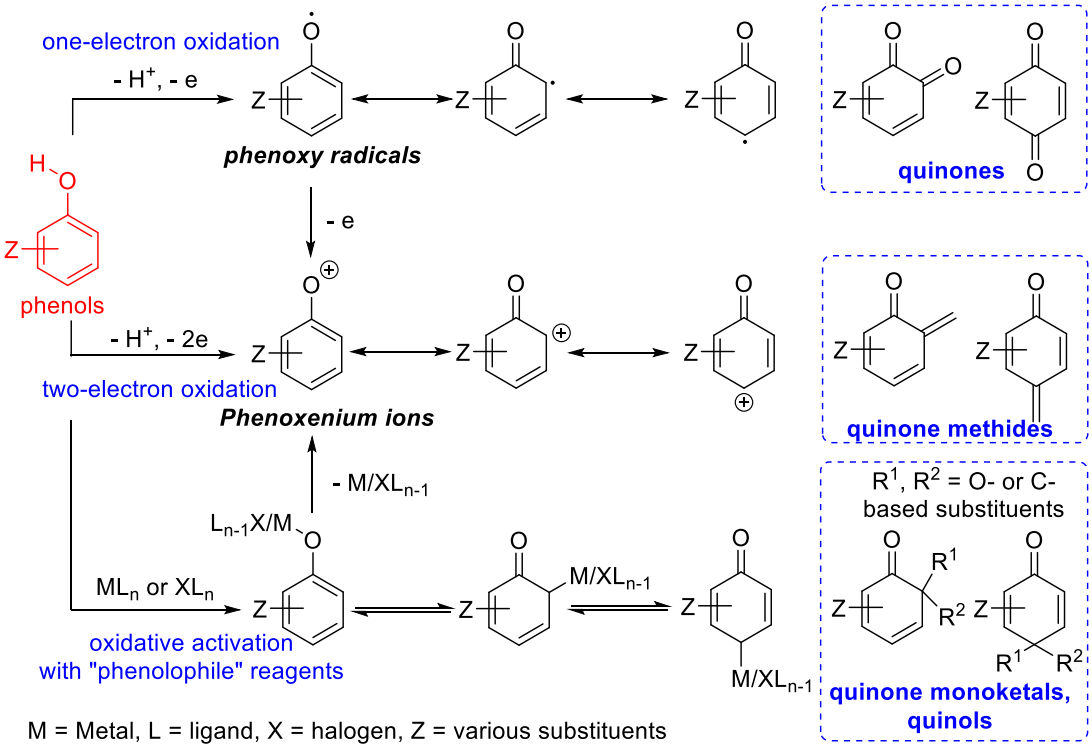


Figure 5-1 Various facets of the dearomatisation of phenols, reprinted from reference [388].

In this Chapter, one type of the dearomatisation product from *para*-substituted phenols, *p*-peroxyquinols, are attractive synthetic targets, given their widespread abundance in nature, with many displaying potent antimalarial and antimicrobial properties,[389-392] as well as being valuable building blocks in organic synthesis.[393]

Although natural products with peroxy functional group are abundant,[394] there are only a few natural derivatives with 4-hydroxy-2,5-cyclohexadienones structure.[395] Cyclisation 1,2,4-trioxane compounds from *p*-peroxyquinol can also have antimalarial activity.[396]

However, how to make them dearomatise efficiently and greenly has been a challenge for chemists for dozens of decades. The synthesis of *p*-peroxyquinols[397] is usually achieved by the reaction of *para*-substituted phenols with singlet oxygen,[398-399] irradiated by ultraviolet light (UV) in the presence of photosensitisers.[78] In addition, various oxidising systems based on heavy metals,[400-401] hypervalent iodine species[402-403] and other halogenated organic reagents,[404] as well as an oxone catalytic system,[405-406] have been developed to mediate the dearomatisation of *para*-substituted phenols.

5.1.2 Oxidation of *p*-alkyl phenol derivatives with transition-metal catalyst

Several strategies have been developed for accessing singlet oxygen involving the use of transition-metal ions in the presence of H_2O_2 or ^{t}BuOOH. In 1966, ruthenium-catalysed selective oxidative dearomatisation of *p*-substituted phenols into 4-(*tert*-butylperoxy)cyclohexadienones without substituents at the 2- or 6-positions in the presence of ^{t}BuOOH was firstly put forward by Murahashi's group; the products can be further reacted to produce 2-substituted quinones under acid conditions.[145] In 2011, the same group investigated the mechanism of this selective oxidation.[407] The mechanism is shown in Figure 5-2. Immediately afterwards, Doyle and co-workers reported the oxidation of phenols by treatment with 70 % aqueous *tert*-butyl hydroperoxide and dirhodium caprolactamate ($Rh_2(cap)_4$) as the catalyst.[408] Using ^{t}BuOOH as an oxidant for the oxidation of 2,4,6-trialkyl substituted phenols to 4-*t*-butylperoxy-2,5-cyclohexadiene-1-ones was achieved in the presence of heteropolyacids ($H_3PMo_{12}O_{40}\cdot nH_2O$) in Takehira's group.[409]

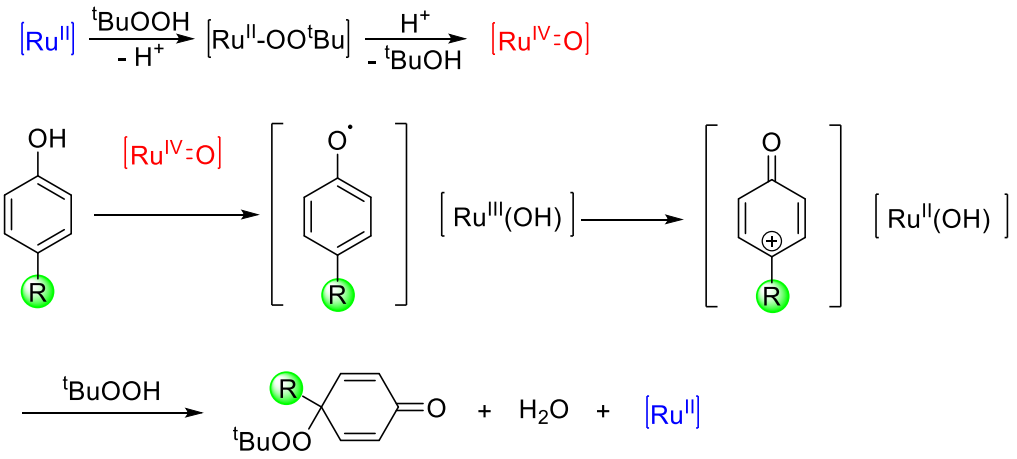


Figure 5-2 Proposed mechanism for ruthenium-catalysed selective oxidation of phenols.

Moreover, Matsuura's group showed that di-(3 - salicyclideneaminopropyl) aminecobalt(II)) could be used for selective catalytic autoxidation of 4-alkyl-2,6-di-t-butyl phenol to introduce oxygen at the *p*-position to give the corresponding *p*-peroxyquinol in good yield (Figure 5-3).[410]

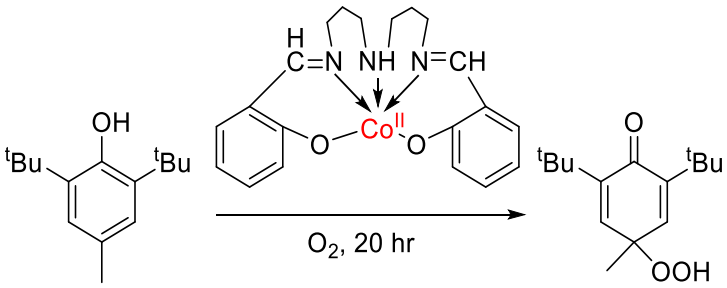


Figure 5-3 Selective oxidation at the p-position of p-substituted phenol with Co complex.

In the 1970s, following from the transition-metal catalysation of *p*-substituted phenols in Matsuura's group, Cr (VI),[411] K_3CrO_8,[412] Ce (IV)-H_2O_2 system,[413] catalysts were prepared for activating the oxidation of *p*-phenols *via* singlet oxygen. Another molybdate-exchanged (Mg, Al) layered doubled hydroxides catalyst, was introduced to generate singlet oxygen in the presence of H_2O_2, which can then perform selective oxygenations.[414] Based on this work, Jacobs and co-workers investigated the

bromide-assisted oxidation of *p*-alkyl phenols to *p*-quinols over WO_4^{2-}-exchanged layered double hydroxides in the presence of H_2O_2. They designed a one-pot metal-catalysed procedure for the high chemoselectivity for the desired quinol products to be reached.[404]

A copper-catalysed intermolecular asymmetric propargylic dearomatisation of *para*-substituted phenol derivatives has been realised.[415] Under catalysis of decorated $(CF_3SO_3Cu)_2 \cdot C_6H_6$, the dearomatisation reaction proceeded smoothly with excellent regioselectitives to produce a variety of optically active cyclohexadienones derivatives. Porco and co-workers developed another copper catalysed oxidative dearomatisation of phenols in the synthesis of bicyclo[2.2.2]octenones.[416] This reaction was dearomatisation to generate quaternary *o*-quinols in moderate yields but limited to 2-methyl-5-substituted phenols. When it was employed on 4-substituted phenols, it afforded dimeric structures.[417] Afterwards, Rooney and co-workers studied the phenol photo-oxidation catalysed by photosensitiser palladium@TiO_2 in a Taylor flow system.[418] In 2018, Cu-ZSM-5 and Fe-Cu-kaolinite catalysts were also prepared for photochemical degradation of *p*-substituted phenols for the treatment of wastewater, sludge, and bottom sediments.[419-420] Moreover, some different groups have also been studying the dearomatisation reactions of naphthol derivatives catalysed by iridium(II),[421-422] palladium(0),[423] and scandium(III).[424]

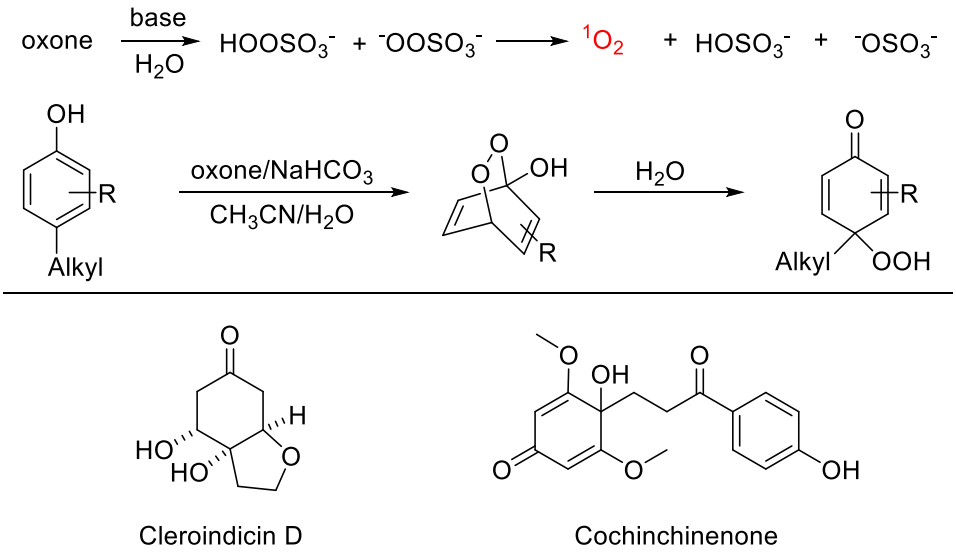
Most of the transition-metal catalytic reactions for the selective dearomatisation of *p*-substituted phenol derivatives involved the presence of H_2O_2 or ^{t}BuOOH. As in ruthenium(III) catalytic system, ^{t}BuOOH was used as co-oxidant.

5.1.3 **Photosensitised dearomatisation of *p*-substituted phenols**

The dearomatisation of phenols has been largely investigated with a transition-metal catalyst or hypervalent iodine catalysts as described above. Iodane-mediated catalysis are usually performed with stoichiometric amounts of iodane reagents, but also the catalytic use of transition-metal compounds together with a simpler terminal

oxidant is possible. Alternative methods using other oxidants have also been reported, such as using the singlet oxygen ($^1O_2$), generated from the oxone[405-406, 425] or photochemically in the presence of photosensitiser.[426-427]

Carreño and co-workers developed an efficient method for the selective oxidative dearomatisation of *p*-alkyl phenols to access *p*-peroxyquinols and *p*-quinols using oxone as a source of $^1O_2$.[428] They proposed a mechanism for the formation of *p*-peroxyquinols and presented evidence that $^1O_2$ is the reactive species from oxone. (Scheme 5-3)[429] This proved to be an interesting way for the synthesis of (±)-cleroindicin D (Scheme 5-3).[430] In 2012, this method was also used successfully for the total synthesis of natural *p*-quinol cochinchinenone, and the oxone-mediated oxidative dearomatisation of the corresponding ketone-containing *p*-substituted phenol was the key step in this synthesis.[395]

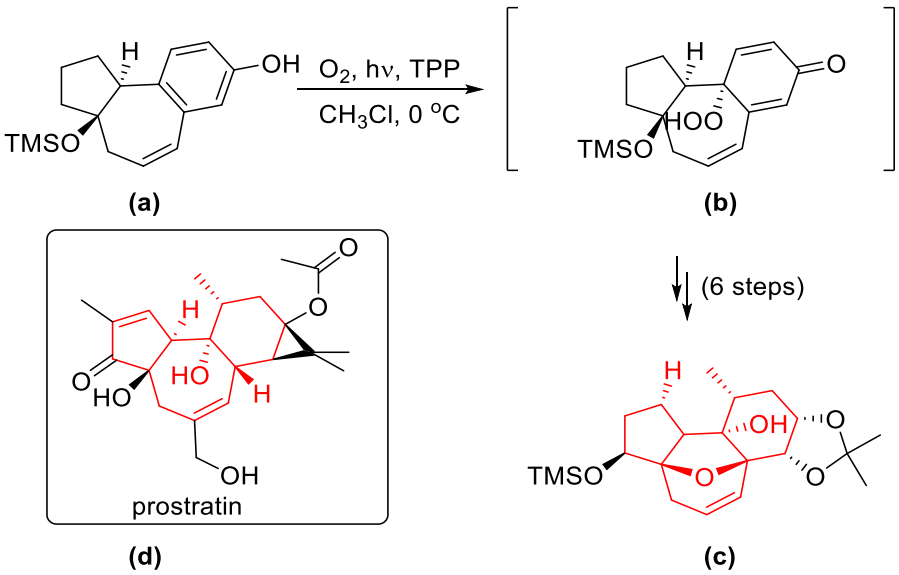


Scheme 5-3 Mechanism for the formation of p-peroxyquinols and generation of $^1O_2$ from oxone and the structures for cleroindicin D and cochinchinenone.

In 1965, Matsuura's group proposed the first photo-induced oxidation of *p*-phenols under the catalysis of photosensitisers.[431] His group examined the photochemical oxidation of hindered phenol, 2, 6-di-t-butyl-phenol using various photosensitisers, such as eosin Y, erythrosine, methylene blue, chlorophyllin, and

methyl orange. This difficult strategy was based on the mechanistic studies of Zwicker's group[432] and irradiation of phenols with ultraviolet light or visible light to form phenoxy radicals.[433] Sedee and co-workers in 1983 found that a bicyclic or steroidal phenol could be irradiated with visible light to form the corresponding hydroperoxide in the presence of methylene blue.[434]

Strategies also have been developed for accessing natural product phenols from $^1O_2$ under irradiation. An approach reported in 2014 used the TPP-sensitised photo - oxidation of phenol Scheme 5-4**(a)**, which led to its dearomatisation (Scheme 5-4)[435]. Singlet oxygen was added selectively access hydroxyperoxy quinol (Scheme 5-4**(b)**), then further leading to model compound (Scheme 5-4**(c)**), which has a [5-7-6] tricyclic core, similar to that for the natural product prostratin, Scheme 5-4**(d)**.



Scheme 5-4 Synthesis of Tigliane and Daphnane-type compounds.

A 2018 report described how the non-planar tetracyclic *p*-peroxyquinols, *p*-quinols, and a pentacyclic double peroxide, showing anticancer properties, were synthesised from the corresponding phenols under the wavelength-controlled irradiation (Blue LEDs) with air in acetone in the absence of an external photosensitiser,[436] as well as the methods used for the dearomatisation of phenol

derivatives, ozone or biocatalytic enzymes, also mediate the dearomatisation of *para*-alkyl phenol derivatives.

The well-known investigation of dearomatisation of *p*-phenols has been extensively studied in different mechanisms, like the transition-metal catalytic system, hypervalent iodine-mediated dearomatisation, as well as oxone and photooxidation in the presence of photosensitisers, described in Section 5.1. Most of them have promoted the application of phenols and can achieve the dearomatisation of phenols to access the different core structure of natural products, as well as for other reactions.

For the work described in this Chapter, the main aim was to develop a green and continuous flow process for the effective dearomatisation of *p*-phenols family. Herein, photo-oxidation of dearomatisation of *p*-phenols will be investigated in the high pressure liquid and supercritical CO_2 system, since the advantages of dense CO_2 being used as a solvent as well as the continuous flow reactor have been discussed in Chapter 1 and Section 3.1.

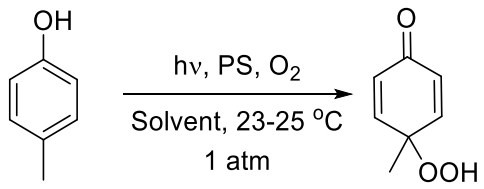
5.2 Photo-oxidation of *p*-cresol in Batch

Before performing the experiments in the high-pressure system with large scale, starting with the dearomatisation of *p*-cresol in a small batch reactor, different traditional solvents were screened. In all the batch experiments, the desired amount of **5.1a** and photosensitiser were dissolving in the required solvent, and oxygen was provided by a balloon filled with pure oxygen at 1 atm; then irradiated by LED light. The LED light source used for the batch experiments in this Chapter is one aluminium block (5 x Citizen Electronics Co. Ltd 1000 lumen white light LED arrays (CL-L233-C13N1-C)) with fan cooled.

5.2.1 **Screening of different organic solvents**

Both the photosensitisers, Rose Bengal and TPFPP (5,10,15,20-tetrakis-(pentafluorophenyl)porphyrin), can promote the production of peroxide in the traditional organic solvents. This reaction was catalysed by CO_2-soluble TPFPP, which is an efficient photosensitiser having been used in our previous work.[237] The results demonstrated that polar and protic solvent, like methanol, increased the yield of peroxide **5.2a** to 81% after irradiation by batch LED light in 5 hours, compared to aprotic solvents, such as acetonitrile or EtOAc (Table 5-1).

Table 5-1 Screen the solvents for the photo-oxidation of p-cresol in conventional solvents at 1 atm pressure.[a]



5.1a **5.2a**

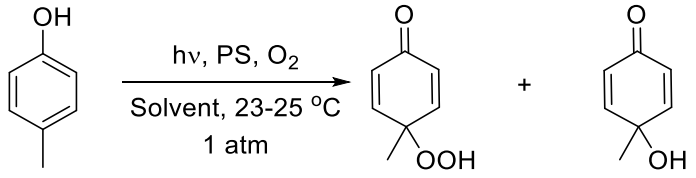
Entry	Solvent	Photosensitiser (mol %)	Reaction Time	Yield of 5.2a (%)[c]
1[b]	MeOH	Rose Bengal (1 mol%)	5 h	64
2	MeOH	TPFPP (0.1 mol%)	5 h	81
3	MeCN	TPFPP (0.1 mol%)	5 h	32
4	MeCN/H_2O (1:1)	TPFPP (0.1 mol%)	5 h	79
5	EtOAc/MeOH (1:1)	TPFPP (0.1 mol%)	4 h	41
6	EtOAc/MeOH (1:1)	TPFPP (0.1 mol%)	5 h	48
7	EtOH	TPFPP (0.1 mol%)	5 h	39
8	EtOH/H_2O (8:2)	TPFPP (0.1 mol%)	5 h	48

[a]: All the experiments were running in a 1 mmol scale *p*-cresol (**5.1a**) (0.067 M), at room temperature and atmospheric pressure, unless otherwise stated. [b]: Conducting the reaction according to the literature.[437] [c] Yield was calculated from ^{1}H NMR spectroscopy using biphenyl as internal standard.

5.2.2 **The screen of different co-catalysts**

Since protic solvents appeared beneficial for the production of peroxide, triethylamine (TEA, 5 mol%) or acetic acid (5 mol%) were added to investigate their effect on this [4+2] cycloaddition reaction. The yield of **5.2a** was 68 % in growth in the presence of TEA (Table 5-2, entry 1), but the presence of acetic acid inhibited the photo-oxidation step (Table 5-2, entry 4), the yield of **5.2a** was reduced to 47 % in 5 h.

*Table 5-2 The effect of co-catalysts on the dearomatisation of **5.1a** in conventional solvent at 1 atm pressure.*[a]



5.1a **5.2a** **5.2aa**

Entry	Solvent	Photosensitiser (mol %)	Co-catalyst[c]	Yield of 5.2a (%)	Yield of 5.2aa (%)[e]
1	EtOAc/	TPFPP (0.1 mol%)	TEA	61	2
2	MeOH(1:1)	TPFPP (0.1 mol%)	TEA	68	2
3	MeOH	TPFPP (0.05 mol%)	-	70	-
4	MeOH	TPFPP (0.05 mol%)	AcOH	47	-
5[b]	MeOH	TPFPP (0.05 mol%)	AcOH	n.d[d]	

[a]: All the experiments were running in a 1 mmol scale p-cresol, **5.1a** (0.067 M) for 5 hours, at room temperature and atmospheric pressure, unless otherwise stated. [b]: Using **5.2a** as a starting material.[c]: 0.5 equivalent for each co-catalyst. [d]: No **5.1a** was detected. [e] Yield was calculated from ^{1}H NMR spectroscopy using biphenyl as internal standard.

However, the addition of TEA also triggered the side reaction to produce a trace amount of **5.2aa** (Table 5-2, entry 1). When using **5.2a** as starting material catalysed by acetic acid, no **5.1a** was detected after stirring for 5 h (Table 5-2, entry 5). This demonstrated that the dearomatisation of **5.2a** was not a reversible reaction in the

presence of acetic acid. The inhibition effect of acetic acid was probably due to the decomposition.

5.3 Dearomatisation of *p*-cresol in high pressure setup

5.3.1 High Pressure Setup

After testing the photo-oxidation of **5.1a** in batch on a small scale, and a good result was obtained, the high-pressure rig was employed for this reaction.[237, 293] It should only be used with the proper safety training, especially for reactions to produce peroxides which are potentially explosive. A simplified schematic for high-pressure setup is shown in Figure 5-4 as below.

To investigate the miscibility of highly polar phenol derivatives in nonpolar supercritical CO_2, a very brief phase behaviour study was carried out with collaboration with Dr Jie Ke in the high-pressure rig within the sapphire tube reactor, and the results are shown in Experimental Section 5.10. A co-solvent is necessary to solubilise the model substrate, *p*-cresol, since it is solid at room temperature. According to the results obtained from the batch reaction conducted in traditional solvents, methanol was the most suitable solvent for the production of peroxide. Hence, methanol was chosen as the co-solvent to make a homogenous **5.1a** solution for being pumped into the CO_2 stream. Investigating different conditions provided the results that the solution of **5.1a**, methanol, and CO_2 was homogeneous. (Further details are presented in Section 5.10.3) It reduces the potential safety risks caused by the large concentration of oxygen in the organic phase.

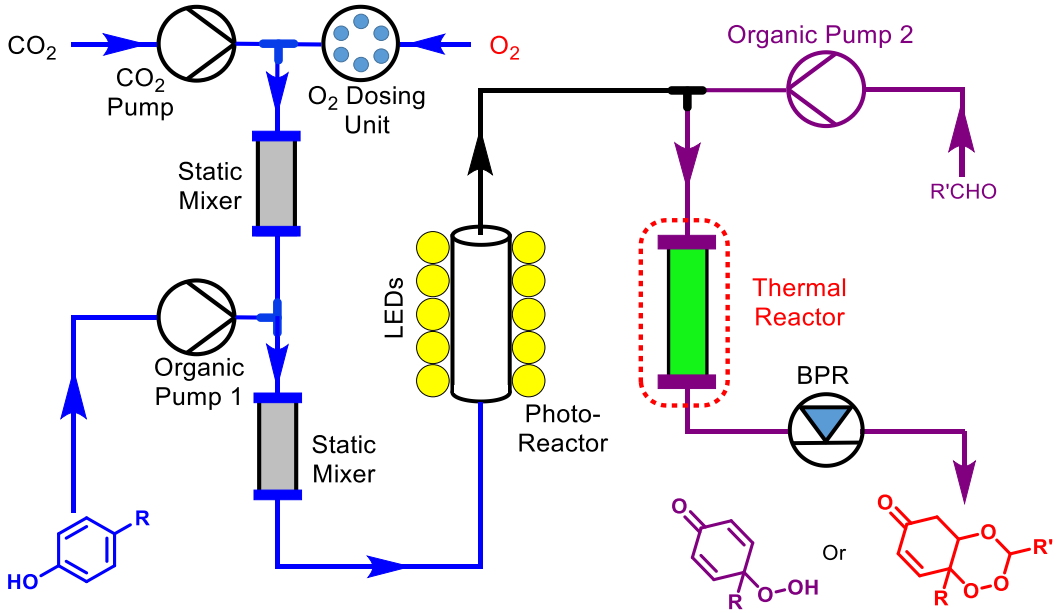


Figure 5-4 Simplified diagram for high pressure continuous flow setup. CO_2 is supplied from a chilled CO_2 pump and O_2 is dosaged at a known amount via a Rheodyne Dosage Unit. Static mixer 1 consists of a stainless steel tubular reactor loaded with sand to promote the mixing of CO_2 and O_2. The reagents and photosensitiser are pumped by organic pump 1 and then mixing with gases in static mixer 2, which is also a stainless steel tube filled with sand. The mixture is then flowed upwards through a high-pressure sapphire tube reactor which filled with glass beads for mixing, irradiated by LED lights. Downstream of the photoreactor is a thermal reactor. This thermal reactor consists of a stainless steel tubular reactor loaded with a solid catalyst and a heating block. A second organic pump is added before the thermal reactor (shown in red). The thermal reactor and second pump are added depending on the reaction. The mixture passes through the back pressure regulator before further analysis is carried out. (A full diagram of each set-up and the information about the LED light set are provided in the Experimental section 5.10).

5.3.2 **Oxidation of *p*-alkyl phenol derivatives by hypervalent iodine**

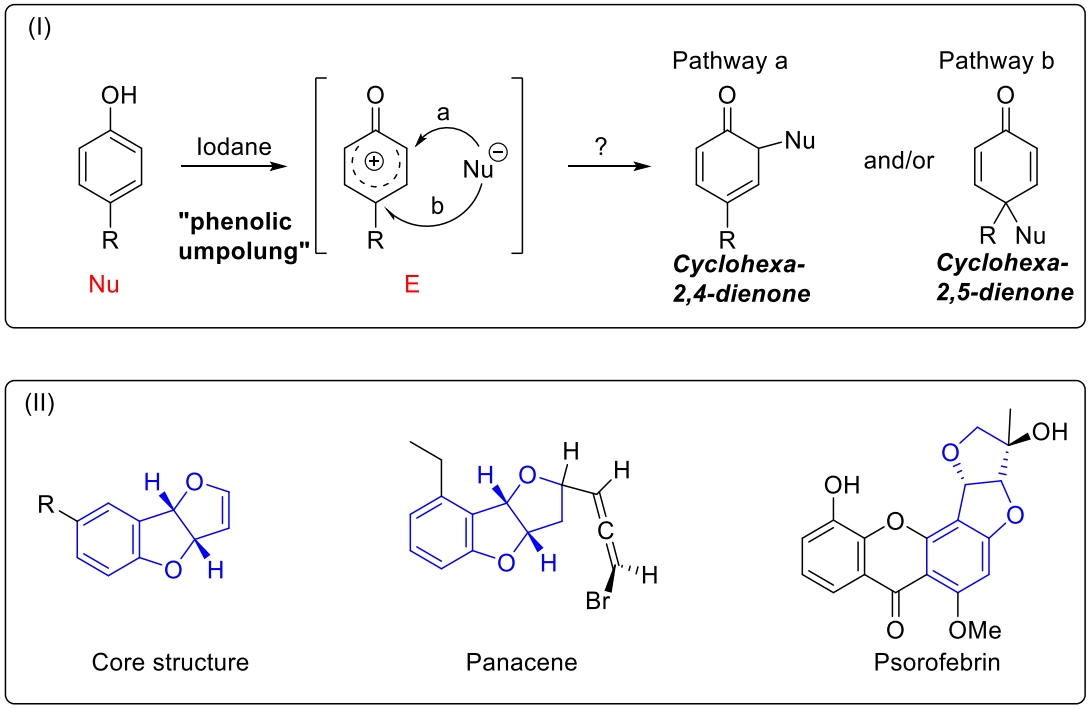
Transition-metal catalysed dearomatisation has been developed in the past few years employing electron transfer. Hypervalent iodine reagents also can be used as oxidants in organic synthesis, and their chemical properties in many aspects are similar to the derivative of heavy metals.[438] However, hypervalent iodine as oxidant is much more attractive in the dearomatisation of *para*-substituted phenols and is

regarded as of low toxicity, in contrast to many metal oxidants.[439] Moreover, iodine compounds are mild, stable, ready availability, easy to handle and eco-compatible reagents, advantageously competing with heavy metals. As such, it is not surprising that iodine catalysis has attracted the interest of the synthetic community in the field of asymmetric synthesis with the aim of developing greener and more environmentally benign chemistry, as well as being popular in the field of the dearomatisation oxidation reaction of phenols.[440]

In pioneering work, Siegel and Antony described the first oxidative dearomatisation of *para*-substituted phenols mediated by iodoarene diacetates.[441] Hypervalent iodine(III) and iodine(V) reagents (i.e., λ^3-iodanes and λ^5-iodanes, respectively) such as phenyliodoso diacetate (PIDA), and [bis(trifluoroacetoxy)iodo]benzene (BTI), and 2-iodoxybenzoic acid (IBX) have been extensively employed in phenolic coupling-mediated product synthesis by White[442] and Schwartz,[443] and further ground-breaking developments by Kita,[444] Lewis,[445] Quideau,[446] and Pelter[447].

A possible approach to extend the application of hypervalent iodine to aromatic derivatives involved the formation of an electrophilic intermediate from the corresponding aromatic ring. The phenolic intermediate then was transferred into cyclohexa-2,4 or -2,5-dienones catalysed by a mild and environmentally acceptable iodane (Scheme 5-5).[381, 448] Such transformations rely on the electrophilic character of the hypervalent iodine centre and conceptually impose a switch to phenols from being nucleophiles to being electrophiles. This ‘phenolic umpolung’, also more generally referred to as ‘aromatic ring umpolung’ has been developed in the work of Kita,[444, 449-450] then facilitates attack of nucleophiles at the *orth*- or *para*-carbon centres of the starting phenol thus oxidatively active. Kita and co-workers have shown that phenols[451, 452]can be activated under the influence of hypervalent iodine reagents such as λ^3-iodane or λ^5-iodane leading to “E” (Scheme 5-5 (I)). The electrophilic species “E” tends to react at the 4-position (e.g. Reaction mode b), at least with

heteronucleophiles. Reaction mode a generally occurs best in solvents such as trifluoroethanol (TFE) or hexafluoroisopropanol (HFIP), just as demonstrated by Kita[453-454] and Canesi's[455] group. In 2010, Canesi and co-workers employed the strategy of "aromatic ring umpolung" to access the main core structure of natural products, such as panacene and psorofebrin (Scheme 5-5 (II)).[456]

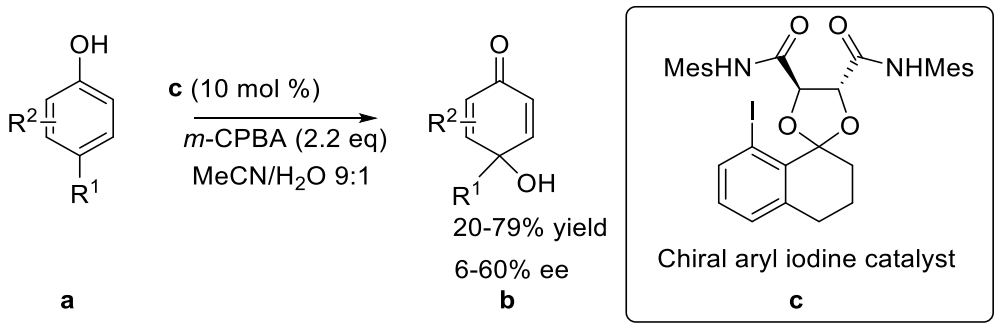


Scheme 5-5 Investigating (I)Iodane-mediated (oxygenation) dearomatisation of phenols into cyclohexadienone; (II) Structures of panacene and psorofebrin.

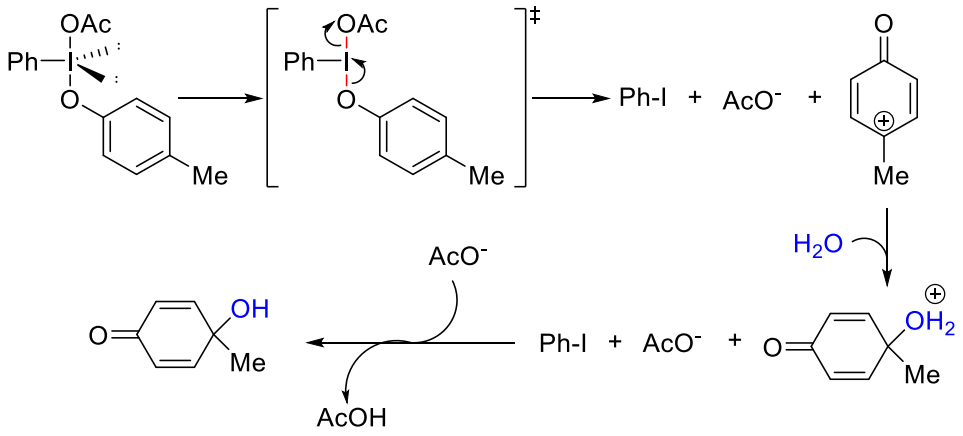
Quideau and co-workers also investigated the formation of orthoquinone monoketals from *para*-substituted phenols and a chiral ethanol unit *O*-tethered to the ortho position of this phenol.[451] In this condition, although PIDA (λ^3-iodane) was used as oxidant in the presence of 2,2,2-trifluoroethanol(TEE) at -35 °C, the active site was at the *ortho*-position, and the substituent at the *para*-position was supposed to prevent or at least retard the self-dimerisation of the dearomatised species through [4+2] cycloaddition events.[457-458] In 2016, Alaniz and co-workers developed a one-pot synthesis of anilines and nitrosobenzene from phenols, which were oxidised by phenyliodoso diacetate (PIDA) in methanol; this strategy can be a green method to

access anilines instead of the use of toxic thallium (III) nitrate.[459-460] As well as the single oxidant λ^3- or λ^5-iodane, oxone also can be used a co-oxidant. For example. Yakura and co-workers investigated oxone oxidised the iodoarene to tri- or pentavalent iodine species, which then oxidised *para*-alkoxyphenol to yield *p*-quinone.[461]

The asymmetric dearomatisation of phenol derivatives by hypervalent iodine catalysts is of particular interest for the synthetic community as it can be a pivotal step in the total synthesis of natural products.[462] In 2013, Harned's group prepared a new aryl iodine reagent (Scheme 5-6 **c**) starting from 8-iodotetralone and tartaric acid. The combination of 10 mol% of catalyst (Scheme 5-6 **c)** and 2.2 equivalent of 3-chloroperbenzoic acid (*m* - CPBA) could promote the conversion of phenols to the corresponding 2,5-cyclohexadienones, Scheme 5-6 **b**, in moderate to good yields.[463] The same group recently studied the mechanism of iodine(III)-mediated oxidative dearomatisation of phenols by DFT. They shed light on the nature of phenol oxidation by iodine(III) reagents and external nucleophiles. Their results showed that the intermediate proceeded through a phenoxenium ion as shown in Scheme 5-7.[403] Asymmetric iodine-mediated catalysis has been used extensively by Singh[402], Fujita[464], and Claraz's group[465].



Scheme 5-6 Asymmetric iodine catalysis-mediated dearomatisation of phenols by m - CPBA.



Scheme 5-7 Suggesting mechanism of iodine(III) - mediated dearomatisation of phenols

The hypervalent iodine(III) and iodine(V) reagents have been extensively employed in the dearomatisation of phenols to access the core structure of many natural products. Also, the mechanism of iodine-mediated catalysis of phenols has been explored. It was observed that the regioselectivity was largely dependent on the nature of the iodine catalytic system. The conclusion is that iodine-mediated catalysts can be used for the asymmetric synthesis to achieve the enantioselective oxidative products, but only the moderate yields and enantioselectivities were obtained.

5.3.3 **The yield of peroxide dependence on the co-catalysts**

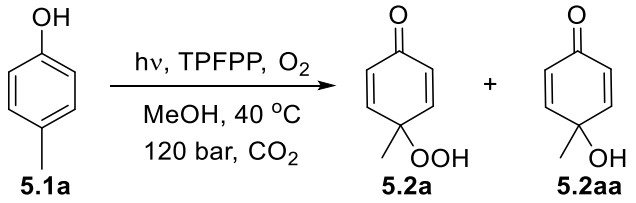
As the effect of a base catalyst on the photo-oxidation of **5.1a** has been explored in batch experiments, the results appeared that different base catalysts could be used to increase the yield of peroxide **5.2a**. Starting with the photo-oxidation of **5.1a** in high-pressure sapphire tube reactor (10 mm o.d., 120 mm length), methanol was used as co-solvent and TPFPP as photosensitiser. These experiments were conducted at 40 °C, 120 bar, the concentration of **5.1a** in co-solvent was 0.1 M, with the ratio of TPFPP to **5.1a**, 0.1 mol %. An example of these numbers for the molar composition and flow rate were depicted in Table 5-3.

*Table 5-3 An example of required parameters to conduct a photo-oxidation experiment in a high-pressure system, specifically in the case of p-cresol (**5.1a**) to peroxide (**5.2a**), using methanol as co-solvent and TPFPP as photosensitiser. For this particular experiment, the ratio of TPFPP to p-cresol was 0.1 mol %; the concentration of **5.1a** in methanol was 0.1 M.*

Parameter	Value	Unit
Volume rate of **5.1a** solution	0.1	mL/min
Volume Rate of CO_2	0.37	mL/min
Percentage of O_2 in CO_2	3.96	mol %
O_2 Cylinder Pressure	180	Bar
System Pressure	120	Bar
Sample Loop Volume	50	µL
Required Switch Rate of Dosage Unit	13.3	seconds
O_2: **5.1a** Ratio	20:1	mol: mol

The experimental results are presented in Table 5-4. Firstly, this experiment was performed without co-catalyst in methanol and CO_2; the yield of **5.2a** was 35% when the residence time in the photoreactor was 7 min (Table 5-4, entry 1). Instead of methanol, EtOAc was used as co-solvent, and no peroxide was observed in this condition (Table 5-4, entry 2). Therefore, compared to the photo-oxidation of cyclopentadiene and fulvenes in Chapter 3 and Chapter 4, the reaction rate of dearomatic oxidation of phenol derivatives was significantly slower. This results from the π-system in the phenol aromatic compounds, which is quite stable and not easy to break. To increase the residence time for the photo-oxidation step, a double-sized volume of photoreactor (10 mm o.d., 240 mm length) was utilised, see details in Section 5.10.2. Different organic and inorganic base catalysts, such as TEA, DBU and K_2CO_3 were screened. The highest peroxide yield of 82% was obtained in the presence of 5 mol% of DBU compared to TEA and K_2CO_3 as co-catalysts (Table 5-4, entries 4-6) when the residence time was 26 minutes. The reason is that pKa of DBU is higher than TEA and K_2CO_3. The yield of **5.2a** was up to 72% even without a base catalyst (Table 5-4, entry 7). In contrast, the presence of base catalysts promotes the

*Table 5-4 The yields of **5.2a** and **5.2aa** dependence on co-catalysts in high-pressure CO_2 system.*[a]



5.1a **5.2a** **5.2aa**

Entry	Co-catalyst	Org. pump (mL/min)	CO_2 pump (mL/min)	Residence time (min)	Yield of 5.2a	Yield of 5.2aa
1[b]	-	0.05	0.37	7	35%	-
2[b, c]	-	0.05	0.37	7	0	-
3[d]	TEA (5 mol%)	0.05	0.15	26	77%	-
4	TEA (5 mol%)	0.05	0.15	26	77%	3%
5	DBU (5 mol%)	0.05	0.15	26	82%	5%
6	K_2CO_3 (5 mol%)	0.05	0.15	26	76%	8%
7	-	0.05	0.15	26	72%	-
8	DBU (20 mol%)	0.05	0.15	26	81%	9%
9	DBU (20 mol%)	0.1	0.45	13	73%	12%
10	DBU (20 mol%)	0.15	0.45	9	53%	13%

[a]: All the experiments were performed using methanol as co-solvent, the concentration of **5.1a** in co-solvent was 0.1 M, and the concentration of TPFPP was 0.1 mol% of **5.1a** unless otherwise stated. [b]: This experiment was conducted in the previous photoreactor (10 mm o. d., 120 mm long). [c]: This experiment was performed in EtOAc. [d]: H_2O (12.5 mol%) was added. The yield was calculated by ^1H NMR spectroscopy using biphenyl as internal standard.

producing of side-product **5.2aa**, the yield of which increased with the increasing amount of base catalysts (Table 5-4, entries 4-10). Increasing the flow rate of the organic pump and CO_2 pump in the presence of 20 mol% of DBU, the yield of

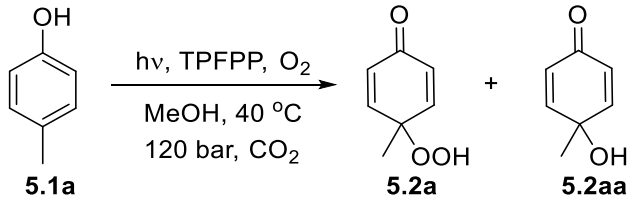
peroxide **5.2a** diminished from 81% to 53%, since the residence time reduced from 26 min to 9 min.

5.3.4 The effect of concentration of *p*-cresol in MeOH

After screening different inorganic and organic base catalysts, increasing the concentration of substrate in methanol from 0.1 M to 2.0 M, keeping the ratio of TPFPP to **5.1a** at 0.1 mol% and using 5 mol% DBU as co-catalyst, the yield of **5.2a** ranged from 82 % to 91 % when the residence time was 26 min. In this process, the yield of **5.2aa** stayed at 5-6 % (Table 5-5, entries 1-4). The yield of **5.2a** increased with increasing concentration of **5.1a** since the production of **5.2a** from **5.1a** was a second-order reaction. It reduced to 77% when the residence time was 13 min by doubling the flow rate of the organic pump and CO_2 pump. However, it decomposed to 45 % in the presence of DBU overnight with polymerisation occurring,[466] with the yield of **5.2aa** increasing from 10 % to 20 % (Table 5-5, entries 5-6).

Since **5.2a** was not stable in the DBU solution, the yield of **5.2a** was up to 91 % without the co-catalyst DBU at 2.0 M (Table 5-5, entry 7), and the yield of by-product **5.2aa** reduced from 6 % to 1 %. The results demonstrated that a high concentration of DBU was not suitable for the synthesis of peroxide **5.2a** from **5.1a** as **5.2a** polymerised with the help of DBU. Increasing the concentration of **5.1a** to 3.0 M gave 96 % of peroxide **5.2a** and 94 % even at 5.0 M (Table 5-5, entries 8 and 10). If reducing the residence time form 26 min to 13 min, the yield of **5.2a** was still 78 % at 3.0 M, but the BPR blocked when using 0.2 mL/min flow rate of CO_2 (Table 5-5, entry 9 and 10). The blockages were caused by the massive evaporation of methanol with a large amount of CO_2 releasing after BPR.

*Table 5-5 Yields of peroxide **5.2a** dependence on the concentration of **5.1a** and residence time.[a]*



5.1a **5.2a** **5.2aa**

Entry	Conc. (M)	Organic. pump (ml/min)	CO_2 pump (ml/min)	Residence time (min)	[d]Yield of 5.2a	[d]Yield of 5.2aa
1	0.1	0.05	0.15	26	82 %	5%
2	0.5	0.05	0.15	26	91 %	5 %
3	1.0	0.05	0.15	26	90 %	5 %
4	2.0	0.05	0.15	26	87 %	6 %
5	2.0	0.1	0.3	13	77 %	10 %
6[b]	2.0	0.1	0.3	13	45 %	20 %
7	2.0	0.05	0.15	26	91 %	1 %
8	3.0	0.05	0.15	26	96 %	<1 %
9	3.0	0.05	0.3	15	Blocked	
10	3.0	0.1	0.3	13	78 %	<1 %
11[c]	5.0	0.05	0.15	26	94 %	-

[a]: Full conversion for entry 4. [b]: Analysis was carried out after leaving the sample of room temperature overnight. [c]: The BPR blocked after running for 4 hours. The concentration of TPFPP was 0.1 mol % of **5.1a** (entries 1-7) and 0.05 mol % of **5.1a** (entries 8-11). Entries 1 - 6: with 5 mol % DBU; entries 7-11: without co-catalyst. [d] Yield was calculated from ^{1}H NMR spectroscopy using biphenyl as internal standard.

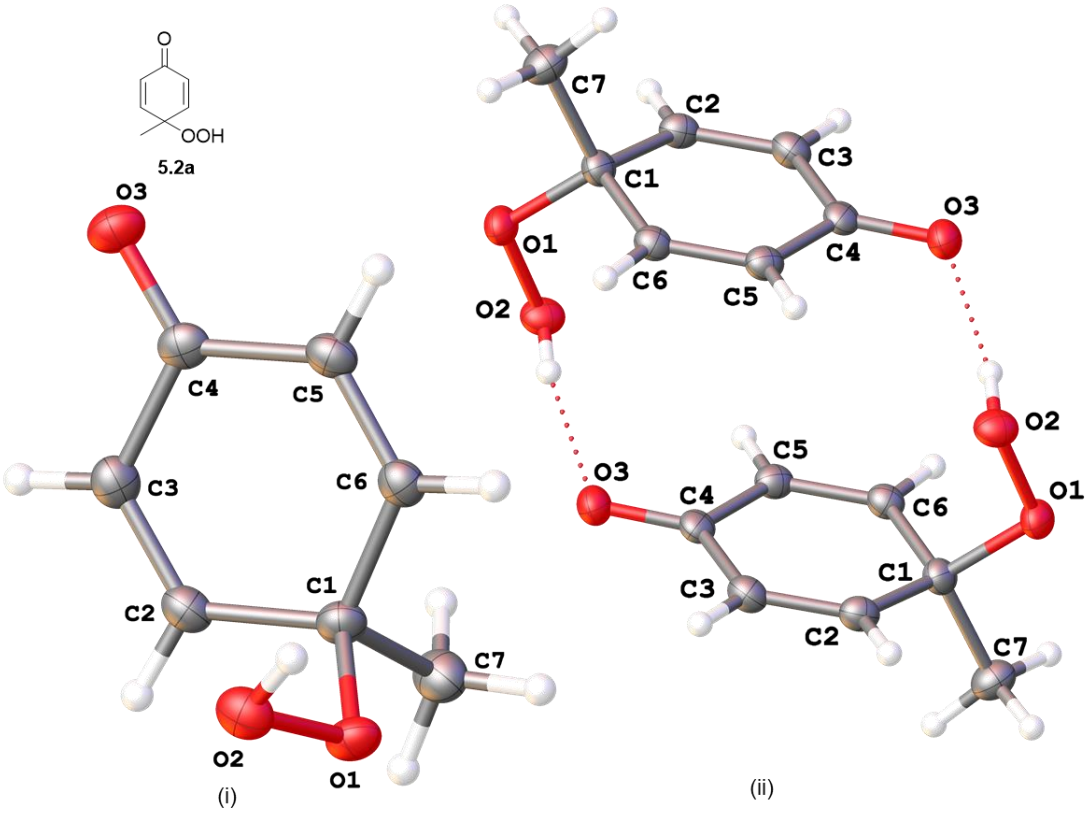


*Figure 5-5 Molecular structure of **5.2a** with anisotropic displacement ellipsoids set at 50% probability, single-crystal X-ray structure obtained from a crystal formed in the crude (i), hydrogen bonding for the single crystal (ii).Selected bond lengths (Å) and angles (°) for **5.2a**. **5.2a**: C(1)-C(2) 1.473(2); C(2)-C(3) 1.335(2); C(3)-C(4) 1.498(2); O(9)-O(10) 2.795(1); O(9)-H-O(10) 167(2); C(2)-C(3)-C(4) 123.49 (12); C(3)-C(2)-C(1) 120.71(12). Other relevant bond length and angles are provided in Appendix.*

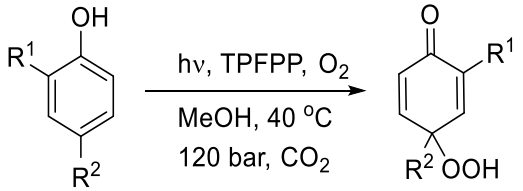
The absolute structure of **5.2a** was confirmed by X-ray crystallography, shown in Figure 5-5. The crystal was obtained directly from the crude after the BPR when the co-solvent was evaporated in the atmosphere. The structure in Figure 5-5 (i) is the single-crystal confirmed by X-ray crystallography. Interesting, this *p*-peroxyquinol was crystalised with two hydrogen bonds between two molecules as depicted in Figure 5-5 (ii). Both the distances of hydrogen bond from H to O3 is 1.96 (2) Å; further details are shown in the Experimental Section 5.10 at the end of this chapter.

5.3.5 **The scope of different phenol derivatives**

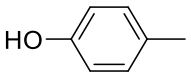
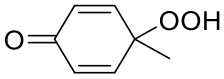
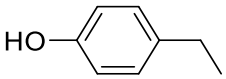
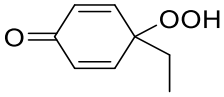
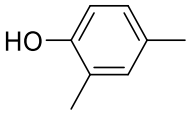
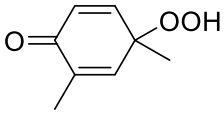
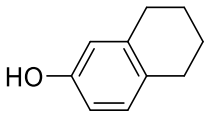
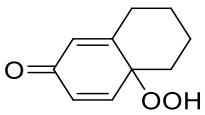
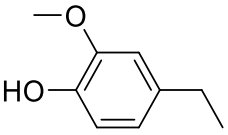
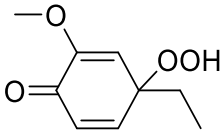
With the optimal dearomatisation of p-cresol conditions in hand, we examined different phenol derivatives in this high-pressure setup. The yield and productivity in two different conditions are shown in Table 5-6. When increasing the flow rate of the organic pump and CO_2 pump, high productivities of **5.2a**-**5.2e** were obtained at the cost of yield to some extent. 96 % yield and 29 g/day of productivity of **5.2a** were achieved under these conditions as specified in the table that the flow rate of the organic pump was 0.05 mL/min and the flow rate of $CO_2$was 0.15 mL/min. However, projected productivity of **5.2a** was 47 g/day at 0.1 mL/min of organic pump and 0.3 mL/min CO_2 pump flow rate because the yield of **5.2a** was reduced by only 18 % even with twice flow rate (Table 5-6, entry 1).The recovery of the product **5.2a** was 92 %, which has been examined by NMR and HPLC. Excellent yields were obtained for substrate **5.1a-5.1d**, which were higher than 90 % under condition **A** (Table 5-6, entries 1-4). In particular, for substrate **5.1d**, near quantitative yield was achieved under conditions **A**, and the projected productivity was up to 67 g/day under condition **B**. This is very promising for scaling up.

When employing the phenol derivative, 2-methoxy-4-ethylphenol (**5.1e**), with methoxy group attached in the *ortho*-position, the yield for **5.2e** was 85 % with residence time 26 min under condition **A**. The yield dropped to only 34 % if decreasing the residence time to 13 min under condition **B**. This resulted from that the methoxy group was an electron donating group, which would affect the electron distribution in the beneze ring. This changed the way of photocycloaddition intermediate after [4+2] isomerisation to peroxide.

Table 5-6 Scope of different phenol derivatives.[a]



1a-1e **2a-2e**

Entry	Substrate (5.1a-5.1e)	Product (5.2a-5.2e)	Condi -tion	Yield of product 5.2a-5.2e	Productivity of product 5.2a-5.2e (/Day)
1			**A**	96 %	29 g
			B	78 %	47 g
2			**A**	93 %	31 g
			B	83 %	55 g
3			**A**	94 %	31 g
			B	83 %	55 g
4			**A**	>99 %	39 g
			B	86 %	67 g
5			**A**	85 %	34 g
			B	34 %	27 g

[a]: Concentration of phenol derivatives in methanol was 3.0 M; concentration of TPFPP was 0.05 mol % of substrate; Condition **A**: organic pump flow rate: 0.05 mL/min; CO_2 pump flow rate: 0.15 mL/min; residence time: 26 min; Condition **B**: organic pump flow rate: 0.1 ml/min; CO_2 pump flow rate:0.3 ml/min; residence time: 13 min.

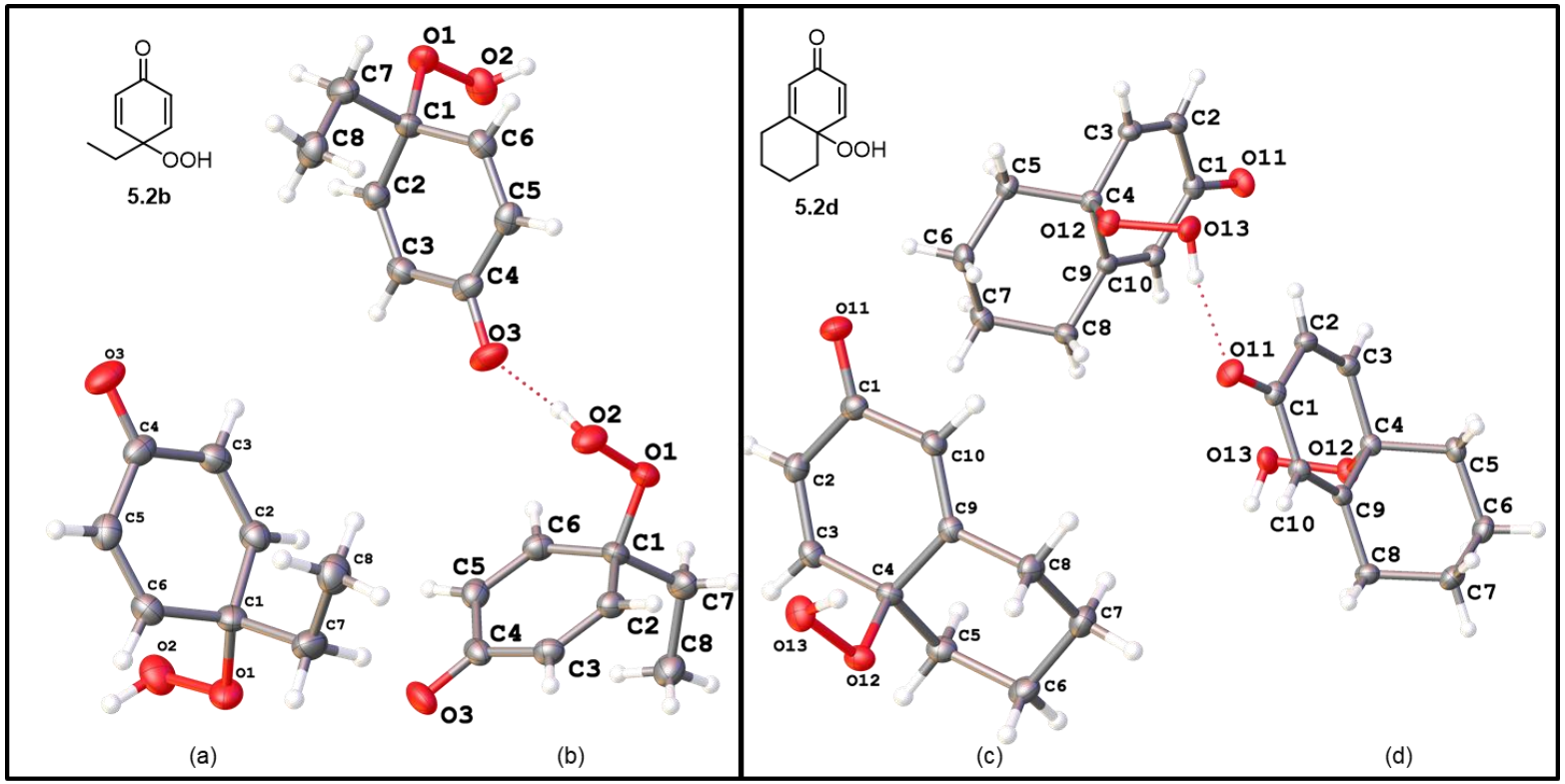


*Figure 5-6 Molecular structure of **5.2b** and **5.2d** with anisotropic displacement ellipsoids set at 50% probability. Structures of (a) and (b) are the single crystal and two units for chain-peroxide **5.2b**. Structures of (c) and (d) are the single crystal and two units for chain-peroxide **5.2d**. Selected bond lengths (Å) and angles (°) for **5.2b** and **5.2d**. **5.2b**: C(1)-C(2) 1.495 (2); C(2)-C(3) 1.330(2); C(3)-C(4) 1.465(2); C(1)-C(2)-C(3) 122.82(11); C(2)-C(3)-C(4) 121.14(11). **5.2d**: C(1)-C(2) 1.466(2); C(2)-C(3) 1.329(2); C(3)-C(4) 1.497(1); O(13)-O(11) 2.747(1); O(13)-H-O(11) 167.5(16); C(1)-C(2)-C(3) 120.92(10); C(2)-C(3)-C(4) 123.10(10) Relevant bond length and angles are provided in Appendix.*

The solvent was left to evaporate at room temperature and atmosphere, yielding single crystals for both **5.2b** and **5.2d**. The structures of **5.2b** and **5.2d** were shown in Figure 5-6. Unlike crystal **5.2a**, which forms dimers between two molecules (Figure 5-5), these compounds (**5.2b** and **5.2d**) form long H-bonded chains. The interaction of these both **5.2b** and **5.2d** are hydrogen bonding, which appeared in crystal **5.2a** as well. However, the interaction of molecular **5.2b**, **5.2d** are bonded by only a single interaction hydrogen bond. The distance of hydrogen bond from H1 to O3 (Figure 5-6 (b)) and H1 to O11 (Figure 5-6 (d)) are 1.86(2) Å and 1.88(2) Å, respectively.

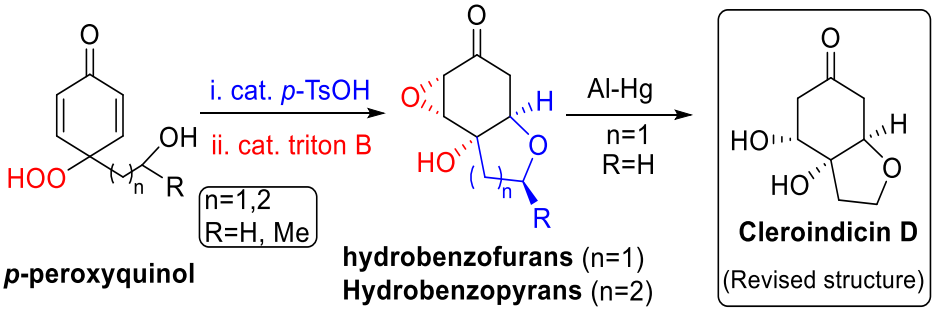
5.4 The application of *p*-peroxyquinol

5.4.1 Access to 1,2,4-trioxane

Phenols are the most frequently utilised substrates for dearomatisation to access complex molecules. A number of dearomatisation strategies have been used by organic chemists to construct fused, bridged and spiro structures.[467] One of the products, cyclohex-2,5-dione, can be obtained from the dearomative oxidation of *p*-phenols, which are considered as good electrophilic substrates in various reactions, such as the Diels-Alder reaction,[468-469] reductions, [3+2] cyclization and Michael addition, which been found widespread use in the chemical synthesis of natural products.[176, 470-472] Additionally, the groups of Feringa,[473] Hayashi,[474] and Rovis[475] have developed catalytic desymmetrization methods to convert the cyclohexadienones motif into useful enantioenriched molecules.[397]

Urbano and co-workers developed an acidic - basic tandem catalytic process on *p* - peroxyquinols with hydroxyl alkyl chains at C - 4 allowed the one-pot synthesis of hydrobenzofuran and hydrobenzopyran tricyclic epoxides.[430] This provides the strategy for the first synthesis and structural revision of natural product cleroindicin D

(Scheme 5-8). *p*-quinol can be accessed from reduced *p*-peroxyquinol, and Carreño and co-workers explored the Morita-Baylis-Hillman reaction of *p*-methylquinols with activated aromatic aldehydes to obtain three different products, including a fused 1,3-dioxolane.[376]

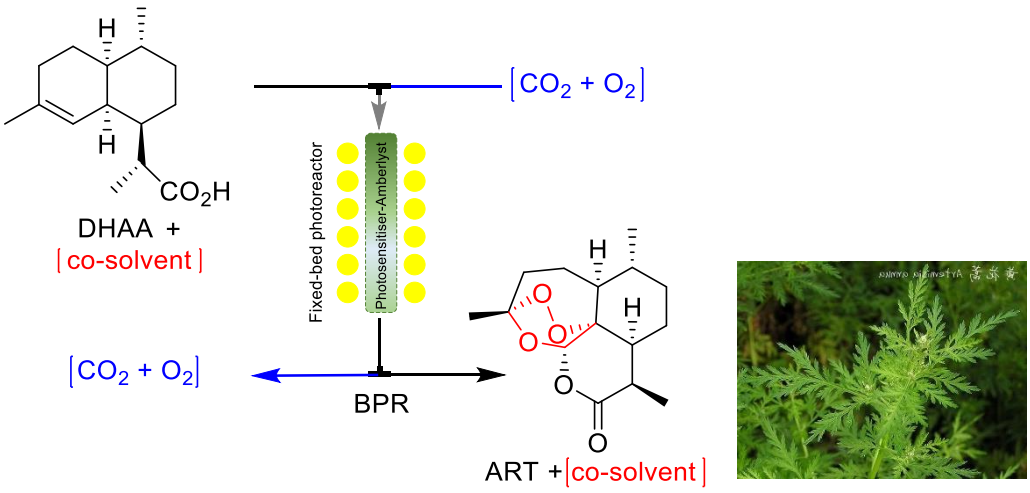


Scheme 5-8 One-pot synthesis of hydrobenzofuran and hydrobenzopyran from p-peroxyquinol.[430]

Besides the application of *p*-peroxyquinol mentioned above, another strategy is to access 1,2,4-trioxane compounds *via* Michael addition, which is the core structure of some antimalarial reagents.[137] The acetalisation/oxa-Michael cascade was first proposed by Jefford.[476] It is well-known that malaria continues to be a major lethal infectious disease of human beings, affecting around 219 million people and causing approximately 435,000 deaths globally in 2017.[477] The naturally occurring sesquiterpene lactone peroxide artemisinin (qinghaosu), which contains a 1,2,4-trioxane subunit, serves as the natural active principle and model compound.[478]

Artemisinin is mainly extracted from a Chinese plant, *Artemisia annua* (Scheme 5-9), and supply does not always meet demand, so supplementing this with a semi-synthetic manufacturing process from more abundant biosynthetic precursors is a promising way.[479] A green and continuous process for dihydroartemisinic acid (DHAA) transformation to artemisinin (ART) was developed in our group in 2015, liquid CO_2 offers possibilities due to its inertness towards oxidation, which is the main step for the synthesis of artemisinin.[39] The use of aqueous mixtures and utilisation of Amberlyst-15 supported photosensitiser also provided opportunities for solvent

manipulation. These approaches proposed in this work hold promise for rapid implementation on a large scale (Scheme 5-9).



Scheme 5-9 One strategy for the one-pot semi-synthesis of artemisinin in liquid CO_2 (Left). The Chinese plant: Artemisia annua (Right).[39]

However, artemisinin-based combination therapies (ACTs) such as artemether/lumefantrine/amodiaquine recommended by WHO for the treatment of malaria have been reported to develop resistance in South-East Asia.[480] Recently, more different novel 1,2,4-trioxane compounds have been synthesised to be potent antimalarial agents.[481-483]

Given the antimalarial properties of 1,2,4-trioxane compounds, it remains worth exploring newer scalable methods for the production of 1,2,4-trioxane chemicals. Herein, a green and scaled up process was investigated in the high-pressure continuous flow system using CO_2 as a solvent, which followed the step of dearomatisation of *p*-phenols under the irradiation in a daisy-chain.

5.4.2 **The reactivity of *p*-peroxyquinol with an aldehyde in methanol**

In the next experiment, a daisy-chained reaction to synthesise a 1,2,4-trioxane in methanol is proposed: step 1: dearomatisation of phenol derivatives; step 2: cyclisation of *p*-peroxyquinol with cyclohexanecarboxaldehyde **5.7** under acid conditions. Herein, the concentration of aldehyde **5.7** was 1.2 M in EtOAc, which was

pumped by an extra organic pump. Unfortunately, 1,2,4- trioxane **5.3a** cannot be synthesised using the mentioned method, due to the protic solvent employed. Instead of 1,2,4-trioxane **5.3a**, acetal **5.3aa** was obtained, since methanol was reactive with an aldehyde under acidic conditions. This is also in accordance with the results in the literature, which used the aprotic solvent, CH_2Cl_2[483] (Figure 5-7).

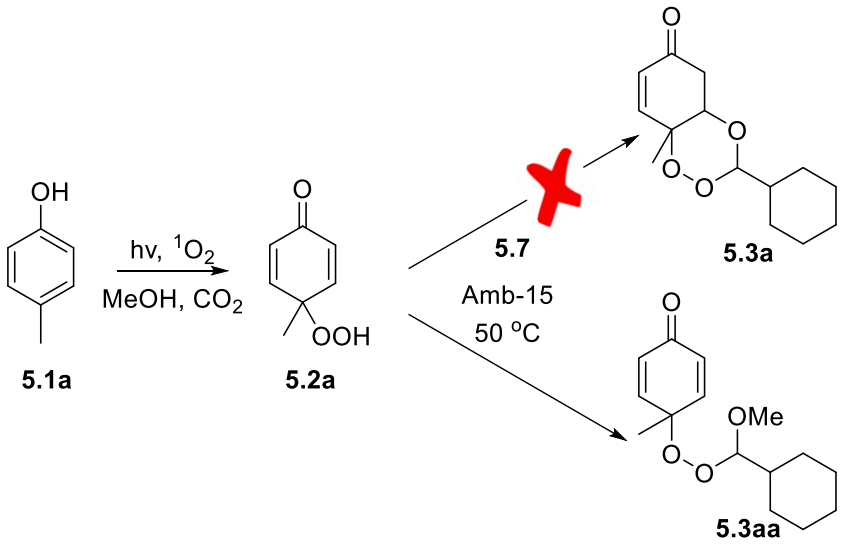


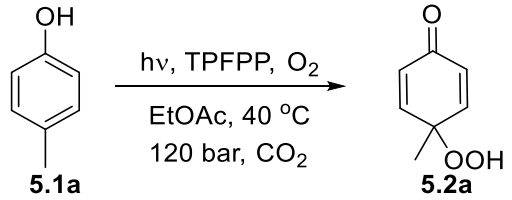
*Figure 5-7 The reactivity of peroxide with aldehyde **5.7** in methanol*

5.5 Dearomatisation of 5.1a using EtOAc as co-solvent

Therefore, in order to synthesise a 1,2,4-trioxane **5.3a** *via* the dearomatisation of phenol derivatives, aprotic solvent, EtOAc, was employed instead of the protic solvent, methanol. EtOAc was chosen as the co-solvent with supercritical CO_2 to conduct the dearomatisation of *p*-cresol, because it is green and sustainable, easily removed, and the lifetime of singlet oxygen in EtOAc is acceptable.[176] The results in Table 5-7 demonstrates that *p*-peroxyquinol **5.2a** could be obtained in a reasonable yield. During this process, polymerisation was also observed when high concentrations (2.0 M and 3.0 M) of **5.1a** were used, probably because of the absence of protic solvent; only *ca*. 54 % yield of **5.2a** was obtained (Table 5-7, entries 2 and 5).

However, the yield of **5.2a** was approaching 68 %, when a 1.0 M concentration of **5.1a** in EtOAc was used (Table 5-7, entry 4). The conversion was less than 100 % in all cases as shown in Table 5-7.

*Table 5-7 Results of dearomatisation of **5.1a** using EtOAc as co-solvent.[a]*



5.1a **5.2a**

Entry	Concentration (M)		Residence Time (min)[d]	Conversion of 5.1a	Yield of 5.2a
	5.1a[b]	TPFPP[c]			
1	3.0	0.05 mol%	21	80 %	41 %
2	3.0	0.05 mol%	35	94 %	54 %
3	1.0	0.1 mol%	21	41 %	41 %
4	1.0	0.1 mol%	35	72 %	68 %
5	2.0	0.1 mol%	21	88 %	51 %

[a]: All experiments were conducted at 40 °C and 120 bar, using CO_2 and EtOAc as solvents, the flow rate of organic pump 1 was 0.05 mL/min, the flow rate of CO_2 was 0.1 - 0.2 mL/min. The photoreactor was 10 mm O. D., 120 mm length, filled with glass beads (6 mm O. D.), the yield and conversion were calculated from ^{1}H NMR spectroscopy, using biphenyl as internal standard. [b]: The concentration of **5.1a** in EtOAc. [c]: The ratio of TPFPP to **5.1a**. [d]: Residence Time of photo-oxidation step in the photoreactor.

Since the conversion was less than 100 %, we investigated whether increasing the amount of TPFPP could increase the conversion of **5.1a** and yield of **5.2a** when the flow rate of the organic pump 1 and CO_2 pump was 0.05 mL/min and 0.3 mL/min, respectively, as shown in Figure 5-8. The yield of **5.2a** increased from 41 % to 69 % when increasing the ratio of TPFPP to **5.1a** from 0.1 mol % to 0.3 mol %. Since the generation of $^1O_2$ dependent on the amount of photosensitiser, TPFPP, more $^1O_2$ can be produced with more TPFPP, at some point, as explained in the Introduction.

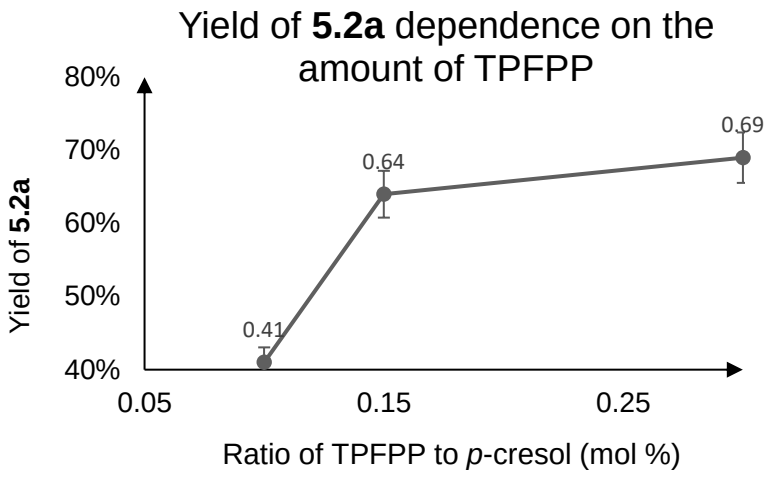


*Figure 5-8 Showing how the yield of **5.2a** depends on the amount of TPFPP in EtOAc and CO_2. These experiments were conducted in the setup shown in Figure 5-4. The system pressure was 120 bar. The photoreactor (40 °C) was 10 mm O. D., 240 mm length, filled with glass beads (6 mm O. D.), the flow rate of organic pump 1 was 0.05 mL/min, the flow rate of CO_2 pump was 0.3 mL/min. The concentration of **5.1a** in EtOAc was 1.0 M, the residence time was 15 min, The switching time of Rheodyne for oxygen was 15.9 seconds; using biphenyl as an internal standard.*

5.6 The reactivity of *p*-peroxyquinol 5.2a with an aldehyde in EtOAc

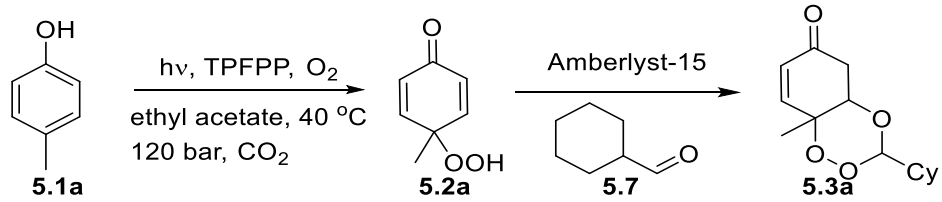
5.6.1 The reactivity of 5.2a using EtOAc as co-solvent

In the following section, we describe experiments using 0.3 mol% TPFPP. A 61 % yield of 1,2,4-trioxane **5.3a** was obtained when the thermal reactor was held at 50 °C, pumping 1.2 M aldehyde **5.7** *via* organic pump 2, see Figure 5-4. This example is described in Table 5-8. During this process, the yield of the cyclisation step was up to 88 %, and no peroxide **5.2a** was observed after passing through the thermal reactor, giving 61 % of overall yield for 1,2,4-trioxane **5.3a** yield.

To further increase the conversion of **5.1a** in EtOAc and CO_2 system, the CO_2 flow rate was reduced from 0.3 mL/min to 0.2 mL/min to increase the residence time in the photoreactor from 15 min to 26 min. The conversion changed from 69 % to

75 %, with a 72 % overall yield of **5.3a**. When 2 equivalents of *tert*-butanol (acting as protic solvent) were employed with EtOAc solution, the conversion of **5.1a** increased further to 86 % at 0.05 mL/min for organic pump 1, 0.15 mL/min for CO_2 pump. The overall yield for **5.3a** was up to 78 %.

*Table 5-8 Summary of the synthesis of **5.3a** in high-pressure EtOAc and CO_2 system.[a]*



Temperature (°C)		Concentration (M)[b]		Flow Rate (mL/min)		
Photo-reactor	**Thermal Reactor**	**5.1a**	**5.7**	**CO_2**	**Organic pump 1**	**Organic pump 2**
40	50	1.0	1.2	0.3	0.05	0.05
Residence Time		**Ratio of TPFPP to 5.1a**	**System Pressure**	**Conversion**	**Cyclisation Yield**	**Overall Yield of 5.3a**
Photo-reactor	**Thermal Reactor**					
15 min	2.7 min	0.3 mol %	120 bar	69 %	88 %	61 %
[a]: Thermal Reactor was loaded with 1 g Amberlyst-15, yield was calculated from ^{1}H NMR, using biphenyl as an internal standard. The switching time of Rheodyne for oxygen was 15.9 seconds. [b]: represents the concentration in EtOAc.						

However, the addition of *tert*-butanol also promoted the yield of the reduced by-product, 4-hydroxy-4-methylcyclohexa-2,5-dien-1-one (**5.2aa**). When we employed more powerful LED lights (8000 lumens for each chip, 3 chips for each LED), one powerful LED and five normal LED (1000 lumens for each chip, each LED with 5 chips) at the same time to irradiate the photoreactor, the conversion of **5.1a** was 89 %. The residence time was 9 min in the photo-oxidation step, with 64 % overall yield of **5.3a**, the flow rates of organic pump 1 and CO_2 pump were held at 0.1 mL/min, 0.45 mL/min,

respectively. Others conditions also were tested, but polymerisation was observed when employing a longer residence time, 26 min as previously shown in Table 5-1.

*Table 5-9 The results of photo-oxidation of **5.1a** with powerful LED light.[a]*

Entry	Flow Rate (mL/min)		Residence Time[b]	Conversion[c]	Yield of 5.2a[c]
	Org. Pump 1	CO_2 Pump			
1	0.05	0.15	26 min	97 %	58%
2	0.05	0.3	15 min	97 %	35 %
3	0.1	0.45	9 min	89 %	69 %
4	0.1	0.6	7 min	89 %	54 %
5	0.15	0.52	8 min	89 %	80 %

[a]: All experiments were performed at 40 °C, 120 bar. The concentration of TPFPP to **5.1a** was 0.3 mol %. The switching time of Rheodyne for oxygen was 15.9 seconds. [b]: represents Residence Time in the photoreactor. [c]: Yield was calculated by ^{1}H NMR spectroscopy, using biphenyl as an internal standard.

The stereochemistry of the structure of **5.3a** was firstly identified by single-crystal X-ray (Figure 5-9 (a)). This crystal was obtained directly after BPR without further purification, which is matching with some of 12 Principles of “Green Chemistry”, such as preventing waste than to treat it after it is formed, and without unnecessary derivatisation, as well as catalytic reagents used instead of stoichiometric reagents. 4.2 grams of crystalline product can also be obtained if recrystallised in diethyl ether (Figure 5-9 (b)).

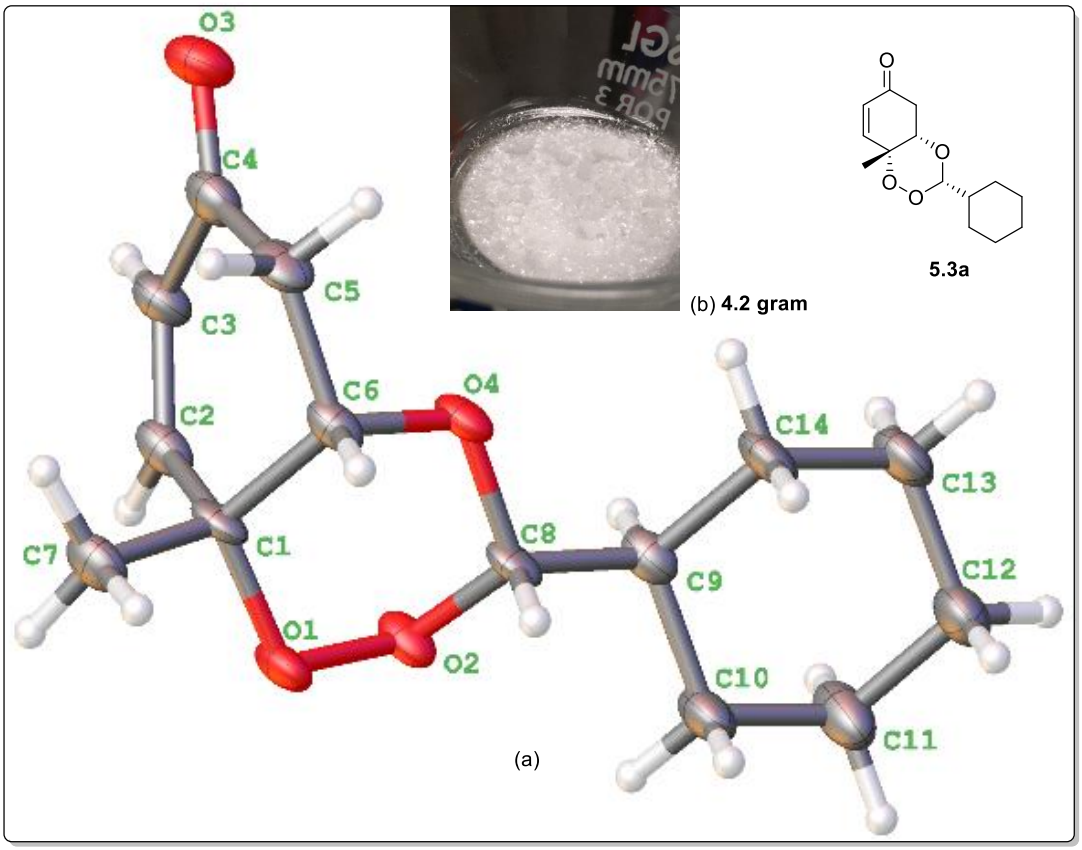


*Figure 5-9 (a) Molecular structure of **5.3a** with anisotropic displacement ellipsoids set at 50% probability. Selected bond lengths (Å) and angles (°) for **5.3a**. **5.3a**: C(1)-C(2) 1.501(6); C(2)-C(3) 1.335(6); C(3)-C(4) 1.471(7); C(1)-O(1) 1.455(5); O(1)-O(2) 1.467(4); O(2)-C(8) 1.426(5); C(1)-C(2)-C(3) 122.6(4); C(2)-C(3)-C(4) 121.6(4); C(1)-O(1)-O(2) 107.4(3); C(8)-O(4)-C(6) 110.6(3); other relevant bond lengths and angles are put in the Appendix. (b) 4.2 grams of **5.3a** were recrystallised from the crude in diethyl ether.*

5.6.2 The reactivity of 5.2a using MeCN/ EtOAc as co-solvent

When employing a mixture of acetonitrile/ethyl acetate (MeCN/EtOAc) as co-solvent, the system pressure was 120 bar, and the temperature of photoreactor was 40 °C, as shown in Table 5-10. The conversion of **5.1a** was 73 %, giving an overall 62 % yield of **5.2a** when the residence time in the photoreactor was 26 min. EtOAc was used in a 1:1 volume ratio with MeCN as EtOAc is known to solubilise TPFPP (0.3 mol% of **5.2a**) in MeCN/CO_2 system. Unfortunately, 1,2,4-trioxane **5.3a** was not observed in the mixture of MeCN/EtOAc as co-solvents when pumping compound **5.7**

(1.2 M, 0.05 mL/min) under acid conditions, with the temperature of thermal reactor held at 50 °C.

*Table 5-10 Results of the dearomatisation of **5.1a** when employing MeCN/EtOAc as co-solvent.*[a]

Entry	Flow Rate (mL/min)		Residence Time[b]	Conversion[c]	Yield of 5.2a[c]
	Org. Pump 1	CO_2 Pump			
1	0.05	0.15	26 min	73 %	62 %
2	0.05	0.3	15 min	51 %	37 %
3[d]	0.05	0.15	26 min	73 %	28 %[d]

[a]: The mixture of Acetonitrile/EtOAc (v/v=1:1) was used as co-solvent to dissolve the starting material **5.1a**, 1.0 M; the system pressure was 120 bar and the temperature was 40 °C in photoreactor; the switching time of Rheodyne for oxygen was 15.9 seconds unless otherwise stated. [b]: Residence Time in Photoreactor, [c]: Yield was calculated from ^{1}H NMR spectroscopy, using biphenyl as an internal standard. [d]: Pumping 1.2 M compound **5.7** in EtOAc with one more organic pump at 0.05 mL/min, the thermal reactor (50 °C) loaded with 1.0 g Amberlyst-15, the residence time in the thermal reactor was 4 min. [d]: No 1,2,4-trioxane **5.3a** was observed, but the yield of **5.2a** reduced to 28 %.

5.6.3 The reactivity of 5.2a dependent on the residence time

Given the results of screening the amount of TPFPP, different co-solvents, with/without the *tert*-butanol, all of these parameters affect the dearomatisation of **5.1a** and synthesis of **5.3a** in this high-pressure setup (Figure 5-4). Then, longer residence time for the photo-oxidation step of **5.1a** in EtOAc *via* increasing the length of the sapphire tube photoreactor was considered, and the results are shown in Table 5-11. Firstly, employing different flow rates of CO_2 pump, keeping the flow rate of organic pump 1 at 0.05 mL/min, the yield of **5.2a** peaked at 95 %, with near full conversion when the residence time in the photoreactor was 52 min in the more extended photoreactor (40 °C, 120 bar) (Figure 5-17, Table 5-11, entries 1 and 2). The conversion of **5.1a** and the yield of **5.2a** decreased as shortening the residence time in the photoreactor, *via* changing the flow rates of organic pump 1 and CO_2 pump

(Table 5-11, entries 1 - 4). An 84 % overall yield of 1,2,4-trioxane **5.3a** was obtained when introducing the1.2 M concentration compound **5.7** between the photoreactor and the thermal

*Table 5-11 Investigating the effect of more extended Photoreactor on the dearomatisation of **5.1a**.*[a]

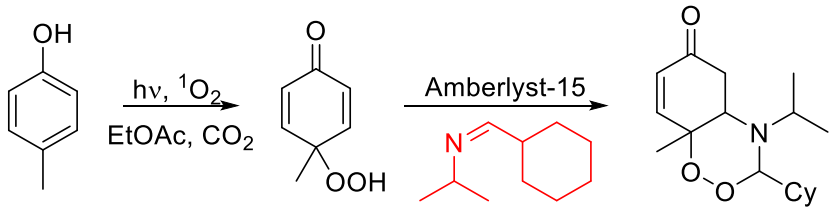
Entry	Flow rate (mL/min)		Residence Time[b]	Conversion[c]	Yield of 5.2a	Overall Yield of 5.3a
	Org. Pump 1	CO_2 Pump				
1	0.05	0.15	52 min	>99 %	95 %	-
2	0.05	0.3	30 min	95 %	87 %	-
3	0.1	0.3	26 min	79 %	74 %	-
4	0.1	0.45	19 min	59 %	52 %	-
5[d]	0.05	0.15	52 min[e]	>99 %	3 %	84 %
6[d]	0.05	0.3	30 min[e]	95 %	6 %	74 %
7[d]	0.1	0.3	26 min[e]	79 %	<1 %	74 %

[a]: The concentration of **5.1a** was 1.0 M in EtOAc, and the system pressure was 120 bar, as well as the temperature of photoreactor was 40 °C. The switching time of Rheodyne for oxygen was 15.9 seconds unless otherwise stated. Yield was calculated by ^{1}H NMR spectroscopy using biphenyl as internal stardand. [b]: Residence Time in Photoreactor(10 mm O. D., 480 mm length, loaded with glass balls, 6 mm O. D.). [c]: Conv.: Conversion of **5.1a**. [d]: Pumping compound **5.7** (1.2 M in EtOAc) at 0.05 mL/min between the photoreactor and the thermal reactor by organic pump 2, the flow rate of organic pump 2 was the same as organic pump 1. The temperature of the thermal reactor (loaded with 1g Amberlyst-15) was 50 °C. [e]: The residence time in the thermal reactor for entries 5, 6, 7 was 3.2 min, 2.0 min, 1.6 min, respectively.

reactor (50 °C) at 0.05 mL/min (Table 5-11, entry 5). When increasing the flow rate of CO_2 pump from 0.15 mL/min to 0.3 mL/min, the overall yield of **5.3a** decreased from 84 % to 74 %. Under these two conditions, 3 - 6 % of **5.2a** was unreacted; the cyclisation yield decreased from 84 % to 78 %. When doubling the flow rate of organic pump 1 from 0.05 mL/min to 0.1 mL/min, 74 % overall yield was obtained, with 27 g/day projected productivity of **5.3a** (Table 5-11, entry 7).

Instead of using aldehyde **5.7**, freshly prepared imine 1-cyclohexyl-N-isopropylmethanimine[484] (compound **5.8**, 1.2 M in EtOAc) was introduced into the rig between the photoreactor and the thermal reactor at 0.05-0.1 mL/min, giving 10 % of tentively asiigned 3-cyclohexyl-4-isopropyl-8a-methyl-3,4,4a,8a-tetrahydrobenzo [*e*] [1,2,4]dioxazin-6 (5*H*)-one (compound **N-3a**), and peroxide **5.2a** was unreacted (Table 5-12), the procedures are described in the Experimental section at the end of this Chapter. The compound N-3a will be further explored in the future. This low yield of **N-3a** was probably the result of the acid catalyst Amberlyst-15 being neutralized by the basic imine preventing catalysis of peroxide **5.2a** to dioxazinone **N-3a**.

*Table 5-12 Testing the reactivity of peroxide **5.2a** with imine **5.8** in the high-pressure system.*[a]



5.1a **5.2a** **5.8** **N-3a**

Entry	Flow rate (mL/min)		Residence Time[b]	Conversion[c]	Yield of 5.2a	Overall Yield of N-3a
	Org. Pump 1	CO_2 Pump				
1[d]	0.05	0.1	69 min[e]	95 %	73 %	9 %
2[d]	0.1	0.2	35 min[e]	79 %	66 %	10 %

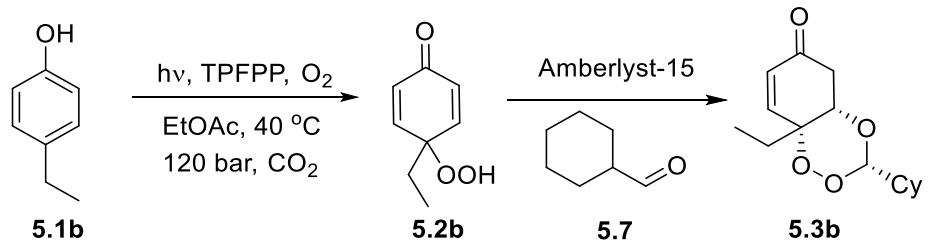
[a]: The concentration of **5.1a** was in ethyl acetate was 1.0 M and the system pressure was 120 bar, as well as the temperature of photoreactor was 40 °C. The switching time of Rheodyne for oxygen was 15.9 seconds unless otherwise stated. The yield was determined according to ^{1}H NMR spectroscopy using biphenyl as internal standard. [b]: Residence Time in Photoreactor (10 mm O. D., 480 mm length, loaded with glass balls, 6 mm O. D.). [c]: Conversion of **5.1a**. [d]: Pumping compound **5.8** (1.2 M, freshly prepared) at 0.05 mL/min after the photoreactor, the temperature of the thermal reactor (loaded with 1g Amberlyst-15) was 50 °C. [e]: The residence time in the thermal reactor for entries 1 and 2 was 4 min and 2.3 min, respectively.

5.6.4 **The scope of different substrates using EtOAc as co-solvent**

With the conditions to investigate the substrate **5.1a** in hand, **5.1b** was examined with these parameters as shown in Table 5-13.

A similar trend was observed as for substrate **5.1a**; higher conversion of **5.1b** and higher yield of **5.2b** were observed when increasing the irradiation time in the photoreactor from 26 min to 52 min (Table 5-13, entries 1 and 2). **5.1b**, with an ethyl group in the *para*-position, was less reactive towards singlet oxygen than **5.1a** under

*Table 5-13 Synthesis of **5.2b** and **5.3b** using EtOAc as co-solvent in the high-pressure CO_2 setup-4.*[a]



Entry	Flow rate (mL/min)		Residence Time[a]	Conversion[b]	Yield of 5.2b[f]	Overall Yield of 5.3b[f]
	Org. Pump 1	CO_2 Pump				
1	0.05	0.15	52 min	84 %	83 %	-
2	0.1	0.3	26 min	71 %	71%	-
3[c]	0.05	0.15	52 min[d]	84 %	0	34 %
4[c]	0.1	0.3	26 min[d]	71 %	0	41 %

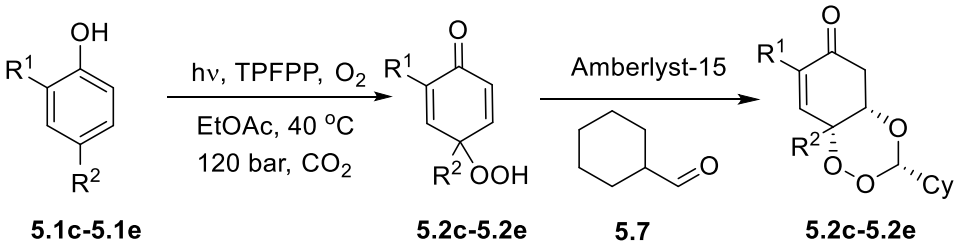
[a]: The concentration of **5.1b** in EtOAc was 1.0 M and the system pressure was 120 bar, as well as the temperature of photoreactor was 40 °C. The switching time of Rheodyne for oxygen was 15.9 seconds unless otherwise stated. [b]: Residence Time in photoreactor(10 mm O. D., 480 mm length, loaded with glass balls, 6 mm O. D.). [c]: Conversion of **5.1b**. [d]: Pumping compound **5.7** (1.2 M) at 0.05-0.1 mL/min between the photoreactor and thermal reactor by organic pump 2, the flow rate of the organic pump 2 was the same as organic pump 1. The temperature of the thermal reactor (loaded with 1g Amberlyst-15) was 50 °C. [e]: The residence time in the thermal reactor for entries 3 and 4 was 3.2 min and 1.6 min, respectively. [f]: Yield was calculated by ^{1}H NMR spectroscopy using biphenyl as internal standard.

the same conditions; the conversion of **5.1b** was 84 % when the radiation time was 52 min (Table 5-13, entry 1), while for **5.1a** was 99 % (Table 5-11, entry 1).

The selectivity for **5.2b** was near 100 % at different irradiation times in the photoreactor. After the photoreactor, compound **5.7** (1.2 M, 0.05 mL/min) was pumped from organic pump 2into the process before the thermal reactor, giving a yield for the cyclisation step, forming **5.3b**, of 41 %. This cyclisation step was catalysed by Amberlyst-15 in the thermal reactor (50 °C), as shown in Table 5-13, entry 3. A cyclisation step yield of 58 % (overall yield was 41 %) was obtained when increasing the flow rate of pumps (Table 5-13, entry 4). That a higher overall yield of **5.3b** was obtained with higher flow rates of both pumps was different from the synthesis of **5.3a** from substrate **5.1a** (Table 5-11, entries 5 and 7).

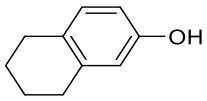
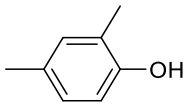
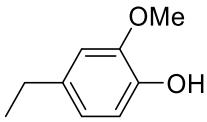
Both conditions **A** and **B** (at 120 bar and 40 °C, *Table 5-14*), having been tested on substrate **5.1a** and **5.1b**, were employed on further *para*-phenol derivatives with different functional groups. The difference between conditions **A** and conditions **B** are the flow rates. The flow rates of organic pump 1, 2 and CO_2 pump was 0.05 mL/min, 0.05 mL/min, 0.15 mL/min, respectively, under conditions **A**; and 0.1 mL/min, 0.1 mL/min, 0.3 mL/min, respectively, under conditions **B**. When investigating the reactivity of 5, 6, 7, 8-tetrahydro-2-2-naphthol, **5.1c**, under conditions **A** as mentioned in *Table 5-14*, entry 1, only 21 % of peroxide **5.2c** was observed, but with the full conversion. This naphthol **5.1c** may be overoxidised in the more extended photoreactor since the rate constant was higher for dearomatisation of naphthol derivatives with singlet oxygen than *p*-cresol **5.1a** with singlet oxygen under the same conditions.[168] Reducing the reaction time in the photoreactor by increasing the flow rate of the organic pump and CO_2 pump to 0.1 mL/min, 0.3 mL/min, respectively, under conditions **B**, the yield of **5.2c** was 47 % (*Table 5-14*, entry 2).

*Table 5-14 Scope of dearomatisation of **5.1a** using EtOAc as co-solvent in high-pressure setup-4.*[a]



5.1c-5.1e **5.2c-5.2e** **5.7** **5.2c-5.2e**

1c: R^1=Me, R^2=Me
1d: R^1=H, R^2=$(CH_2)_4$
1e: R^1=OMe, R^2=Et

Entry	Substrate	Condition	Conversion[b]	Yield of Peroxide[c]	Overall Yield of trioxane[c]
1	 **5.1c**	**A**	>99 %	21 %	4 %
		B	>99 %	47 %	9 %
2	 **5.1d**	**A**	96 %	41 %	55%
		B	95 %	88 %	53%
3	 **5.1e**	**A**	>99%	16 %	5 %

[a]: The concentration of substrate was 1.0 M in EtOAc fed by organic pump 1, compound **5.7** (1.2 M) was introduced into the rig by organic pump 2 between photoreactor (10 mm O. D., 480 mm length, loaded with glass balls, 6 mm O. D.) and thermal reactor, and thermal reactor was loaded with 1.0 g Amberlys-15, 50 °C. Condition **A**: Flow rate of organic pump 1, 2 and CO_2 pump was 0.05 mL/min, 0.05 mL/min, 0.15 mL/min; respectively; condition **B**: Flow rate of organic pump 1, 2 and CO_2 pump was 0.1 mL/min, 0.1 mL/min, 0.3 mL/min, respectively; the switching time of Rheodyne for oxygen was 15.9 seconds unless otherwise stated. [b]: Conversion of the substrate. [c]: Yield was calculated from ^{1}H NMR spectroscopy, using biphenyl as an internal standard.

Peroxide **5.2c** reacted with compound **5.7** in the daisy chained reactor to synthesise 1,2,4-trioxane motif, at a yield of just 9 % **5.3c** being observed under conditions **B**. This is thought to be because the 6-membered ring attached on the *para*- and *meta*-position hindered the formation of trioxane **5.3c**. Moreover, substrates **5.1d** and **5.1e** were used for synthesising 1,2,4-trioxanes with different functional groups. A moderate yield of **5.3d** was obtained, but with a quite low yield of **5.3e** being observed, since the yield of **5.2e** was not promising, merely 16 % (*Table 5-14*)

As described in Table 5-13, the overall yield for **5.3b** was 34 % and 41 %, respectively (Table 5-13, entries 3 and 4); with the cyclisation step yields were 40 % and 58 % respectively. Surprisingly, these results were in contrast to the yields of cyclisation step for the model substrate **5.1a**. We suspected that both the amount of loaded catalyst (Amberlyst-15) and the temperature for the cyclisation step affect this.

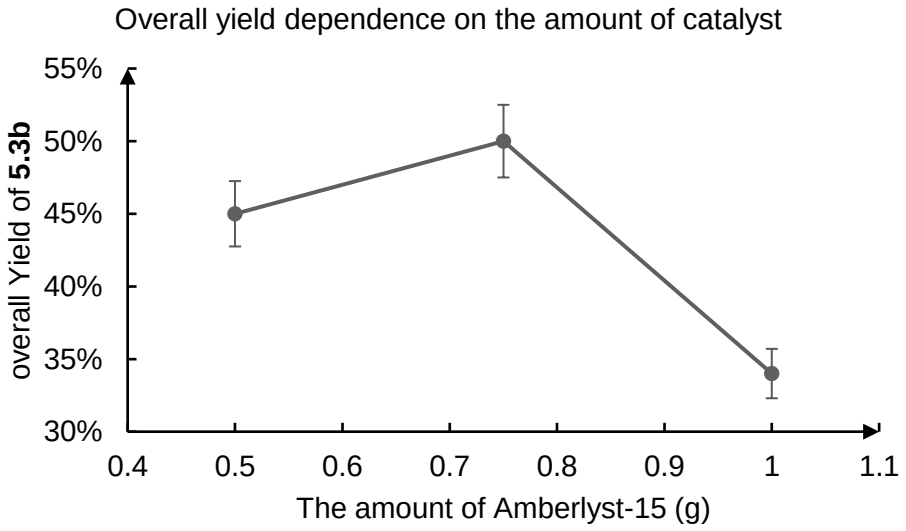
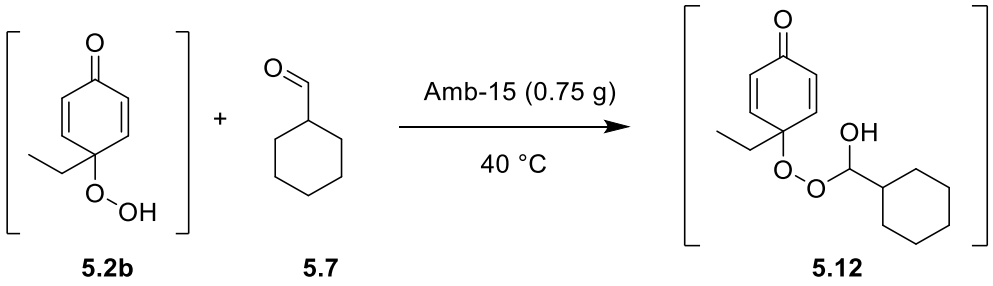


*Figure 5-10 Yield of 1,2,4-trioxane **5.3a** depends on the amount of Amberlyst-15. The concentration of substrate was 1.0 M in EtOAc pumped by organic pump 1 (0.05 mL/min), and compound **5.7** (1.2 M) was introduced into the rig by organic pump 2 (0.05 mL/min) between photoreactor (40 °C, 10 mm O. D., 480 mm length, loaded with glass balls, 6 mm O. D.) and thermal reactor (1/4 inch O. D., 156 mm); and the temperature of the thermal reactor was 50 °C. The flow rate of CO_2 was 0.15 mL/min. Up flow was used for the thermal reactor, 0.5 g, 0.75 g, and 1 g Amberlyst-15 was loaded in the bottom, respectively and glass balls (1.5 -2 mm) were loaded at the top of the tubular thermal reactor in Figure 5-4 unless otherwise stated.*

Therefore, different amounts of Amberlyst-15 were pre-loaded at the bottom of the tubular thermal reactor, with the remaining filled with glass beads (1.5 -2 mm) at the top. At 50 °C, the overall yield of 1,2,4-trioxane **5.3b** was 45 %, 50 %, and 34 % when increasing the amount of Amberlyst-15 from 0.5 g to 0.75 g and 1.0 g (Figure 5-10). The best yield was obtained with 0.75 g Amberlyst-15 (50 °C). Then, we observed that the yield of **5.3b** increased to 53 % when decreasing the temperature of the thermal reactor from 50 C to 40 °C (0.75 g Amberlyst-15 pre-loaded). The yield for **5.3b** increased further to 62 % when pre-loading the 0.75 g Amberlyst-15 at the top, filled with glass beads (1.5 -2 mm) in the bottom, providing for pre-mixing the peroxide **5.2b** with aldehyde **5.7** to form an intermediate compound **5.12** before obtaining the desired 1,2,4- trioxane **5.3b**.*via* Michael addition (Figure 5-11). This presumably reduces the decomposition of **5.2b** when interacting with acid Amberlyst - 15 in the thermal reactor.



5.2b **5.7** **5.12**

*Figure 5-11 The formation of intermediate **5.12** in the high-pressure setup-4.*

Next, the effect of temperature on the cyclisation step was investigated. 0.75 g Amberlyst - 15 was loaded in the thermal reactor, keeping the flow rate of organic pump 1 (1.0 M **5.1b** solution in EtOAc), organic pump 2 (1.2 M compound **5.7** in EtOAc) and CO_2 pump at the 0.05 mL/min, 0.05 mL/min and 0.15 mL/min, respectively; results are presented in Figure 5-12. The yield of **5.3b** peaked at 62 % when the temperature of the cyclisation step was 40 °C, and it decreased to 27 % by increasing the temperature to 60 °C. This illustrated that the temperature also affected

the synthesis of trioxane **5.3b**. A better yield of **5.3b** was obtained at 40 °C than other temperatures studied when 0.75 g Amberlyst-15 was used.

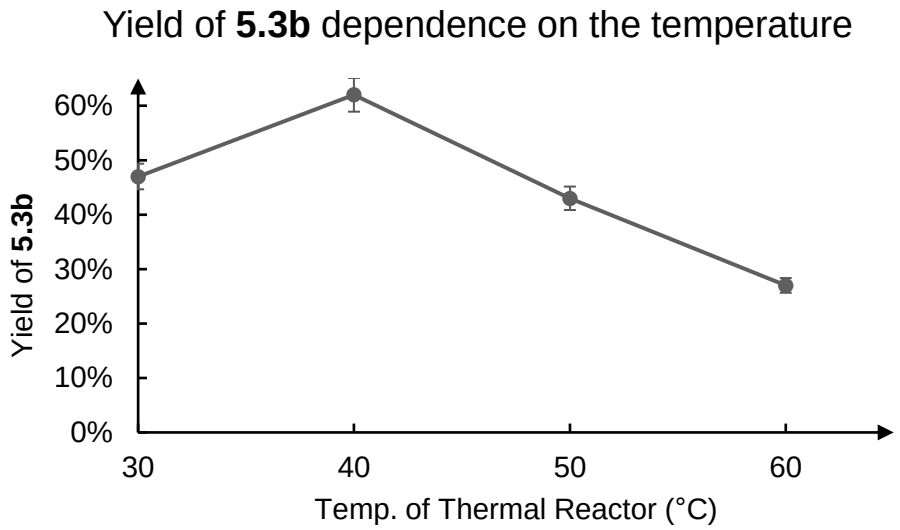


*Figure 5-12 Yield of **5.3b** dependence on the temperature of the thermal reactor. The concentration of substrate was 1.0 M in EtOAc fed by organic pump 1 (0.05 mL/min), compound **5.7** (1.2 M) was introduced into the rig by organic pump 2 (0.05 mL/min) between photoreactor (40 °C, 10 mm O. D., 480 mm length, loaded with glass balls, 6 mm O. D.) and thermal reactor. The flow rate of CO_2 was 0.1 mL/min. 0.75 g Amberlyst-15 was loaded at the top of the tubular reactor (1/4 inch O. D., 156 mm), glass balls (1.5 -2 mm) were loaded in the bottom.*

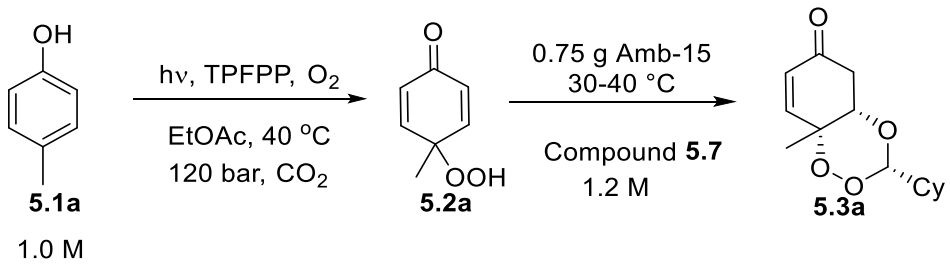


*Figure 5-13 Investigating the synthesis of trioxane **5.3a** when catalysed by 0.75 g Amberlyst - 15 at 40 °C. The concentration of 1a in EtOAc was 1.0 M (0.05 mL/min); the flow rate of CO_2 was 0.1 mL/min. Compound **5.7** (1.2 M in EtOAc) was introduced into the rig by organic pump 2 (0.05 mL/min) after photoreactor (10 mm O. D., 480 mm length, loaded with glass balls, 6 mm O. D.). 0.75 g Amb-15 was loaded at the top of the tubular reactor (1/4 inch O. D., 156 mm), glass balls (1.5 -2 mm) were loaded in the bottom.*

With this information about the dearomatisation of *p*-phenol derivatives in hand, an excellent yield 88 - 89 % for the 1,2,4-trioxane **5.3a** was obtained when using 0.75 g Amberlyst - 15 and 30 - 40 °C for the thermal reactor, as shown in Figure 5-13. The reason was that substrate **5.1a** has smaller spatial hindrance compared to 4-ethylphenol **5.1b** and 5,6,7,8-tetrahydro-2-naphthol **5.1c** in the *para* - position, which would affect the 1,2,4-trioxane compound formation with an aldehyde in the presence of acid.

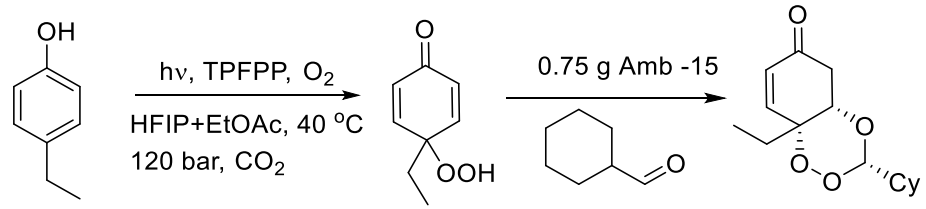
5.7 The effect of HFIP on the dearomatisation of 5.1b

To increase the efficiency of dearomatisation and the yield of 1,2,4-trioxane compounds, a different protic solvent Hexafluoro-2-propanol (HFIP), besides *tert*-butanol, was added into the reaction to be investigated. HFIP is a protic solvent with lower pKa than methanol and *tert*-butanol. The two trifluoromethyl groups make HFIP less-nucleophilic.[485] Since an excellent yield and productivity for **5.3a** from **5.1a** had been achieved in the EtOAc and CO_2 system; substrate **5.1b** was taken as an example.

To further increase the conversion of **5.1b** to access higher yield of **5.2b**, eventually, to obtain a better yield for **5.3b**, we introduced HFIP into the dearomatisation system. 2 equivalents HFIP were added into the starting **5.1b** solution (1.0 M); surprisingly, full conversion of **5.1b** was obtained in the mixture of CO_2, EtOAc and 2 equivalent HFIP. Moreover, a quantitative yield of **5.2b** was observed with the addition of 2 equivalents HFIP, although no **5.3b** was observed without Amberlyst – 15 (Table 5-15, entry 1). Compared to the experiment without HFIP, the conversion and the yield increased from 83% (Table 5-13, entry 1 and Table 5-15, entry 1) to 99 % when the residence time in the photoreactor was prolonged from 26 min to 52 min. Compound **5.7** (1.2 M in EtOAc) was pumped at 0.05 mL/min to mix with photo-oxidation product, catalysed by 0.75 g Amberlyst-15 in the thermal

reactor, giving a 71 % yield of **5.3b** at 30 °C, which was higher than 61 % at 40 °C without HFIP (Table 5-15, entries 2 and 3). This is probably due to a synergistic effect between the acidity[486] of HFIP and Amberlyst - 15 in the cyclisation step to promote the synthesis of **5.3b**.

*Table 5-15 The effect of HFIP on the dearomatisation of **5.1b**[a]*



5.1b **5.2b** **5.7** **5.3b**

Entry	Flow rate (mL/min)		HFIP	Temp[b] (°C)	Yield of 5.2b	Overall Yield of 5.3b
	Org. Pump 1/2	CO_2 Pump				
1[c]	0.05/0.05	0.1	2 equiv.	40	>99%	0
2	0.05/0.05	0.1	2 equiv.	30	2%	71%
3	0.05/0.05	0.1	2 equiv.	40	2%	61%
4	0.05/0.05	0.1	1 equiv.	30	8%	60%
5	0.05/0.05	0.1	1 equiv.	40	4%	55%

[a]: The concentration of **5.1b** in EtOAc and HFIP was 1.0 M. Photo reactor was 10 mm O. D., 480 mm length, loaded with glass balls (6 mm O. D). [b]: Temp.: The temperature for the thermal reactor (loaded with 0.75 g Amberlyst-15), yields were calculated from ^{1}HMR spectroscopy using biphenyl as internal standard, unless otherwise stated. [c]: Without pre-loading Amb - 15 in the thermal reactor, instead of glass balls (1.5 - 2 mm). Compound **5.7** (1.2 M) was pumped at 0.05 mL/min after the photoreactor by organic pump 2. Full conversion for all these entries.

However, we still obtained the full conversion of **5.1b** by adding 1 equivalent of HFIP, but only 60 % of the overall yield of **5.3b** was observed at 30 °C, catalysed by 0.75 g Amberlyst-15 (Table 5-15, entry 4), compared to 71 % (2 equivalents of HFIP). Moreover, the decreased yield of 55 % of **5.3b** was obtained when the temperature of the thermal step was raised to 40 °C (Table 5-15, entry 5). These results demonstrate that the addition of HFIP could promote the dearomatisation of **5.1b** in the mixture of EtOAc and supercritical CO_2 system. Meanwhile, it can also have a

synergistic effect with Amberlyst-15 for the production of **5.3b** at 30 °C in the high-pressure CO_2 system.

From the results obtained in Table 5-13 and Table 5-15, both methods, adding HFIP and prolonging the residence time, can increase the conversion of **5.1b** to access *p*-peroxyquinol **5.2b**. Another experiment for the photo-oxidation of **5.1a** was conducted in a shorter photoreactor (240 mm length) with 2 equivalents HFIP; other conditions were as same as the experiment (480 mm length for photoreactor, without HFIP) in Figure 5-13. Surprisingly, the yield of **5.3a** was similar to the experiment in Figure 5-13, but with 26 min residence time in this photoreactor. Using fewer LEDs for shorter photoreactor (240 mm length) reduces energy consumption comparing to more LEDs used in longer photoreactor (480 mm length).

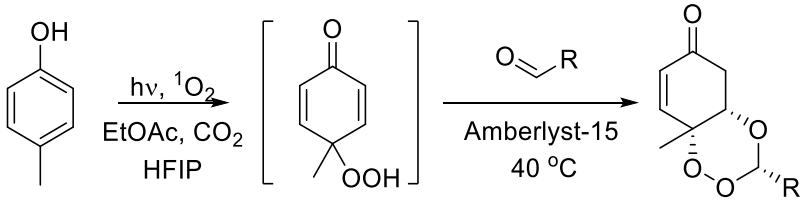
5.8 The scope of different aldehydes reacting with 5.2a

In a strategy for the synthesis 1,2,4-trioxanes from *p*-phenol derivatives, different aldehydes, **5.9**, **5.10**,**5.11** reacting with **5.2a**, were explored for the scope of this library synthesis in the high-pressure system (Figure 5-4). These experiments were carried out in collaboration with PhD student Bruna Lacerda Da Silva Abreu, and results are shown in Table 5-16.

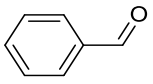
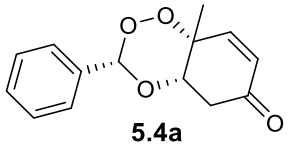
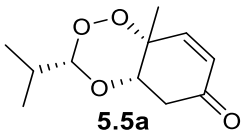
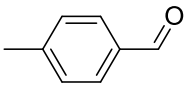
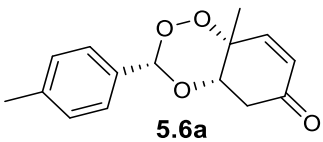
Aldehydes containing different alkyl, aromatic and hindered aliphatic groups were investigated. When the system was 120 bar, and the temperatures of the photoreactor and thermal reactor were 40 °C, aldehydes containing alkyl and aliphatic groups were tolerated, reacting with **5.2a** to afford most 1,2,4-trioxanes with excellent yields. (Figure 5-13 and Table 5-16, entry 2). The yield of **5.5a** was 92 % when **5.2a** was reacting with alkyl aldehyde **5.10** (1.2 M in EtOAc). Aromatic aldehydes also can participate in the reaction, but with decreased yields (Table 5-16, entries 1 and 3). The reduction in yield for electron-rich aryl aldehydes may be the result of a

thermodynamically less favourable peroxy hemiacetal formation,[487] as well as the polymerisation of the aldehydes.

*Table 5-16 Scope of different aldehydes (**5.9**, **5.10**, **5.11**) with p-peroxyquinol **5.2a** in high-pressure setup-2.[a]*



5.1a **5.2a** **5.4a-5.6a**

Entry	Aldehyde (5.9-5.11)	Products (5.4a-5.6a)[b]	Yield[b]
1	 **5.9**	 **5.4a**	-[c]
2	 **5.10**	 **5.5a**	92 %
3	 **5.11**	 **5.6a**	20 %

[a]: All experiments were carried out at 120 bar, 40 °C (photoreactor). The concentration of **5.1a** was 1.0 M in EtOAc, with adding 2 equivalent HFIP. Residence time in the photoreactor (10 mm O.D., 240 mm length, loaded with glass balls, 6 mm O.D.) was 26 min. The flow rate of organic pump 1 and CO_2 pump was 0.05 mL/min and 0.15 mL/min, respectively. Reagents **5.9**, **5.10**, **5.11** solutions (1.2 M, freshly prepared in EtOAc, respectively) was pumped by organic pump 2 at a flow rate of 0.05 mL/min between the photoreactor and thermal reactor, respectively. The temperature of the thermal reactor (loaded with 0.75 g Amberlyst-15 and 0.87 g glass beads, 1.5-2 mm O.D.), the residence time in the thermal reactor was 3.2 min. [b]: Yield was calculated by ^{1}H NMR, using biphenyl as an internal standard. [c]: Product **5.4a** formed in small amounts but the yield could not be fully quantified due to problems with the internal standard.

5.9 Conclusion and Future work

In summary, the photoinitiated dearomatisation of *p*-phenol derivatives with singlet oxygen and the synthesis of 1,2,4-trioxane compounds from *p*-phenol derivatives *via* photo-oxidation products have been successfully conducted and scaled up in high-pressure continuous flow CO_2 systems. This methodology is much greener than in the traditional methods with oxone or hypervalent iodine catalysts, including greener reagent (singlet oxygen), greener solvent (supercritical CO_2) as well as using the continuous flow reactor.

Taking *p*-cresol (**5.1a**) as a model substrate, phase behaviour studies demonstrated that the polar substrate **5.1a** was highly soluble in a high-pressure CO_2 system when using methanol as co-solvent. A quantitative yield of the *p*-peroxyquinol **5.2a** was obtained in methanol and CO_2 system when the residence time in the photoreactor was 26 min. The reactivity of dearomatisation of phenol derivatives in the CO_2 system was lower than the photo-oxidation of cyclopentadiene and fulvene in the CO_2 system as discussed inChapter 3 and Chapter 4.[237, 293] However, it is much higher than the literature work, and the projected productivity of **5.2a** was scaled up to 47 g/day when the concentration of **5.2a** in methanol was 3.0 M, with a space time yield of 753 $g \cdot L^{-1} \cdot h^{-1}$, comparing to the 1.9 g/day in the previous work.[488]

Five different *para*-substituted phenol derivatives, with alkyl groups/aromatic groups bulky groups, were investigated in the high-pressure system using methanol as co-solvent, 67 g/day projected productivity was successfully obtained from 5,6,7,8-Tetrahydro-2-naphthol (**5.1d**). (See Table 5-6)

When using EtOAc as co-solvent instead of methanol, the reaction rate for dearomatisation of *p*-cresol **5.1a** was lower than that utilising methanol as co-solvent. Changing the concentration of photosensitiser, photo-oxidation time, adding protic solvent *tetra*-butanol/HFIP, a good yield for *p*-peroxyquinols **5.2a – 5.2e** was obtained. Furthermore, 1,2,4-trioxane compound **5.3a – 5.3e** and **5.4a – 5.6a** were successfully

and efficiently synthesised catalysed by solid catalyst Amberlyst-15, by varying the *para*-phenol substrates and different aldehydes, respectively. The overall yield of **5.3a** was up to 90 % in the daisy-chain EtOAc and CO_2 system, when the concentration of **5.1a** in EtOAc solution was 1.0 M, and 4.2 gram crystalline **5.3a** was obtained in 8 hours.

The good productivities for *p*-peroxyquinol and 1,2,4-trioxane are very promising to be applied for further scale-up, which is very important for the building of antimalarial and anticancer drugs.[137]

In the future, more *p*-phenol derivatives with different functional groups, such as *para*-substituted with bulky groups, electron withdrawing groups, will be explored in the high-pressure CO_2 system to access more valuable and antimalarial compounds. Furthermore, the antimalarial activity of 1,2,4-trioxanes probably should be tested *in vitro*.

5.10 Experimental data

5.10.1 Procedure for batch reaction

In a round bottle flask, 1 mmol of *p*-cresol (**5.1a**) was dissolved in the desired solvent to prepare 0.067 M of the solution. To this solution, 0.05-0.1 mol % of TPFPP to **5.1a** was added. Oxygen was provided from a balloon loaded with pure oxygen at atmospheric pressure. This solution was irradiated by white LED light at room temperature for a time period of 4-5 hours. The crude was purified with eluent (Cyclohexane/EtOAc) by autosampler Flash Chromatography after removing the solvent. For the reaction with co-catalyst, 0.5 equivalent co-catalyst was added into the solution before irradiation.

5.10.2 **Procedure for the high-pressure setup**

The high pressure rig was described in Figure 5-14 to Figure 5-17. The details for the high-pressure rig were described in the Experimental Section 2.1.2.

The fluid mixture then entered into the high-pressure sapphire tube reactor (Saint-Gobain Crystals, 10 mm O.D., 1 mm wall thickness, 120-480 mm long; loaded with glass beads, 6 mm O. D.) following an up-flow method. The sapphire tube was irradiated with white light by LEDs, which were controlled by a LED controller. The LED lights consisted of three banks of water-cooled LED aluminium blocks each containing five chips (Citizen Electronics Co. Ltd) irradiating for 1000/8000 lumen per chip. The blocks were cooled with chillers. Due to the heat generated by the LED lights, a secondary cooling bath was used to pump coolant around the sapphire tube to ensure the desired temperature (40 °C) in the reactor. Thus, LEDs can be positioned as close as possible to the sapphire tube assuring highly efficient irradiation. Photoreactor 1 refers to the association of the sapphire tube, LEDs and aluminium blocks.

Procedure for the synthesis of *p*-peroxyquinol derivatives: The desired concentration of starting material was pumped into the rig by organic pump 1 at the desired flow rate; a second pump delivered more solvent after the photoreactor to avoid the blockage in the BPR. The *p*-peroxyquinol derivatives crude could be collected after BPR, ready to be purified and identified.

Procedure for the synthesis of 1,2,4-trioxane derivatives: As described in the procedure for the synthesis of *p*-peroxyquinol derivatives, instead of pumping the pure solvent from the second pump, the desired aldehyde dissolved in the solvent was pumped at the same flow rate as organic pump 1.

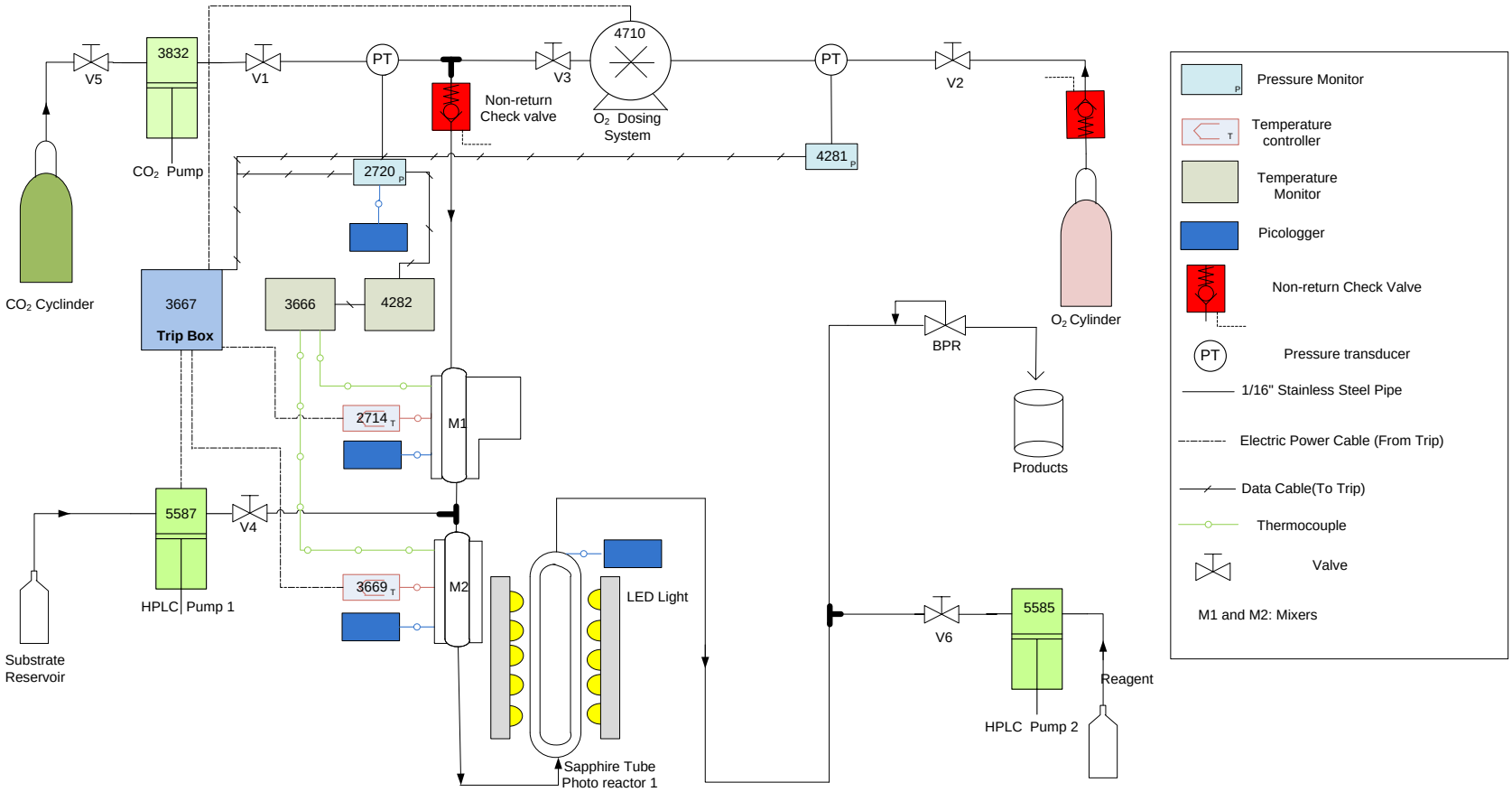


Figure 5-14 The diagram of the high-pressure rig for the synthesis of products-setup-1. This is a general high-pressure continuous flow reactor using CO_2 as a solvent. CO_2 and O_2 were mixed in M1, then the organic solution was introduced by organic pump 1 meeting the gases in the

second mixer M2. A second organic pump was used to pump more solvent to avoid the blockage in the BPR. The solution was irradiated by white LEDs in the photoreactor (Saint-Gobain Crystals, 10 mm O.D., 1 mm wall thickness, 240 mm long) before flowing out from BPR. Non-return check valves were used to prevent the organic stream from large amount of oxygen. Pressure and temperature monitors were connected to the Piclogger. Trip box was installed in case of an emergency.

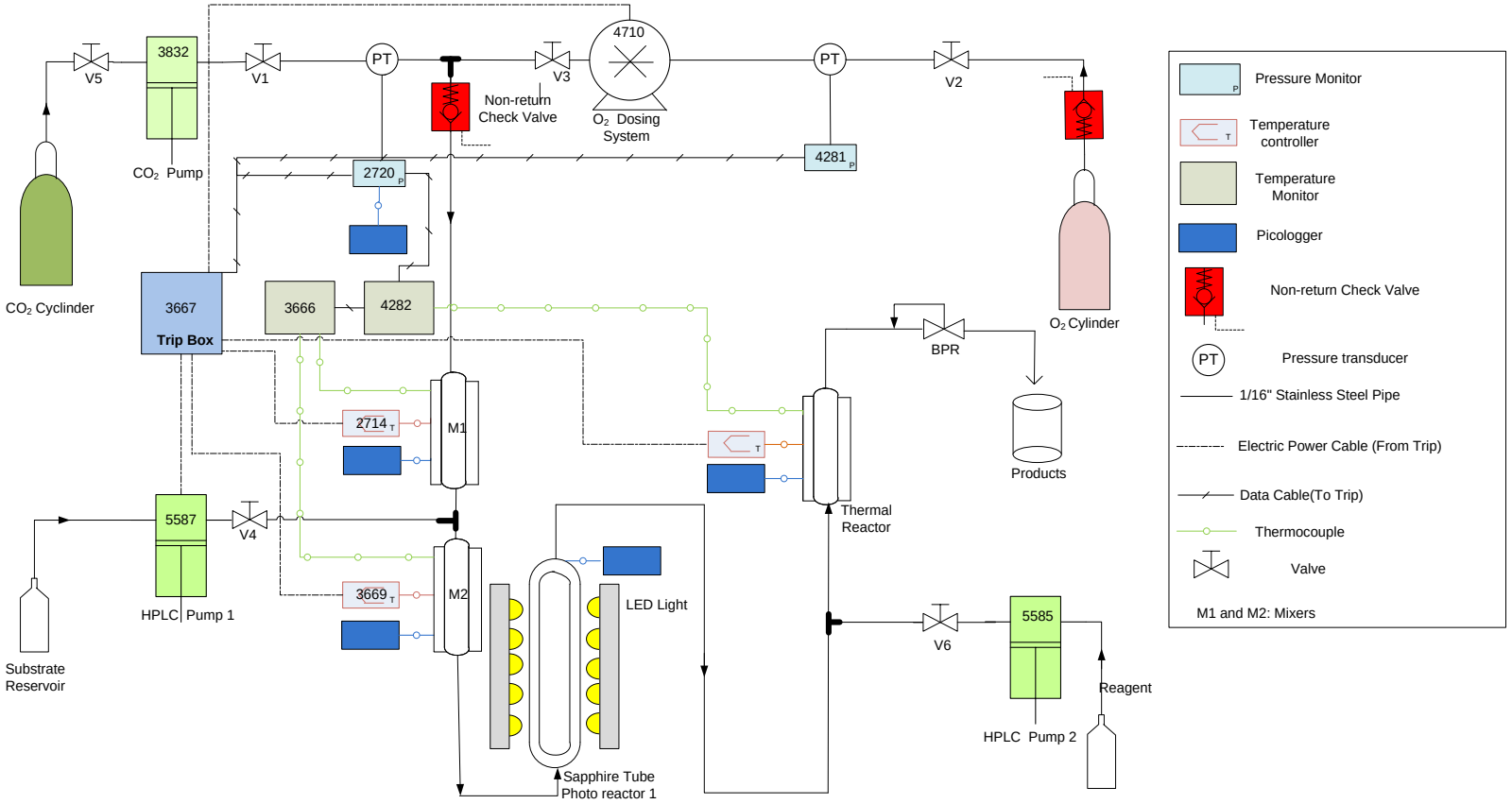


Figure 5-15 The diagram of the high-pressure rig for the synthesis of products-setup-2. The difference between setup-2 and setup-1 was that a thermal reactor (78 mm, ¼ inch O. D., SS316 tubes) was added between photoreactor and BPR, for the cyclisation of p-peroxylquinol derivatives with different aldehydes.

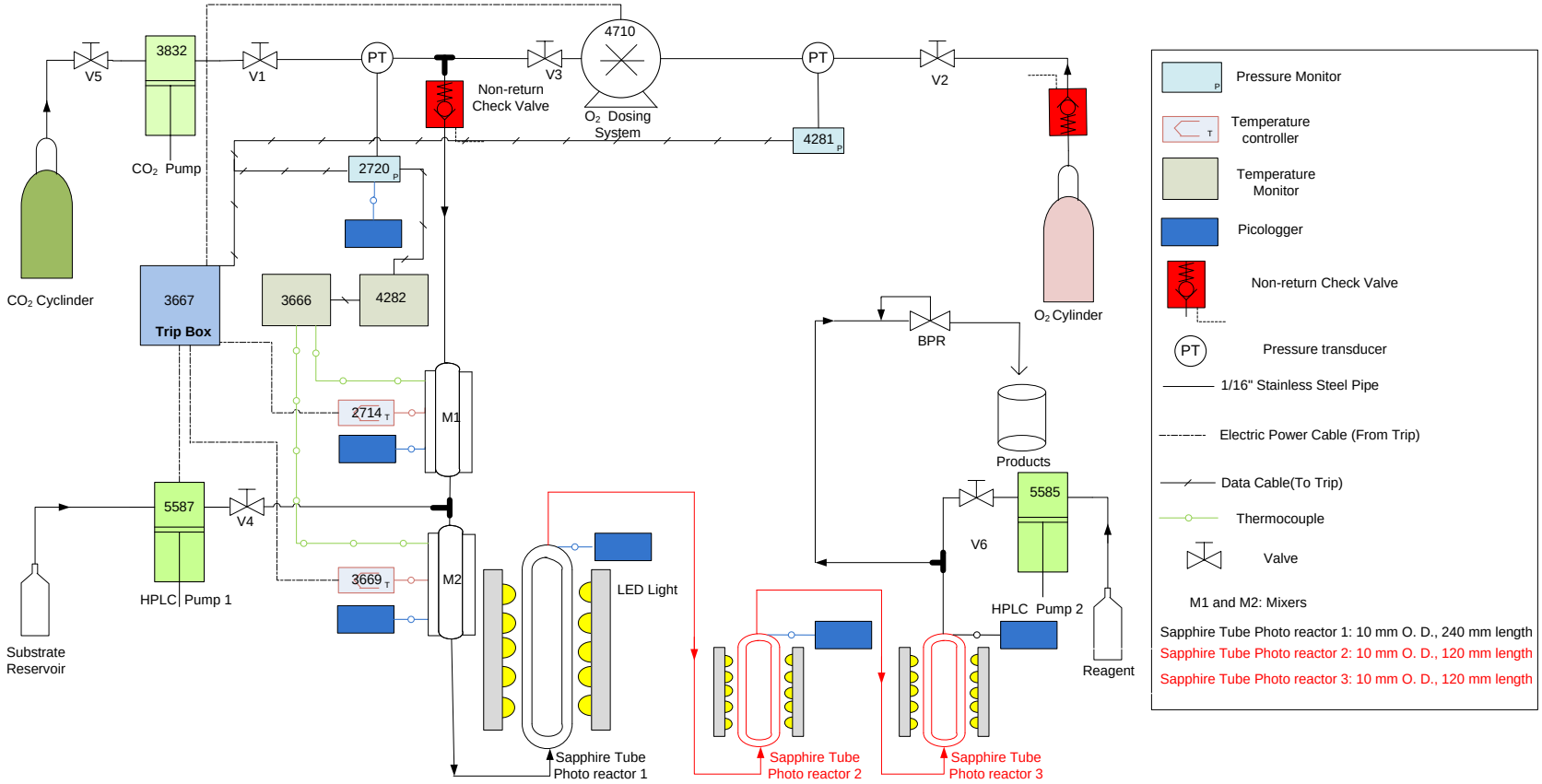


Figure 5-16 The diagram of the high-pressure rig for the synthesis of products-setup-3. The difference between setup-3 and setup-1 was that two extra photoreactors (Saint-Gobain Crystals, 10 mm O.D., 1 mm wall thickness, 120 mm long) were connected with previous photoreactor 1 in series to extend the irradiation time in the photoreactor.

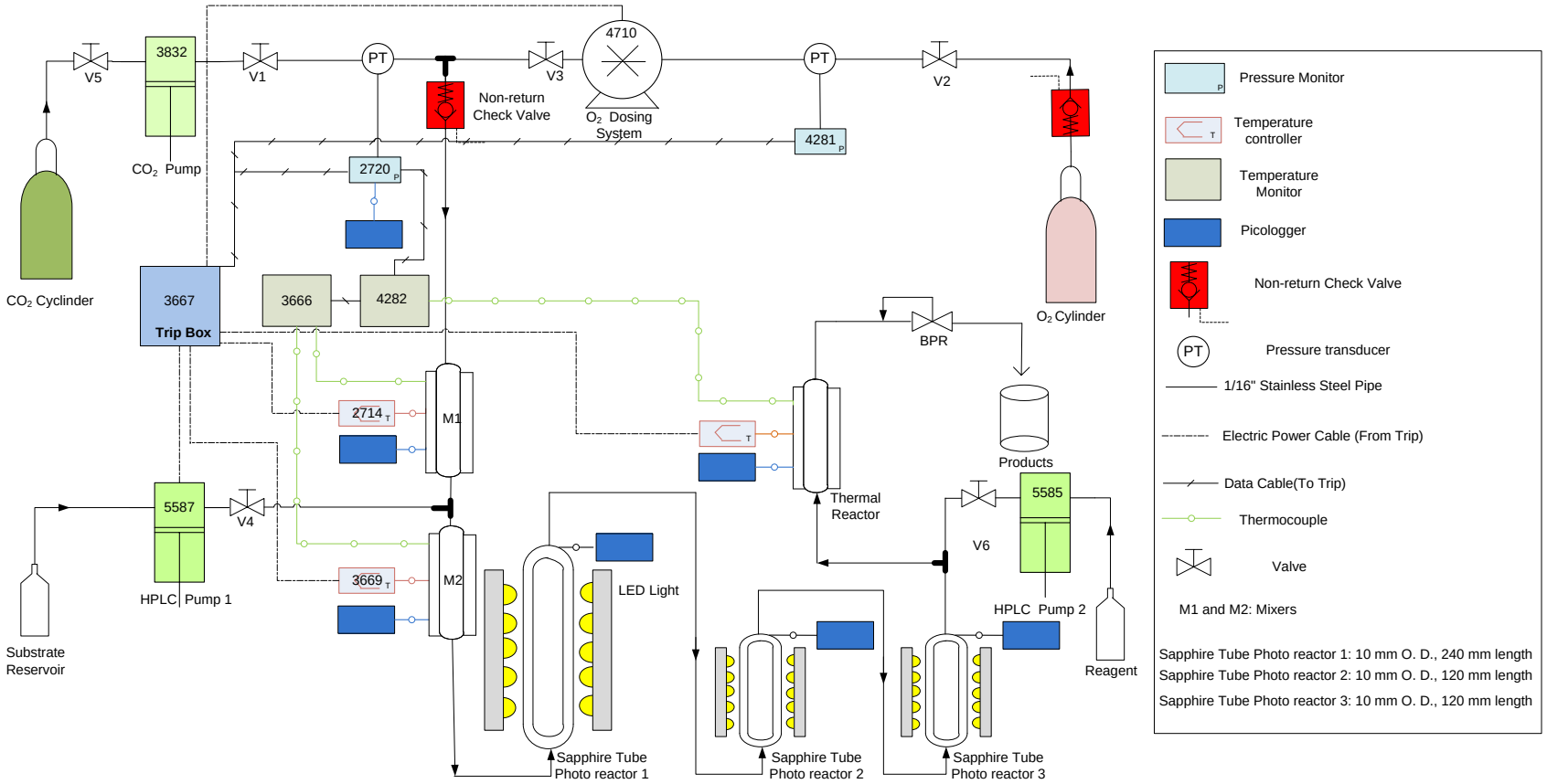


Figure 5-17 The diagram of the high-pressure rig for the synthesis of products-setup-4. The difference between setup-4 and setup-1 was that a thermal reactor and two photoreactors were connected in series as shown in the diagram to obtain longer irradiation time and cyclisation of p-peroxylquinol derivatives with different aldehydes.

5.10.3 **Phase Behaviour study**

In order to mimic the conditions in the process of dearomatisation, the phase behaviour was studied in the high-pressure continuous flow reactor (Figure 5-4), without irradiation by LED light, at 120 bar and 40 °C when the sapphire tube (240 mm length, 10 mm O. D.) was loaded with glass beads as the same as in the reaction state. The results are shown in Table 5-17.

Firstly, CO_2/methanol system was studied, 62 % of CO_2 and 38 % of methanol were miscible well, the molar ratio of the substrate (*p*-cresol) to oxygen was 1:1. Only a single phase would be observed (entry 1). Then, pumping the *p*-cresol solution at 3.9 %, CO_2 (59.6 %) and methanol (36.5 %), under this condition, the equivalent concentration of *p*-cresol in methanol was 3.0 M, *p* - cresol, CO_2 and methanol were still in a single phase (entry 2). However, if we introduced oxygen (3.8 %) and p-cresol (3.8 %), two phases (for example in Figure 5-18) were observed for these components (CO_2, methanol, oxygen and *p*-cresol) (entries 3-4).

Then, decreasing the mole fraction of oxygen in CO_2/methanol from 3.8 % to 2.0 %, we found a single phase occurred under the conditions with 2.0 % of oxygen, even adding 2 % of *p*-cresol.(entries 5–8) During of all these processes, *p*-cresol was soluble very well in methanol and CO_2 system. However, two phases were observed when the mole fraction of oxygen was higher than 2.7 %. This problem was avoided since the oxygen was consuming, even starting with high oxygen concentration.

Table 5-17 The results for phase behaviour studies in the CO_2 system (Figure 5-15).

Entry	Equivalent Concentration of 5.1a in MeOH, O_2:Sub=1:1 (mol:mol)	Mole fraction of each component %				Phase behaviour	Pressure (bar)	Temperature (°C)
		CO_2	MeOH	O_2	Substrate			
1	-	62.0	38	0	0	A single phase	120	40
2	3.0 M	59.6	36.5	0	3.9	A single phase	120	40
3	3.0 M	59.6	36.5	3.9	0	Two phases[a]	120	40
4	3.0 M	57.3	35.1	3.8	3.8	Two phases[a]	120	40
5	2.5 M	60.3	36.3	3.3	0	Two phases[a]	120	40
6	2.0 M	61.1	36.2	2.7	0	Two phases[a]	120	40
7	1.5 M	62	36	2	0	A single phase	120	40
8	1.5 M	60.7	35.3	2	2	A single phase	120	40

[a]: "*Two phases*" means some bubbles would be observed in the up-flow sapphire tube reactor.

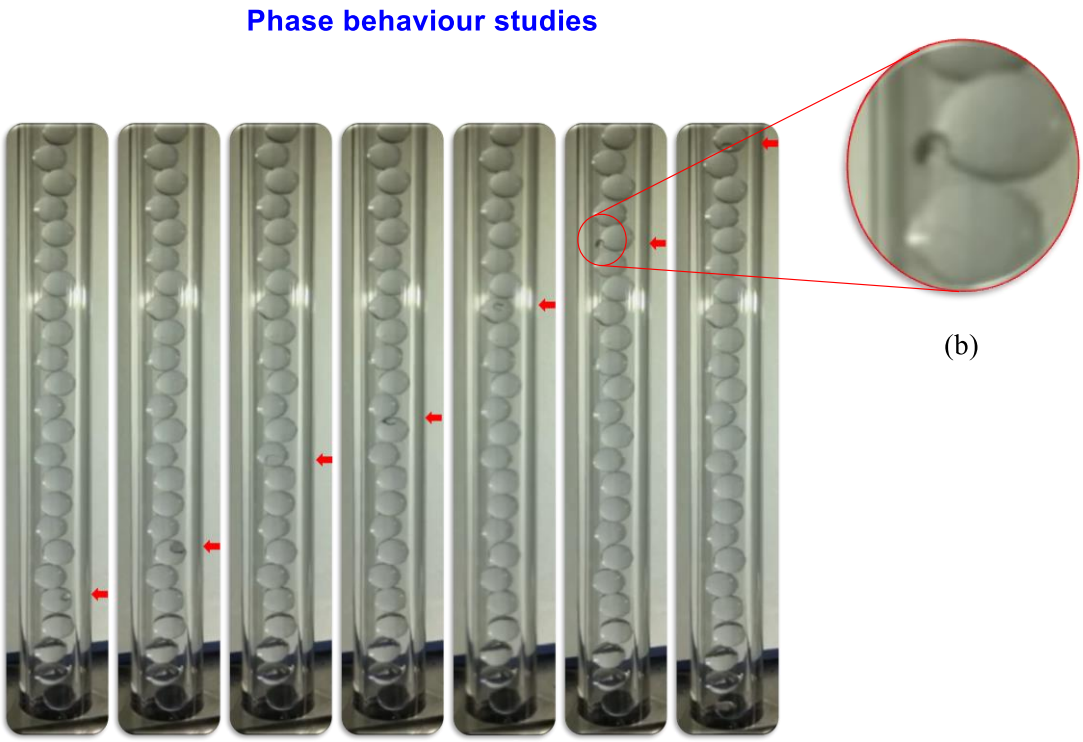
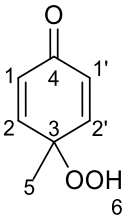


Figure 5-18 An example of two phases under the condition of Table 5-17, entry 4. (a) A bubble is flowing upwards as the time evolves from left to right; (b)Magnified picture to show the bubble.

5.10.4 NMR Data

4-hydroperoxy-4-methylcyclohexa-2,5-dien-1-one (5.2a)

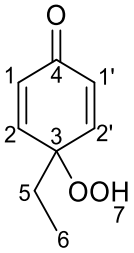


^{1}H NMR (400 MHz, Chloroform-*d*) δ 8.34 (s, 1H, -OOH), 6.94 – 6.87 (m, 2H, H2 + H2'), 6.33 – 6.26 (m, 2H, H1 + H1'), 1.42 (s, 3H, CH3).

^{13}C NMR (101 MHz, Chloroform-*d*) δ = 185.5 (C4), 149.7 (C2+ C2'), 130.5 (C1 + C1'), 78.7 (C3), 22.9 (C5).

HRMS (ESI): for $C_7H_8O_3$, $[M]^+$ calculated *m/z* = 140.0473, found *m/z* = 140.0472.

4-ethyl-4-hydroperoxycyclohexa-2,5-dien-1-one (5.2b)[483]

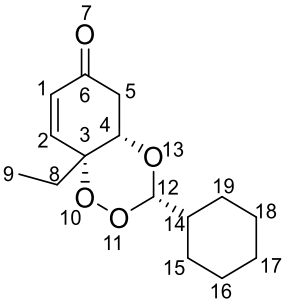


^{1}H NMR (400 MHz, Chloroform-*d*) δ 8.75 (s, 1H, -OOH), 6.96 – 6.75 (m, 2H, H2 + H2'), 6.39 – 6.30 (m, 2H, H1 + H1'), 1.74 (q, *J* = 7.6 Hz, 2H, CH2), 0.85 (t, *J* = 7.6 Hz, 3H, CH3).

^{13}C NMR (101 MHz, Chloroform-*d*) δ = 186.2 (C4), 149.4 (C2 + C2'), 131.4 (C1 + C1'), 82.4 (C3), 29.0 (C5), 7.9 (C6).

HRMS (ESI): for $C_8H_{10}O_3$, $[M-H]^-$ calculated *m/z* = 153.0557, found *m/z* = 153.0551.

3-cyclohexyl-8a-ethyl-4a,8a-dihydrobenzo[e][1,2,4]trioxin-6(5H)-one (5.3b)

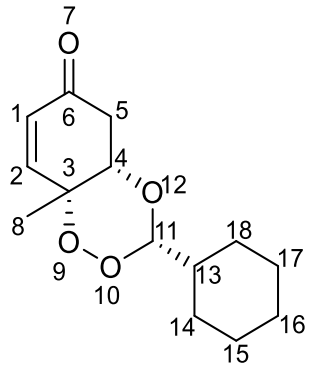


^{1}H NMR (400 MHz, Chloroform-*d*) δ 6.90 (d, *J* = 10.4, 1H, H2), 6.10 (d, *J* = 10.4 Hz, 1H, H1), 4.99 (d, *J* = 5.5 Hz, 1H, H12), 4.18 (q, *J* = 2.9 Hz, 1H, H4), 2.68 (m, 2H, 2×H5), 1.79 (m, 1H, H14), 1.74 – 1.57 (m, 8H, 2×H15 + 2×H19 + 2×H16 + 2×H18), 1.49 (m, 2H, 2×H8), 1.17 – 1.04 (m, 2H, 2×H17), 1.00 (t, *J* = 7.6 Hz, 3H, CH3).

^{13}C NMR (101 MHz, Chloroform-*d*) δ = 195.5 (C6), 150.9 (C2), 130.0 (C1), 106.6 (C12), 80.0 (C4), 75.3 (C3), 41.0 (C5), 40.5 (C14), 28.8 (C8), 27.0 (C15 + C19), 26.3 (C17) , 25.7 (C16 + C18), 7.3 (C9).

HRMS (ESI): for $C_{15}H_{22}O_4$, $[M+H]^+$ calculated *m/z* = 267.1596, found *m/z* = 267.1574.

3-cyclohexyl-8a-methyl-4a, 8a-dihydrobenzo[e][1,2,4]trioxin-6(5H)-one (5.3a)[483]

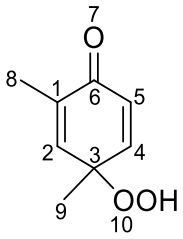


^{1}H NMR (400 MHz, Chloroform-*d*) δ 6.84 (d, *J* = 10.3, 1H, H2), 6.07 (dd, *J* = 10.3, Hz, 1H, H1), 5.02 (d, *J* = 5.4 Hz, 1H, H11), 4.14 (q, *J* = 3.0 Hz, 1H, H4), 2.70 (m, 2H, 2×H5), 1.74 – 1.58 (m, 5H, H13 + 2×H14 + 2×H18), 1.33 (s, 3H, CH3), 1.22 – 0.98 (m, 6H, 2×H15 + 2×H16 + 2×H17).

^{13}C NMR (101 MHz, Chloroform-*d*) δ = 195.3 (C6), 151.3 (C2), 129.7 (C1), 106.7 (C11), 78.0 (C4), 76.5 (C3), 41.2 (C5), 40.5 (C13), 27.1 (C14), 27.0 (C18), 26.3 (C16), 25.8 (C15 + C17), 20.7 (C8).

HRMS (ESI): for $C_{14}H_{20}O_4$, $[M+Na]^+$ calculated *m/z* = 275.1254, found *m/z* = 275.1254.

4-hydroperoxy-2,4-dimethylcyclohexa-2,5-dien-1-one (5.2c)[428]

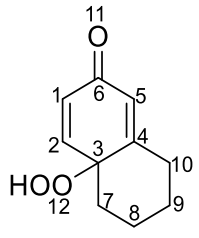


^{1}H NMR (400 MHz, Chloroform-*d*) δ 8.16 (s, 1H, -OOH), 6.87 (d, *J* = 10.0 Hz, 1H, H4), 6.66 (q, 1.5 Hz, 1H, H2), 6.28 (d, *J* = 10.0 Hz, 1H, H5), 1.92 (s, 3H, H8 (CH3)), 1.40 (s, 3H, H9 (CH3)).

^{13}C NMR (101 MHz, Chloroform-*d*) δ = 186.3 (C6), 149.4 (C4), 144.8 (C2), 137.2 (C1), 130.2 (C5), 79.0 (C3), 23.0 (C8), 15.9 (C9).

HRMS (ESI): for $C_8H_{10}O_3$, $[M-H]^-$ calculated *m/z* = 153.0557, found *m/z* = 153.0541.

4a-hydroperoxy-5,6,7,8-tetrahydronaphthalen-2(4aH)-one (5.2d)[428]

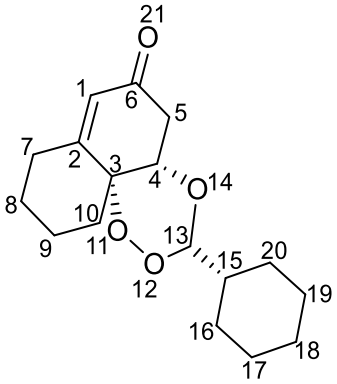


white solid, **^{1}H NMR** (400 MHz, Chloroform-*d*) δ 7.85 (s, 1H, -OOH), 6.81 (d, *J* = 9.9 Hz, 1H, H2), 6.31 (d, *J* = 9.9 Hz, 1H, H1), 6.19 (s, 1H, H5), 2.70 – 2.59 (m, 1H, 2×H7), 2.24 – 2.00 (m, 2H, 2×H10), 2.09 – 2.00 (m, 2H, 2×H9), 1.52 – 1.34 (m, 2H, 2×H8).

^{13}C NMR (101 MHz, Chloroform-*d*) δ = 186.5 (C6), 161.4 (C4), 149.2 (C2), 131.1 (C1), 126.4 (C5), 79.8 (C3), 37.0 (C7), 32.4 (C10), 28.0 (C8), 20.6 (C9).

HRMS (ESI): for $C_{10}H_{12}O_3$, $[M+H]^+$ calculated *m/z* = 181.0859, found *m/z* = 181.0855.

3-cyclohexyl-4a,5,8,9,10,11-hexahydro-6H-naphtho[1,8a-e][1,2,4]trioxin-6-one (5.3d)

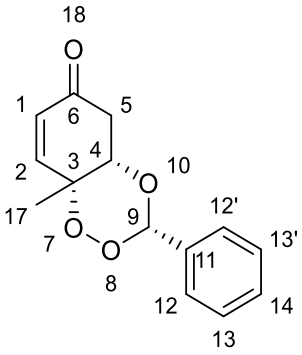


Yellow oil, **^{1}H NMR** (400 MHz, Chloroform-*d*) δ 5.99 (t, J = 1.3 Hz, 1H, H1), 5.02 (d, J = 5.5 Hz, 1H, H13), 4.04 (t, J = 3.0 Hz, 1H, H4), 2.73 – 2.58 (m, 2H, 2×H5), 2.29 (m, 1H, H15), 2.12 – 1.90 (m, 2H, 2×H10), 1.71 – 1.65 (m, 6H, 2H7 + 2H8 + 2H9), 1.42-1.40 (m, 8H, 2×H16 + 2×H17 + 2×H19 + 2×H20), 1.32 – 1.22 (m, 2H, 2×H18).

^{13}C NMR (101 MHz, Chloroform-*d*) δ = 195.8 (C6), 163.6 (C2), 125.1 (C1), 106.2 (C13), 79.2 (C4), 75.5 (C3), 42.1 (C15), 40.5 (C5), 34.7 (C10), 32.2 (C7), 29.7 (C8), 29.0 (C9), 27.1 (C16 + C20), 26.3 (C17), 25.7 (C19), 20.2 (C18).

HRMS (ESI): for $C_{17}H_{24}O_4$, $[M+H]^+$ calculated *m/z* = 293.1747, found *m/z* = 293.1749.

8a-methyl-3-phenyl-4a, 8a-dihydrobenzo[e][1,2,4]trioxin-6(5H)-one (5.4a)

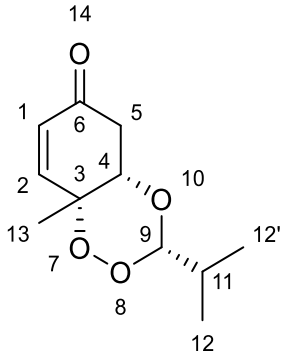


White solid, , **^{1}H NMR** (400 MHz, Chloroform-*d*) δ= 7.43 – 7.33 (m, 5H, Hs on benzene group), 6.95 (d, *J* = 10.4 Hz, 1H, H2), 6.22 (s, 1H, H9), 6.17 (d, *J* = 10.4 Hz, 1H, H1), 4.41 (q, *J* = 2.9 Hz, 1H, H4), 2.79 (m, 2H, 2×H5), 1.44 (s, 3H, CH3).

^{13}C NMR (101 MHz, Chloroform-*d*) δ = 195.0 (C6), 151.2 (C2), 133.6 (C11), 130.4 (C14), 129.9 (C1), 128.6 (C12 + C12‘), 127.3 (C13 + C13‘), 103.8 (C9), 78.1 (C4), 77.1 (C3), 41.2 (C5), 20.8 (C17).

HRMS (ESI): for $C_{14}H_{14}O_4$, $[M+Na]^+$ calculated *m/z* = 269.0784, found *m/z* = 269.0783.

3-isopropyl-8a-methyl-4a,8a-dihydrobenzo[e][1,2,4]trioxin-6(5H)-one (5.5a)[483]

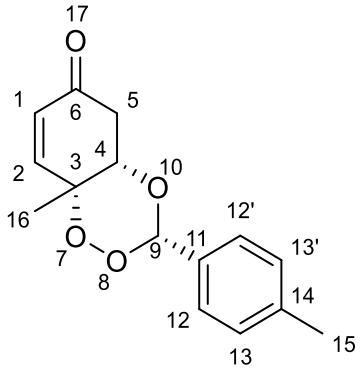


White solid, **^{1}H NMR** (400 MHz, Chloroform-*d*) δ= 6.84 (d, *J* = 10.4 Hz, 1H, H2), 6.06 (d, *J* = 10.4 Hz, 1H, H1), 5.00 (d, *J* = 5.1 Hz, 1H, H9), 4.15 (q, *J* = 2.9 Hz, 1H, H4), 2.78 – 2.64 (m, 2H, 2×H5), 1.76 (m, 1H, H11), 1.33 (s, 3H, H13 (CH3)), 0.88 (d, *J* = 6.9 Hz, 6H, H12 (CH3) + H12‘ (CH3)).

^{13}C NMR (101 MHz, Chloroform-*d*) δ = 195.3 (C6), 151.2 (C2), 129.7 (C1), 107.2 (C9), 77.9 (C4), 76.5 (C3), 41.1 (C5), 31.0 (C11), 20.7 (C13), 16.7 (C12 + C12‘).

HRMS (ESI): for $C_{11}H_{16}O_4$, $[M+Na]^+$ calculated *m/z* = 235.0941,found *m/z* = 235.0934.

8a-methyl-3-(*p*-tolyl)-4a,8a-dihydrobenzo[*e*][1,2,4]trioxin-6(5*H*)-one (5.6a)

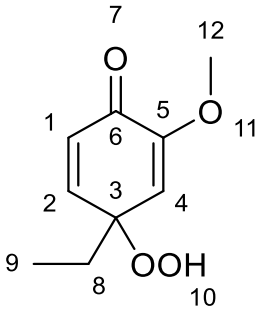


White solid, ^{1}H NMR (400 MHz, Chloroform-*d*) δ= 7.29 (d, *J* = 8.2 Hz, 2H, H12 + H12‘), 7.16 (d, *J* = 7.9 Hz, 2H, H13 + H13‘), 6.94 (d, *J* = 10.3 Hz, 1H, H2), 6.18 (s, 1H, H9), 6.16 (d, *J* = 10.3 Hz, 1H, H1), 4.39 (q, *J* = 2.9 Hz, 1H, H4), 2.88 – 2.75 (m, 2H, 2×H5), 2.34 (s, 3H, H15 (CH3)), 1.43 (s, 3H, H16 (CH3)).

^{13}C NMR (101 MHz, Chloroform-*d*) δ = 195.0 (C6), 151.3 (C2), 140.5 (C11), 130.8 (C14), 129.9 (C1), 129.3 (C12 + C12‘), 127.2 (C13 + C13‘), 103.8 (C9), 80.0 (C4), 77.1 (C3), 41.2 (C5), 21.5 (C15), 20.8 (C16).

HRMS (ESI): for $C_{15}H_{16}O_4$, $[M+Na]^+$ calculated *m/z* = 283.0941,found *m/z* = 283.0942.

4-ethyl-4-hydroperoxy-2-methoxycyclohexa-2,5-dien-1-one (5.2e)



Yellow solid, **^{1}H NMR** (400 MHz, Chloroform-*d*) δ 8.23 (s, 1H, -OOH), 6.85 (d, *J* = 10.0 Hz, 1H, H2), 6.35 (d, *J* = 10.0 Hz, 1H, H1), 5.66 (s, 1H, H4), 3.70 (s, 3H, H12 (CH3)), 1.79 (q, *J* = 7.7 Hz, 2H, 2×H8), 0.87 (t, *J* = 7.6 Hz, 3H, 3×H9).

^{13}C NMR (101 MHz, Chloroform-*d*) δ = 181.3 (C6), 152.9 (C2), 149.6 (C4), 130.5 (C1), 114.5 (C5), 84.2 (C3), 55.2 (C12), 29.9 (C8), 8.1 (C9).

HRMS (ESI): for $C_9H_{12}O_4$, $[M+H]^+$ calculated *m/z* = 185.0808, found *m/z* = 185.0800.

Chapter 6. Conclusion and Future Work

Chapter 1 outlined the aims of this Thesis, and the aims are repeated as follows for convenience. The goals of this work were:

1. To improve and rebuild a safer high-pressure continuous flow photo-oxidation reactor in order to perform multistep experiments.
2. To investigate the synthesis of a range of valuable products from a single feedstock in a new daisy-chained reactor, such as from combining the photoreactor and thermal reactor in series.
3. To investigate the principle of how to efficiently perform a multistep experiment to realise high reaction yields and productivities, such as synthesis of a range of individualised chemicals.
4. To explore a green photochemical route as an alternative to the traditional, harsh method (using stoichiometric reagents to obtain high efficiency), such as the dearomatisation of phenols *via* photo-oxidation.
5. To investigate the heterogeneous catalyst in continuous fixed-bed thermal reactor daisy-chaining with photoreactor in order to conduct a sequence of steps to give a target molecule, such as the synthesis of 1,2,4-trioxanes following dearomatisation of phenols.

In this Chapter, the progress towards meeting each of these aims is discussed. For each aim, the underlying rationale is discussed together with the progress conducted to meet the relevant aim, conclusions which can be drawn from the work presented. In addition, possible future work is proposed.

6.1 Aim 1 and Aim 3

Aim 1 and Aim 3, repeated as follows, were closely related to each other, as the development of Aim 1 is for realising Aim 3. Both of them were fulfilled in the Thesis.

"**Aim 1**: To improve and rebuild a safer high-pressure continuous flow photo-oxidation reactor in order to perform multistep experiments."

"**Aim 3**: To investigate the principle of how to efficiently perform a multistep experiment to realise high reaction yields and productivities, such as synthesis of a range of individualised chemicals."

6.1.1 Rationale

The high-pressure photo-oxidation in $scCO_2$ has been studied in the Clean Technology Group since 2008,[203] and then it was adapted to continuous flow reactor. Consequently, although Dr Bellamy developed it in the current photoreactor with high light penetration and better temperature control,[202] it has been limited only for the oxidation step in the sapphire tube reactor and relatively fast photo-oxidation reactions. The previous high-pressure continuous photo-oxidation setup was working safely, but without a check valve to avoid the mixture of oxygen and organic stream returning back to the pure oxygen stream, even back to the oxygen cylinder, which is a potential risk.

In order to conduct more interesting photo-oxidation and multistep reactions safely in a daisy-chained mode in the high-pressure continuous flow CO_2 system, a

high-pressure equipment with appropriate check valve which can be used for multistep reactions was the ultimate goal.

6.1.2 **Progress**

Chapter 2 describes the new high-pressure continuous flow CO_2 equipment (Figure 2-4) for general multistep reactions in a daisy-chained mode. Two more check valves were added into the system, as shown in Figure 2-4. These check valves can avoid the mixture of organic and oxygen stream going back to the pure oxygen stream when an emergency occurred. A sapphire tube reactor coupled with a thermal reactor, besides other components, having been discussed in Chapter 2.

Both the sapphire tube reactor and the thermal reactor can be easily modified to adapt to relevant multistep experiments. Chapter 3 describes four higher value compounds being produced from a single feedstock, **3.1**, in this newly designed equipment by coupling the sapphire photoreactor with a stainless steel thermal reactor. It also includes the modification of thermal reactor to yield compound **3.5** by using a thermal reactor consisting of 4 normal size tubular stainless steel tubes in series to obtain an excellent yield for **3.5**, and the simplified diagrams were shown in Section 3.9.3. Chapter 4 demonstrated the synthesis of caprolactone in this daisy-chained mode equipment by the combination of a photoreactor and thermal reactors, as shown in Figure 4-3. Chapter 5 further proved the advantages of the high-pressure continuous flow CO_2 setup used for multistep reactions. The dearomatisation of *para*-phenols and cyclisation of the products which were obtained in the photoreactor were performed in the photoreactor and thermal reactor in series. Since the reaction rate for dearomatisation of phenols by using $^1O_2$ is much slower than that of cyclopentadiene and fulvene, an elongated sapphire tube reactor was used for the dearomatisation step of phenols in order to obtain relatively more light radiation and longer residence time in the photoreactor (240 mm in length, 2 × that of the reactors

previously described or three sapphire tube reactors in series), as shown in Figure 5-14.

As in the discussion of all these reactive systems, good yields and productivities are important for the scaling up in industry. In our current multistep equipment, 99 % yield of **3.5** was obtained by tuning the parameters properly and the productivity achieved was approximately 50 times higher compared to the literary work; 4.2 g of crystal **5.3a** was obtained in 8 hours.

Through the three reaction systems, four products obtained from cyclopentadiene, caprolactones obtained from fulvenes and dearomatisation of phenol to further obtain 1,2,4-trioxane compounds, the developed high-pressure continuous flow CO_2 equipment for multistep reactions was shown to be working very well. The appropriate reaction conditions for both photo-oxidation and thermal step are realised in the current system, allowing to obtain relatively high yield and productivity.

6.1.3 **Further directions**

The high-pressure continuous flow CO_2 setup can be further modified to adapt more challenging experiments, such as installing several thermal reactors in parallel loading same or different solid catalysts to meet the demand for the catalyst deactivation during the experiment.

It is possible to install an online analysis to realise self-optimisation for meeting the production of numbers of individualised products to better fulfil the new challenges in Pharma.

6.2 Aim 2

"To investigate the synthesis of a range of valuable products from a single feedstock in a new daisy-chained reactor, such as from combining the photoreactor and thermal reactor in series."

6.2.1 **Rationale**

Photo-oxidation of cyclopentadiene (**3.1**, presented in Chapter 3) with $^1O_2$ after irradiation by visible light to product **3.3** usually occurred under harsh conditions (-20~-130 °C) and on a small scale (0.01 mmol), since the intermediate **3.2** is highly reactive with a potential for explosion when large amounts of **3.2** gatherings in a batch reactor. This reaction usually was conducted in organic solvents, such as CH_2Cl_2 or CCl_4, because these solvents provide a relatively long lifetime for reactive $^1O_2$, though they are not environmental-friendly. The use of these solvents resulted in the scaling up of experiments involving this photo-oxidation of **3.1** having been limited. In addition, four higher value products, **3.3** - **3.6**, can be formed from the photo-oxidation of **3.1** *via* facile transformations of active intermediate **3.2** upon treatment under a variety of conditions.

As shown in Scheme 3-2, product **3.3** can be obtained by reduction of intermediate **3.2** from the photo-oxidation of **3.1**, while **3.4** can be formed when the photo-oxidation was carried out in dilute alkaline alcoholic solutions at atmospheric pressure and room temperature. Both products **3.3** and **3.4** are attractive to organic chemists since they can be used as starting materials for a variety of applications, most notably in one of the popular routes to prostaglandins. Whereas, active aldehyde **3.5** was made *via* thermal isomerisation of intermediate **3.2** at an appropriate temperature and has a unique structure comprising two active sites (α,β-conjugated ketone and a terminal epoxide) susceptible to undergo a reaction when subjected to agents to useful compounds, such as, **3.6**, a versatile compound being used as a fuel.

Other than the production of **3.3** from **3.1** on a small scale in organic solutions, the other products mentioned above have been relatively less studied. Due to the highly reactive nature of $^1O_2$, the choice of suitable solvents for the scale-up of such photo-oxidation is limited as they are required to be non-flammable and inefficient $^1O_2$ quenchers. Dense CO_2 provides many attractive properties for oxidation as it is fully-oxidised, non-flammable and non-toxic. Using inert supercritical fluids as reaction solvents is a greener alternative to using traditional, flammable and toxic solvents. Moreover, oxygen is entirely miscible with CO_2 and $^1O_2$ has a relatively longer lifetime in $scCO_2$.

Continuous flow reactors are relatively smaller compared to batch reactors for scaling up, only small amounts of chemicals react at any given instant, which can avoid a large amount of potentially hazardous compounds gathering, more advantages have been discussed in Section 1.3.

Also, photo-oxidation of fulvenes to access caprolactones are underdeveloped, even though caprolactones have found broad applications as critical molecules for the synthesis of important bioactive compounds, natural products and polymers and have been the most widely studied lactones in enzymatic polymerisation for the synthesis of biocompatible and biodegradable polymers. The ε-caprolactone is usually synthesised *via* Baeyer-Villiger reaction with Caro's acid or organic peracids, which has a high economic and environmental cost, together with a high risk of explosion due to the need for organic solvents and unstable reagents.

Therefore, these valuable products can be synthesised efficiently in the multistep continuous flow CO_2 setup in a daisy-chained mode. For the synthesis of caprolactones, a co-solvent is required either for pumping the starting material, such as fulvenes in Chapter 4 or for avoiding the blockages during the process because the fuleves are viscous or solid at room temperature. However, a co-solvent has been considered to be green and, in the case of synthetic **3.6**, a reagent required for the final step is suitable for this purpose.

6.2.2 **Progress**

Synthesis of four products from a single feedstock, cyclopentadiene

Firstly, the photo-oxidation of **3.1** was monitored by FT-IR in a high-pressure batch cell, using $scCO_2$ as a solvent. The freshly prepared solution of TPFPP solubilising in **3.1**, and then feeding CO_2/O_2 mixture, was irradiated by visible light every 20 seconds, at 120 bar and 40 °C. The reaction was confirmed by FT-IR spectroscopy recorded in 19 min. Three compounds, **3.1**, **3.2** and **3.3** were observed from the spectra of the mixture by comparison with the spectra recorded of the corresponding pure compound of **3.1** and **3.5**, respectively, because pure **3.2** only can be isolated at **-**100 °C. Based on the assignment of characteristic peaks of 1369 cm^{-1} (**3.1**), 1330 cm^{-1} (**3.2**) and 1616 cm^{-1} (**3.5**), these peaks in size varied upon the photolysis time. After 19 min irradiation, the results showed that the photo-oxidation of **3.1** to **3.2** proceed with zero-order kinetics under these conditions. We can further demonstrate that: (i) Product **3.2** and **3.5** were produced under these conditions (120 bar, 40 °C); (ii) **3.2** can be detected before decaying into **3.5**.

Then, the isomerisation of **3.2** to **3.5** was monitored by NMR for 5 hours at 20 °C, atmospheric pressure. Chemical shifts at 10.18~10.22 ppm and 5.29~5.32 ppm represent compound **3.5** and **3.2**, respectively. The concentration of **3.5** increased as that of **3.2** decreased. The results proved that this thermal isomerisation was the first-order reaction, and the half-life is a couple of hours at 20 °C.

Following the small-scale batch reactions and monitoring by FT-IR and NMR, these results suggested that it might be used for the production of **3.3**, **3.4**, **3.5**, **3.6** after the photo-oxidation of **3.1** in $scCO_2$ in a scaled-up daisy-chain continuous flow setup. The photo-oxidation of **3.1** with $^1O_2$ was optimised by varying the temperature of photoreactor, the flow rates of CO_2 pump and organic pump, the concentrations of **3.1** and TPFPP or using methanol as co-solvent. Full conversion of **3.1** were obtained under both in liquid CO_2 (0 °C) and $scCO_2$ (40 °C) with or without co-solvent. However,

intermediate **3.2** was much more stable in liquid CO_2 than in $scCO_2$. Treatment of **3.2** by introducing a thiourea solution (1.0 M in methanol) downstream of photoreactor (0 °C), 94 % of **3.3** was obtained, with 5.94 mmol/h productivity when the thermal reactor was kept at room temperature, while the highest productivity of **3.3** in vortex reactor was 4.26 mmol/h. Both the productivities in high-pressure daisy-chained CO_2 setup and vortex reactor are higher than the literature work (3.06 mmol/h).

Treatment of endoperoxides **3.2** with a base leads to the formation of an α, β-unsaturated carbonyl moiety containing an attached hydroxyl group, HCP (**3.4**). Different base catalyst (NaOH solution (0.1 M), solid catalyst Amberlite IR 120 Na^+ form and TEA solution (0.8 M)) were tested, yielding 81 % of **3.4** when pumping neat **3.1** into the system and catalysed by TEA in the thermal reactor, with a productivity of 30.9 mmol/h, much higher than the previous work (5.0 mmol/h).

A quantitative yield of **3.5** was achieved in continuous flow daisy-chained reactor (Figure 3-13) using $scCO_2$ as a solvent, and the temperature was 40 °C for both photoreactor and thermal reactor. The productivity of **3.5** reached 36.3 mmol/h, almost 50 times compared to the published work. Further treatment of **3.5** by acid catalyst yielded 85 % of **3.6** when introducing TFA solution (50 mM) downstream of thermal reactor 1 (Figure 3-14), with productivity of 31.6 mmol/h, which is 26 times higher than that of in the previous work.

Synthesis of caprolactones from fulvenes

In terms of the synthesis of caprolactones form fulvenes, starting with 6,6-dimethyl fulvene (**4.1a**), the photo-oxidation of **4.1a** and thermal isomerisations were optimised in the high-pressure $scCO_2$ system using either ethyl acetate or methanol as co-solvent by varying the concentration of **4.1a**, the flow rates of CO_2 and organic pump and temperature of the thermal reactor. Different products ratios of **4.2a**: **4.3a**: **4.4a** could be obtained merely by changing the parameters of the flow reactor, but with caprolactone **4.2a** (76 % yield) as the major product by increasing the CO_2 flow

rate to 0.75 mL/min (hence lowering the concentration of **4.1a** in the reactor as the organic flow rate remained constant).

With the optimised conditions in hand, we surveyed several different functionalised fulvenes (**4.1a**-**4.1g**) as starting materials to access a variety of caprolactone derivatives and obtained good yields for most of the caprolactones (**4.2a**-**4.2g**). The reactivity of fulvenes with $^1O_2$ depends on the substitutents attached to the fulvene, either electron withdrawing groups or electron donating groups, even with easily removed allylic hydrogen atoms or hydroxyl groups. For example, an unexpected product **4.5g** was obtained when fulvene with a hydroxyl group subjected to the experiment.

Some of these caprolactone have been demonstrated that they can be used for the further reaction to add value on them, such as quantitative hydrogenation yield of **4.6** from **4.2c** was obtained in a small batch reactor.

These results demonstrated that a variety of valuable products were scaled-up in the high-pressure continuous flow daisy-chained reactors, using dense CO_2 as solvent *via* safe and green routes.

6.2.3 Future Directions

This has been studied in Chapter 3 has provided a starting point for the green continuous flow synthesis of a variety of higher value chemicals in multistep equipment to meet the demand for more personalised drugs in the future. It also can be further developed by adding value to the current products.

In terms of the choice of starting material, cyclopentadiene derivatives should be investigated to scale up the practicality of the daisy-chained mode equipment. A thermal reactor could be added before upstream of the photoreactor to realise the cracking of dicyclopentadiene to **3.1** directly monitored by self-optimisation, due to its easy dimerisation to its dimer at room temperature, there will be no extra distillation required before the reaction, and useful products can be produced from cheap

dicyclopentadiene. Moreover, more functionalised cyclopentadiene derivatives will be explored in the high-pressure continuous flow reactor using CO_2 as a solvent, such as 1,2,3,4-Tetramethyl-1,3-cyclopentadiene or 1,2,3,4-Tetraphenyl-1,3-cyclopentadiene.

The enantiomer of **3.4** is attractive to organic chemists and is also an important precursor for the synthesis of prostaglandin. Synthesis of chiral base catalyst should be explored for the transformation of endoperoxide **3.2** to chiral **3.4**. These possible chiral bases can be synthesised from, such as quinine derivatives and cinchonidine derivatives.

Inspired by the production of furfuryl alcohol, **3.6**, from aldehyde **3.5**, the synthesis of pyrrole derivatives should be explored from aldehyde **3.5**, since they are components of more complex macrocycles, including porphyrin and chlorophyll. This can start with the synthesis of imine from aldehyde **3.5** reacting with an amine, such as n-butylamine, and then further treated with an acid to access pyrroles.

In terms of the utilization of caprolactone, further polymerisation should be performed to synthesise polymers which might be biodegradable. Since all the lactones we obtained are unsaturated lactones, some of them can be hydrogenated successfully in a batch reactor. We should explore coupling the setup for the synthesis of caprolactone from fulvenes with hydrogenation step *via* hydrogen atom transfer by reacting with hydrogen donating alcohols rather than using hydrogen since hydrogen and oxygen are not allowed to be provided in the same setup.

6.3 Aim 4

"To explore a green photochemical route as an alternative to the traditional, harsh method (using stoichiometric reagents to obtain high efficiency), reactions such as the dearomatisation of phenols *via* photo-oxidation."

6.3.1 **Rationale**

Phenol and its derivatives are pervasive in natural products, bioactive molecules and, the most frequently utilised, substrates for the synthetic complex natural products *via* dearomatisation with $^1O_2$. These dearomative routes include the oxidation of phenols catalysed by transition-metal catalysts with the help of H_2O_2 or ^{t}BuOOH, or conducted in the presence of oxone as well as photosensitised dearomatisation, which have been discussed in Chapter 5.

Under the conditions with transition-metal catalyst, often, Ruthenium- or Rhodium-based catalysts, Cr (VI), K_3CrO_8, and Ce (IV) have been investigated, in the presence of H_2O_2 or ^{t}BuOOH. The latter was used as co-oxidant, which usually were added in a stoichiometric, or more than stoichiometric quantities, of precursors. Unfortunately, byproducts from this process need to be separated from the reaction mixtures, making the process laborious and expensive. These problems have also been faced in the oxone oxidation system. In addition, the procedure involved with H_2O_2 cannot be used for substrates that react with H_2O_2 or cannot tolerate water or alcohol as solvents. Although dearomatisation with $^1O_2$ was photosensitised under visible light, most of them were conducted in a chlorinated solvent on a minimal scale, this limited its applications in industry, which have been described in Chapter 1.

The dearomatisation of phenol derivatives with $^1O_2$ should be conducted in a greener and more efficient way to avoid or reduce the production of byproducts as well as scale up the amount of dearomative products for further value added in a photochemically continuous flow reactor.

6.3.2 **Progress**

In the case of the dearomatisation of phenol derivatives, the photo-oxidation of *p*-presol (**5.1a**) was initially investigated in the CO_2 system. First, a suitable solvent was required to allow for the pumping of the solid substrate **5.1a** into the photoreactor and to be sure the mixture system was homogeneous. It was found that both

methanol and ethyl acetate are suitable for this purpose, and methanol improves the process of dearomatisation from a reaction rate aspect, although ethyl acetate is preferable from a green chemistry standpoint and a further daisy-chained reactions, which have been discussed in Chapter 5 for the Aim 5.

Subsequently, the dependence of **5.1a** reacting with $^1O_2$ is based on: co-catalysts, the concentrations of **5.1a**, the flow rates of CO_2 pump and organic pumps. These were investigated in the high-pressure continuous flow photoreactor using $scCO_2$ as a solvent and methanol as a co-solvent. This photo-oxidation was photosensitised by TPFPP. This is the same photosensitiser used in the photo-oxidation of cyclopentadiene and fulvenes. The yield of peroxyquinol **5.2a** reached 82 % when 5 mol % of DBU was added, and the concentration of **5.1a** was kept at 0.1 M, but the decomposition of **5.2a** occurred in the presence of 20 mol % DBU. Following this, the concentration of **5.1a** in methanol was varied from 0.1 M to 5.0 M, with an increasing yield of **5.2a** to 96 % even without the addition of base co-catalyst, since the molar ratio of **5.1a** in the $scCO_2$ system increased. Next, *para*-phenols with different functional groups (**5.1a-5.1e**) were investigated under the optimised condition of substrate **5.1a**. The yield of these peroxyquinol derivatives (**5.2a-5.2e**) ranged from 85-96 % when the residence time in the photoreactor was 26 min, with relatively high productivity of 67 g/day for **5.2d** when the irradiation time was 13 min as specified in Table 5-6.

The photo-oxidation of phenol derivatives with $^1O_2$ under irradiation by visible light in the high-pressure CO_2 system provides a promising route to scale up the production of peroxyquinol derivatives for further synthesis of natural products in a greener mode.

6.3.3 Future Directions

In the future, variable *para*-phenol derivatives with different functional groups, such as *para*-substituted with bulky groups, electron withdrawing groups, will be

explored in the high-pressure CO_2 system to discover the effect of substitutes attached to the aromatic structure of phenols. This can give a chance to explore more motifs for the synthesis of chemicals with the antimalarial property. First year PhD student Bruna Lacerda Da Silva Abreu is currently investigating the dearomatisation of phenols with different functional groups in this high-pressure continuous flow CO_2 setup, and the author would like to wish her the best of success in this project.

6.4 Aim 5

"To investigate the heterogeneous catalyst in continuous fixed-bed thermal reactor daisy-chaining with photoreactor in order to conduct a sequence of steps to give a target molecule, such as the synthesis of 1,2,4-trioxanes following dearomatisation of phenols."

6.4.1 Rationale

One of the applications of *p*-peroxyquinol is to access 1,2,4-trioxane chemicals *via* Michael addition, which is the core structure of some antimalarial reagents. It is well-known that malaria continues to be a major lethal infectious disease of human beings. Artemisinin serves as the natural active principle and model compound, which contains a 1,2,4-trioxane subunit. It is mainly extracted from a Chinese plant, but the supply does not always meet the demand, with a semi-synthetic process from more abundant biosynthetic precursors emerged. However, artemisinin-based combination therapies (ACTs, in Chapter 5) such as artemether/lumefantrine/amodiaquine recommended by WHO for the treatment of malaria have been reported to develop resistance in South-East Asia. Recently, different novel 1,2,4-trioxane compounds have been synthesised to be potent antimalarial agents. A greener and more sustainable process should be explored to scale up the production of 1,2,4-trioxane chemicals with potential antimalarial activity. Compared to the liquid catalyst, solid

catalysts have many advantages. Often, the heterogeneous catalysts are stable, reusable and can be used as in the fixed beds, as well as produce fewer waste materials with an easy separation. Amberlyst-15 was frequently used due to its high acidity and low cost. It is a good choice to use Ambelyst-15 instead of some homogenous acid to achieve good productivity in industry.

6.4.2 **Progress**

Following on the dearomatisation of phenol derivatives (Chapter 5) in the high-pressure continuous CO_2 system using methanol as co-solvent, a daisy-chained reaction to synthesise 1,2,4-trioxane chemicals using methanol as co-solvent was proposed. The first step of photo-oxidation of phenols with $^1O_2$ occurred in the photoreactor, and a cyclisation of *p*-peroxyquinol with cyclohexanecarboxaldehyde **5.7** occurred downstream of photo-oxidation solutions catalysed by pre-loaded Amberlyst-15 in the thermal reactor. The first attempt to prepare 1,2,4-trioxane **5.3a** was not successful since the protic solvent methanol was employed, resulting in acetal compound **5.3aa** produced instead of **5.3a** under acid conditions. This is also consistent with the results in the literature, which used aprotic solvent, CH_2Cl_2 as the solvent.

EtOAc was as an alternative co-solvent instead of methanol to avoid the production of **5.3aa**. Since the optimisation of photo-oxidation of **5.1a** was performed in this high-pressure CO_2 using methanol as solvent, we attempted to do optimisation of photo-oxidation of **5.1a** with $^1O_2$ using EtOAc as co-solvent by varying the concentration of **5.1a** in EtOAc, the concentration of TPFPP, the flow rates of CO_2 pump and organic pumps, the temperatures of thermal reactor and the power of LED lights. The yield of **5.2a** in EtOAc was lower than that in methanol unless increasing the residence time in the photoreactor from 26 min to 52 min by prolonging the size of photoreactor. An 84 % yield **5.3a** was obtained when pre-loading 1.0 g Amberlyst-15 in the thermal reactor (40 °C) (Figure 5-4).

To further increase the reaction rate in the photoreactor when using EtOAc as co-solvent, the addition of another protic solvent Hexafluoro-2-propanol (HFIP) was investigated, since HFIP is a protic solvent with lower pKa than methanol. Since the yield of **5.2a** was 95 % in EtOAc without HFIP, 4-ethylphenol (**5.1b**) was used as the model substrate to study the effect of HFIP on both photo-oxidation and thermal cyclisation. The initial attempt was conducted with 2 equivalent of HFIP in the EtOAc solution, without thermal reactor, and the results showed that the yield of **5.2b** indeed increased from 83 % to 99 %. When coupling the photoreactor and thermal reactor, the yield of **5.3b** was 71 %.

The pre-loaded Amberlyst -15 was continually used for the different *p*-peroxyquinol derivatives with variable aldehyde, **5.7**, **5.9**. **5.10**, **5.11**, the yields of 1,2,4-trioxane (**5.3a**-**5.6a**, **5.3b**-**5.3e**) ranged from 20 % to 92 % even without further optimisation for all synthetic 1,2,4-trioxanes. The products 1,2,4-trioxane can be crystallised by collecting after the BPR; it reduced the cost for the further separation with a solid acid catalyst. 4.2 g crystalline **5.3a** was obtained in 8 hours.

6.4.3 Future directions

In the future, more *p*-phenol derivatives with different functional groups, such as *para*-substituted with bulky groups, electron withdrawing groups, will be explored in the high-pressure CO_2 system to access more valuable and antimalarial compounds. Furthermore, the antimalarial activity of 1,2,4-trioxanes probably should be tested in vitro.

6.5 Final Words

Although much progress has been made towards the development of high-pressure continuous flow photo-oxidation process in dense CO_2, as well as of scaling up the synthesis of some more challenging organic compounds, there is still a long

way to go in terms of further investigation of this process on a larger scale. This process also provides an idea, in some extent, to fulfil the demand for the production of personalised drugs in the pharmaceutical industry. I would like to wish first year PhD student Bruna Abreu who continues this research the best of luck and hope to see some of these ideas to be applied to industrial processes in the not too distant future.

知者不惑，仁者不忧，勇者不惧。

Reference

1. Whitesides, G. M., Reinventing Chemistry. *Angew. Chem. Int. Ed.* **2015,** *54*, 3196-3209.
2. Leker, J.; Gelhard, C.; Delft, S. v., *Business Chemistry: How to Build and Sustain Thriving Businesses in the Chemical Industry*. Wiley: USA, 2018.
3. Linkova-Nijs, M. https://cefic.org/media-corner/newsroom/chemical-industry-contributes-5-7-trillion-to-global-gdp-and-supports-120-million-jobs-new-report-shows/ (accessed March 11, 2019).
4. *UK Chemical and Pharmaceutical Industry Facts and Figures*; Chemical Industries Association: 2015.
5. *The Pharmaceutical Industry: a key asset to scientific and medical progress*; European Federation of Pharmaceutical Industries and Associations: 2018.
6. Global Pharmaceutical Industry - Statistics & Facts. https://www.statista.com/topics/1764/global-pharmaceutical-industry/ (accessed 2017).
7. Hermann, M.; Pentek, T.; Otto, B. In *Design Principles for Industrie 4.0 Scenarios*, 2016 49th Hawaii International Conference on System Sciences (HICSS), 5-8 Jan. 2016; 2016; pp 3928-3937.
8. Gaertner, R. *Pharma 4.0 – time to rethink manufacturing and quality*; Manufacturing Chemist Pharma: 2016.
9. Ding, B. Y., Pharma Industry 4.0: Literature review and research opportunities in sustainable pharmaceutical supply chains. *Process Saf. Environ. Prot.* **2018,** *119*, 115-130.
10. Dunn, P.; Wells, A.; Williams, M. T., *Green Chemistry in the Pharmaceutical Industry*. Wiley-VCH: Germany, 2010.
11. Lee, S. L.; O'Connor, T. F.; Yang, X.; Cruz, C. N.; Chatterjee, S.; Madurawe, R. D.; Moore, C. M. V.; Yu, L. X.; Woodcock, J., Modernizing Pharmaceutical Manufacturing: from Batch to Continuous Production. *J. Pharm. Innov.* **2015,** *10*, 191-199.
12. Klán, P.; Wirz, J., *Photochemistry of organic compounds: from concepts to practice*. Wiley: UK, 2009.
13. Xie, Y.; Breen, L., Greening community pharmaceutical supply chain in UK: a cross boundary approach. *Supply Chain Manag.* **2012,** *17*, 40-53.

14. Pfoertner, K. H., Photochemistry in industrial synthesis. *J. Photochem. Photobiol., A* **1990,** *51*, 81-86.
15. Coyle, E. Green Photochemistry: The synthesis of fine chemicals with sunlight. PhD Thesis, Dublin City University, Dublin, 2010.
16. Scholes, G. D.; Fleming, G. R.; Olaya-Castro, A.; van Grondelle, R., Lessons from nature about solar light harvesting. *Nat. Chem.* **2011,** *3*, 763-734.
17. Demmig-Adams, B.; Stewart, J. J.; Burch, T. A.; Adams, W. W., Insights from Placing Photosynthetic Light Harvesting into Context. *J. Phys. Chem. Lett.* **2014,** *5*, 2880-2889.
18. Hashemi, M. M.; Akhbari, M., Efficient Solvent-Free Oxidation of Phenols to p-Quinones with Iodic Acid on the Surface of K10 Montmorillonite. *Russ. J. Org. Chem.* **2005,** *41*, 935-936.
19. Takizawa, S.-y.; Aboshi, R.; Murata, S., Photooxidation of 1,5-dihydroxynaphthalene with iridium complexes as singlet oxygen sensitizers. *Photochem. Photobiol. Sci.* **2011,** *10*, 895-903.
20. Oelgemöller, M.; Jung, C.; Ortner, J.; Mattay, J.; Zimmermann, E., Green photochemistry: solar photooxygenations with medium concentrated sunlight. *Green Chem.* **2005,** *7*, 35-38.
21. Cambie, D.; Bottecchia, C.; Straathof, N. J.; Hessel, V.; Noel, T., Applications of Continuous-Flow Photochemistry in Organic Synthesis, Material Science, and Water Treatment. *Chem. Rev.* **2016,** *116*, 10276-10341.
22. Ciamician, G., The Photochemistry of the Future. *Science* **1912,** *36*, 385-394.
23. Nebbia, G.; Kauffman, G., Prophet of Solar Energy: A Retrospective View of Giacomo Luigi Ciamician (1857-1922), the Founder of Green Chemistry, on the 150th Anniversary of His Birth. *Chem. Educ* **2007,** *12*, 362–369.
24. Oelgemöller, M.; Jung, C.; Mattay, J., Green photochemistry: Production of fine chemicals with sunlight. *Pure Appl. Chem.* **2007,** *79*, 1939-1947.
25. Schiel, C.; Oelgemöller, M.; Ortner, J.; Mattay, J., Green photochemistry: the solar-chemical 'Photo–Friedel–Crafts acylation' of quinones. *Green Chem.* **2001,** *3*, 224-228.
26. Schiavello, M., *Photoelectrochemistry, Photocatalysis and Photoreactors Fundamentals and Developments*. Springer Netherlands: 1985.
27. Schultz, D. M.; Yoon, T. P., Solar synthesis: prospects in visible light photocatalysis. *Science* **2014,** *343*, 985-995.
28. Yoon, T. P.; Ischay, M. A.; Du, J., Visible light photocatalysis as a greener approach to photochemical synthesis. *Nat. Chem.* **2010,** *2*, 527-532.
29. Zeitler, K., Photoredox catalysis with visible light. *Angew. Chem. Int. Ed.* **2009,** *48*, 9785-9789.
30. Pottier, R. H.; Russell, D. A., Quantum Yield of a Photochemical Reaction. In *Photobiological Techniques*, Valenzeno, D. P.; Pottier, R. H.; Mathis, P.; Douglas, R. H., Eds. Springer US: Boston, MA, 1991; pp 45-57.

31. Ravelli, D.; Protti, S.; Neri, P.; Fagnoni, M.; Albini, A., Photochemical technologies assessed: the case of rose oxide. *Green Chem.* **2011,** *13*, 1876-1884.
32. Ong, P. K. C.; Acree, T. E., Similarities in the Aroma Chemistry of Gewürztraminer Variety Wines and Lychee (Litchi chinesis Sonn.) Fruit. *J. Agric. Food Chem.* **1999,** *47*, 665-670.
33. Small, E.; Canada, N. R. C., *Culinary Herbs*. NRC Research Press: Canada, 2006.
34. Günther, S., O.; Ziegler, K., The synthesis of ascaridol. *The Science of Nature* **1944,** *32*, 157-157.
35. Klayman, D., Qinghaosu (artemisinin): an antimalarial drug from China. *Science* **1985,** *228*, 1049-1055.
36. White, N. J., Assessment of the pharmacodynamic properties of antimalarial drugs in vivo. *Antimicrob. Agents Chemother.* **1997,** *41*, 1413-1422.
37. O'Neill, P. M.; Posner, G. H., A Medicinal Chemistry Perspective on Artemisinin and Related Endoperoxides. *J. Med. Chem.* **2004,** *47*, 2945-2964.
38. Tang, Y.; Dong, Y.; Vennerstrom, J. L., Synthetic peroxides as antimalarials. *Med. Res. Rev.* **2004,** *24*, 425-448.
39. Amara, Z.; Bellamy, J. F. B.; Horvath, R.; Burgar, A.; Rossen, K.; Poliakoff, M.; J.Miller, S.; George, M.; Beeby, A., Applying green chemistry to the photochemical route to artemisinin. *Nat. Chem.* **2015,** *7*, 489-495.
40. Olivucci, M.; Santoro, F., Chemical Selectivity through Control of Excited-State Dynamics. *Angew. Chem. Int. Ed.* **2008,** *47*, 6322-6325.
41. Schapiro, I.; Melaccio, F.; Laricheva, E. N.; Olivucci, M., Using the computer to understand the chemistry of conical intersections. *Photochem. Photobiol. Sci.* **2011,** *10*, 867-886.
42. Ghogare, A. A.; Greer, A., Using Singlet Oxygen to Synthesize Natural Products and Drugs. *Chem. Rev.* **2016,** *116*, 9994-10034.
43. Karkas, M. D.; Porco, J. A., Jr.; Stephenson, C. R., Photochemical Approaches to Complex Chemotypes: Applications in Natural Product Synthesis. *Chem. Rev.* **2016,** *116*, 9683-9747.
44. Ramamurthy, V.; Sivaguru, J., Supramolecular Photochemistry as a Potential Synthetic Tool: Photocycloaddition. *Chem. Rev.* **2016,** *116*, 9914-9993.
45. Romero, N. A.; Nicewicz, D. A., Organic Photoredox Catalysis. *Chem. Rev.* **2016,** *116*, 10075-10166.
46. Skubi, K. L.; Blum, T. R.; Yoon, T. P., Dual Catalysis Strategies in Photochemical Synthesis. *Chem. Rev.* **2016,** *116*, 10035-10074.
47. Lancaster, M.; Chemistry, *Green Chemistry: An Introductory Text*. Royal Society of Chemistry: UK, 2002.
48. Su, Y.; Straathof, N. J. W.; Hessel, V.; Noël, T., Photochemical Transformations Accelerated in Continuous-Flow Reactors: Basic Concepts and Applications. *Chem. Eur. J.* **2014,** *20*, 10562-10589.

49. Dietliker, K.; Braig, A.; Ricci, A., Industrial applications of photochemistry: automotive coatings and beyond. In *Photochemistry: Volume 38*, The Royal Society of Chemistry: 2010; Vol. 38, pp 344-368.
50. Fischer, M., Industrial Applications of Photochemical Syntheses. *Angew. Chem. Int. Ed. Engl* **1978,** *17*, 16-26.
51. Coyle, E. E.; Oelgemöller, M., Micro-photochemistry: photochemistry in microstructured reactors. The new photochemistry of the future? *Photochem. Photobiol. Sci.* **2008,** *7*, 1313-1322.
52. Oelgemoeller, M., Highlights of Photochemical Reactions in Microflow Reactors. *Chem. Eng. Technol.* **2012,** *35*, 1144-1152.
53. Elliott, L. D.; Knowles, J. P.; Koovits, P. J.; Maskill, K. G.; Ralph, M. J.; Lejeune, G.; Edwards, L. J.; Robinson, R. I.; Clemens, I. R.; Cox, B.; Pascoe, D. D.; Koch, G.; Eberle, M.; Berry, M. B.; Booker-Milburn, K. I., Batch versus Flow Photochemistry: A Revealing Comparison of Yield and Productivity. *Chem. Eur. J.* **2014,** *20*, 15226-15232.
54. Jähnisch, K.; Dingerdissen, U., Photochemical Generation and [4+2]-Cycloaddition of Singlet Oxygen in a Falling-Film Micro Reactor. *Chem. Eng. Technol.* **2005,** *28*, 426-427.
55. Lee, D. S.; Amara, Z.; Clark, C. A.; Xu, Z.; Kakimpa, B.; Morvan, H. P.; Pickering, S. J.; Poliakoff, M.; George, M. W., Continuous Photo-Oxidation in a Vortex Reactor: Efficient Operations Using Air Drawn from the Laboratory. *Org. Process Res. Dev.* **2017,** *21*, 1042-1050.
56. Yavorskyy, A.; Shvydkiv, O.; Hoffmann, N.; Nolan, K.; Oelgemöller, M., Parallel Microflow Photochemistry: Process Optimization, Scale-up, and Library Synthesis. *Org. Lett.* **2012,** *14*, 4342-4345.
57. Glasnov, T., *Continuous-flow chemistry in the research laboratory: Modern organic chemistry in dedicated reactors at the dawn of the 21st century*. Springer: Switzerland, 2016; p 1-114.
58. Zhou, G.; Emerson, K.; Majusiak, E.; Anderson, C.; Sudah, O., Safe Scale-Up of Processes Containing Hazardous Species in the Headspace with Inline IR. *Org. Process Res. Dev.* **2012,** *16*, 204-213.
59. Acke, D. R. J.; Stevens, C. V., A HCN-based reaction under microreactor conditions: industrially feasible and continuous synthesis of 3,4-diamino-1H-isochromen-1-ones. *Green Chem.* **2007,** *9*, 386-390.
60. Martin, B.; Lehmann, H.; Yang, H.; Chen, L.; Tian, X.; Polenk, J.; Schenkel, B., Continuous manufacturing as an enabling tool with green credentials in early-phase pharmaceutical chemistry. *Curr. Opin. Green Sustain. Chem.* **2018,** *11*, 27-33.
61. Tinder, R.; Farr, R.; Heid, R.; Zhao, R.; Rarig, R. S.; Storz, T., A Convenient and Stable Synthon for Ethyl Azide and Its Evaluation in a [3 + 2]-Cycloaddition Reaction under Continuous-Flow Conditions. *Org. Process Res. Dev.* **2009,** *13*, 1401-1406.

62. Pelleter, J.; Renaud, F., Facile, Fast and Safe Process Development of Nitration and Bromination Reactions Using Continuous Flow Reactors. *Org. Process Res. Dev.* **2009,** *13*, 698-705.
63. Gemoets, H. P. L.; Su, Y.; Shang, M.; Hessel, V.; Luque, R.; Noël, T., Liquid phase oxidation chemistry in continuous-flow microreactors. *Chem. Soc. Rev.* **2016,** *45*, 83-117.
64. Hessel, V.; Noel, T., *Chim. Oggi.* **2015,** *33*, 44-49.
65. In, S.-i.; Nielsen, M. G.; Vesborg, P. C. K.; Hou, Y.; Abrams, B. L.; Henriksen, T. R.; Hansen, O.; Chorkendorff, I., Photocatalytic methane decomposition over vertically aligned transparent TiO_2 nanotube arrays. *Chem. Commun.* **2011,** *47*, 2613-2615.
66. Windaus, A.; Linsert, O., About the ultraviolet radiation of dehydro-ergosterol. *Eur. J. Org. Chem.* **1928,** *460*, 148-166.
67. Newman, S. G.; Jensen, K. F., The role of flow in green chemistry and engineering. *Green Chem.* **2013,** *15*, 1456-1472.
68. Lane, N., *Oxygen: The Molecule that Made the World*. Oxford University Press: Oxford, 2003.
69. Nonell, S.; Flors, C., *Singlet Oxygen: Applications in Biosciences and Nanosciences Volume 2*. Royal Society of Chemistry: 2016.
70. Hoffmann, N., Photochemical Reactions as Key Steps in Organic Synthesis. *Chem. Rev.* **2008,** *108*, 1052-1103.
71. Redmond, R. W.; Gamlin, J. N., A Compilation of Singlet Oxygen Yields from Biologically Relevant Molecules. *Photochem. Photobiol.* **1999,** *70*, 391-475.
72. Orel, V. E., Singlet oxygen therapy. *Klinichna khirurhiia* **1997**, 47-8.
73. Greer, A., Christopher Foote's Discovery of the Role of Singlet Oxygen [$^1O_2$ ($^1\Delta g$)] in Photosensitized Oxidation Reactions. *Acc. Chem. Res.* **2006,** *39*, 797-804.
74. Zakharov, S. D.; Ivanov, A. V., Light-oxygen effect in cells and its potential applications in tumour therapy (review). *Quantum Electron.* **1999,** *29*, 1031-1053.
75. Lewis, G. N., The Magnetochemical Theory. *Chem. Rev.* **1924,** *1*, 231-248.
76. Mulliken, R. S., Interpretation of the Atmospheric Oxygen Bands; Electronic Levels of the Oxygen Molecule. *Nature* **1928,** *122*, 505-505.
77. Foote, C. S., Photosensitized oxygenations and the role of singlet oxygen. *Acc. Chem. Res.* **1968,** *1*, 104-110.
78. Maria C. DeRosa; Crutchley, R. J., Photosensitized singlet oxygen and its applications. *Coord. Chem. Rev.* **2002,** *233-234*, 351-371.
79. Mulliken, R. S., The Interpretation of Band Spectra Part III. Electron Quantum Numbers and States of Molecules and Their Atoms. *Rev. Mod. Phys.* **1932,** *4*, 1-86.
80. Arnold, S. J.; Kubo, M.; Ogryzlo, E. A., Relaxation and Reactivity of Singlet Oxygen. In *Oxidation of Organic Compounds*, American chemical society: 1968; Vol. 77, pp 133-142.
81. Merkel, P. B.; Kearns, D. R., Remarkable solvent effects on the lifetime of 1.DELTA.g oxygen. *J. Am. Chem. Soc.* **1972,** *94*, 1029-1030.

82. Schweitzer, C.; Schmidt, R., Physical Mechanisms of Generation and Deactivation of Singlet Oxygen. *Chem. Rev.* **2003,** *103*, 1685-1758.
83. Kautsky, H.; de Bruijn, H., The elucidation of the photoluminescence attenuation of fluorescent systems by oxygen: The formation of active, diffusible oxygen molecules by sensitization. *The Science of Nature* **1931,** *19*, 1043-1043.
84. Kautsky, H., Quenching of luminescence by oxygen. *Trans. Faraday Soc.* **1939,** *35*, 216-219.
85. Gollnick, K.; Schenck, G. O., Mechanism and stereoselectivity of photosensitized oxygen transfer reactions. *Pure and Applied Chemistry* **1964,** *9*, 507.
86. Khan, A. U.; Kasha, M., Red Chemiluminescence of Molecular Oxygen in Aqueous Solution. *J. Chem. Phys.* **1963,** *39*, 2105-2106.
87. Khan, A. U.; Kasha, M., Rotational Structure in the Chemiluminescence Spectrum of Molecular Oxygen in Aqueous Systems. *Nature* **1964,** *204*, 241-243.
88. Khan, A. U.; Kasha, M., Chemiluminescence arising from simultaneous transitions in pairs of singlet oxygen molecules. *J. Am. Chem. Soc.* **1970,** *92*, 3293-3300.
89. Foote, C. S.; Wexler, S., Singlet Oxygen. A Probable Intermediate in Photosensitized Autoxidations. *J. Am. Chem. Soc.* **1964,** *86*, 3880-3881.
90. Foote, C. S.; Wexler, S., Olefin Oxidations with Excited Singlet Molecular Oxygen. *J. Am. Chem. Soc.* **1964,** *86*, 3879-3880.
91. Long, C. A.; Kearns, D. R., Radiationless decay of singlet molecular oxygen in solution. II. Temperature dependence and solvent effects. *J. Am. Chem. Soc.* **1975,** *97*, 2018-2020.
92. Khan, A. U.; Kasha, M., Direct spectroscopic observation of singlet oxygen emission at 1268 nm excited by sensitizing dyes of biological interest in liquid solution. *Proc. Natl. Acad. Sci.* **1979,** *76*, 6047-6049.
93. Wasserman, E.; Murray, R. W.; Kaplan, M. L.; Yager, W. A., Electron paramagnetic resonance of 1.DELTA. oxygen from a phosphite-ozone complex. *J. Am. Chem. Soc.* **1968,** *90*, 4160-4161.
94. Corney, A., *Atomic and Laser Spectroscopy*. OUP Oxford: Oxford, 2006.
95. Krupenie, P. H., The Spectrum of Molecular Oxygen. *J. Phys. Chem. Ref. Data* **1972,** *1*, 423-534.
96. Cristina, F.; G., G. A.; Georgios, V., Singlet Oxygen: Chemistry, Applications and Challenges Ahead. *ChemPhotoChem* **2018,** *2*, 510-511.
97. C. S. Foote; S. Wexler; Ando, W.; Higgins, R., Chemistry of singlet oxygen. IV. Oxygenations with hypochlorite-hydrogen peroxide. *J. Am. Chem. Soc.* **1968,** *90*, 975-981.
98. Foote, C. S., Mechanisms of Photosensitized Oxidation. *Science* **1968,** *162*, 963-970.
99. Ogilby, P. R., Singlet oxygen: there is indeed something new under the sun. *Chem. Soc. Rev.* **2010,** *39*, 3181-3209.

100. Schmidt, R., Photosensitized Generation of Singlet Oxygen. *Photochem. Photobiol.* **2006,** *82*, 1161-1177.
101. Rong-rong, C.; Lie-zheng, D.; Wen-bo, S.; He-ping, Y.; Guo-he, S.; Cun-hao, Z., Liquid-liquid reaction of hydrogen peroxide and sodium hypochlorite for the production of singlet oxygen in a centrifugal flow singlet oxygen generator. *Quantum Electron.* **2011,** *41*, 139-144.
102. Foote, C. S.; Wexler, S.; Ando, W.; Higgins, R., Chemistry of singlet oxygen. IV. Oxygenations with hypochlorite-hydrogen peroxide. *J. Am. Chem. Soc.* **1968,** *90*, 975-981.
103. Thompson, Q. E., Ozone Oxidation of Nucleophilic Substances. I. Tertiary Phosphite Esters1. *J. Am. Chem. Soc.* **1961,** *83*, 845-851.
104. Higgins, R.; Foote, C. S.; Cheng, H., Chemistry of Singlet Oxygen. In *Oxidation of Organic Compounds*, American chemical society: 1968; Vol. 77, pp 102-117.
105. Fudickar, W.; Linker, T., Release of Singlet Oxygen from Organic Peroxides under Mild Conditions. *ChemPhotoChem* **2018,** *2*, 548-558.
106. Prein, M.; Adam, W., The Schenck ene reaction: Diastereoselective oxyfunctionalization with singlet oxygen in synthetic applications. *Angew. Chem. Int. Ed.* **1996,** *35*, 477-494.
107. Clennan, E. L., Synthetic and mechanistic aspects of 1,3-diene photooxidation. *Tetrahedron* **1991,** *47*, 1343-1382.
108. Gollnick, K.; Koegler, S., (4+2)-cycloaddition of singlet oxygen to oxazoles formation of oxazole endoperoxides. *Tetrahedron Lett.* **1988,** *29*, 1003-1006.
109. Lin, Y.-Y.; Li, G.-B.; Zhang, Y.-H.; Leung, H.-K., A Novel Singlet Oxygen Reaction. *Photochem. Photobiol. Sci.* **1997,** *65*, 82-84.
110. Bayer, P.; Pérez-Ruiz, R.; Jacobi von Wangelin, A., Stereoselective Photooxidations by the Schenck Ene Reaction. *ChemPhotoChem* **2018,** *2*, 559-570.
111. Gupta, S.; Ramamurthy, V., Characterization and Singlet Oxygen Oxidation of 1-Alkyl Cyclohexenes Encapsulated Within a Water-Soluble Organic Capsule. *ChemPhotoChem* **2018,** *2*, 655-666.
112. Ponce, M. A.; Ramirez, J. A.; Galagovsky, L. R.; Gros, E. G.; Erra-Balsells*, R., A new look into the reaction between ergosterol and singlet oxygen in vitro. *Photochem. Photobiol. Sci.* **2002,** *1*, 749-756.
113. Ivana, P.; Silvestre, B.; Antonio, P. P.; Andrea, P., Photochemically Produced Singlet Oxygen: Applications and Perspectives. *ChemPhotoChem* **2018,** *2*, 535-547.
114. Sevin, F.; McKee, M. L., Reactions of 1,3-Cyclohexadiene with Singlet Oxygen. A Theoretical Study. *J. Am. Chem. Soc.* **2001,** *123*, 4591-4600.
115. McCarrick, M. A.; Wu, Y. D.; Houk, K. N., Hetero-Diels-Alder reaction transition structures: reactivity, stereoselectivity, catalysis, solvent effects, and the exo-lone-pair effect. *J. Org. Chem.* **1993,** *58*, 3330-3343.
116. Bloodworth, A. J.; Eggelte, H. J., Endoperoxides, in Singlet oxygen Vol. II In *(A. A. Frimer, Ed.), CRC Press, Boca Raton*, 1985; pp 93-203.

117. de Souza, J. M.; Brocksom, T. J.; McQuade, D. T.; de Oliveira, K. T., Continuous Endoperoxidation of Conjugated Dienes and Subsequent Rearrangements Leading to C–H Oxidized Synthons. *J. Org. Chem.* **2018,** *83*, 7574-7585.
118. Clennan, E. L.; L'Espereance, R. P., The addition of singlet oxygen to alkoxy and trimethysiloxybutadienes. The synthesis of novel new peroxides. *Tetrahedron Lett.* **1983,** *24*, 4291-4294.
119. Coughlin, D. J.; Salomon, R. G., Synthesis and thermal reactivity of some 2,3-dioxabicyclo[2.2.1]heptane models of prostaglandin endoperoxides. *J. Am. Chem. Soc.* **1977,** *99*, 655-657.
120. Balci, M., Bicyclic endoperoxides and synthetic applications. *Chem. Rev.* **1981,** *81*, 91-108.
121. Di Mascio, P.; Martinez, G. R.; Miyamoto, S.; Ronsein, G. E.; Medeiros, M. H. G.; Cadet, J., Singlet Molecular Oxygen Reactions with Nucleic Acids, Lipids, and Proteins. *Chem. Rev.* **2019,** *119*, 2043-2086.
122. Jones, K. M.; Hillringhaus, T.; Klussmann, M., A singlet oxygen approach to oxaspirocycles. *Tetrahedron Lett.* **2013,** *54*, 3294-3297.
123. Hamri, S.; Rodríguez, J.; Basset, J.; Guillaumet, G.; Dolors Pujol, M., A convenient iodination of indoles and derivatives. *Tetrahedron* **2012,** *68*, 6269-6275.
124. Stratakis, M.; Rabalakos, C., Chemoselective hydroperoxidation of alkenylarenes within thionin-supported zeolite Na-Y. *Tetrahedron Lett.* **2001,** *42*, 4545-4547.
125. Clennan, E. L.; Mehrsheikh-Mohammadi, M. E., Mechanism of endoperoxide formation. 3. Utilization of the Young and Carlsson kinetic techniques. *J. Am. Chem. Soc.* **1984,** *106*, 7112-7118.
126. Mauger, A.; Farjon, J.; Nun, P.; Coeffard, V., One-Pot Synthesis of Functionalized Fused Furans via a BODIPY-Catalyzed Domino Photooxygenation. *Chem. - Eur. J.* **2018,** *24*, 4790-4793.
127. Montagnon, T.; Kalaitzakis, D.; Triantafyllakis, M.; Stratakis, M.; Vassilikogiannakis, G., Furans and singlet oxygen – why there is more to come from this powerful partnership. *Chemical communications* **2014,** *50*, 15480-15498.
128. Ishibe, N.; Odani, M.; Sunami, M., Photosensitized oxygenation of 4H-pyran-4-thiones and 4H-thiopyran-4-thiones. *J. Chem. Soc. D* **1971**, 118-119.
129. H. Wasserman, H.; R. Scheffer, J.; L. Cooper, J., Singlet oxygen reactions with 9,10-diphenylanthracene peroxide. *J. Am. Chem. Soc.* **1972,** *94*, 4991-4996.
130. van den Heuvel, C. J. M.; Steinberg, H.; de Boer, T. J., The photo-oxidation of hexamethylbenzene by singlet oxygen. *Recl.: J. R. Neth. Chem. Soc.* **2010,** *96*, 157-159.
131. Foote, C. S.; Clennan, E. L., Properties and Reactions of Singlet Dioxygen. In *Active Oxygen in Chemistry*, Foote, C. S.; Valentine, J. S.; Greenberg, A.; Liebman, J. F., Eds. Springer Netherlands: Dordrecht, 1995; pp 105-140.

132. Erden, I.; Öcal, N.; Song, J.; Gleason, C.; Gärtner, C., Unusual endoperoxide isomerizations: a convenient entry into 2-vinyl-2-cyclopentenones from saturated fulvene endoperoxides. *Tetrahedron* **2006,** *62*, 10676-10682.
133. Pibiri, I.; Buscemi, S.; Palumbo Piccionello, A.; Pace, A., Photochemically Produced Singlet Oxygen: Applications and Perspectives. *ChemPhotoChem* **2018,** *2*, 535-547.
134. Boyd, J. D.; Foote, C. S.; Imagawa, D. K., Synthesis of 1,2:3,4-Diepoxides by Catalyzed Rearrangement of 1,4-Endoperoxides. *J. Am. Chem. Soc.* **1980,** *102:10*, 3641-3642.
135. Chaturvedi, D.; Goswami, A.; Pratim Saikia, P.; Barua, N. C.; Rao, P. G., Artemisinin and its derivatives: a novel class of anti-malarial and anti-cancer agents. *Chem. Soc. Rev.* **2010,** *39*, 435-454.
136. Gilmore, K.; Kopetzki, D.; Lee, J. W.; Horvath, Z.; McQuade, D. T.; Seidel-Morgenstern, A.; Seeberger, P. H., Continuous synthesis of artemisinin-derived medicines. *Chem. Commun.* **2014,** *50*, 12652-12655.
137. Rudrapal, M.; Chetia, D.; Singh, V., Novel series of 1,2,4-trioxane derivatives as antimalarial agents. *J. Enzyme Inhib. Med. Chem.* **2017,** *32*, 1159-1173.
138. Fanny, F.; W., T. S., Tuning the Key Properties of Singlet Oxygen-Responsive Acene-Doped Conjugated Polymer Nanoparticles. *ChemPhotoChem* **2018,** *2*, 632-639.
139. Matsumoto, M.; Dobashi, S.; Kuroda, K.; Kondo, K., Sensitized photo-oxygenation of acyclic conjugated dienes. *Tetrahedron* **1985,** *41*, 2147-2154.
140. Dewar, M. J. S.; Thiel, W., MINDO/3 study of the addition of singlet oxygen to 1,3-butadiene. *J. Am. Chem. Soc.* **1977,** *99*, 2338-2339.
141. Grdina, M. B.; Orfanopoulos, M.; Stephenson, L. M., Stereochemical dependence of isotope effects in the singlet oxygen-olefin reaction. *J. Am. Chem. Soc.* **1979,** *101*, 3111-3112.
142. Delogu, G.; Fabbri, D.; Fabris, F.; Sbrogiò, F.; Valle, G.; De Lucchi, O., syn and anti Cycloaddition of singlet oxygen to bisdialine. *J. Chem. Soc., Chem. Commun.* **1995**, 1887-1888.
143. Rigaudy, J.; Capdevielle, P.; Combrisson, S.; Maumy, M., Ouverture concertee des adduits du bis-benzylidene-1,2 (E,E) diphenyl-3,4 cyclobutane cis. Rectification des structures des produits derives. *Tetrahedron Lett.* **1974,** *15*, 2757-2760.
144. Jacquot, C. *Cycloadditions with singlet oxygen mechanism and substituent directing effects*; 2004; pp 17-24.
145. Murahashi, S.-I.; Naota, T.; Miyaguchi, N.; Noda, S., Ruthenium-Catalyzed Oxidation of Phenols with Alkyl Hydroperoxides. A Novel, Facile Route to 2-Substituted Quinones. *J. Am. Chem. Soc.* **1996,** *118*, 2509-2510.
146. Patrick, B.; Raúl, P.-R.; Axel, J. v. W., Stereoselective Photooxidations by the Schenck Ene Reaction. *ChemPhotoChem* **2018,** *2*, 559-570.

147. Orfanopoulos, M.; Stephenson, L. M., Stereochemistry of the singlet oxygen olefin-ene reaction. *J. Am. Chem. Soc.* **1980,** *102*, 1417-1418.
148. Griesbeck, A. G.; Adam, W.; Bartoschek, A.; El-Idreesy, T. T., Photooxygenation of allylic alcohols: kinetic comparison of unfunctionalized alkenes with prenol-type allylic alcohols, ethers and acetates. *Photochem. Photobiol.* **2003,** *2*, 877-881.
149. Alberti, M. N.; Vougioukalakis, G. C.; Orfanopoulos, M., Electronic effects in the regioselectivity of the singlet oxygen and 4-methyl-1,2,4-triazoline-3,5-dione ene reactions with isobutenylarenes. *Tetrahedron Lett.* **2003,** *44*, 903-905.
150. Orfanopoulos, M.; Sister, M. B. G.; Stephenson, L. M., Site specificity in the singlet oxygen-trisubstituted olefin reaction. *J. Am. Chem. Soc.* **1979,** *101*, 275-276.
151. Stratakis, M.; Orfanopoulos, M., Anti “cis effect” selectivity in the reaction of singlet oxygen with trisubstituted alkenes. *Tetrahedron Lett.* **1995,** *36*, 4291-4294.
152. Kleczka, M.; But, D.; Dylong, D.; Fendinger, C.; Marmann, V.; Wartke, C.; Griesbeck, A. G., Two Useful Directing Modes in Singlet Oxygen Reactivity: Electrostatic Effects in the Ene Reaction with Allylic Alcoholates and a Chemoselectivity Change with α-Alkoxy Michael Esters. *ChemPhotoChem* **2018,** *2*, 964-975.
153. Lévesque, F.; Seeberger, P. H., Continuous-Flow Synthesis of the Anti-Malaria Drug Artemisinin. *Angew. Chem. Int. Ed.* **2012,** *51*, 1706-1709.
154. Sy, L.-K.; Brown, G. D., The mechanism of the spontaneous autoxidation of dihydroartemisinic acid. *Tetrahedron* **2002,** *58*, 897-908.
155. Hall, J. F. B. Continuous Photo-oxidation with $^1O_2$ in CO_2. PhD Thesis, The University of Nottingham, Nottingham, 2014.
156. Adam, W.; Bosio, S. G.; Turro, N. J., Control of the Mode Selectivity (Ene Reaction versus [2 + 2] Cycloaddition) in the Photooxygenation of Ene Carbamates: Directing Effect of an Alkenylic Nitrogen Functionality. *J. Am. Chem. Soc.* **2002,** *124*, 14004-14005.
157. Cermola, F.; Guaragna, A.; Iesce, M. R.; Palumbo, G.; Purcaro, R.; Rubino, M.; Tuzi, A., New Insight into the Reaction of Singlet Oxygen with Sulfur-Containing Cyclic Alkenes: Dye-Sensitized Photooxygenation of 5,6-Dihydro-1,4-dithiins. *J. Org. Chem.* **2007,** *72*, 10075-10080.
158. Poplata, S.; Tröster, A.; Zou, Y.-Q.; Bach, T., Recent Advances in the Synthesis of Cyclobutanes by Olefin [2 + 2] Photocycloaddition Reactions. *Chem. Rev.* **2016,** *116*, 9748-9815.
159. Sivaguru, J.; Solomon, M. R.; Poon, T.; Jockusch, S.; Bosio, S. G.; Adam, W.; Turro, N. J., The Reaction of Singlet Oxygen with Enecarbamates: A Mechanistic Playground for Investigating Chemoselectivity, Stereoselectivity, and Vibratioselectivity of Photooxidations. *Acc. Chem. Res.* **2008,** *41*, 387-400.
160. Li, J.; Cai, S.; Chen, J.; Zhao, Y.; Wang, D. Z., Visible Light Induced Photocatalytic Conversion of Enamines into Amides. *Synlett* **2014,** *25*, 1626-1628.

161. Celaje, J. A.; Zhang, D.; Guerrero, A. M.; Selke, M., Chemistry of trans-Resveratrol with Singlet Oxygen: [2 + 2] Addition, [4 + 2] Addition, and Formation of the Phytoalexin Moracin M. *Org. Lett.* **2011,** *13*, 4846-4849.
162. Le Bechec, M.; Pigot, T.; Lacombe, S., Chemical Quenching of Singlet Oxygen and Other Reactive Oxygen Species in Water: A Reliable Method for the Determination of Quantum Yields in Photochemical Processes? *ChemPhotoChem* **2018,** *2*, 622-631.
163. Ogilby, P. R., Solvent Effects on the Radiative Transitions of Singlet Oxygen. *Acc. Chem. Res.* **1999,** *32*, 512-519.
164. Clough, R. L.; Dillon, M. P.; Iu, K. K.; Ogilby, P. R., Behavior of singlet molecular oxygen in a polymer matrix: effects of temperature, matrix rigidity, and molecular composition. *Macromolecules* **1989,** *22*, 3620-3628.
165. Bregnhøj, M.; Westberg, M.; Jensen, F.; Ogilby, P. R., Solvent-dependent singlet oxygen lifetimes: temperature effects implicate tunneling and charge-transfer interactions. *Phys. Chem. Chem. Phys.* **2016,** *18*, 22946-22961.
166. Badger, R. M.; Wright, A. C.; Whitlock, R. F., Absolute Intensities of the Discrete and Continuous Absorption Bands of Oxygen Gas at 1.26 and 1.065 μ and the Radiative Lifetime of the 1Δg State of Oxygen. *J. Chem. Phys.* **1965,** *43*, 4345-4350.
167. Scurlock, R. D.; Nonell, S.; Braslavsky, S. E.; Ogilby, P. R., Effect of Solvent on the Radiative Decay of Singlet Molecular Oxygen. *J. Phys. Chem.* **1995,** *99*, 3521-3526.
168. Wilkinson, F.; Helman, W. P.; Ross, A. B., Rate Constants for the Decay and Reactions of the Lowest Electronically Excited Singlet State of Molecular Oxygen in Solution. An Expanded and Revised Compilation. *J. Phys. Chem. Ref. Data* **1995,** *24*, 663-677.
169. Lancaster, J. R.; Martí, A. A.; López-Gejo, J.; Jockusch, S.; O'Connor, N.; Turro, N. J., Nonradiative Deactivation of Singlet Oxygen ($^1O_2$) by Cubane and Its Derivatives. *Org. Lett.* **2008,** *10*, 5509-5512.
170. Clennan, E. L.; Noe, L. J.; Szneler, E.; Wen, T., Hydrazines: new charge-transfer physical quenchers of singlet oxygen. *J. Am. Chem. Soc.* **1990,** *112*, 5080-5085.
171. Abdel-Shafi, A. A.; Wilkinson, F., Electronic to vibrational energy conversion and charge transfer contributions during quenching by molecular oxygen of electronically excited triplet states. *Phys. Chem. Chem. Phys.* **2002,** *4*, 248-254.
172. Singh, J. P.; Setser, D. W., Electronic-to-vibrational energy-transfer studies of singlet molecular oxygen. *J. Phys. Chem.* **1985,** *89*, 5353-5358.
173. Foote, C. S.; Chang, Y. C.; Denny, R. W., Chemistry of singlet oxygen. XI. Cis-trans isomerization of carotenoids by single oxygen and a probable quenching mechanism. *J. Am. Chem. Soc.* **1970,** *92*, 5218-5219.
174. Conn, P. F.; Schalch, W.; Truscott, T. G., The singlet oxygen and carotenoid interaction. *J. Photochem. Photobiol., B* **1991,** *11*, 41-47.

175. Hurst, J. R.; Schuster, G. B., Nonradiative relaxation of singlet oxygen in solution. *J. Am. Chem. Soc.* **1983,** *105*, 5756-5760.
176. Rodgers, M. A. J., Solvent-induced deactivation of singlet oxygen: additivity relationships in nonaromatic solvents. *J. Am. Chem. Soc.* **1983,** *105*, 6201-6205.
177. Losev, A. P.; Nichiporovich, I. N.; Byteva, I. M.; Drozdov, N. N.; Jghgami, I. F. A., The perturbing effect of solvents on the luminescence rate constant of singlet molecular oxygen. *Chem. Phys. Lett.* **1991,** *181*, 45-50.
178. Hurst, J. R.; McDonald, J. D.; Schuster, G. B., Lifetime of singlet oxygen in solution directly determined by laser spectroscopy. *J. Am. Chem. Soc.* **1982,** *104*, 2065-2067.
179. Ogilby, P. R.; Foote, C. S., Chemistry of singlet oxygen. 36. Singlet molecular oxygen ($^1O_2$) luminescence in solution following pulsed laser excitation. Solvent deuterium isotope effects on the lifetime of singlet oxygen. *J. Am. Chem. Soc.* **1982,** *104*, 2069-2070.
180. Scurlock, R. D.; Ogilby, P. R., Effect of solvent on the rate constant for the radiative deactivation of singlet molecular oxygen. *J. Phys. Chem.* **1987,** *91*, 4599-4602.
181. Henderson, R. K.; Jiménez-González, C.; Constable, D. J. C.; Alston, S. R.; Inglis, G. G. A.; Fisher, G.; Sherwood, J.; Binks, S. P.; Curzons, A. D., Expanding GSK's solvent selection guide – embedding sustainability into solvent selection starting at medicinal chemistry. *Green Chem.* **2011,** *13*, 854-862.
182. Prat, D.; Pardigon, O.; Flemming, H.-W.; Letestu, S.; Ducandas, V.; Isnard, P.; Guntrum, E.; Senac, T.; Ruisseau, S.; Cruciani, P.; Hosek, P., Sanofi's Solvent Selection Guide: A Step Toward More Sustainable Processes. *Org. Process Res. Dev.* **2013,** *17*, 1517-1525.
183. Diorazio, L. J.; Hose, D. R. J.; Adlington, N. K., Toward a More Holistic Framework for Solvent Selection. *Org. Process Res. Dev.* **2016,** *20*, 760-773.
184. Reichardt, C., Solvents and Solvent Effects: An Introduction. *Org. Process Res. Dev.* **2007,** *11*, 105-113.
185. Dunn, P. J., The importance of Green Chemistry in Process Research and Development. *Chem. Soc. Rev.* **2012,** *41*, 1452-1461.
186. koteswararao, P. R.; S.L.Tulasi; Y.Pavani, Impact of solvents on environmental pollution. *J. Chem. Pharm. Sci.* **2014**, 132-135.
187. Tzschucke, C. C.; Markert, C.; Bannwarth, W.; Roller, S.; Hebel, A.; Haag, R., Modern Separation Techniques for the Efficient Workup in Organic Synthesis. *Angew. Chem. Int. Ed.* **2002,** *41*, 3964-4000.
188. Constable, D. J. C.; Jimenez-Gonzalez, C.; Henderson, R. K., Perspective on Solvent Use in the Pharmaceutical Industry. *Org. Process Res. Dev.* **2007,** *11*, 133-137.
189. Singh, R.; Kumar, S., *Green Technologies and Environmental Sustainability*. Springer International Publishing: Switzerland, 2017.

190. Clark, J. H.; Farmer, T. J.; Hunt, A. J.; Sherwood, J., Opportunities for Bio-Based Solvents Created as Petrochemical and Fuel Products Transition towards Renewable Resources. *Int. J. Mol. Sci.* **2015,** *16*, 17101-17159.
191. Ismail, O. M. S.; Hameed, R. S. A., Environmental effects of volatile organic compounds on ozone layer. *Adv. Appl. Sci. Res.* **2013,** *4*, 264-268.
192. Jessop, P. G., Searching for green solvents. *Green Chem.* **2011,** *13*, 1391-1398.
193. Prat, D.; Hayler, J.; Wells, A., A survey of solvent selection guides. *Green Chem.* **2014,** *16*, 4546-4551.
194. Chatel, G.; Pereira, J. F. B.; Debbeti, V.; Wang, H.; Rogers, R. D., Mixing ionic liquids – "simple mixtures" or "double salts"? *Green Chem.* **2014,** *16*, 2051-2083.
195. Prat, D.; Wells, A.; Hayler, J.; Sneddon, H.; McElroy, C. R.; Abou-Shehada, S.; Dunn, P. J., CHEM21 selection guide of classical- and less classical-solvents. *Green Chem.* **2016,** *18*, 288-296.
196. Gu, Y.; Jérôme, F., Bio-based solvents: an emerging generation of fluids for the design of eco-efficient processes in catalysis and organic chemistry. *Chem. Soc. Rev.* **2013,** *42*, 9550-9570.
197. Leitner, W.; Jessop, P. G., *Chemical Synthesis Using Supercritical Fluids*. Wiley: Germany, 1999.
198. Baiker, A., Supercritical Fluids in Heterogeneous Catalysis. *Chem. Rev* **1999,** *99*, 453-473.
199. J. Fraga-Dubreuil; E. Garcia-Verdugo; P. A. Hamley; E. M. Vaquero; L. M. Dudd; I. Pearson; D. Housley; W. Partenheimer; W. B. Thomas; K. Whiston; M. Poliakoff, *Green Chem.* **2007,** *9*, 1238-1245.
200. Seki, T.; Baiker, A., Catalytic Oxidations in Dense Carbon Dioxide. *Chemical Reviews* **2009,** *109*, 2409-2454.
201. Worrall, D. R.; Abdel-Shafi, A. A.; Wilkinson, F., Factors Affecting the Rate of Decay of the First Excited Singlet State of Molecular Oxygen O_2 in Supercritical Fluid Carbon Dioxide. *J. Phys. Chem. A* **2001,** *105*, 1270-1276.
202. B, H. J. F. Continuous Photo-Oxidation with $^1O_2$ in CO_2. PhD Thesis, The University of Nottingham, 2014.
203. Bourne, R. A.; Han, X.; Chapman, A. O.; Arrowsmith, N. J.; Kawanami, H.; Poliakoff, M.; George, M. W., Homogeneous photochemical oxidation via singlet O_2 in supercritical CO_2. *Chem. Commun.* **2008**, 4457-4459.
204. Bourne, R. A.; Han, X.; Poliakoff, M.; George, M. W., Cleaner continuous photo-oxidation using singlet oxygen in supercritical carbon dioxide. *Angew. Chem. Int. Ed.* **2009,** *48*, 5322-5325.
205. Han, X.; Bourne, R. A.; Poliakoff, M.; George, M. W., Strategies for cleaner oxidations using photochemically generated singlet oxygen in supercritical carbon dioxide. *Green Chem.* **2009,** *11*, 1787-1792.

206. Hall, J. F. B.; Bourne, R. A.; Han, X.; Earley, J. H.; Poliakoff, M.; George, M. W., Synthesis of antimalarial trioxanes via continuous photo-oxidation with $^1O_2$ in supercritical CO_2. *Green Chem.* **2013,** *15*, 177-180.
207. Sheldon, R. A., Green solvents for sustainable organic synthesis: state of the art. *Green Chem.* **2005,** *7*, 267-278.
208. Brunner, G., Applications of Supercritical Fluids. *Annu. Rev. Chem. Biomol. Eng.* **2010,** *1*, 321-342.
209. Leitner, W., Supercritical Carbon Dioxide as a Green Reaction Medium for Catalysis. *Acc. Chem. Res.* **2002,** *35*, 746-756.
210. Licence, P.; Ke, J.; Sokolova, M.; Ross, S. K.; Poliakoff, M., Chemical reactions in supercritical carbon dioxide: from laboratory to commercial plant. *Green Chemistry* **2003,** *5*, 99-104.
211.Anastas, P. T.; Zimmerman, J. B., Peer Reviewed: Design Through the 12 Principles of Green Engineering. *Environ. Sci. Technol.* **2003,** *37*, 94A-101A.
212. Kümmerer, K.; Clark, J., Green and Sustainable Chemistry. In *Sustainability Science: An Introduction*, Heinrichs, H.; Martens, P.; Michelsen, G.; Wiek, A., Eds. Springer Netherlands: Dordrecht, 2016; pp 43-59.
213. Poliakoff, M.; Licence, P.; George Michael, W., A New Approach to Sustainability: A Moore's Law for Chemistry. *Angew. Chem. Int. Ed.* **2018,** *57*, 12590 – 12591.
214. Anastas, P.; Warner, J., *Green Chemistry: Theory and Practice*. Oxford University Press: Oxford, 1998.
215. Anastas, P.; Eghbali, N., Green Chemistry: Principles and Practice. *Chem. Soc. Rev.* **2010,** *39*, 301-312.
216. Trost, B., The atom economy--a search for synthetic efficiency. *Science* **1991,** *254*, 1471-1477.
217. Pagliaro, M., Renewable Resources and Renewable Energy. A Global Challenge. Edited by Mauro Graziani and Paolo Fornasiero. *Angew. Chem. Int. Ed.* **2007,** *46*, 9143-9143.
218. Phan, T. V. T.; Gallardo, C.; Mane, J., GREEN MOTION: a new and easy to use green chemistry metric from laboratories to industry. *Green Chem.* **2015,** *17*, 2846-2852.
219. Keijer, T.; Bakker, V.; Slootweg, J. C., Circular chemistry to enable a circular economy. *Nat. Chem.* **2019,** *11*, 190-195.
220. Sheldon, R. A., The E Factor: fifteen years on. *Green Chem.* **2007,** *9*, 1273-1283.
221. Zhu, J.-B.; Watson, E. M.; Tang, J.; Chen, E. Y.-X., A synthetic polymer system with repeatable chemical recyclability. *Science* **2018,** *360*, 398-403.
222. Sardon, H.; Dove, A. P., Plastics recycling with a difference. *Science* **2018,** *360*, 380-381.

223. Curzons, A. D.; Constable, D. J. C.; Mortimer, D. N.; Cunningham, V. L., So you think your process is green, how do you know?—Using principles of sustainability to determine what is green–a corporate perspective. *Green Chem.* **2001,** *3*, 1-6.
224. Communication, N. R. C. C. R. P., *Improving Risk Communication*. National Academy Press: 1989.
225. Winterton, N., News and Views/ Twelve more green chemistry principles. *Green Chem.* **2001,** *3*, G73-G81.
226. Tang, S. L. Y.; Smith, R. L.; Poliakoff, M., Principles of green chemistry: PRODUCTIVELY. *Green Chem.* **2005,** *7*, 761-762.
227. Martin G. Hitzler; Poliakoff, M., Continuous hydrogenation of organic compounds in supercriticalfluids. *Chem. Commun.* **1997,** *17*, 1667-1668.
228. Bourne, R. A. Automated reactions in supercritical carbon dioxide. PhD Thesis, The University of Nottingham, Nottingham, 2008.
229. Han, X.; Bourne, R. A.; Poliakoff, M.; George, M. W., Immobilised photosensitisers for continuous flow reactions of singlet oxygen in supercritical carbon dioxide. *Chem. Sci.* **2011,** *2*, 1059-1067.
230. Poliakoff, M.; S. M. Howdle; Kazarian, S. G., Vibrational Spectroscopy in Supercritical Fluids From Analysis and Hydrogen Bonding to Polymers and Synthesis. *Angew. Chem. Int. Ed.* **1995,** *34*, 1275-1295.
231. Lewis, B.; Elbe, G. v., *Combustion, flames and explosions of gases*. 3rd ed.; Orlando : Academic Press: Orlando, 1987.
232. Han, X. Singlet Oxygen Reactions in Supercritical CO_2. PhD Thesis, University of Nottingham, 2010.
233. Chapman, A. O. Reactions of molecular oxygen in supercritical carbon PhD Thesis, The University of Nottingham, Nottingham, 2007.
234. Fulmer, G. R.; Miller, A. J. M.; Sherden, N. H.; Gottlieb, H. E.; Nudelman, A.; Stoltz, B. M.; Bercaw, J. E.; Goldberg, K. I., NMR Chemical Shifts of Trace Impurities: Common Laboratory Solvents, Organics, and Gases in Deuterated Solvents Relevant to the Organometallic Chemist. *Organometallics* **2010,** *29*, 2176-2179.
235. Lange, H.; Carter, C. F.; Hopkin, M. D.; Burke, A.; Goode, J. G.; Baxendale, I. R.; Ley, S. V., A breakthrough method for the accurate addition of reagents in multi-step segmented flow processing. *Chem. Sci.* **2011,** *2*, 765-769.
236. Mikami, K., *Green Reaction Media in Organic Synthesis*. Blackwell Publishing: 2005.
237. Wu, L.; Abada, Z.; Lee, D. S.; Poliakoff, M.; George, M. W., Combining engineering and chemistry for the selective continuous production of four different oxygenated compounds by photo-oxidation of cyclopentadiene using liquid and supercritical CO_2 as solvents. *Tetrahedron* **2018,** *74*, 3107-3112.
238. Summerton, L.; Summerton, L.; Sneddon, H. F.; Sneddon, H. F.; Jones, L. C.; Clark, J. H.; Clark, J. H.; Brown, M.; Sherwood, J.; Hunt, A. J.; Kummerer, K.; Hayler, J.; Messinger, J.; Moseley, J.; Fairlamb, I.; Blacker, J.; Whiting, A.; Glieder, A.; Wells, A.; Maes, B.; Pattison, G., *Green and sustainable medicinal chemistry :*

methods, tools and strategies for the 21st Century pharmaceutical industry. Royal Society of Chemistry,: Cambridge, 2016.
239. Baumann, M.; Baxendale, I.; Filipponi, P.; Hu, T., Sustainable Flow Synthesis of a Versatile Cyclopentenone Building Block. *Org. Process Res. Dev.* **2017,** *21*, 2052-2059.
240. Plutschack, M. B.; Pieber, B.; Gilmore, K.; Seeberger, P. H., The Hitchhiker's Guide to Flow Chemistry. *Chem. Rev.* **2017,** *117*, 11796-11893.
241. Ingham, R. J.; Battilocchio, C.; Fitzpatrick, D. E.; Sliwinski, E.; Hawkins, J. M.; Ley, S. V., A Systems Approach towards an Intelligent and Self-Controlling Platform for Integrated Continuous Reaction Sequences. *Angew. Chem. Int. Ed.* **2015,** *54*, 144-148.
242. Gutmann, B.; Cantillo, D.; Kappe, C. O., Continuous-flow technology-a tool for the safe manufacturing of active pharmaceutical ingredients. *Angew. Chem. Int. Ed. Engl* **2015,** *54*, 6688-6728.
243. Jin, J.; Guidi, S.; Abada, Z.; Amara, Z.; Selva, M.; George, M. W.; Poliakoff, M., Continuous niobium phosphate catalysed Skraup reaction for quinoline synthesis from solketal. *Green Chem.* **2017,** *19*, 2439-2447.
244. Streng, E. S.; Lee, D. S.; George, M. W.; Poliakoff, M., Continuous N-alkylation reactions of amino alcohols using γ-Al_2O_3 and supercritical CO_2: unexpected formation of cyclic ureas and urethanes by reaction with CO_2. *Beilstein J. Org. Chem.* **2017,** *13*, 329-337.
245. Service, R. F., The synthesis machine. *Science* **2015,** *347*, 1190-1193.
246. Mascia, S.; Heider, P. L.; Zhang, H.; Lakerveld, R.; Benyahia, B.; Barton, P. I.; Braatz, R. D.; Cooney, C. L.; Evans, J. M. B.; Jamison, T. F.; Jensen, K. F.; Myerson, A. S.; Trout, B. L., End-to-End Continuous Manufacturing of Pharmaceuticals: Integrated Synthesis, Purification, and Final Dosage Formation. *Angew. Chem. Int. Ed.* **2013,** *52*, 12359-12363.
247. Kaneko, C., Design Of New Reactions And Its Application To Creative Drug Research. *Yakugaku Zasshi-J. Pharm. Soc. Jpn.* **1993,** *113*, 627-646.
248. Jas, G.; Kirschning, A., Continuous Flow Techniques in Organic Synthesis. *Chem. Eur. J.* **2003,** *9*, 5708-5723.
249. Pozzi, G.; Mercs, L.; Holczknecht, O.; Martimbianco, F.; Fabris, F., Straightforward Synthesis of a Fluorous Tetraarylporphyrin: an Efficient and Recyclable Sensitizer for Photooxygenation Reactions. *Adv. Synth. Catal.* **2006,** *348*, 1611-1620.
250. Maraş, A.; Seçen, H.; Sütbeyaz, Y.; Balcı, M., A Convenient Synthesis of (±)-talo-Quercitol (1-Deoxy-neo-Inositol) and (±)-vibo-Quercitol (1-Deoxy-myo-Inositol) via Ene Reaction of Singlet Oxygen. *J. Org. Chem.* **1998,** *63*, 2039-2041.
251. Baran, A.; Aydin, G.; Savran, T.; Sahin, E.; Balci, M., Trisequential Photooxygenation Reaction: Application to the Synthesis of Carbasugars. *Org. Lett.* **2013,** *15*, 4350-4353.

252. Han, X.; Poliakoff, M., Continuous reactions in supercritical carbon dioxide: problems, solutions and possible ways forward. *Chem. Soc. Rev.* **2012,** *41*, 1428-1436.
253. Hiroto, N.; Hiroaki, M.; Yasuji, Y., Total synthesis of (+)-halimedatrial: The absolute configuration of halimedatrial. *Tetrahedron Lett.* **1990,** *31*, 1573-1576.
254. Rybicka-Jasińska, K.; Shan, W.; Zawada, K.; Kadish, K. M.; Gryko, D., Porphyrins as Photoredox Catalysts: Experimental and Theoretical Studies. *J. Am. Chem. Soc.* **2016,** *138*, 15451-15458.
255. Hall, J. F.; Han, X.; Poliakoff, M.; Bourne, R. A.; George, M. W., Maximising the efficiency of continuous photo-oxidation with singlet oxygen in supercritical CO_2 by use of fluorous biphasic catalysis. *Chem. Commun (Camb)* **2012,** *48*, 3073-3075.
256. Worrall, D. R.; Abdel-Shafi, A. A.; Wilkinson, F., Factors Affecting the Rate of Decay of the First Excited Singlet State of Molecular Oxygen in Supercritical Fluid Carbon Dioxide. *J. Phys. Chem. A* **2001,** *105*, 1270-1276.
257. Walsh, B.; Hyde, J. R.; Licence, P.; Poliakoff, M., The automation of continuous reactions in supercritical CO_2: the acid-catalysed etherification of short chain alcohols. *Green Chem.* **2005,** *7*, 456-463.
258. Amandi, R.; Licence, P.; Ross, S. K.; Aaltonen, O.; Poliakoff, M., Friedel−Crafts Alkylation of Anisole in Supercritical Carbon Dioxide: A Comparative Study of Catalysts. *Org. Process Res. Dev.* **2005,** *9*, 451-456.
259. Hitzler, M. G.; Smail, F. R.; Ross, S. K.; Poliakoff, M., Selective Catalytic Hydrogenation of Organic Compounds in Supercritical Fluids as a Continuous Process. *Org. Process Res. Dev.* **1998,** *2*, 137-146.
260. Licence, P.; Ke, J.; Sokolova, M.; Ross, S. K.; Poliakoff, M., Chemical reactions in supercritical carbon dioxide: from laboratory to commercial plant. *Green Chem.* **2003,** *5*, 99-104.
261. Stevens, J. G.; Bourne, R. A.; Twigg, M. V.; Poliakoff, M., Real-Time Product Switching Using a Twin Catalyst System for the Hydrogenation of Furfural in Supercritical CO_2. *Angew. Chem. Int. Ed.* **2010,** *49*, 8856-8859.
262. Schenck, G. O.; Dunlap, D. E., Photosynthese von Cyclopentadien-endoperoxyd bei −100°C und Hydrierung von Endoperoxyden mit Thioharnstoff Verwendung von Na-Dampflampen in der präparativen Photochemie. *Angew. Chem.* **1956,** *68*, 248-249.
263. Kaneko, C.; Sugimoto, A.; Tanaka, S., A Facile One-step Synthesis of cis-2-Cyclopentene- and cis-2-Cyclohexene-1,4-diols from the Corresponding Cyclodienes. *Synlett* **1974,** *1974*, 876-877.
264. Carmona, R. C.; Correia, C. R. D., Stereoselective Synthesis of 3-Hydroxy-4-arylcyclopentanones and 4-Arylcyclopentenones through a Heck-Matsuda Desymmetrization ofmeso cis-4-Cyclopentene-1,3-diol. *Adv. Synth. Catal.* **2015,** *357*, 2639-2643.
265. Adams, W. R.; Trecker, D. J., The dye-sensitized photooxidation of cyclopentadiene. *Tetrahedron* **1971**.

266. Nagaoka, H.; Miyakoshi, T.; Yamada, Y., Total synthesis of marine prostanoids clavulones. *Tetrahedron Lett.* **1984,** *25*, 3621-3624.
267. Lis, L. G.; Zheldakova, T. A., New marine prostanoids, clavulones, halogenovulones, and punaglandins. *Chemistry of Natural Compounds* **1993,** *29*, 259-274.
268. Hornung, C. H.; Hallmark, B.; Baumann, M.; Baxendale, I. R.; Ley, S. V.; Hester, P.; Clayton, P.; Mackley, M. R., Multiple Microcapillary Reactor for Organic Synthesis. *Ind. Eng. Chem. Res.* **2010,** *49*, 4576-4582.
269. Zhang, D.; Wu, L. Z.; Yang, Q. Z.; Li, X. H.; Zhang, L. P.; Tung, C. H., Versatile photosensitization system for O-1(2)-mediated oxidation of alkenes based on Nafion-supported platinum(II) terpyridyl acetylide complex. *Org. Lett.* **2003,** *5*, 3221-3224.
270. Moffett, R. B., Cyclopentadiene and 3-Chlorocyclopentene. *Org. Synth.* **1952,** *32*, 41-46.
271. Jahnisch, K.; Dingerdissen, U., Photochemical Generation and [4+2]-Cycloaddition of Singlet Oxygen in a Falling-Film Micro Reactor. *Chem. Eng. Technol* **2005,** *28*, 426-427.
272. Directive 67/548/EEC or Directive 1999/45/EC. European Union Council 2008.
273. Sharpless, K. B.; Snyder, T. E.; Sharpless, K. B.; Snyder, T. E.; Clayton, R. B., The Mechanism of the Addition of ‘A, Excited Oxygen to Olefins. Evidence for a 1,2-Dioxetane Intermediate. *J. Am. Chem. Soc.* **1969,** *91:12*, 3396-3398.
274. Tiwari, M. S.; Gawade, A. B.; Yadav, G. D., Magnetically separable sulfated zirconia as highly active acidic catalysts for selective synthesis of ethyl levulinate from furfuryl alcohol. *Green Chem.* **2017,** *19*, 963-976.
275. Collins, P. W.; Djuric, S. W., Synthesis of therapeutically useful prostaglandin and prostacyclin analogs. *Chem. Rev.* **1993,** *93*, 1533-1564.
276. Nicolaou, K. C.; Sorensen, E. J., Classics in Total Synthesis. *Recueil des Travaux Chimiques des Pays-Bas* **1996,** *115*, 552-552.
277. Ricciotti, E.; FitzGerald Garret, A., Prostaglandins and Inflammation. *Arterioscler., Thromb., Vasc. Biol.* **2011,** *31*, 986-1000.
278. Poliakoff, M.; S. M. Howdle, S. G. K., Vibrational Spectroscopy in Supercritical Fluids From Analysis and Hydrogen Bonding to Polymers and Synthesis. *Angew. Chem. Int. Ed.* **1995,** *34*, 1275-1295.
279. Adams, W. R.; Trecker, D. J., The dye-sensitized photooxidation of cyclopentadiene. *Tetrahedron* **1971,** *27*, 2631-2637.
280. Chapman, A. O.; Akien, G. R.; Arrowsmith, N. J.; Licence, P.; Poliakoff, M., Continuous heterogeneous catalytic oxidation of primary and secondary alcohols in $scCO_2$. *Green Chem.* **2010,** *12*, 310-315.
281. Lee, D. S.; Amara, Z.; Poliakoff, M.; Harman, T.; Reid, G.; Rhodes, B.; Brough, S.; McInally, T.; Woodward, S., Investigating Scale-Up and Further Applications of DABAL-Me_3 Promoted Amide Synthesis. *Org. Process Res. Dev.* **2015,** *19*, 831-840.

282. Spivey, A. C.; Mañas, C. G.; Mann, I., Polystyrene-supported N-methylthiourea: a convenient new reagent for the hydrogenolysis of bicyclic endoperoxides. *Chem. Commun.* **2005**, 4426-4428.
283. Jessop, P.; Wynne, D. C.; DeHaai, S.; Nakawatase, D., Carbon dioxide gas accelerates solventless synthesis. *Chem. Commun.* **2000**, 693-694.
284. Avery, T. D.; Jenkins, N. F.; Kimber, M. C.; Lupton, D. W.; Taylor, D. K., First examples of the catalytic asymmetric ring-opening of meso 1,2-dioxines utilising cobalt(ii) complexes with optically active tetradentate Schiff base ligands: formation of enantio-enriched cyclopropanes. *Chem. Commun.* **2002**, 28-29.
285. Priest, J.; Longland, M. R.; Elsegood, M. R. J.; Kimber, M. C., An Asymmetric Synthesis of trans-Fused Butyrolactones from Endoperoxides. *J. Org. Chem.* **2013,** *78*, 3476-3481.
286. Staben, S. T.; Linghu, X.; Toste, F. D., Enantioselective Synthesis of γ-Hydroxyenones by Chiral Base-Catalyzed Kornblum DeLaMare Rearrangement. *J. Am. Chem. Soc.* **2006,** *128*, 12658-12659.
287. Trabanco, A. A.; Montalban, A. G.; Rumbles, G.; Barrett, A. G. M.; Hoffman, B. M., A seco-Porphyrazine: Superb Sensitizer for Singlet Oxygen Generation and Endoperoxide Synthesis. *Synlett* **2000,** *2000*, 1010-1012.
288. Sitthisa, S.; Resasco, D. E., Hydrodeoxygenation of Furfural Over Supported Metal Catalysts: A Comparative Study of Cu, Pd and Ni. *Catal. Lett.* **2011,** *141*, 784-791.
289. Clark, C. A.; Lee, D. S.; Pickering, S. J.; Poliakoff, M.; George, M. W., A Simple and Versatile Reactor for Photochemistry. *Org. Process Res. Dev.* **2016,** *20*, 1792-1798.
290. Dickson, R. S.; Dobney, B. J.; Eastwood, F. W., Preparation of cyclopentadiene from its dimer. *J. Chem. Educ.* **1987,** *64*, 898.
291. Holland, D.; Stoddart, F. J., Regioselective and Stereoselective Methods for the Synthesis of the pentitols. *J. Chem. Soc., Perkin Trans. 1* **1983**, 1553-1571.
292. Teles, J. H.; Hermans, I.; Franz, G.; Sheldon, R. A., Oxidation. In *Ullmann's Encyclopedia of Industrial Chemistry*, Wiley-VCH Verlag GmbH & Co. KGaA, Weinheim: 2015.
293. Wu, L.; Lee, D. S.; Boufroura, H.; Poliakoff, M.; George, M. W., Photooxidation of Fulvenes in a Continuous Flow Photoreactor using Carbon Dioxide as a Solvent. *ChemPhotoChem* **2018,** *2*, 580-585.
294. Hopf, H.; Sherburn, M. S., *Cross conjugation: Modern Dendralene, Radialene and Fulvene Chemistry*. Wiley: New York, 2016; p 459.
295. Thiele, J., Ueber Ketonreactionen bei dem Cyclopentadiën. *Berichte der deutschen chemischen Gesellschaft* **1900,** *33*, 666-673.
296. Thiele, J.; Balhorn, H., 4. Condensationsproducte des cyklopentadiëns. *Justus Liebigs Annalen der Chemie* **1906,** *348*, 1-15.
297. Mueller-Westerhoff, U., Metallocenes from fulvenes : A new synthesis of functionally substituted ferrocenes. *Tetrahedron Lett.* **1972,** *13*, 4639-4642.

298. Day, J. H., The Fulvenes. *Chem. Rev.* **1953,** *53*, 167-189.
299. Tacke, M.; Cuffe, L. P.; Gallagher, W. M.; Lou, Y.; Mendoza, O.; Müller-Bunz, H.; Rehmann, F.-J. K.; Sweeney, N., Methoxy-phenyl substituted ansa-titanocenes as potential anti-cancer drugs derived from fulvenes and titanium dichloride. *J. Inorg. Biochem.* **2004,** *98*, 1987-1994.
300. Ebner, C.; Carreira, E. M., Pentafulvene for the Synthesis of Complex Natural Products: Total Syntheses of (±)-Pallambins A and B. *Angew. Chem. Int. Ed Engl* **2015,** *54*, 11227-11230.
301. Godman, N. P.; Balaich, G. J.; Iacono, S. T., First preparation of low band gap fulvene-modified polynorbornene via ring-opening metathesis polymerization. *Chem. Commun.* **2016,** *52*, 5242-5245.
302. Hafner, K.; Häfner, K. H.; König, C.; Kreuder, M.; Ploss, G.; Schulz, G.; Sturm, E.; Vöpel, K. H., Fulvenes as Isomers of Benzenoid Compounds. *Angew. Chem. Int. Ed. Engl* **1963,** *2*, 123-134.
303. Wheland, G. W.; Mann, D. E., The Dipole Moments of Fulvene and Azulene. *J. Chem. Phys.* **1949,** *17*, 264-268.
304. Day, J. H.; Oestreich, C., Fulvenes. III. Heat of Combustion and Resonance Energy1. *J. Org. Chem.* **1957,** *22*, 214-216.
305. Nair, V.; Anilkumar, G.; Radhakrishnan, K. V.; Sheela, K. C.; Rath, N. P., Diels-Alder reactions of a 6-arenyl fulvene with dienes and dienophiles and related chemistry. *Tetrahedron* **1997,** *53*, 17361-17372.
306. Tamke, S.; Daniliuc, C.; Paradies, J., Frustrated Lewis Pair catalyzed Hydrosilylation and Hydrosilane mediated Hydrogenation of Fulvenes. *Org. Biomol. Chem.* **2014,** *12*.
307. Antczak, K.; Kingston, J. F.; Fallis, A. G., Addition initiated ring closure: synthesis of substituted spiro[2.4]hepta-4,6-dienes via cyclopentadiene intermediates from fulvene precursors. *Can. J. Chem.* **1984,** *62*, 2451-2455.
308. Mains, H.; Day, J. H., Polymers of dimethyl fulvene. *J. Polym. Sci., Part B: Polym. Lett.* **1963,** *1*, 347-349.
309. Schulz, S.; Hötling, S., The use of the lactone motif in chemical communication. *Nat. Prod. Rep.* **2015,** *32*, 1042-1066.
310. Mander, L.; Liu, H.-W., *Comprehensive Natural Products II: Chemistry and Biology: Chemical Ecology*. Elsevier Science: 2010; Vol. 4.
311. Dickschat, J. S., Quorum sensing and bacterial biofilms. *Nat. Prod. Rep.* **2010,** *27*, 343-369.
312. B., G.; A., K.; A., S., Lactones with a fragrance properties. *CHEMIK* **2015,** *69*, 342-349.
313. C., G.; D., P.; S., G., A Biotechnological Approach to Microbial Based Perfumes and Flavours. *J. Microbiol Exp.* **2015,** *2*, 34-41.
314. Zinck, P., Synthetic Strategies for Biomedical Polyesters Specialties. In *Trends in Materials Science*, Mr Anthony Laskovski (Ed.) ed.; 2011.

315. Albertsson, A.-C.; Srivastava, R. K., Recent developments in enzyme-catalyzed ring-opening polymerization. *Adv. Drug Delivery Rev.* **2008,** *60*, 1077-1093.
316. Kobayashi, S., Enzymatic ring-opening polymerization and polycondensation for the green synthesis of polyesters. *Polym. Adv. Technol.* **2015,** *26*, 677-686.
317. Kobayashi, S., Recent Developments in Lipase-Catalyzed Synthesis of Polyesters. *Macromol. Rapid Commun.* **2009,** *30*, 237-266.
318. Uyama, H.; Takamoto, T.; Kobayashi, S., Enzymatic Synthesis of Polyesters in Ionic Liquids. *Polym. J. (Tokyo, Jpn.)* **2002,** *34*, 94-96.
319. Zhao, H., Enzymatic ring-opening polymerization (ROP) of polylactones: roles of non-aqueous solvents. *J. Appl. Chem. Biotechnol.* **2018,** *93*, 9-19.
320. Tsuji, H.; Nishikawa, M.; Osanai, Y.; Matsumura, S., New Strategy for Controlling Biodegradability of Biodegradable Polyesters by Enzyme-Catalyzed Surface Grafting. *Macromol. Rapid Commun.* **2007,** *28*, 1651-1656.
321. Fortunati, T.; D'Acunto, M.; Caruso, T.; Spinella, A., Chemoenzymatic preparation of musky macrolactones. *Tetrahedron* **2015,** *71*, 2357-2362.
322. Wisse, E.; Renken, R. A. E.; Roosma, J. R.; Palmans, A. R. A.; Meijer, E. W., Poly(caprolactone-co-oxo-crown ether)-Based Poly(urethane)urea for Soft Tissue Engineering Applications. *Biomacromolecules* **2007,** *8*, 2739-2745.
323. de Geus, M.; Peeters, J.; Wolffs, M.; Hermans, T.; Palmans, A. R. A.; Koning, C. E.; Heise, A., Investigation of Factors Influencing the Chemoenzymatic Synthesis of Block Copolymers. *Macromolecules* **2005,** *38*, 4220-4225.
324. Peeters, J. W.; Palmans, A. R. A.; Meijer, E. W.; Koning, C. E.; Heise, A., Chemoenzymatic Synthesis of Branched Polymers. *Macromol. Rapid Commun.* **2005,** *26*, 684-689.
325. Jiang, Y.; Loos, K., Enzymatic Synthesis of Biobased Polyesters and Polyamides. *Polymers* **2016,** *8*, 243-295.
326. Baeyer, A.; Villiger, V., Einwirkung des Caro'schen Reagens auf Ketone. *Berichte der deutschen chemischen Gesellschaft* **1899,** *32*, 3625-3633.
327. Krow, G. R., The Baeyer–Villiger Oxidation of Ketones and Aldehydes. In *Organic Reactions*, 2004.
328. Sinhamahapatra, A.; Sinha, A.; Pahari, S. K.; Sutradhar, N.; Bajaj, H. C.; Panda, A. B., Room temperature Baeyer–Villiger oxidation using molecular oxygen over mesoporous zirconium phosphate. *Catal. Sci. Technol.* **2012,** *2*, 2375-2382.
329. Göttlich, R.; Yamakoshi, K.; Sasai, H.; Shibasaki, M., A New and Selective Metal-Catalyzed Baeyer-Villiger Oxidation Procedure. *Synlett* **1997,** *1997*, 971-973.
330. Del Todesco Frisone, M.; Pinna, F.; Strukul, G., Baeyer-Villiger oxidation of cyclic ketones with hydrogen peroxide catalyzed by cationic complexes of platinum(II): selectivity properties and mechanistic studies. *Organometallics* **1993,** *12*, 148-156.
331. Strukul, G.; Varagnolo, A.; Pinna, F., New (old) hydroxo complexes of platinum(II) as catalysts for the Baeyer-Villiger oxidation of ketones with hydrogen peroxide. *J. Mol. Catal. A: Chem.* **1997,** *117*, 413-423.

332. Caron, S.; Dugger, R. W.; Ruggeri, S. G.; Ragan, J. A.; Ripin, D. H. B., Large-Scale Oxidations in the Pharmaceutical Industry. *Chem. Rev.* **2006,** *106*, 2943-2989.
333. Otomo, R.; Kosugi, R.; Kamiya, Y.; Tatsumi, T.; Yokoi, T., Modification of Sn-Beta zeolite: characterization of acidic/basic properties and catalytic performance in Baeyer–Villiger oxidation. *Catal. Sci. Technol.* **2016,** *6*, 2787-2795.
334. Fukuda, O.; Sakaguchi, S.; Ishii, Y., A new strategy for catalytic Baeyer–Villiger oxidation of KA-oil with molecular oxygen using N-hydroxyphthalimide. *Tetrahedron Lett.* **2001,** *42*, 3479-3481.
335. Gusso, A.; Baccin, C.; Pinna, F.; Strukul, G., Platinum-Catalyzed Oxidations with Hydrogen Peroxide: Enantiospecific Baeyer-Villiger Oxidation of Cyclic Ketones. *Organometallics* **1994,** *13*, 3442-3451.
336. Strukul, G., Transition Metal Catalysis in the Baeyer–Villiger Oxidation of Ketones. *Angew. Chem. Int. Ed.* **1998,** *37*, 1198-1209.
337. ten Brink, G.-J.; Vis, J.-M.; Arends, I. W. C. E.; Sheldon, R. A., Selenium-Catalyzed Oxidations with Aqueous Hydrogen Peroxide. 2. Baeyer−Villiger Reactions in Homogeneous Solution1. *J. Org. Chem.* **2001,** *66*, 2429-2433.
338. ten Brink, G. J.; Arends, I. W. C. E.; Sheldon, R. A., The Baeyer−Villiger Reaction: New Developments toward Greener Procedures. *Chem. Rev.* **2004,** *104*, 4105-4124.
339. Corma, A.; Nemeth, L. T.; Renz, M.; Valencia, S., Sn-zeolite beta as a heterogeneous chemoselective catalyst for Baeyer–Villiger oxidations. *Nature* **2001,** *412*, 423-425.
340. Neimann, K.; Neumann, R., Electrophilic Activation of Hydrogen Peroxide: Selective Oxidation Reactions in Perfluorinated Alcohol Solvents. *Org. Lett.* **2000,** *2*, 2861-2863.
341. Du, R.; Yuan, H.; Yao, J.; Li, H., Oxidation of KA oil to caprolactone with molecular oxygen using N-hydroxyphthalimide-mediated $Ce(NH_4)_2(NO_3)_6$ catalyst. *Mol. Catal.* **2019,** *467*, 24-29.
342. Skorianetz, W.; SchulteW-Elte, K. H.; Ohloff, G., Farbstoffsensibilisierte Photo-Oxygenierung von 6,6-Dimethylfulven. Eine neue 1,2-Dioxolan-Umlagerung. *Helv. Chim. Acta* **1971,** *54*, 1913-1922.
343. Straus, F., Johannes Thiele (1865–1918). *Berichte der deutschen chemischen Gesellschaft (A and B Series)* **1927,** *60*, A75-A132.
344. Stone, K. J.; Little, R. D., An exceptionally simple and efficient method for the preparation of a wide variety of fulvenes. *J. Org. Chem.* **1984,** *49*, 1849-1853.
345. Harada, N.; Suzuki, S.; Uda, H.; Ueno, H., Photochemical oxidation of 6,6-disubstituted fulvenes. *J. Am. Chem. Soc.* **1972,** *94*, 1777-1778.
346. Harada, N.; Uda, H.; Ueno, H., Solvent dependence in the photochemical oxidation of 6,6-dimethylfulvene and isolation of 5-isopropenyl-4-hydroxy-2-cyclopentenone. *Chem. lett.* **1972,** *1*, 663-666.

347. Milas, N. A.; Golubovic, A., Studies in Organic Peroxides. XXVI. Organic Peroxides Derived from Acetone and Hydrogen Peroxide. *J. Am. Chem. Soc.* **1959,** *81*, 6461-6462.
348. Nobuyuki, H.; Shukuko, S.; Hisashi, U.; Hiroshi, U., Photochemical Oxidation Of 6,6-Dimethylfulvene In Alkaline Methanolic Solution. *Chem. Lett.* **1972,** *1*, 803-806.
349. Nobuyuki, H.; Hisashi, U.; Hiroshi, U.; Shun-ichi, U., Isolation And Properties Of 6,6-Dimethylfulvene 1,4-Epidioxide. *Chem. lett.* **1973,** *2*, 1173-1176.
350. Akira, K.; Hiroshi, K.; Hisashi, U., 2(7H)-Oxepinones: Photochemical Oxidation Of 6-Monosubstituted Fulvenes. *Chem. Lett.* **1972,** *1*, 807-810.
351. Erden, I.; Drummond, J.; Alstad, R.; Xu, F., Chemistry of singlet oxygen: Isolation and characterization of a stable allene oxide from a fulvene endoperoxide. *Tetrahedron Lett.* **1993,** *34*, 1255-1258.
352. Camp, R. L.; Greene, F. D., 1,3-Di-tert-butylallene oxide. Isolation and isomerization to trans-2,3-di-tert-butylcyclopropanone. *J. Am. Chem. Soc.* **1968,** *90*, 7349-7349.
353. Erden, I.; Amputch, M. A., Thermal decomposition of 7-isopropylidene-2,3-dioxabicyclo[2.2.1]heptane: Evidence for allene oxide and cyclopropanone intermediates. *Tetrahedron Lett.* **1987,** *28*, 3779-3782.
354. Erden, I.; Basada, J.; Poli, D.; Cabrera, G.; Xu, F.; Gronert, S., Unusual hydroxyl effect on fulvene endoperoxide decompositions. *Tetrahedron Lett.* **2016,** *57*, 2190-2193.
355. Coşkun, N.; Erden, I., An efficient catalytic method for fulvene synthesis. *Tetrahedron* **2011,** *67*, 8607-8614.
356. Reynaud, C.; Fall, Y.; Feuerstein, M.; Doucet, H.; Santelli, M., Synthesis of cis,cis,cis-1-alkylidene-2,3,4,5-tetrakis(diphenylphosphinomethyl)cyclopentanes. *Tetrahedron* **2009,** *65*, 7440-7448.
357. Adam, W.; Erden, I., Trapping of Unstable Fulvene/Singlet Oxygen Adducts by Reduction with Diazene. *Angew. Chem. Int. Ed. Engl* **1978,** *17*, 210-210.
358. Bonneau, R.; Pottier, R.; Bagno, O.; Joussot-Dubien, J., pH dependence of singlet oxygen production in aqueous solutions using thiazine dyes as photosensitizers. *Photochem. Photobiol. Sci.* **1975,** *21*, 159-163.
359. Li, Y.; Junge, K.; Beller, M., Zinc-Catalyzed Reductions of Unsaturated Compounds. In *Zinc Catalysis*, 2015.
360. Peluso, A.; Improta, R.; Zambelli, A., Polymerization Mechanism of Conjugated Dienes in the Presence of Ziegler−Natta Type Catalysts: Theoretical Study of Butadiene and Isoprene Polymerization with $CpTiCl_3$−MAO Initiator. *Organometallics* **2000,** *19*, 411-419.
361. Suzuki, T.; Tanaka, K.; Toyoshima, I.; Okuhara, T.; Tanaka, K.-i., Hydrogenation of conjugated dienes and isomerization of butenes on CdO, Co_3O_4 and Cr_2O_3. *J. Chem. Soc., Faraday Trans. 1* **1987,** *83*, 1213-1226.

362. Hamer, J., *1,4-Cycloaddition Reaction: The Diels-Alder Reaction in Heterocyclic Syntheses: The Diels-Alder Reaction in Heterocyclic Syntheses*. Elsevier Science: UK, 2013.
363. McMurry, J. E., *Study Guide with Student Solutions Manual for McMurry's Organic Chemistry, 8th*. Cengage Learning: 2011.
364. Yang, Y.; Ge, Y.; Zhao, H.; Shi, W.; Li, Q., Lipase-catalyzed synthesis of poly(ε-caprolactone) and characterization of its solid-state properties. *Biocatal. Biotransform.* **2011,** *29*, 337-343.
365. Kerep, P.; Ritter, H., Influence of Microwave Irradiation on the Lipase-Catalyzed Ring-Opening Polymerization of ε-Caprolactone. *Macromol. Rapid Commun.* **2006,** *27*, 707-710.
366. Yang, Y.; Ge, Y.; Zhao, H.; Shi, W.; Li, Q., Lipase-catalyzed synthesis of poly(ε-caprolactone) and characterization of its solid-state properties. *Biocatal. Biotransform.* **2011,** *29*, 337-343.
367. Biotechnology LettersWu, C.; Zhang, Z.; He, F.; Zhuo, R., Enzymatic synthesis of poly(ε-caprolactone) in monocationic and dicationic ionic liquids. *Biotechnol. Lett.* **2013,** *35*, 879-885.
368. Amara, Z.; Poliakoff, M.; Duque, R.; Geier, D.; Franciò, G.; Gordon, C. M.; Meadows, R. E.; Woodward, R.; Leitner, W., Enabling the Scale-Up of a Key Asymmetric Hydrogenation Step in the Synthesis of an API Using Continuous Flow Solid-Supported Catalysis. *Org. Process Res. Dev.* **2016,** *20*, 1321-1327.
369. Stevens, J. G.; Gómez, P.; Bourne, R. A.; Drage, T. C.; George, M. W.; Poliakoff, M., Could the energy cost of using supercritical fluids be mitigated by using CO_2 from carbon capture and storage (CCS)? *Green Chem.* **2011,** *13*, 2727-2733.
370. Bourne, R. A.; Stevens, J. G.; Ke, J.; Poliakoff, M., Maximising opportunities in supercritical chemistry: the continuous conversion of levulinic acid to [gamma]-valerolactone in CO_2. *Chem. Commun.* **2007**, 4632-4634.
371. Hoshi, N.; Uda, H.; Sato, K.; Hagiwara, H., Temperature dependence in the sensitized photoreaction of 3,3-dimethyloxepin-2(3H)-one and 2,2,7,7-tetramethylcyclohepta-3,5-dien-1-one. *J. Chem. Soc., Perkin Trans. 1* **1984,** *I*, 769-773.
372. DeLaney, E. N.; Lee, D. S.; Elliott, L. D.; Jin, J.; Booker-Milburn, K. I.; Poliakoff, M.; George, M. W., A laboratory-scale annular continuous flow reactor for UV photochemistry using excimer lamps for discrete wavelength excitation and its use in a wavelength study of a photodecarboxlyative cyclisation. *Green Chem.* **2017,** *19*, 1431-1438.
373. Wollenberg, R. H., Efficient conversion of carbonyl compounds to conjugated dienals. *Tetrahedron Lett.* **1978,** *19*, 717-720.
374. Wang, X.; Porco, J. A., Synthesis of the Tetracyclic Core of the Tetrapetalones through Transannular Oxidative [4+3] Cyclization. *Angew. Chem., Int. Ed.* **2006,** *45*, 6607-6607.

375. Wang, X.; Porco, J. A., Synthesis of the Tetracyclic Core of the Tetrapetalones through Transannular Oxidative [4+3] Cyclization. *Angew. Chem. Int. Ed.* **2005,** *117*, 3127-3131.
376. Redondo, M. C.; Ribagorda, M.; Carreño, M. C., Exploring Morita−Baylis−Hillman Reactions of p-Quinols. *Org. Lett.* **2010,** *12*, 568-571.
377. Berry, J. M.; Bradshaw, T. D.; Fichtner, I.; Ren, R.; Schwalbe, C. H.; Wells, G.; Chew, E.-H.; Stevens, M. F. G.; Westwell, A. D., Quinols as Novel Therapeutic Agents. 2. 4-(1-Arylsulfonylindol-2-yl)-4-hydroxycyclohexa-2,5-dien-1-ones and Related Agents as Potent and Selective Antitumor Agents. *J. Med. Chem.* **2005,** *48*, 639-644.
378. Pape, A. R.; Kaliappan, K. P.; Kündig, E. P., Transition-Metal-Mediated Dearomatization Reactions. *Chem. Rev.* **2000,** *100*, 2917-2940.
379. López Ortiz, F.; Iglesias, M. J.; Fernández, I.; Andújar Sánchez, C. M.; Ruiz Gómez, G., Nucleophilic Dearomatizing (DNAr) Reactions of Aromatic C,H-Systems. A Mature Paradigm in Organic Synthesis. *Chem. Rev.* **2007,** *107*, 1580-1691.
380. Chun-Xiang, Z.; Wei, Z.; Shu-Li, Y., Catalytic Asymmetric Dearomatization Reactions. *Angew. Chem., Int. Ed.* **2012,** *51*, 12662-12686.
381. Quideau, S.; Pouységu, L.; Deffieux, D., Oxidative Dearomatization of Phenols: Why, How and What For? *Synlett* **2008,** *2008*, 467-495.
382. Roche, S. P.; Porco, J. A., Dearomatization Strategies in the Synthesis of Complex Natural Products. *Angew. Chem., Int. Ed.* **2011,** *50*, 4068-4093.
383. Rappoport, Z., *The chemistry of phenols*. John Wiley & Sons Ltd: 2003.
384. Astruc, D., *Modern Arene Chemistry: Concepts, Synthesis, and Applications*. Wiley-VCH: Germany, 2002.
385. You, S.-L., *Asymmetric dearomatization reactions*. Wiley-VCH: New Jersey, 2016.
386. Todd, M. A.; Sabat, M.; Myers, W. H.; Harman, W. D., [2+2] Cycloaddition Reactions with a Tungsten-Stabilized 2H-Phenol. *J. Am. Chem. Soc.* **2007,** *129*, 11010-11011.
387. Mehta, G.; Pan, S. C., Total Synthesis of the Novel Antifungal Agent (±)-Jesterone. *Org. Lett.* **2004,** *6*, 811-813.
388. Quideau, S.; Pouysegu, L.; Peixoto, P. A.; Deffieux, D., Phenol Dearomatization with Hypervalent Iodine Reagents. In *Hypervalent Iodine Chemistry*, Wirth, T., Ed. 2016; Vol. 373, pp 25-74.
389. Valery, M. D.; Tatyana, A. G.; Vladimir, V. P., Natural Peroxy Anticancer Agents. *Mini-Rev. Med. Chem.* **2007,** *7*, 571-589.
390. Dembitsky, V. M., Bioactive peroxides as potential therapeutic agents. *Eur. J. Med. Chem.* **2008,** *43*, 223-251.
391. Muraleedharan, K. M.; Avery, M. A., Progress in the development of peroxide-based anti-parasitic agents. *Drug Discovery Today* **2009,** *14*, 793-803.
392. Gandhi, H.; O'Reilly, K.; Gupta, M. K.; Horgan, C.; O'Leary, E. M.; O'Sullivan, T. P., Advances in the synthesis of acyclic peroxides. *RSC Adv.* **2017,** *7*, 19506-19556.

393. Esguerra, K. V. N.; Lumb, J.-P., Selectivity in the Aerobic Dearomatization of Phenols: Total Synthesis of Dehydronornuciferine by Chemo- and Regioselective Oxidation. *Angew. Chem., Int. Ed.* **2018,** *57*, 1514-1518.
394. Quideau, S.; Pouységu, L., Synthetic Uses Of Orthoquinone Monoketals And Their Orthoquinol Variants. A Review. *Org. Prep. Proced. Int.* **1999,** *31*, 617-680.
395. Barradas, S.; Hernández-Torres, G.; Urbano, A.; Carreño, M. C., Total Synthesis of Natural p-Quinol Cochinchinenone. *Org. Lett.* **2012,** *14*, 5952–5955.
396. Park, B. K.; O'Neill, P. M.; Maggs, J. L.; Pirmohamed, M., Safety assessment of peroxide antimalarials: clinical and chemical perspectives. *Br. J. Clin. Pharmacol.* **1998,** *46*, 521-529.
397. Magdziak, D.; Meek, S. J.; Pettus, T. R. R., Cyclohexadienone Ketals and Quinols: Four Building Blocks Potentially Useful for Enantioselective Synthesis. *Chem. Rev.* **2004,** *104*, 1383-1430.
398. Gersmann, H. R.; Bickel, A. F., 543. Autoxidation of hindered phenols in alkaline media. Part I. *J. Chem. Soc.* **1959**, 2711-2716.
399. Adam, W.; Kıç, H.; Saha-Möller, C. R., An Efficient Regioselective and Diastereoselective Synthesis of the Epoxy-quinol Functionality as Building Block for the Manumycin Antibiotics by the Sequence of Photooxygenation, Reduction and Weitz-Scheffer Epoxidation. *Synlett* **2002,** *2002*, 510-512.
400. Zhang, K.; Liu, Y.; Deng, J.; Xie, S.; Zhao, X.; Yang, J.; Han, Z.; Dai, H., Co–Pd/$BiVO_4$: High-performance photocatalysts for the degradation of phenol under visible light irradiation. *Appl. Catal. B Environ.* **2018,** *224*, 350-359.
401. Sahoo, D. P.; Patnaik, S.; Rath, D.; Parida, K. M., Synergistic effects of plasmon induced Ag@Ag_3VO_4/ZnCr LDH ternary heterostructures towards visible light responsive O_2 evolution and phenol oxidation reactions. *Inorg. Chem. Front.* **2018,** *5*, 879-896.
402. Singh, F. V.; Kole, P. B.; Mangaonkar, S. R.; Shetgaonkar, S. E., Synthesis of spirocyclic scaffolds using hypervalent iodine reagents. *Beilstein J. Org. Chem.* **2018,** *14*, 1778-1805.
403. Harned, A. M., Concerning the mechanism of iodine(III)-mediated oxidative dearomatization of phenols. *Org. Biomol. Chem.* **2018,** *16*, 2324-2329.
404. Sels, B. F.; De Vos, D. E.; Jacobs, P. A., Bromide-Assisted Oxidation of Substituted Phenols with Hydrogen Peroxide to the Corresponding p-Quinol and p-Quinol Ethers over WO_4^{2-}-Exchanged Layered Double Hydroxides. *Angew. Chem. Int. Ed Engl* **2005,** *44*, 310-313.
405. Ramya, P. V. S.; Angapelly, S.; Babu, B. N.; Digwal, C. S.; Nagarsenkar, A.; Gannoju, S.; Prasanth, B.; Arifuddin, M.; Kanneboina, K.; Rangan, K.; Kamal, A., Metal-Free C−C Bond Cleavage: One-Pot Access to 1,4-Benzoquinone-linked N-Formyl Amides/Sulfonamides/Carbamates using Oxone. *Asian J. Org. Chem.* **2017,** *6*, 1008-1013.
406. Uyanik, M.; Mutsuga, T.; Ishihara, K., IBS-Catalyzed Regioselective Oxidation of Phenols to 1,2-Quinones with Oxone®. *Molecules* **2012,** *17*, 8604-8616.

407. Murahashi, S.-I.; Miyaguchi, N.; Noda, S.; Naota, T.; Fujii, A.; Inubushi, Y.; Komiya, N., Ruthenium-Catalyzed Oxidative Dearomatization of Phenols to 4-(tert-Butylperoxy)cyclohexadienones: Synthesis of 2-Substituted Quinones from p-Substituted Phenols. *Eur. J. Org. Chem.* **2011,** *2011*, 5355-5365.

408. Ratnikov, M. O.; Farkas, L. E.; McLaughlin, E. C.; Chiou, G.; Choi, H.; El-Khalafy, S. H.; Doyle, M. P., Dirhodium-Catalyzed Phenol and Aniline Oxidations with T-HYDRO. Substrate Scope and Mechanism of Oxidation. *J. Org. Chem.* **2011,** *76*, 2585-2593.

409. Masao, S.; Hideo, O.; Takashi, H.; Yoshihito, W.; Katsuomi, T., The Oxidation of p-Substituted Phenols Using a t-Butyl Hydroperoxide–Heteropolyacid System. *Bull. Chem. Soc. Jpn.* **1991,** *64*, 2583-2584.

410. Matsuura, T.; Watanabe, K.; Nishinaga, A., Autoxidation of 4-alkyl-2,6-di-t-butylphenols with di-(3-salicylideneaminopropyl)aminecobalt(II) catalyst. *J. Chem. Soc. D* **1970**, 163-164.

411.Chan, H. W. S., Oxygenation reactions of diperoxychromium(VI) oxide etherate (CrO_5–OEt_2). Possible role of singlet oxygen in the isolation of 1,2,3,4-tetraphenyl-5,6-dioxabicyclo[2,2,1]hept-2-en-7-one (tetracyclone endoperoxide). *J. Chem. Soc. D* **1970**, 1550-1551.

412. Peters, J. W.; Pitts, J. N.; Rosenthal, I.; Fuhr, H., New and unique chemical source of singlet molecular oxygen. Potassium perchromate. *J. Am. Chem. Soc.* **1972,** *94*, 4348-4350.

413. Barton, D. H. R.; Magnus, P. D.; Quinney, J. C., Experiments on the synthesis of tetracycline. Part XIII. Oxidation of ring A model phenols to p-hydroxycyclohexadienones. *J. Chem. Soc., Perkin Trans. 1* **1975**, 1610-1614.

414. van Laar, F. M. P. R.; De Vos, D. E.; Pierard, F.; Kirsch-De Mesmaeker, A.; Fiermans, L.; Jacobs, P. A., Generation of Singlet Molecular Oxygen from H_2O_2 with Molybdate-Exchanged Layered Double Hydroxides: Effects of Catalyst Composition and Reaction Conditions. *J. Catal.* **2001,** *197*, 139-150.

415. Shao, L.; Hu, X. P., Copper-catalyzed intermolecular asymmetric propargylic dearomatization of phenol derivatives. *Chemical communications* **2017,** *53*, 8192-8195.

416. Dong, S.; Zhu, J.; Porco, J. A., Enantioselective Synthesis of Bicyclo[2.2.2]octenones Using a Copper-Mediated Oxidative Dearomatization/[4 + 2] Dimerization Cascade. *Journal of the American Chemical Society* **2008,** *130*, 2738-2739.

417. Dong, S.; Hamel, E.; Bai, R.; Covell, D. G.; Beutler, J. A.; Porco Jr., J. A., Enantioselective Synthesis of (+)-Chamaecypanone C: A Novel Microtubule Inhibitor. *Angew. Chem., Int. Ed.* **2009,** *48*, 1494-1497.

418. Yilleng, M. T.; Rooney, D.; Manyar, H.; Gimba, E.; Ndukwe, G. In *Enhancing phenol photo-oxidation with palladium core-shell in TiO_2 on Taylor flow system*, American Chemical Society: 2017; p 491.

419. Zhou, S. W.; Xu, R.; He, J. Z.; Huang, Y. C.; Cai, Z. J.; Xu, M. G.; Song, Z. G., Preparation of Fe-Cu-kaolinite for catalytic wet peroxide oxidation of 4-chlorophenol. *Environ. Sci. Pollut. Res.* **2018,** *25*, 4924-4933.
420. He, D.; Zhang, H.; Yan, Y., Preparation of Cu-ZSM-5 catalysts by chemical vapour deposition for catalytic wet peroxide oxidation of phenol in a fixed bed reactor. *R. Soc. Open Sci.* **2018,** *5*, 172364-172378.
421. Shen, D.; Chen, Q. L.; Yan, P. P.; Zeng, X. F.; Zhong, G. F., Enantioselective Dearomatization of Naphthol Derivatives with Allylic Alcohols by Cooperative Iridium and Bronsted Acid Catalysis. *Angew. Chem., Int. Ed.* **2017,** *56*, 3242-3246.
422. Wu, Q.-F.; Liu, W.-B.; Zhuo, C.-X.; Rong, Z.-Q.; Ye, K.-Y.; You, S.-L., Iridium-Catalyzed Intramolecular Asymmetric Allylic Dearomatization of Phenols. *Angew. Chem., Int. Ed.* **2011,** *50*, 4455-4458.
423. Xu, R. Q.; Gu, Q.; You, S. L., Construction of the Benzomesembrine Skeleton: Palladium(0)-Catalyzed Intermolecular Arylative Dearomatization of alpha-Naphthols and Subsequent Aza-Michael Reaction. *Angew. Chem., Int. Ed.* **2017,** *56*, 7252-7256.
424. Zhang, Y.; Liao, Y. T.; Liu, X. H.; Xu, X.; Lin, L. L.; Feng, X. M., Catalytic asymmetric hydroxylative dearomatization of 2-naphthols: synthesis of lacinilene derivatives. *Chem. Sci.* **2017,** *8*, 6645-6649.
425. Hussain, H.; Green, I. R.; Ahmed, I., Journey Describing Applications of Oxone in Synthetic Chemistry. *Chem. Rev.* **2013,** *113*, 3329-3371.
426. Matsuura, T.; Nishinaga, A.; Matsuo, K.; Omura, K.; Oishi, Y., Photo-induced reactions. VIII. Photosensitized ozidation of 3,5-dihalophloretic acids. *J. Org. Chem.* **1967,** *32*, 3457-3461.
427. Saito, I.; Chujo, Y.; Shimazu, H.; Yamane, M.; Matsuura, T.; Cahnmann, H. J., Photoinduced reactions. LXXXVII. Nonenzymic oxidation of p-hydroxyphenylpyruvic acid with singlet oxygen to homogentisic acid. Model for the action of p-hydroxyphenylpyruvate hydroxylase. *J. Am. Chem. Soc.* **1975,** *97*, 5272-5277.
428. Carreno, M. C.; Gonzalez-Lopez, M.; Urbano, A., Oxidative de-aromatization of para-alkyl phenols into para-peroxyquinols and para-quinols mediated by oxone as a source of singlet oxygen. *Angew. Chem., Int. Ed. Engl.* **2006,** *45*, 2737-2741.
429. Ball, D. L.; Edwards, J. O., The Kinetics and Mechanism of the Decomposition of Caro's Acid. I. *J. Am. Chem. Soc.* **1956,** *78*, 1125-1129.
430. Barradas, S.; Carreño, M. C.; González-López, M.; Latorre, A.; Urbano, A., Direct Stereocontrolled Synthesis of Polyoxygenated Hydrobenzofurans and Hydrobenzopyrans from p-Peroxy Quinols. *Org. Lett.* **2007,** *9*, 5019-5022.
431. Teruo, M.; Kanji, O.; Ruka, N., Photo-induced Reaction. II. The Photo-sensitized Oxidation of Hindered Phenols. *Bull. Chem. Soc. Jpn.* **1965,** *38*, 1358-1362.
432. Zwicker, E. F.; Grossweiner, L. I., Transient Measurements Of Photochemical Processes In Dyes. Ii. The Mechanism Of The Photosensitized Oxidation Of Aqueous Phenol By Eosin1. *J. Phys. Chem.* **1963,** *67*, 549-555.

433. Land, E. J.; Porter, G., Primary photochemical processes in aromatic molecules. Part 7.—Spectra and kinetics of some phenoxyl derivatives. *Trans. Faraday Soc.* **1963,** *59*, 2016-2026.

434. Sedee, A. G. J.; van Henegouwen, G. M. J. B., A synthesis for p-quinol compounds from phenols fused with other saturated rings. *Tetrahedron Lett.* **1983,** *24*, 5779-5780.

435. Tong, G.; Liu, Z.; Li, P., Stereocontrolled Construction of the Tricyclic Framework of Tiglianes and Daphnanes by an Oxidative Dearomatization Approach. *Org. Lett.* **2014,** *16*, 2288-2291.

436. Cabrera-Afonso, M. J.; Lucena, S. R.; Juarranz, Á.; Urbano, A.; Carreño, M. C., Selective Oxidative Dearomatization of Angular Tetracyclic Phenols by Controlled Irradiation under Air: Synthesis of an Angucyclinone-Type Double Peroxide with Anticancer Properties. *Org. Lett.* **2018,** *20*, 6094-6098.

437. Endo, K.; Seya, K.; Hikino, H., Biogenesis-like transformation of salidroside to rengyol and its related cyclohexyletanoids of forsythia suspensa. *Tetrahedron* **1989,** *45*, 3673-3682.

438. Wirth, T., *Hypervalent Iodine Chemistry: Modern Developments in Organic Synthesis*. Springer-Verlag Berlin Heidelberg: Germany, 2003.

439. Zhdankin, V. V., *Hypervalent Iodine Chemistry: Preparation, Structure, and Synthetic Applications of Polyvalent Iodine Compounds*. Wiley: New Jersey, 2013.

440. Wu, W. T.; Zhang, L. M.; You, S. L., Catalytic asymmetric dearomatization (CADA) reactions of phenol and aniline derivatives. *Chem. Soc. Rev.* **2016,** *45*, 1570-1580.

441. Siegel, A.; Antony, F., About the oxidation of phenols with iodosoacetates. *Monatshefte fur Chemie* **1955,** *86*, 292-300.

442. White, J. D.; Chong, W. K. M.; Thirring, K., Phenolic oxidative coupling with hypervalent iodine. A synthesis of 6a-epipretazettine. *J. Org. Chem.* **1983,** *48*, 2300-2302.

443. Schwartz, M. A.; Pham Phuong Thi, K., Oxidative coupling of cis-3,N-bis(methoxycarbonyl)-N-norreticuline. An approach to the asymmetric synthesis of morphine alkaloids. *J. Org. Chem.* **1988,** *53*, 2318-2322.

444. Tamura, Y.; Yakura, T.; Haruta, J.; Kita, Y., Hypervalent iodine oxidation of p-alkoxyphenols and related compounds: a general route to p-benzoquinone monoacetals and spiro lactones. *J. Org. Chem.* **1987,** *52*, 3927-3930.

445. Lewis, N.; Wallbank, P., Formation of Quinol Ethers using (Diacetoxyiodo)benzene. *Synthesis* **1987,** *1987*, 1103-1106.

446. Quideau, S.; Pouységu, L.; Ozanne, A.; Gagnepain, J., Oxidative Dearomatization of Phenols and Anilines via λ^3- and λ^5-Iodane-Mediated Phenylation and Oxygenation. *Molecules* **2005,** *10*, 201-216.

447. Pelter, A.; Elgendy, S. M. A., Phenolic oxidations with phenyliodonium diacetate. *J. Chem. Soc., Perkin Trans. 1* **1993**, 1891-1896.

448. Pouységu, L.; Deffieux, D.; Quideau, S., Hypervalent iodine-mediated phenol dearomatization in natural product synthesis. *Tetrahedron* **2010,** *66*, 2235-2261.
449. Kita, Y.; Tohma, H.; Hatanaka, K.; Takada, T.; Fujita, S.; Mitoh, S.; Sakurai, H.; Oka, S., Hypervalent Iodine-Induced Nucleophilic Substitution of para-Substituted Phenol Ethers. Generation of Cation Radicals as Reactive Intermediates. *J. Am. Chem. Soc.* **1994,** *116*, 3684-3691.
450. Dohi, T.; Maruyama, A.; Takenaga, N.; Senami, K.; Minamitsuji, Y.; Fujioka, H.; Caemmerer, S. B.; Kita, Y., A Chiral Hypervalent Iodine(III) Reagent for Enantioselective Dearomatization of Phenols. *Angew. Chem., Int. Ed.* **2008,** *47*, 3787-3790.
451. Pouységu, L.; Chassaing, S.; Dejugnac, D.; Lamidey, A.-M.; Miqueu, K.; Sotiropoulos, J.-M.; Quideau, S., Highly Diastereoselective Synthesis of Orthoquinone Monoketals through λ^3-Iodane-Mediated Oxidative Dearomatization of Phenols. *Angew. Chem., Int. Ed.* **2008,** *47*, 3552-3555.
452. Pouységu, L.; Sylla, T.; Garnier, T.; Rojas, L. B.; Charris, J.; Deffieux, D.; Quideau, S., Hypervalent iodine-mediated oxygenative phenol dearomatization reactions. *Tetrahedron* **2010,** *66*, 5908-5917.
453. Kita, Y.; Tohma, H.; Kikuchi, K.; Inagaki, M.; Yakura, T., Hypervalent iodine oxidation of N-acyltyramines: synthesis of quinol ethers, spirohexadienones, and hexahydroindol-6-ones. *J. Org. Chem.* **1991,** *56*, 435-438.
454. Hamamoto, H.; Anilkumar, G.; Tohma, H.; Kita, Y., A Novel and Useful Oxidative Intramolecular Coupling Reaction of Phenol Ether Derivatives on Treatment with a Combination of Hypervalent Iodine(III) Reagent and Heteropoly Acid. *Chem. Eur. J.* **2002,** *8*, 5377-5383.
455. Jean, A.; Cantat, J.; Bérard, D.; Bouchu, D.; Canesi, S., Novel Method of Aromatic Coupling between N-Aryl Methanesulfonamide and Thiophene Derivatives. *Org. Lett.* **2007,** *9*, 2553-2556.
456. Guérard, K. C.; Sabot, C.; Beaulieu, M.-A.; Giroux, M.-A.; Canesi, S., 'Aromatic ring umpolung', a rapid access to the main core of several natural products. *Tetrahedron* **2010,** *66*, 5893-5901.
457. Deffieux, D.; Fabre, I.; Titz, A.; Léger, J.-M.; Quideau, S., Electrochemical Synthesis of Dimerizing and Nondimerizing Orthoquinone Monoketals. *J. Org. Chem.* **2004,** *69*, 8731-8738.
458. Lai, C.-H.; Shen, Y.-L.; Wang, M.-N.; Kameswara Rao, N. S.; Liao, C.-C., Intermolecular Diels−Alder Reactions of Brominated Masked o-Benzoquinones with Electron-Deficient Dienophiles. A Detour Method to Synthesize Bicyclo[2.2.2]octenones from 2-Methoxyphenols. *J. Org. Chem.* **2002,** *67*, 6493-6502.
459. St. Amant, A. H.; Frazier, C. P.; Newmeyer, B.; Fruehauf, K. R.; Read de Alaniz, J., Direct synthesis of anilines and nitrosobenzenes from phenols. *Org. Biomol. Chem.* **2016,** *14*, 5520-5524.

460. Peter, A. L. J.; Viraraghavan, T., Thallium: a review of public health and environmental concerns. *Environ. Int.* **2005,** *31*, 493-501.
461. Yakura, T.; Omoto, M.; Yamauchi, Y.; Tian, Y.; Ozono, A., Hypervalent iodine oxidation of phenol derivatives using a catalytic amount of 4-iodophenoxyacetic acid and Oxone® as a co-oxidant. *Tetrahedron* **2010,** *66*, 5833-5840.
462. Wang, D.-S.; Chen, Q.-A.; Lu, S.-M.; Zhou, Y.-G., Asymmetric Hydrogenation of Heteroarenes and Arenes. *Chem. Rev* **2012,** *112*, 2557-2590.
463. Volp, K. A.; Harned, A. M., Chiral aryl iodide catalysts for the enantioselective synthesis of para-quinols. *Chem. Commun.* **2013,** *49*, 3001-3003.
464. Fujita, M., Enantioselective Heterocycle Formation Using Chiral Hypervalent Iodine(III). *Heterocycles* **2018,** *96*, 563-594.
465. Claraz, A.; Masson, G., Asymmetric iodine catalysis-mediated enantioselective oxidative transformations. *Org. Biomol. Chem.* **2018,** *16*, 5386-5402.
466. Platzer, N. A. J., *Addition and Condensation Polymerization Processes*. Am. Chem. Soc.: 1969; Vol. 91, p 796.
467. Ding, Q. P.; Ye, Y.; Fan, R. H., Recent Advances in Phenol Dearomatization and Its Application in Complex Syntheses. *Synthesis-Stuttgart* **2013,** *45*, 1-16.
468. Gagnepain, J.; Castet, F.; Quideau, S., Total Synthesis of (+)-Aquaticol by Biomimetic Phenol Dearomatization: Double Diastereofacial Differentiation in the Diels–Alder Dimerization of Orthoquinols with a C2-Symmetric Transition State. *Angew. Chem., Int. Ed.* **2007,** *46*, 1533-1535.
469. Breuning, M.; Corey, E. J., Catalytic Enantioselective Diels−Alder Reactions of 1,4-Quinone Monoketals. *Org. Lett.*
2001, *3*, 1559-1562.
470. Eske, A.; Ecker, S.; Fendinger, C.; Goldfuss, B.; Jonen, M.; Lefarth, J.; Neudörfl, J.-M.; Spilles, M.; Griesbeck, A. G., Spirofused and Annulated 1,2,4-Trioxepane-, 1,2,4-Trioxocane-, and 1,2,4-Trioxonane-Cyclohexadienones: Cyclic Peroxides with Unusual Ring Conformation Dynamics. *Angew. Chem., Int. Ed.* **2018,** *57*, 13770-13774.
471. Sun, W.; Li, G.; Hong, L.; Wang, R., Asymmetric dearomatization of phenols. *Org. Biomol. Chem.* **2016,** *14*, 2164-2176.
472. Scheffler, G.; Seike, H.; Sorensen, E. J., An Enantiospecific Synthesis of the Potent Immunosuppressant FR901483. *Angew. Chem., Int. Ed.* **2000,** *39*, 4593-4596.
473. Imbos, R.; Minnaard, A. J.; Feringa, B. L., A Highly Enantioselective Intramolecular Heck Reaction with a Monodentate Ligand. *J. Am. Chem. Soc.* **2002,** *124*, 184-185.
474. Hayashi, Y.; Gotoh, H.; Tamura, T.; Yamaguchi, H.; Masui, R.; Shoji, M., Cysteine-Derived Organocatalyst in a Highly Enantioselective Intramolecular Michael Reaction. *J. Am. Chem. Soc.* **2005,** *127*, 16028-16029.
475. Liu, Q.; Rovis, T., Asymmetric Synthesis of Hydrobenzofuranones via Desymmetrization of Cyclohexadienones Using the Intramolecular Stetter Reaction. *J. Am. Chem. Soc.* **2006,** *128*, 2552-2553.

476. Jefford, C. W.; Jaggi, D.; Boukouvalas, J.; Kohmoto, S., Reaction of bicyclic endo peroxides with carbonyl compounds. A new approach to 1,2,4-trioxanes. *J. Am. Chem. Soc.* **1983,** *105*, 6497-6498.
477. Organization, W. H. *World Malria Report*; Geneva, Switzerland, 2018.
478. Haynes, R. K.; Vonwiller, S. C., From Qinghao, Marvelous Herb of Antiquity, to the Antimalarial Trioxane Qinghaosuand Some Remarkable New Chemistry. *Acc. Chem. Res.* **1997,** *30*, 73-79.
479. Westfall, P. J.; Pitera, D. J.; Lenihan, J. R.; Eng, D.; Woolard, F. X.; Regentin, R.; Horning, T.; Tsuruta, H.; Melis, D. J.; Owens, A.; Fickes, S.; Diola, D.; Benjamin, K. R.; Keasling, J. D.; Leavell, M. D.; McPhee, D. J.; Renninger, N. S.; Newman, J. D.; Paddon, C. J., Production of amorphadiene in yeast, and its conversion to dihydroartemisinic acid, precursor to the antimalarial agent artemisinin. *Proc. Natl. Acad. Sci.* **2012,** *109*, E111-E118.
480. Kyle, D. E.; Teja-Isavadharm, P.; Li, Q.; Leo, K., Pharmacokinetics and pharmacodynamics of qinghaosu derivatives: how do they impact on the choice of drug and the dosage regimens? *Med Trop (Mars)* **1998,** *58*, 38-44.
481. Rudrapal, M.; Chetia, D., Endoperoxide antimalarials: development, structural diversity and pharmacodynamic aspects with reference to 1,2,4-trioxane-based structural scaffold. *Drug Des., Dev. Ther.* **2016,** *2016:10*, 3575-3590.
482. García-García, C.; Redondo, M. C.; Ribagorda, M.; Carreño, M. C., Reactions of p-Quinols with Aldehydes and Imines: Stereoselective Access to Polyheterobicyclic and Tricyclic Systems. *Eur. J. Org. Chem.* **2014,** *2014*, 7377-7388.
483. Rubush, D. M.; Morges, M. A.; Rose, B. J.; Thamm, D. H.; Rovis, T., An asymmetric synthesis of 1,2,4-trioxane anticancer agents via desymmetrization of peroxyquinols through a Bronsted acid catalysis cascade. *J. Am. Chem. Soc.* **2012,** *134*, 13554-13557.
484. Nagae, H.; Shibata, Y.; Tsurugi, H.; Mashima, K., Aminomethylation Reaction of ortho-Pyridyl C–H Bonds Catalyzed by Group 3 Metal Triamido Complexes. *J. Am. Chem. Soc.* **2015,** *137*, 640-643.
485. Eberson, L.; Hartshorn, M. P.; Persson, O., 1,1,1,3,3,3-Hexafluoropropan-2-ol as a solvent for the generation of highly persistent radical cations. *J. Chem. Soc., Perkin Trans. 2* **1995**, 1735-1744.
486. Vo, N. T.; Pace, R. D. M.; O'Har, F.; Gaunt, M. J., An Enantioselective Organocatalytic Oxidative Dearomatization Strategy. *J. Am. Chem. Soc.* **2008,** *130*, 404-405.
487. Tsai, C.-Y.; Chen, L.-A.; Sung, K., $TiCl_4$-catalyzed synthesis of peroxyacetals from aldehydes. *Can. J. Chem.* **2012,** *90*, 321-325.
488. Endo, K.; Seya, K.; Hikino, H., Biogenesis-like Transformation of Salidroside to Rengyol and its Related Cyclohexyletanoids of Forsythia Suspensa. *Tetrahedron* **1989,** *45*, 3673-3682.

Appendix

Standard Operation Procedure for Batch cell Reaction in CO_2

Below are the procedures used to perform photo-oxidation batch reactions in CO_2 and CO_2-based solvent mixture. The start-up procedure, shutdown procedure and rest conditions are included. More details about the components are described in Section 2.1.3.

After checking O_2 cylinder pressure

(Should be high enough for the desired reaction condition):

- Start-up procedure:

1. Use the Excel spreadsheet file in the Appendix to calculate the required pump flow rates, Rheodyne switching time and sample loop sizes for the reaction to be performed.
2. Ensure that all valves, except valve V5, are closed; set the BPR to the required pressure (e.g. 140 bar).
3. Check that the CO_2 pump is flowing correctly and can pressurise against a closed valve V5 (i.e. check that the valves are working correctly).
4. Ensure that the CO_2 pump (4272) shows adequate bottle pressure (i.e. > 45 bar), then open V1 and allow the CO_2 pump (at 2 ml/min) to fill the system to the desired pressure. The reading on the system pressure monitor (5358) should increase.
5. Flush the system with CO_2 for no less than 30 minutes at this pressure.

6. Ensure that all thermocouples are correctly attached, that all pressure transducers are calibrated and working, and that the pressure and temperature trips are working and set correctly (including pumps).

7. Attach the correct sample loops to the Rheodyne dosing unit (5700).

8. Start the Picologger recording on the PC.

9. Set the trip of system pressure (5358) and oxygen pressure (5091).

10. Increase the BPR (4272) setting to hold the desired reaction pressure.

11. After 30 minutes, set the CO_2 pump (4385) to the desired flow rate for the reaction.

12. Set the mixer heater A (2714).

13. Allow the system time to reach the desired temperature.

14. Set the correct switching time on the Rheodyne dosing unit (5224) (switching time should be around 4-14 seconds, which can be reached using an appropriate sample loop).

15. Start the Rheodyne dosing unit (5224), and open valve V3 to allow oxygen to enter the system.

16. While the system is flushing with CO_2, remove the thermocouple and load materials *via* injection to be photo-oxidised, including photosensitiser and any co-solvent into the batch cell using an appropriately sized Hamilton Syringe.

17. Replace the thermocouple and reseal the batch cell.

18. Allow the system to equilibrate with CO_2/O_2 mixture for 30 minutes fully. Then it is possible to charge the photochemical batch cell slowly with CO_2/O_2 mixture. Ensure that V7 and V8 are closed and partially open V6. Carefully open V7 such that the CO_2/O_2 mixture flow into the batch cell at a rate of approximately 3-5 psi/s. Once the desired pressure is reached, V6 and V7 are closed, and leaving for about 10 minutes to ensure that the batch cell system pressure is stable, without leakage, by observing the stability of the internal cell pressure and testing with Snoop liquid leak detector.

19. The rig is now under starting conditions. Switch on the chosen light source. The O_2 dosage unit can be switched off, V3 and V4 should be closed, and the CO_2

flow should be maintained for *ca*. 30 minutes to flush O_2 from the system. Ensure V6 and V7 are closed, and the batch cell now can be disconnected between V6 and V7 from the rest of the system for further analysis.

- **Shutdown procedure:**

1. Switch off the light source.
2. Ensure Rheodyne dosing unit (5224), valve V3, V4 and O_2 cylinder are closed.
3. After 10 minutes, turn off mixer heater A (2714).
4. Allow the system to flush with CO_2 for *ca*. 30 minutes.
5. Close valve V1 and stop the CO_2 pump (4385).
6. Release the pressure slowly by reducing the set pressure at the BPR (4272) to atmospheric pressure in 20 bar increments, allowing approximately 10 seconds in each setting number.
7. Depressurise the cell carefully by slowly opening V8 and venting the contents into a container for further analysis (such as for analysis by NMR).
8. The cell should then be flushed with a non-halogenated solvent (e.g. 2-propanol) for approximately 30 minutes (at 1 mL/min) by connecting it to an extra HPLC pump (5822). After this procedure, the cell is connected between the CO_2 pump and BPR, and flushed with CO_2 at pressure (e.g. 140 bar) for approximately 1 hour to ensure that no potentially flammable solvent remains before the next oxidation experiment to perform.
9. Ensure that the system pressure has reached atmospheric pressure before leaving the rig unattended.

Rest Conditions

When not in use the rig was left in a rest state, as described below:

- All the pumps are stopped.
- All heating and cooling are ceased.

- All light sources are turned off.
- Valves V1, V3, V4, V6, V7 and V8 are closed, valves V2 and V5 are open.
- The Rheodyne dosing unit (5224) are turned off.
- All other units left on, particularly the BPR (4272), CO_2 pump (4385) and system pressure (5358)/temperature monitors (2717).

Standard Operating Procedure for Flow photo-oxidation

Below is the procedure used to perform photo-oxidation reactions in CO_2 and CO_2-based solvent mixture. The start-up procedure and shutdown procedure are included. More details about the components are described in Section 2.1.

After checking O_2 cylinder pressure

(Should be high enough for the desired reaction condition):

- **Start-up procedure:**

1. Use the Excel spreadsheet file in the Appendix to calculate the required pump flow rates, Rheodyne switching time and sample loop sizes for the reaction to be performed.
2. Ensure that all thermocouples are correctly attached, that all pressure transducers are calibrated and working, and that the pressure and temperature trips are working and set correctly (including pumps).
3. Attach the correct sample loops to the Rheodyne dosing unit (4710).
4. Start the Picologger recording on the PC.
5. Set the trip of system pressure (2720) and oxygen pressure (4281).
6. Set the BPR (3835) to hold 60 bar.
7. Set the CO_2 pump (3832) to 5 ml/min.
8. Open valve V1 to allow CO_2 to enter the system. The reading on the system pressure monitor (2720) should increase.
9. Start the CO_2 pump (3832).

10. Increase the BPR (3835) setting to hold at the desired reaction pressure, typically at 120 bar.

11. Allow the system time to reach the required pressure.

12. Set the CO_2 pump (3832) to the desired flow rate for the reaction.

13. Allow the system time to settle.

14. Set the mixer heaters (2714) and (3669), and two cooling bath to the desired temperatures.

15. Allow the system to reach the setting temperatures.

16. Set the correct switching time on the Rheodyne dosing unit (4710) (switching time should be around 4-14 seconds, which can be reached by using an appropriate sample loop).

17. Start the Rheodyne dosing unit (4710), and open valve V2 and V3 to allow oxygen to enter the system.

18. Allow the system to equilibrate.

19. Make a solution of any reagents and co-solvents and use it to prime HPLC pump 1 (5587).

20. Start the chosen light source.

21. Set HPLC pump (5587) to the required flow rate.

22. Start HPLC pump (5587) then soon afterwards open valve V4 to allow organic material to enter the rig.

23. Allow the system to equilibrate.

24. The rig is now under starting conditions.

Shutdown procedure:

1. Switch off the light source.
2. Close valve V4 then stop HPLC pump (5587).
3. Close valve V2 and V3 then turn off the Rheodyne dosing unit (4710).
4. After 10 minutes, turn off mixer heaters (2714) and (3669), and cooling bath.

5. Allow the system to flush with CO_2 and cool the temperature to room temperature.

6. Close valve V1 and stop the CO_2 pump (3832).

7. Release the pressure slowly by reducing the set pressure at the BPR (3835) to atmospheric pressure in 20 bar increments, allowing approximately 10 seconds in each setting pressure.

Emergency shutdown procedure

In the event of an emergency where the system is not automatically tripped, the following procedure should be followed:

1. Hit the red emergency stop button located on the trip box (3667). This will turn off the heaters (2714) and (3669), the substrate pump (5587) and the Rheodyne dosing unit (4710).

2. Close valves V3 and V4. The CO_2 (3832)) will stay on to aid with flushing and cooling the system. These pumps will trip independently if the pressure exceeds their set values.

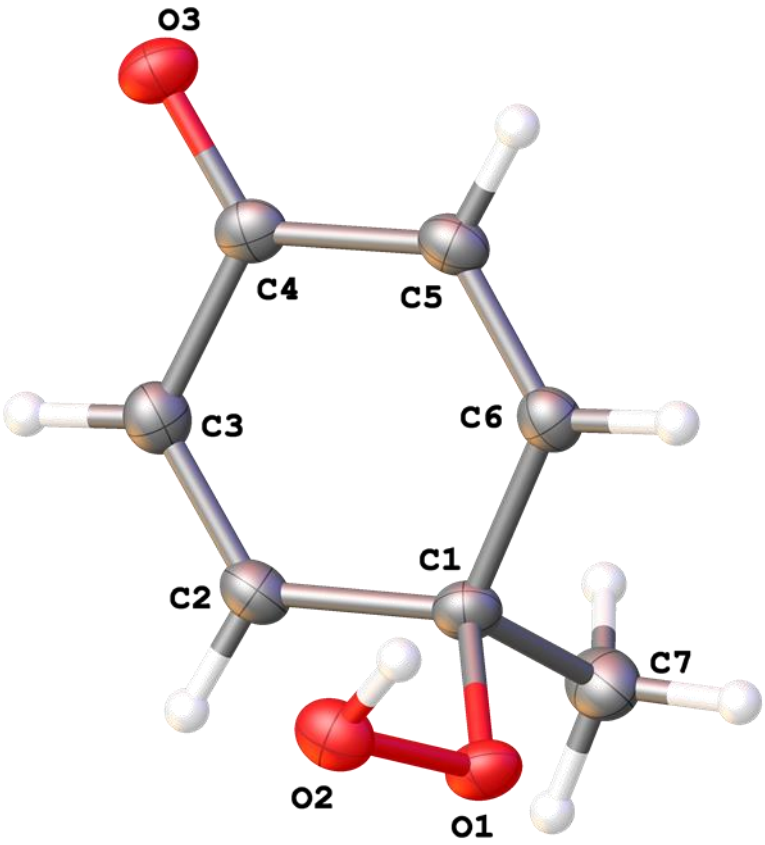
3. The system must be allowed to cool for as long as is necessary. Do not remove the blast shield or attempt to release the pressure before the temperature readings are both below 40 °C.

4. Release the pressure slowly by reducing the set pressure at the BPR (3835) in 20 bar increments, allowing approximately 10 seconds in each setting pressure.

5. If a blockage has occurred, sections of the rig may still be under pressure. Undo any connections very carefully and with the fume hood sash as low as is practical.

6. When the pressure and temperature hazards have been dealt with, press the square reset button on the side of the trip box (3667) to allow full power back to the rig.

Crystal Data



Experimental

Single crystals of $C_7H_8O_3$ [**2a**] were slow evaporation from ethyl acetate. A suitable crystal was selected and in a fomblin on a micromount on a XtalLAB PRO MM007, PILATUS3 R 200K diffractometer. The crystal was kept at 120(2) K during data collection. Using Olex2,[i] the structure was solved with the olex2.solve structure solution program using Charge Flipping and refined with the olex2.refine refinement package using Gauss-Newton minimisation.

Crystal data (2a)

Crystal Data for $C_7H_8O_3$ (*M* =140.13 g/mol): monoclinic, space group $P2_1/c$ (no. 14), *a* = 10.1442(5) Å, *b* = 10.4033(5) Å, *c* = 6.3880(3) Å, *β* = 104.154(5)°, *V* = 653.68(6) Å^3, *Z* = 4, *T* = 120(2) K, μ(CuKα) = 0.946 mm^{-1},*Dcalc* = 1.424 g/cm^3, 2408

[i]Dolomanov, O.V., Bourhis, L.J., Gildea, R.J, Howard, J.A.K. & Puschmann, H. (2009), *J. Appl. Cryst.* 42, 339-341.

reflections measured (8.99° ≤ 2Θ ≤ 145.826°), 1257 unique (R_{int} = 0.0217, R_{sigma} = 0.0277) which were used in all calculations. The final R_1 was 0.0376 (I > 2σ(I)) and wR_2 was 0.1053 (all data).

*Table **2a**-1 Crystal data and structure refinement for 2a.*

Empirical formula	$C_7H_8O_3$
Formula weight	140.13
Temperature/K	120(2)
Crystal system	monoclinic
Space group	$P2_1/c$
a/Å	10.1442(5)
b/Å	10.4033(5)
c/Å	6.3880(3)
α/°	90
β/°	104.154(5)
γ/°	90
Volume/Å^3	653.68(6)
Z	4
ρ_{calc}g/cm^3	1.424
μ/mm^{-1}	0.946
F(000)	296.0
Crystal size/mm^3	0.221 × 0.173 × 0.102
Radiation	CuKα (λ = 1.54184)
2Θ range for data collection/°	8.99 to 145.826
Index ranges	-8 ≤ h ≤ 12, -11 ≤ k ≤ 12, -7 ≤ l ≤ 7
Reflections collected	2408
Independent reflections	1257 [R_{int} = 0.0217, R_{sigma} = 0.0277]
Data/restraints/parameters	1257/1/95
Goodness-of-fit on F^2	1.095
Final R indexes [I>=2σ (I)]	R_1 = 0.0376, wR_2 = 0.1021
Final R indexes [all data]	R_1 = 0.0409, wR_2 = 0.1053
Largest diff. peak/hole / e Å^{-3}	0.27/-0.24

*Table **2a**-2 Fractional Atomic Coordinates (×10^4) and Equivalent Isotropic Displacement Parameters (Å^2×10^3) for HBMWGB. U_{eq} is defined as 1/3 of of the trace of the orthogonalised U_{IJ} tensor.*

$Atom$	x	y	z	$U(eq)$
C1	3960.4 (13)	5787.8 (13)	2232(2)	19.8(3)
C2	2768.2 (14)	6475.7 (13)	2601(2)	22.2(3)
C3	1838.9 (13)	5861.5 (13)	3387(2)	20.8(3)
C4	1875.2 (13)	4444.5 (13)	3816(2)	19.9(3)
C5	3154.3 (13)	3810.6 (13)	3560(2)	19.4(3)
C6	4088.2 (13)	4413.3 (13)	2771(2)	20.0(3)
C7	644.8 (14)	3782.8 (14)	2342(2)	26.8(3)
O8	1688.7 (9)	4191.0 (10)	5957.7(15)	22.8(3)
O9	2681.0 (10)	4954.1 (10)	7515.7(16)	25.4 (3)
O10	4842.1 (10)	6361.6 (10)	1564.1(16)	24.6 (3)

*Table **2a**-3 Anisotropic Displacement Parameters ($Å^2×10^3$) for **2a**. The Anisotropic displacement factor exponent takes the form: -2π2[h2a*2U11+2hka*b*U12+…].*

$Atom$	U_{11}	U_{22}	U_{33}	U_{23}	U_{13}	U_{12}
C1	21.4(6)	25.3(7)	12.3(6)	-0.2(5)	3.3(5)	-1.2(5)
C2	26.0(7)	21.6(6)	18.4(6)	1.4(5)	4.2(5)	2.2(5)
C3	20.6(6)	23.3(7)	18.1(6)	-1.2(5)	4.3(5)	4.2(5)
C4	20.8(6)	23.5(7)	16.4(6)	0.6(5)	6.4(5)	-0.1(5)
C5	22.0(6)	20.4(6)	15.7(6)	-0.9(5)	4.2(5)	1.5(5)
C6	19.8(6)	24.6(7)	15.7(6)	-1.8(5)	4.4(5)	2.3(5)
C7	21.9(7)	29.2(7)	28.2(7)	-4.6(6)	4.3(5)	-1.5(6)
O8	22.5(5)	28.7(5)	18.7(5)	0.5(4)	8.0(4)	-3.2(4)
O9	25.3(5)	31.1(5)	18.9(5)	-3.2(4)	3.7(4)	1.7(4)
O10	24.4(5)	30.3(5)	20.1(5)	3.2(4)	7.3(4)	-3.1(4)

*Table **2a**-4 Bond Lengths for **2a**.*

Atom	Atom	Length/Å	Atom	Atom	Length/Å
C1	C2	1.4729(19)	C4	C5	1.4997(18)
C1	C6	1.4691(18)	C4	C7	1.5307(19)
C1	O10	1.2351(16)	C4	O8	1.4506(16)
C2	C3	1.335(2)	C5	C6	1.3333(19)
C3	C4	1.4981(18)	O8	O9	1.4643(14)

Table **2a**-*5 Bond Angles for* ***2a****.*

Atom	Atom	Atom	Angle/˚	Atom	Atom	Atom	Angle/˚
C6	C1	C2	117.67(11)	C5	C4	C7	109.41(11)
O10	C1	C2	120.85(12)	O8	C4	C3	110.37(11)
O10	C1	C6	121.43(12)	O8	C4	C5	109.80(11)
C3	C2	C1	120.71(12)	O8	C4	C7	102.91(10)
C2	C3	C4	123.49(12)	C6	C5	C4	123.23(12)
C3	C4	C5	113.33(11)	C5	C6	C1	121.07(12)
C3	C4	C7	110.51(11)	C4	O8	O9	108.42(9)

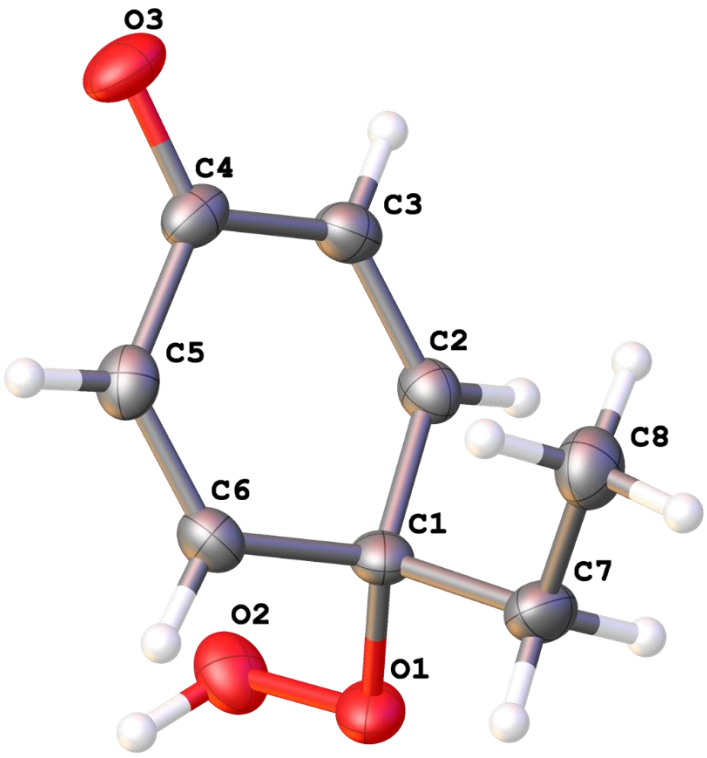
Table ***2a***-*6 Hydrogen Bonds for* ***2a****.*

D	H	A	d(D-H)/Å	d(H-A)/Å	d(D-A)/Å	D-H-A/°
O9	H9	O101	0.848(16)	1.960(16)	2.7946(14)	167(2)

Table ***2a***-*7 Hydrogen Atom Coordinates (Å×104) and Isotropic Displacement Parameters (Å^2×10^3) for* ***2a****.*

Atom	x	y	z	$U(eq)$
H2	2659.53	7366.22	2275.1	27
H3	1115.92	6348.78	3691.89	25
H5	3306.7	2936.53	3980.07	23
H6	4848.56	3946.29	2554.15	24
H7A	656.98	2865.69	2697.35	40
H7B	682.36	3886.36	833.28	40
H7C	-192.73	4172.54	2553.39	40
H9	3362(18)	4454(19)	7810(30)	38

Crystal (2b)



Experimental

Single crystals of $C_8H_{10}O_3$ [**2b**] were Slow evaporation from ethyl acetate. A suitable crystal was selected and in a fomblin film on a micromount on a XtalLAB PRO MM007, PILATUS3 R 200Kdiffractometer. The crystal was kept at 120(2) K during data collection. Using Olex2[i], the structure was solved with the ShelXS[ii] structure solution program using Direct Methods and refined with the ShelXL[iii] refinement package using Least Squares minimisation.

Crystal Data

Crystal Data for $C_8H_{10}O_3$ (M =154.16 g/mol): orthorhombic, space group Pbca (no. 61), a = 7.13195(11) Å, b = 11.8244(2) Å, c = 18.2107(3) Å, V =

[i] Dolomanov, O.V., Bourhis, L.J., Gildea, R.J, Howard, J.A.K. & Puschmann, H. (2009), J. Appl. Cryst. 42, 339-341.

[ii] Sheldrick, G.M. (2008). Acta Cryst. A64, 112-122.

[iii] Sheldrick, G.M. (2015). Acta Cryst. C71, 3-8.

1535.72(5) $Å^3$, Z = 8, T = 120(2) K, μ(CuKα) = 0.853 mm^{-1}, Dcalc = 1.334 g/cm^3, 8253 reflections measured (9.714° ≤ 2Θ ≤ 155.514°), 1614 unique (R_{int} = 0.0269, R_{sigma} = 0.0160) which were used in all calculations. The final R_1 was 0.0381 (I > 2σ(I)) and wR_2 was 0.1031 (all data).

*Table **2b**-1 Crystal data and structure refinement for **2b**.*

Empirical formula	$C_8H_{10}O_3$
Formula weight	154.16
Temperature/K	120(2)
Crystal system	orthorhombic
Space group	Pbca
a/Å	7.13195(11)
b/Å	11.8244(2)
c/Å	18.2107(3)
α/°	90
β/°	90
γ/°	90
Volume/$Å^3$	1535.72(5)
Z	8
$\rho_{calc}g/cm^3$	1.334
μ/mm^{-1}	0.853
F(000)	656.0
Crystal size/mm^3	0.317 × 0.105 × 0.049
Radiation	CuKα (λ = 1.54184)
2Θ range for data collection/°	9.714 to 155.514
Index ranges	-4 ≤ h ≤ 9, -13 ≤ k ≤ 14, -22 ≤ l ≤ 23
Reflections collected	8253
Independent reflections	1614 [R_{int} = 0.0269, R_{sigma} = 0.0160]
Data/restraints/parameters	1614/0/105
Goodness-of-fit on F^2	1.076
Final R indexes [I>=2σ (I)]	R_1 = 0.0381, wR_2 = 0.1021
Final R indexes [all data]	R_1 = 0.0393, wR_2 = 0.1031
Largest diff. peak/hole / e $Å^{-3}$	0.27/-0.18

*Table **2b**-2 Fractional Atomic Coordinates (×10^4) and Equivalent Isotropic Displacement Parameters (Å^2×10^3) for **2b**. U_{eq} is defined as 1/3 of of the trace of the orthogonalised U_{IJ} tensor.*

Atom	*x*	*y*	*z*	U(eq)
O1	588.8(14)	597.3(7)	4032.9(5)	31.1(2)
O3	144.5(14)	-3337.9(8)	2648.6(5)	36.8(3)
O2	-1232.9(15)	660.5(8)	3662.9(6)	35.3(3)
C5	1452.0(17)	-1504.2(10)	2680.7(7)	26.4(3)
C1	1387.8(18)	-496.5(9)	3877.3(7)	23.9(3)
C4	442.7(17)	-2462.3(10)	3000.3(7)	25.7(3)
C6	1851.4(17)	-592.6(10)	3079.1(7)	25.5(3)
C3	-257.1(17)	-2336.0(10)	3752.4(7)	25.8(3)
C2	127.4(17)	-1417.5(10)	4146.4(7)	24.5(3)
C7	3204(2)	-470.2(10)	4342.7(8)	32.6(3)
C8	4323(2)	-1561.2(12)	4310.5(8)	35.1(3)

*Table **2b**-3 Anisotropic Displacement Parameters (Å^2×10^3) for **2a**. The Anisotropic displacement factor exponent takes the form: -2π^2[h^{2}a*^{2}U$_{11}$+2hka*b*U$_{12}$+…].*

Atom	U_{11}	U_{22}	U_{33}	U_{23}	U_{13}	U_{12}
O1	42.7(5)	20.4(4)	30.3(5)	-3.8(3)	-5.7(4)	7.4(4)
O3	40.2(5)	28.2(5)	41.9(6)	-15.2(4)	-9.2(4)	3.4(4)
O2	37.1(5)	33.6(5)	35.1(5)	4.2(4)	-0.4(4)	12.5(4)
C5	25.2(6)	31.3(6)	22.8(6)	-2.3(4)	1.1(5)	6.0(5)
C1	30.5(6)	16.1(5)	25.0(6)	-1.2(4)	-1.0(5)	2.2(4)
C4	23.4(6)	23.5(6)	30.3(6)	-6.1(5)	-6.3(5)	4.7(5)
C6	25.7(6)	23.8(6)	27.0(6)	4.2(5)	2.7(5)	1.2(5)
C3	25.2(6)	22.2(6)	29.9(6)	2.9(5)	-1.1(5)	-1.2(5)
C2	26.9(6)	23.6(6)	23.2(6)	1.3(4)	2.0(5)	3.1(5)
C7	35.9(7)	25.1(6)	36.9(7)	-1.2(5)	-9.4(6)	-3.6(5)
C8	33.8(7)	38.6(7)	33.1(7)	-0.3(6)	-7.3(6)	6.0(6)

*Table **2b**-4 Bond Lengths for **2b**.*

Atom	Atom	Length/Å	Atom	Atom	Length/Å
O1	O2	1.4654(14)	C1	C2	1.4947(17)
O1	C1	1.4415(13)	C1	C7	1.5481(18)
O3	C4	1.2359(15)	C4	C3	1.4654(18)
C5	C4	1.4629(18)	C3	C2	1.3302(17)
C5	C6	1.3302(17)	C7	C8	1.5180(18)
C1	C6	1.4949(17)			

*Table **2b**-5 Bond Angles for **2b**.*

Atom	Atom	Atom	Angle/˚	Atom	Atom	Atom	Angle/˚
C1	O1	O2	107.81(8)	O3	C4	C5	121.82(12)
C6	C5	C4	121.06(11)	O3	C4	C3	120.74(12)
O1	C1	C6	110.29(9)	C5	C4	C3	117.42(10)
O1	C1	C2	110.58(10)	C5	C6	C1	122.99(11)
O1	C1	C7	101.83(9)	C2	C3	C4	121.14(11)
C6	C1	C7	110.41(11)	C3	C2	C1	122.82(11)
C2	C1	C6	113.35(10)	C8	C7	C1	113.68(10)
C2	C1	C7	109.77(10)				

*Table **2b**-6 Hydrogen Atom Coordinates (Å×10^4) and Isotropic Displacement Parameters (Å^2×10^3) for **2b**.*

Atom	x	y	z	U(eq)
H5	1820.19	-1532.98	2191.18	32
H6	2446.09	12.55	2850.75	31
H3	-982.62	-2907.79	3957.88	31
H2A	-411.06	-1345.24	4609.11	29
H7A	3988.85	146.06	4172.14	39
H7B	2875.01	-316.84	4849.81	39
H8A	4610.56	-1737.22	3808.4	53
H8B	3598.7	-2164.47	4520.49	53
H8C	5466.44	-1471.96	4582.38	53
H2	-860(30)	1035(17)	3248(13)	63(6)

Crystal (2c)

Experimental

Single crystals of $C_{10}H_{12}O_3$ [**2c**] were slow evaporation of a methanol solution. A suitable crystal was selected and in a fomblin film on a micromount on a SuperNova, Atlas S2 diffractometer. The crystal was kept at 120(2) K during data collection. Using Olex2[i], the structure was solved with the olex2.solve[ii] structure solution program using Charge Flipping and refined with the ShelXL[iii] refinement package using Least Squares minimisation.

Crystal structure determination of 2c

Crystal Data for $C_8H_{10}O_3$ (M =154.16 g/mol): orthorhombic, space group Pbca (no. 61), a = 7.13195(11) Å, b = 11.8244(2) Å, c = 18.2107(3) Å, V = 1535.72(5) Å^3, Z = 8, T = 120(2) K, μ(CuKα) = 0.853 mm^{-1}, Dcalc = 1.334 g/cm^3,

[i] Dolomanov, O.V., Bourhis, L.J., Gildea, R.J, Howard, J.A.K. & Puschmann, H. (2009), J. Appl. Cryst. 42, 339-341.

[ii] Sheldrick, G.M. (2008). Acta Cryst. A64, 112-122.

[iii] Sheldrick, G.M. (2015). Acta Cryst. C71, 3-8.

8253 reflections measured (9.714° ≤ 2Θ ≤ 155.514°), 1614 unique (R_{int} = 0.0269, R_{sigma} = 0.0160) which were used in all calculations. The final R_1 was 0.0381 (I > 2σ(I)) and wR_2 was 0.1031 (all data).

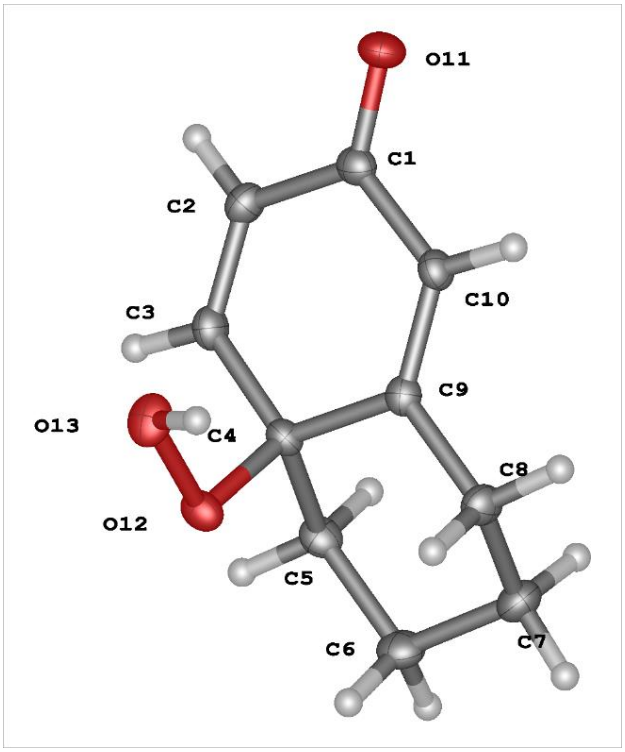


*Table **2c**-1 Crystal data and structure refinement for **2c**.*

Empirical formula	$C_{10}H_{12}O_3$
Formula weight	180.20
Temperature/K	120(2)
Crystal system	monoclinic
Space group	$P2_1/n$
a/Å	8.29297(16)
b/Å	7.41007(12)
c/Å	14.8813(3)
α/°	90
β/°	105.2902(19)
γ/°	90
Volume/Å^3	882.11(3)
Z	4

ρ_{calc}g/cm^3	1.357
μ/mm^{-1}	0.825
F(000)	384.0
Crystal size/mm^3	0.321 × 0.205 × 0.111
Radiation	CuKα (λ = 1.54184)
2Θ range for data collection/°	11.152 to 148.578
Index ranges	-10 ≤ h ≤ 10, -9 ≤ k ≤ 8, -18 ≤ l ≤ 18
Reflections collected	9460
Independent reflections	1783 [R_{int} = 0.0210, R_{sigma} = 0.0138]
Data/restraints/parameters	1783/0/121
Goodness-of-fit on F^2	1.037
Final R indexes [I>=2σ (I)]	R_1 = 0.0329, wR_2 = 0.0865
Final R indexes [all data]	R_1 = 0.0346, wR_2 = 0.0879
Largest diff. peak/hole / e Å^{-3}	0.28/-0.20

*Table **2c**-2 Fractional Atomic Coordinates (×10^4) and Equivalent Isotropic Displacement Parameters (Å^2×10^3) for **2c**. U_{eq} is defined as 1/3 of of the trace of the orthogonalised U_{IJ} tensor.*

Atom	*x*	*y*	*z*	U(eq)
C1	2833.6(13)	4979.1(15)	3496.4(7)	18.7(2)
C2	3899.8(13)	6394.1(14)	3271.0(7)	19.6(2)
C3	5414.3(13)	6011.2(14)	3179.6(7)	18.9(2)
C4	6173.0(12)	4167.7(14)	3343.7(7)	16.3(2)
C5	7865.7(13)	4270.8(15)	4083.5(8)	20.1(2)
C6	8693.3(13)	2426.8(16)	4316.5(8)	23.8(3)
C7	7531.0(14)	1081.3(16)	4601.8(8)	24.5(3)
C8	5862.2(14)	937.7(14)	3847.5(8)	20.6(2)
C9	5080.9(13)	2766.8(14)	3633.9(7)	16.3(2)
C10	3558.3(13)	3181.2(14)	3718.7(7)	18.2(2)
O11	1365.3(10)	5281.2(12)	3491.2(6)	25.7(2)
O12	6616.1(9)	3572.4(11)	2513.5(5)	20.1(2)
O13	5104.8(10)	3631.2(12)	1736.0(5)	24.8(2)
C1	2833.6(13)	4979.1(15)	3496.4(7)	18.7(2)
C2	3899.8(13)	6394.1(14)	3271.0(7)	19.6(2)
C3	5414.3(13)	6011.2(14)	3179.6(7)	18.9(2)

*Table **2c**-3 Anisotropic Displacement Parameters ($Å^2×10^3$) for **2c**. The Anisotropic displacement factor exponent takes the form: $-2π^2[h^2a^{*2}U_{11}+2hka^*b^*U_{12}+…]$.*

Atom	U_{11}	U_{22}	U_{33}	U_{23}	U_{13}	U_{12}
C1	17.7(5)	22.6(5)	15.9(5)	-0.6(4)	4.5(4)	1.4(4)
C2	21.7(5)	16.1(5)	19.9(5)	0.6(4)	3.9(4)	1.5(4)
C3	21.1(5)	17.0(5)	19.0(5)	0.6(4)	6.0(4)	-3.4(4)
C4	15.6(5)	17.7(5)	16.7(5)	-1.2(4)	6.2(4)	-1.2(4)
C5	16.3(5)	23.0(5)	20.6(5)	-2.6(4)	4.0(4)	-3.1(4)
C6	16.6(5)	28.5(6)	24.6(5)	0.2(5)	2.4(4)	2.9(4)
C7	23.5(6)	23.5(6)	25.1(6)	4.3(4)	4.0(5)	5.3(4)
C8	21.1(5)	15.9(5)	24.9(5)	1.0(4)	6.4(4)	0.6(4)
C9	17.7(5)	16.1(5)	14.7(5)	-0.6(4)	3.2(4)	-1.7(4)
C10	17.7(5)	18.9(5)	18.8(5)	1.4(4)	5.9(4)	-2.4(4)
O11	17.8(4)	29.8(4)	31.2(4)	3.4(3)	9.5(3)	5.1(3)
O12	17.6(4)	25.9(4)	17.3(4)	-2.7(3)	5.5(3)	-1.2(3)
O13	27.3(4)	26.2(4)	17.4(4)	-0.9(3)	-0.6(3)	-4.0(3)

*Table **2c**-4 Bond Lengths for **2c**.*

Atom	Atom	Length/Å	Atom	Atom	Length/Å
C1	C2	1.4663(15)	C4	O12	1.4475(12)
C1	C10	1.4631(15)	C5	C6	1.5274(16)
C1	O11	1.2360(13)	C6	C7	1.5230(16)
C2	C3	1.3291(16)	C7	C8	1.5386(15)
C3	C4	1.4969(14)	C8	C9	1.4998(14)
C4	C5	1.5405(14)	C9	C10	1.3373(15)
C4	C9	1.5135(14)	O12	O13	1.4651(10)

*Table **2c**-5 Bond Angles for **2c**.*

Atom	Atom	Atom	Angle/˚	Atom	Atom	Atom	Angle/˚
C10	C1	C2	117.80(9)	O12	C4	C9	109.89(8)
O11	C1	C2	121.43(10)	C6	C5	C4	112.83(9)
O11	C1	C10	120.76(10)	C7	C6	C5	111.68(9)
C3	C2	C1	120.92(10)	C6	C7	C8	110.82(9)
C2	C3	C4	123.10(10)	C9	C8	C7	110.32(9)
C3	C4	C5	109.63(8)	C8	C9	C4	115.01(9)
C3	C4	C9	114.52(9)	C10	C9	C4	121.36(9)
C9	C4	C5	109.34(8)	C10	C9	C8	123.60(10)
O12	C4	C3	109.23(8)	C9	C10	C1	121.97(10)
O12	C4	C5	103.68(8)	C4	O12	O13	107.95(7)

*Table **2c**-6 Torsion Angles for **2c**.*

A	B	C	D	Angle/˚	A	B	C	D	Angle/˚
C1	C2	C3	C4	-3.20(16)	C5	C6	C7	C8	54.94(12)
C2	C1	C10	C9	-6.53(15)	C6	C7	C8	C9	-54.87(12)
C2	C3	C4	C5	-123.93(11)	C7	C8	C9	C4	55.87(12)
C2	C3	C4	C9	-0.62(15)	C7	C8	C9	C10	-121.92(11)
C2	C3	C4	O12	123.10(11)	C8	C9	C10	C1	-179.51(9)
C3	C4	C5	C6	177.92(9)	C9	C4	C5	C6	51.61(11)
C3	C4	C9	C8	-177.02(8)	C9	C4	O12	O13	69.67(10)
C3	C4	C9	C10	0.82(14)	C10	C1	C2	C3	6.67(15)
C3	C4	O12	O13	-56.74(10)	O11	C1	C2	C3	-172.64(10)
C4	C5	C6	C7	-54.20(12)	O11	C1	C10	C9	172.79(10)
C4	C9	C10	C1	2.83(15)	O12	C4	C5	C6	-65.55(11)
C5	C4	C9	C8	-53.56(11)	O12	C4	C9	C8	59.62(11)
C5	C4	C9	C10	124.29(10)	O12	C4	C9	C10	-122.54(10)
C5	C4	O12	O13	-173.55(7)					

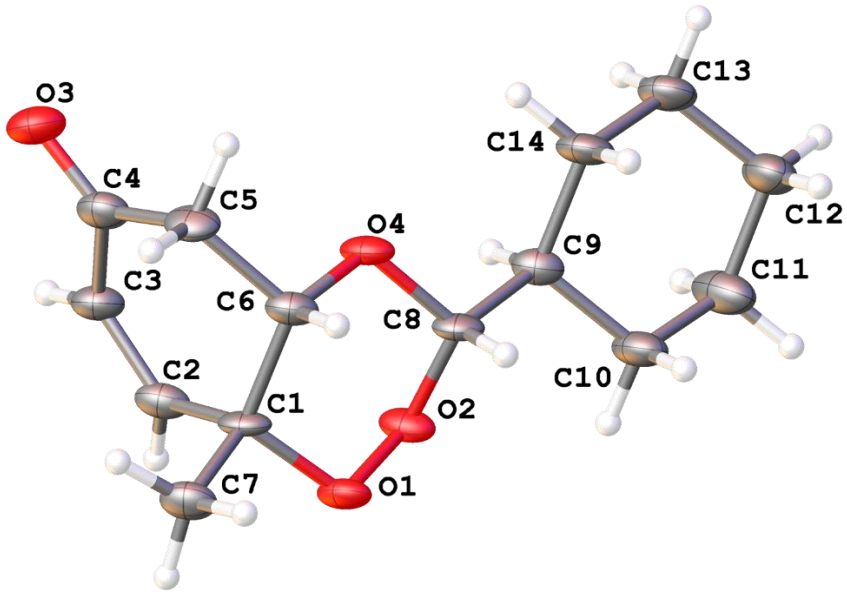
*Table **2c**-7 Hydrogen Bonds for **2c**.*

D	H	A	d(D-H)/Å	d(H-A)/Å	d(D-A)/Å	D-H-A/°
O13	H13	O111	0.883(18)	1.878(18)	2.7470(12)	167.5(16)

*Table **2c**-8 Hydrogen Atom Coordinates (Å×10^4) and Isotropic Displacement Parameters (Å^2×10^3) for **2c**.*

Atom	x	y	z	U(eq)
H2	3502.5	7601.36	3189.24	23
H3	6044.94	6951.94	3001.79	23
H5A	8625.63	5071.82	3853.66	24
H5B	7693.13	4813.63	4658.91	24
H6A	9016.91	1957.21	3766.02	29
H6B	9722.95	2560.53	4830.81	29
H7A	7317.1	1471.74	5196.17	29
H7B	8074.06	-118.55	4701.68	29
H8A	6058.25	408.58	3274.59	25
H8B	5092.77	131.33	4066.56	25
H10	2928.43	2281.18	3929.57	22
H13	4740(20)	2510(30)	1743(11)	37

Crystal (3a)



Experimental

Single crystals of $C_{14}H_{20}O_4$ [**3a**] were recrystallised in diethyl ether. A suitable crystal was selected and loaded on a SuperNova, Titan S2 diffractometer. The crystal was kept at 120(2) K during data collection. Using Olex2[i], the structure was solved with the ShelXT[ii] structure solution program using Intrinsic Phasing and refined with the ShelXL[iii] refinement package using Least Squares minimisation.

Crystal structure determination of 3a

Crystal Data for $C_{14}H_{20}O_4$ (M =252.30 g/mol): monoclinic, space group $P2_1/c$ (no. 14), a = 5.8033(5) Å, b = 38.0676(19) Å, c = 6.4898(5) Å, β = 115.253(10)°, V = 1296.70(16) Å^3, Z = 4, T = 120(2) K, μ(CuKα) = 0.767 mm^{-1}, *Dcalc* = 1.292 g/cm^3, 16445 reflections measured (4.642° ≤ 2Θ ≤ 135.918°), 2323 unique (R_{int} = 0.0786, R_{sigma} = 0.0361) which were used in all calculations. The final R_1 was 0.1103 (I > 2σ(I)) and wR_2 was 0.2938 (all data).

[i] Dolomanov, O.V., Bourhis, L.J., Gildea, R.J, Howard, J.A.K. & Puschmann, H. (2009), J. Appl. Cryst. 42, 339-341.

[ii] Sheldrick, G.M. (2015). Acta Cryst. A71, 3-8.

[iii] Sheldrick, G.M. (2015). Acta Cryst. C71, 3-8.

*Table **3a**-1 Crystal data and structure refinement for **3a**.*

Empirical formula	$C_{14}H_{20}O_4$
Formula weight	252.30
Temperature/K	120(2)
Crystal system	monoclinic
Space group	$P2_1/c$
a/Å	5.8033(5)
b/Å	38.0676(19)
c/Å	6.4898(5)
α/°	90.0
β/°	115.253(10)
γ/°	90.0
Volume/Å^3	1296.70(16)
Z	4
ρ_{calc}g/cm^3	1.292
μ/mm^{-1}	0.767
F(000)	544.0
Crystal size/mm^3	0.573 × 0.129 × 0.026
Radiation	CuKα (λ = 1.54184)
2Θ range for data collection/°	4.642 to 135.918
Index ranges	$-6 \le h \le 6$, $-45 \le k \le 45$, $-6 \le l \le 7$
Reflections collected	16445
Independent reflections	2323 [R_{int} = 0.0786, R_{sigma} = 0.0361]
Data/restraints/parameters	2323/0/164
Goodness-of-fit on F^2	1.137
Final R indexes [I>=2σ (I)]	R_1 = 0.1103, wR_2 = 0.2895
Final R indexes [all data]	R_1 = 0.1164, wR_2 = 0.2938
Largest diff. peak/hole / e Å^{-3}	0.64/-0.42

*Table **3a**-2 Fractional Atomic Coordinates (×10^4) and Equivalent Isotropic Displacement Parameters (Å^2×10^3) for **3a**. U_{eq} is defined as 1/3 of of the trace of the orthogonalised U_{IJ} tensor.*

Atom	*x*	*y*	*z*	U(eq)
O1	5021(6)	3554.7(8)	586(5)	28.9(8)

O2	3991(6)	3691.2(8)	2137(5)	28.6(8)
O3	10561(7)	2652.5(9)	7466(6)	36.3(9)
O4	7874(6)	3621.8(8)	5260(5)	26.7(8)
C1	6850(8)	3281.4(12)	1798(7)	24.1(10)
C2	5545(9)	2986.6(12)	2417(7)	27.6(10)
C3	6724(9)	2790.6(12)	4281(7)	28.6(10)
C4	9404(9)	2851.9(13)	5863(8)	30.4(11)
C5	10736(8)	3164.6(12)	5444(8)	30.3(11)
C6	8954(8)	3444.4(12)	3920(7)	26.1(10)
C7	7843(9)	3166.4(13)	79(8)	30.6(11)
C8	6030(8)	3870.6(12)	3917(7)	24.8(10)
C9	4870(8)	4056.8(12)	5312(7)	26.1(10)
C10	3045(10)	4342.0(14)	3857(8)	36.1(12)
C11	1827(11)	4540.9(16)	5181(9)	46.7(15)
C12	3838(11)	4696.7(14)	7384(8)	40.9(13)
C13	5635(10)	4410.1(14)	8820(8)	36.5(12)
C14	6880(10)	4216.7(14)	7503(8)	34.6(11)

*Table **3a**-3 Anisotropic Displacement Parameters ($Å^2×10^3$) for **3a**. The Anisotropic displacement factor exponent takes the form: $-2π^2[h^2a^{*2}U_{11}+2hka^*b^*U_{12}+…]$.*

Atom	U_{11}	U_{22}	U_{33}	U_{23}	U_{13}	U_{12}
O1	26.5(17)	44.7(19)	12.8(15)	-1.7(12)	5.9(13)	6.2(13)
O2	17.2(15)	46.9(19)	17.7(15)	-6.5(13)	3.6(12)	1.0(13)
O3	33.7(19)	50(2)	20.7(18)	5.1(14)	7.3(15)	4.1(15)
O4	19.0(16)	43.8(18)	12.6(15)	-1.5(12)	2.4(12)	2.3(12)
C1	15(2)	42(2)	10(2)	-1.5(16)	0.3(17)	1.2(17)
C2	20(2)	44(3)	18(2)	-4.8(17)	8.0(18)	-0.9(18)
C3	25(2)	41(3)	17(2)	-1.1(17)	6.1(19)	0.0(18)
C4	30(3)	41(3)	19(2)	-2.9(18)	10(2)	3.0(19)
C5	16(2)	46(3)	21(2)	-2.2(18)	-0.2(18)	1.9(18)
C6	21(2)	40(2)	16(2)	-2.6(17)	6.1(18)	-2.4(18)
C7	27(2)	47(3)	20(2)	-2.7(18)	11.9(19)	0.5(19)
C8	17(2)	39(2)	12(2)	-1.9(16)	0.3(16)	-0.9(17)
C9	20(2)	39(2)	19(2)	-2.6(17)	7.9(18)	-1.7(17)
C10	35(3)	49(3)	18(2)	-4.7(19)	5(2)	9(2)
C11	39(3)	66(4)	28(3)	-12(2)	7(2)	15(3)
C12	48(3)	46(3)	23(3)	-6(2)	10(2)	6(2)
C13	39(3)	51(3)	17(2)	-3.5(19)	10(2)	4(2)
C14	34(3)	50(3)	14(2)	-5.0(19)	5(2)	2(2)

*Table **3a**-4 Bond Lengths for **3a**.*

Atom	Atom	Length/Å	Atom	Atom	Length/Å
O1	O2	1.467(4)	C3	C4	1.471(7)
O1	C1	1.455(5)	C4	C5	1.506(7)
O2	C8	1.426(5)	C5	C6	1.520(6)
O3	C4	1.230(6)	C8	C9	1.515(6)
O4	C6	1.439(5)	C9	C10	1.529(6)
O4	C8	1.416(5)	C9	C14	1.529(6)
C1	C2	1.501(6)	C10	C11	1.526(7)
C1	C6	1.529(6)	C11	C12	1.528(7)
C1	C7	1.522(6)	C12	C13	1.522(7)
C2	C3	1.335(6)	C13	C14	1.523(7)

*Table **3a**-5 Bond Angles for **3a**.*

Atom	Atom	Atom	Angle/˚	Atom	Atom	Atom	Angle/˚
C1	O1	O2	107.4(3)	O4	C6	C1	110.4(3)
C8	O2	O1	106.6(3)	O4	C6	C5	106.7(3)
C8	O4	C6	110.6(3)	C5	C6	C1	111.2(4)
O1	C1	C2	110.1(3)	O2	C8	C9	106.3(3)
O1	C1	C6	108.4(3)	O4	C8	O2	109.0(3)
O1	C1	C7	103.1(3)	O4	C8	C9	110.9(3)
C2	C1	C6	111.3(3)	C8	C9	C10	109.3(4)
C2	C1	C7	111.9(4)	C8	C9	C14	112.6(4)
C7	C1	C6	111.7(4)	C14	C9	C10	110.1(4)
C3	C2	C1	122.6(4)	C11	C10	C9	111.7(4)
C2	C3	C4	121.6(4)	C10	C11	C12	111.6(5)
O3	C4	C3	121.7(4)	C13	C12	C11	110.2(4)
O3	C4	C5	120.2(4)	C12	C13	C14	111.6(4)
C3	C4	C5	118.1(4)	C13	C14	C9	111.0(4)
C4	C5	C6	114.3(4)				

*Table **3a**-6 Hydrogen Atom Coordinates (Å×10^4) and Isotropic Displacement Parameters (Å^2×10^3) for **3a**.*

Atom	x	y	z	U(eq)
H2	3813.36	2937.58	1442.95	33
H3	5809.43	2607.19	4594.49	34
H5A	11852.89	3081.97	4739.64	36
H5B	11838.18	3272.42	6928.03	36
H6	9948.77	3615.72	3452.55	31
H7A	6416.43	3085.72	-1316.87	46
H7B	9066.33	2974.33	724	46
H7C	8684.49	3365.1	-276.92	46
H8	6817.45	4045.29	3258.24	30
H9	3864.28	3881.35	5736.85	31
H10A	3988.69	4509.44	3333.94	43
H10B	1691.25	4232.74	2493.26	43
H11A	720.93	4378.98	5548.76	56
H11B	745.74	4732.16	4217.65	56
H12A	4819.73	4879.29	7018.01	49
H12B	2992.49	4808.66	8256.89	49
H13A	4672.07	4240.28	9306.05	44
H13B	6974.2	4516.33	10205.36	44
H14A	7992.68	4028.05	8468.94	42
H14B	7955.1	4382.29	7121.6	42

NMR Data (Chapter 4)

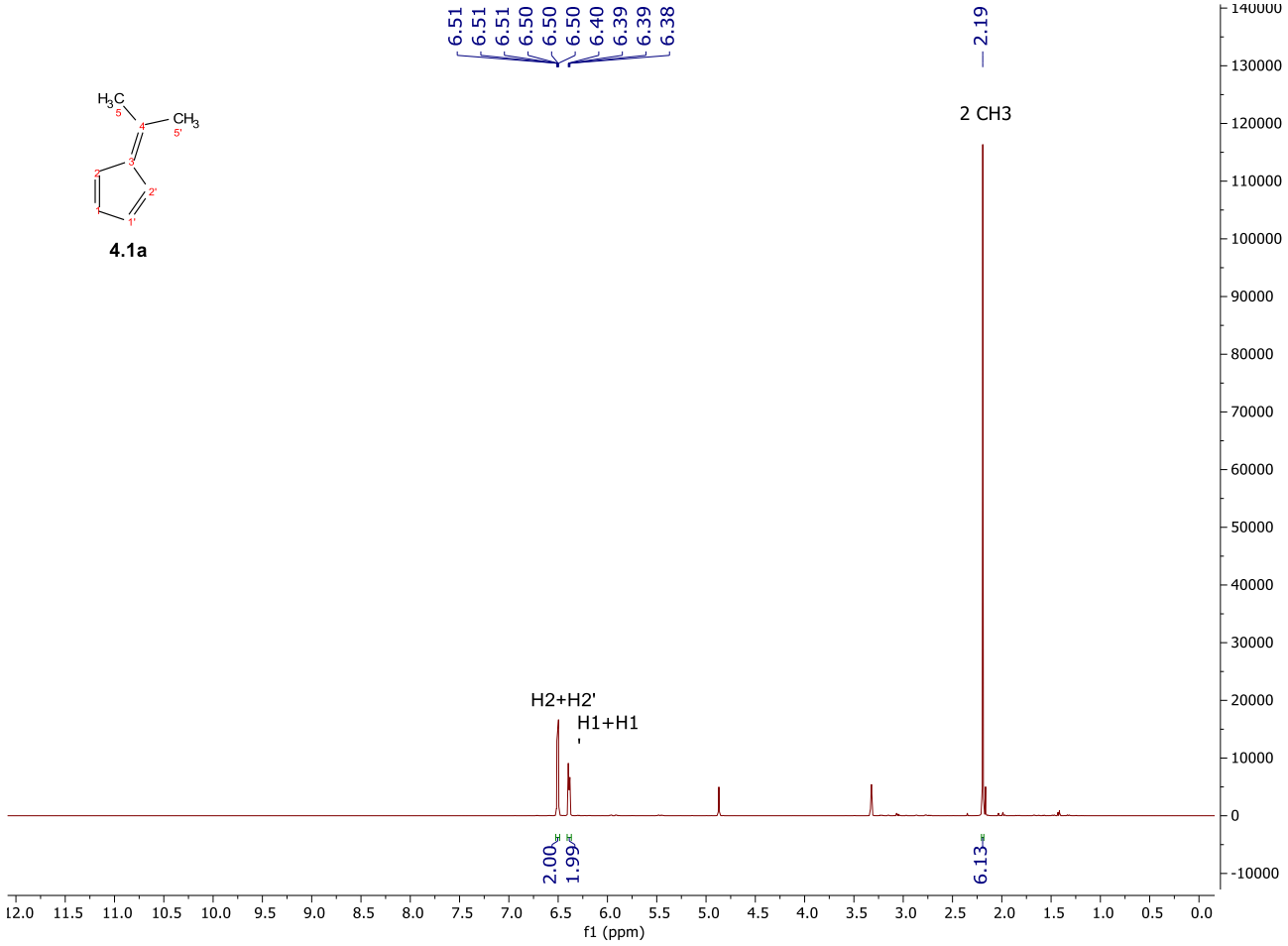


*Figure 4 - 1 ^{1}H NMR of compound **4.1a** in methanol-d_4.*

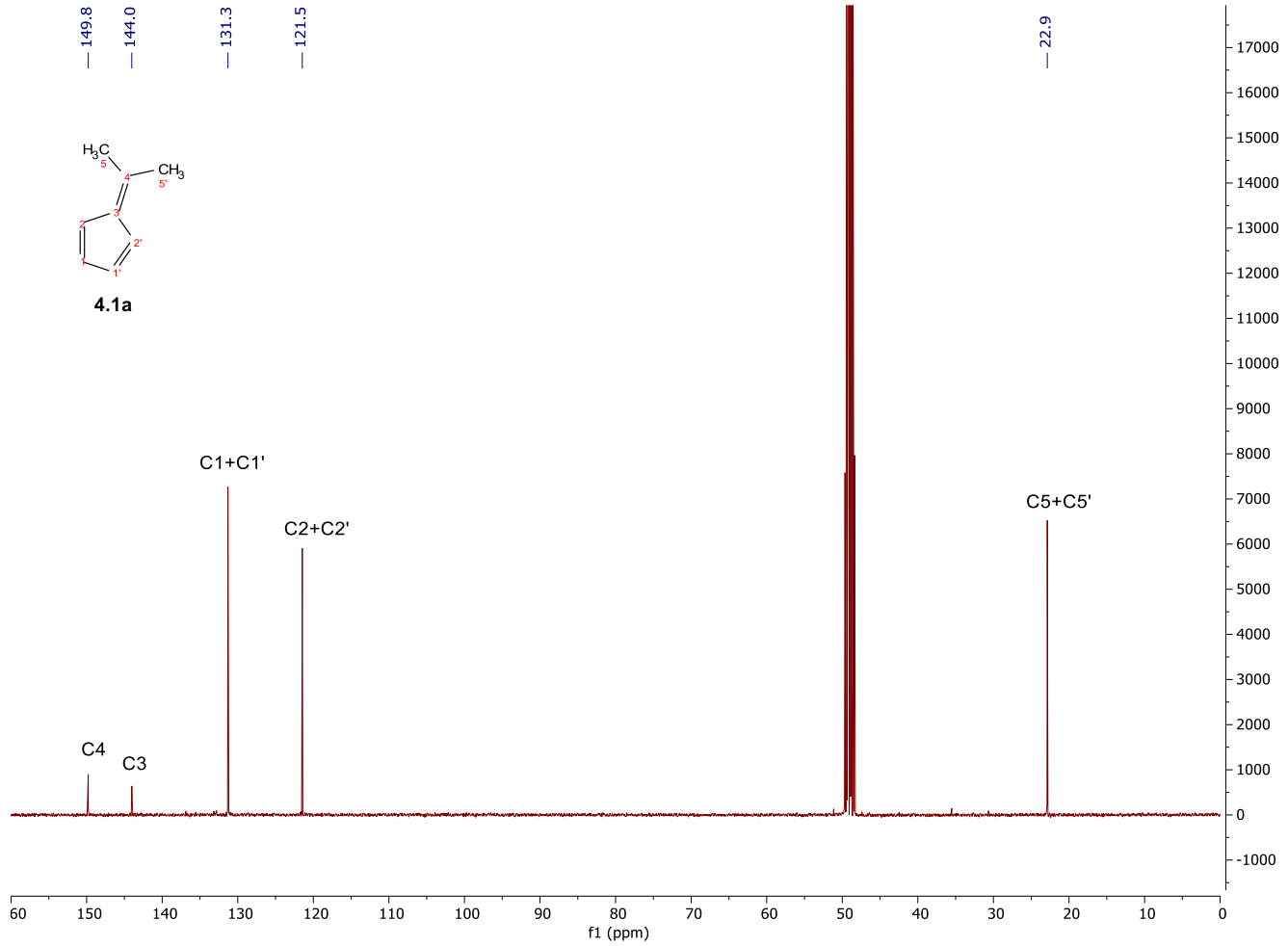


*Figure 4 - 2 ^{13}C NMR of compound **4.1a** in methanol-d_4.*

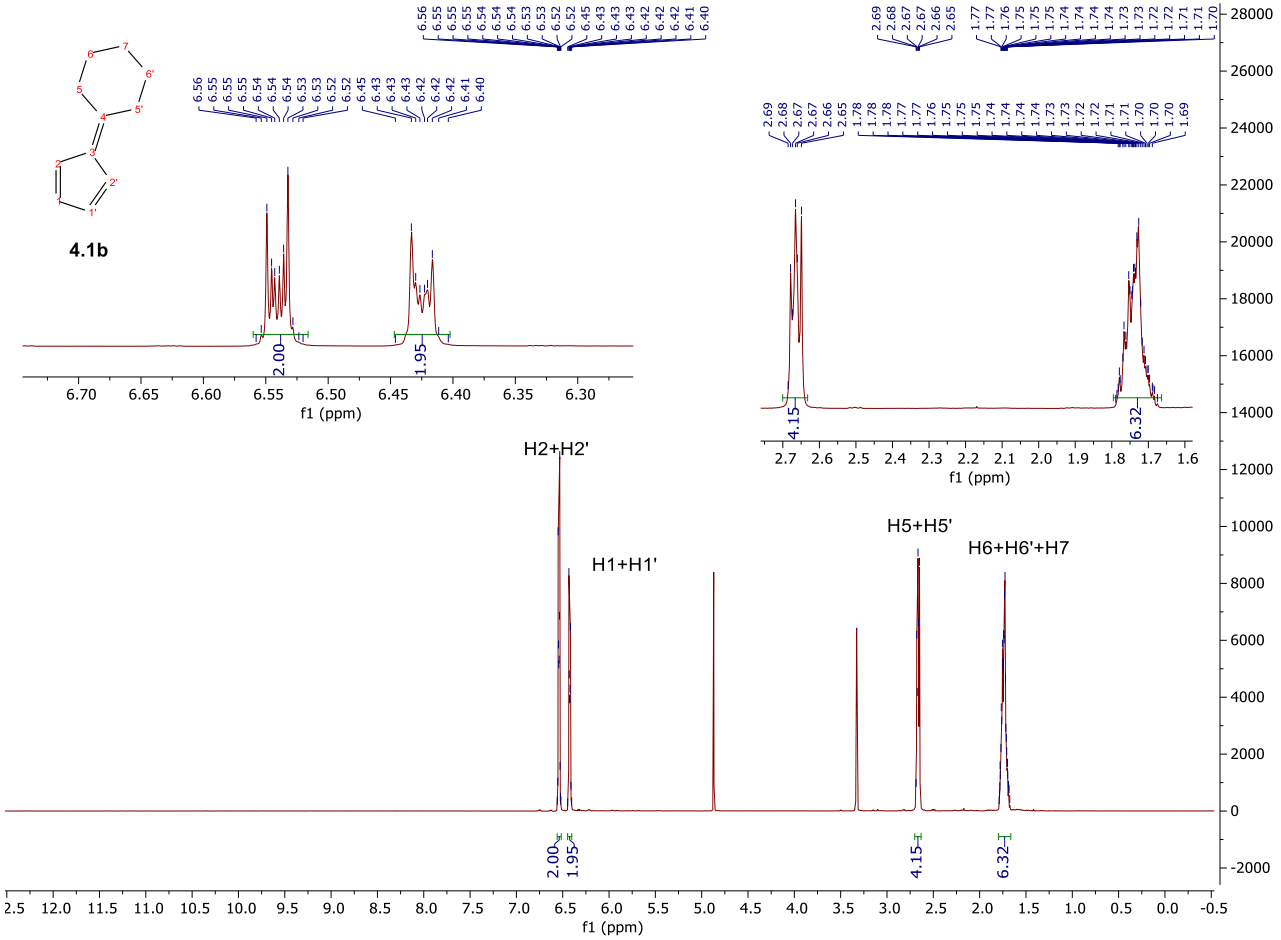


*Figure 4 - 3 ^{1}H NMR of compound **4.1b** in methanol-d_4.*

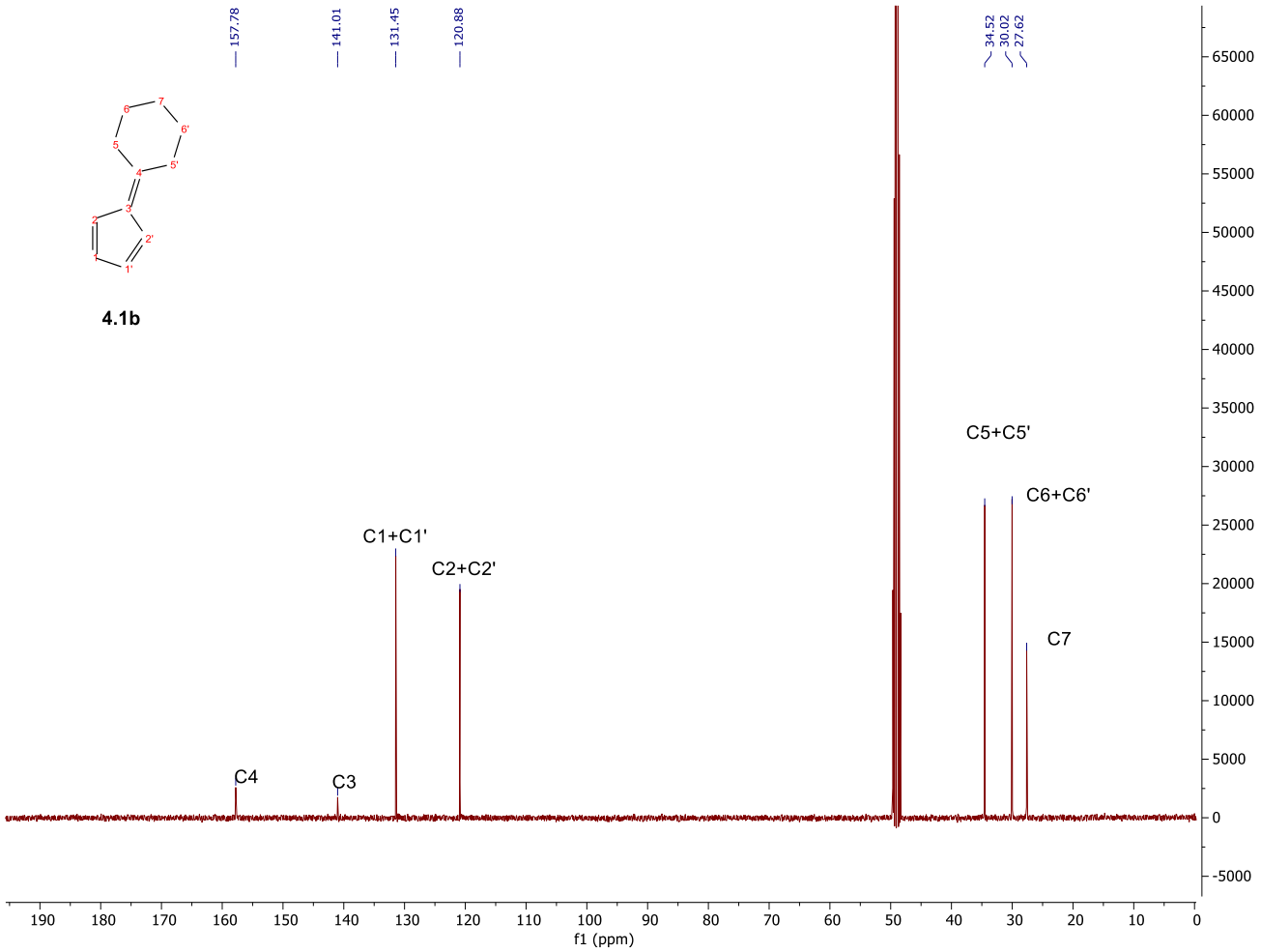


*Figure 4 - 4 ^{13}C NMR of compound **4.1b** in methanol-d_4.*

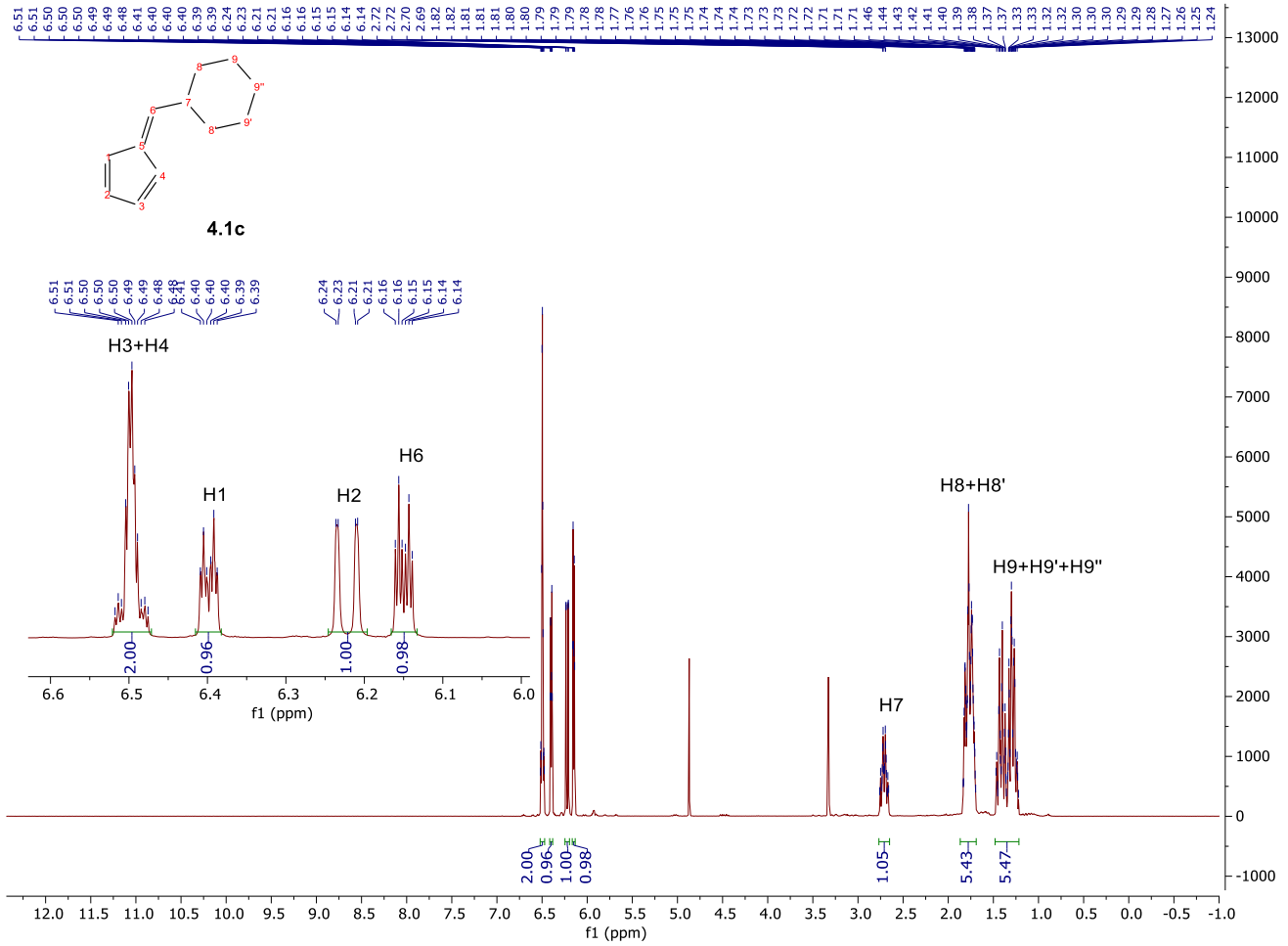


*Figure 4 - 5 ^{1}H NMR of compound **4.1c** in methanol-d_4*

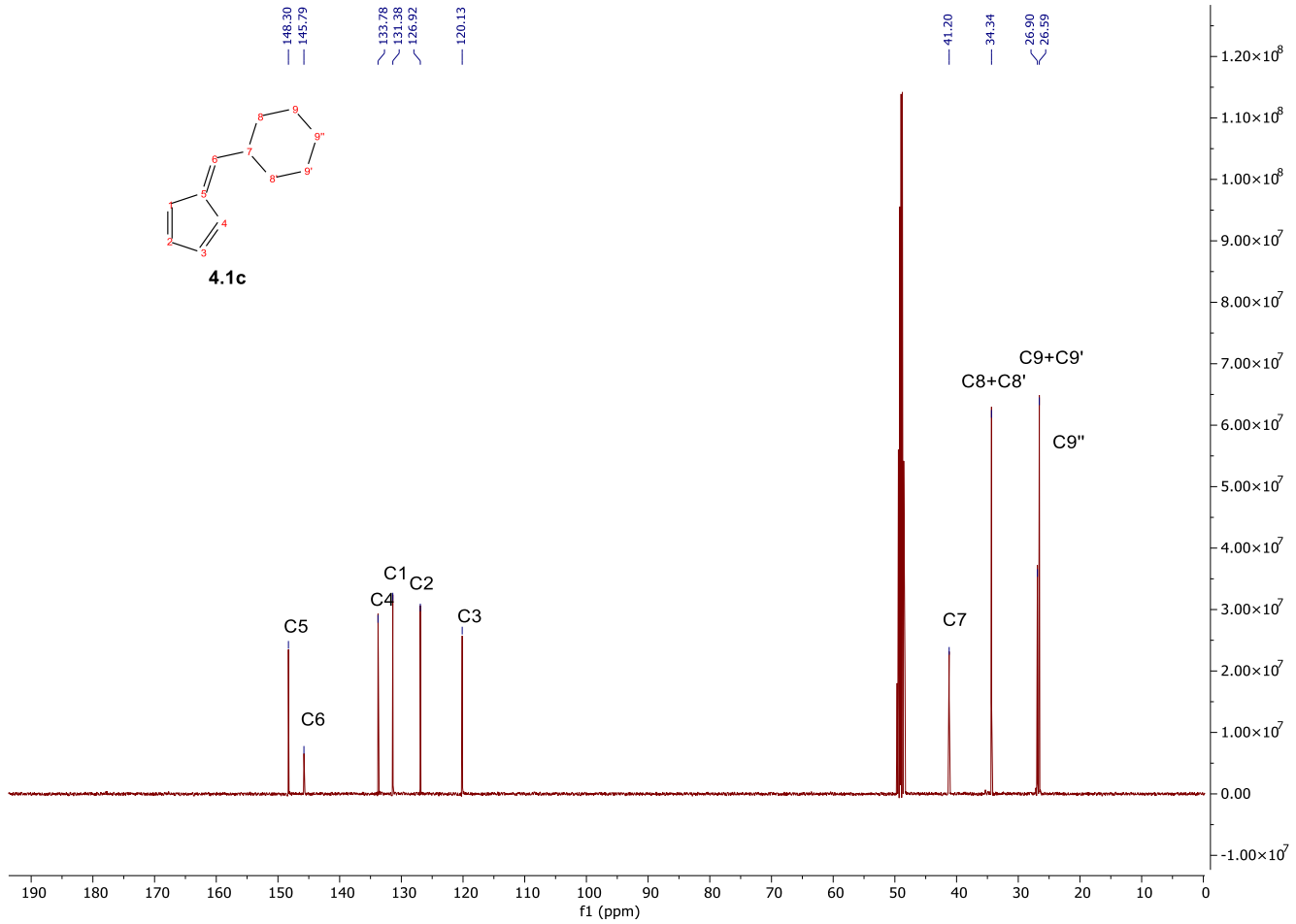


*Figure 4 - 6 ^{13}C NMR of compound **4.1c** in methanol-d_4.*

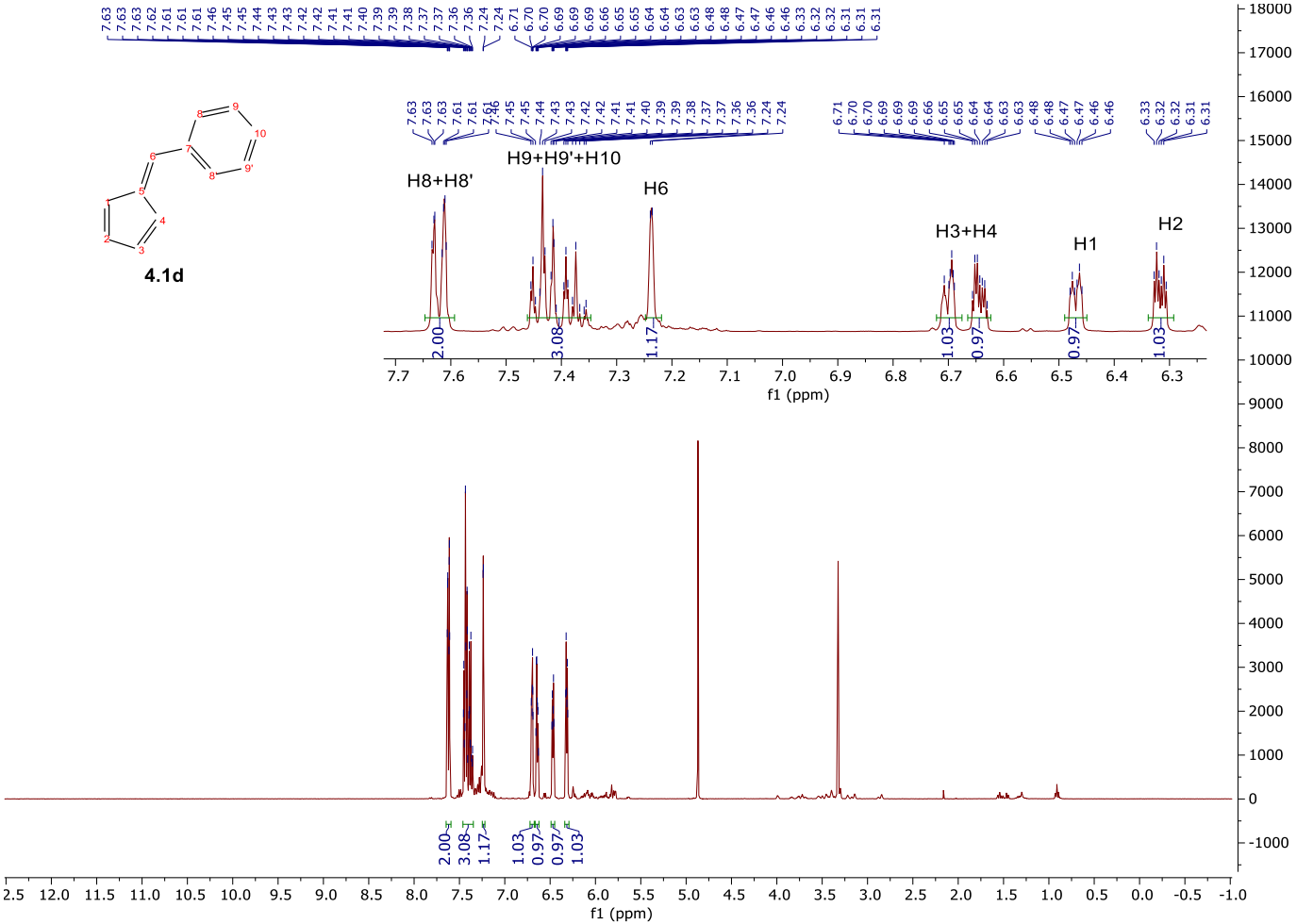


*Figure 4 - 7 ^{1}H NMR of compound **4.1d** in methanol-d_4.*

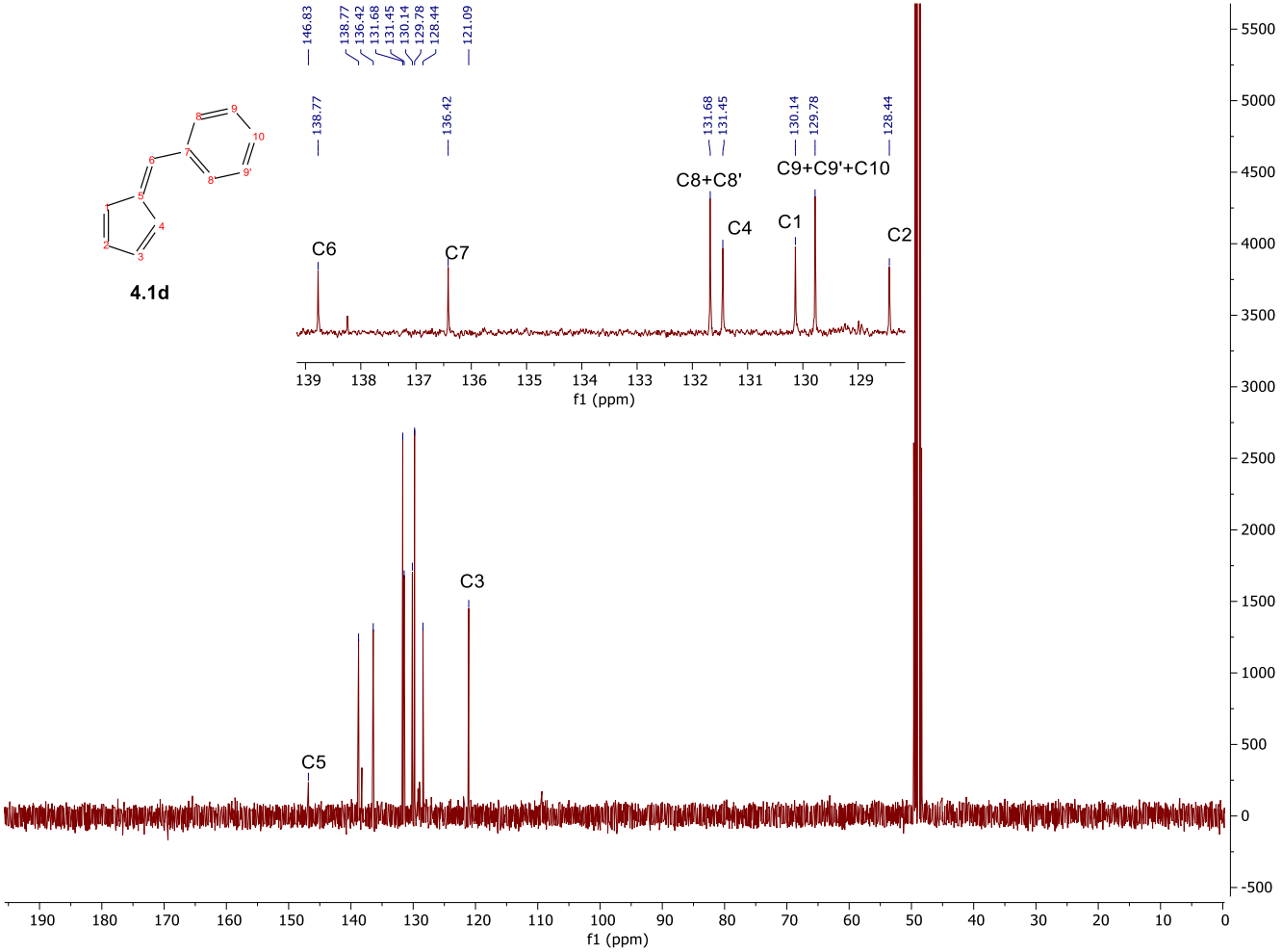


*Figure 4 - 8 ^{13}C NMR of compound **4.1d** in methanol-d_4.*

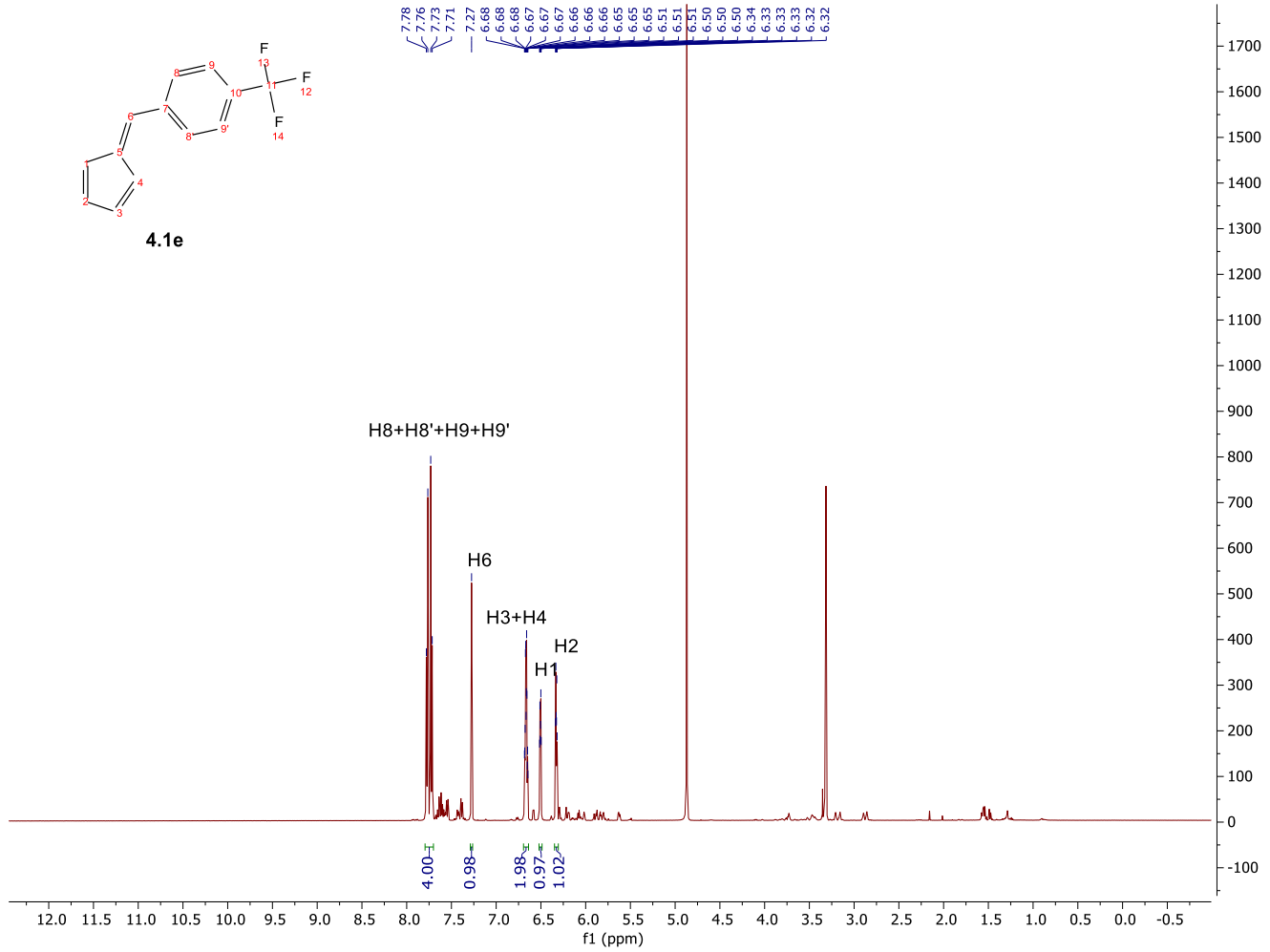


*Figure 4 - 9 ^{1}H NMR of compound **4.1e** in methanol-d_4.*

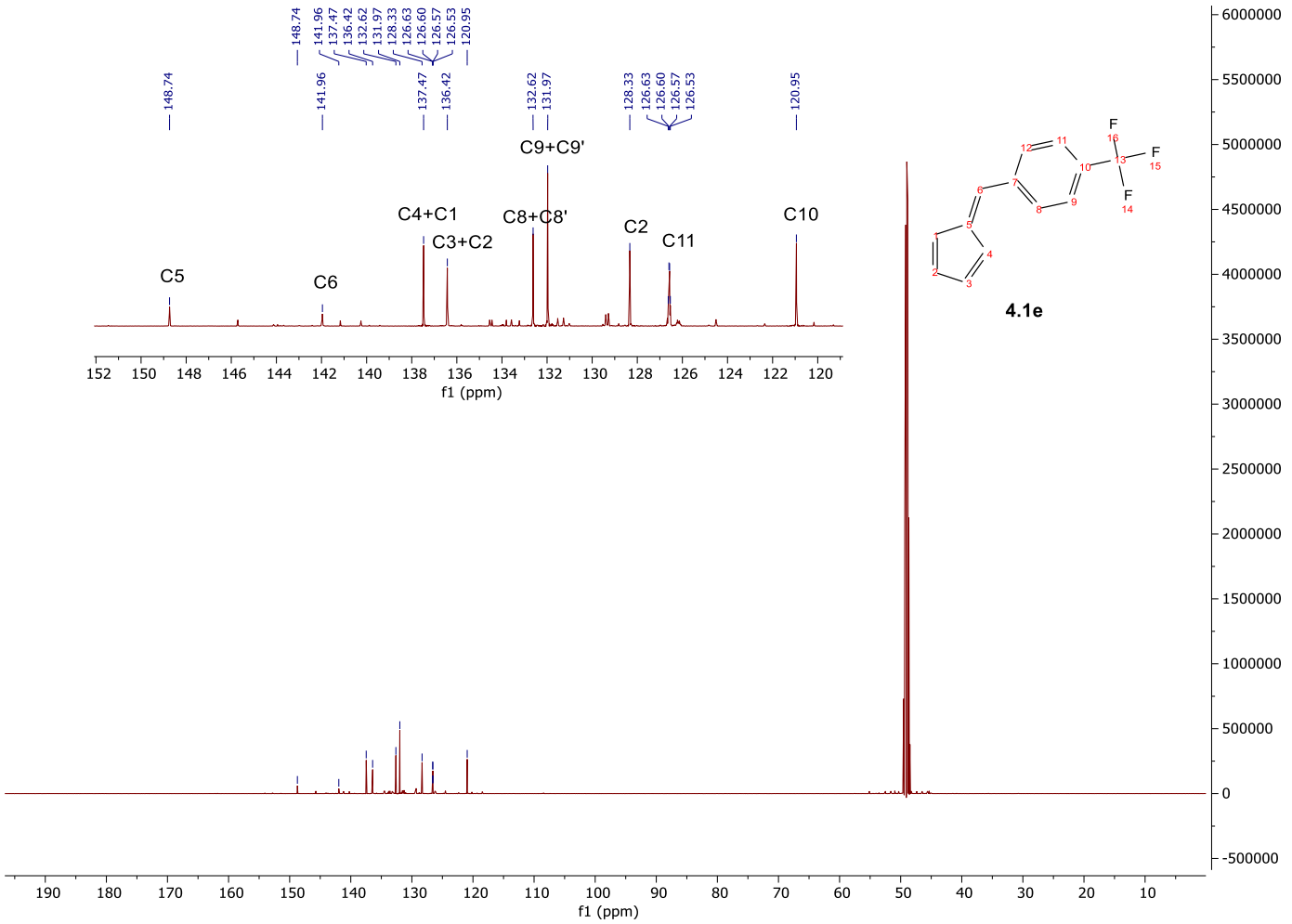


*Figure 4 - 10 ^{13}C NMR of compound **4.1e** in methanol-d_4.*

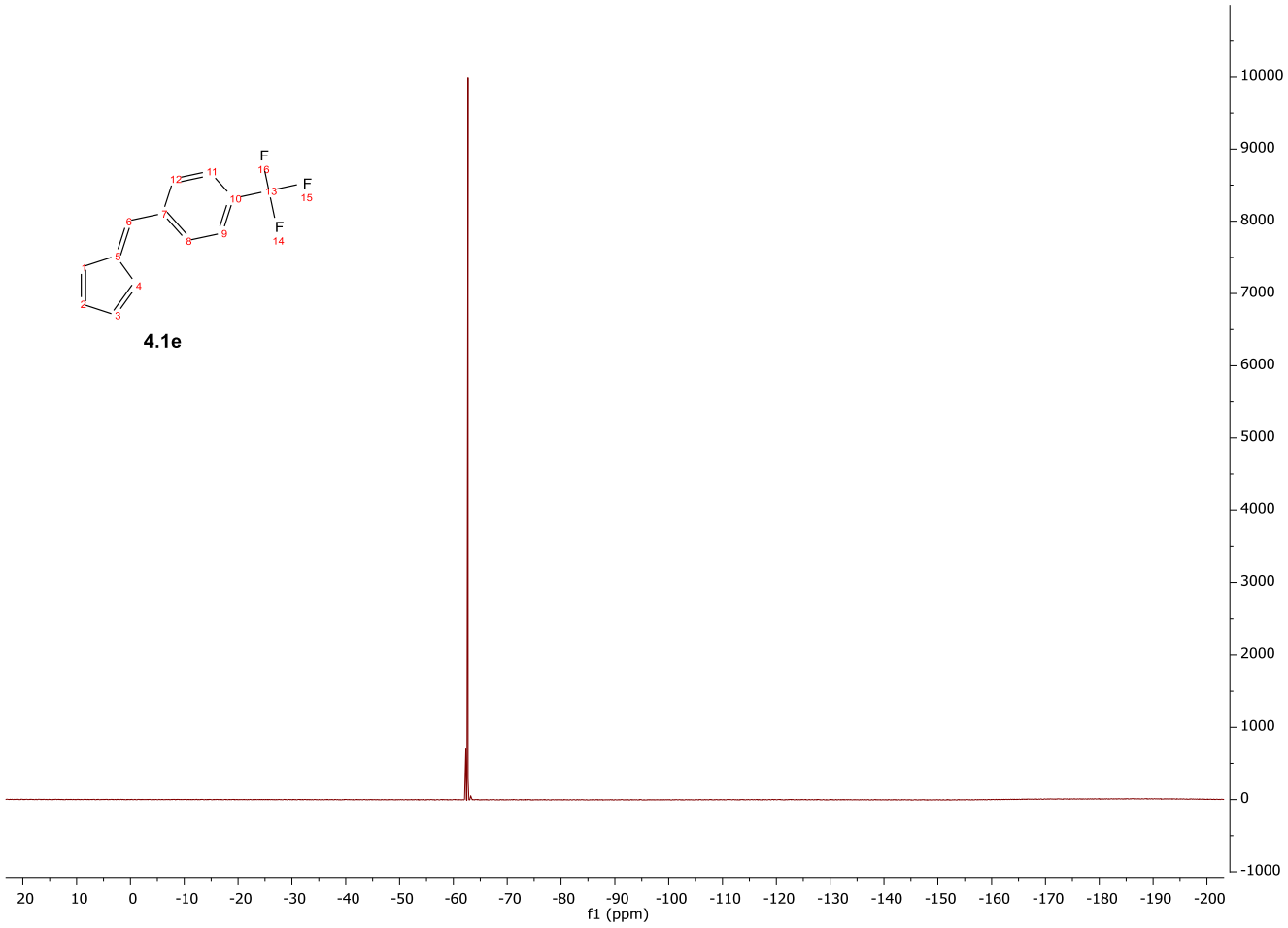


*Figure 4 - 11 ^{19}F NMR of compound **4.1e** in methanol-d_4.*

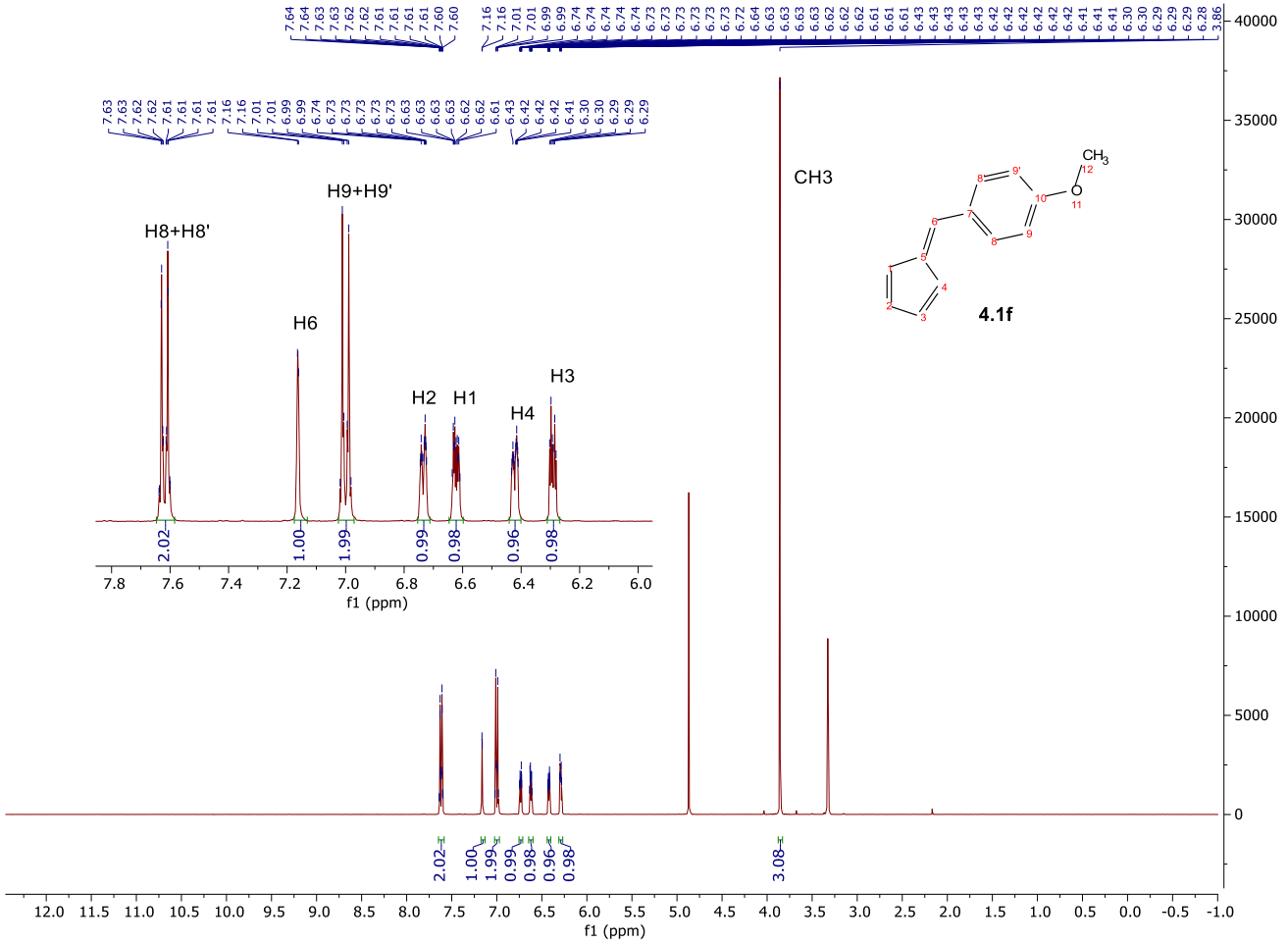


*Figure 4 - 12 ^{1}H NMR of compound **4.1f** in methanol-d$_4$.*

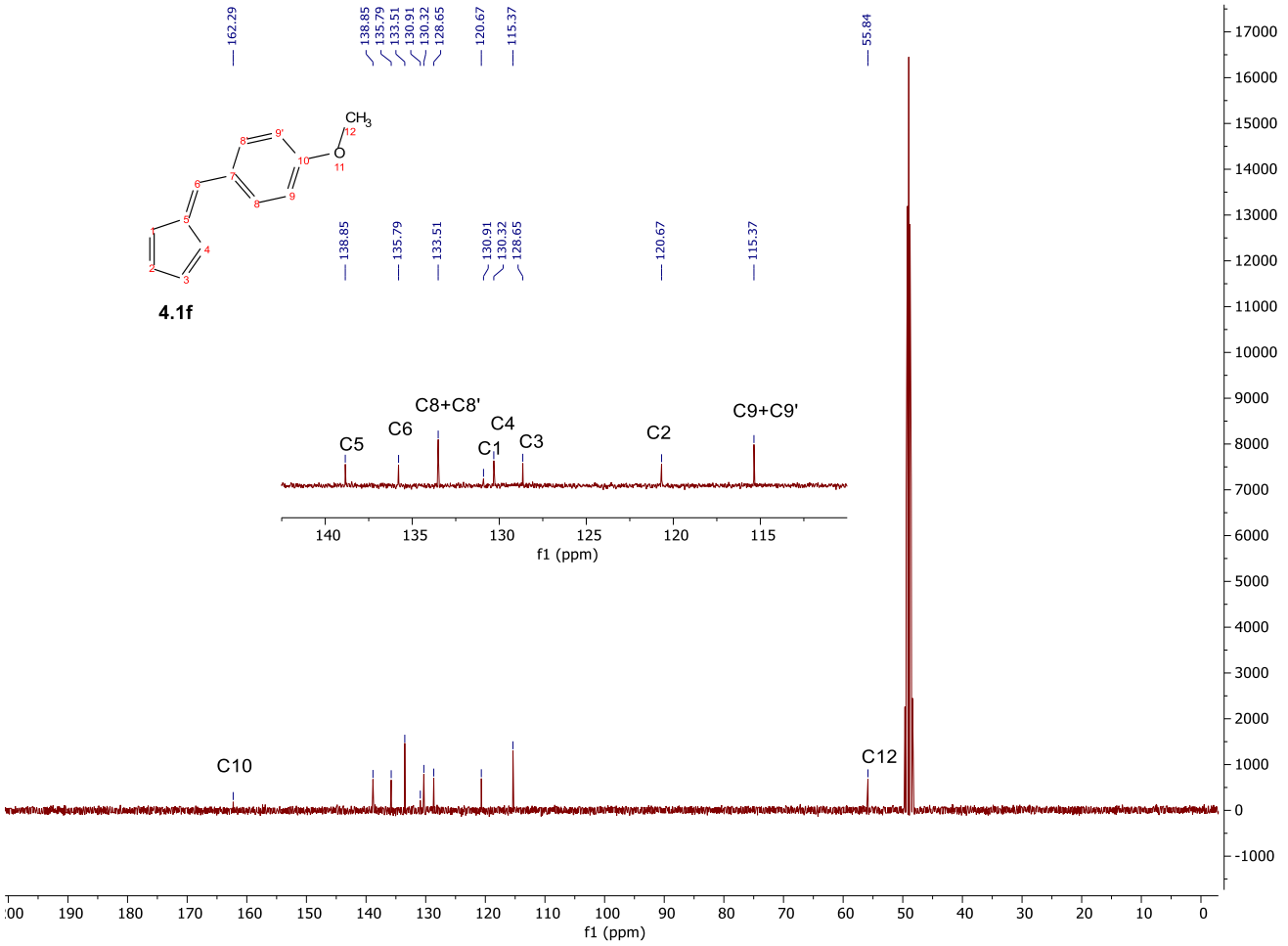


*Figure 4 - 13 ^{13}C NMR of compound **4.1f** in methanol-d_4.*

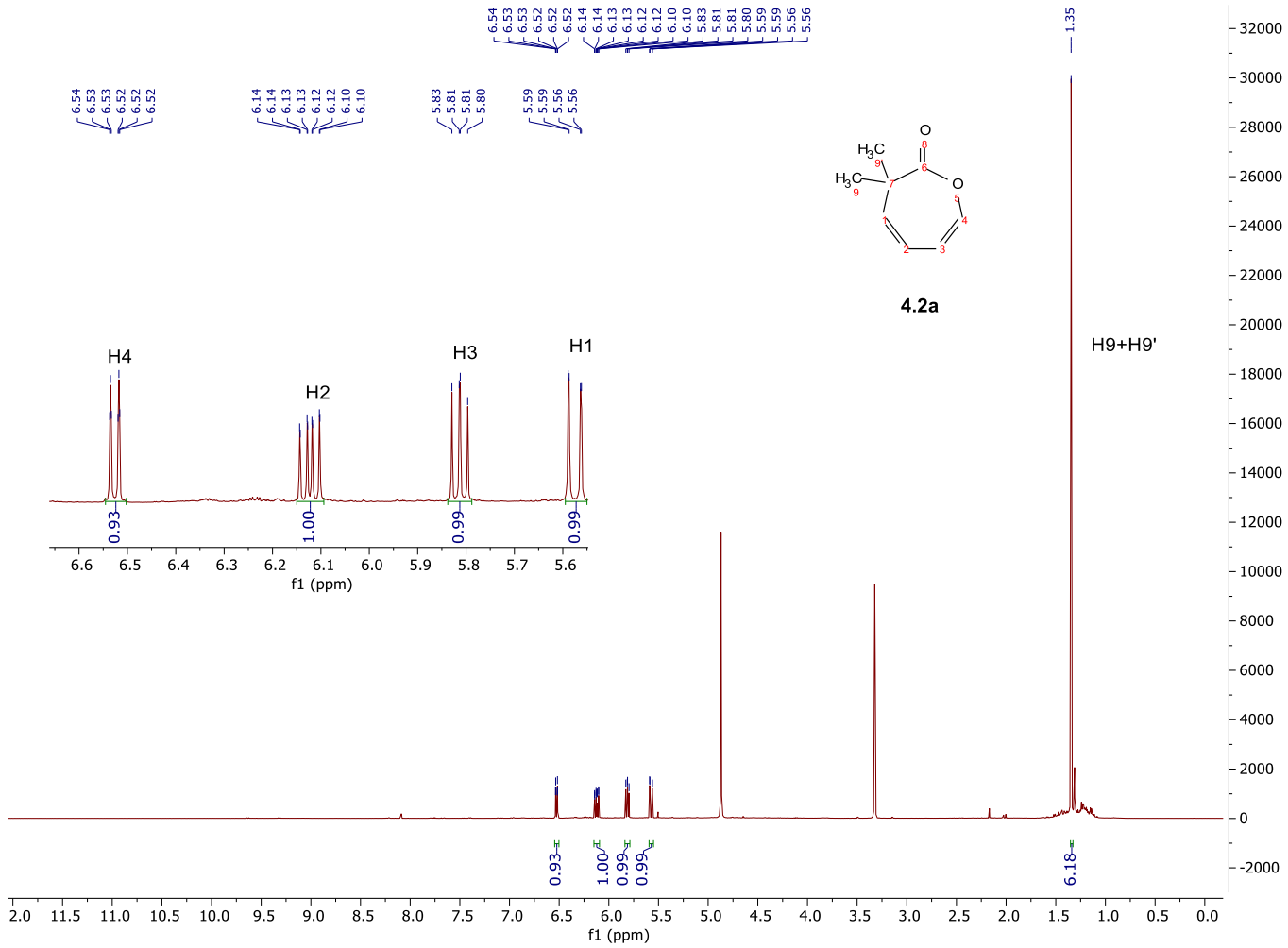


*Figure 4 - 14 ^{1}H NMR of compound **4.2a** in methanol-d_4.*

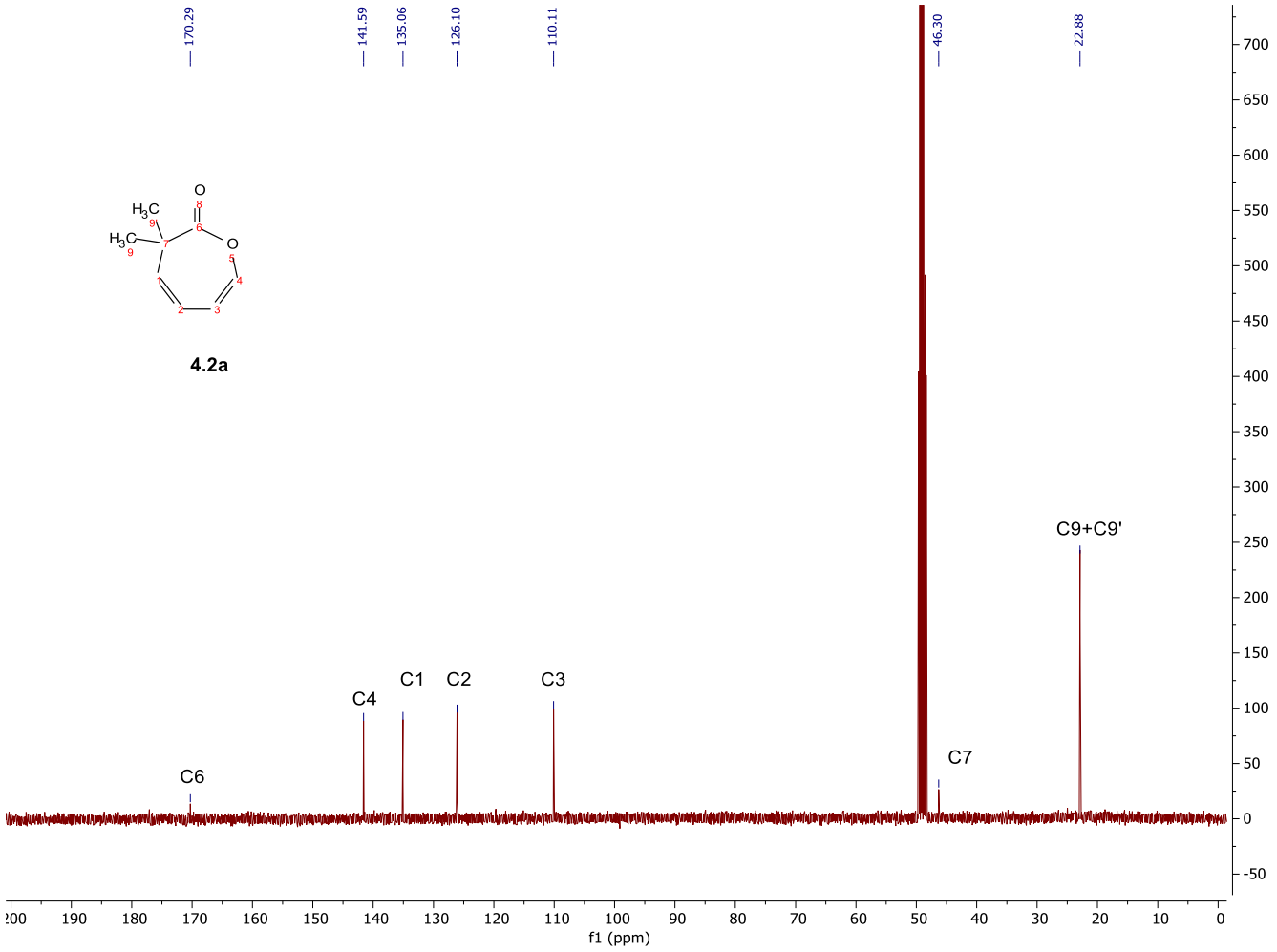


*Figure 4 - 14 ^{13}C NMR of compound **4.2a** in methanol-d_4.*

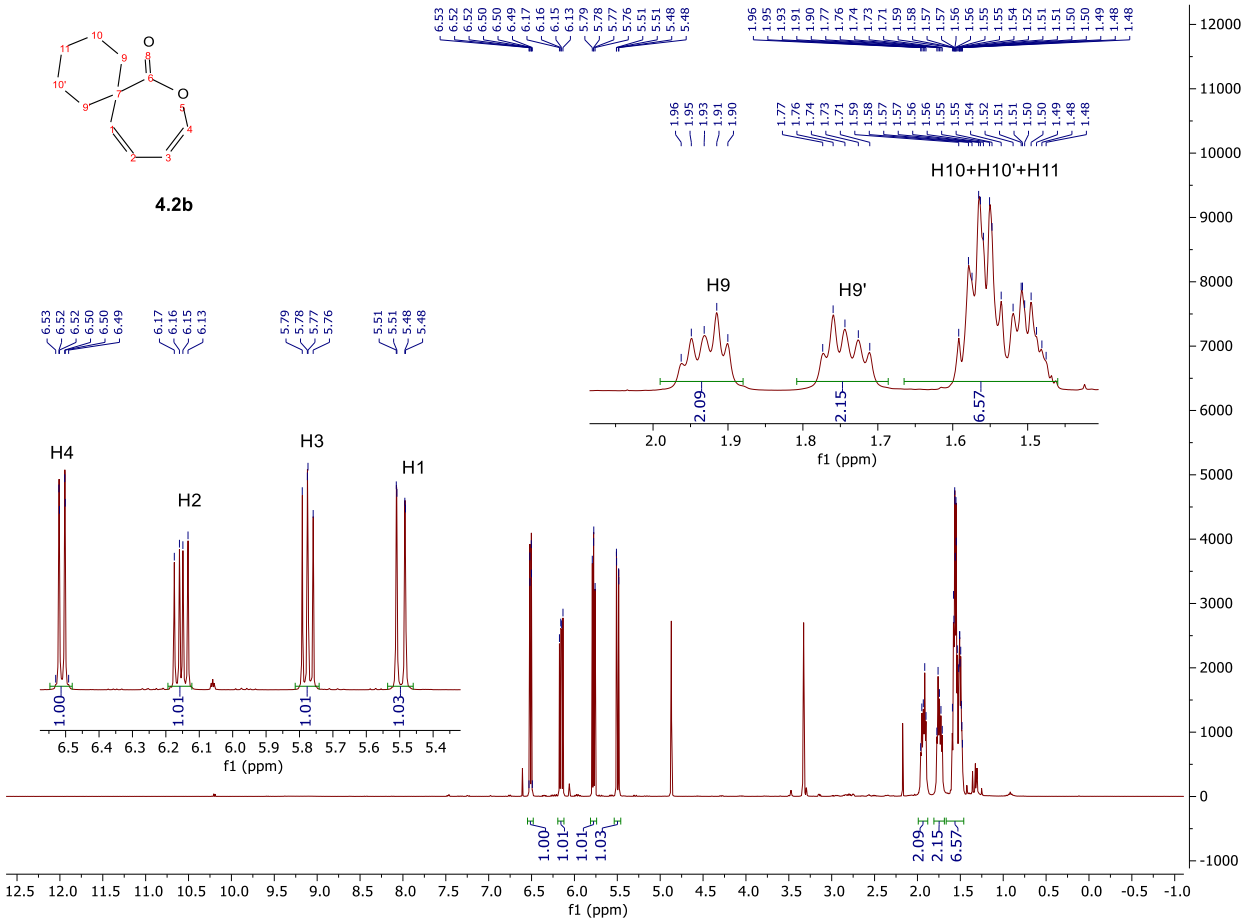


*Figure 4 - 15 ^{1}H NMR of compound **4.2b** in methanol-d_4.*

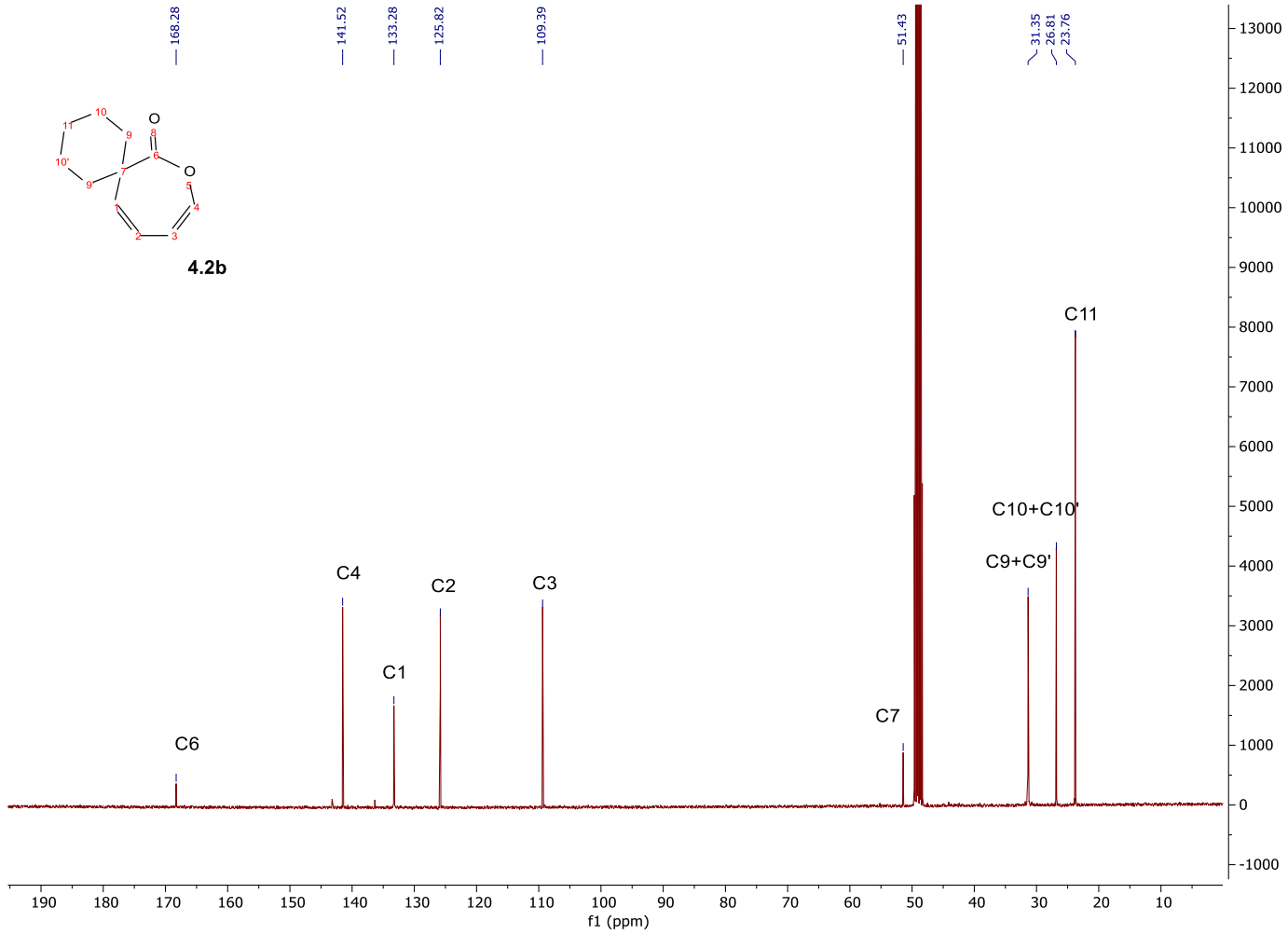


*Figure 4 - 16 ^{13}C NMR of compound **4.2b** in methanol-d_4.*

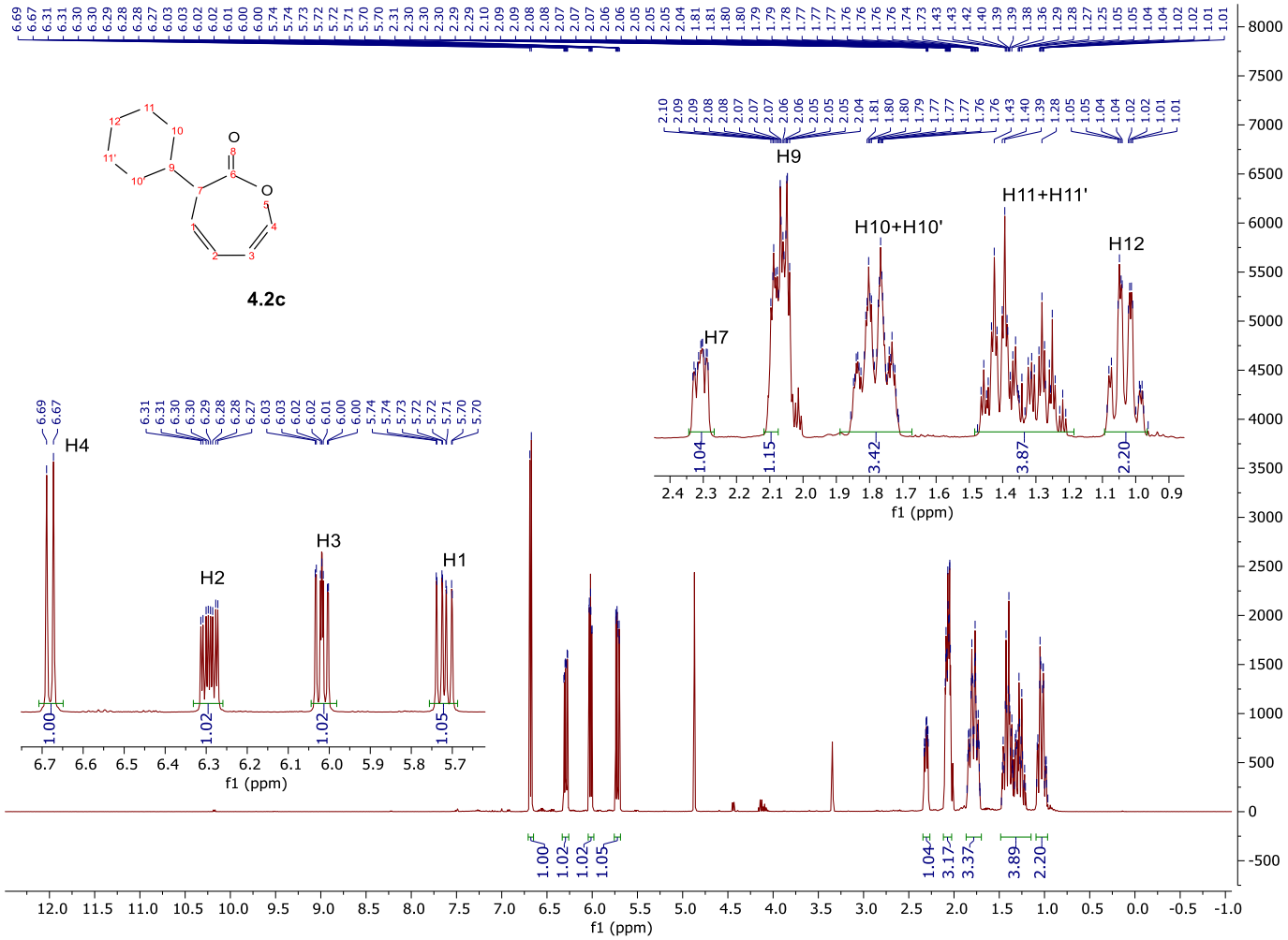


*Figure 4 - 127 ^{1}H NMR of compound **4.2c** in methanol-d_4.*

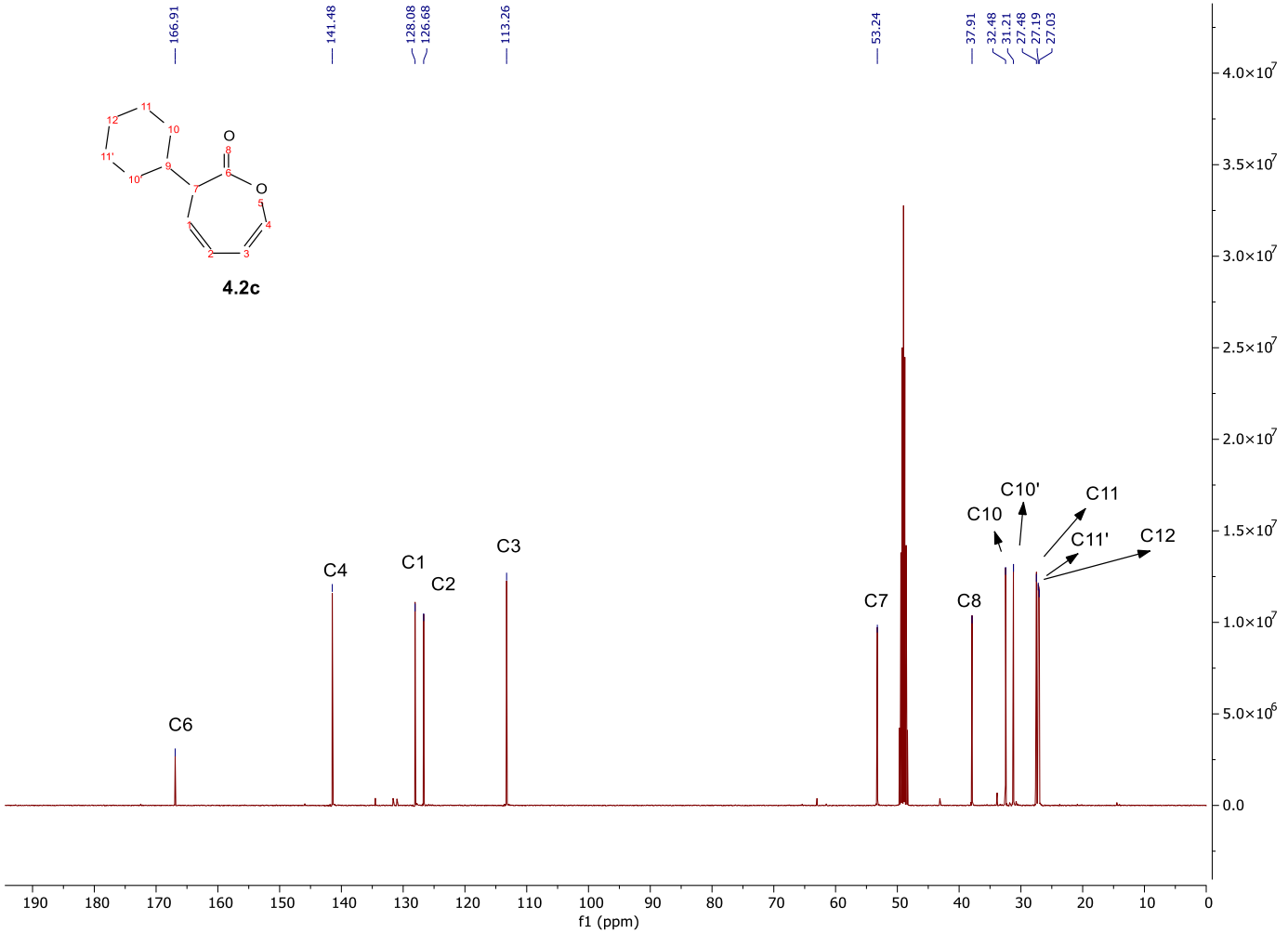


*Figure 4 - 18 ^{1}H NMR of compound **4.2c** in methanol-d_4.*

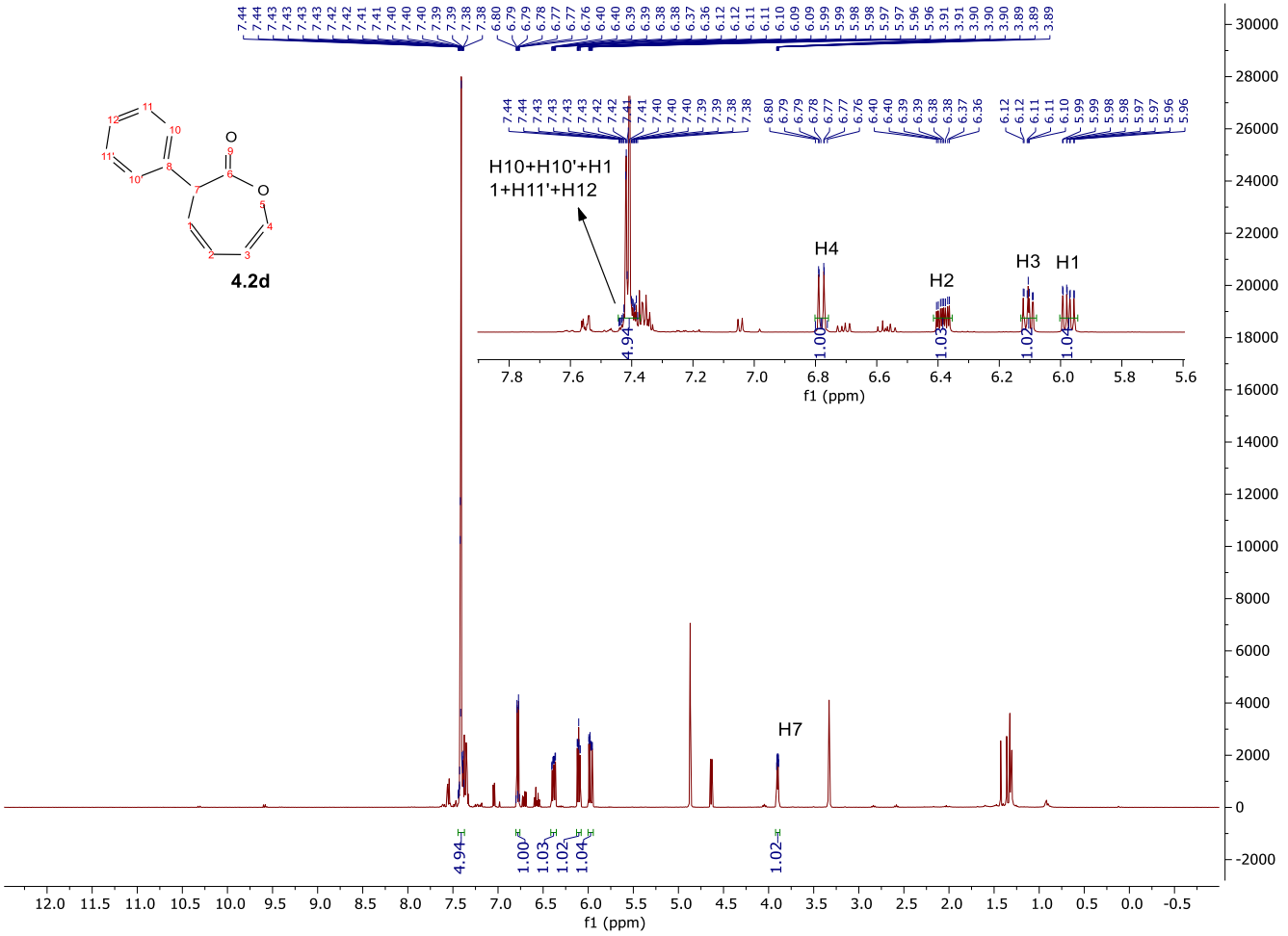


*Figure 4 - 19 ^{1}H NMR of compound **4.2d** in methanol-d_4.*

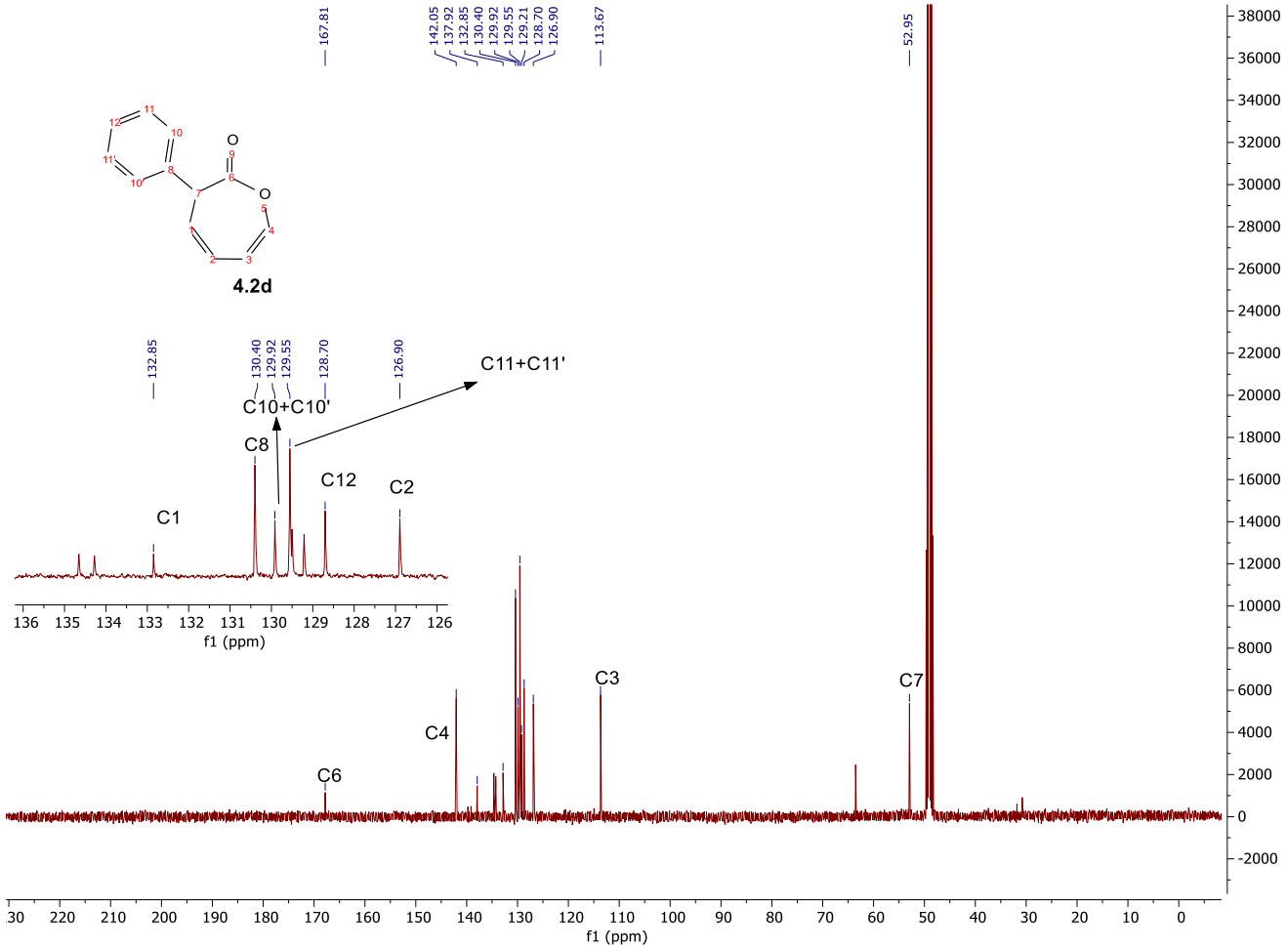


*Figure 4 - 20 ^{13}C NMR of compound **4.2d** in methanol-d_4.*

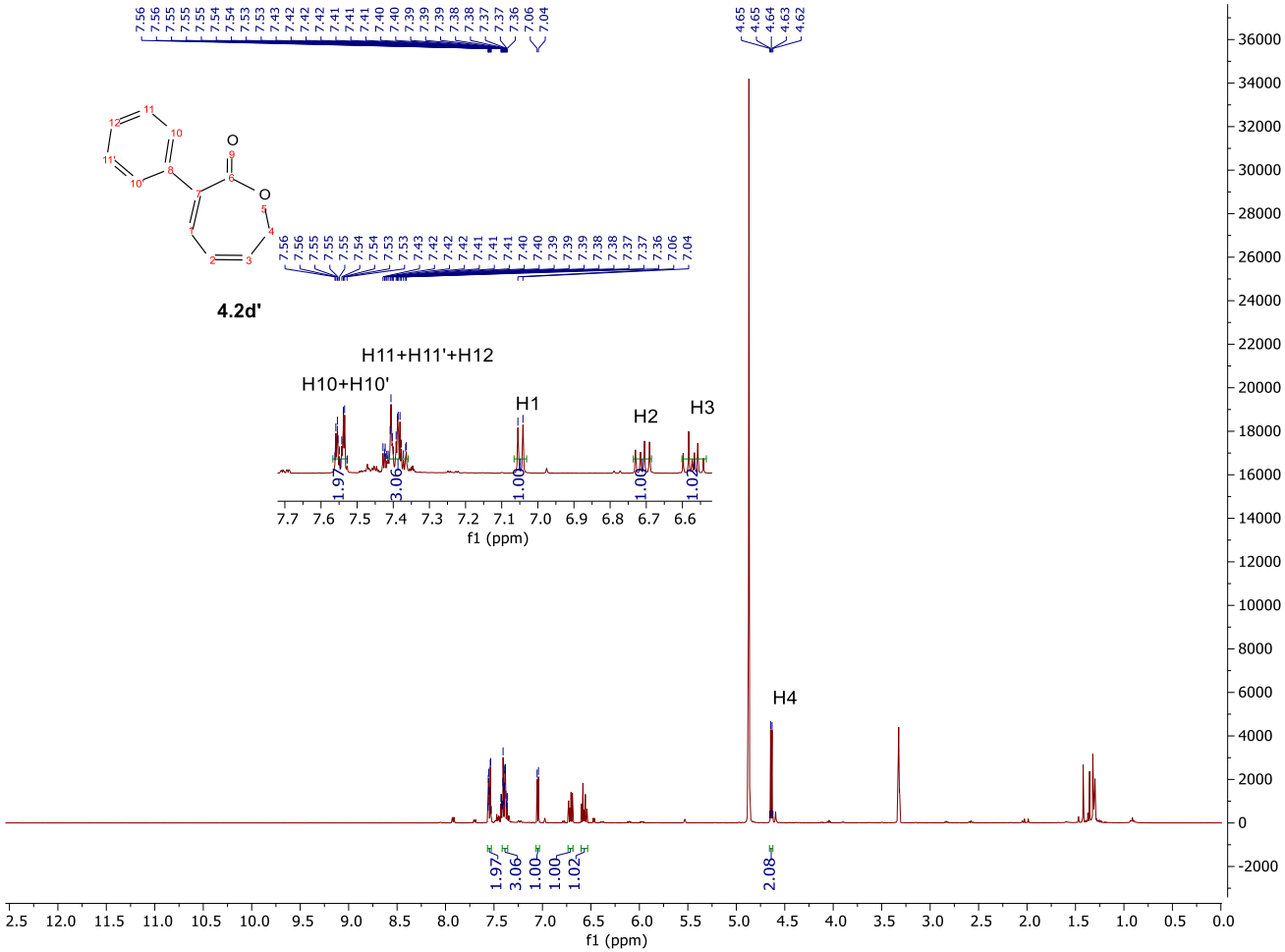


*Figure 4 - 21 ^{1}H NMR of compound **4.2d'** in methanol-d_4.*

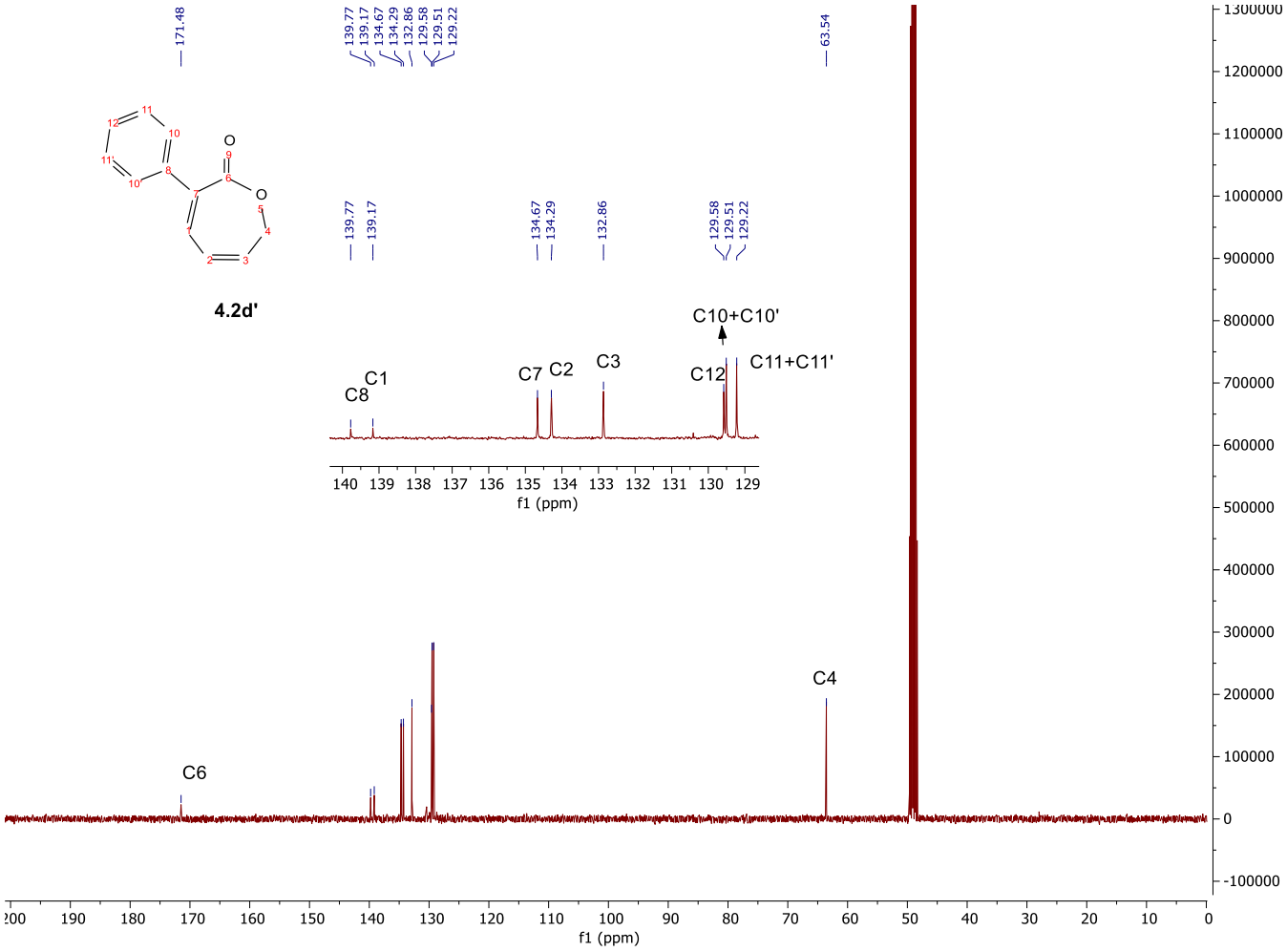


*Figure 4 - 22 ^{13}C NMR of compound **4.2d'** in methanol-d_4.*

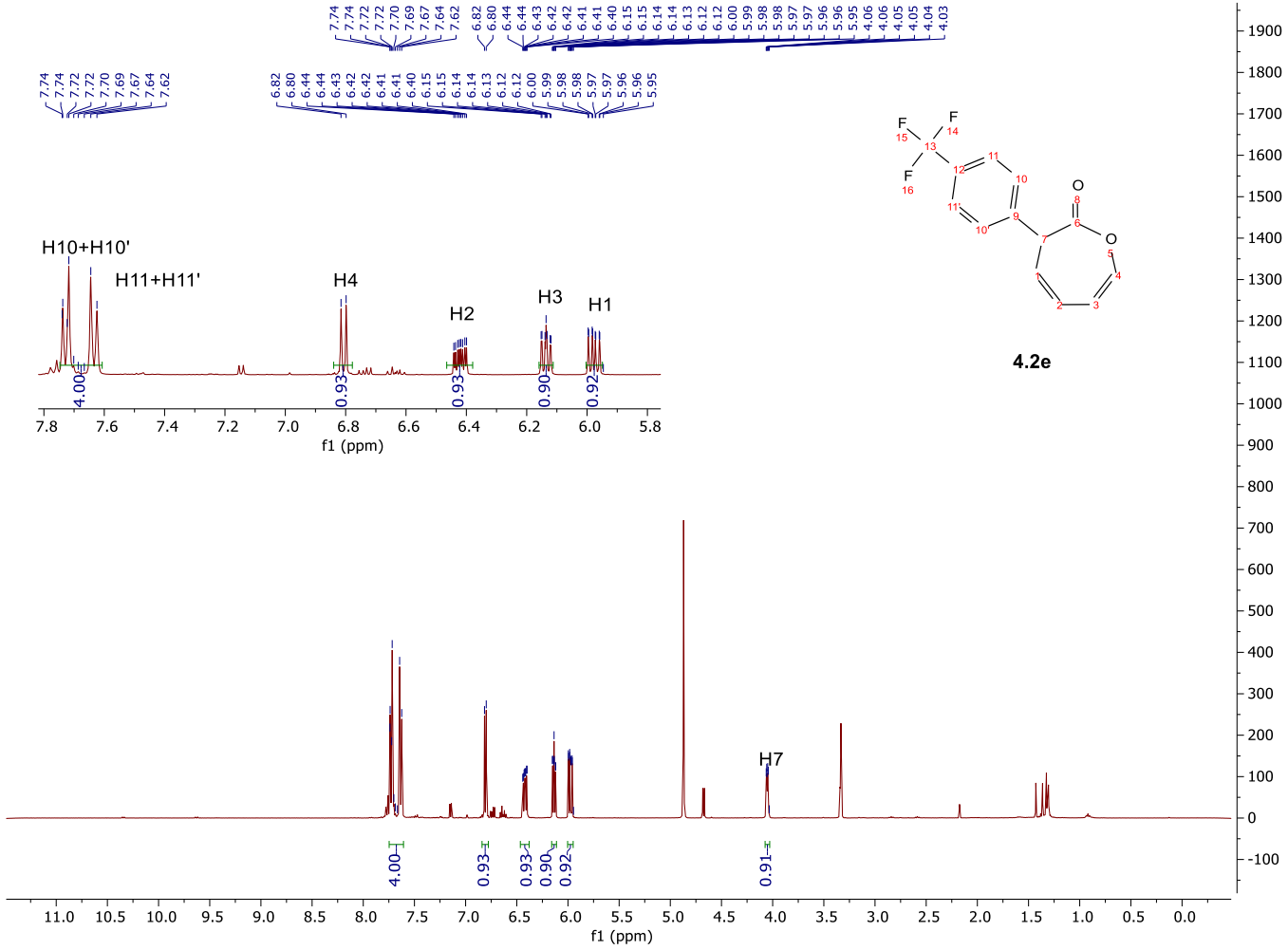


*Figure 4 - 133 ^{1}H NMR of compound **4.2e** in methanol-d_4.*

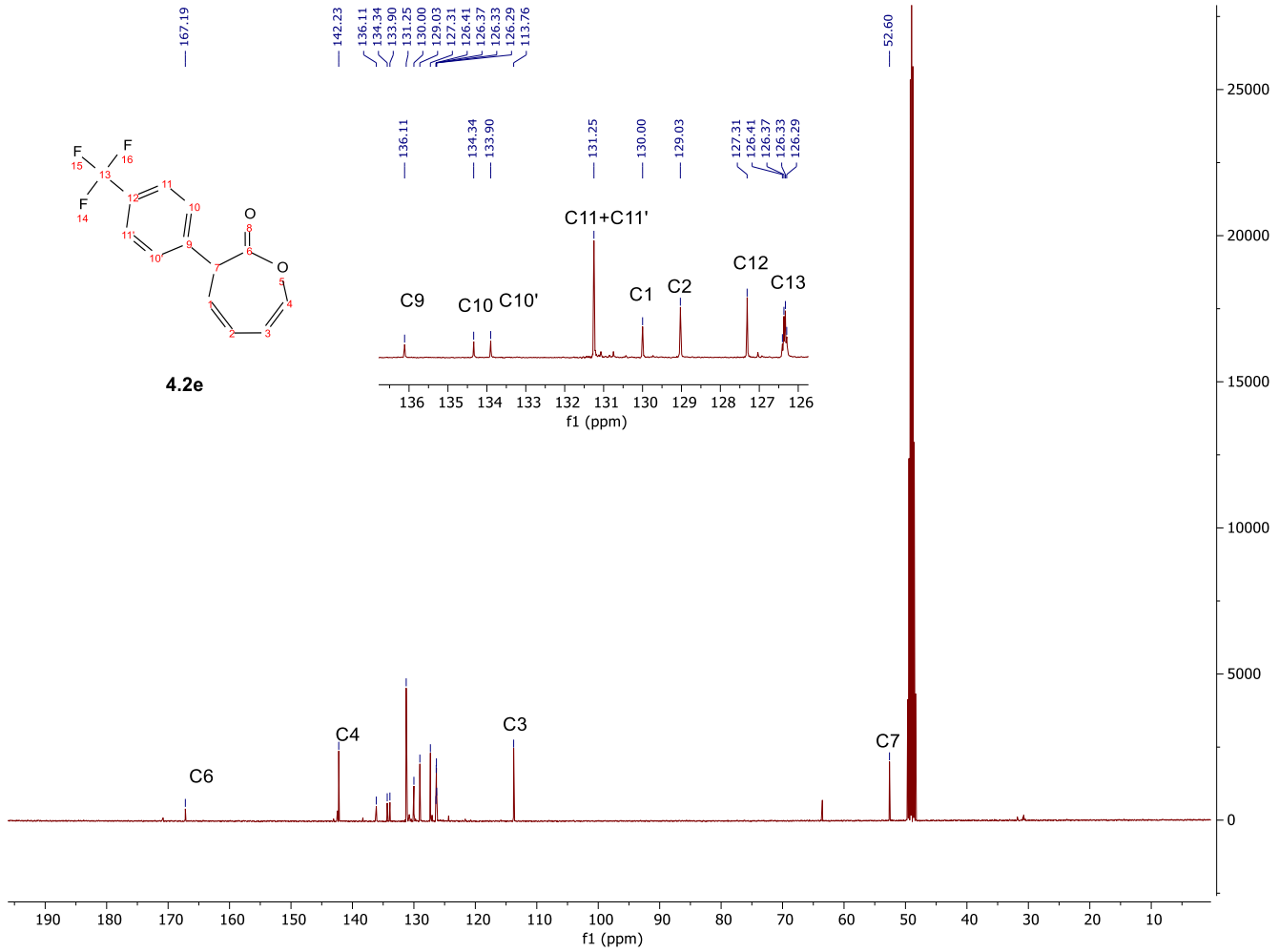


*Figure 4 - 144 ^{13}C NMR of compound **4.2e** in methanol-d_4.*

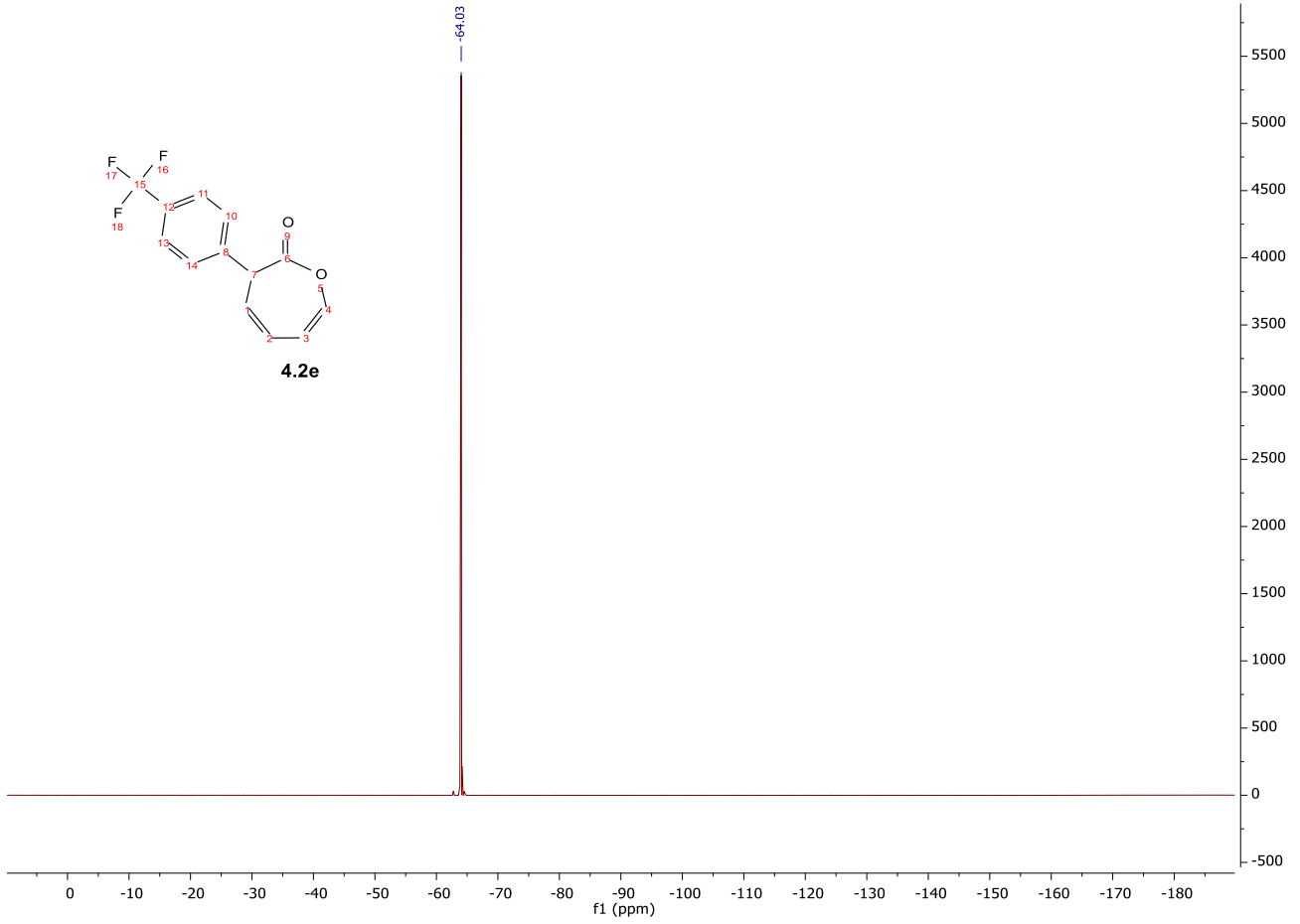


*Figure 4 - 155 ^{19}F NMR of compound **4.2e** in methanol-d_4.*

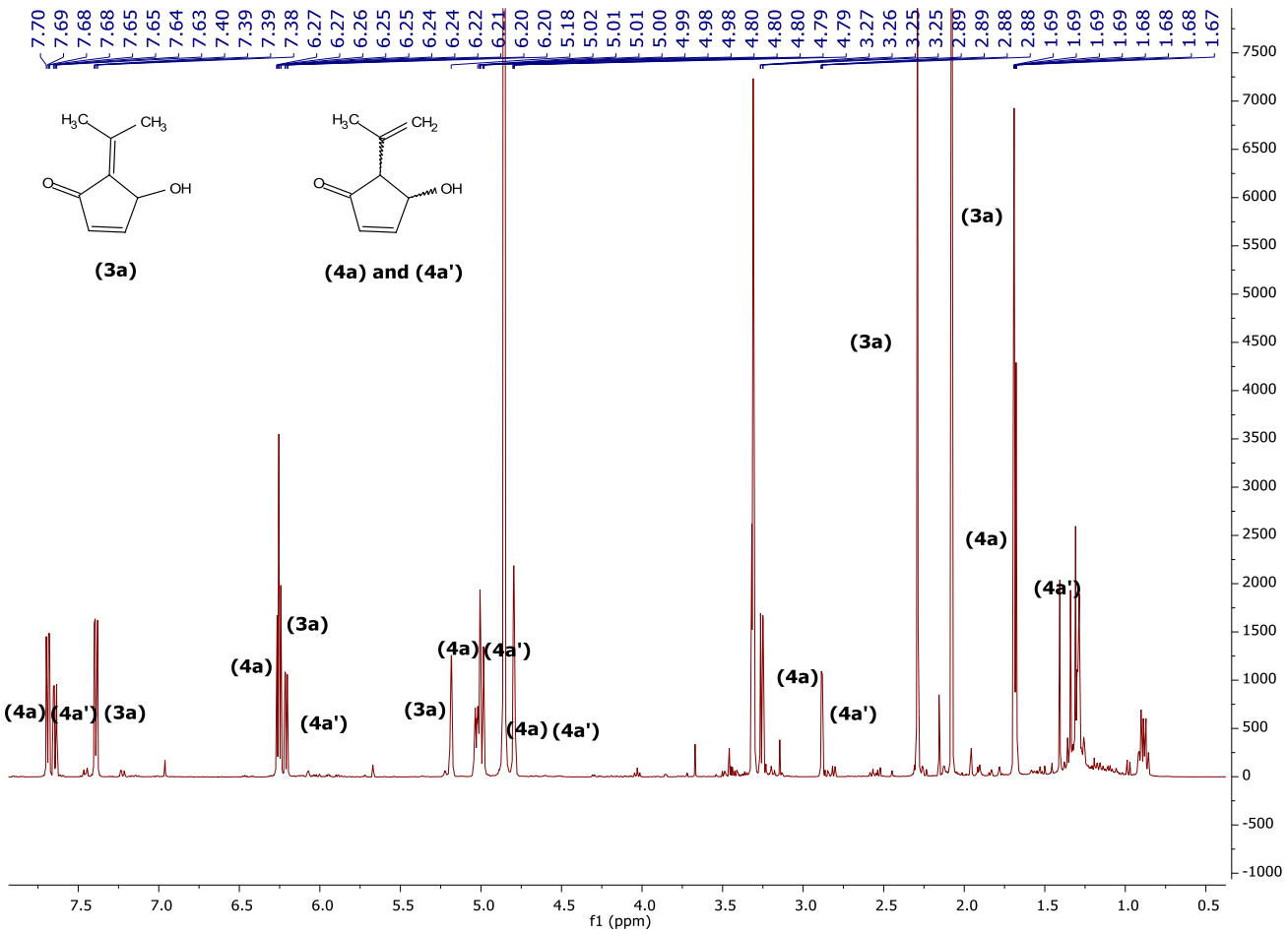


*Figure 4 - 26 ^{1}H NMR of the mixture of compounds **3a** (**4.3a**), **4a** (**4.4a**) and **4a'** (**4.4a'**) in methanol-d$_4$.*

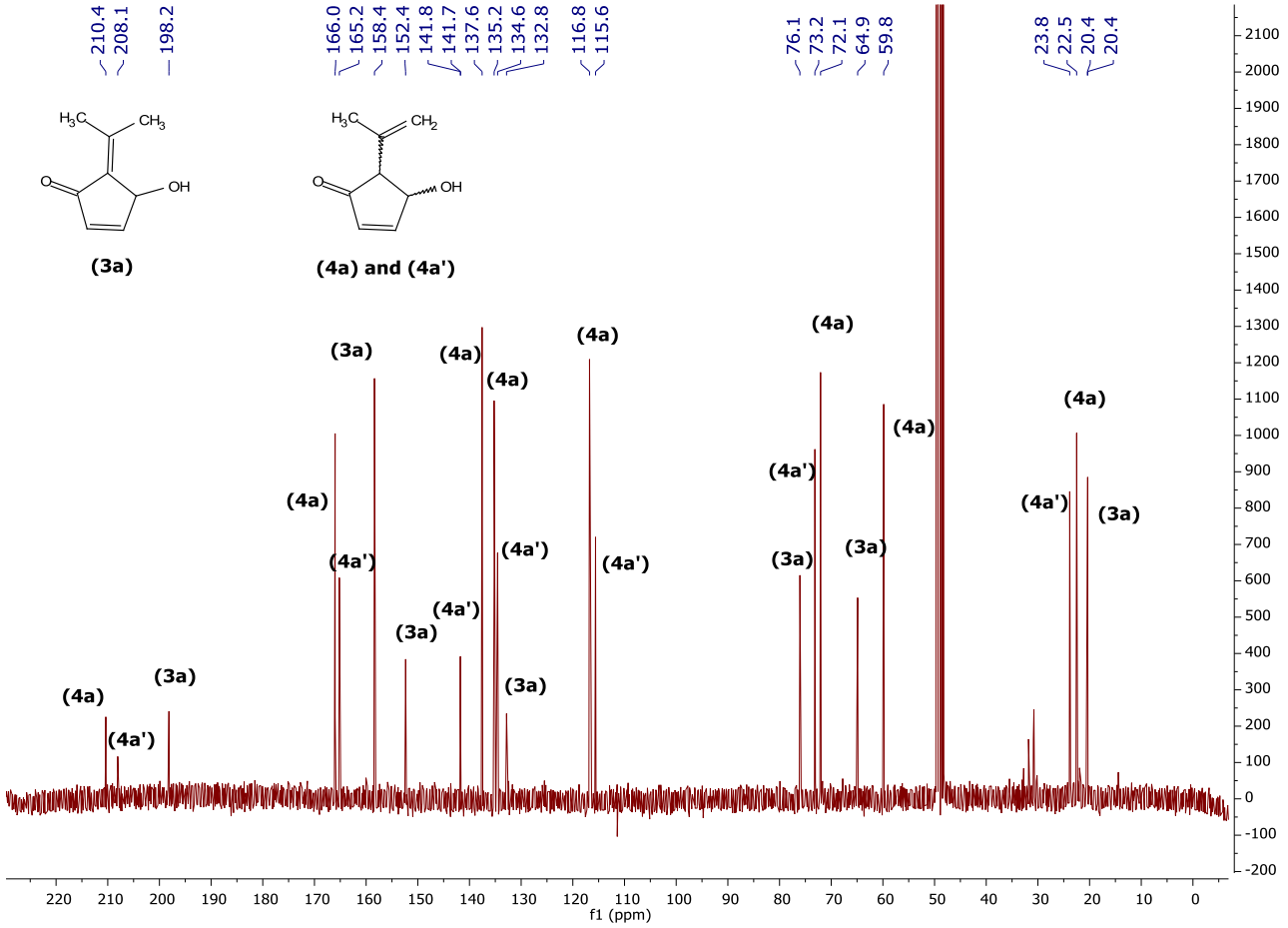


*Figure 4 - 27 ^{13}C NMR of the mixture of compounds **3a** (**4.3a**), **4a** (**4.4a**) and **4a'** (**4.4a'**) in methanol-d_4.*

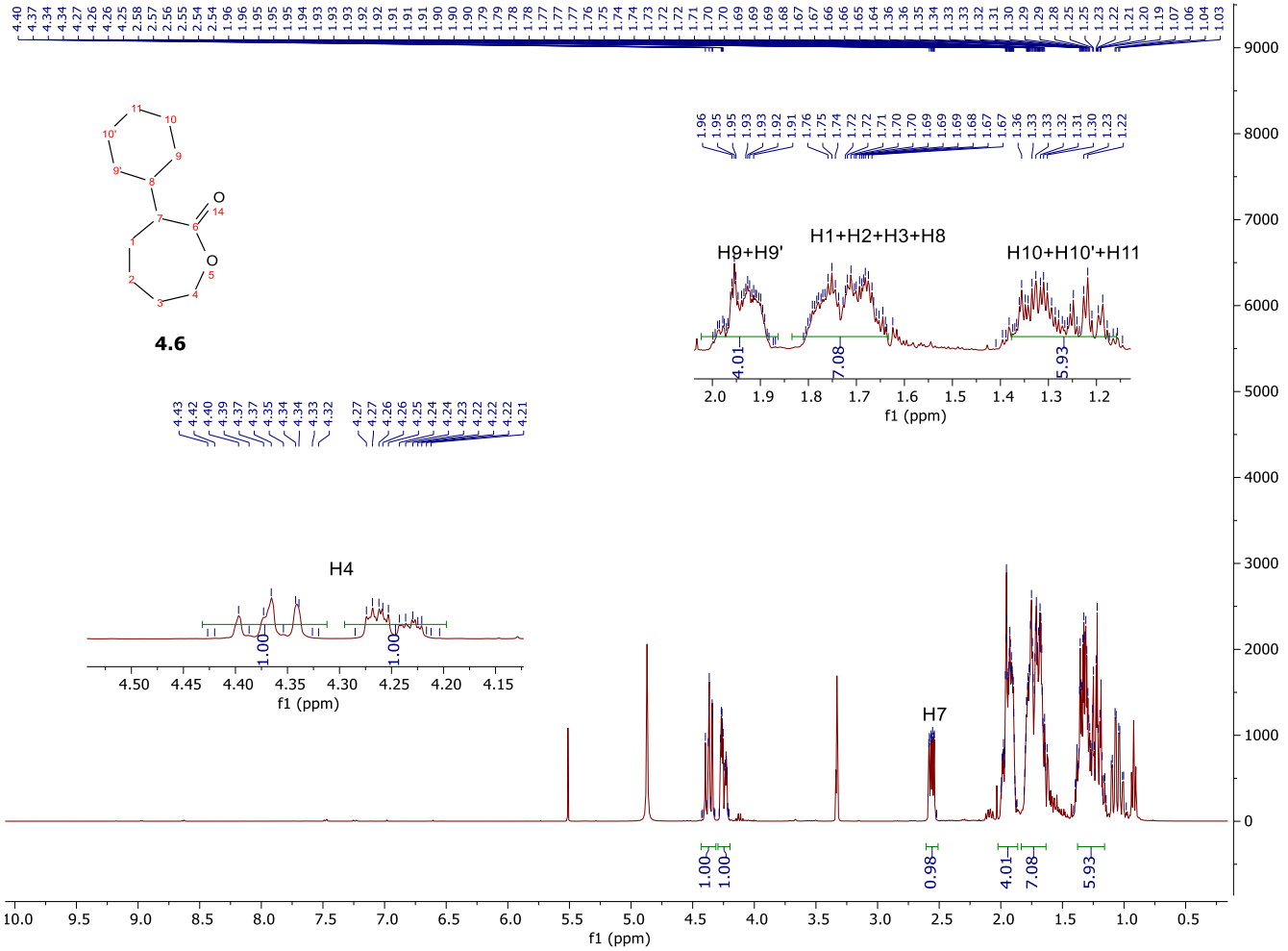


*Figure 4 - 168 ^{1}H NMR of compound **4.6** in methanol-d_4.*

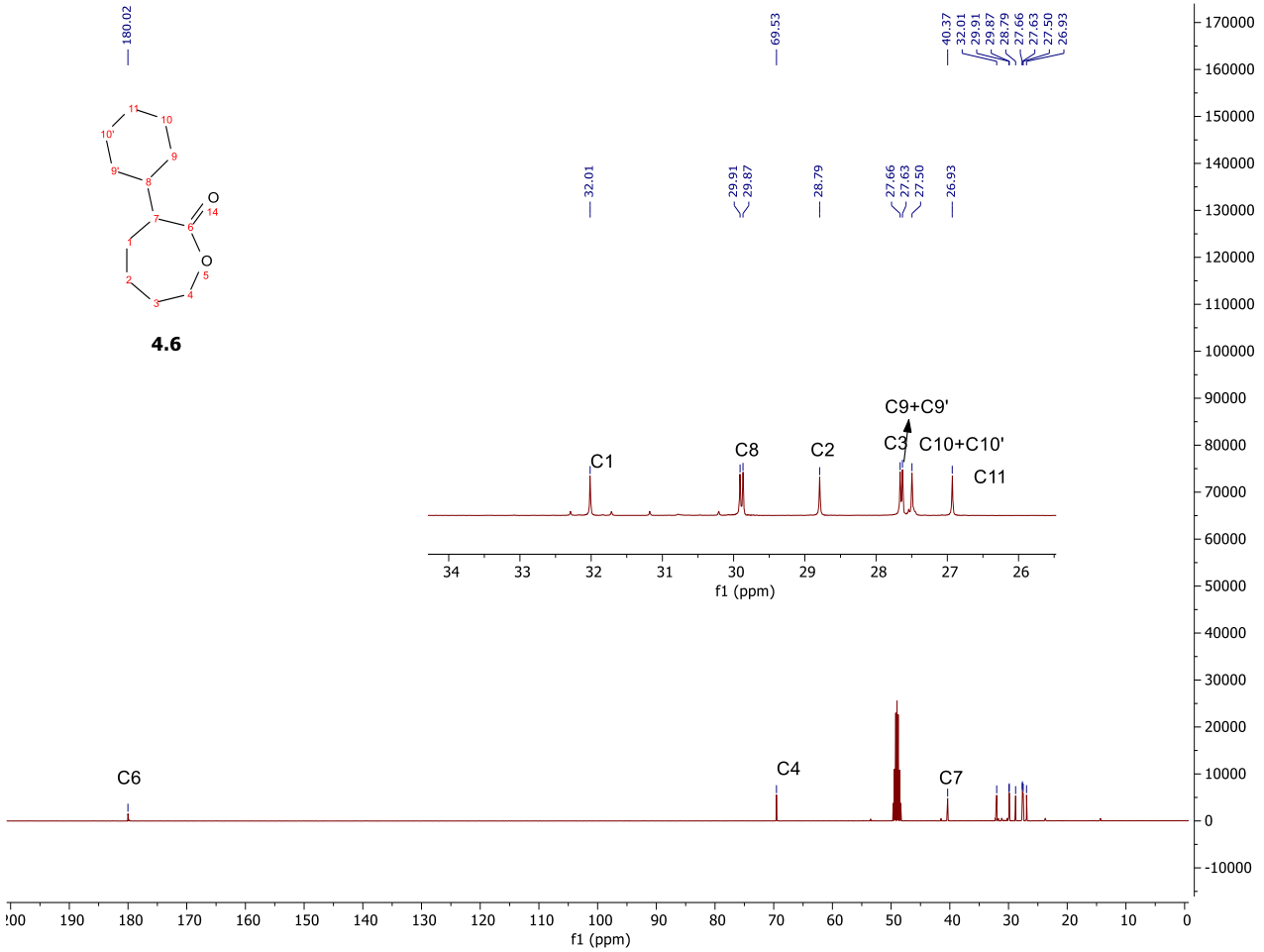


*Figure 4 - 29 ^{13}C NMR of compound **4.6** in methanol-d_4..*

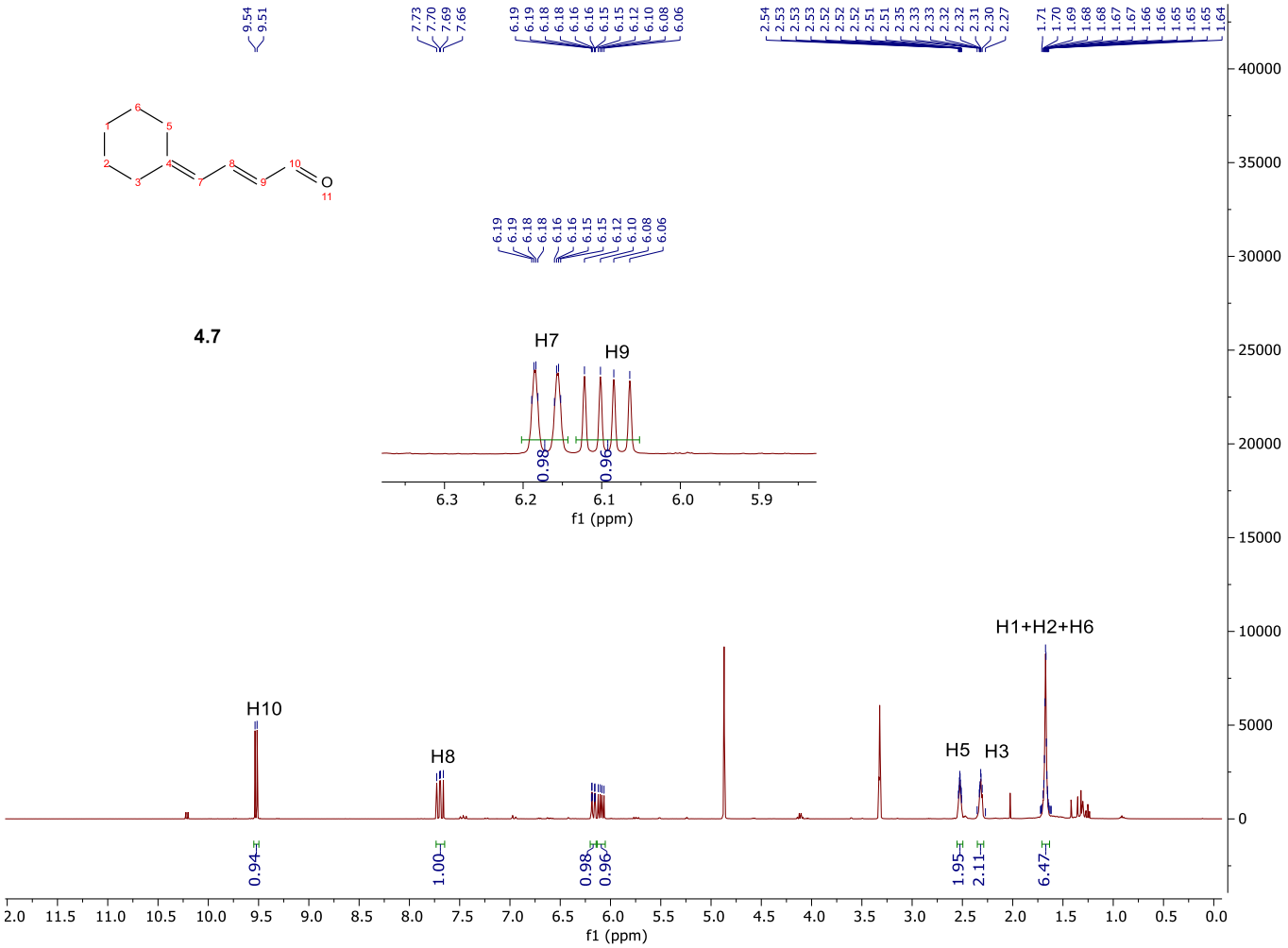


*Figure 4 - 30 ^{1}H NMR of compound **4.7** in methanol-d_4.*

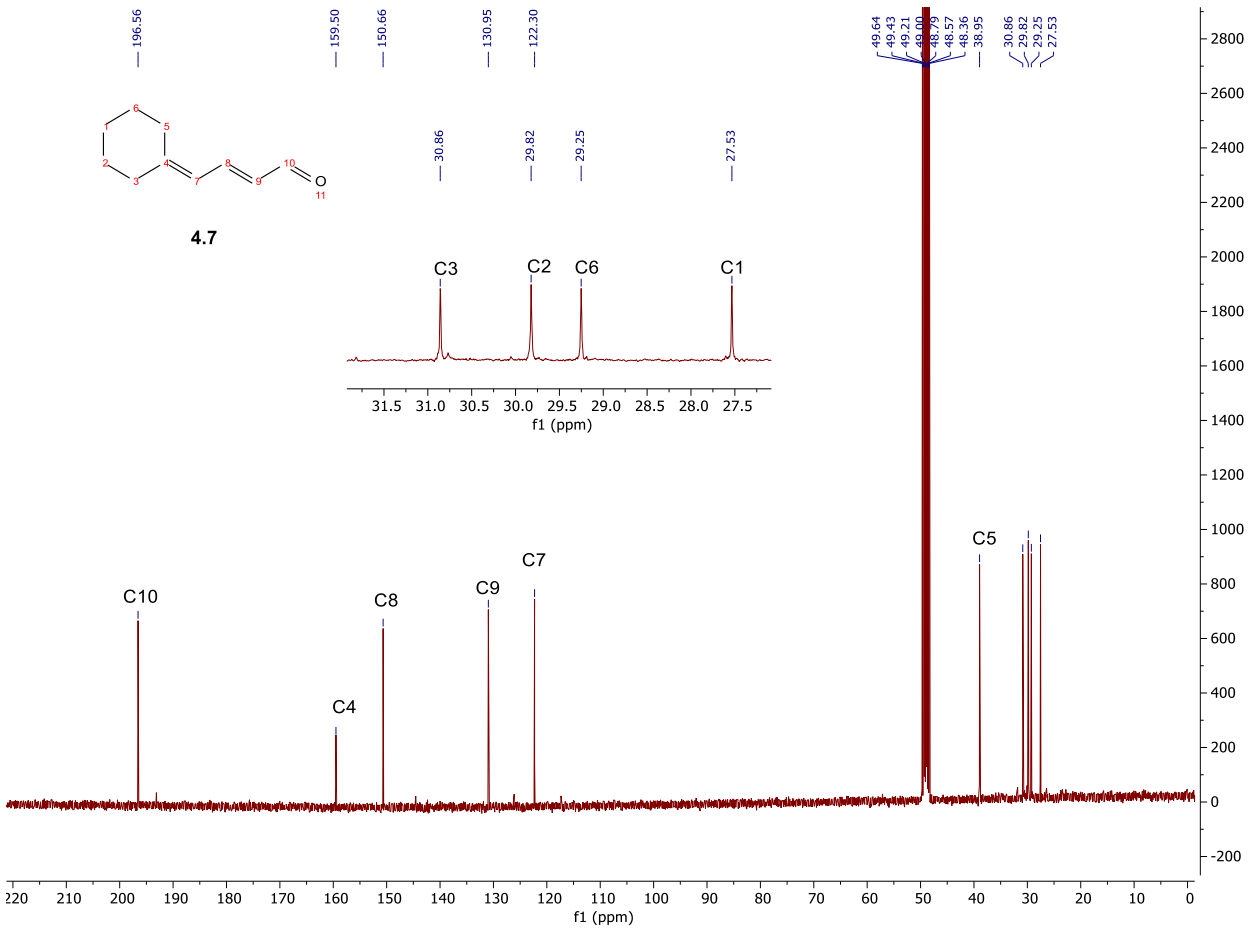


*Figure 4 - 31 ^{13}C NMR of compound **4.7** in methanol-d_4.*

NMR Data (Chapter 5)

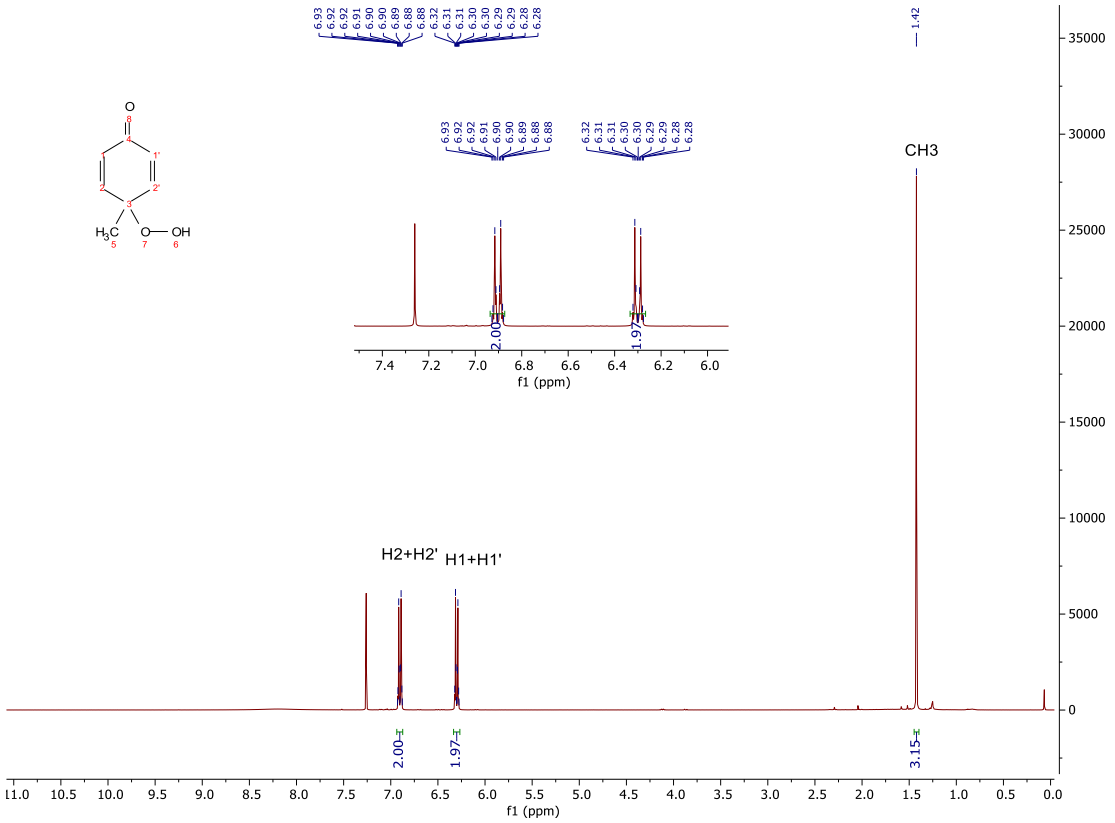


*Figure 5 - 1[1]H NMR of **5.2a** in $CDCl_3$.*

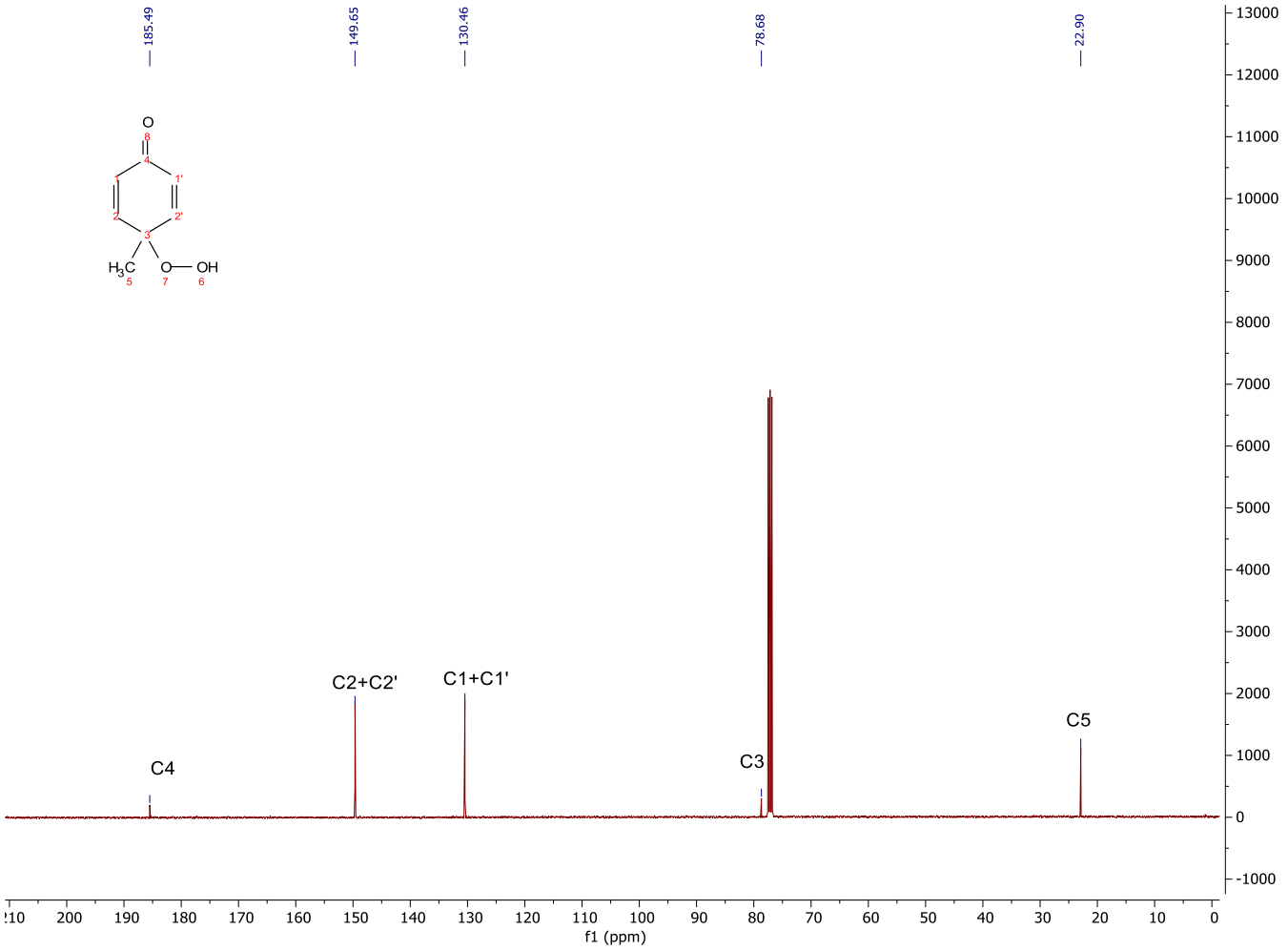


*Figure 5 - 2 ^{13}C NMR of **5.2a** in $CDCl_3$.*

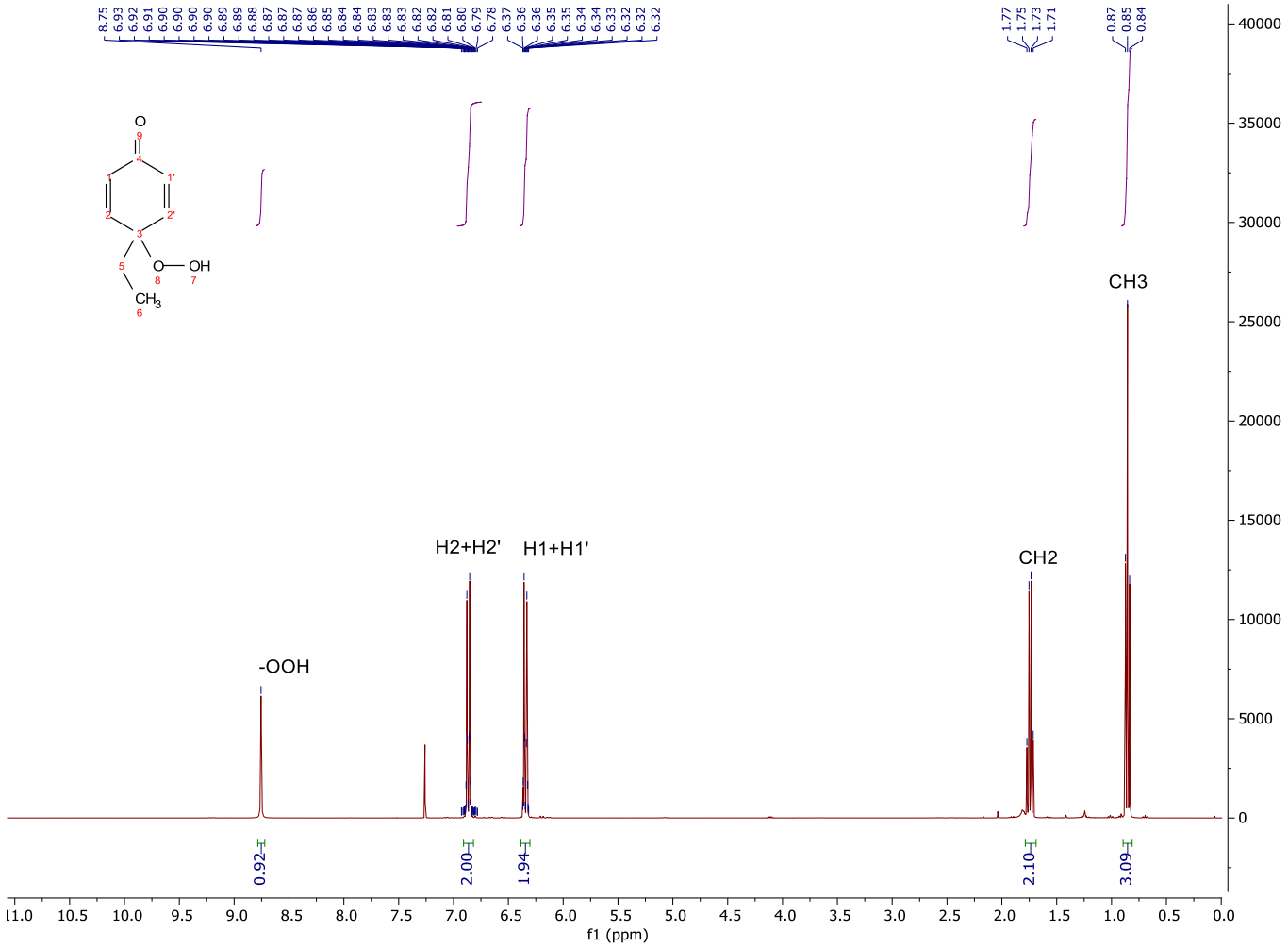


*Figure 5 - 3 ^{1}H NMR of **5.2b** in $CDCl_3$.*

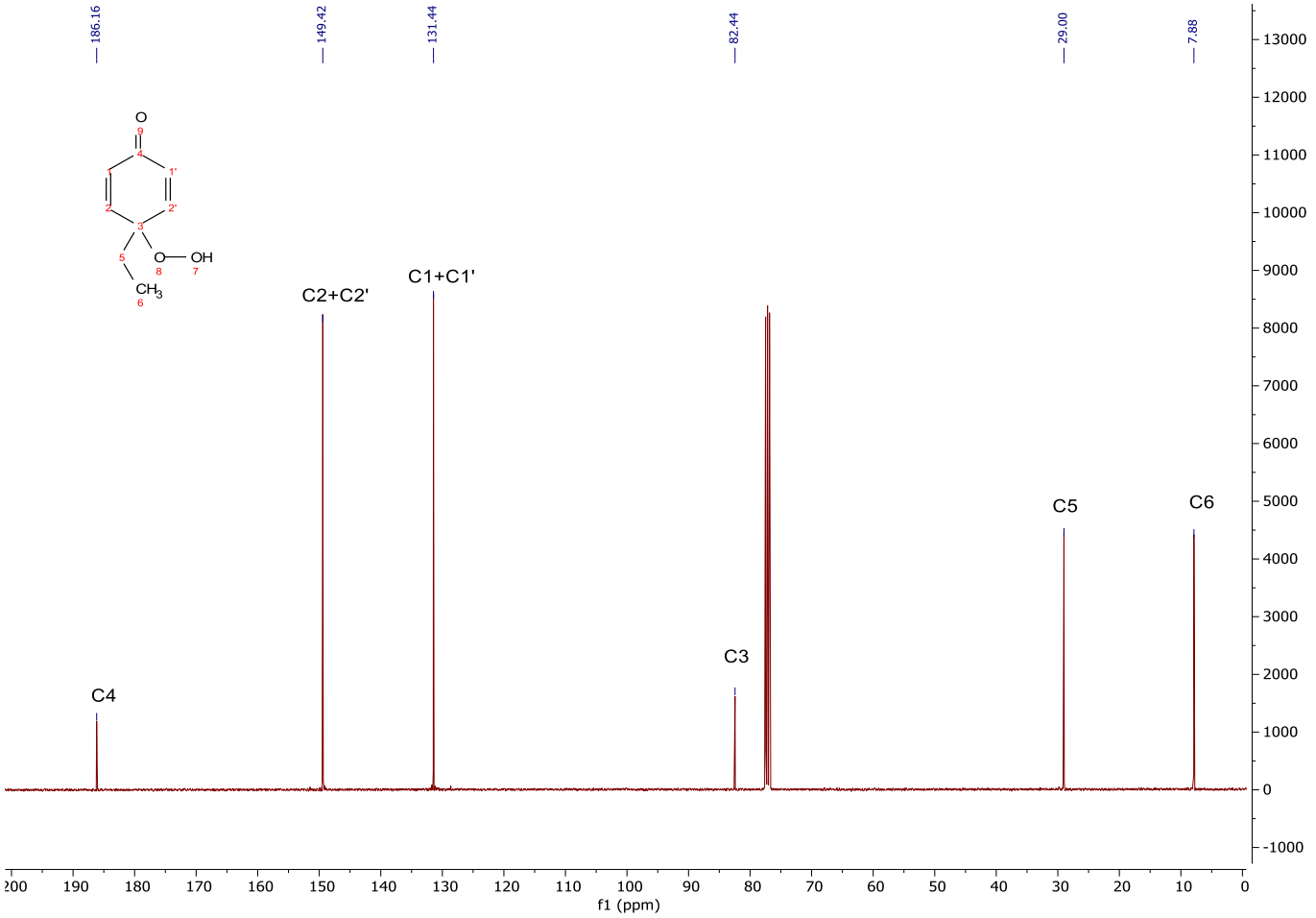


*Figure 5 - 4 ^{13}C NMR of **5.2b** in $CDCl_3$.*

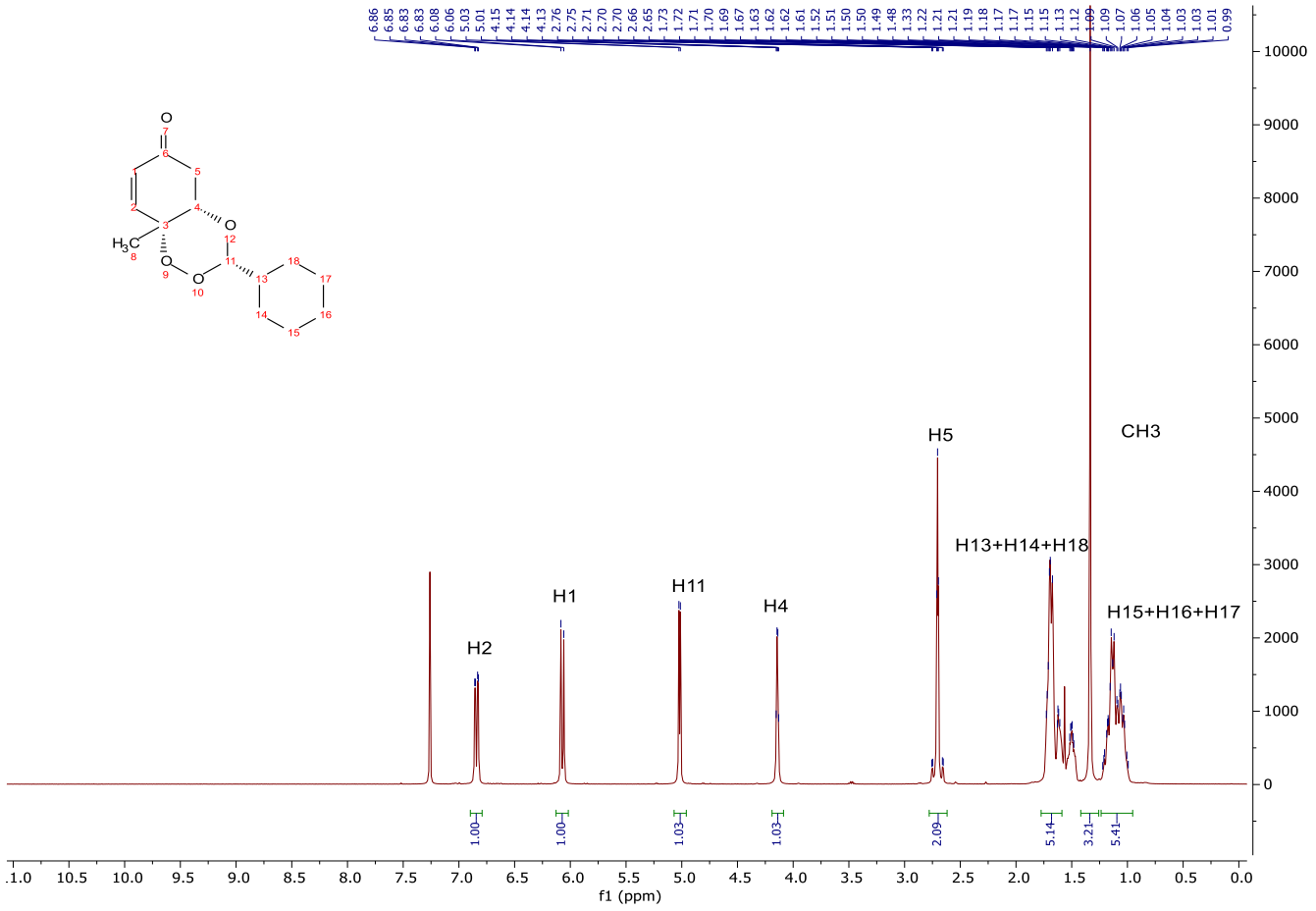


*Figure 5 - 5 ^{1}H NMR of **5.3a** in $CDCl_3$.*

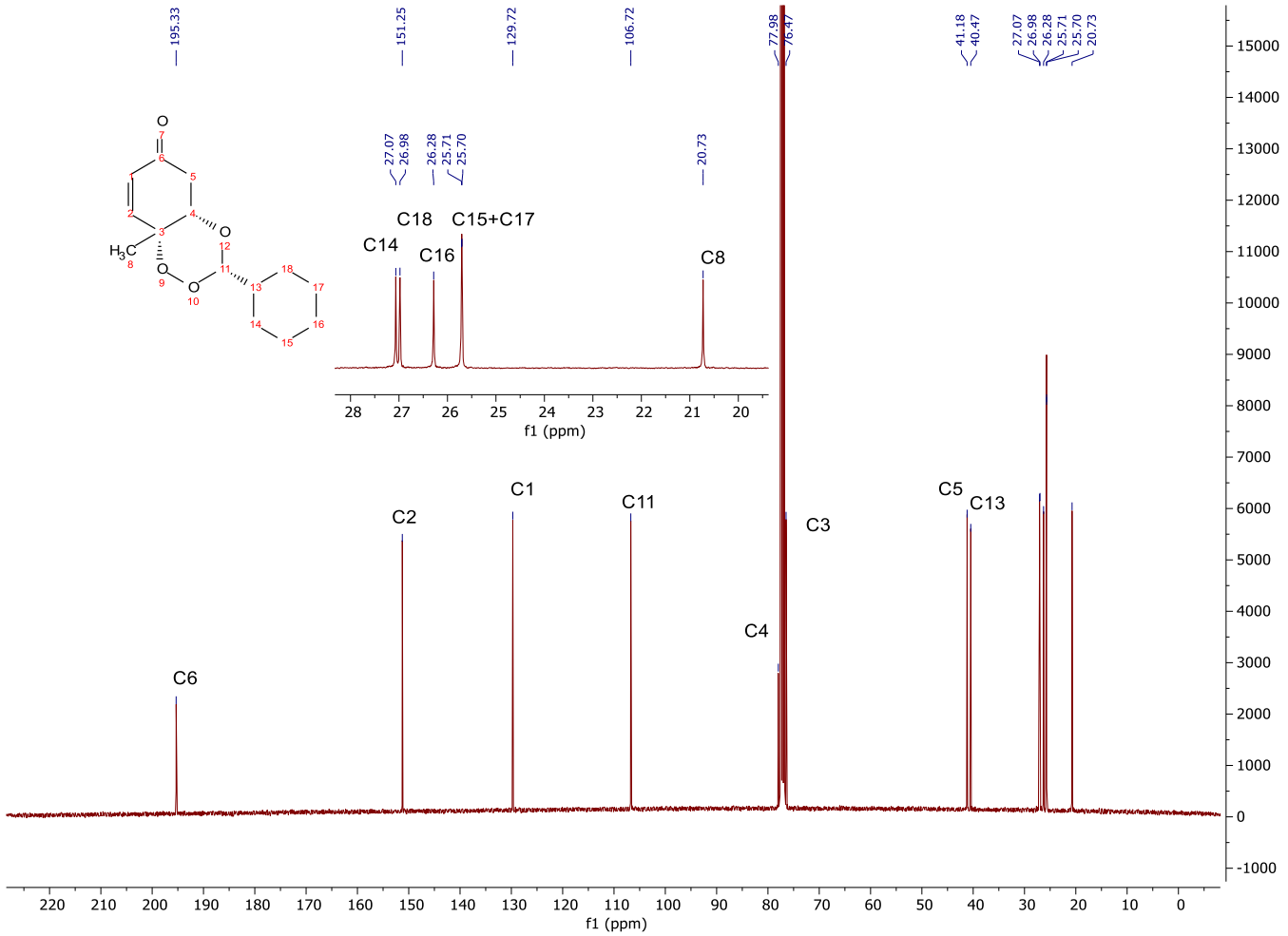


Figure 5 - 6 *^{13}C NMR of **5.3a** in $CDCl_3$.*

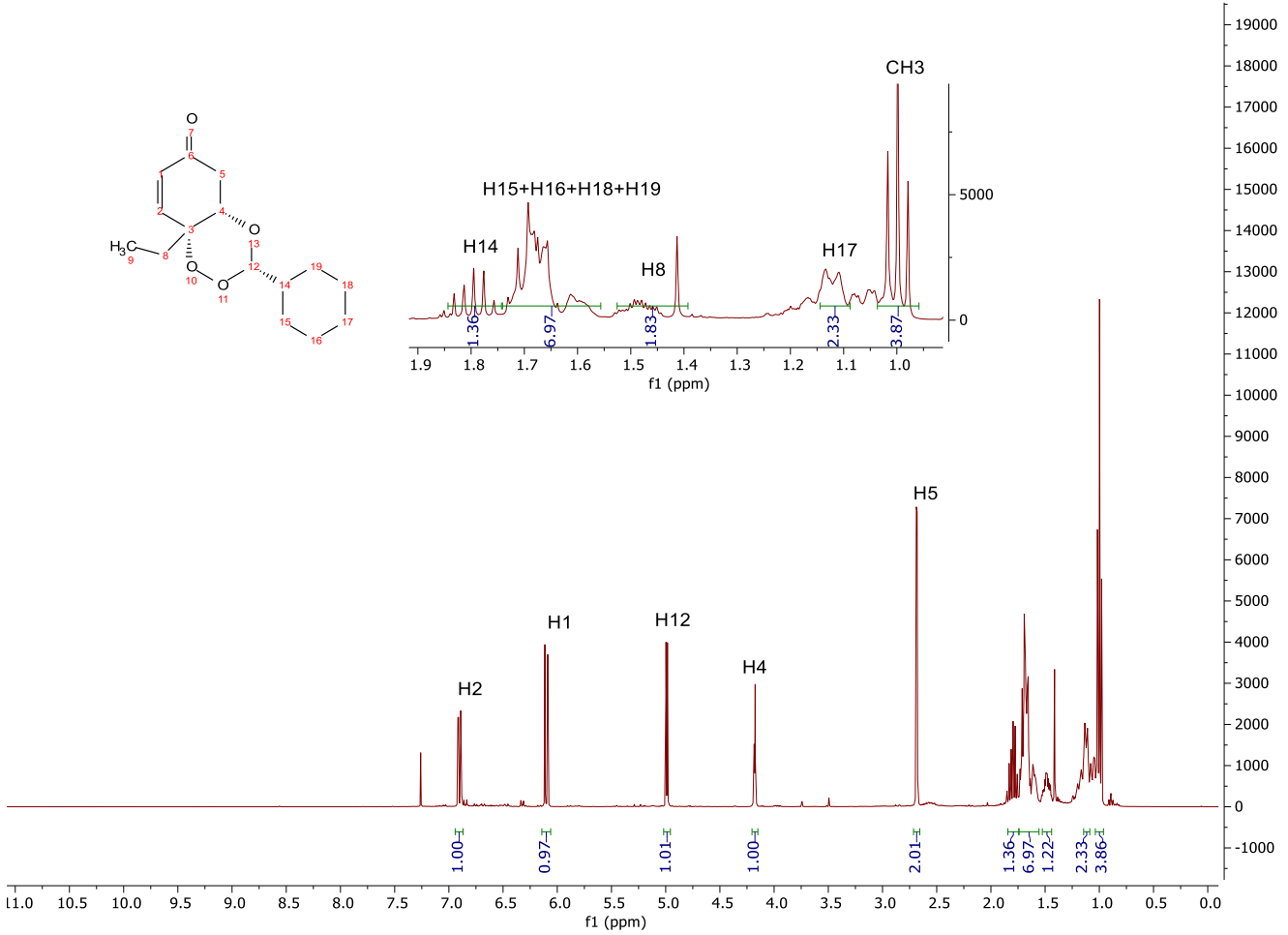


*Figure 5 - 7 ^{1}H NMR of **5.3b** in $CDCl_3$.*

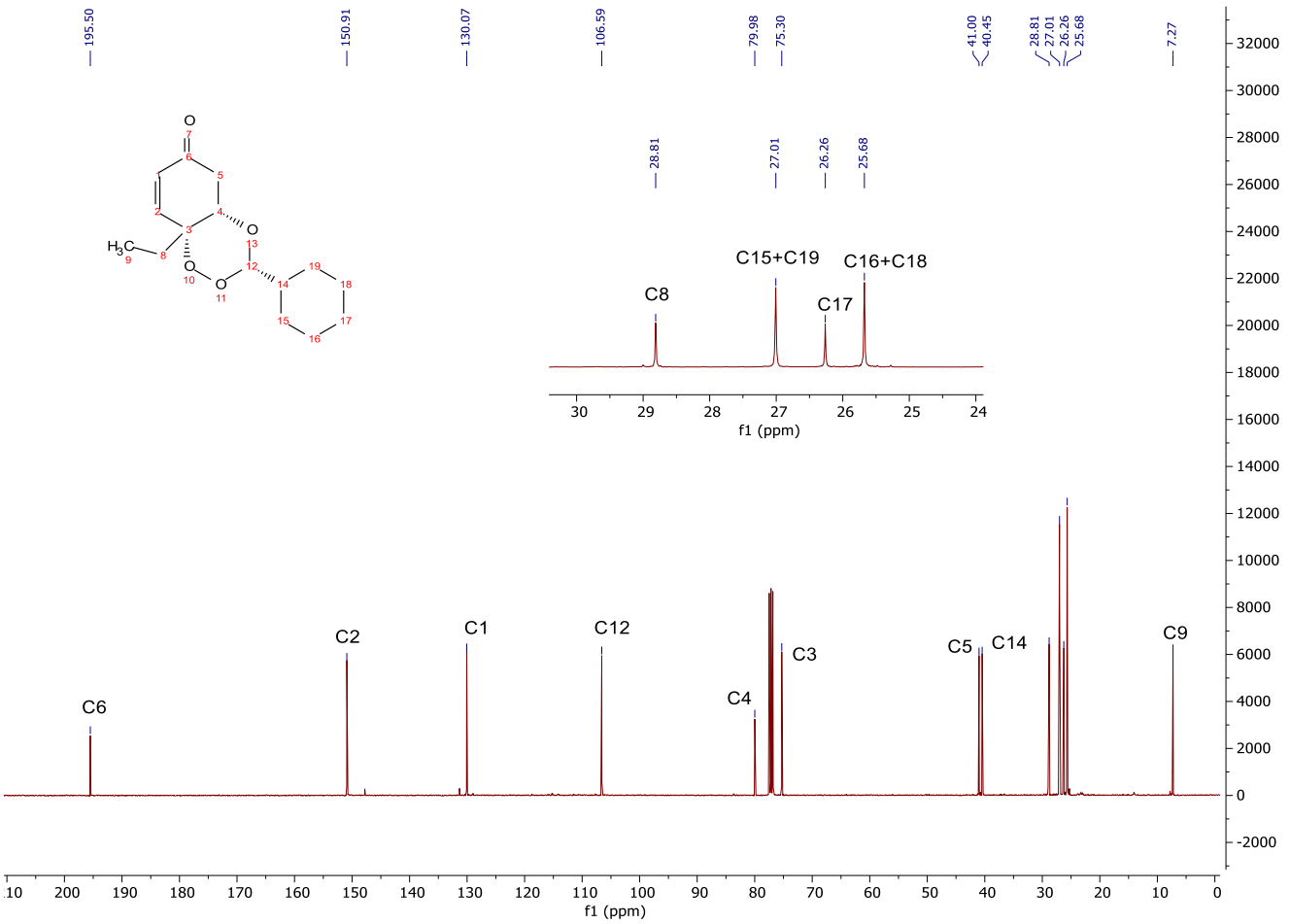


*Figure 5 - 8 ^{13}C NMR of **5.3b** in $CDCl_3$.*

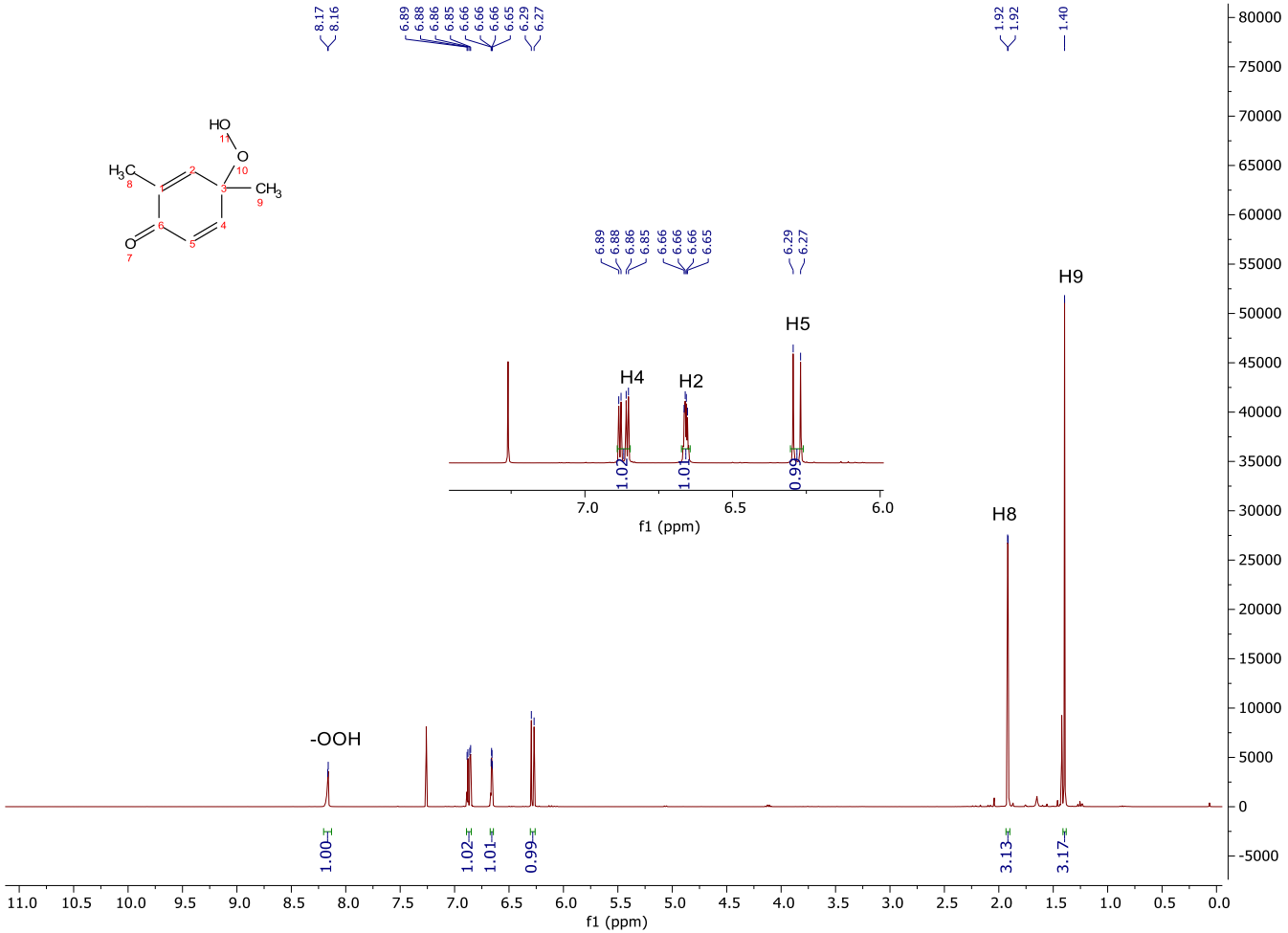


*Figure 5 - 9 ^1H NMR of **5.2c** in $CDCl_3$.*

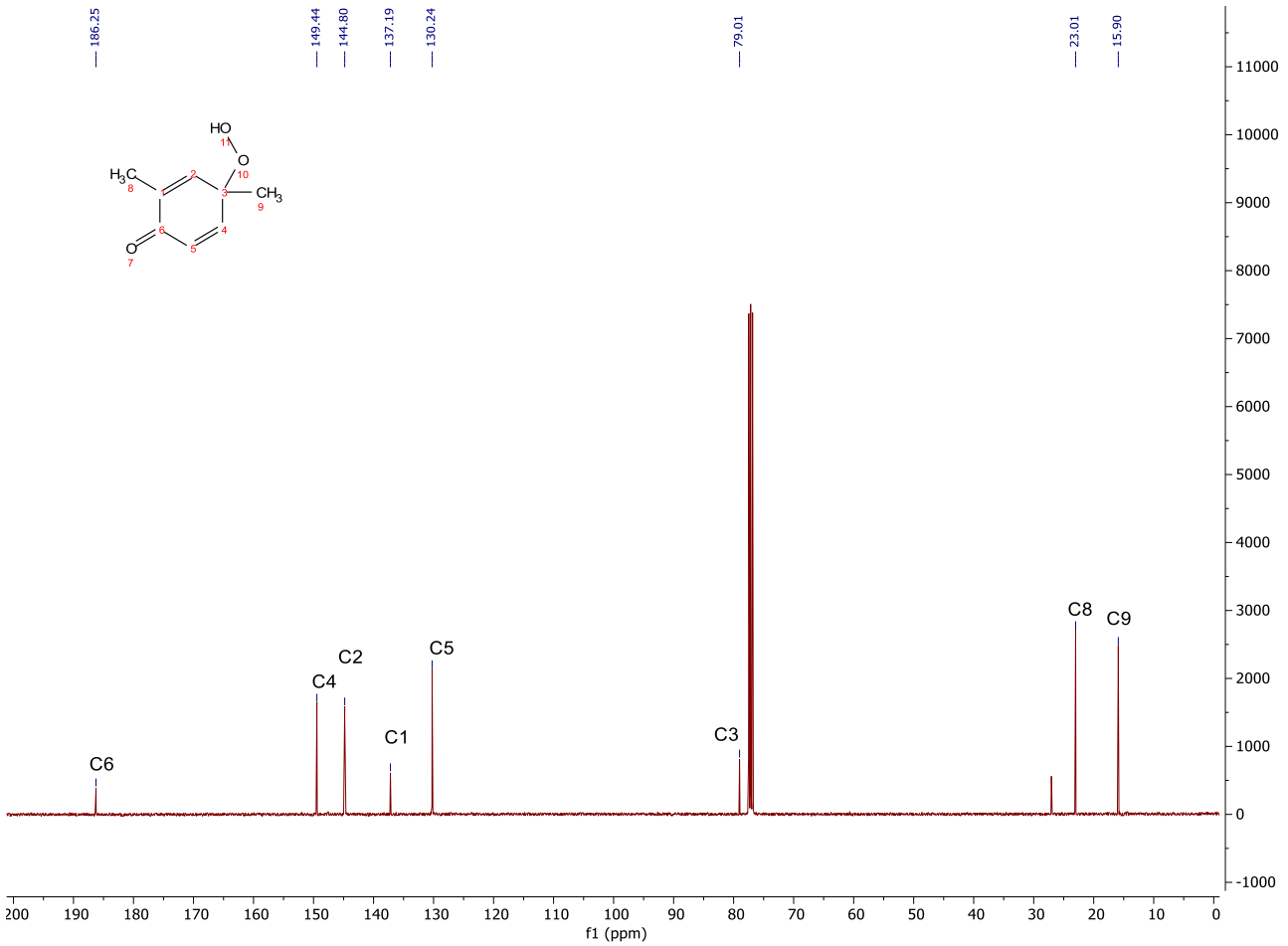


*Figure 5 - 10 ^{13}C NMR of **5.2c** in $CDCl_3$.*

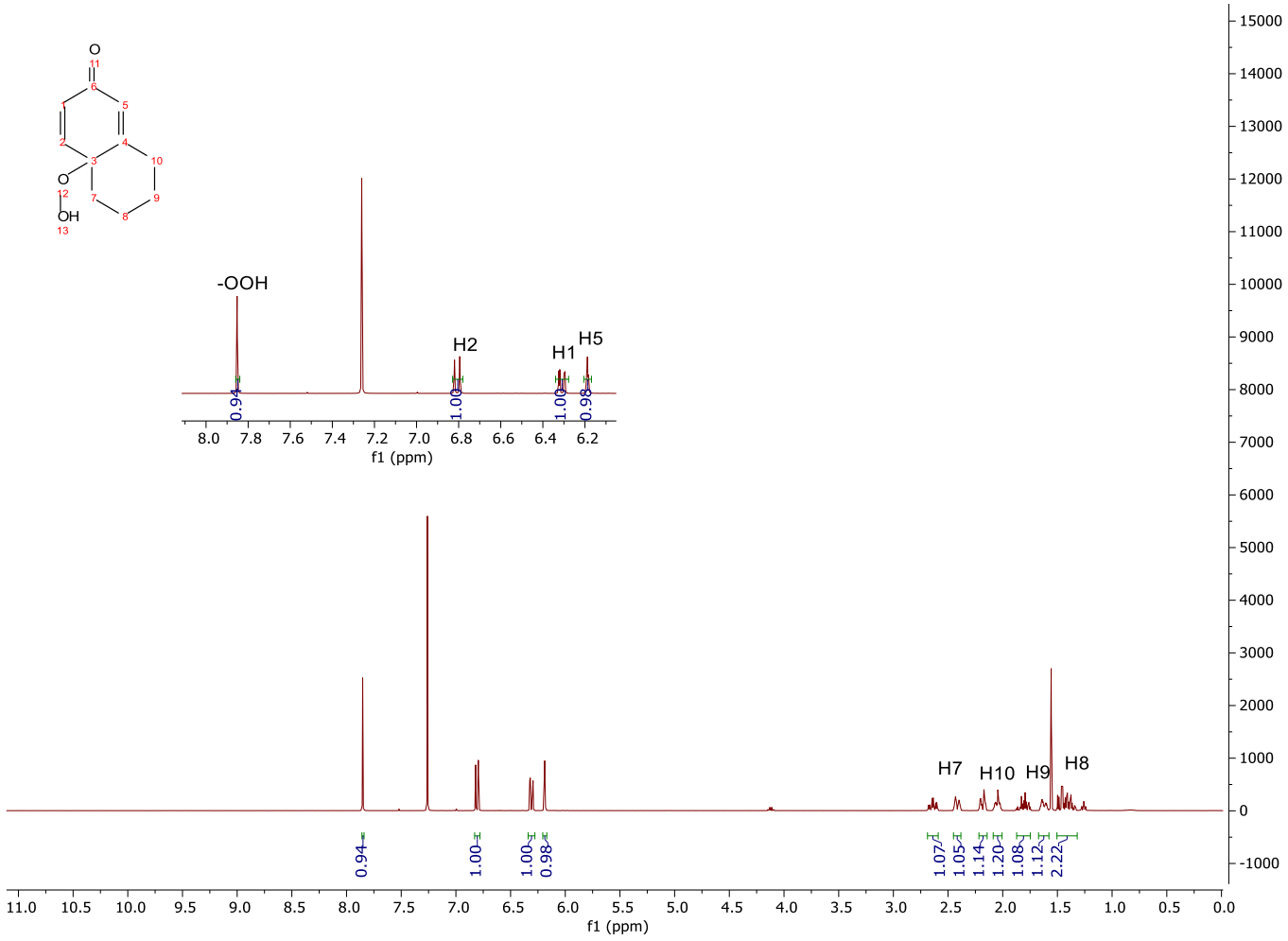


*Figure 5 - 11 ^{1}H NMR of **5.2d** in $CDCl_3$.*

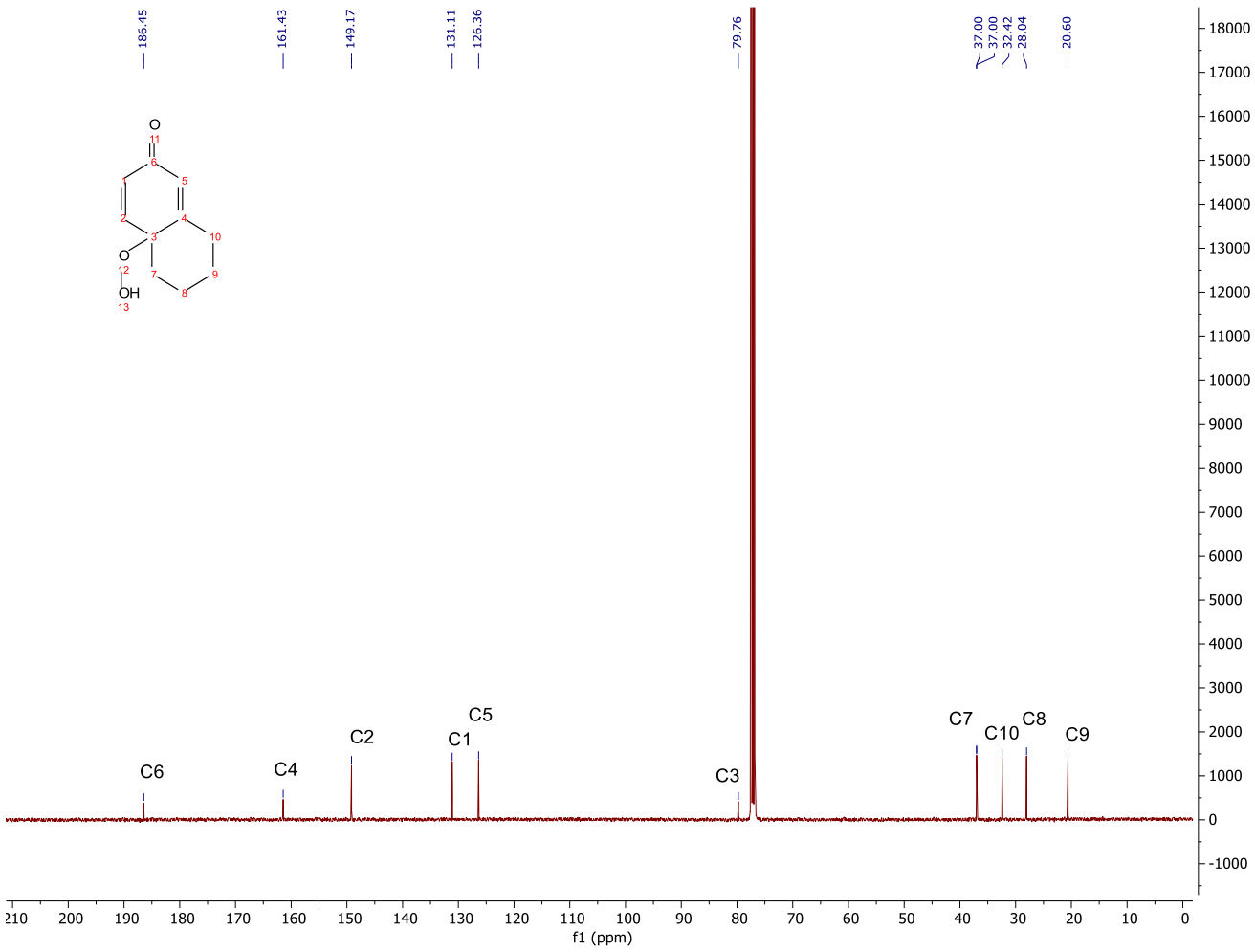


*Figure 5 - 12 ^{13}C NMR of **5.2d** in $CDCl_3$.*

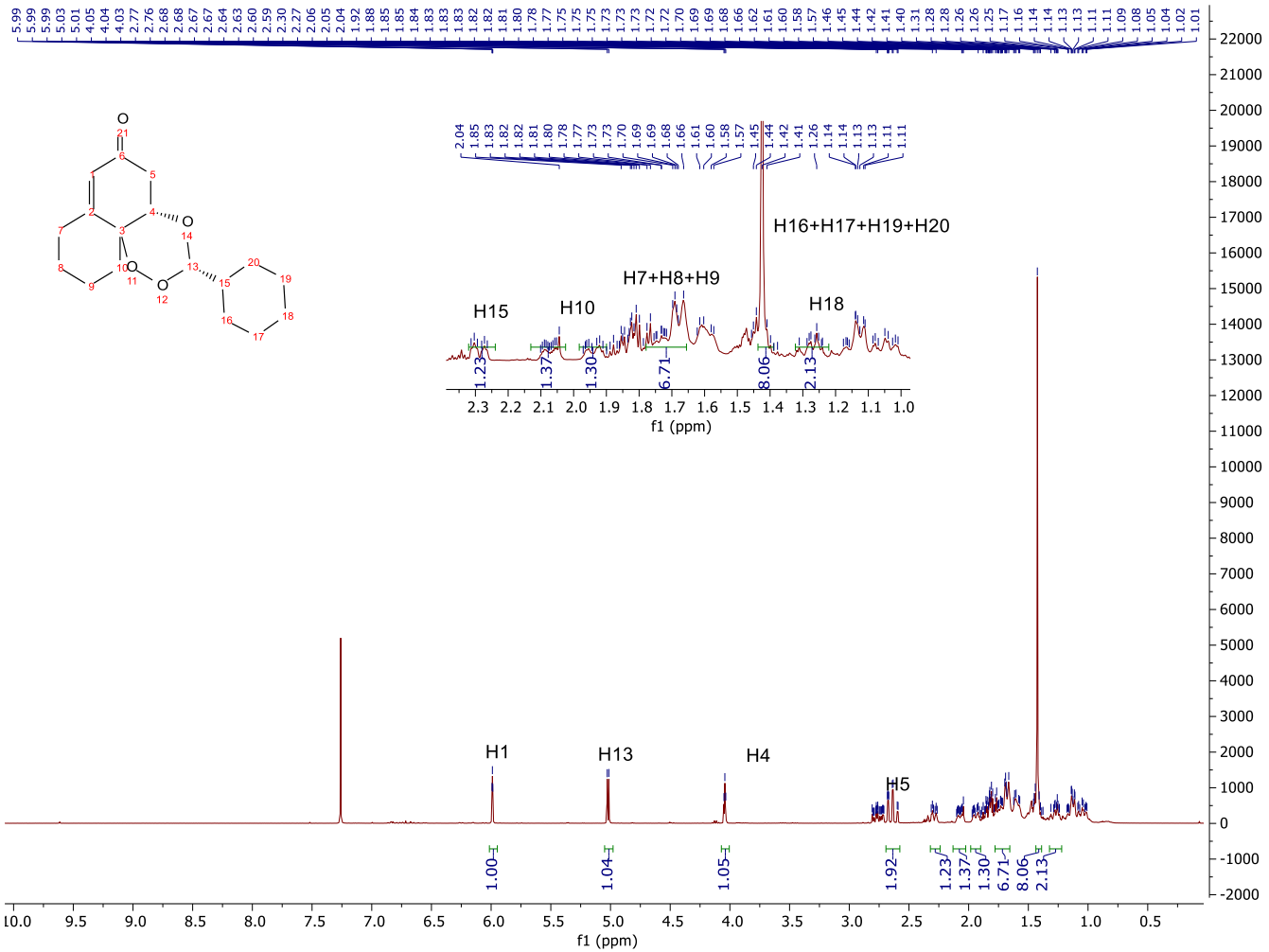


*Figure 5 - 13 ^{1}H NMR of **5.3d** in $CDCl_3$.*

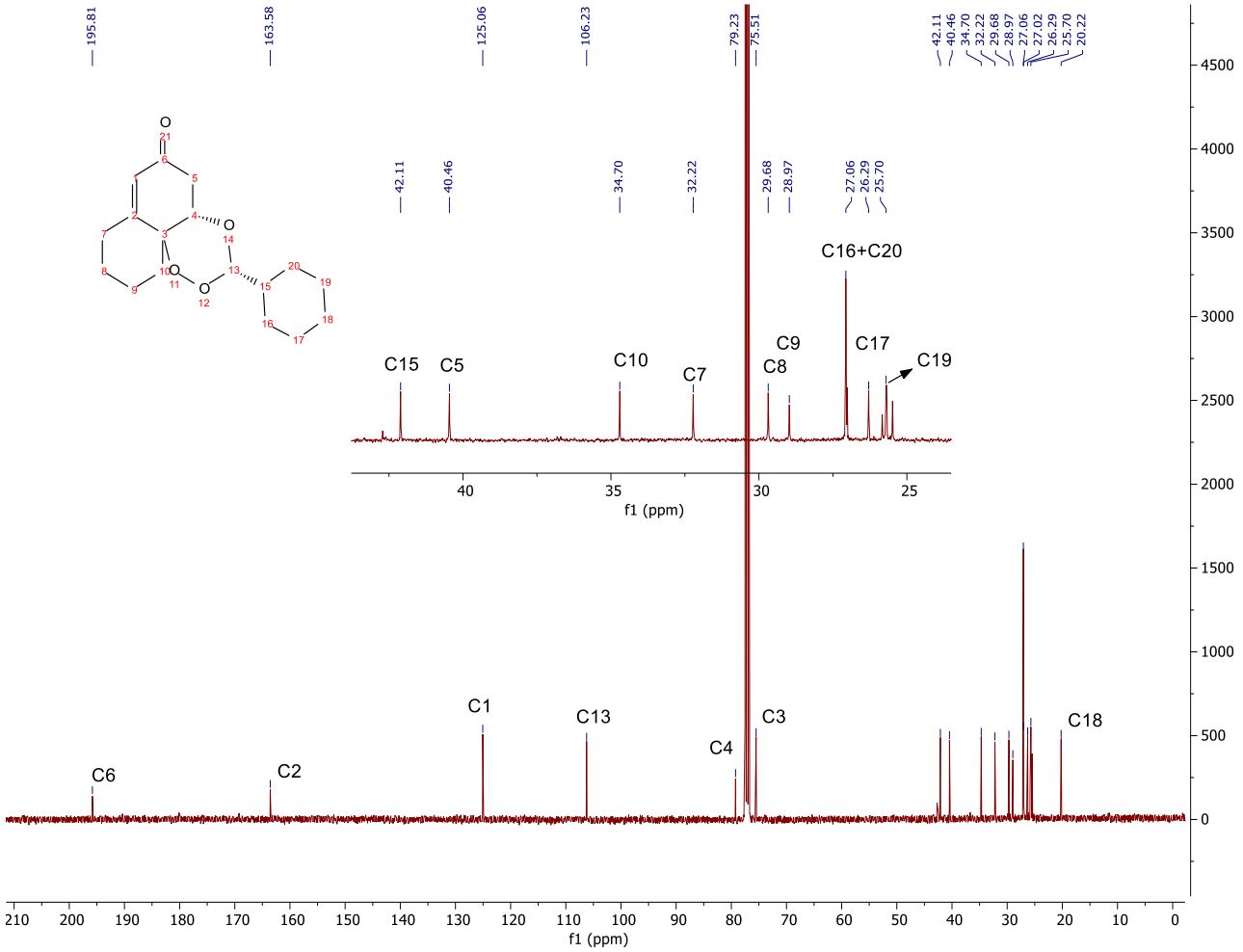


*Figure 5 - 14 ^{13}C NMR of **5.3d** in $CDCl_3$.*

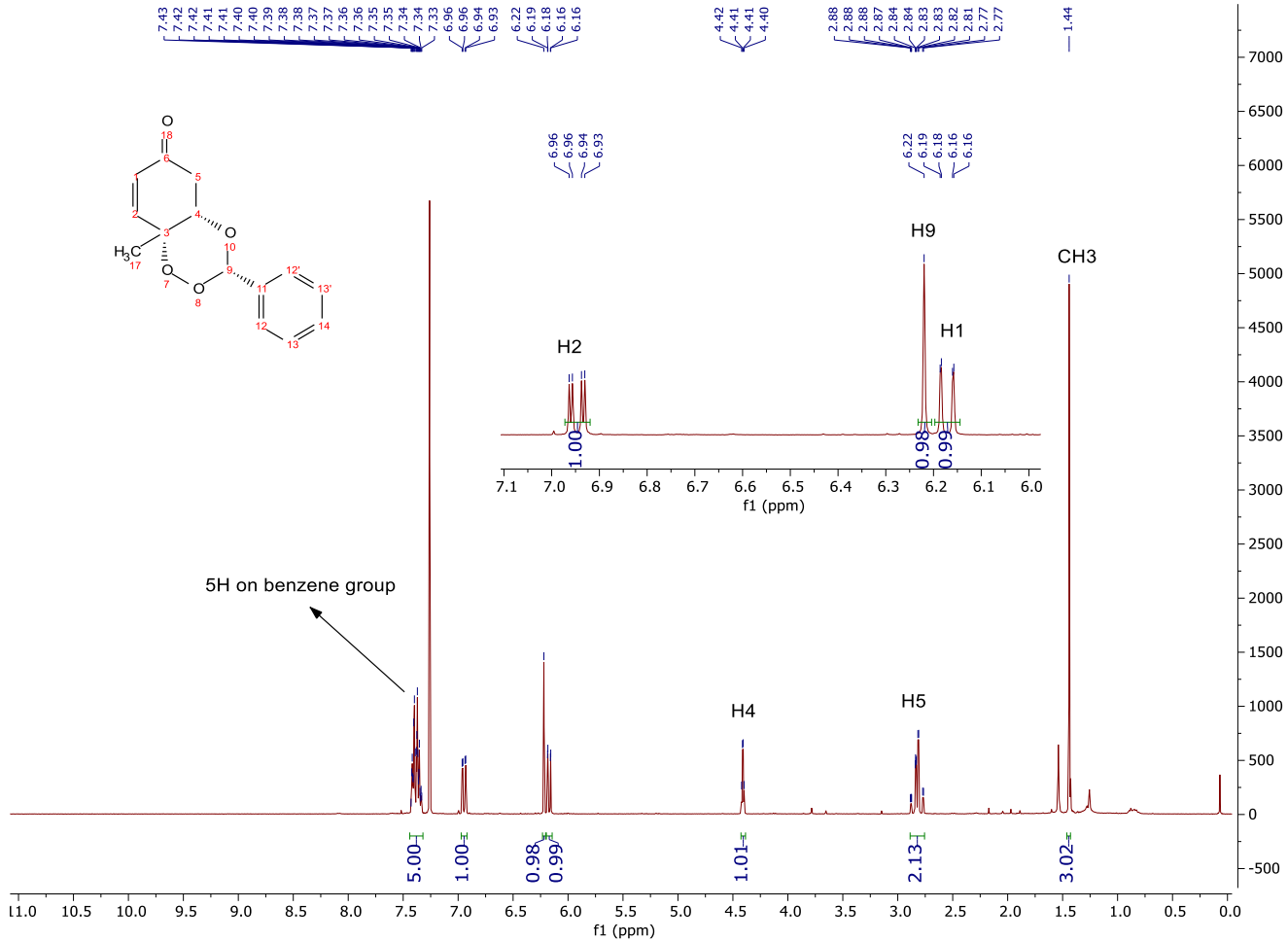


*Figure 5 - 15 ^{1}H NMR of **5.4a** in $CDCl_3$.*

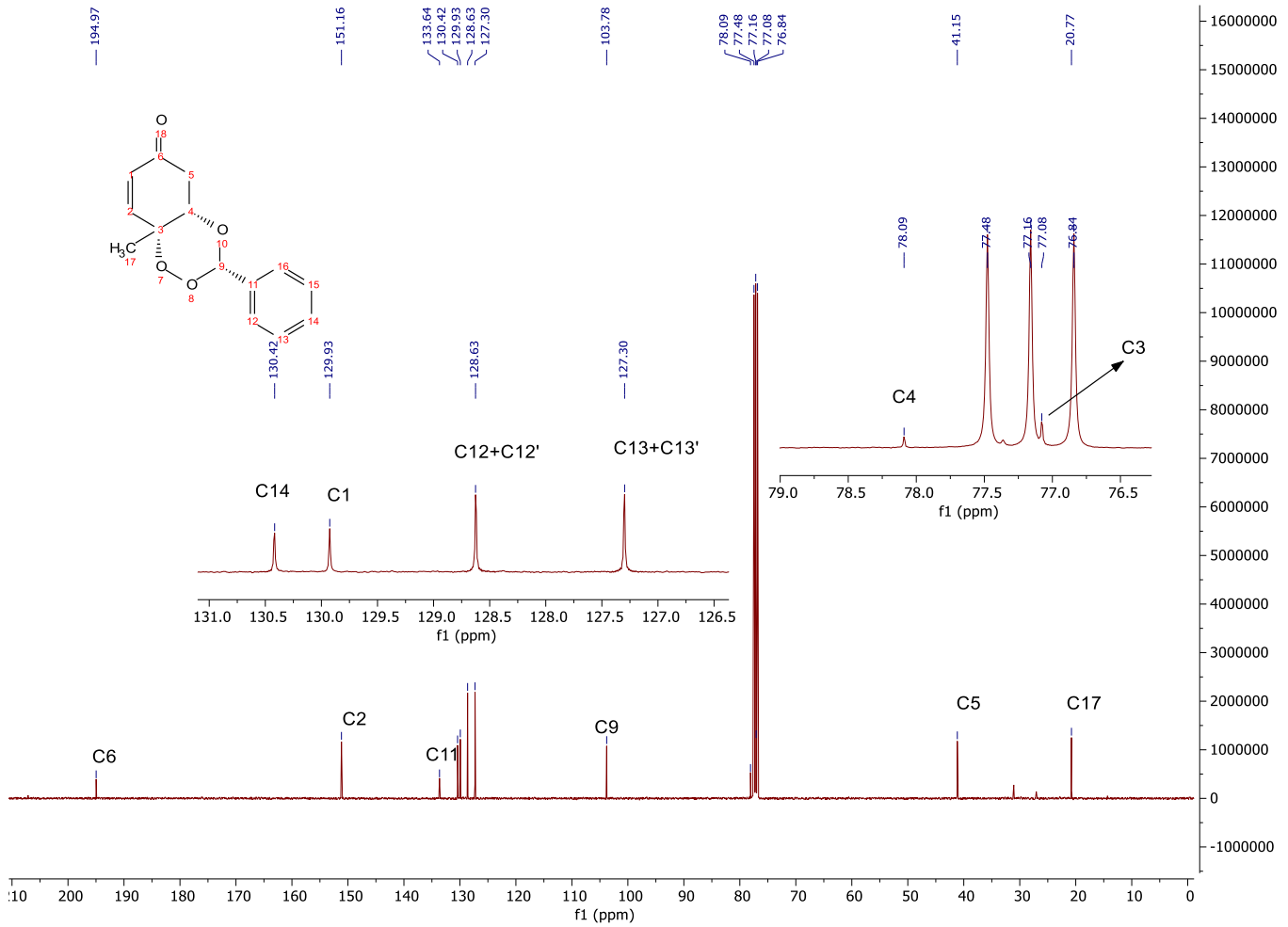


*Figure 5 - 16 ^{13}C NMR of **5.4a** in $CDCl_3$.*

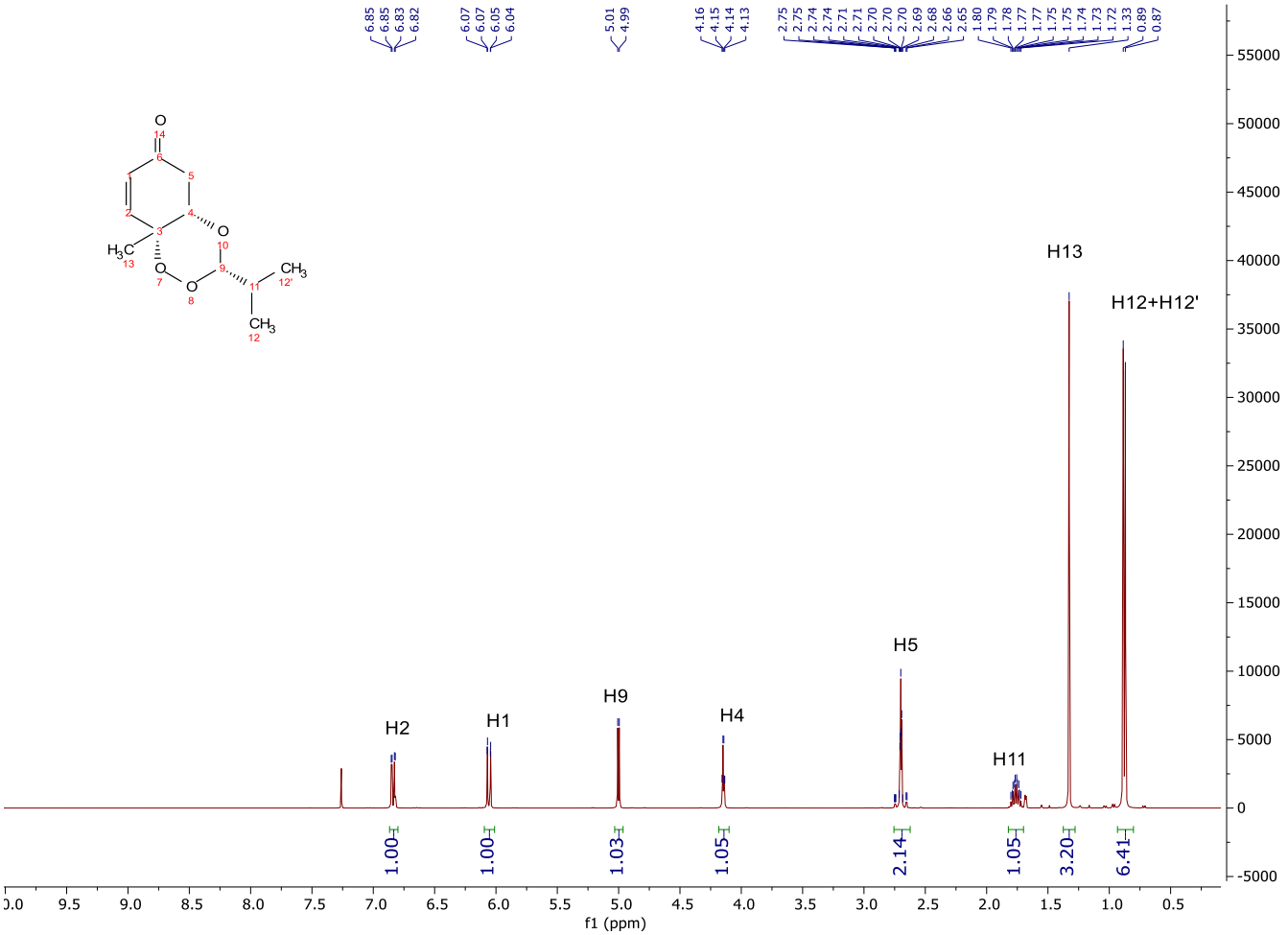


*Figure 5 - 17 ^{1}H NMR of **5.5a** in $CDCl_3$.*

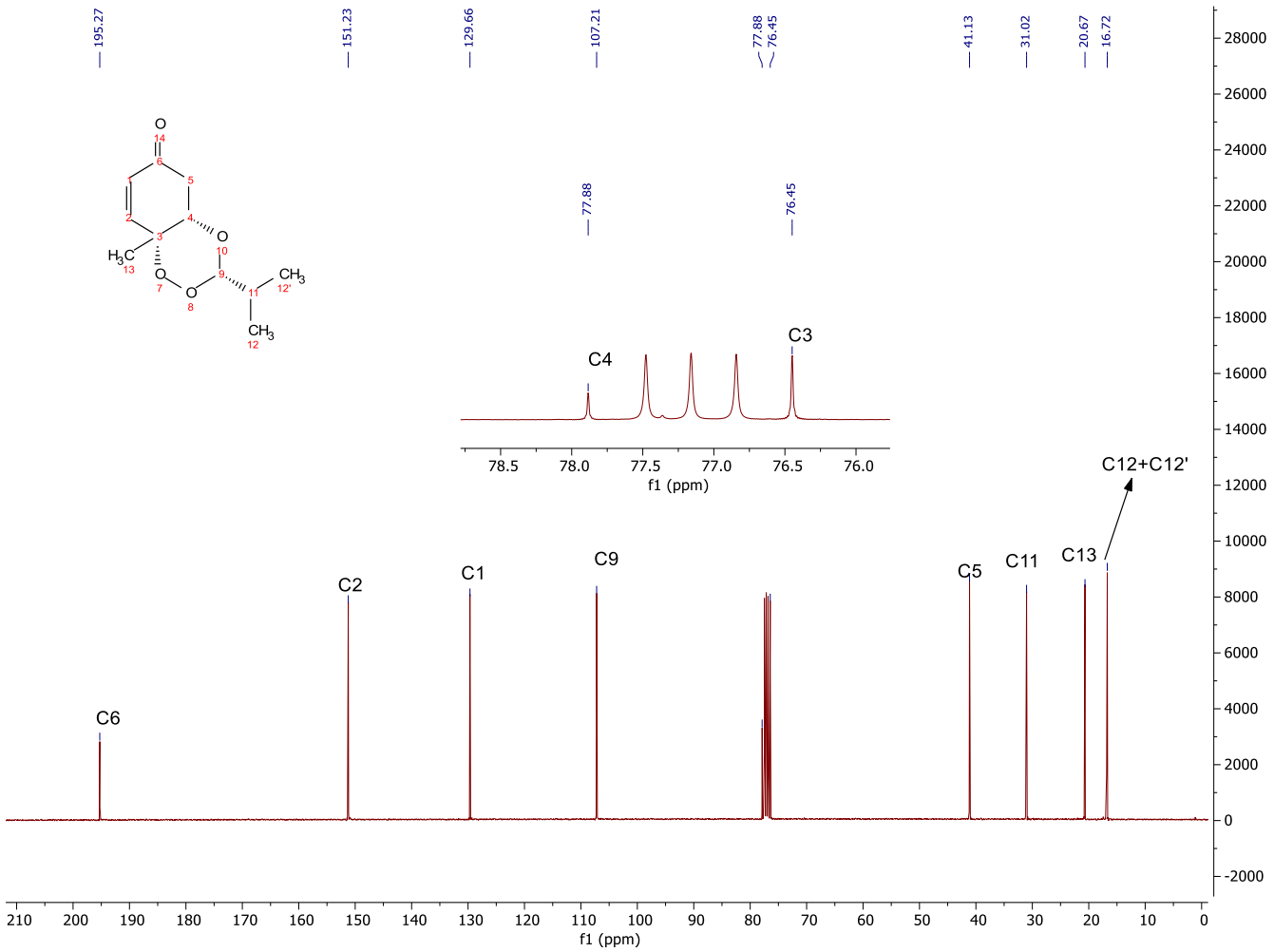


*Figure 5 - 18 ^{13}C NMR of **5.5a** in $CDCl_3$.*

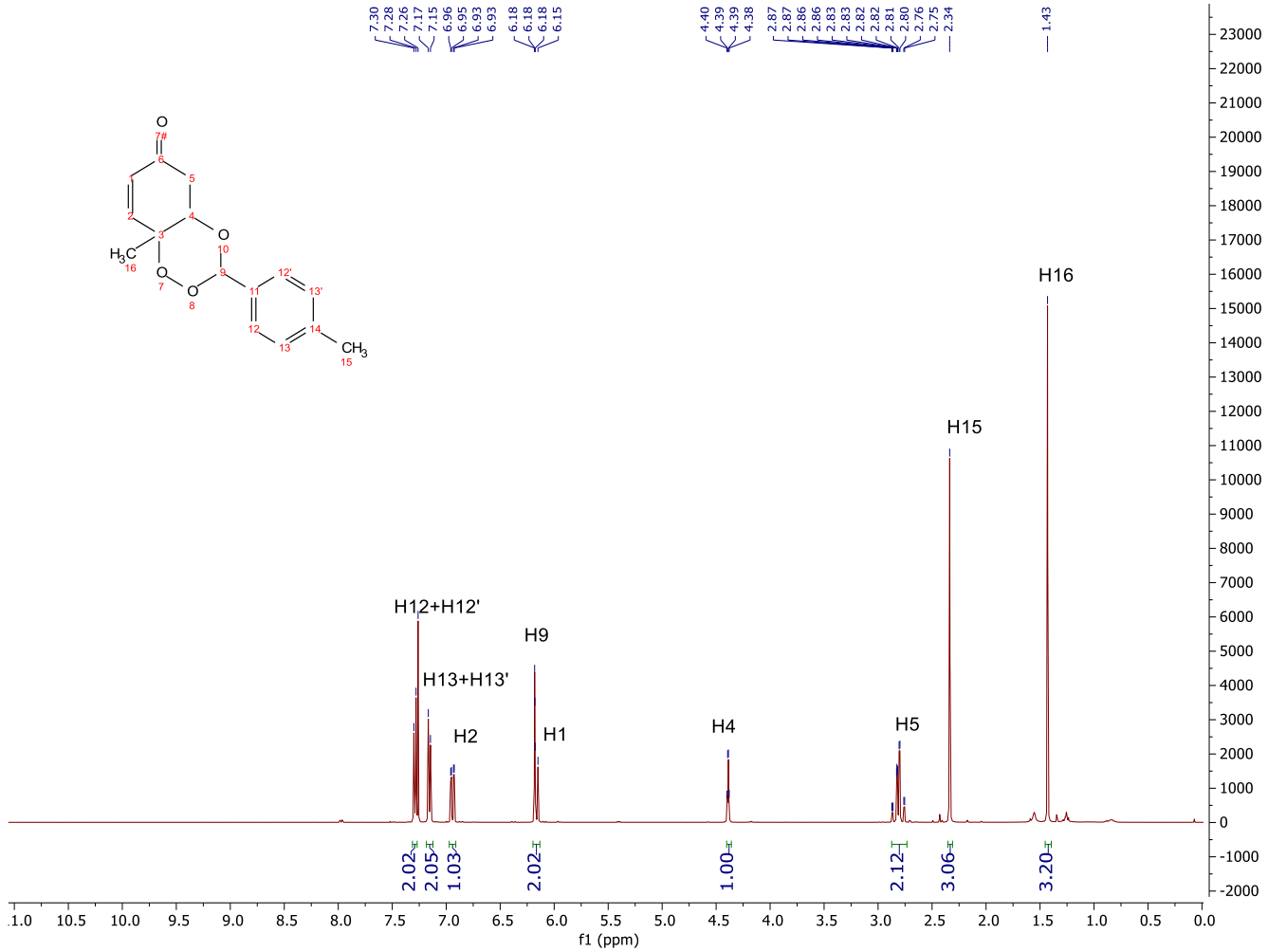


*Figure 5 - 19 ^{1}H NMR of **5.6a** in $CDCl_3$.*

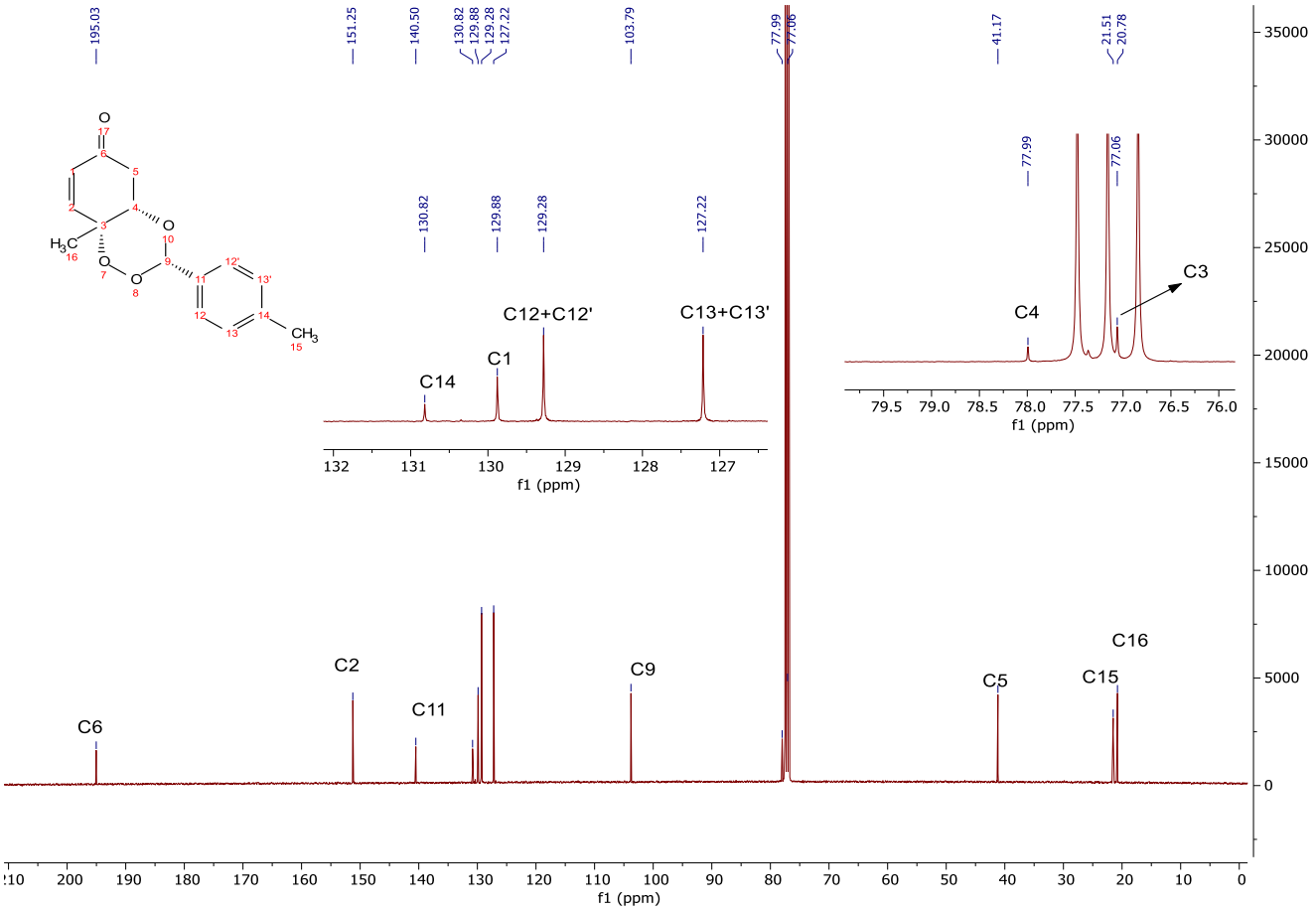


*Figure 5 - 20 ^{13}C NMR of **5.6a** in $CDCl_3$.*

Excel spreadsheet for data caculations

Key:	
	Data to be Altered Readily
	Numbers to Check Manually
	Numbers to be Recorded
	Switch Rate
	Warning
	Calculated values - do not edit

0.075

0.225

Parameter	Value	Units	Notes
CO_2			
Desired Flow Rate	0.15	$mLmin^{-1}$	
Pump Efficency	0.89	%	
Set Flow Rate	0.17	$mLmin^{-1}$	
Density at pump pressure	0.98391	gcm^{-3}	*Assumes Pump at -7C and 55 Bar pressure in cyclinder*

Publications

- *"Combining engineering and chemistry for the selective continuous production of four different oxygenated compounds by photo-oxidation of cyclopentadiene using liquid and supercritical CO_2 as solvents*," **L. Wu**, Z. Abada, D. Lee, M. Poliakoff,* M. George,* ***Tetrahedron*, 2018**, 74, 3107.
- "Photo-oxidation of fulvenes in a continuous flow photoreactor using carbon dioxide as a solvent," **L. Wu**, D. Lee,* H. Boufroura, M. Poliakoff,* M. George,* ***ChemPhotoChem*, 2018**, 2, 580. (**Cover paper**)